



**TARGETING ANTIBIOFILM COMPOUNDS FROM ENDOPHYTIC
FUNGI FROM INDIGENOUS NIGERIAN MEDICINAL PLANTS USING
A METABOLOMICS APPROACH**

BY

ELIZABETH CHIKA NWAGWU

B.Sc., M.Sc.

Strathclyde Institute of Pharmacy and Biomedical Sciences (SIPBS)

University of Strathclyde, Glasgow, UK.

A thesis submitted to The University of Strathclyde in fulfilment of the
requirements for the degree of Doctor of Philosophy.

September 2024.

Declaration

This thesis is the result of the author's original research. It is composed by the author and has not been previously submitted for examination which has led to award of the degree. The copyright of the thesis belongs to the author under the terms of the United Kingdom Copyright Acts as qualified by the University of Strathclyde regulation 3.50. Due acknowledgment must always be made of the use of any material contained in or derived from this thesis.

Signed:

Date:

Acknowledgements

My appreciation first goes to God Almighty for giving me the direction and enablement to carry out this work. I am grateful to God for his mercies and for being with me throughout this journey. I thank God for giving me a good supervisor.

I would like to express my utmost gratitude to my supervisor, Dr RuAngelie Edrada-Ebel, for accepting me as her student, for the knowledge she impacted on me, her patience, love, care, guidance, counsel, and encouragement during my study. She remains the best supervisor a student can rely on from start to finish. I thank my second supervisor, Mrs Louise Young, for her help and guidance in the biological assay work. I am grateful to Dr Rothwelle Tate for his help in PCR and ITS gene sequencing, Mr Craig Irving for his help in the NMR tests, Jessica Bame and Graeme Anderson for their support with the HR-LCMS tests.

I am extremely grateful to my father, Sir Emmanuel Osuji for sponsoring my PhD program and to my mother Lady Grace Osuji.

I thank my previous and current lab-mates in the NPs Metabolomics Group: Dr. Gustavo, Dr. Dana, Dr. Saif, Sanju, Roberth, Fadiyah, Dinesh, Farida, and Beatris. My thanks also go to Kirsty and Marcella. A very special thanks goes to Dr Christopher Lawson for standing by me at the early stages of the purification work. My appreciation goes to my sisters Blessing Ayininuola and Emmanuella Bioseh. I am also grateful to Pastor Chukwuemeka and Dr. Olivia Chinagorom.

Finally, I am grateful to my husband Ifeanyi Nwagwu who helped me take care of my children, so that I can do my laboratory work. My thanks also go to my children (Miracle and Breakthrough), who endured the long times I was away due to the PhD programme.

Publication, Posters and Conferences

Singh, Sanju, **Elizabeth Nwagwu**, Louise Young, Pankaj Kumar, Pramod B. Shinde, and RuAngelie Edrada-Ebel. 2024. "Targeted Isolation of Antibiofilm Compounds from Halophytic Endophyte *Bacillus velesensis* 7NPB-3B Using LC-HR-MS-Based Metabolomics," *Microorganisms* 12, no. 2: 413. <https://doi.org/10.3390/microorganisms12020413>

Scottish Metabolomics Network Symposium 2022. Oral conference presentation, P&J Live, Aberdeen - 3 and 4 November 2022.

Elizabeth Nwagwu, Farida Sobahy, Tabassum Ara, Rothwelle Tate, Louise Young, RuAngelie Edrada-Ebel. Using an NMR and MS based metabolomics approach to assess and optimise the antimicrobial and antibiofilm potential of a fungal endophyte DGS2 via OSMAC.

2nd Annual Mass Spectrometry User Group Meeting, 19th of April 2023. Oral conference presentation, University of Strathclyde, Glasgow.

Elizabeth Nwagwu, Farida Sobahy, Tabassum Ara, Rothwelle Tate, Louise Young, RuAngelie Edrada-Ebel. Using an NMR and MS based metabolomics approach to assess and optimise the antimicrobial and antibiofilm potential of a fungal endophyte DGS2 via OSMAC.

BIOACTIVE NPS RESEARCH MEETING July 13-14, 2023 | Lisbon, Portugal and Online (A Hybrid Conference).

Elizabeth Nwagwu, Beatris Bergamo, **RuAngelie Edrada-Ebel**. Metabolomic Profiling of Mixed Endosymbiotic Fungal Culture in the Enhancement of Anti-biofilm Activity.

Scottish Metabolomics Network Symposium 2023. East Kilbride, Glasgow- 15 and 16 November 2023. Poster.

Elisabeth Nwagwu, Beatris Bergamo, Louise Young, RuAngelie Edrad-Ebel. **Application of Metabolomic tools in the co-culture of two fungal endophytes and assessing their antibiofilm potentials (Poster).**

Elizabeth Nwagwu, Dinesh Rangadesh, Tabassum Ara, Rothwelle Tate, Louise Young, RuAngelie Edrada-Ebel. **A metabolomic approach in assessing the anti-Biofilm potentials of *F. proliferatum*-a fungal endophyte isolated from an indigenous Nigerian medicinal plant. (Poster)**

15th APS PharmSci 2024 international conference, University of Huddersfield-6th September 2024.

Table of Contents

List of Figures	10
List of Tables	22
Abbreviations	26
Abstract	28
CHAPTER 1	30
1 Introduction	30
1.1 Antimicrobial Resistance	30
1.1.1 MRSA as a global health challenge	31
1.1.2 Drug Resistance in <i>P. aeruginosa</i>	32
1.1.3 Microbial biofilms as a major cause of drug resistance.....	33
1.2 Medicinal Plants	33
1.3 NPs	34
1.3.1 Advantages of NPs	35
1.3.2 Disadvantages of NPs	36
1.4 Application of metabolomics in NPs drug agents	36
1.4.1 Liquid chromatography-mass spectrometry (LC-MS) based metabolomics	37
1.4.2 Nuclear Magnetic Resonance (NMR)	37
1.4.3 Limitations of metabolomics	38
1.4.4 Multivariate Analysis	39
1.5 Antimicrobials from NPs	39
1.6 Fungal Endophytes	40
1.7 Co-culturing of microorganisms	41
1.8 Hypothesis, study aims and objectives	42
CHAPTER 2	44
2 Materials and methods	44
2.1 Isolation and identification of endophytes from Nigerian medicinal plants ...	44
2.1.1 Plant Collection.....	45
2.2 Microbiological methods	45
2.2.1 Preparation of malt extract agar (MEA) media and fungal inoculation from 5 Nigerian medicinal plants.....	45
2.2.2 Initial inoculation of endophytic fungi from plants.....	46
2.2.3 Fungal culture purification step	46
2.2.4 Cryopreservation of isolated fungal endophyte	46
2.2.5 Screening of fungal endophytes for the presence of active secondary metabolites	46

2.2.6 Extracts test against planktonic, prebiofilm and postbiofilm MRSA and <i>P. aeruginosa</i>	48
2.3 NMR spectroscopy	52
2.4 LC-HRMS spectrometry.....	52
2.5 Identification of bio-active endophytic fungi by ITS gene sequencing.....	52
2.5.1 DNA Extraction	53
2.5.2 Internal Transcribed Spacer Polymerase Chain Reaction.....	53
2.5.3 Electrophoresis and Gel Purification of ITS PCR products	53
2.5.4 DNA Sequencing.....	54
2.6 Media optimisation	54
2.6.1 Reactivation and Culturing of active fungi.....	54
2.6.2 Media preparation to optimise the production of active crude extracts.....	54
2.7 Chemical analysis: Extraction, chromatographic separation, and structure elucidation	59
2.7.1 Scale-up fermentation and extraction of active fungal endophytes.....	59
2.7.2 Medium pressure liquid chromatography (MPLC).....	62
2.7.3 Thin layer chromatography (TLC).....	63
2.7.4 Preparative thin layer chromatography (PTLC).....	63
2.7.5 Anisaldehyde- sulphuric acid spray reagent composition.....	64
2.7.6 Fractionation of scale-up crude extracts.....	64
2.7.7 Purification of active fractions.....	68
CHAPTER 3.....	71
3 Isolation and Screening of Fungal Endophytes.....	71
3.1 Literature background on five selected plants for this study.....	71
3.1.1. <i>Vernonia amygdalina</i> as a source of NPs	71
3.1.2. <i>Ocimum gratissimum</i> as a source of NPs	71
3.1.3. <i>Fungal isolates indica</i> as a source of NPs	72
3.1.4. <i>Azadirachta indica</i> as a source of NPs	72
3.1.5. <i>Moringa oleifera</i> as a source of NPs	73
3.2 Fungal extraction.....	74
3.3 Bioassay screening of fungal extracts.....	75
3.3.1 Crude extract test results against MRSA.....	76
3.3.2 Crude extract test results against <i>P. aeruginosa</i>	76
3.3.3 Minimum inhibitory concentration (MIC) and Minimum biofilm eradication bacteria (MBEC) assay.....	77
3.4 NMR analysis of 34 fungal crude extracts.....	78
3.5 MVA of LC-HRMS data.....	85

3.6	ITS gene sequencing	95
3.7	Review of the crude extract screening results	96
CHAPTER 4.....		97
4	Secondary metabolites of <i>F. proliferatum</i> isolated from <i>Vernonia amygdalina</i>	97
4.1	Metabolites of <i>F. proliferatum</i>	97
4.2	Results and Discussion.....	99
4.2.1	Media optimisation and identification of metabolite production from <i>F. proliferatum</i>	99
4.2.2	<i>F. proliferatum</i> extract yields on 4 different media.	99
4.2.3	Extracts test against MRSA.....	101
4.2.4	Multivariate analysis of LC-HRMS data	102
4.2.5	Fractionation of <i>F. proliferatum</i> Scale-up crude extracts	120
4.2.6	Bioactivity test results of <i>F. proliferatum</i> fractions.....	121
4.2.7	NMR spectroscopy for <i>F. proliferatum</i> fractions	121
4.2.8	LC-HRMS analysis of <i>F. proliferatum</i> fractions	130
4.2.9	Pure compound isolation.....	139
4.2.10	Structure elucidation and identification of isolated metabolites	141
4.2.11	Bioactivity test results	145
4.3	Summary and conclusion	151
4.3.1	Isolation of fungi and extraction	151
4.3.2	Media optimisation and metabolomics bioassay guided isolation	151
4.3.3	Pure compounds isolation.....	152
4.3.4	Isolation of new compounds	153
CHAPTER 5.....		155
5	Secondary metabolites of <i>F. falciforme</i> isolated from <i>Moringa oleifera</i>	155
5.1	Metabolites of <i>F. falciforme</i>	155
5.2	Results and Discussion.....	156
5.2.1	Media optimisation and identification of metabolite production from <i>F. falciforme</i>	156
5.2.2	<i>F. falciforme</i> extract yields on 4 different media.....	156
5.2.3	Extract test against MRSA.....	158
5.2.4	Multivariate analysis of LC-HRMS data	159
5.2.5	Scale up fermentation and extraction of <i>F. falciforme</i> in the production of bioactive metabolites.....	176
5.2.6	Results obtained from Solvent – Solvent partitioning of <i>F. falciforme</i>	176
5.2.7	Bioactivity test results of <i>F. falciforme</i> fractions.....	177
5.2.8	NMR spectroscopy for <i>F. falciforme</i> fractions.....	178

5.2.9	LC-HRMS analysis of <i>F. falciforme</i> fractions	183
5.3	Summary and conclusion	195
5.3.1	Isolation of fungi and extraction	195
5.3.2	Media optimisation and metabolomics guided fractionation	196
5.3.3	Scale up and loss of bioactivity	196
CHAPTER 6	198
6	Secondary metabolites of <i>A. alternata</i> isolated from <i>A. indica</i>.	198
6.1	Metabolites of <i>Alternaria alternata</i>	198
6.2	Results and Discussion.....	198
6.2.1	Media optimisation and identification of metabolite production from <i>A. alternata</i>	198
6.2.2	<i>A. alternata</i> extract yields on 4 different media.	199
6.2.3	Extract test against MRSA	201
6.2.4	MVA of LC-HRMS data	202
6.2.5	Fractionation of <i>A. alternata</i> Scale-up crude extracts.....	214
6.2.6	Bioactivity test results of <i>A. alternata</i> fractions	215
6.2.7	NMR spectroscopy for <i>A. alternata</i> fractions	215
6.2.8	LC-HRMS analysis of <i>A. alternata</i> fractions.....	223
6.2.9	Pure compound isolation.....	233
6.2.10	Bioactivity test results	239
6.3	Summary and conclusion	245
6.3.1	Isolation of fungi and extraction	245
6.3.2	Media optimisation and metabolomics bioassay guided isolation	245
6.3.3	Pure compounds isolation.....	246
CHAPTER 7	247
7.1	Secondary metabolites from co-culture of isolated fungal endophytes and MRSA.....	247
7.2.	Results and Discussion.....	249
7.2.1	Co-culture extract yields on solid malt extract agar media	249
7.2.3	Multivariate analysis of LC-HRMS data	251
7.2.4	Co-culture extract yields on liquid malt extract media	265
7.2.5	Crude extract biological assay screening.....	267
7.2.6	Multivariate analysis of LC-HRMS data	267
7.2.7	Fractionation of <i>F. proliferatum</i> -MRSA Scale-up crude extracts	279
7.2.8	Bioactivity test results of <i>F. proliferatum</i> -MRSA fractions	280
7.2.9	NMR spectroscopy for <i>F. proliferatum</i> -MRSA fractions	280

7.2.10	LC-HRMS analysis of <i>F. proliferatum</i> -MRSA fractions	287
7.2.11	Pure compound isolation	294
7.2.12:	Bioactivity test results	295
7.3	Summary and conclusion	300
7.3.1	Media optimisation and metabolomics bioassay guided isolation	300
7.3.2	Pure compounds isolation.....	300
CHAPTER 8	302
8.1	Secondary metabolites from the co-culture of two fungal endophytes	302
8.2	Results and Discussion.....	304
8.2.1	Co-culture extract weights on solid malt extract agar media.....	304
8.2.2	Crude extract biological assay screening	305
8.2.3	Multivariate analysis of LC-HRMS data	306
8.2.4	Co-culture extract yields on liquid malt extract media	316
8.2.5	Crude extract biological assay screening	317
8.2.6	Multivariate analysis of LC-HRMS data	318
8.2.7:	Fractionation of <i>F. proliferatum</i> - <i>F. falciforme</i> crude extracts.....	327
8.2.8	Bioactivity test results of <i>F. proliferatum</i> - <i>F. falciforme</i> fractions.....	328
8.2.9	NMR spectroscopy for <i>F. proliferatum</i> - <i>F. falciforme</i> co-culture fractions	329
8.2.10	LC-HRMS analysis of <i>Fusarium</i> fractions	335
8.2.11	Pure compound isolation	341
8.2.12:	Bioactivity test results	344
8.3	Summary and conclusion	353
8.3.1	Media optimisation and metabolomics bioassay guided isolation	353
8.3.2	Pure compounds isolation.....	353
8.3.3	Proposed biosynthetic pathway of 1,4-Naphthoquinones.....	354
CHAPTER 9	357
Overall summary and future recommendations		357
10	References	362
11	APPENDIX	382

List of Figures

Figure 2.1: Flow diagram for the extraction of fungal endophytes.....	48
Figure 2.2: Plate map for 96-well plate use in MIC and MBEC.....	51
Figure 2.3: Summary diagram showing extraction protocol for both liquid and solid media..	58
Figure 2.4: Experimental workflow for <i>F. falciforme</i> (MgS3A) scale up from frozen state to extract.....	60
Figure 2.5: Summary diagram of solvent-solvent partitioning of <i>F. falciforme</i> extract grown on malt extract broth.....	61
Figure 2.6: Summary workflow of applying metabolomics in the search for antimicrobial agents.....	70
Figure 3.1: Average extract yields produced by isolated endophytic fungi. The purple bars represent the bioactive extracts against MRSA.....	74
Figure 3.2: Summary workflow showing the 5 plants used, and the 34 fungi endophyte isolated from them.....	75
Figure 3.3: (A) MIC and (B) MBEC results of BLS1.....	78
Figure 3.4: Stacked ¹ H NMR (400 MHz) data obtained from media (1), and 34 fungi crude extracts (2 to 35), isolated from 5 medicinal plants, measured in DMSO-d ₆	79
Figure 3.5: Stacked ¹ H NMR (400 MHz) data obtained from the 3 bioactive fungi extracts.....	80
Figure 3.6: (A) PCA scores and (B) loadings plots of the NMR spectra data of fungi crude extracts.....	82
Figure 3.7: PLS-DA of the NMR spectra data of fungi crude extracts.....	83
Figure 3.8: VIP scores of the 3 bioactive fungi extracts from Simca® showing the chemical shifts of 20 most discriminating metabolites with VIP scores above 1.....	84
Figure 3.9A: Heatmap analysis of the NMR spectral data of the 3 bioactive fungal extracts generated by MetaboAnalyst®.....	84
Figure 3.9B: Heatmap analysis of the NMR spectral data of the 3 bioactive fungal endophytes generated by MetaboAnalyst®.....	85
Figure 3.10: (A) PCA scores and (B) loadings plots of the LC-HRMS data of fungi crude extracts.....	86
Figure 3.11: (A) PCA scores and (B) loadings plots of the LC-HRMS data of 3 active fungi crude extracts. R ₂ X= 0.995 and Q ₂ X = 0.811. The difference between group R ₂ Xo [1] is equal to 60.2% and the difference within groups R ₂ X [2] is 17.5%.....	89
Figure 3.12: PCA Structures of compounds that were putatively identified through dereplication studies of 3 active fungi extracts listed in Table 3.3.....	93

Figure 3.13: Total Ion Chromatogram (TIC) of both positive and negative modes produced from active and blank extracts.....	94
Figure 3.14: Electrophoresis gel image of the PCR products of three fungi samples. The ITS PCR products were resolved on a 1% (w/v) agarose gel and visualised by ethidium bromide staining.	95
Figure 4.1: A summary workflow for isolation, identification, and culture of <i>F. proliferatum</i> ..	98
Figure 4.2: Histogram showing average weight of extracts from three respective replicates of <i>F. proliferatum</i> obtained from four different media and incubated at 7, 15, and 30 days....	101
Figure 4.3: (A) PCA scores and (B) loading plots of LC-HRMS data of <i>F. proliferatum</i> extracts from four media incubated at 7, 15, and 30 days. $R_2X= 0.831$ and $Q_2X = 0.611$. Encircled features represent the discriminating ion peaks for the outlying extracts obtained from malt and potato media incubated for 15 and 30 days.....	104
Figure 4.4: (A) PLS-DA scores and (B) loading plots of LC-HRMS of <i>F. proliferatum</i> extract obtained from different media. The encircled box indicated the discriminating feature for the respective fungal extracts from various media. $R_2 = 0.965$ and $Q_2 = 0.895$. The difference between group R_2X_0 [1] is equal to 29.8% and the difference within groups R_2X [2] is 23.5%.....	106
Figure 4.5: PLS-DA Structures of the discriminating metabolites from <i>F. proliferatum</i> extract obtained from different media.....	110
Figure 4.6: (A) OPLS-DA scores and (B) S- plots of LC-HRMS of <i>F. proliferatum</i> extracts obtained from different media. The encircled metabolites on S-plot indicated the discriminating feature for each media extracts. $R_2 = 0.912$ and $Q_2 = 0.759$. The difference between group R_2X_0 [1] is equal to 67.4% and the difference within groups R_2X [2] is 25.5%.....	113
Figure 4.7: Structures of the discriminating active metabolites from <i>F. proliferatum</i> extract obtained from four different media.....	116
Figure 4.8: Heatmap analysis of the mass spectral data of <i>F. proliferatum</i> extracts with their m/z values, obtained from different media, generated by MetaboAnalyst®.	117
Figure 4.9: Total ion chromatogram (TIC) (A= Positive, B= Negative) of the bioactive extracts of <i>F. proliferatum</i> from different media. The ion peaks that represent the discriminating features listed in Table 4.4 and 4.5 have been labelled (Schmid <i>et al.</i> , 2023).....	118
Figure 4.10: Summary TLC Plate of <i>F. proliferatum</i> pooled fractions after spraying with anisaldehyde-sulphuric acid. The TLC plate showed fractions from the non-polar solvent of hexane to the more polar solvent of ethylacetate (100% Hexane- 100% ethylacetate). Bioactive fractions are highlighted in red box.....	120

Figure 4.11: Stacked ¹ H NMR spectra of the bioactive <i>F. proliferatum</i> fractions ranging from fraction 8 to 14.....	122
Figure 4.12: (A) PCA scatter and (B) loading plots of the NMR spectral data of the active fractions. The R ₂ X and Q ₂ X values were 1.00 and 0.99, respectively.....	123
Figure 4.13: OPLS-DA scores (A) and loadings (B) plots of the NMR spectral data of <i>F. proliferatum</i> fractions grouped according to their bioactivity against MRSA. R ₂ and Q ₂ values were 0.996 and 0.915, respectively. The difference between group R ₂ X _o [1] is equal to 36.9 % and the difference within groups R ₂ X [2] is 6.0 %. The chemical shift of the discriminating features were labelled.....	125
Figure 4.14: VIP scores of <i>F. proliferatum</i> fractions from Simca® showing the chemical shifts of 20 most discriminating metabolites with VIP scores above 1.....	127
Figure 4.15: DMod X results to test the occurrence of true outliers. Variables above the red line are the true outliers that includes only fraction 8.....	127
Figure 4.16A: Heatmap analysis of the NMR spectral data of <i>F. proliferatum</i> fractions generated by MetaboAnalyst®. The purple boxed fractions (F8-F14) are those biologically active against MRSA along with the discriminating chemical shifts.....	128
Figure 4.16B: Heatmap analysis of the NMR spectral data of <i>F. proliferatum</i> fractions generated by MetaboAnalyst®. The red boxed fractions (F8-F14) are those biologically active against MRSA along with the discriminating chemical shifts.....	129
Figure 4.17: PCA scores (A) and loadings (B) plots of the LC-HRMS data of <i>F. proliferatum</i> fractions. Labelled features represent the discriminating ion peaks for the outlier F11 to F14. The R ₂ and Q ₂ values were 1.0 and 0.997 respectively.....	131
Figure 4.18: OPLS-DA scores (A) and S-plot (B) of the LC-HRMS data of <i>F. proliferatum</i> fractions. Labelled features represent the discriminating active fractions. The R ₂ and Q ₂ values were 0.999 and 0.788 respectively. The difference between group R ₂ X _o [1] is equal to 21.5 % and the difference within groups R ₂ X [2] is 14.1 %.....	132
Figure 4.19: Structures of dereplicated compound hits showing PCA and OPLSDA active discriminating metabolites obtained from <i>F. proliferatum</i> fractions, as listed in Table 4.8 and 4.9.....	134
Figure 4.20: DMod X results to confirm the occurrence of true outliers. Variables above the red line are the true outliers, that includes extracts fraction 1, 2 and 4.....	136
Figure 4.21: Total ion chromatogram (TIC) (A = Positive, B = Negative) of the bioactive fractions of <i>F. proliferatum</i>	137
Figure 4.22: Summary workflow of <i>F. proliferatum</i> scale-up crude extract to isolated compounds.....	140
Figure 4.23: Effect of pure compounds isolated from <i>F. proliferatum</i> . Left-planktonic (A), prebiofilm (B), and postbiofilm (C) MRSA. Right- planktonic (A) and prebiofilm (B) SA-NCTC	

8325 at 100µg/mL. The blue line indicates the bioactivity threshold which is 30% viability (70% inhibition).....	146
Figure 4.24: Distribution of the isolated compounds on the active quadrant by OPLS-DA showing predicted compounds with their molecular weights.....	147
Figure 4.25: Distribution of the isolated compounds on the active quadrant by OPLS-DA showing predicted compounds with their molecular weights.....	148
Figure 5.1: Histogram of extract average weights of <i>F. falciforme</i> obtained from four different media and incubated at 7, 15, and 30 days.....	158
Figure 5.2: (A) PCA scores (B) loading plots of LC-HRMS data of <i>F. falciforme</i> extracts from four media incubated at 7, 15, and 30 days. $R_2X = 0.935$ and $Q_2X = 0.824$	161
Figure 5.3: PCA Structures of the discriminating metabolites from <i>F. falciforme</i> extract obtained from malt media and listed in Table 5.4.....	164
Figure 5.4: (A) PLS-DA scores and (B) loading plots of LC-HRMS of <i>F. falciforme</i> extract obtained from different media. The encircled box indicated the discriminating feature for each media extracts. $R_2 = 0.923$ and $Q_2 = 0.973$. The difference between group $R_2X_0 [1]$ is equal to 59.8% and the difference within groups $R_2X [2]$ is 4.5%.....	166
Figure 5.5: PLS-DA Structures of the discriminating metabolites from <i>F. falciforme</i> extract obtained from potato, rice, and oat media and listed in Table 5.4.....	168
Figure 5.6: (A) OPLS-DA scores and (B) S- plots of LC-HRMS of <i>F. falciforme</i> extracts obtained from different media. $R_2 = 0.978$ and $Q_2 = 0.907$. The difference between group $R_2X_0 [1]$ is equal to 54.6% and the difference within groups $R_2X [2]$ is 12.3%.....	170
Figure 5.7: Structures of the discriminating bioactive metabolites of <i>F. falciforme</i> extracts from different media and listed in Table 5.5.....	173
Figure 5.8: Heatmap analysis of the mass spectral data of <i>F. falciforme</i> extracts with their Mzmine values, obtained from different media, generated by MetaboAnalyst®.	174
Figure 5.9: Total ion chromatogram (TIC) of the bioactive extracts of <i>F. falciforme</i> from different media.....	175
Figure 5.10: Effect of <i>F. falciforme</i> MeOH and Hexane fractions against MRSA.....	177
Figure 5.11: Stacked 1H NMR spectra of <i>F. falciforme</i> malt 15 days crude extract, MeOH and hexane fractions.....	179
Figure 5.12: (A) PCA scatter and (B) loading plots of the NMR spectral data of <i>F. falciforme</i> malt 15 days crude extract, MeOH and hexane fractions. The R_2X and Q_2X values were 1.00 and 0.997, respectively.....	180

Figure 5.13: OPLS-DA scores (A) and S (B) plots of the NMR spectral data of <i>F. falciforme</i> extracts grouped according to their bioactivity against MRSA. R_2 and Q_2 values were both 1. The difference between group R_2X_0 [1] is equal to 61.4 % and the difference within groups R_2X [2] is 38.6 %.....	181
Figure 5.14: VIP scores of <i>F. falciforme</i> malt 15 extract, MeOH and hexane fractions from Simca® showing the chemical shifts of 20 most discriminating metabolites with VIP scores above 1.....	182
Figure 5.15: PCA scores (A) and loadings (B) plots of the LC-HRMS data of <i>F. falciforme</i> MeOH and hexane fractions. The R_2 and Q_2 values were 0.990 and 0.950 respectively.....	184
Figure 5.16: Structures of dereplicated compound hits showing PCA discriminating metabolites obtained from <i>F. falciforme</i> MeOH (green box) and Hexane (purple box) fractions, as listed in Table 5.8 and 5.9.....	188
Figure 5.17: PCA scores (A) and loadings (B) plots of the LC-HRMS data of <i>F. falciforme</i> Malt 15 days extracts, MeOH and hexane fractions. The R_2 and Q_2 values were 0.984 and 0.937 respectively.....	190
Figure 5.18: PLS-DA scores (A) and loadings (B) plots of the LC-HRMS data of <i>F. falciforme</i> malt 15 days extracts, MeOH and hexane fractions. The R_2 and Q_2 values were 0.995 and 0.992 respectively.....	191
Figure 5.19: Effect of <i>F. falciforme</i> fractions (MeOH + Hexane) on (A) Planktonic and (B) Post biofilm MRSA. The combination of 50% MeOH and 50% hexane fractions restored <i>F. falciforme</i> bioactivity.....	195
Figure 6.1: Histogram showing average weight of extracts from three respective replicates of <i>A. alternata</i> obtained from four different media and incubated at 7, 15, and 30 days.....	201
Figure 6.2: (A) PCA scores and (B) loading plots of LC-HRMS data of <i>A. alternata</i> extracts from four media incubated at 7, 15, and 30 days. $R_2X= 0.727$ and $Q_2X = 0.374$. Encircled features represent the discriminating ion peaks for the outlying extracts obtained from malt 30, potato 30 and rice 30 days.....	204
Figure 6.3: PCA Structures of the discriminating metabolites from <i>A. alternata</i> extract obtained from different media and listed in Table 6.3.....	207
Figure 6.4: (A) OPLS-DA scores and (B) S- plots of LC-HRMS of <i>A. alternata</i> extracts obtained from different media. The labelled metabolites on S-plot indicated the discriminating active extracts as listed under Table 6.4. $R_2 = 0.998$ and $Q_2 = 0.869$. The difference between group R_2X_0 [1] is equal to 60.8% and the difference within groups R_2X [2] is 24.1%.....	209

Figure 6.5: Heatmap analysis of the mass spectral data of <i>A. alternata</i> extracts with their Mzmine values, obtained from different media, generated by MetaboAnalyst®.....	212
Figure 6.6: Total ion chromatogram (TIC) of the bioactive extracts of <i>A. alternata</i> from different media. The ion peaks that represent the discriminating features listed in Table 6.4 have been labelled.....	213
Figure 6.7: Summary TLC Plate of <i>A. alternata</i> pooled fractions after spraying with anisaldehyde-sulphuric acid.....	214
Figure 6.8: Stacked ¹ H NMR spectra of the bioactive <i>A. alternata</i> fractions ranging from fraction F4 to F9 and F31-P.....	216
Figure 6.9: PCA scores (A) and loadings (B) plots of the LC-HRMS data of <i>A. alternata</i> fractions. Labelled features represent the discriminating ion peaks for the outlier F4, F5, F30P and F31P. The R ₂ and Q ₂ values were 0.995 and 0.787 respectively.....	217
Figure 6.10: OPLSDA scores (A) and S (B) plots of the LC-HRMS data of <i>A. alternata</i> fractions. Labelled features represent the discriminating bioactive metabolites listed under Table 6.8. The R ₂ and Q ₂ values were 0.866 and 0.599 respectively. The difference between group R ₂ X ₀ [1] is equal to 27.4 % and the difference within groups R ₂ X [2] is 16.2 %.....	219
Figure 6.11: DMod X results to test the occurrence of true outliers. Variables above the red line are the true outliers that includes only fraction 5.....	221
Figure 6.12: VIP scores of <i>A. alternata</i> fractions from Simca® showing the chemical shifts of 20 most discriminating metabolites with VIP scores above 1.....	221
Figure 6.13: Heatmap analysis of the NMR spectral data of <i>A. alternata</i> fractions generated by MetaboAnalyst®. The purple boxed fractions (F4-F9, F31-P) are those biologically active against MRSA along with the discriminating chemical shifts. The green boxed fractions were F2 and F3 which was discriminatory but inactive. Highlighted chemical shifts on the Y-axis indicate common metabolites observed on the heatmap and VIP.....	222
Figure 6.14: PCA scores (A) and loadings (B) plots of the LC-HRMS data of <i>A. alternata</i> fractions. Labelled features represent the discriminating ion peaks for the outlier F4, F5, F30P and F31P. The R ₂ and Q ₂ values were 0.995 and 0.787 respectively.....	224
Figure 6.15: OPLSDA scores (A) and S (B) plots of the LC-HRMS data of <i>A. alternata</i> fractions. Labelled features represent the discriminating bioactive metabolites listed under Table 6.8. The R ₂ and Q ₂ values were 0.866 and 0.599 respectively. The difference between group R ₂ X ₀ [1] is equal to 27.4 % and the difference within groups R ₂ X [2] is 16.2 %.....	226
Figure 6.16: Structures of dereplicated compound hits showing MVA discriminating metabolites obtained from <i>A. alternata</i> fractions, as listed in Table 6.7 and 6.8.....	231

Figure 6.17: Total ion chromatogram (TIC) of the bioactive fractions of <i>A. alternata</i> . The ion peaks that represent the discriminating features listed in Table 6.8 have been labelled.....	232
Figure 6.18: Summary workflow of <i>A. alternata</i> scale-up crude extract showing isolated and re-isolated compounds.....	234
Figure 6.19: Effect of pure compounds isolated from <i>A. Alternaria</i> against planktonic (A), prebiofilm (B), and postbiofilm (C) MRSA at 100µg/mL. The blue line indicates the bioactivity threshold.....	240
Figure 6.20: (A) MIC of alternariol and altenuisol, (B) MBEC results 9-O-acetylalternariol..	241
Figure 6.21: Distribution of the isolated compounds on the active quadrant by OPLS-DA S-plot for the fractionation stage.....	242
Figure 6.22: Distribution of the isolated compounds on the active quadrant by OPLS-DA S-plot during the media optimisation stage.....	243
Figure 7.1: A summary workflow for crude extract screening, media optimisation and scaling up of three fungal isolates co-cultured with MRSA.....	248
Figure 7.2: Histogram showing average weight of extracts from three respective replicates of <i>F. proliferatum</i> + MRSA, <i>F. falciforme</i> + MRSA and <i>A. alternata</i> + MRSA co-cultures obtained from malt extract media and incubated for 4 and 10 days.....	250
Figure 7.3: (A) PCA scores and (B) loadings plots of LC-HRMS data of co-culture extracts from malt extract media incubated at 4 and 10 days. $R_2X= 0.481$ and $Q_2X = 0.274$	253
Figure 7.4: Structures of dereplicated compound hits showing PCA discriminating metabolites obtained from co-culture extracts, as listed in Table 7.4.....	256
Figure 7.5: PLSDA scores of LC-HRMS data of co-culture extracts from malt extract media incubated at 4 and 10 days. $R_2X= 0.992$ and $Q_2X = 0.911$. The variation between groups R_2X_0 [1] was 29.3 % and within group R_2X [2] was 17.3%.....	257
Figure 7.6: (A) OPLS-DA scores and (B) S- plots of LC-HRMS of co-culture extracts obtained from malt extract media. The labelled metabolites on S-plot indicated the discriminating feature for each media extracts. $R_2 = 0.987$ and $Q_2 = 0.889$. The difference between group R_2X_0 [1] is equal to 27.2% and the difference within groups R_2X [2] is 18.3%.....	259
Figure 7.7: Heatmap analysis of the mass spectral data of co-culture crude extracts with their m/z values, obtained from malt extract media, generated by MetaboAnalyst®.....	263
Figure 7.8: Total ion chromatogram (TIC) of the bioactive extracts of <i>F. proliferatum</i> -MRSA co-culture from malt extract media.....	264

Figure 7.9: Histogram showing average weight of extracts from three respective replicates of <i>F. proliferatum</i> + MRSA, <i>F. falciforme</i> + MRSA and <i>A. alternata</i> + MRSA co-cultures obtained from malt extract media and incubated for 15 and 30 days.....	266
Figure 7.10: (A) PCA scores and (B) loadings plots of LC-HRMS data of co-culture extracts from malt extract media incubated at 15 and 30 days. $R_2X= 0.939$ and $Q_2X = 0.647$	269
Figure 7.11: Structure of dereplicated compound hit showing PCA discriminating metabolite obtained from 15- and 30-days co-culture extracts, as listed in Table 7.8 and 7.9.....	272
Figure 7.12: (A) OPLS-DA scores and (B) S- plots of LC-HRMS of co-culture extracts obtained from malt extract media. The labelled metabolites on S-plot indicated the discriminating feature for each media extracts. $R_2 = 0.989$ and $Q_2 = 0.943$. The difference between group R_2X_0 [1] is equal to 28.3% and the difference within groups R_2X [2] is 17.5%.....	274
Figure 7.13: Heatmap analysis of the mass spectral data of co-culture crude extracts with their Mzmine values, obtained from malt extract media, generated by MetaboAnalyst®.....	277
Figure 7.14: Total ion chromatogram (TIC) of the bioactive extracts of <i>F. proliferatum</i> -MRSA co-culture from malt extract media.....	278
Figure 7.15: Summary TLC Plate of <i>F. proliferatum</i> -MRSA pooled fractions before (UV bands) and after spraying with anisaldehyde-sulphuric acid. The TLC plate showed fractions from the non-polar solvent of hexane to the more polar solvent of ethylacetate (100% Hexane- 100% ethylacetate).....	279
Figure 7.16: Stacked 1H NMR spectra of the bioactive <i>F. proliferatum</i> -MRSA fractions consisting of F2, F3, F5, F6.....	281
Figure 7.17: (A) PCA scatter and (B) loadings plots of the NMR spectral data of the active fractions. The R_2X and Q_2X values were 0.982 and 0.888, respectively.....	282
Figure 7.18: OPLS-DA scores (A) and loadings (B) plots of the NMR spectral data of <i>F. proliferatum</i> -MRSA fractions grouped according to their bioactivity against MRSA. R_2 and Q_2 values were 1.000 and 0.779, respectively. The difference between group R_2X_0 [1] is equal to 26.6 % and the difference within groups R_2X [2] is 16.7 %.....	283
Figure 7.19: DMod X results to test the occurrence of true outliers. Variables above the red line are the true outliers that includes only fraction 3.....	284
Figure 7.20: VIP scores of <i>F. proliferatum</i> -MRSA fractions from Simca® showing the chemical shifts of 20 most discriminating metabolites with VIP scores above 1.....	285
Figure 7.21: Heatmap analysis of the NMR spectral data of <i>F. proliferatum</i> -MRSA fractions generated by MetaboAnalyst®.....	286

Figure 7.22: PCA scores (A) and loadings (B) plots of the LC-HRMS data of <i>F. proliferatum</i> -MRSA fractions. Labelled features represent the discriminating ion peaks. The R_2 and Q_2 values were 1.0 and 0.999 respectively.....	288
Figure 7.23: Structures of dereplicated compound hits showing PCA discriminating metabolites obtained from fractions of <i>F. proliferatum</i> -MRSA co-culture extract, as listed in Table 7.13.....	290
Figure 7.24: OPLS-DA scores (A) and S-plot (B) of the LC-HRMS data of <i>F. proliferatum</i> -MRSA fractions. Labelled features represent the discriminating active fractions. The R_2 and Q_2 values were 1 and 0.953 respectively. The difference between group R_2X_0 [1] is equal to 39.9 % and the difference within groups R_2X [2] is 16.2 %.....	291
Figure 7.25: Total ion chromatogram (TIC) of the bioactive fractions of <i>F. proliferatum</i> -MRSA.....	293
Figure 7.26: Summary workflow of <i>F. proliferatum</i> -MRSA scale-up crude extract to isolated compounds.....	294
Figure 7.27: Effect of pure compounds isolated from <i>F. proliferatum</i> -MRSA. Left plots are the planktonic (A), prebiofilm (B), and postbiofilm (C) activity against MRSA. Right plots are the planktonic (A) and prebiofilm (B) activity on SA-NCTC 8325 at 100 μ g/mL. The blue line indicates the bioactivity threshold which is 30% viability (70.0% inhibition).....	296
Figure 7.28: Distribution of the isolated compounds detected on the left active quadrant of the OPLS-DA loadings plot of the co-culture extracts generated during the media optimisation stage.....	298
Figure 7.29: Distribution of the isolated compounds on the right active quadrant of the OPLS-DA loadings plot of the chromatographic fractions.....	298
Figure 8.1: A summary workflow for crude extract screening, media optimisation and scale-up of co-cultures of two fungal strains.....	302
Figure 8.2: Source and co-cultures of <i>Fusarium proliferatum</i> + <i>Fusarium falciforme</i> , <i>Fusarium falciforme</i> + <i>Alternaria alternata</i> , <i>Fusarium proliferatum</i> + <i>Alternaria alternata</i> on solid malt extract agar.....	303
Figure 8.3: Histogram showing average weight of extracts from three respective replicates of <i>F. proliferatum</i> + <i>F. falciforme</i> , <i>F. proliferatum</i> + <i>A. alternata</i> , <i>A. alternata</i> + <i>F. falciforme</i> co-cultures obtained from malt extract media and incubated for 7 days.....	305
Figure 8.4: (A) PLS-DA scores and (B) loading plots of LC-HRMS data of co-culture fungal extracts from malt extract media incubated at 7 days. $R_2X= 0.994$ and $Q_2X = 0.888$. The difference between groups R_2X_0 [1] is equal to 45.1 % and the difference within groups R_2X [2] is 21.4%.....	307
Figure 8.5: Structures of dereplicated compound hits showing PLS-DA discriminating metabolites obtained from co-culture extracts, as listed in Table 8.4.....	309

Figure 8.6: (A) OPLS-DA scores and (B) S- plots of LC-HRMS of co-culture extracts obtained from malt extract media. The labelled metabolites on S-plot indicated the discriminating feature for the active extracts. $R_2 = 0.983$ and $Q_2 = 0.886$. The difference between group R_2X_0 [1] is equal to 47.9% and the difference within groups R_2X [2] is 7.6%.....	311
Figure 8.7: Structure of dereplicated compound hit showing OPLS-DA discriminating metabolite obtained from bioactive co-culture extracts, as listed in Table 8.5.....	313
Figure 8.8: Heatmap analysis of the mass spectral data of co-culture crude extracts with their Mzmine values, obtained from malt extract media, generated by MetaboAnalyst®.....	314
Figure 8.9: Total ion chromatogram (TIC) of the bioactive co-culture extracts from malt extract agar media.....	315
Figure 8.10: Histogram showing average weight of extracts from two respective replicates of co-cultures of <i>F. proliferatum</i> + <i>F. falciforme</i> and <i>F. proliferatum</i> + <i>A. alternata</i> obtained from malt extract media and incubated for 15 and 30 days.....	317
Figure 8.11: (A) PCA scores and (B) loading plots of LC-HRMS data of co-culture fungal extracts from malt extract media incubated at 15 and 30 days. $R_2X = 0.898$ and $Q_2X = 0.651$	319
Figure 8.12: Structures of dereplicated compound hits showing PCA discriminating metabolites obtained from fungi-to-fungi co-culture extracts, as listed in Table 8.8.....	321
Figure 8.13: (A) OPLS-DA scores and (B) S- plots of LC-HRMS of co-culture extracts obtained from malt extract media. The labelled metabolites on S-plot indicated the discriminating feature for each media extracts. $R_2 = 0.996$ and $Q_2 = 0.989$. The difference between group R_2X_0 [1] is equal to 57.0% and the difference within groups R_2X [2] is 15.6%.....	323
Figure 8.14: Heatmap analysis of the mass spectral data of fungi-to-fungi co-culture crude extracts with their Mzmine values, obtained from malt extract media, generated by MetaboAnalyst®.....	325
Figure 8.15: Total ion chromatogram (TIC) of the bioactive extracts of <i>F. proliferatum</i> - <i>F. falciforme</i> co-culture from malt extract media.....	326
Figure 8.16: Summary TLC Plate of <i>F. proliferatum</i> - <i>F. falciforme</i> pooled fractions before (UV bands) and after spraying with anisaldehyde-sulphuric acid. The TLC plate showed fractions from the non-polar solvent of hexane to the more polar solvent of ethylacetate (100% Hexane-100% ethylacetate).....	327
Figure 8.17: Stacked 1H NMR spectra of the bioactive <i>F. proliferatum</i> - <i>F. falciforme</i> fractions consisting of F3, F4, F5, F6, F7, F8, W1.....	330
Figure 8.18: (A) PCA scatter and (B) loading plots of the NMR spectral data of the active fractions. The R_2X and Q_2X values were 0.972 and 0.514, respectively.....	331

Figure 8.19: OPLS-DA scores (A) and (B) S plots of the NMR spectral data of <i>F. proliferatum</i> - <i>F. falciforme</i> fractions grouped according to their bioactivity against MRSA. R_2 and Q_2 values were 1.0 and 0.318, respectively. The difference between group R_2X_0 [1] is equal to 11.9 % and the difference within groups R_2X [2] is 1.1 %.....	332
Figure 8.20: VIP scores of <i>F. proliferatum</i> - <i>F. falciforme</i> fractions from Simca® showing the chemical shifts of 20 most discriminating metabolites with VIP scores above 1. The top 20 VIP showed that the discriminatory metabolites mostly consisted of aliphatics and sugars ranging between 0.81 to 3.53 ppm.....	333
Figure 8.21: Heatmap analysis of the NMR spectral data of <i>F. proliferatum</i> - <i>F. falciforme</i> fractions generated by MetaboAnalyst®.....	334
Figure 8.22: PCA scores (A) and loadings (B) plots of the LC-HRMS data of <i>F. proliferatum</i> - <i>F. falciforme</i> fractions.....	336
Figure 8.23: OPLS-DA scores (A) and S-plot (B) of the LC-HRMS data of <i>F. proliferatum</i> - <i>F. falciforme</i> fractions.....	338
Figure 8.24: Total ion chromatogram (TIC) of the bioactive fractions of <i>F. proliferatum</i> - <i>F. falciforme</i> . The ion peaks that represent the discriminating features listed in Table 8.13 have been labelled.....	340
Figure 8.25: Summary workflow of <i>F. proliferatum</i> - <i>F. falciforme</i> co-culture crude extract to isolated compounds.....	341
Figure 8.26: Comparison of the ^1H -NMR data of linoleic acid isolated from <i>Alternaria</i> (DGS2) and the <i>Fusarium</i> co-culture.....	344
Figure 8.27: Mass and NMR spectral data of F3-6 indicating the occurrence of a methyl-ether derivative of javanicin. A) TIC of F3-6, B) EIC for ion peak at m/z 305.101 $[\text{M}+\text{H}]^+$ and TLC band for F3-6. C) Mass spectrum for ion peak at m/z 305.101 $[\text{M}+\text{H}]^+$ for $\text{C}_{16}\text{H}_{17}\text{O}_6$. D) ^1H NMR spectrum of F3-6 showing the proton assignments for a methyl-ether derivative of javanicin in DMSO-d_6	345
Figure 8.28: Effect of pure compounds isolated from <i>F. proliferatum</i> - <i>F. falciforme</i> . Left plots are the planktonic (A), prebiofilm (B), and postbiofilm (C) activity against MRSA. Right plots are the planktonic (A) and prebiofilm (B) activity on SA-NCTC 8325 at 100 $\mu\text{g}/\text{mL}$. The blue line indicates the bioactivity threshold which is 20% viability (80.0% inhibition).....	347
Figure 8.29: (Top) MIC and (Down) MBEC results of compounds with bioactivity above 80.00%.....	348
Figure 8.30: Distribution of the isolated compounds on the right active quadrant of the OPLS-DA loadings plot of the chromatographic fractions.....	350
Figure 8.31: Distribution of the isolated compounds on the right active quadrant of the OPLS-DA loadings plot of the crude extracts.....	351

Figure 8.32: Schematic diagram of proposed naphthoquinone biosynthetic pathway in the fungi genus *Fusarium*.....355

List of Tables

Table 2.1: Materials.....	44
Table 2.2: Equipment.....	45
Table 2.3: Sample concentration required for screening.....	47
Table 2.4: Experimental set up for media optimisation.....	55
Table 2.5: The components of anisaldehyde/sulfuric acid spray reagent.....	64
Table 2.6: Elution gradient for fractionation of <i>F. proliferatum</i> extracts obtained from scale-up with Rice media.....	65
Table 2.7: Elution gradient for the fractionation of <i>A. alternata</i> obtained from scale-up with Potato media.....	66
Table 2.8: Elution gradient for fractionation of <i>F. proliferatum</i> and MRSA co-culture Scale-up obtained from malt broth media.....	67
Table 2.9: Elution gradient used in fractionating co-culture of <i>F. proliferatum</i> and <i>F. falciforme</i>	68
Table 3.1: Summary of Planktonic, prebiofilm, and postbiofilm percentage inhibition of active crude extracts against MRSA.....	76
Table 3.2: Summary of Planktonic, prebiofilm, and postbiofilm percentage viability of active crude extracts against <i>P. aeruginosa</i>	77
Table 3.3: Loadings plot – compound hits for the discriminatory 3 active fungi metabolites isolated from 5 medicinal plants.....	90
Table 4.1: Extract yields of <i>F. proliferatum</i> , grown on different media and incubated for 7, 15, and 30 days. All cultures were incubated at 27°C.....	100
Table 4.2: Types of media and incubation days.....	100
Table 4.3: Summary activity of <i>F. proliferatum</i> extracts from different media against Planktonic, Prebiofilm, and Post biofilm MRSA at concentrations of 100 µg/ml.....	102
Table 4.4: PLS-DA loadings plot–dereplicated compound hits from discriminating metabolites for (A) Malt, (B) Potato, (C) Rice, and (D) Oat.....	107
Table 4.5: OPLSDA S-plot – compound hits for the discriminating bio-active metabolites of <i>F. proliferatum</i> from different media.....	114
Table 4.6: Extract yields of <i>F. proliferatum</i> fractions.....	120
Table 4.7: Summary of bioactivity of <i>F. proliferatum</i> fractions against MRSA Planktonic, prebiofilm, and postbiofilm percentage viability.....	121
Table 4.8: PCA loadings- Plot– dereplicated compound hits for the discriminating metabolites of <i>F. proliferatum</i> fractions.....	133
Table 4.9: OPLSDA S- Plot– dereplicated compound hits for the discriminating antibacterial and antibiofilm- active metabolites of <i>F. proliferatum</i> fractions.....	135

Table 4.10: Isolated pure compounds from <i>F. proliferatum</i> . For fraction source, underlined fractions were used for structural elucidation.....	142
Table 4.11: Isolated compounds observed on OPLS-DA active quadrant. Highlighted rows represent the bioactive metabolites.....	149
Table 5.1: Extract yield of <i>F. falciforme</i> , grown on different media and incubated for 7, 15, and 30 days. All cultures were incubated at 27°C.....	157
Table 5.2: Summary activity of <i>F. falciforme</i> extracts from different media against Planktonic, Prebiofilm, and Post biofilm MRSA at concentrations of 100 µg/ml.....	159
Table 5.3: PCA loadings plot – dereplicated compound hits from bioactive discriminatory and active metabolites from Malt media.....	162
Table 5.4: PLSDA- Scores plot – dereplicated compound hits from bioactive discriminating metabolites for potato, rice, and oat media.....	167
Table 5.5: OPLSDA S- Plot– dereplicated compound hits for the discriminating planktonic and pre-biofilm active metabolites of <i>F. falciforme</i>	171
Table 5.6: Weight of fractions after solvent-solvent partition.....	176
Table 5.7: Summary of bioactivity of <i>Fusarium falciforme</i> fractions against MRSA Planktonic, prebiofilm, and postbiofilm percentage viability.....	178
Table 5.8: PCA scores Plot– dereplicated compound hits for the discriminating metabolites of <i>F. falciforme</i> MeOH and hexane fractions. Highlighted rows in green are those earlier defined biomarkers for bioactivity during the optimisation stage.....	185
Table 5.9: Dereplicated compound hits for the discriminating metabolites of <i>F. falciforme</i> malt 15 days extract.....	192
Table 5.10: Comparison of dereplicated compound hits for the discriminatory metabolites of <i>F. falciforme</i> extracts obtained from malt broth 15 days, MeOH and hexane fractions.....	194
Table 6.1: Extract yields of <i>A. alternata</i> grown on different media and incubated for 7, 15, and 30 days. All cultures were incubated at 27°C.....	200
Table 6.2: Summary activity of <i>A. alternata</i> extracts from different media against Planktonic, Prebiofilm, and Post biofilm MRSA at concentrations of 100 µg/ml.....	202
Table 6.3: PCA loadings plot – Dereplicated compound hits from discriminating metabolites of <i>A. alternata</i> from potato, malt, and rice media 30 days.....	205
Table 6.4: OPLSDA S-plot – compound hits for the discriminating bio-active metabolites of <i>A. alternata</i> from different media.....	210
Table 6.5: Extract yields of <i>A. alternata</i> fractions.....	214
Table 6.6: Summary of bioactivity of <i>A. alternata</i> fractions against MRSA Planktonic, prebiofilm, and postbiofilm percentage viability.....	215
Table 6.7: PCA loadings- Plot– dereplicated compound hits for the discriminating metabolites of <i>A. alternata</i> fractions.....	227

Table 6.8: Dereplicated compound hits for the discriminating antibacteria and antibiofilm-active metabolites of <i>A. alternata</i> fractions obtained from the OPLS-DA S-Plot.....	229
Table 6.9: Isolated pure compounds from <i>A. alternata</i> . For fraction source, underlined fractions were used for structural elucidation.....	236
Table 6.10: IC ₅₀ (μM) for the bioactive isolated compounds against MRSA.....	241
Table 6.11: Isolated compounds observed on OPLS-DA active quadrant (fig. 6.15 and 6.4). Highlighted rows represent the bioactive metabolites.....	244
Table 7.1: Co-culture extracts weights incubated for 4 and 10 days as illustrated in Figure 7.4.	249
Table 7.2: Sample codes.....	250
Table 7.3: Dereplicated compound hits from discriminating metabolites from co-culture of fungus and MRSA incubated for 4 and 10 days obtained from the PCA loadings plot.....	254
Table 7.4: Dereplicated compound hits from discriminating metabolites from co-culture of fungi and MRSA incubated for 4 and 10 days obtained from the OPLS-DA S-plot.....	260
Table 7.5: Co-culture extracts weights incubated for 15 and 30 days as illustrated in Figure 7.20. All cultures were incubated at 27°C.....	265
Table 7.6: Sample codes.....	266
Table 7.7: Summary activity of active co-culture extract against MRSA at concentrations of 100 μg/ml.....	267
Table 7.8: PCA loadings plot – dereplicated compound hits from discriminating metabolites from co-culture of fungi and MRSA incubated for 15 and 30 days.....	270
Table 7.9: OPLS-DA S-plot – dereplicated compound hits from discriminating metabolites from co-culture of fungi and MRSA incubated for 15 and 30 days.....	275
Table 7.10: Extract yields of <i>F. proliferatum</i> -MRSA co-culture fractions.....	279
Table 7.11: Summary of bioactivity of fractions obtained from <i>Fusarium proliferatum</i> -MRSA co-cultures against Planktonic MRSA, along with their prebiofilm, and postbiofilm stages indicated by their percentage viability.....	280
Table 7.12: PCA loadings- Plot– dereplicated compound hits for the discriminating metabolites of <i>F. proliferatum</i> -MRSA fractions.	289
Table 7.13: Dereplicated compound hits for the discriminating active metabolites of <i>F. proliferatum</i> -MRSA fractions detected from the OPLS-DA loadings plot.	292
Table 7.14: Isolated pure compounds from co-culture of <i>F. proliferatum</i> -MRSA.....	295
Table 7.15: Isolated compounds observed on OPLS-DA active quadrant.....	299
Table 8.1: Co-culture extracts weights incubated for 7 days as illustrated in Figure 8.3.	304

Table 8.2: Sample codes.....	304
Table 8.3: Summary activity of active co-culture extract against MRSA at concentrations of 100 µg/ml.....	306
Table 8.4: PLS-DA loadings plot – dereplicated compound hits from discriminating metabolites from co-culture of fungi to fungi incubated for 7 days.....	308
Table 8.5: OPLS-DA S-plot – dereplicated compound hits from discriminating metabolites from co-culture of fungi to fungi incubated for 7 days.....	312
Table 8.6: Weights of crude extracts of Fungal co-cultures after 15- and 30-days incubation on malt extract broth media.....	316
Table 8.7: Summary activity of active fungi to fungi co-culture extract against MRSA at concentrations of 100 µg/ml.....	318
Table 8.8: PCA loadings plot – dereplicated compound hits from discriminating metabolites from co-culture of fungi to fungi incubated for 15 and 30 days.....	320
Table 8.9: OPLS-DA S-plot – dereplicated compound hits from discriminating active metabolites from co-culture of fungi to fungi incubated for 15 and 30 days.....	324
Table 8.10: Extract yields of <i>F. proliferatum</i> - <i>F. falciforme</i> co-culture fractions.....	328
Table 8.11: Summary of bioactivity of <i>Fusarium proliferatum</i> - <i>F. falciforme</i> fractions against MRSA Planktonic, prebiofilm, and postbiofilm percentage viability.....	329
Table 8.12: PCA loadings- Plot– dereplicated compound hits for the discriminating metabolites of <i>F. proliferatum</i> - <i>F. falciforme</i> fractions.....	337
Table 8.13: OPLS-DA-S Plot– Dereplicated compound hits for the discriminating active metabolites of <i>F. proliferatum</i> - <i>F. falciforme</i> fractions.....	339
Table 8.14: Isolated pure compounds from co-culture of <i>F. proliferatum</i> - <i>F. falciforme</i>	342
Table 8.15: IC ₅₀ (µM) for the bioactive isolated compounds against MRSA.....	349
Table 8.16: Isolated compounds observed on OPLS-DA active quadrant (fig. 8.23 and 8.13).....	352

Abbreviations

¹³ C NMR	Carbon NMR
¹ H NMR	Proton NMR
ACN	Acetonitrile
BLAST	Basic Local Alignment Search Tool
bp	Base pair
COSY	Correlation spectroscopy
D	doublet
DCM	Dichloromethane
DMSO	Dimethyl sulfoxide
DNA	Deoxyribonucleic acid
DNP	Dictionary of NPs
ELSD	Evaporative Light Scattering Detector
EtOAc	Ethyl acetate
FA	Fatty acid
FC	Flash chromatography
HMBC	Heteronuclear Multiple-Bond Correlation
HPLC	High Performance Liquid Chromatography
HSQC	Heteronuclear Single Quantum Correlation
HR-LCMS	High Resolution- Liquid Chromatography Mass Spectrometry
ITS	Internal Transcribed Spacer
JMod	J-Modulated Spin
MEA	Malt Extract Agar
MBEC	Minimum Bacterial Eradication Concentration
MeOH	Methanol
Mg	Magnesium
MHB	Mueller Hinton broth
MIC	Minimum inhibitory concentration
mins	Minute
MPLC	Medium Pressure Liquid Chromatography
MRSA	Methicillin Resistance <i>Staphylococcus aureus</i>
MWt	Molecular Weight
<i>m/z</i>	mass to charge ratio
MS	Mass spectrometry
NCBI	National Center for Biotechnology
NMR	Nuclear Magnetic Resonance
OPLS-DA	Orthogonal Partial Least Squares Discriminant Analysis
OSMAC	One Strain Many Compounds
<i>P. aeruginosa</i>	<i>Pseudomonas aeruginosa</i>
PBS	Phosphate buffer saline
PC	Principal Component
PCA	Principal Component Analysis
PCR	Polymerase Chain Reaction
PLS-DA	Partial Least Squares, or Projections to Latent Structures-Discriminant Analysis

PTLC	Preparative Thin Layer Chromatography
Q	quartet
rRNA	Ribosomal Ribonucleic Acid
ROESY	Rotating-Frame NOE Spectroscopy
s	Singlet
<i>S. aureus</i>	<i>Staphylococcus aureus</i>
SIMCA	Soft Independent Modelling by Class Analogy
Stdev	Standard deviation
t	triplet
TLC	Thin Layer Chromatography
Tocsy	Total Correlation Spectroscopy
UV	Ultraviolet
VIP	Variable Importance in Projection

Abstract

Infectious diseases remain the second leading source of death worldwide despite the success of antibiotic discovery, while resistance to antibiotics is among the prominent health issues in the twenty-first century. Fungal endophytes are very rich in phytochemicals which can be processed into new drugs. Thirty-four fungal endophytes were isolated from five Nigerian medicinal plants namely, *Vernonia amygdalina*, *Moringa oleifera*, *Magnifera indica*, *Azadirachta indica* and *Ocimum gratissimum*, which are used in Nigeria for the treatment of various ailments. The isolated endophytes were tested against methicillin resistant *Staphylococcus aureus* (MRSA) and *Pseudomonas aeruginosa* but showed inactivity for *P. aeruginosa*. Each extract was tested against planktonic, prebiofilm and postbiofilm MRSA. Bioactive endophytes were identified using ITS gene sequencing. Three fungal endophytes namely, *F. proliferatum*, *F. falciforme* and *A. alternata* were identified and subjected for media optimisation work using rice solid media, oat solid media, malt extract broth and potato dextrose broth. Bio-active co-cultures were subjected to media optimisation work using malt extract broth incubated for 15 and 30 days. Extracts obtained from monocultures and co-cultures were tested against MRSA. Based on the media optimisation result, *F. proliferatum* was scaled up on rice media for 15 days, *F. falciforme* was scaled up on malt extract broth for 15 days, *A. alternata* was scaled up on potato dextrose broth for 30 days.

F. proliferatum-F. falciforme, *F. proliferatum-A. alternata*, *F. falciforme-A. alternata*, and *F. proliferatum-MRSA*, *F. Falciforme-MRSA*, *A. Alternata-MRSA* were co-cultured on malt extract agar. According to the best bioactivity results against MRSA ($\geq 80.0\%$ inhibition), co-culture of *F. proliferatum-MRSA* was scaled up on malt extract broth for 15 days. Due to limited time, co-culture of *F. proliferatum-F. falciforme* was not scaled up but the extracts obtained from media optimisation were pooled together and purified as they showed similar bioactivity and chemical profiles.

The scaled-up extracts of *F. falciforme* were subjected to solvent-solvent partitioning and lost their bioactivity, therefore no further chromatographic isolation work was carried out. Other scaled up extracts were fractionated using either a flash chromatographic technique or medium pressure flash chromatography. All extracts from the crude to the initial fractionation stages were tested against MRSA and analysed using ^1H NMR and High-Resolution Mass Spectrometry (HR-LCMS). HR-LCMS data was processed using Mzmine followed by dereplication using in-house macro excel. The data were exported to SIMCA for analysis using Principal component analysis and orthogonal partial least square-discriminant analysis. A total

of 45 compounds were isolated in this study. *F. proliferatum* bioactive fractions were purified and afforded 13 known compounds and 6 new compounds, out of which one compound named, 3-dihydroxy-6-methoxy-8-methylxanthone inhibited planktonic MRSA by 65.81%. *A. alternata* afforded 11 known compounds with alternariol and altenuisol inhibiting planktonic MRSA with an MIC (Minimum Inhibitory Concentration) of 25 and 50 µg/mL, respectively. Co-culture of *F. proliferatum* and MRSA afforded 6 known compounds of weak antibacterial activities while co-culture of *F. proliferatum* and *F. falciforme* afforded 10 known compounds out of which 3 naphthoquinones namely solaniol, dihydrojavanicin and javanicin inhibited planktonic MRSA with MIC values of 12.5 µg/mL and MBEC values of 6.5 µg/mL for solaniol, 25 µg/mL for both javanicin congeners. This study revealed the efficacy of endophytic fungi and their co-cultures as a potential source of antibiotics for alternative therapy in combating and curtailing the development and survival of multidrug-resistant pathogens.

CHAPTER 1

1 Introduction

1.1 Antimicrobial Resistance

The number of multi-drug resistant bacteria is on the increase, and the treatment of infections caused by these microbes is becoming a great challenge (Rice, 2008). The traditional methods used for drug discovery is time consuming and labour-intensive. The rediscovery rates are also becoming increasingly demotivating (Cooper and Shlaes, 2011). The field of natural product discovery has started to shift away from traditional activity-guided approaches and is beginning to take advantage of increasingly available metabolomics and genomics datasets to explore chemical space that has not been discovered. Major steps have been taken and now enable-omics-informed prioritisation of chemical structures for discovery, including the prospect of confidently linking metabolites to their biosynthetic pathways (Caesar *et al.*, 2021).

Antibiotics had been effective against the prevention and prevalence of infections in the yesteryears, but recently there has been a complication of resistance adapted by most of the pathogenic organisms in the pipeline of available antibiotics. The resistance has been linked to under usage and over usage of antibiotics leading to gene, molecular, cellular and community level resistance. Antibiotics have high affinity to the targets if there is a single point of mutation could trigger the surface leading to resistance and proliferation as well as transfer of resistance gene by transformation. Enzyme catalysed inactivation of antibiotics by hydrolysis has been the main reason for the failure of β lactam antibiotics preventing cell penetration, alteration of targets and resisting the action of antibiotics (Gabrani *et al.*, 2015).

One of the major reasons for antibiotic failure is the formation of biofilms. Microbes merge to form biofilms leading to irreversible attachment to the biotic/abiotic surface. Biofilms help consortia of microbes against increase in specific efflux pumps, oxidative stress, and protection by providing an outer layer of extracellular polysaccharide layer. Also, the transfer of antibiotic resistance genes by horizontal gene transfer has been found to be at increased levels (Blair *et al.*, 2015, Bazzini S., 2014, Chandra Mohana *et al.*, 2018).

One well-established approach to promote the identification of novel antibiotics, is the modification of culture conditions such as pH, temperature, and nutrient sources. This strategy could result in the activation of silent gene clusters, thereby promoting production of different secondary metabolites. The One Strain Many Compounds (OSMAC) approach was invented about 20 years ago (Schiewe and Zeeck, 1999), but the concept has a longer history (Zähner,

1977, Atanasov *et al.*, 2021), with its use commonly applied in industrial microbiology since the 1960s (Newman, 2017).

1.1.1 MRSA as a global health challenge

MRSA infection is a global health problem. It is one of the leading causes of hospital-acquired infections with significant rate of mortality. The annual frequency of deaths from MRSA has surpassed those caused by human immunodeficiency virus/acquired immune deficiency syndrome (Zouhir *et al.*, 2016). MRSA infections can be further split into community-acquired infections and hospital-acquired infections. They differ with respect to their clinical features, molecular biology, their antibiotic susceptibility, and treatment (Elward *et al.*, 2009, Lakhundi and Zhang, 2018, Shahkarami *et al.*, 2014). The history of MRSA infection dates to 1961 when it was first identified. Since then, the prevalence and incidence of MRSA infection have been increasing dramatically across the United States. The reported incidence of MRSA infection ranges from 7 percent to 60 percent (Sabbagh *et al.*, 2019, Khan *et al.*, 2018, Ko and Moon, 2018).

Methicillin resistance has occurred in *S. aureus* by mutation of a chromosome-encoded protein, known as penicillin-binding protein. This type of resistance is conveyed by *S. aureus* organisms with the aid of bacteriophages (Lakhundi and Zhang, 2018). The major factor for MRSA resistance to beta-lactam antibiotics is due to the presence of the *mecA* gene sequence, which is known to generate transpeptidase PB2a, which has the capacity to lower the affinity of the organism to bind to beta-lactam antibiotics (Shahkarami *et al.*, 2014).

Commonly associated risk factors for MRSA infection are recent hospitalisation, prolonged hospitalisation, intensive care admission, invasive procedures, MRSA colonisation, open wounds, haemodialysis, admission to nursing homes and long-term use of urinary catheter (Siddiqui and Koirala, 2022). Even though advancement in age is not considered a risk factor for MRSA infection, age greater than 65 years is an important risk factor for hospitalisation. Thus, advancement in age is indirectly linked to MRSA acquisition. Also, admission to a hospital with a high prevalence of hospital acquired-MRSA or living in an area with a high prevalence of community acquired-MRSA is considered a significant risk factor for MRSA colonisation (National Nosocomial Infections Surveillance, 2004). Finally, about sixty percent of patients do acquire MRSA within 48 hours despite having no healthcare risks (Khan *et al.*, 2018, Kavanagh *et al.*, 2018, Kengen *et al.*, 2018).

MRSA can cause various organ-specific infections, the most common being the skin and subcutaneous tissues, followed by invasive infections like meningitis, osteomyelitis,

pneumonia, empyema, and lung abscess. Infective endocarditis caused by MRSA can result in increased morbidity and fatality rate compared to other organisms. *S. aureus* is a causative agent of bacteraemia, and this has been reported to be associated with mortality rates of 15% to 60%. MRSA bacteraemia is mostly seen in intensive care unit patients with central line insertions. The effect of MRSA bacteraemia in humans are worse than other MRSA infections, due to the decline in response to vancomycin in these patients (Siddiqui and Koirala, 2022).

1.1.2 Drug Resistance in *P. aeruginosa*

P. aeruginosa is one of the six bacterial pathogens (*Enterococcus faecium*, *S. aureus*, *Klebsiella pneumoniae*, *Acinetobacter baumannii*, *P. aeruginosa*, and *Enterobacter* sp.) denoted by their acronym ESKAPE, which are commonly associated with antimicrobial resistance, (Ciofu and Tolker-Nielsen, 2019). *P. aeruginosa* is an opportunistic pathogen that is a leading cause of morbidity and mortality in immune-compromised individuals, and cystic fibrosis patients. Total eradication of *P. aeruginosa* has become more difficult due to its ability to resist antibiotics. Adaptive antibiotic resistance of *P. aeruginosa*, includes formation of multidrug-tolerant and biofilm-mediated cell resistance. This is responsible for the relapse and recalcitrance of infections. The discovery and development of therapeutic approaches that present novel channels against *P. aeruginosa* infections are in increasing demand and gaining more and more attention (Pang *et al.*, 2019).

P. aeruginosa has specific characteristics that contribute to its virulence, including pili to attach to tissue surfaces, flagella to promote motility, and lipopolysaccharide to act as an endotoxin. It can proliferate on surfaces in the clinical environments and has become a major cause of nosocomial infections. When *P. aeruginosa* replicates enough, it forms a biofilm that attaches to a surface and is difficult to eradicate. Infection can occur when *P. aeruginosa* adheres to a tissue surface and then replicates to the point of having a mass capable of infection, and finally damages the tissue using the toxins it produces. Exotoxin A, which is a virulence factor, work by colonising the host cell, inhibiting protein synthesis, and attacking the structural proteins of the cell (Fajardo and Martínez, 2008).

P. aeruginosa is resistant to antibiotics as well as disinfectants. Resistance develops in a similar fashion as a MRSA infection, as the bacterium is exposed to different kinds of medication. Its rapid reproduction combined with low susceptibility result in continual adaptation to the antibodies and high bacterial diversity. It undergoes mutations and acquires resistance genes that enhance its survival in the presence of antibiotics. Its genome was entirely sequenced in 2000 and was recorded as having 6.3 million base pairs. Such a notably

large genome encodes many proteins which contributes to its versatility in adaptation, antimicrobial resistance, and virulence function (Stover *et al.*, 2000).

1.1.3 Microbial biofilms as a major cause of drug resistance

One of the most significant characteristics of microbial biofilms is that the bacteria are able to survive antibiotic treatment administered at high doses (Costerton *et al.*, 1999). The planktonic bacteria will show sensitivity to antibiotics and display low minimal inhibitory concentration (MIC) values if the biofilm is dispersed. Mechanistically, resistance is due to acquired mutations and usually involves efflux pumps, antibiotic-modulating enzymes, or mutations that eliminate the molecular target of the antibiotic and allows bacteria to survive the antibiotic treatment irrespective of it not being embedded in a biofilm. In contrast, the antibiotic-tolerant cells in biofilms have the capacity to survive the high antibiotic concentrations only if they are embedded in the biofilms. Resistance and tolerance are both associated in the recalcitrance of biofilms to antibiotic treatment (Lebeaux *et al.*, 2014).

Biofilms are the cause of persistent infections associated with a variety of medical implants, and are also linked with diseases such as chronic obstructive pulmonary disease, chronic wounds, cystic fibrosis and urinary tract infections (Costerton *et al.*, 1999, Tolker-Nielsen, 2015, Ciofu *et al.*, 2015, Rybtke *et al.*, 2015). The ability of microbial biofilms to tolerate antibiotics and components of the host immune system is the main reason for the challenging infections they are causing (Høiby *et al.*, 2015). The primary clinical consequence of tolerance of biofilms to antibiotics is that, the high concentration of antibiotics required for the eradication of biofilm infections (Macià *et al.*, 2014) cannot be achieved *in vivo* by systemic administration without leading to toxicity (Hengzhuang *et al.*, 2012).

1.2 Medicinal Plants

Medicinal plants have been used in past and modern times for the treatment of various ailments. They are used as traditional medicines. Traditional medicines can treat various infections and chronic conditions. In sub-Saharan Africa, traditional herbal medicine is still an important component of healthcare. This is largely due to poverty, inadequacy of health services and shortage of health workers, and even when the facilities exist, there is rampant shortage of drugs and equipment (Kipkore *et al.*, 2014). Today, many indigenous herbal remedies in Nigeria largely remain unrecognised and undocumented as potential forms of treatment, and as a result, they continue to be used by only small groups of indigenous populations (Thirumalai, 2009).

More than 25% of prescribed medicines in industrialised countries are derived directly or indirectly from plants, despite the remarkable progress in synthetic organic medicinal products of the twentieth century (Newman *et al.*, 2000, Abd El-Ghani, 2016). There is a wide range of medicinal plants in Nigeria, and research has confirmed the efficacy of these plants. Most of these plants have been shown to have antimicrobial and anticancer properties. Previous and on-going studies on Nigerian plants have proven to contain, terpenes, alkaloids, glycosides, polyphenols, with therapeutic potentials (Ugboko *et al.*, 2020). Abd El-Ghani reported that different plant families and species, were identified and recognised as being used by the people of Nigeria for the treatment of various common diseases (Abd El-Ghani, 2016). Some of these plants grow in the wild, while others are cultivated by the people themselves.

There are people that rely on *Vernonia amygdalina* for sexually transmitted disease and vagina itch and *Azadirachta indica* for syphilis. Diarrhoea and dysentery are treated with *Ocimum gratissimum* (Abd El-Ghani, 2016). This study will test the efficacy of bioactive compounds isolated from the fungal endophytes of Nigerian medicinal plants in inhibiting the growth of MRSA and *P. aeruginosa*.

1.3 NPs

Compounds which are derived from natural sources like plants, animals, and microorganisms, are defined as natural products (NPs) (Baker *et al.*, 2007). Many NPs show pharmacological or biological activities. They are a crucial source of inspiration for development of potential novel drugs (Xie *et al.*, 2015). Therefore, understanding the activity mechanism of NPs is crucial.

Several NPs include small molecules that result from metabolic reactions. NPs have evolved over a long period of time, and acquired a novel chemical diversity, which invariably results in the diversity of their biological activities and therapeutic properties. Therefore, even before the evolution of modern chemical pharmacology, NPs have been used many years ago as components of traditional medicines, particularly as active components of herbal remedies. Recently, some of the traditional healing practices, such as traditional Chinese medicine or African herbal medicines, and Indian Ayurveda remain the main treatment option for many people across the world, due to economic reasons, personal beliefs or due to the difficulty in accessing therapeutic products. NPs have become one of the most important resources for developing new lead compounds and scaffolds in modern medicine (Mirza *et al.*, 2015, Newman and Cragg, 2016, Khalifa *et al.*, 2019, Sorokina and Steinbeck, 2020).

Unconventional medicines have been used since the beginning of human history, providing cure and treatments for a variety of diseases (Newman and Cragg, 2020, Petrovska, 2012). Bacteria, fungi, and plants have a centuries-old connection with humankind, producing both harmful and beneficial metabolites, with an effect on human health. These secondary metabolites, also referred to as specialised metabolites, are formed by diverse enzymatic machinery evolutionarily primed over millennia to assist the organism secure its environmental niche (Bernardini *et al.*, 2018) and have become an important source of inspiration for new pharmaceutical drugs active against various ailments (Cragg and Pezzuto, 2016, Roemer *et al.*, 2011). Even though hundreds of life-saving drugs have been discovered from, and inspired by nature, the fact remains that, there are still major secondary metabolites contributing to the biological activity of those organisms which are yet to be discovered (Genilloud, 2019, Bills and Gloer, 2016).

Irrespective of the decrease of the pharmaceutical industry to pursue NPs in their pipelines, statistical findings show that NPs still play a major role in drug discovery with over fifty percent of FDA-approved drugs being derived from NPs. However, NPs research has been found to be too time-consuming, laborious, and uneconomical, which may have led to the declining trend. Nevertheless, with the emergence of new and more advanced technologies such as genomics, proteomics, transcriptomics, metabolomics, and bioinformatics, NPs research has become more competent in finding promising novel drugs (Newman and Cragg, 2012, Challis, 2008, Góngora-Castillo and Buell, 2013, Yang *et al.*, 2011, Kamal *et al.*, 2017).

1.3.1 Advantages of NPs

NPs utilise special enzymatic machinery to biosynthesise an inspiring diversity of secondary metabolites. They make up the competitive advantage for the producers of these secondary metabolites which have widespread human impacts such as antibiotics, anti-inflammatories, and antifungal drugs. Over the years, researchers have been provided with integrated strategies that are useful for the identification of expressed secondary metabolites. NPs have structures that have evolved to serve biological functions, including the regulation of endogenous defence mechanisms and the interaction (often competition) with other organisms, which explains their importance as therapeutics for infectious diseases. Also, their use in unconventional medicine may provide insights regarding efficacy and safety. NPs have been the centre of attention in science over the last decades, and the interest around them continues to improve rapidly. This has resulted in the rapid multiplication of different databases and collections, as a general resource for NP information (Sorokina and Steinbeck, 2020).

Scientific articles in peer-reviewed journals are published periodically, describing the positive effects of NPs on the healing process of different human and animal diseases. Major classes of antifungals, and antibiotics have their roots on NPs isolated from microorganisms. Drugs used in the treatment of diabetes, cancers, cardiovascular diseases, and more are often isolated from NPs or their derivatives. For example, over fifty percent of newly developed drugs were developed from NPs between 1981 and 2019 (Newman and Cragg, 2016, Terreni *et al.*, 2021). In summary, NPs are enriched with 'bioactive' compounds covering a wider area of chemical space compared with typical synthetic small-molecule libraries (Lachance *et al.*, 2012, Atanasov *et al.*, 2021).

1.3.2 Disadvantages of NPs

NP screening usually involve a library of extracts from natural sources, which may not be compatible with traditional target-based assays (Henrich and Beutler, 2013, Atanasov *et al.*, 2021). Identifying the bioactive compounds of interest are often challenging, and dereplication tools have to be used, to avoid rediscovery of known compounds. Accessing sufficient biological material to isolate and characterise a bioactive NP may also be challenging (Cragg *et al.*, 1993). In addition, gaining intellectual property rights for new NPs exhibiting relevant bioactivities can be a huge task, since naturally occurring compounds in their primary form may not always be patented (legal frameworks are different and are changing between countries) (Harrison, 2014), but simple derivatives can be patent protected.

1.4 Application of metabolomics in NPs drug agents

A metabolite can be defined as any molecule that is less than 1.5 kDa in size. Metabolites can be substrates, intermediates, or products of metabolism (Wishart *et al.*, 2007). Metabolomics is therefore the scientific study of chemical processes involving metabolites, the little molecule substrates, intermediates and products of cell metabolism (Daviss, 2005). The metabolome represents the entire set of metabolites in a biological cell, tissue, organ or organism, which are the final products of cellular processes (Jordan *et al.*, 2009). Messenger RNA (mRNA), gene expression data and proteomic analyses identifies the set of gene products being produced in the cell, and data that represents one aspect of cellular function. This invariably means that, metabolic profiling can give an immediate snapshot of the physiology of that cell (Villate *et al.*, 2021).

Natural extracts are mostly composed of hundreds to thousands of metabolites, whereby the bioactivity of natural extracts can be represented by synergism between several metabolites. However, isolating every single compound from a natural extract is not always possible due

to the chemical complexity, and presence of secondary metabolites at very low levels. Metabolomics has emerged in recent years as an imperative tool for the analysis of thousands of metabolites from crude natural extracts, resulting in a paradigm shift in NPs drug research. Analytical methods like mass spectrometry, and nuclear magnetic resonance are used to generally annotate the constituents of plant NPs for screening, drug discovery and quality control purposes (Salem *et al.*, 2016). Metabolomics could therefore be a powerful tool in the analysis and identification of metabolites responsible for biological properties. Regarding natural product chemistry, it can be a possible strategy to streamline the classic and laborious process of isolating NPs, which regularly involves the re-isolation and identification of known compounds (Demarque *et al.*, 2020). Therefore, its objective includes metabolite identification by searching spectral databases (Johnson and Lange, 2015).

1.4.1 Liquid chromatography-mass spectrometry (LC-MS) based metabolomics

Mass spectrometry is most likely to be employed in metabolic fingerprinting and is favoured for its sensitivity in more global metabolic profiling applications, but generally requires upstream chromatographic separations due to the limited molecular-weight diversity of metabolites (Chan *et al.*, 2009, Goodacre *et al.*, 2003, Wu *et al.*, 2008). LC-MS based metabolomics could have a major impact in the study of NPs, especially in its metabolism, toxicity, and activity (Zhao *et al.*, 2018).

LCMS does not require prior sample treatment, and crude extracts obtained by simple extraction can be introduced directly to the LC-MS. The choice of columns such as ion exchange, reversed phase, and hydrophobic interaction provides metabolite separation based on differential chemical properties. Nowadays, reversed-phase columns such as C18 or C8 are the most used in LC gradient separation (De Vos *et al.*, 2007). The development of ultra-performance LC rendered the approach even more potent in the areas of sensitivity, resolution, and throughput. LCMS is a unique method for measuring plant secondary metabolites such as alkaloids and flavonoids (Iijima *et al.*, 2008, Matsuda *et al.*, 2010), membrane lipids (Salem *et al.*, 2016, Salem and Giavalisco, 2018, Okazaki *et al.*, 2009) and primary metabolites like amino acids (Gu *et al.*, 2007). The limitations of LCMS are that metabolites with poor ionising capability cannot be detected.

1.4.2 Nuclear Magnetic Resonance (NMR)

NMR spectroscopy is a powerful analytical tool that has traditionally occupied an important position for structure elucidation of NPs (Kim *et al.*, 2010a, Kim *et al.*, 2011, Grkovic *et al.*, 2014, Mahrous and Farag, 2015, Starks *et al.*, 2012). NMR is not discriminatory, and is less

biased, as the results do not rely on the type of ionisation condition or the preferences of the used instruments (Wang *et al.*, 2007). Therefore, this technique allows for the detection of the abundant primary metabolites such as amino acids, organic acids, and sugars alongside secondary metabolites like terpenoids, alkaloids, and flavonoids as typically found in plant natural extracts (Kim *et al.*, 2010a).

In addition, NMR is a very useful technique for the structure elucidation of novel and/or unexpected compounds including those with identical masses and/or different isotope distributions (Tawfike *et al.*, 2013). Moreover, NMR-based methods are highly consistent, nonintrusive, non-destructive, and require little sample preparation as the sample does not get in physical contact with the device as in MS (Zhang *et al.*, 2016). Another advantage of NMR spectroscopy lies in the direct proportionality between the NMR spectrum signals and the corresponding real molar levels of the detected metabolites, making absolute quantification of all detected metabolites possible without the need for calibration curves of individual analytes, posing it as a powerful tool in quality control purposes of drug extracts (Simmler *et al.*, 2014).

Also, in metabolomic analysis of biofluids, blood, urine, and culture extracts, NMR has an edge over other methods, as it allows the introduction of samples directly into the instrument with very easy sample-preparation procedures (Beckonert *et al.*, 2007, Kim *et al.*, 2010b).

1.4.3 Limitations of metabolomics

Difficulties can be encountered in metabolomics experiment. The small-molecule metabolites in a biofluid, cell lysate, tissues or organ differs wildly depending on the organism studied (Dunn and Ellis, 2005). Metabolomics is a new discipline, and as a result a complete list of the human metabolome, and the metabolomes of other organisms is not available (Pearson, 2007). Therefore, it is common to encounter unknown metabolites, and complications in the analysis and interpretation of metabolic changes. Furthermore, the exhibited diversity of physical and chemical properties of compounds within the metabolome, makes true metabolomics unattainable when using current instrumental capabilities (Lindon *et al.*, 2000, Dunn and Ellis, 2005, Dettmer *et al.*, 2007). For instance, the limited molecular-weight distribution of the metabolome, prevents a comprehensive and detailed analysis by mass spectrometry and generally requires the additional use of chromatography (Kell, 2004, Viswanadhan *et al.*, 2011). The analysis of metabolomic data is further complicated due to the inherent variability found in each sample, as each cell, tissue, organ, or organism is unique (Rubakhin *et al.*, 2011).

Finally, complexity of metabolomic data, makes optimal information retrieval challenging, therefore up-to-date computational and mathematical approaches for accurate data interpretation are urgently needed (Shestakova *et al.*, 2023).

Despite, these challenges, the use of NMR or MS-based metabolomics is an efficient potential approach to find antimicrobials in single-microbial cultures or co-cultures (Wu *et al.*, 2015).

1.4.4 Multivariate Analysis

Metabolomics data can be meaningful after the application of MVA, such as PCA, PLS, and OPLSDA, where spectral features contributing mostly to variation or separation are identified for further analysis. (Worley and Powers, 2013).

The aim of metabolic fingerprinting analysis is to formulate the corresponding discrepancies between the metabolomes of two or more systems to deduce a biological relationship. This implies that, the hallmark of metabolic fingerprinting is the use of multivariate analysis methods to spot those biologically relevant spectral features for further targeted analyses (Lindon *et al.*, 2000, Dettmer *et al.*, 2007, Ellis and Goodacre, 2006) with two of the most popular methods being principal component analysis (PCA) (Pearson, 1901., Hotelling, 1933., Worley and Powers, 2013) and partial least squares projection to latent structures (PLS) (Wold *et al.*, 2001, Wold *et al.*, 1993, Wold *et al.*, 1994). In other words, the goal of PCA and PLS is to differentiate between classes in highly complex data sets, despite within class variability (Worley and Powers, 2013).

Principal component analysis (PCA) is notably the most widely used multivariate analysis method for metabolic fingerprinting and, in fact, chemometrics in general. The aim of PCA is to reach a linear transformation that preserves as much of the variance in the original data as possible in the lower dimensionality output data (Jolliffe, 2002). It also shows the similarity and discrepancies amongst groups of metabolites. Although, the unsupervised nature of the PCA algorithm provides a means to get unbiased dimensionality reduction, its application only reveals group structure when within-group variation is sufficiently less than between-group variation. Thus, supervised types of discriminant analysis like PLS and OPLSDA, that depend on the category of each observation are usually applied in metabolic fingerprinting experiments (Chan *et al.*, 2009, Barker and Rayens, 2003).

1.5 Antimicrobials from NPs

The need for a brand new antibiotic pipeline to tackle the threat imposed by resistant pathogens has become a significant global concern for human health. There is restored

interest in nature towards exploring untapped microorganisms to bring about new drug agents, due to the negative effects associated with synthetic drugs (Chandra Mohana *et al.*, 2018). NPs have served as powerful therapeutics against pathogenic bacteria for many years. However, the increasing frequency of antibiotic-resistant infections clearly demonstrates that new antibiotics are critical for contemporary medicine. Since combinatorial approaches have not yielded effective drugs, it is proposed that the development of new antibiotics around proven natural scaffolds is the best short-term solution to the rising crisis of antibiotic resistance (Rossiter *et al.*, 2017).

Microbial NPs has been of critical importance in therapeutically viable drugs against cancer, infectious diseases, diabetes, and antioxidants (Naman *et al.*, 2017). Food and Drug administration (FDA) assessment of NPs reveals that almost one-quarter of antibiotics has been derived from microbial sources (Patridge *et al.*, 2016, Naman *et al.*, 2017). Microbial NPs have replaced plant-derived compounds as a source of therapeutic agents and has been a possible source for the discovery of novel therapeutics within the past decades (Chandra Mohana *et al.*, 2018, Bleicher *et al.*, 2003).

1.6 Fungal Endophytes

Plants harbour a wide array of microorganisms such as bacteria, fungi, algae, protists, and archaea both within and outside of their tissues. As a result of long-term evolution, complicated interactions have gradually formed between these species. This has led to the symbiotic relationship between them (Hassani *et al.*, 2018). It has been estimated that over one million endophytic fungal species are occurring in nature. Endophytic fungi were classified into three main ecological groups namely; mycorrhizal, balansicaeous, and non-pasture endophytic fungi (Faeth and Fagan, 2002).

Fungal endophytes are a diverse group of eukaryotes. They are ubiquitous and possess the ability to synthesise secondary metabolites that are of clinical significance (Hasnahana *et al.*, 2019). They possess favourable effects on their host plants, some of which include disease-resistance improvement, growth promotion, and secondary metabolite induction. Endophytes are a group of microorganisms, which are endosymbiotic, that colonise host plants and microbes. They are reservoirs of novel bioactive compounds like, alkaloids, steroids, saponins, tannins, phenolic acids, and terpenoids, which serve as potential candidates for anticancer, antimicrobial, and anti-insect properties. While plant sources are being exploited for new chemical compounds for therapeutic purposes, endophytic microbes also constitute an important source for new drug discovery (Gouda *et al.*, 2016). Endophytes make a myriad of biologically active compounds due to the relationship they have with their host plants. These

compounds can be classified as, antioxidants, anticancer agents, antibiotics, immunosuppressive compounds, volatile antimicrobial agents, plant growth-promoting agents, and insecticides (Strobel, 2018). Endophytes possess the ability to produce similar chemicals as those originating from their host plants (Ebada *et al.*, 2016). Many endophytic fungi produce bioactive substances that protect plants against pathogens, herbivores, and biotic and abiotic stresses. Many of these compounds isolated from fungal endophytes are recognised as novel discoveries in the fields of pharmaceuticals and health care. It could be an answer to many diseases (Pant *et al.*, 2021).

Phyostimulation, biofertilisations, and biocontrol are various mechanisms fungal endophytes use to promote plant growth (Hassan, 2017, Eid *et al.*, 2019). Plant growth-promoting fungi (PGPF) directly promote plant growth by the production of phytohormones such as gibberellic acid, and indole-3-acetic acid (IAA) (Hashim *et al.*, 2020). Plant growth is stimulated by the synergistic reaction between Fungal IAA and endogenous plant IAA. PGPF also promotes plant growth by phosphate solubilisations, and nitrogen fixation (Zamin *et al.*, 2020), different enzyme production, such as protease, amylase, catalase, and urease (Hassan, 2017, El-Esawi *et al.*, 2019) including ammonia production (Fouda *et al.*, 2015). In addition, endophytic fungi have a high potential to protect plants against different pathogens, thereby reducing crop loss. This is carried out by the secretion of different bioactive compounds such as antibiotics (Murali *et al.*, 2017).

Compounds isolated from endophytic fungi includes; a complex diterpene alkaloid, Taxol (paclitaxel), produced by the endophyte *Metarhizium anisopliae*, found on the bark of Taxus tree (Visalakchi and Johnpaul, 2010, Jalgaonwala *et al.*, 2011), camptothecin, developed from *Nothapodytes foetida*, known to have antifungal and cytotoxic properties (Zhang *et al.*, 2012, Joseph and Priya, 2011), phomoenamides, an antifungal compound and a new enamide dimer, produced by a *Phomopsis* sp. isolated from the leaves of *Garcinia dulcis* (Rukachaisirikul *et al.*, 2008), and Kheiric acid, a new aliphatic compound, isolated from an endophytic fungus *Curvularia papendorfii* inhabiting *Vernonia amygdalina*, which was found active against MRSA (Khiralla *et al.*, 2020).

1.7 Co-culturing of microorganisms

Microbial co-culture is a biological system in which two or more microorganisms are grown together in the same medium and growth conditions. Advantages of microbial co-culture are stated below.

- To elicit the production of novel compounds.

- To elicit the production of known compounds that were not isolated in the pure culture.
- To improve the extract weight which can lead to an increase in pure compound yield.
- To improve the bioactivity of extracts.

1.8 Hypothesis, study aims and objectives

Study question: Are endophytic fungi derived from Nigerian medicinal plants good sources of new bioactive compounds, with antibacterial antibiofilm activity against biofilm-forming MRSA?

Hypothesis: Implementing metabolomics processes such as dereplication, PCA, PLS-DA OPLS-DA, to search for antibacterial and anti-biofilm bioactive compounds from endophytic fungi associated with Nigerian plants will help to putatively identify bioactive compounds in the first fractionation step. These compounds will be targeted, isolated, identified, and tested against the pathogen of concern (MRSA and *P. aeruginosa*) to certify their bioactivity.

Aim: The aim of this study is to isolate active antibacterial compounds from plants associated endophytes. Five Nigerian plants – *Vernonia amygdalina*, *Moringa oleifera*, *Azadirachta indica*, *Ocimum gratissimum*, and *Magnifera indica*, were chosen for this purpose.

Objectives: This research is specifically designed to achieve the following objectives

Monoculture

- 1) To isolate fungal endophytes from Nigerian medicinal plants.
- 2) To determine bioactive fungal endophytes, by performing biological assays against biofilm forming MRSA and *P. aeruginosa*.
- 3) To identify bioactive fungal endophytes using ITS gene sequencing.
- 4) To optimise the best media for the growth of bioactive fungal endophytes. The media optimisation will show the best yield and the most potent biological activity for each endophytic fungus.
- 5) To scale-up cultures of bioactive fungal endophytes using the optimum media.
- 6) To fractionate and isolate compounds obtained from scale-up crude extract.
- 7) To determine bioactive compounds by performing biological assay on isolated compounds.
- 8) To structurally elucidate and identify isolated compounds using NMR and LCMS.

Co-culture

- 1) To optimise the best condition for the co-culture of fungi-MRSA and fungi-fungi.
- 2) To scale-up the cultivation of bioactive co-cultures using the optimum media.
- 3) To fractionate and isolate compounds obtained from scale-up crude extract.
- 4) To determine bioactive compounds by performing biological assay on isolated compounds.
- 5) To structurally elucidate and identify isolated compounds obtained from co-culture using NMR and LCMS.

CHAPTER 2

2 Materials and methods

2.1 Isolation and identification of endophytes from Nigerian medicinal plants

Table 2.1: Materials

Materials	Source
Malt extract (ME) powder and agar	Oxoid, Manchester, UK
Chloramphenicol	Acros Organics, Geel, Belgium
HPLC grade ethanol	Sigma-Aldrich, Posnań, Poland
Sagrotan® spray	Sagrotan, Heidelberg, Germany
NaOH	Sigma-Aldrich Posna, Poland
UltraPure™ TBE buffer 10X	Life technologies, Cramlington, UK
Agarose-Molecular Grade	Bioline, Camarillo, USA
Ethidium bromide	Sigma-Aldrich, St. Louis, MO, USA
Water Molecular Biology reagent	Sigma-Aldrich, Dorset, UK
PCR ReadyMix™	Sigma-Aldrich, Dorset, UK
Extraction and Dilution solution	Sigma-Aldrich, Dorset, UK
ITS primers	Integrated DNA Technologies, Leuven, Belgium
Hyperladder 50bp DNA ladder	Bioline, London, UK
1x Tris/Borate/EDTA (TBE) buffer	Fisher Scientific, Leicestershire, UK
Monarch DNA Gel Extraction Kit	New England Biolabs, Hitchin, UK
DMSO	Fisher Scientific, Waltham, MA, USA

Table 2.2: Equipment

Equipment	Source
pH meter	Jenway, Staffordshire, UK
Incubator	Vindon Scientific, Oldham Lancashire, UK
Magnetic mixer	Stuart, Stone, UK
Vortex Genie 2	Scientific Industries Inc, London, UK
Petri dishes	Thermo Scientific, Waltham, MA, USA
UV gel-documentation system	Syngene, Cambridge, UK
Microbiological safety cabinet-BioMAT2	Medical Air Technology, Manchester, UK
Disposable sterile scalpel	Swann-Morton, Sheffield, UK
Rotary evaporator	Buchi, Flawil, Switzerland
Plate reader	Molecular Devices, San Jose, CA, USA
TLC silica gel 60 F ₂₅₄	Merck, Darmstadt, Germany
Silica column	VersaFlash, Bellefonte, PA, USA
Grace Reveleris	W.R. Grace, Columbia, MD, USA
Biotage Isolera One	Biotage, Uppsala, Sweden

2.1.1 Plant Collection

Whole plants were purchased from Abdulrahaman Greenland flower garden, located at Gobarau road, by NNPC Sonal office, Kaduna, Nigeria, in June 2021. Plants were confirmed by Prof. Ajibade Gabriel, a botanist, of the Biological Sciences Department, Nigerian Defence Academy, Nigeria. There was no voucher of the collected plants, as the plants were identified only through photos.

2.2 Microbiological methods

2.2.1 Preparation of malt extract agar (MEA) media and fungal inoculation

The media was prepared by weighing 7.5g of malt extract powder and 7.5g of agar followed by addition of 0.1g of chloramphenicol in a 500 ml jar. The mixture was dissolved in 500 ml of ultrapure water while pH of the mixture was adjusted to between 7.4 and 7.8 with 1M sodium hydroxide and a pH meter. The prepared media was then autoclaved for 1h and 30mins at 121°C under 15psi. The laminar flow was cleaned and disinfected using Sagrotan™ spray to ensure sterility. The autoclaved agar-based media was poured into 100mm×15mm Petri dishes plates in a microbiological safety cabinet-BioMAT2. The stems and roots of each plant was dipped into a beaker containing autoclaved distilled water to wash off plant debris, then into another beaker containing 70% ethanol to remove the epiphytes living on the surface of

it, and finally into the last beaker containing autoclaved distilled water to get rid of any ethanol residues. Using a disposable sterile scalpel, a small section of the stem and root of each plant were then cut, and the inner tissues inoculated onto petri dishes containing malt extract agar, supplemented with chloramphenicol to suppress bacterial growth. This was carried out in duplicate. The plates were incubated for 5-6 days at a temperature of 24°C – 31°C, until fungal growth was observed.

2.2.2 Initial inoculation of endophytic fungi from plants

MEA plates were again prepared as described in section 2.2.1. A small part of each of the fungal colony from the incubated plates from section 2.2.1 were transferred to the new MEA plates. The re-inoculated plates were labelled according to their host origin. The colour and morphology of each transferred colony were observed. The newly inoculated plates were incubated at 27°C until sufficient fungal growth was available for the 2nd inoculation for further purification.

2.2.3 Fungal culture purification step

MEA plates were again prepared as in section 2.2.2 but without addition of chloramphenicol. An aliquot cut of each of the pure fungal colonies from section 2.2.2 were re-inoculated on new plates and were incubated at 27°C. Plates were continuously sub-cultured on MEA to obtain pure cultures of the fungal endophytes. The isolated endophytes were coded according to their host plant names and plant parts and were grouped into fast, moderate, and slow growing.

2.2.4 Cryopreservation of isolated fungal endophyte

Malt extract broth: glycerol (70:30) media of about 1 mL was introduced into 2 mL cryovials. Small sections of the fungal endophytes were cut and put into the cryogen vials. The vials and contents were preserved in the -80°C freezer until further use.

2.2.5 Screening of fungal endophytes for the presence of active secondary metabolites

Fast, moderate, and slow growing fungal endophytes were cultured for 11, 15, and 30 days respectively. Each purified fungus was re-inoculated on nine MEA plates as prepared in section 2.2.3 to make a triplicate from each fungal extract. The isolates were introduced into 500 mL of conical flask, 250 mL of ethyl acetate was added to the conical flask containing the organism, and the conical flask was closed using aluminium foil. The preparation was left overnight.

2.2.5.1 Extraction process

Fungal endophytes that were left overnight in ethyl acetate were homogenised for 2 mins using a homogeniser, whose rod was sterilised with 250 mL of 70% ethanol. Filtration to get a clear solvent was carried out with the aid of a Buchner funnel and filter paper. A volume of 250 mL ethyl acetate was added to the residue in a conical flask, the mixture was stirred for 1 hour with a magnetic stirrer and filtered. This was repeated for the second time on the filtered mycelial, then the filtrates were pooled together. A rotary evaporator was used to concentrate the extract in a round bottom flask. The extract in the round bottom flask was sonicated for 2 mins to ensure extracts were removed from the flask's walls. The extracts were then introduced into tared vials. Further drying of the extract was performed with Nitrogen generation dryer with the samples set on a heat block at 40°C. The dried extracts were prepared for NMR (Section 2.3), MS (Section 2.4), and antibacterial antibiofilm assay (Section 2.2.6) against MRSA.

2.2.5.2. Sample preparation of fungal crude extracts for screening

Three screening tests namely, NMR, HR-LCMS and biological assay were performed on the crude fungi extracts. The spectral data was processed and subjected to MVA using SIMCA 17.0 software. Sample concentrations for each screening test are summarised in Table 2.3. Flow diagram for the extraction of fungal endophytes is shown in Figure 2.1.

Table 2.3: Sample concentration required for screening.

Screening test	Concentration	Solvent use
LC-HRMS	1 mg/mL	ACN: Methanol (50:50)
NMR	5 mg/600µL	DMSO-d ₆
Bioassay	1 mg/mL	DMSO

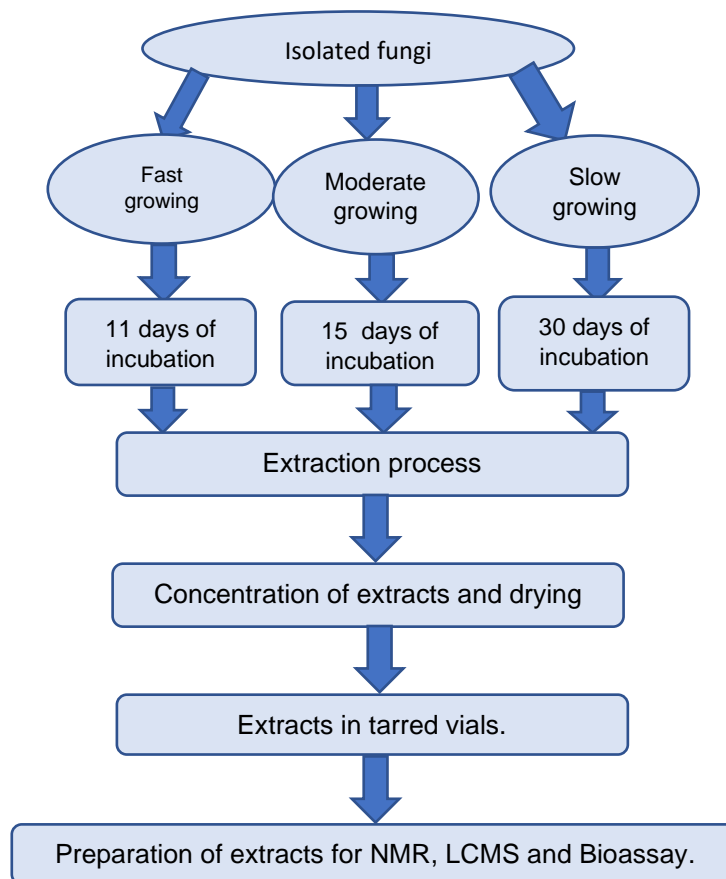


Figure 2.1: Flow diagram for the extraction of fungal endophytes

2.2.6 Extracts test against planktonic, prebiofilm and postbiofilm MRSA and *P. aeruginosa*

2.2.6.1. Bacterial concentration preparation:

S. aureus (ATCC 43300), and *P. aeruginosa* (ATCC 27853) were separately inoculated into 25 mL of Mueller-Hinton broth (MHB) media supplemented with 2 mL of glucose solution, 1 mL of calcium, and 500 µl of magnesium, using a 50 mL centrifuge tube. The bacterial suspension was incubated at 35°C in a shaking incubator, 140 rpm for 16 hours (MRSA), and 40 hours for (*P. aeruginosa*). Thereafter, 250 µl of the grown bacterial suspension was inoculated into 15 mL of MHB. This was incubated at 35°C in a shaking incubator (140 rpm) for 3 hours for the bacterial suspension to attain exponential phase.

2.2.6.1.1 Planktonic assay

Fungi extracts obtained from 2.2.5.2, at concentration of 100 µg/ml was pipetted into wells A2-A11 through H80 of 96 well plate. Sterile MHB of 1.5 mL and bacterial suspension of 1.5 mL was pipetted into 2 different cuvettes, and the optical density (OD₆₀₀) was read using a Cell

Density Meter. The measured optical density was used to calculate the volume of bacterial suspension needed to make a bacterial concentration of 500,000 CFU/mL, using [www.labtools.us/bacterial-cell-number- OD₆₀₀/](http://www.labtools.us/bacterial-cell-number-OD600/).

The formular used was:

$$\text{Volume of Bacterial Suspension (mL)} = \frac{\text{New Wanted Conc.}}{\text{Current Bacterial Conc.}} \times \text{Total Volume of Media}$$

Bacterial suspension of 100 µl, was added into wells already containing fungal extracts at a concentration of 500,000 CFU/mL. The control wells were A1 to D1 (100 µl of bacterial suspension), E1 to H1 (100 µl of sterile MHB), A12-H12 contained double dilution series of ciprofloxacin at a concentration of 25 µg/ml to 0.195 µg/mL, mixed with 100 µl of bacterial suspension. DMSO was used as a negative control, while ciprofloxacin was used as a positive control with double dilution concentrations between. The plate was incubated for 24 hours at a temperature of 35°C, in a shaking incubator at 140 rpm. The optical density readings were then taking at OD₆₀₀ using plate reader.

2.2.6.1.2 Prebiofilm assay

A prebiofilm assay was first performed as described in sections 2.2.6.1 and 2.2.6.1.1 After 24 hours of incubation, the floating planktonic bacteria was pipetted out by adjusting the pipette to 115 µl PBS (100 µL) was added to the wells, to wash the MRSA once, and the *P. aeruginosa* twice. After washing, 90 µL of Dubecco's Modified Eagle Medium (DMEM), and 10 µL of AlamarBlue®, was added to the wells. The plate was covered with aluminium foil and incubated in a shaking incubator at 35°C, 140 rpm. The fluorescence readings were taken after 90 mins of incubation for MRSA, and after 150 mins for *P. aeruginosa* at excitation of 560 nm and emission of 590 nm.

2.2.6.1.3 Postbiofilm assay

Postbiofilm assay was initially performed as in 2.2.6.1, then bacterial suspension of 100 µl, at a concentration of 500,000 CFU/mL, was added into each well with no extracts. The plate was incubated for 24 hours at a temperature of 35°C, in a shaking incubator at 140 rpm, to enable the formation of biofilm. After incubation, the floating planktonic bacteria was pipetted out by adjusting the pipette to 115 µl. Fungi extracts at concentration of 100 µg/ml was pipetted into separate well plates. Wells A12-H12 contained double dilution series of ciprofloxacin, starting at a concentration of 100 µg/ml to 0.78 µg/ml for MRSA, and 66.67 µg/ml for *P. aeruginosa*, mixed with 100 µl of bacteria suspension. The mixtures were transferred to the previous plate

containing pre-formed biofilms. The plate was incubated for 24 hours at a temperature of 35 °C, in a shaking incubator at 140 rpm.

After incubation, the floating planktonic bacteria was pipetted out by adjusting the pipette to 115 µl and the wells were washed as in 2.2.6.1.2. After washing, 90 µL of DMEM and 10 µL of AlamarBlue®, was added to the wells. The plates were covered with aluminium foil and incubated in a shaking incubator at 35°C, 140 rpm. The fluorescence readings were taking after 90 mins for MRSA and after 120 mins for *P. aeruginosa* at excitation of 560 nm and emission of 590 nm.

2.2.6.1.4 Data Processing for planktonic, prebiofilm and postbiofilm of *S. aureus* and *P. aeruginosa*.

Microsoft Excel was used to calculate the percentage viability (Eq. 1) or inhibition (Eq. 2) for each tested crude extract and control.

$$\text{Bacteria Viability (\%)} = \frac{(\mu_{\text{treated well}} - \mu_{\text{min}})}{(\mu_{\text{max}} - \mu_{\text{min}})} \quad (1)$$

$$\text{Bacteria Inhibition (\%)} = \frac{(\mu_{\text{max}} - \mu_{\text{treated well}})}{(\mu_{\text{max}} - \mu_{\text{min}})} \quad (2)$$

Where:

$\mu_{\text{treated well}}$ = the AlamarBlue® count or optical density for the extract treated well

μ_{max} = the average of AlamarBlue® count or optical density for biofilm or planktonic well

μ_{min} = the average of AlamarBlue® count or optical density for the plain LB broth.

GraphPad Prism 9.5 was used to plot the graph.

2.2.6.1.5 Minimum biofilm eradication Concentration (MBEC) and Minimum inhibitory concentration (MIC) assay:

Active fungal extracts with a minimum of 80% bioactivity against bacterial growth (planktonic) and prebiofilm formation, were again tested in both planktonic and prebiofilm assays to calculate the MIC and MBEC at a concentration of 100µg/ml. Assays were carried out in triplicate. A dilution plate was prepared for each extract with a concentration range of 200 µg/ml to 1.56 µg/ml by double dilution method. Test solutions at 200 µg/ml were prepared in column 2 by pipetting 4 µl of 10 mg/mL test stock solution and 196 µl of bacterial suspension into each well, 100 µl of bacterial suspension were pipetted into columns 2 to 10. Column 11 contained negative control DMSO, while column 12 contained the positive control ciprofloxacin. After double dilution was carried out on the plate wells, the remaining MIC and MBEC procedure was as described above in the planktonic and prebiofilm assays in sections 2.2.5.6.2 and 2.2.5.6.3, respectively. After the experiment, readings were taken, and the processed data were plotted on GraphPad Prism 10.1.0. Plate map for MIC and MBEC is shown Figure 2.2 below.

To validate and confirm the MIC readings, 10 µl of AlamarBlue® was added to the wells and incubated for about 90 mins. Samples that remained blue were confirmed to be active, while samples that turned pink were confirmed to be inactive.

		Extracts in ug/ml.									DMSO control	Ciprofloxacin control ug/ml
	1	2	3	4	5	6	7	8	9	10	11	12
A	B B control	200	200	200	200	200	200	200	200	200	200	25
B	B B control	100	100	100	100	100	100	100	100	100	100	12.5
C	B B control	50	50	50	50	50	50	50	50	50	50	6.25
D	B B control	25	25	25	25	25	25	25	25	25	25	3.13
E	S B control	12.5	12.5	12.5	12.5	12.5	12.5	12.5	12.5	12.5	12.5	1.56
F	S B control	6.25	6.25	6.25	6.25	6.25	6.25	6.25	6.25	6.25	6.25	0.78
G	S B control	3.125	3.125	3.125	3.125	3.125	3.125	3.125	3.125	3.125	3.125	0.39
H	S B control	1.56	1.56	1.56	1.56	1.56	1.56	1.56	1.56	1.56	1.56	0.20

Figure 2.2: Plate map for 96-well plate use in MIC and MBEC. BB= Bacterial Broth, SB= Sterile Broth.

2.3 NMR spectroscopy

The extracts were dissolved in 600µl DMSO-d₆ and transferred into 5mm NMR tubes at a concentration of 5 mg/mL, while the entire amount obtained (up to 20 mg) was used for pure compounds. For structure elucidation, all compounds were submitted for NMR using the 400MHz Bruker NMR instruments. This was carried out to perform ¹H, COSY, HMBC, HSQC, TOCSY. ¹³C was only performed for compounds with extract weight of 5mg and above. All experiments were processed using MestReNova 14.2, which involved smoothing with Whittaker Smoother, baseline correction with Whittaker Smoother, and manual phase correction. While COSY analysis, smoothing with Whittaker Smoother, reducing t1 noise and symmetrising as COSY-like were carried out. For the crude extracts, the ¹H NMR spectra data were analysed and processed, then exported to an excel file, converted to csv (comma delimited), then imported to SIMCA 17.0 for MVA.

2.4 LC-HRMS spectrometry

HPLC grade Acetonitrile (ACN) and MeOH were used to dissolve the fungal extract at a concentration of 1 mg/mL. The sample was analysed on a Thermo Vanquish UPLC and an Exactive-Plus Orbitrap high-resolution mass spectrometer. A methanol blank was also analysed. The column attached to the UPLC was an Accucore C18, 100mm x 3mm, 2.8mm column. The mobile phase consisted of micropore water (A) and acetonitrile (B) with 0.1 % formic acid for each solvent. The gradient program started with 10% B linearly increased to 100% B within 30 mins at a flow rate of 300 µL/min and remained isocratic for 5 min before linearly decreasing back to 10 % B in 1 min. The column was equilibrated again with 10% B for 9 mins before the next injection. The total analysis time for each sample was 45 mins. The injection volume was 10 µL and the tray temperature was maintained at 20°C. High-resolution mass spectrometry was carried out in both positive and negative ESI ionisation switch modes with a spray voltage of 4.1 kV and capillary temperature at 320°C. The mass range was set from *m/z* 100-1500 for ESI-MS range. The data was analysed using Mzmine 2.53, Excel-MACRO, and SIMCA 17.0 software.

2.5 Identification of bio-active endophytic fungi by ITS gene sequencing

Based on the Bioassay results, fungi Identification and molecular work was carried out for 3 bioactive fungal endophytes.

2.5.1 DNA Extraction

The voucher specimens of isolated fungi strains were deposited at the Natural Product Metabolomics Laboratory (SIPBS, University of Strathclyde). Three fungi strains were chosen based on their bioactivity against MRSA and processed for DNA extraction, PCR amplification, DNA sequencing. Each fungi strain was processed and sequenced separately. A RED Extract-N-Amp Plant™ PCR kit was used for the single-step extraction of the fungi genomic DNA. A small section of active growing mycelium of the fungi was cut and transferred into a 2 mL microcentrifuge tube using a sterile scalpel and 100 µL of REExtract-N-Amp extraction solution was added to the microcentrifuge tube and briefly vortexed. The sample was incubated at 95°C for 10 mins, after which 100 µL of REExtract-N-Amp dilution solution was added to the extraction solution and vortexed to mix.

2.5.2 Internal Transcribed Spacer Polymerase Chain Reaction

Efforts to help identify the fungi species used polymerase chain reaction (PCR) and PCR primers designed against a hypervariable internal transcribed spacer (ITS) region of the fungal ribosomal DNA (rDNA) (Bellemain *et al.*, 2010). For this study, ITS1 (5'-TCCGTAGGTGAACCTGCGG-3') and ITS4 (5'-TCCTCCGCTTATTGATATGC-3') PCR primers were used. Individual 20µL PCR reactions to amplify the fungi ITS1, 5.8s, and ITS4 regions consisted of the following, in 200µl PCR microtubes: 10 µL REExtract-N-Amp PCR ReadyMix; 1 µL ITS1 Primer (10pmol/ µL); 1 µL ITS4 Primer (10pmol/ µL); 6 µL of nuclease-free water; and 2 µL of the extracted fungi DNA solution. All pipetting steps used aerosol-resistant filter pipette tips. Thermocycling of the ITS1/ITS4 PCRs were conducted on a Primus-96 PCR system under the following cycling conditions: an initial denaturation of 95°C for 3 mins, followed by 40 cycles of denaturation for 1 min; annealing at 56°C for 30s; and extension at 72°C for 1 min. A final extension was carried out for 10 mins at 72°C, and a reaction hold at 8°C.

2.5.3 Electrophoresis and Gel Purification of ITS PCR products

The ITS PCR products from each of the fungi samples were gel purified on 1% (w/v) agarose gels. The gels, with ethidium bromide staining for DNA visualisation (0.4µg/mL), underwent electrophoresis at 60 V for 45 mins in 1x Tris/Borate/EDTA (TBE) buffer (Fisher Scientific, UK). A Hyperladder 50bp DNA ladder was used as a size marker for the gel. The PCR products were visualised and photographed on an ultra-violet (UV) gel-documentation system.

The individual PCR products were sliced out from the agarose gel and transferred into 1.5mL microcentrifuge tubes for purification using a Monarch DNA Gel Extraction Kit. Each gel slice was mixed with 400 µL of Monarch gel dissolving buffer and incubated in a dry block heater

at 55°C for 10 min until the slice is completely dissolved. The solubilised sample solution was then transferred into the Monarch DNA clean-up column and centrifuged for 1 min at 16,000g. The supernatant was discarded. The column was re-inserted into the collection tube and 200 µL of DNA wash buffer was added and then centrifuged for 1 minute. The flow through was discarded. The washing was repeated twice. 20 µL of DNA Elution buffer was pipetted on the centre of the spin column matrix and incubated for 1 minute. Elution of the purified PCR product was carried out by centrifugation for 1 minute at 16,000 g.

2.5.4 DNA Sequencing

Sanger sequencing of each of the fungi ITS PCR products was carried out by Eurofins Genomics (Germany). The gene sequences of each isolate obtained in this study was compared with the GenBank nucleotide database at the National Center for Biotechnology Information (NCBI), by using their Basic Local Alignment Search Tool (BLAST) (<http://blast.ncbi.nlm.nih.gov/Blast.cgi>), and using the 'BLASTN' option (Altschul *et al.*, 1990).

2.6 Media optimisation

Media optimisation was carried out to determine the best media for upscale fermentation of the active fungi. Based on Bioassay result of the crude extracts, media optimisation was carried out for 3 active fungal endophytes: BLS1, MGS3A, and DGS2.

2.6.1 Reactivation and Culturing of active fungi

The fungal endophyte which had been stored in cryovials in the -80°C freezer was brought out and kept in -20°C fridge to defrost overnight. Defrosted fungal endophyte was cultured on petri dish and incubated for 2 days, they were transferred into petri dishes containing MEA and incubated for 7 days at 27°C. Each sample was prepared in triplicate. After 7 days of incubation, the fungi endophyte, was inoculated unto 500 mL flask containing malt extract broth, potato dextrose broth, rice media, and oat media (section 2.6.2).

2.6.2 Media preparation to optimise the production of active crude extracts

2.6.2.1 Malt extract broth

Malt extract broth was prepared by mixing 15 g of malt extract powder with 1000 mL of ultrapure water in 1L glass jar. The pH of the mixture was adjusted to 7.4 – 7.8 using 1M NaOH, 200 mL of the prepared media was poured into 500 mL flask. This was then autoclaved.

2.6.2.2 Potato Dextrose Broth

Potato dextrose broth was prepared by cutting 100 g of sliced (cut in small pieces), unpeeled washed potatoes. This was boiled in 500 mL of ultrapure water, in a stainless-steel pot for 30 mins. Effluent (potato infusion) was filtered, through cheesecloth to a 1-Litre beaker, 10g of dextrose was added and boiled to dissolve completely. After cooling, water was added to the effluent until the 500 mL mark. The pH of the mixture was adjusted to 7.4 -7.8 using 1M NaOH. The 200 mL each of the prepared media was then transferred to a 500 mL Erlenmeyer flask and autoclaved.

2.6.2.3 Rice media

Rice media was prepared by mixing 100g of easy cook rice, produced by Island Sun™ with 150 mL of ultrapure water in 500 mL Erlenmeyer flask then autoclaved.

2.6.2.4 Oat media

For oat media, a 100 %w/v of oat was prepared by mixing 100g of Aldi Everyday Essentials™ porridge oats, with 100 mL of ultrapure water in 500 mL Erlenmeyer flask then autoclaved.

2.6.2.5 Fungal inoculation

A quarter of the petri dish fungal culture was added to the respective media described above. The inoculated media were incubated at 27°C in three time periods at 7, 15, and 30 days. Each sample at different incubation periods were prepared in triplicates. Controls, prepared in triplicates, were also set up for rice, oat, malt, and potato media without fungi inoculation. Experimental set up for media optimisation is shown in Table 2.4.

Table 2.4: Experimental set up for media optimisation

Media	Malt			Potato			Rice			Oat			total
Number of days	7	15	30	7	15	30	7	15	30	7	15	30	
Fungi 1	3	3	3	3	3	3	3	3	3	3	3	3	36
Fungi 2	3	3	3	3	3	3	3	3	3	3	3	3	36
Fungi 3	3	3	3	3	3	3	3	3	3	3	3	3	36
Number of 500 mL flasks													108

2.6.2.6 Extraction from fungal cultures

Extraction was carried out by introducing 250 mL of EtOAc into each flask after 7, 15, and 30 days of fungal growth. This was left overnight. Homogenisation was carried out for 2 mins and 3 mins for the liquid and solid media respectively. The solid and liquid media were filtered. A separating funnel was used to separate the extract from the liquid media. This was carried out thrice to get an extract volume of 750 mL. Filtration was also carried out thrice on the solid media to get an extract volume of 750 mL. Extracts obtained were then concentrated using a rotary evaporator. Sonication was carried out for 1 minute to loosen the concentrated extracts from the round bottom flask, then the concentrated extracts were transferred to tared vials. Extracts were dried using a nitrogen dryer, then prepared for NMR, LCMS, and antibacterial antibiofilm assays against MRSA.

2.6.2.7 Co-culture media optimisation

Co-culture is the process of culturing two types of cells in the same medium. In this study, co-culture was carried out in the manner below.

F. proliferatum was co-cultured with *F. falciforme*

F. proliferatum was co-cultured with *A. alternata*

A. alternata was co-cultured with *F. falciforme*

F. proliferatum was co-cultured with MRSA

F. falciforme was co-cultured with MRSA

A. alternata was co-cultured with MRSA

2.6.2.7.1 First optimisation co-culture of fungi with MRSA on malt agar

MRSA suspension was prepared at a concentration of 500 CFU/mL in a similar manner as explained in 2.2.6.1. Bacterial suspension of 10 mL was introduced unto the centre of each petri dish. Malt extract agar was poured, and the petri dish swirled. This was allowed to solidify, then 4 days cultures (1 cm x 1 cm) each of BLS1, MgS3A, and DgS2 was inoculated by the side of the petri dish. This was incubated at 27°C for 4 days. This was carried out in triplicate with control. Another batch was similarly prepared and incubated for 10 days at 27°C.

Extraction was carried out for both batches by cutting contents of the petri dish into 8 sections, and introducing them into 1 L Flask, 500 mL of EtOAc was added, and left overnight. Homogenisation was carried out the next day, and the filtrate decanted. This was repeated twice, and filtered at the 3rd extraction, to give a total volume of 1,500 mL. The extract was concentrated, and dried to obtain their weights. Extract was prepared for NMR (section 2.3), MS (section 2.4), and antibacterial antibiofilm assay (section 2.2.6) against MRSA.

2.6.2.7.2 Second optimisation co-culture of fungi with MRSA on malt extract broth

Malt extract broth was prepared using a similar method as explained in section 2.6.2.1. One quarter of 4 days culture of BLS1, MgS3A, and DgS2 was inoculated, and incubated at 27°C for 1 day. MRSA suspension of 20 mL, prepared in a similar method as 2.2.6.2.1, was introduced into each flask. Each fungi replicate was duplicated to maximise the yield. A control was also prepared without inoculation. The experimental set-up was incubated at 27°C for 15 days and 30 days. This was followed by extraction and drying of extracts. Extracts were prepared for NMR (section 2.3), LCMS (section 2.4), and antibacterial antibiofilm assays (section 2.2.6) against MRSA.

2.6.2.7.3 First optimisation co-culture of fungi to fungi on malt agar

BLS1 and Mgs3A, BLS1 and DgS2, DgS2 and MgS3A were co-cultured on malt agar plates (1 cm x 1 cm each of BLS1, MgS3A, and DgS2 was inoculated by the side of the petri dish). Experimental control with no fungi inoculation was also set up. The experimental set-up was incubated at 27°C for 7 days. This was followed by extraction and drying of extracts to obtain the weights. Extracts was prepared for NMR (section 2.3), LCMS (section 2.4), and antibacterial antibiofilm assays (section 2.2.6) against MRSA.

2.6.2.7.4 Second Optimisation co-culture of fungi-fungi on malt extract broth

Malt extract broth was prepared using a similar method as explained in section 2.6.2.1 above. One quarter of 4 days old culture of BLS1 with MgS3A, and BLS1 with DgS2 was inoculated as co-cultures, and incubated at 27°C for 15 days and 30 days. The replicates were prepared in duplicates to obtain higher extract yield. Experimental control with no fungi inoculation was also prepared and incubated. This was followed by extraction and drying of extracts to obtain the weights. Extracts were prepared for NMR (section 2.3), LCMS (section 2.4), and antibacterial antibiofilm assays (section 2.2.6) against MRSA. Summary diagram showing extraction protocol for both liquid and solid media is shown in Figure 2.3.

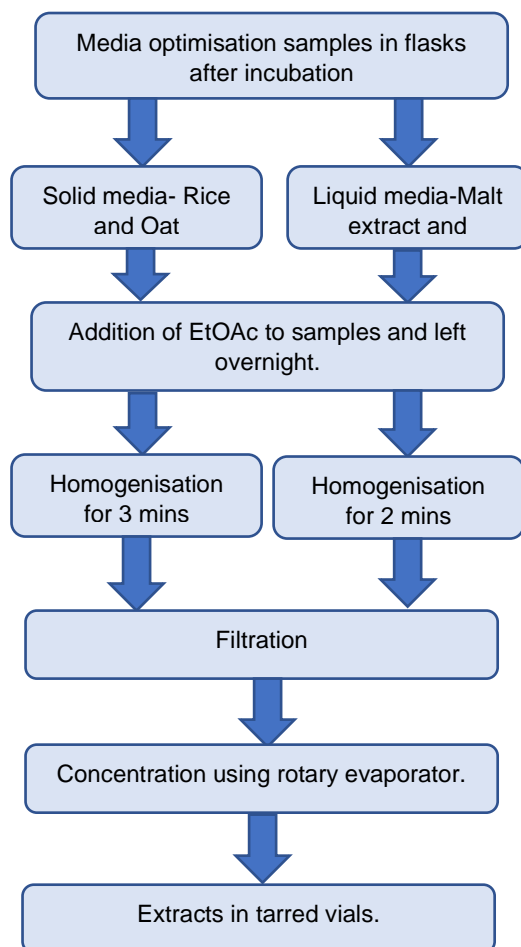


Figure 2.3: Summary diagram showing extraction protocol for both liquid and solid media.

2.6.2.8 Sample Preparation

NMR, HR-LCMS, and bioassay samples were prepared to provide the spectral and biological data necessary to select the media for the scale-up work for both monocultures and co-cultures. The spectral data generated was processed then subjected to MVA using SIMCA 17.0 software.

2.7 Chemical analysis: Extraction, chromatographic separation, and structure elucidation

2.7.1 Scale-up fermentation and extraction of active fungal endophytes

2.7.1.1 Scale-up fermentation and extraction of *F. proliferatum*.

Rice media was chosen to scale up *F. proliferatum* due to the high extract weight of 1.56g, and excellent percentage bioactivity of 89.49% obtained. This was carried out in 36 flasks. The flasks were incubated at 27°C for 15 days. At the end of the 15 days, 250 mL of EtOAc was added to each flask and left overnight to macerate, homogenisation was carried out for 3 mins on each flask, followed by filtration. Four flasks were pooled together, 1 L of EtOAc was added, they were stirred for 1 hour in a metal beaker, followed by filtration. This was repeated twice to get the extracts. The extracts were concentrated with a rotary evaporator, further dried with nitrogen dryer, to obtain the dry weights of extracts, and kept for fractionation.

2.7.1.2 Scale up fermentation and extraction of *F. falciforme*

Malt extract broth was chosen to scale up MGS3A, as MGS3A was found to be more stable in malt extract broth when compared to other media. It showed activity at 7 days, 15 days, and 30 days on malt extract broth. On SIMCA, MGS3A on malt extract broth, was also seen to be producing discriminating metabolites as compared to other 3 media.

Scale up of MGS3A was done in malt extract broth using 72 flasks. Fungal inoculum for scale-up cultures of *F. falciforme* was prepared as described in section 2.6.1 and inoculation was accomplished as described in section 2.6.2.5. The flasks were incubated at 27°C for 15 days. At the end of the 15 days, 250 mL of EtOAc was added to each flask, and kept overnight to macerate, homogenisation was carried out for 2 mins on each flask. A funnel was used to separate EtOAc containing the extracts from the media. This was carried out thrice to obtain the extracts. The extracts were concentrated with a rotary evaporator and further dried with nitrogen dryer. The experimental workflow for *F. falciforme* (MGS3A) scale up from frozen state to extract is shown in Figure 2.4.

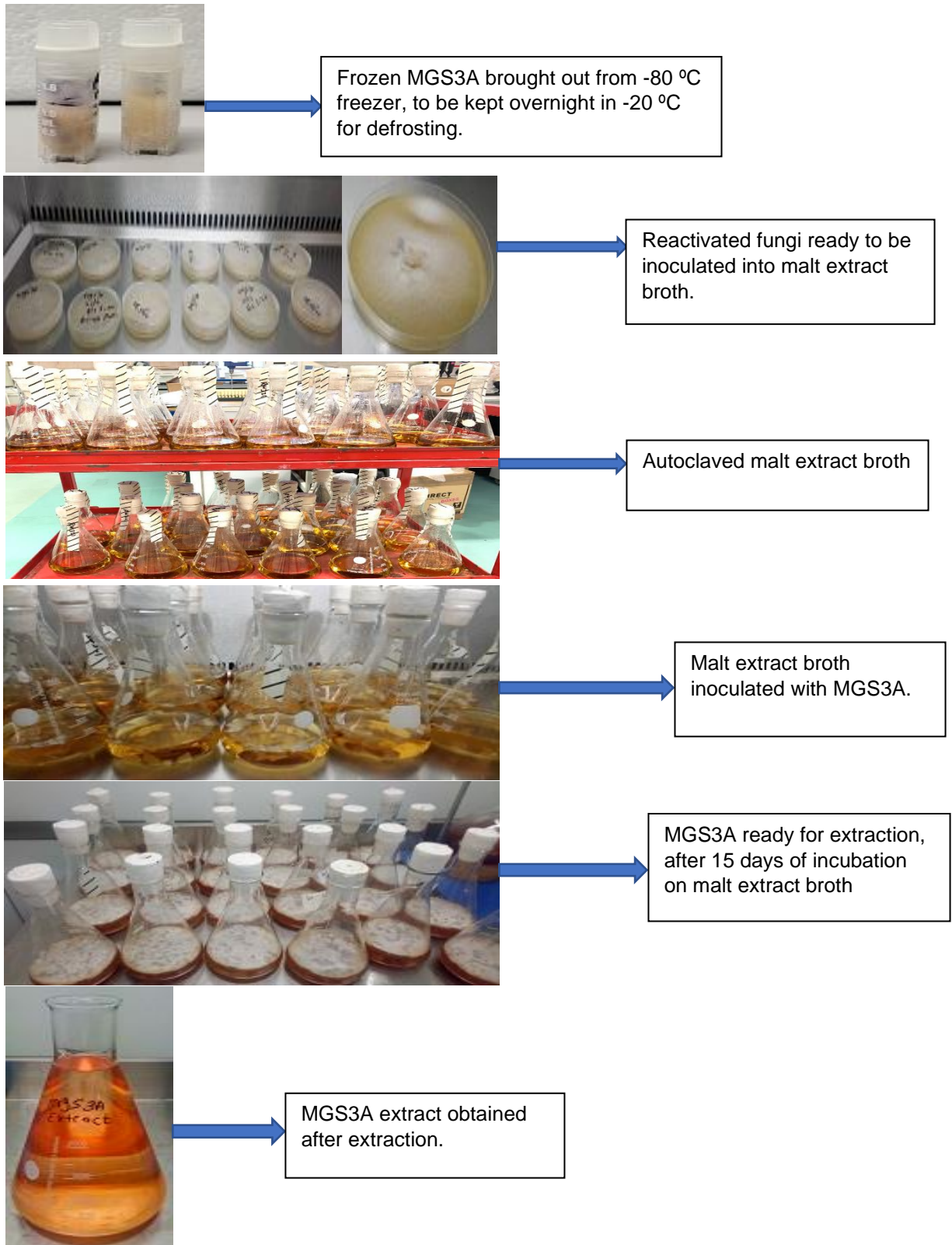


Figure 2.4: Experimental workflow for *F. falciforme* (MgS3A) scale up from frozen state to extract.

2.7.1.3 Solvent – Solvent partitioning of *F. falciforme* scale-up crude extract

Solvent partitioning was done to eliminate the lipids in *F. falciforme* scale-up extract (15.18g). A 100% v/v of aq MeOH and hexane was prepared by reconstituting the crude extracts with 100 mL of 10% aqueous methanol and extracting thrice with 100 mL of n-hexane. The multiple batches of hexane and aqueous methanol extracts were pooled, concentrated, and subjected to NMR (section 2.3), HR-LCMS (section 2.4), and antibacterial antibiofilm assay (section 2.2.6) against MRSA. Summary diagram of solvent-solvent partitioning of *F. falciforme* extract grown on malt extract broth shown in Figure 2.5.

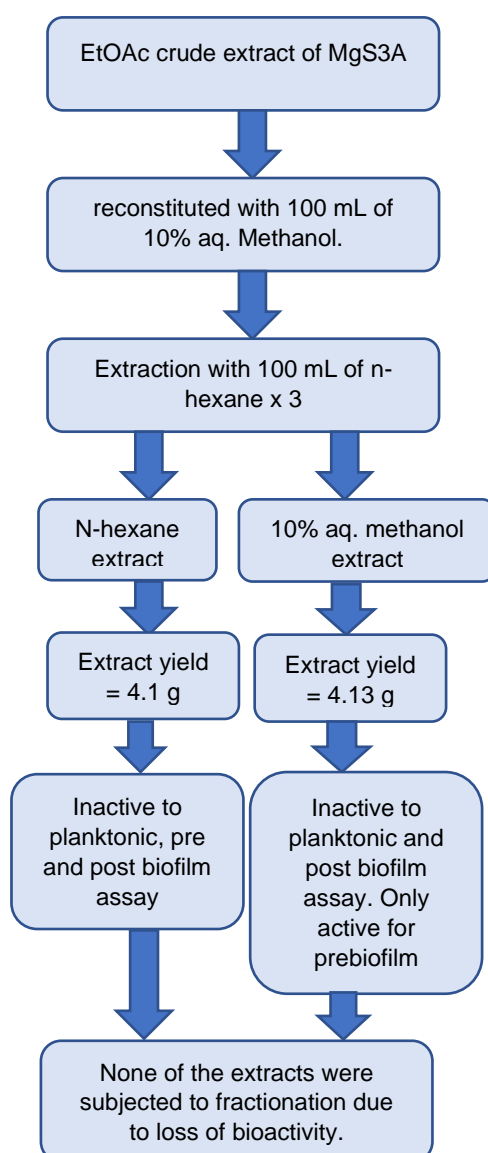


Figure 2.5: Summary diagram of solvent-solvent partitioning of *F. falciforme* extract grown on malt extract broth.

2.7.1.4 Scale up fermentation and extraction of *A. alternata*

Potato dextrose broth was chosen for the scale-up of DGS2, because DGS2 showed highest inhibition rate against MRSA on potato dextrose broth at 30 days, with an average yield of 365.3 mg. The work was carried out using 76 flasks.

Fungal inoculum for scale-up cultures of *A. alternata* was prepared as described in section 2.6.1 and inoculation was accomplished as described in section 2.6.2.5. The flasks were incubated at 27°C for 30 days. At the end of the 30 days, 250 mL of EtOAc was added to each flask, and left overnight to macerate, homogenisation was done for 2 mins on each flask. A separatory funnel was used to separate EtOAc containing the extracts from the media. The extraction was carried out thrice. The extracts were concentrated with a rotary evaporator, further dried with nitrogen dryer, and kept for fractionation.

2.7.1.5 Scale up fermentation and extraction of co-culture of *F. proliferatum* and MRSA

Malt extract broth was chosen to scale up co-culture of *F. proliferatum* with MRSA. One hundred and three flasks were used for the work. The samples were prepared in a similar manner with 2.6.2.7.2. The flasks were incubated at 27°C for 15 days. At the end of the 15 days, 250 mL of EtOAc was added to each flask, and kept overnight. Two flasks were combined into one flask, and homogenisation done for 2 mins, and the sample was filtered using a vacuum pump. A funnel was used to separate EtOAc containing the extracts, from the media. Extraction was done thrice, with 500 mL of EtOAc added at the second and third extraction. The extracts were concentrated with a rotary evaporator and dried.

2.7.2 Medium pressure liquid chromatography (MPLC)

MPLC is a separation technique like open column chromatography but uses pressure to elute the sample from the column faster. It is also known as flash chromatography. The solvent system to be used is first optimised on a TLC plate. Before loading dry samples that were combined with celite, normal phase columns were applied in both the Buchi and Reveleris® flash Forward systems, and they were conditioned with the beginning solvent solution. A silica column with dimensions of 4 x 150 mm and a particle size of 20-45 µm was used for the work. Fractions were collected manually in 100 mL Erlenmeyer flasks, if the Buchi system was used, while fractions were collected automatically in test tubes, if the Reveleris® flash forward system was used. After that, TLC analysis (section 2.7.3) was performed on all fractions, and similar fractions were pooled together. The pooled fractions were concentrated by a rotary evaporator. Further isolation and purification of the active fractions or fractionation of small

quantities of crude extracts were performed using either conventional gravity column or by flash chromatography, which can be either normal or reverse phase fitted with the respective commercially available prepacked column. After separation, sub-fractions obtained were pooled together by TLC using 10x20 silica TLC plates, with DCM: MeOH (90: 10) as the mobile phase.

2.7.3 Thin layer chromatography (TLC)

Thin layer chromatography (TLC) was applied as an analytical tool to aid in identification of compounds based on their R_f (retention factor) value and colour either under UV light or upon reaction with different spraying reagents. It was used in the optimisation of solvent systems for column chromatography. It also served as a very important technique to determine the purity of a sample and to estimate the number of compounds in a mixture. Furthermore, it was used as a preparative tool to purify compounds. To ensure a proper separation of compounds on the column, MPLC system were chosen after they were optimised on TLC silica gel 60 F₂₅₄ plates. The R_f values were used to obtain the method for separation. The R_f value of the components should be between 0.3 and 0.5 to avoid a fast elution rate, which could lead to inappropriate separation. The appropriate mobile phase was selected based on the R_f values of first eluting component. For analytical TLC purposes, fractions were dissolved in EtOAc and spotted 0.5 cm apart, 1 cm above and at the bottom edge of the TLC plate. The TLC chamber was equilibrated with the mobile phase to which the plates were added and left to develop. The plate size used for mobile solvent optimisation was cut in pieces of 2.5x 10 cm, while 10 x 20 cm was used to monitor and pool the fractions. The eluted spots for pure compounds or crude extracts were detected under short or long UV lights. Under the short UV light, dark spots could be indicative of compounds that quenched fluorescence or phosphorescence, while aromatics and conjugated double bond systems could be detected as coloured spots. Other metabolites such as alkaloids or flavonoids could be detected under long UV light. After development, TLC plates were sprayed with anisaldehyde/sulfuric acid reagent (Table 2.5) and heated to 300°C with a heat gun.

2.7.4 Preparative thin layer chromatography (PTLC)

PTLC was used to purify fractions or subfractions with weights less than 100 mg. About 10 to 15 mg of sample was dissolved in 150µL of EtOAc and applied to each TLC silica gel 60 F₂₅₄ (aluminium sheets) plates with 20x20 cm dimension, with 1 cm above and the bottom edge of the plate marked out for the bands not to exceed. Filter papers were placed inside the TLC chamber for equilibration. Few spots were applied to the TLC plate on the 1 cm marked below and was left to airdry, then placed in the equilibrated TLC chamber to develop. After the TLC

plates were developed, the bands were viewed under UV light. The bands were marked with a pencil and cut. The compounds were recovered by sonicating the cut bands thrice for 15mins using EtOAc. The extracts were filtered with a filter paper, concentrated, and put in tared vials. A summary plate was prepared using DCM: MeOH (90:10) as the mobile phase. NMR was carried out to determine the purity of the compounds.

2.7.5 Anisaldehyde- sulphuric acid spray reagent composition

Anisaldehyde- sulphuric acid spray reagent is used to detect phenolic compounds, essential oils, steroids, sugars, terpenes and sapogenins in crude extracts, fractions or pure compounds separated on TLC plates. To check for non-UV compounds that appear in various colours, the TLC plate was sprayed with the reagent and heated at 300°C. The spray reagent was stored in a glass bottle covered with aluminium foil packed to avoid light and kept in a refrigerator prior to use. The components of anisaldehyde/sulfuric acid spray reagent are listed in Table 2.5.

Table 2.5: The components of anisaldehyde/sulphuric acid spray reagent.

Component	Volume (mL)
<i>P</i> - Anisaldehyde	0.5
Methanol	85
Glacial acetic acid	10
concentrated sulfuric acid	5

2.7.6 Fractionation of scale-up crude extracts

2.7.6.1 Fractionation of *F. proliferatum* scale-up crude extract

Solvent optimisation for chromatographic separation was first carried out to determine the best mobile phase using EtOAc (100%), Hexane (100%), EtOAc: MeOH (7:3), Hexane: EtOAc (95:5, 97:3, 99:1, 9:1, 8:2, 7:3, 5:5, 3:7), and DCM: Isopropanol (95:5) on TLC silica gel plate (cut 10x20). The total crude extract obtained from *F. proliferatum* weighed 53.1 g, out of which 19.98 g was reconstituted in EtOAc and used for fractionation. Celite was added to obtain a homogeneous mixture, then left to dry overnight under the fume hood. A prepacked column of silica was used as a stationary phase solvent. The column was equilibrated with 100% hexane for 15 min at a flow rate of 100 mL/min. The chromatographic separation was accomplished by stepwise gradient elution using hexane and EtOAc at a flow rate of 100 mL/min. The fractions were collected in 50 mL and 100 mL flasks. The column was first

washed with EtOAc: Methanol 70:30 (collected in four 500 mL flask), then a final wash was carried out manually with acetone and MeOH 70:30 (collected in three 500 mL flask). The fractions obtained were thereafter pooled together by TLC using DCM: Isopropanol (95:5) at 0.5 cm apart. The fractions were pooled together using the same solvent ratio and placed in tared vials. The fractions were combined based on TLC profiles to give 18 fractions. The fractions obtained were analysed for NMR (2.3), HR-LCMS (2.4), dereplication studies and antibacterial antibiofilm assays (2.2.6) against MRSA. The elution gradient is seen in the Table 2.6 below:

Table 2.6: Elution gradient for fractionation of *F. proliferatum* extracts obtained from scale-up with rice media.

Time (min)	Solvent	Flow rate (mL/min)
0 to 15 min:	100 – 100 % hex	100
15 to 65 min:	100 Hex – 0: 100 Hex: EtOAc	100
65 to 75 min:	100 % EtOAc	100
75 to 90 min:	EtOAc: MeOH (70:30)- First washing	100
Manual washing	Acetone: MeOH (70:30) – Final washing (1.5 L)	100

2.7.6.2 Fractionation of *A. alternata* scale-up crude extract

Solvent optimisation was first carried out to determine the best mobile phase using EtOAc (100%), Hexane (100%), EtOAc: MeOH (7:3), Hexane: EtOAc (95:5, 97:3, 99:1, 9:1, 8:2, 7:3, 5:5, 3:7), and DCM: Isopropanol (95:5) on TLC silica gel plate (used 10 x 20 cut 2.5 x 10). The extract weighing 33.18 g was reconstituted with EtOAc, mixed with 11.80 g of celite, and left in the fume hood for 3 days to dry. A prepacked column of silica was used as a stationary phase solvent. The column was equilibrated with 100% hexane for 15 min at a flow rate of 100 mL/min. The chromatographic separation was accomplished by stepwise gradient elution using hexane and EtOAc at a flow rate of 100 mL/min. The fractions were collected in 50 mL, 100 mL, and 250 mL flask (200 mL). The column was washed manually with acetone and MeOH 70:30 (collected in one 500 mL flask). The fractions obtained were thereafter pooled together by TLC using DCM: Isopropanol (95:5) at 0.5 cm apart. Summary TLC plates using the same solvent ratio was prepared after the fractions were pooled together. The fractions

obtained were prepared for NMR (section 2.3), LCMS (section 2.4), and antibacterial antibiofilm assays (section 2.2.6) against MRSA. The elution gradient is seen in 2.7 below:

Table 2.7: Elution gradient for the Fractionation of *A. alternata* obtained from scale up with potato media.

Time (min)	Solvent	Flow rate (mL/min)
0 to 15 min:	100 %– 100 % hex	100
15 to 65 min:	100 Hex – 0: 100 hex (B): EtOAc (A)	100
65 to 75 min:	100 % EtOAc	100
0 min:	100% EtOAc – 0% MeOH	100
5 min	100% EtOAc – 0% MeOH	100
60 mins	70% EtOAc – 30% MeOH	100
15 mins	70% EtOAc – 30% MeOH	100

2.7.6.3 Fractionation of *F. proliferatum* and MRSA co-culture scale up crude extract

Solvent optimisation was first carried out to determine the best mobile phase using EtOAc (100%), Hexane (100%), EtOAc: MeOH (7:3, 6:4, 5:5, 4:6, 3:7), Hexane: EtOAc (95:5, 97:3, 99:1, 9:1, 8:2, 7:3, 6:4, 5:5, 4:6, 3:7, 2:8, 1:9), and DCM: Isopropanol (95:5) on TLC silica gel plate (used cut 10x20).

Scale-up crude extract obtained weighed 4.15 g, which was reconstituted in EtOAc and used for fractionation. Celite (4 g) was added to obtain a homogeneous mixture, then left to dry for 2 nights under the fume hood. A prepacked column of silica was used as a stationary phase solvent. The column was equilibrated with 100% hexane for 7.45 min. The chromatographic separation was accomplished by stepwise gradient elution using hexane and EtOAc at a flow rate of 60 ml/min. ELSD bands were collected, and UV bands were collected at 254-320 nm. Generic flash column silica-CS 80 g cartridge was used, with a flow rate of 60 mL/min. The fractions were collected in test tubes (20 mL). The column was washed with acetone and isopropanol 50:50, collected in flasks. The fractions obtained were thereafter pooled together by TLC using DCM: MeOH (90:10) at 0.5 cm apart. A summary TLC plates using DCM: MeOH (90:10) was prepared after the fractions were pooled together. The fractions obtained were

prepared for NMR, LCMS, and antibacterial antibiofilm assays against MRSA. The elution gradient is seen in Table 2.8 below:

Table 2.8: Elution gradient for fractionation of *F. proliferatum* and MRSA co-culture Scale-up obtained from malt broth media.

Time (min)	Solvents	Flow rate (mL/min)
5 min:	100 – 100 % Hex	60
60 min:	100% Hex – 100% EtOAc	60
30 min:	70% EtOAc: 30% MeoH	60
10-12 min	Acetone: Isopropanol (50:50)	60

2.7.6.4 Fractionation of *F. proliferatum* and *F. falciforme* co-culture crude extract.

Solvent optimisation was first done to determine the best mobile phase using Hexane: EtOAc (10:90, 20:80, 30:70, 40:60, 50:50, 60:40, 70:30, 80:20, 10:90) on TLC silica gel plate.

Due to similarity in chemical profile and bioassay results, the extracts obtained from replicates of *F. proliferatum* and *F. falciforme* co-culture media optimisation, incubated for 15 and 30 days were merged, dried, and weighed, to give an extract weight of 770 mg. The extract was reconstituted in EtOAc and used for fractionation. The extract was injected into a samplet, then left to dry for 2 nights under the fume hood. The column was manually equilibrated with 100% hexane for 4.84 min. The chromatographic separation was accomplished by linear gradient elution using hexane and EtOAc at a flow rate of 100 ml/min. ELSD bands were collected, and UV bands were collected at 220-280 nm. Biotage flash column of 50 g was used for the work. The fractions were collected in test tubes (18 mL). The fractions obtained were thereafter pooled together by TLC using DCM: MeOH (90:10) at 0.5 cm apart. A summary TLC plates using DCM: MeOH (9:1) was prepared after the fractions were pooled together. The fractions obtained were prepared for NMR, LCMS, and antibacterial antibiofilm assays against MRSA. The elution gradient used is seen in the Table 2.9 below.

Table 2.9: Elution gradient used in fractionating co-culture of *F. proliferatum* and *F. falciforme*.

	Solvents	Percentage mix	Time (min)	Flow rate (mL/min)
	Hexane: EtOAc			
Equilibration	Hexane: EtOAc	0%	2:42	100
1	Hexane: EtOAc	0%	5:00	100
2	Hexane: EtOAc	0%-100%	60:00	100
3	Hexane: EtOAc	100%	5:00	100
4	Hexane: EtOAc	100%	17:30	100
5	EtOAc: MeOH	70%:30%	10:00	100
6	Acetone: Isopropanol	50%:50%	15:00	100
7	Acetone: MeOH	80%:20%	10:00	100

2.7.7 Purification of active fractions

Based on the bioassay results, active fractions were further purified. Purification method used was decided based on the fraction weight. Solvent optimisation was first carried out to determine the best mobile phase for purification.

2.7.7.1 MVA of the crude extract and fractions

The extracts were subjected to proton ¹H NMR and HR-LCMS. MVA was used to correlate the chemical profile and bioactivity pattern of the extracts. PCA SIMCA scores plot of ¹H NMR and HR-LCMS showed the patterns, trends, outliers of the extracts, their similarity, variability, and discrepancies in terms of their chemical profile.

OPLSDA was used to compare 2 groups of samples. For example, the scores plot was used to analyse the samples based on their bioactivity (active versus inactive). It helped in identifying the metabolites that were present in the active extract, by separating the active from the inactive extracts. The active and inactive extracts shown in the OPLS-DA plots of NMR-SIMCA and HRLCMS-SIMCA, were based on the results of the planktonic and prebiofilm biological assay.

The LCMS loadings plot for PCA and OPLSDA gave information about the metabolites that were discriminatory with reference to the positioning of the extract in the scores plot. ^1H NMR loadings plot, grouped the extracts according to their functional groups based on their chemical shifts (PPM), which gave information about the chemical profile of the extracts and their discriminatory metabolites.

In the plot, R_2 estimated goodness of fit and Q_2 showed the predictability. R_2 described the correlation or the linearity between two variables. High R_2 and high Q_2 values, brought about better separation between groups. To produce a good fit, R_2 value should be greater than Q_2 , and the difference between R_2 and Q_2 should not be greater than 0.3.

$R_2 X(1)$ explained the variation between 2 groups of extracts, while $R_2 X_o(1)$ explained the variation within groups of extracts. The $R_2 X(1)$ should be greater than $R_2 X_o(1)$.

2.7.7.2 Dereplication studies by using HR-LCMS

Dereplication study on the total crude extract and fractions of samples were performed using HR-LCMS, and then processed with Mzmine software, an in-house macro coupled with the Dictionary of NPs (DNP) 2021. The mass spectral data was processed using the procedure established in the Natural Products Metabolomics Group Laboratory at SIPBS as described by (Macintyre *et al.*, 2014). HR-LCMS raw data were initially splitted into negative and positive data sets using the MassConvert software package from Proteowizard (pwis). The sliced data sets were subsequently exported into Mzmine 2.53. The peaks in the samples and solvent media blanks were detected using the chromatogram builder. By using a centroid detector threshold that is greater than the noise level which was set at $1.0\text{E}4$, with an MS level of 1, the mass ion peaks were isolated. Chromatogram builder was performed by setting the minimum height and m/z tolerance at $1.0\text{E}4$ and $0.001 m/z$ or 5.0 ppm , respectively, while the minimum time span was set at 0.2 min. Chromatogram deconvolution was done to detect the individual peaks. The local minimum search algorithm was performed by setting search minimum in RT range of 0.4 min, chromatographic threshold was set at 5 %, minimum absolute height of $1.0\text{E}4$, ($1.0\text{E}5$ for the positive files), and minimum relative height was set for 5 %. Minimum ratio of peak top/edge was 2, and peak duration range was set at 0.2-5 mins. Isotopes were also identified using the isotopic peaks grouper (m/z tolerance: $0.001 m/z$ or 5.0 ppm , retention time tolerance: 0.2 absolute (min), maximum charge: 2, and representative isotope: most intense). Using the join aligner parameters set at m/z tolerance of $0.001 m/z$ or 5.0 ppm , weight for m/z was set at 20, retention time tolerance was set at 5.0 relative (%), and weight for RT: 20, the peak list was aligned. Using the gap-filling peak finder (intensity tolerance: 25.0%, m/z tolerance: $0.001 m/z$ or 5.0 ppm , and retention time tolerance

of 0.5 absolute (min), the missing peaks were detected. An adduct search was performed for positive mode (Na and NH₃). A complex search was performed with ionisation method [M-H]⁻ for the negative mode, and a complex search was performed with ionisation method [M+H]⁺ for the positive mode, *m/z* tolerance was set at 0.001 *m/z* or 5.0 ppm, retention time tolerance was 0.2 absolute (min), while maximum complex peak height was set at 50.0%. The processed data was then subjected to molecular formula prediction and peak identification. The positive and negative data sets were exported to csv (comma delimited) to be imported to the in-house macro excel sheet. All processed data from different fractions and samples were combined in the macro, the media was removed, and dereplication was performed to identify putative compound hits. The combined data sets were imported into SIMCA 17.0 for MVA. PCA and OPLS-DA were performed with pareto scaling and used to compare the metabolomic profiles of different samples. The summary workflow of metabolomics applied in the search for antimicrobial agents is shown in Figure 2.6.

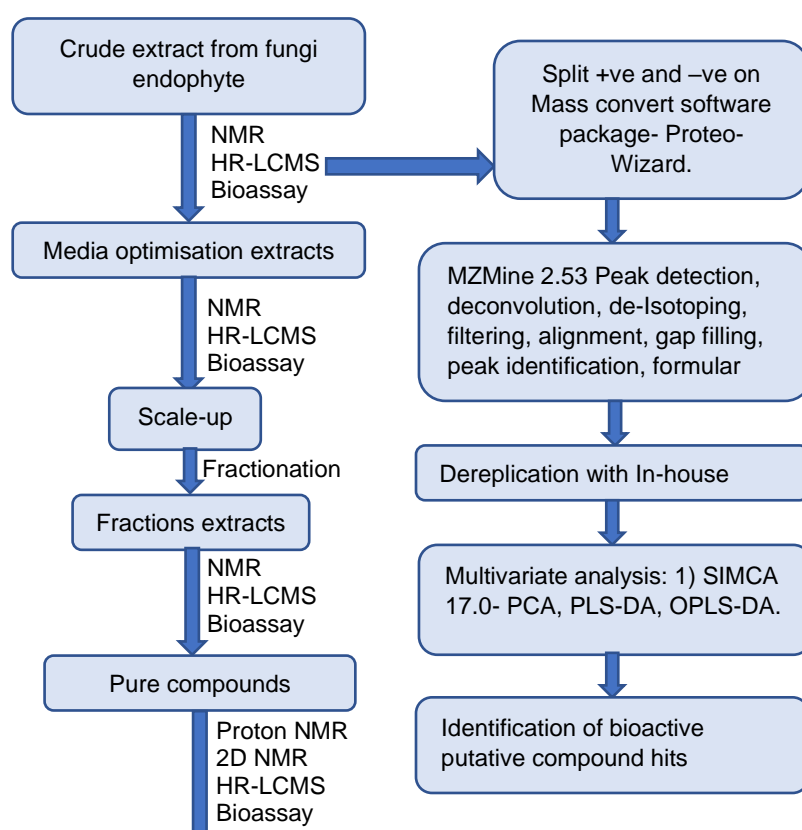


Figure 2.6: Summary workflow of metabolomics applied in the search for antimicrobial agents.

CHAPTER 3

3 Isolation and Screening of Fungal Endophytes

3.1 Literature background on five selected plants for this study

3.1.1. *Vernonia amygdalina* as a source of NPs

V. amygdalina, which belongs to the Asteraceae family, is a major food plant in Nigeria with the common name as bitter leaf and serves as an important diet among several ethnic groups in the country (Oriakhi *et al.*, 2013). It is widely distributed in Asia and tropical Africa, and most abundant in natural forest. It has a long history in traditional medicine and the plant leaves, stem and roots have been exploited in the treatment of various ailments. The leaves are mostly used in the treatment of diabetes mellitus, venereal diseases, malaria, wounds, hepatitis, and cancer (Ibrahim *et al.*, 2000, Erasto *et al.*, 2007, Hamill *et al.*, 2003). It has also been found to exert anthelmintic properties (Kambizi and Afolayan, 2001). The roots and the leaves are used in traditional medicine to treat stomach problems, fever, kidney problems, and hiccups. Extracts from *V. amygdalina* leaves possess several secondary metabolites which include polyphenols, flavonoids, tannins, saponins, and terpenoid (Alara *et al.*, 2018). These phytochemicals might be responsible for its antimicrobial action against drug resistant microorganisms and its anticancer, antioxidant, anti-inflammatory, and antiviral activities (Amaning Danquah *et al.*, 2012, Akinpelu, 1999).

3.1.2. *Ocimum gratissimum* as a source of NPs

O. gratissimum, which is commonly called scent leaf by traders in the open market is a medicinal plant indigenous to Nigerians. It is called Nchanwu by the Igbos, Effirin by the Yorubas, Daidoya by Hausas, and Ntong by the Effiks. Its common name is African Basil. The cold leaf infusions of the plant are used for the relief of stomach upset and haemorrhoids, while the leaf extract is used in the treatment of diarrhoea by the tribals of Nigeria (Akinyemi *et al.*, 2005). The seeds can be used in urinary disorders when infused. The plant is commonly used in herbal medicine to treat different diseases such as upper respiratory tract infections, skin diseases, diarrhoea, and headache, diseases of the eye, cough, pneumonia, and fever (Adebolu and Salau, 2005). There is a belief, that *O. gratissimum* can be used to keep the baby's cord and wound surfaces sterile (Iwu, 1986). It is used to ease the pain of childbirth and expel the after birth. It increases milk in nursing mothers. It is used as a treatment of urinary and respiratory ailments. It is used to reduce indigestion and bad breath (Lowry *et al.*, 1992). It is used for inflammation and ringworm, nausea, cramps, vomiting (Iwu, 1986, Onajobi,

1986). The plants are used to lower stress-related high blood pressure. It is used to control difficult skin diseases like leprosy and infection of the skin (El-Mahmood *et al.*, 2008). It is also suggested as antimicrobial, antifungal, antibacterial, antimalarial, antiviral, anaesthetic, antiprotozoal, and anthelmintic agents (Monga *et al.*, 2017). It has anti-stress, antidiabetic, anti-inflammatory and antifertility activity (Cohen, 2014). The phytochemical components of *O. gratissimum* are phenols, tannins, alkaloids, saponins, phlobatannins, glycosides, terpenoids, flavonoids, and anthraquinones (Olamilosoye *et al.*, 2019).

3.1.3. Fungal isolates of *M. indica* as a source of NPs

M. indica is a fruit belonging to the Anacardiaceae family, grown in many parts of the world, particularly in tropical areas. It is important for its nutritional value, attributable to the presence of health-enhancing compounds; it is considered a good source of carbohydrates, ascorbic acid, dietary fibre, carotenoids, organic acids, and phenolic compounds (Schieber *et al.*, 2000). Mango leaves fed at high percentage could cause poisoning for cattle (Orwa *et al.*, 2009); however, it can form an important part of feed given to domestic animals (Lowry *et al.*, 1992). *M. indica* have been the focus of intense research in search of new metabolites from different parts of the plants such as leaves, stems, fruits, and seed kernels. Its medicinal value is well established and has been used for centuries for the treatment of different kinds of ailments (Shah *et al.*, 2010). It has been found to possess different pharmacological properties including antibacterial property (Hamel and Manzara, 2008).

Previous research on the phytochemical screening of the leaves of *M. indica* revealed the presence of phenols, saponins, tannins, steroids, flavonoids, anthraquinone, and glycosides (Hamel and Manzara, 2008, Aiyelaagbe and Osamudiamen, 2009). Mangiferin, a pharmacologically active hydroxylated xanthone C-glycoside, has been extracted from mango at high concentrations from the young leaves (172 g/kg), bark (107 g/kg), and from old leaves (94 g/kg) (Barreto *et al.*, 2008).

3.1.4. *Azadirachta indica* as a source of NPs

A. indica, also known as the neem tree, is a member of the mahogany family, Meliaceae. Botanically, it is known as *A. indica*, A. Juss. Ingredients obtained from *A. indica* are applied in homeopathy, ayurveda, Unani and modern medicine for the treatment of many infectious diseases (Alzohairy, 2016). The plant species possesses anti-inflammation, bactericidal and growth-disrupting properties, immune stimulation, blood purification, antitumor, and insect repulsion (Singh and Sharma, 2020). Neem has been useful in treating many known and unknown diseases. The plant is known to contain several thousands of secondary metabolites,

which are crucial for multifunctional properties like anti-inflammation, anti-oxidation, antimalarial, and anticarcinogenic activities. Over three hundred compounds have been isolated from different parts of the neem plant. One-third of the compounds belong to the limonoid group of NPs, which are the major cause for their widespread bioactivities. These compounds have a low toxicity against beneficial, and non-target organisms and cause less disruption to ecosystems than conventional insecticides (Tiwari *et al.*, 2014). About 250 neem secondary metabolites have been documented in the NeeMDB (Hatti *et al.*, 2014). Neem metabolites include azadirachtin, salanin, nimbin, azadiradione, epoxy/hydroxy-azadiradione, isolated from different parts of neem plants (leaf, bark, and seed) (Rangiah and Gowda, 2019).

3.1.5. *Moringa oleifera* as a source of NPs

M. oleifera, also known as the miracle tree is well recognised for its rich nutritional value and use in the treatment of various disorders that is attributed to its diverse phytochemical content (Goyal *et al.*, 2007). The tree serves as a food resource specially in India, China, and African countries for its edible tree parts such as leaves, seeds, and pods (Stohs and Hartman, 2015). Different parts of this plant contain a rich profile of macro or micronutrients, like protein, vitamins, and minerals leading to its use in diets and supplements, especially in developing nations that may suffer from malnourishment (Gopalakrishnan *et al.*, 2016). In Africa, *M. oleifera* is now increasingly consumed as a multipurpose plant for its nutritional value (Ayeleso *et al.*, 2020). Previous studies on *M. oleifera* secondary metabolism revealed the presence of several phytochemical classes such as alkaloids, flavonoids, steroids, saponins, anthraquinones, glucosinolates, tannins, phenolic acids, and terpenes among others (Goyal *et al.*, 2007). Metabolites analyses of *M. oleifera* cultured in different countries revealed that different environmental factors affect its phytochemical content both quantitatively, qualitatively (Gopalakrishnan *et al.*, 2016). This complex chemical composition contributes to the various pharmacological effects of *M. oleifera* plant such as antimicrobial, antioxidant, anticancer, antiviral, antiulcer, lactagogue, antihyperlipidemic, hypotensive, antidiabetic, hepatoprotective, CNS depressant and antipyretic (Chen *et al.*, 2020, Fathy and Mahmoud, 2021, Gopalakrishnan *et al.*, 2016). Compounds isolated from *M. oleifera* includes niasinin A, niasinin B, niasimicin and niasinin A + B (Vergara-Jimenez *et al.*, 2017), and *N*, α -L-rhamnopyranosyl vincosamide, phenylacetonitrile pyrrolemarumine, 4'-hydroxyphenylethanamide- α -L-rhamnopyranoside and its glucopyranosyl derivative (Panda *et al.*, 2013).

3.2 Fungal extraction

Thirty-four isolated fungal endophytes were classified as fast, moderate, and slow-growing fungi depending on their growth rates. Each fungus was inoculated on nine malt agar petri dish plates. One extract was prepared by putting together three plates of malt extract media containing fungus. The average weight of extracts from each triplicate is shown in Figure 3.1.

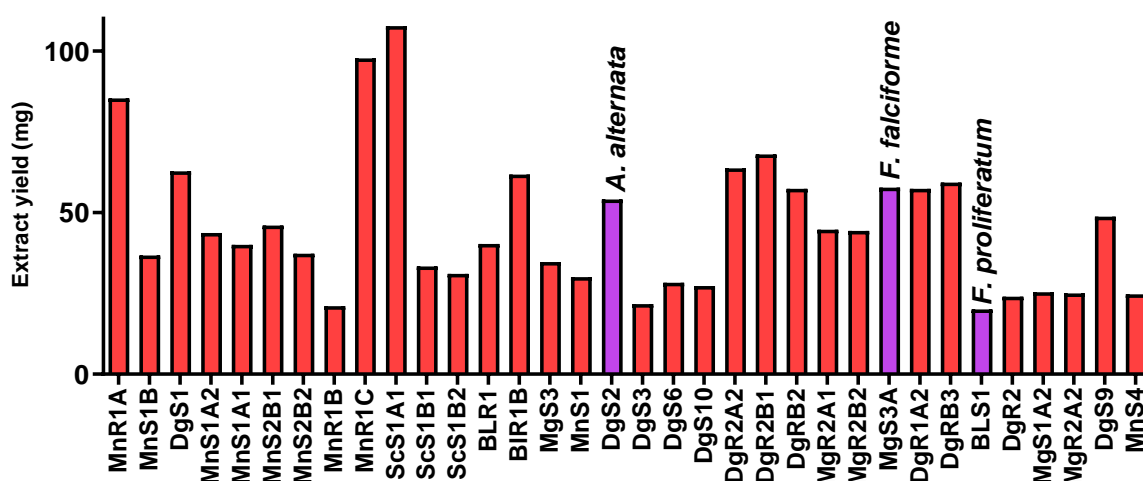


Figure 3.1: Average extract weights generated by isolated endophytic fungi. The purple bars represent the bioactive extracts against MRSA.

To ensure enough extract quantity could be subjected for further microbial assay and chemical profiling, the moderate and slow-growing fungi were incubated for 15 and 30 days respectively, while the fast-growing fungal isolates were incubated for only 11 days to avoid biomass overgrowth, which could lead to the depletion of its media and its own secondary metabolites. The weights of the fungal extracts varied between 20.0 mg and 107.7 mg. All replicates from the three incubation periods were analysed using HR-LCMS and tested against biofilm forming MRSA and *P. aeruginosa*. Figure 3.2 shows summary workflow of the 5 plants used, and the 34 fungal endophytes isolated from them.

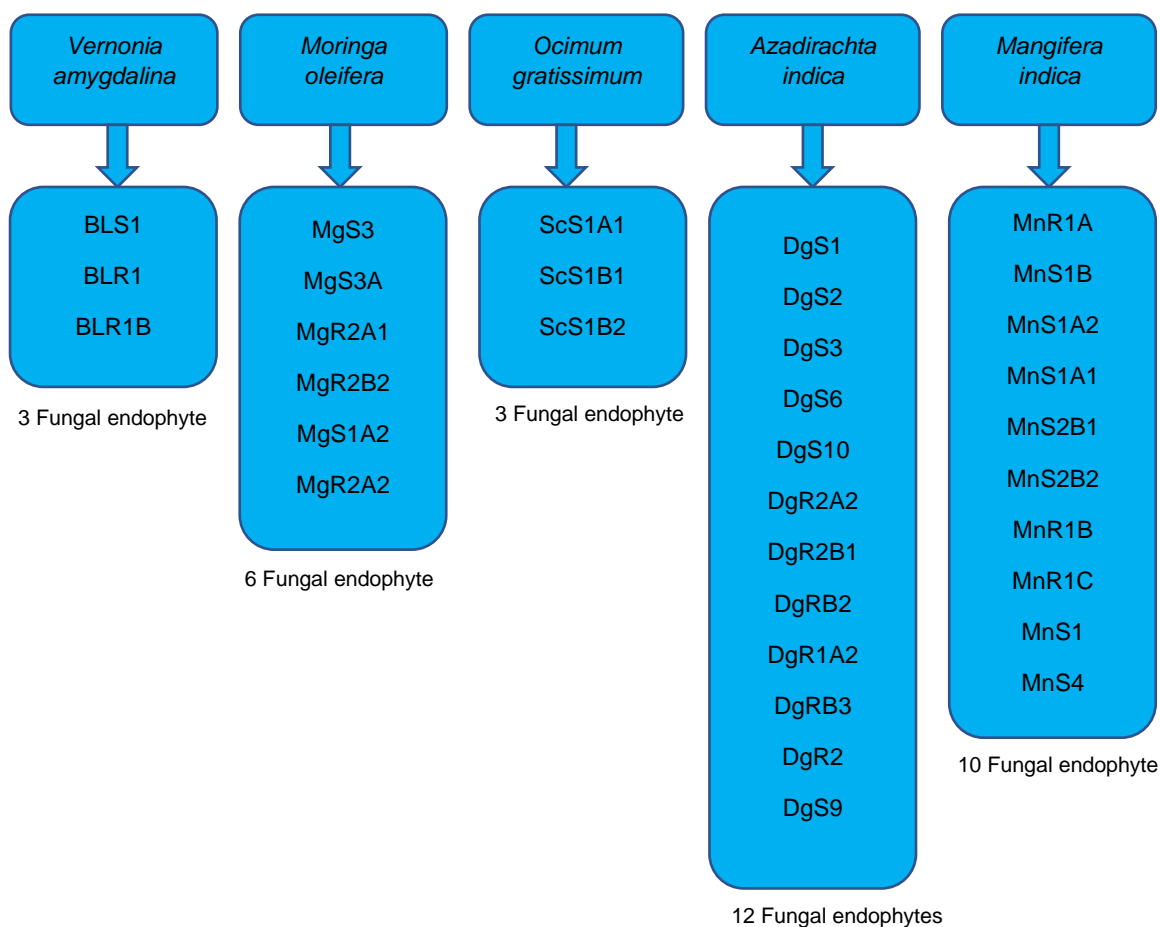


Figure 3.2: Summary workflow showing the 5 plants used, and the 34 fungal endophytes isolated from them.

3.3 Bioassay screening of fungal extracts

Antibacterial antibiofilm assay against MRSA was carried out on crude extracts of 34 fungal endophytes isolated from 5 Nigerian medicinal plants to determine which fungal endophytes was active against bacterial growth of biofilm forming MRSA and *P. aeruginosa*. Planktonic, prebiofilm and postbiofilm assay methods were used to test the ability of the fungal extracts to inhibit bacterial growth, prevent biofilm formation and eradicate preformed biofilm respectively. Screening for antibiofilm activity has been essential to curb bacterial resistance. Threshold for activity was capped at 50%.

3.3.1 Crude extract test results against MRSA

The bioactivity threshold was set at 50% cell viability (50% inhibition). The results showed that only BLS1 and MGS3A showed planktonic (96.3% and 86.98% respectively) and prebiofilm activity (99.8% and 89.26%) against biofilm forming MRSA, while DGS2 showed only planktonic activity (58.66%) against MRSA. Other extracts were inactive to both planktonic and prebiofilm assays. Selection of extracts for further work was based on planktonic and prebiofilm activity. Mns1, ScS1B1, MnS4, and DgS3 showed only postbiofilm activity, therefore, they were not chosen for further work. Their postbiofilm percentage eradication rate is as shown in Table 3.1.

3.3.2 Crude extract test results against *P. aeruginosa*

Bioactivity threshold was set at 50% cell viability (50% inhibition). None of the 34 extracts were active against planktonic *P. aeruginosa* bacteria. MnS2B1, MnR1C, ScS1A1, ScS1B2, BLR1, DgS6, DgS10, DgR2B1, and DgRB2 showed prebiofilm activity of 60.68%, 63.24%, 67.22%, 71.85%, 64.20%, 62.31%, 63.97%, 56.53%, and 63.72 respectively. None of the 34 extracts were active against postbiofilm *P. aeruginosa* bacteria. For extracts to be chosen for further work against *P. aeruginosa* bacteria, they need to also be active against the planktonic cells. Since no extract were active against planktonic *P. aeruginosa* bacteria, further work on this bacterium was paused. Summary bioactivity test result is shown in Table 3.2.

Table 3.1: Summary of planktonic, prebiofilm, and postbiofilm percentage inhibition of active crude extracts against MRSA

Fungi isolates	Antimicrobial % Inhibition	Stdev	Prebiofilm % Inhibition	Stdev	Postbiofilm % Inhibition	Stdev
BLS1	96.30	0.71	99.80	0.16	67.31	16.55
MgS3A	86.98	18.53	89.26	12.44	53.57	17.80
DgS2	58.66	3.76	< 0.00	6.94	< 0.00	94.45
MnS1	54.29	11.79	38.78	43.16	76.80	0.68
ScS1B1	40.57	3.54	< 0.00	5.52	67.87	2.22
MnS4	15.98	15.51	< 0.00	15.51	60.51	7.99
DgS3	36.93	3.64	1.54	11.12	58.89	13.06

*Cells highlighted in blue colour indicates extracts with consistent bioactivity for all replicates, cells with white colour represents inactive extracts, while gold-coloured cells indicate active extracts with inconsistent bioactivity amongst replicates and therefore

Table 3.2: Summary of planktonic, prebiofilm, and postbiofilm percentage viability of active crude extracts against *P. aeruginosa*.

Fungal isolates	Antimicrobial % Inhibition	Prebiofilm % Inhibition	Postbiofilm % Inhibition
MnS2B1	< 0	60.68	< 0
MnR1C	< 0	63.24	< 0
ScS1A1	< 0	67.22	< 0
ScS1B2	< 0	71.85	< 0
BLR1	< 0	64.20	< 0
DgS6	< 0	62.31	< 0
DgS10	< 0	63.97	< 0
DgR2B1	< 0	56.53	< 0
DgRB2	< 0	63.72	< 0

*Cells highlighted in blue indicates bioactive extracts, while cells in white were inactive.

3.3.3 Minimum inhibitory concentration (MIC) and Minimum biofilm eradication bacteria (MBEC) assay

MIC was carried out to determine the lowest concentration of active extracts that will inhibit the growth of planktonic MRSA, while MBEC was done to determine the lowest concentration of active extracts that will prevent the formation of biofilms on the 96 well plates.

The MIC and MBEC values were calculated for the most active fungi endophyte (BLS1) which exhibited 90% activity and above. The MIC and MBEC for BLS1 was 25 µg/mL as shown in Figure 3.3.

MIC of planktonic and MBEC of prebiofilm and postbiofilm were also done for ciprofloxacin (positive control), against MRSA and *P. aeruginosa*. Gentamycin was used as the positive control for *P. aeruginosa* postbiofilm. Ciprofloxacin MIC for planktonic and MBEC of prebiofilm against MRSA was 1.56 µg/mL, while MBEC for postbiofilm was 6.25 µg/mL. Ciprofloxacin MIC for planktonic and MBEC of prebiofilm against *P. aeruginosa* was 0.78 µg/mL and 0.78 µg/mL /1.56 µg/mL, while MBEC for postbiofilm was 4.17 µg/mL,

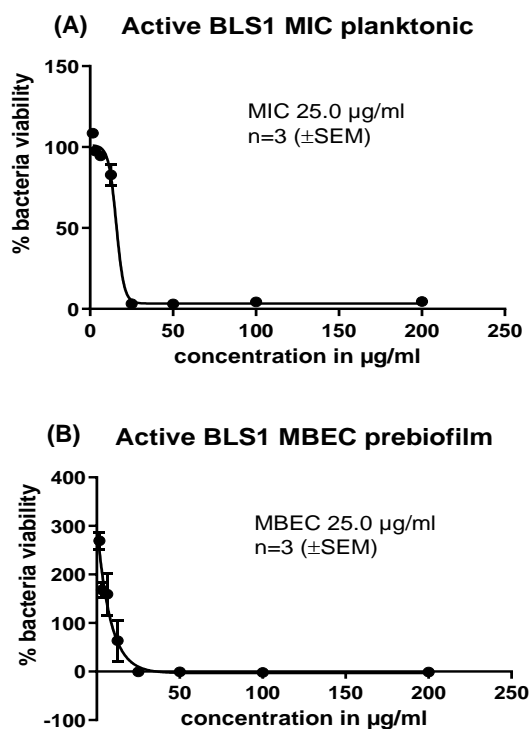


Figure 3.3: (A) MIC and (B) MBEC results of BLS1

3.4 NMR analysis of 34 fungal crude extracts

Figure 3.4 shows there was significant difference between NMR spectra of the fungal extracts and blank media extract, except at the aliphatic region 0.7 to 1.20 ppm (yellow box) where similar peaks were observed for both media blank and fungi extracts. More aliphatic peaks extended beyond 1.20 ppm to 2.30 ppm (yellow box), which was afforded by most of the fungal extracts, without media blank. Hence, most of the signals observed in the ^1H NMR spectra of the fungal extracts were not derived from the medium components. However, among the fungi extracts, similar peaks (blue boxes) could be observed at 4.0 ppm, 5.0 to 5.5 ppm, and 6.5 to 7 ppm, indicating the presence of sugars, olefinic protons, and aromatics, which was not observed in the blank media extract. It could also be observed that fungal isolates from *A. indica* (red boxes) were resonating similar discriminatory peaks at 6.0 to 6.5 ppm, 8.5 to 9.0 ppm, and 10.0 to 11.5 ppm, representing aromatics and carboxylic acids. Fungal isolates from *M. indica* also produced discriminatory peaks at 4.5 to 5.0 ppm and 7.0 to 7.5 ppm, indicating the presence of sugars and aromatics. In general, a diverse range of metabolites from 0.7 to 11.5 ppm (aliphatic systems to carboxylic acids) were observed from the 34 endophytic fungi.

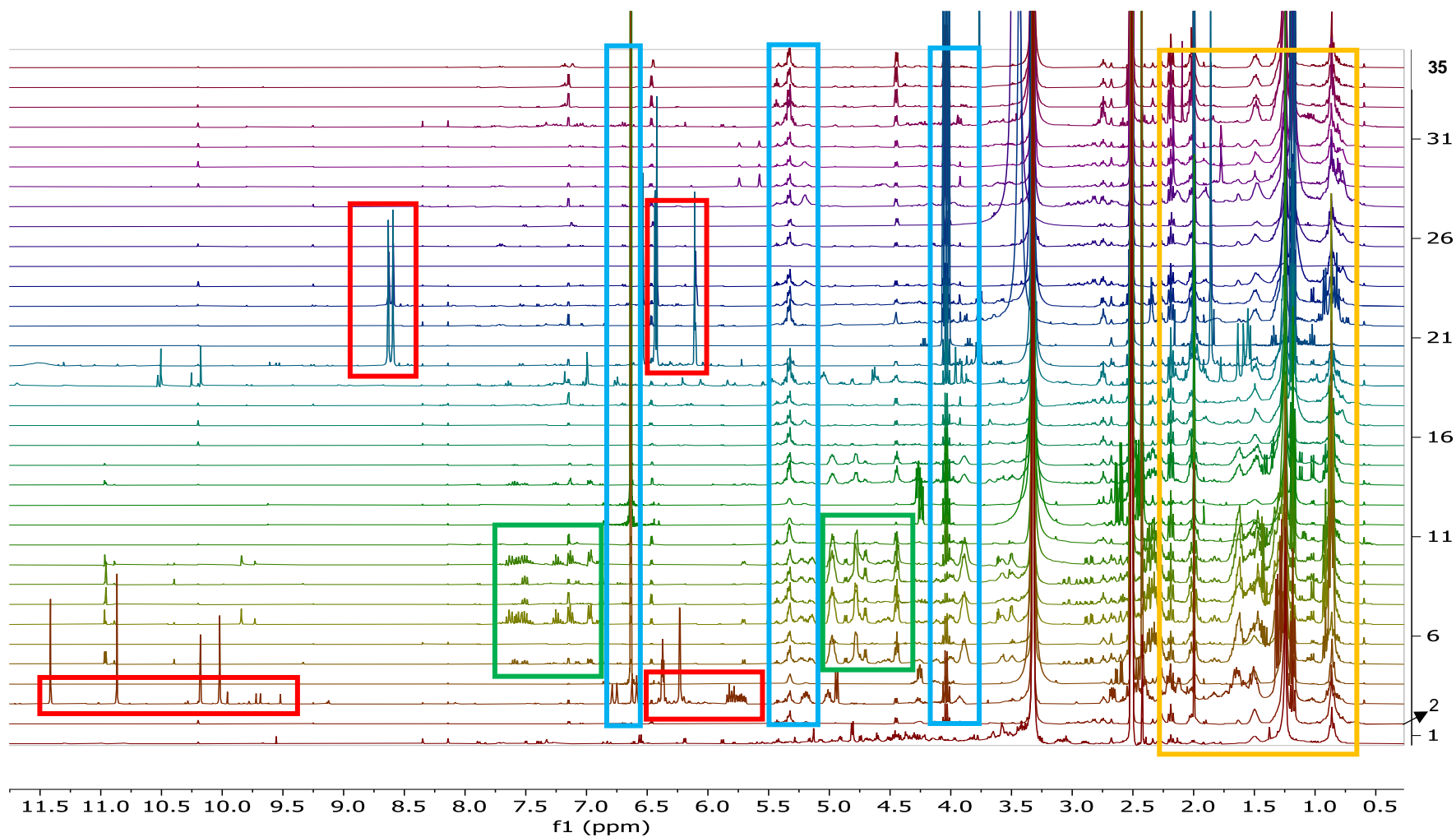


Figure 3.4: Stacked ^1H NMR (400 MHz) data obtained from media (1), and 34 fungi crude extracts (2 to 35), isolated from 5 medicinal plants, measured in DMSO-d_6 . Blue boxes highlighted fungi extracts with similar chemical shifts. Red boxes highlighted fungi extracts from discriminatory *A. indica*, while green boxes highlight fungi extracts from discriminatory *M. indica*.

Figure 3.5 presents a stacked ^1H NMR (400 MHz) data obtained from the 3 bioactive fungi extracts and media blank extract. At the aliphatic region between 0.7 to 1.5 ppm, similar peaks were observed for the blank medium and the 3 fungi extracts, which could indicate that the peaks observed at that region for the fungi extracts, were derived from the medium components. A low intensity peak was observed at the olefinic region 5.0 to 5.5 ppm (blue box) for the 3 fungi extracts but wasn't observed for the blank media extract. All 3 fungi extracts showed the presence of sugars at 4.0 ppm, with DgS2 having a higher peak intensity. BLS1 and MgS3A showed little or no peaks at the aromatic region, but DgS2 showed a high peak intensity at 6.0 to 6.5 ppm and at 8.5 to 9.0 ppm (red box). In summary, DgS2 exhibited a discriminatory and dominance nature, when compared to other fungi extracts.

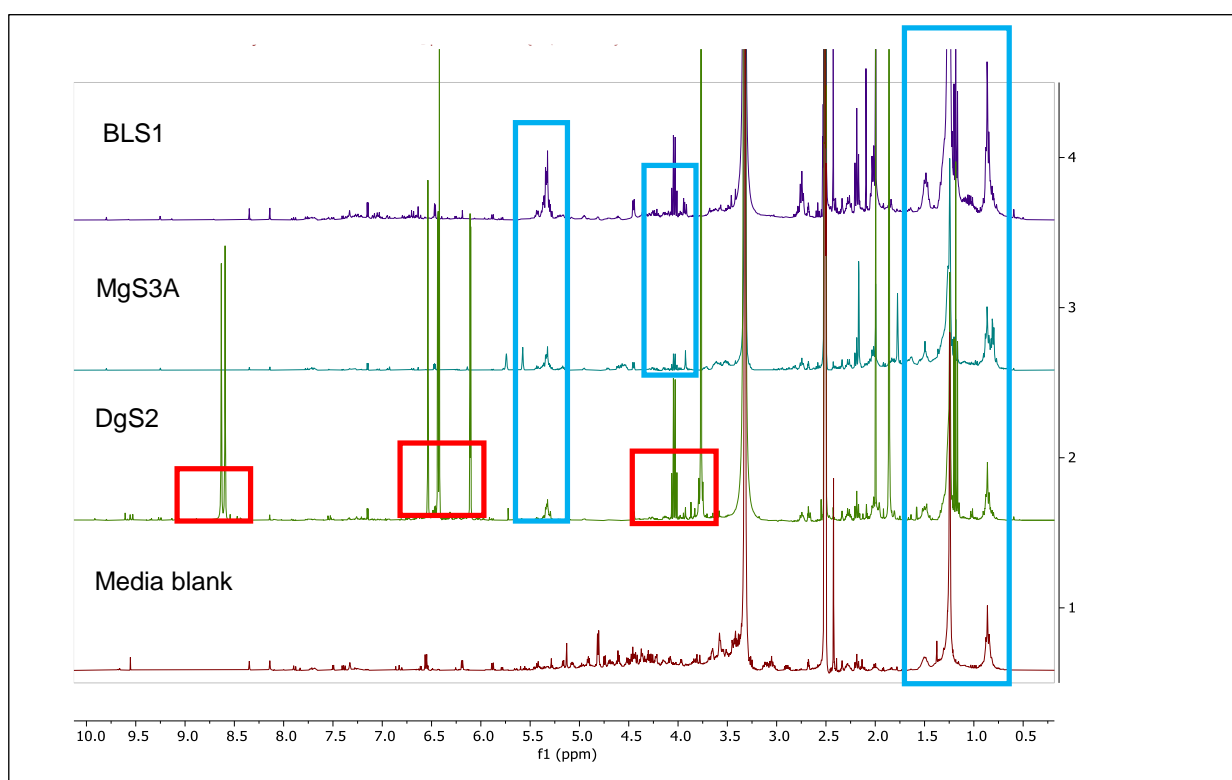


Figure 3.5: Stacked ^1H NMR (400 MHz) data obtained from the 3 bioactive fungi extracts. Blue boxes highlighted fungi extracts with similar chemical shifts. Red boxes highlighted fungi extracts from discriminatory *A. indica*.

The PCA scatter plot (Figure 3.6A) of the NMR spectral data of the fungal extracts showed the unique discriminatory feature of DgS2, which was positioned as an outlier (dark blue circles). The extracts were categorised according to their plants from which they were isolated. The generated PCA scores plot showed the diverse chemical profile observed from the fungal isolates. The metabolites of *A. indica* fungal isolates were distributed in the upper and lower left quadrant, and on the upper right quadrant (metabolites in blue circles). Metabolites of *M. indica* fungal isolates were distributed in the upper and lower left quadrant, and on the lower right quadrant (metabolites in red circles). Metabolites of *M. oleifera* fungal isolates were mostly clustered on the lower left and partially on the right quadrant (metabolites in green circles). Metabolites of *O. gratissimum* fungal isolates were distributed in the upper left quadrant, and on the upper and lower right quadrant (metabolites in yellow circles). The metabolites of *V. amygdalina* fungal isolates were distributed on the lower left quadrant, and on the upper and lower right quadrant (metabolites in light blue circles). The generated PCA-loadings plot (Figure 3.6B) depicted the type of functional groups present in the fungi crude extracts. Most of the discriminatory fungi extracts were observed on the lower right quadrant, upper right and lower left quadrant, which belongs to the aliphatic systems (metabolites in yellow and green circle). An aromatic metabolite, observed at 6.6 ppm was discriminatory.

A PLS-DA (Figure 3.7) analysis was performed to show a clearer illustration of the differences in metabolic profiles between crude extracts of the fungi isolated from 5 different plants. Metabolites of *M. indica* and *O. gratissimum* were majorly distributed on the upper and lower left quadrant of the plot (metabolites in red and yellow circles), while metabolites of *V. amygdalina*, *M. oleifera* and *A. indica* were mostly distributed on the upper and lower right quadrant (metabolites in light blue, green, and dark blue). Fungi extracts isolated from *A. indica* and *M. indica* was positioned as an outlier (dark blue circle and red circle). This corresponds with the NMR spectra in Figure 3.4 which showed the high intensity and unique peaks observed in extracts of fungal isolates from *A. indica* and *M. indica*.

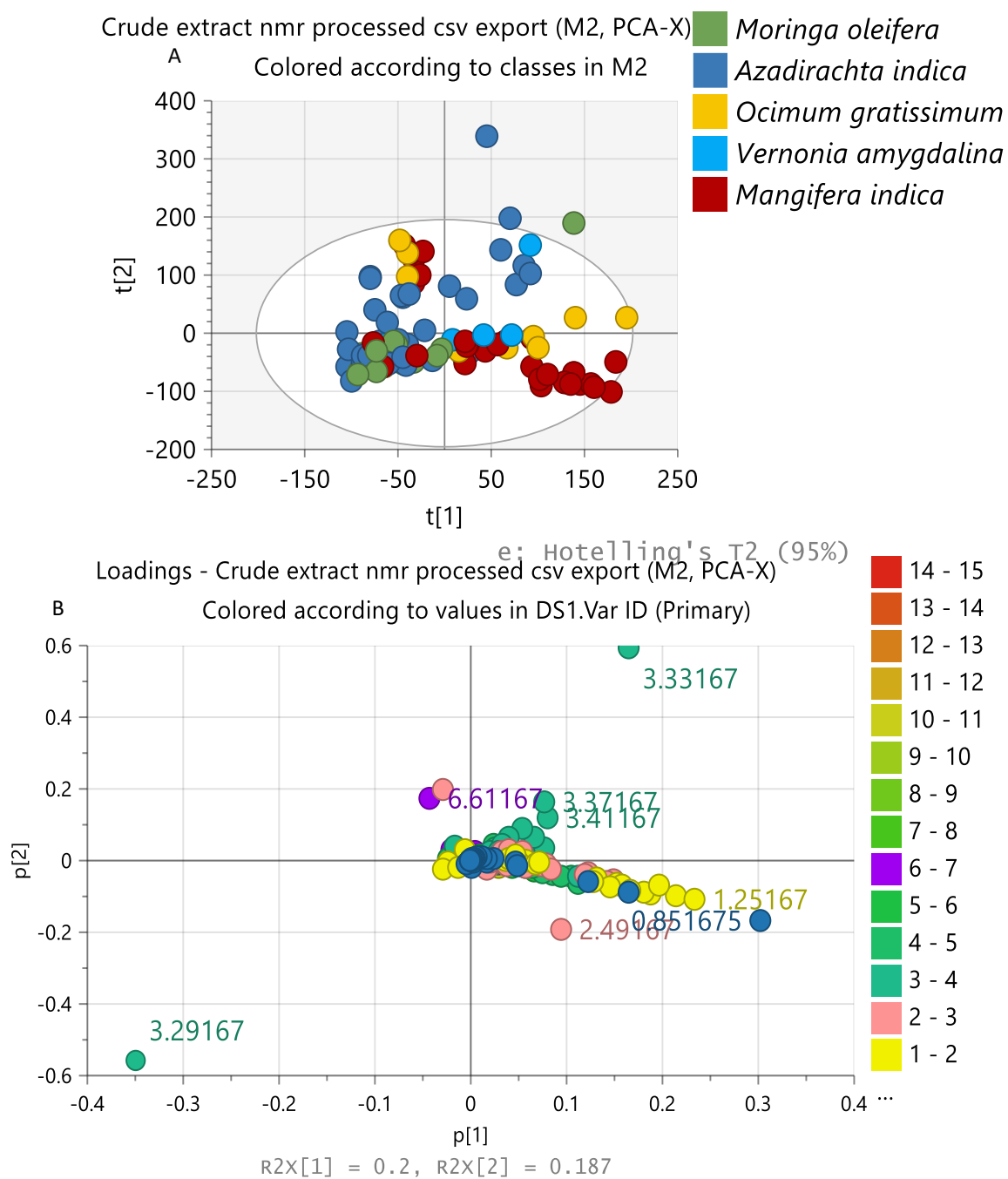


Figure 3.6: (A) PCA scores and (B) loadings plots of the NMR spectra data of fungi crude extracts. The numbers in plot B represent the chemical shifts of the crude extract.

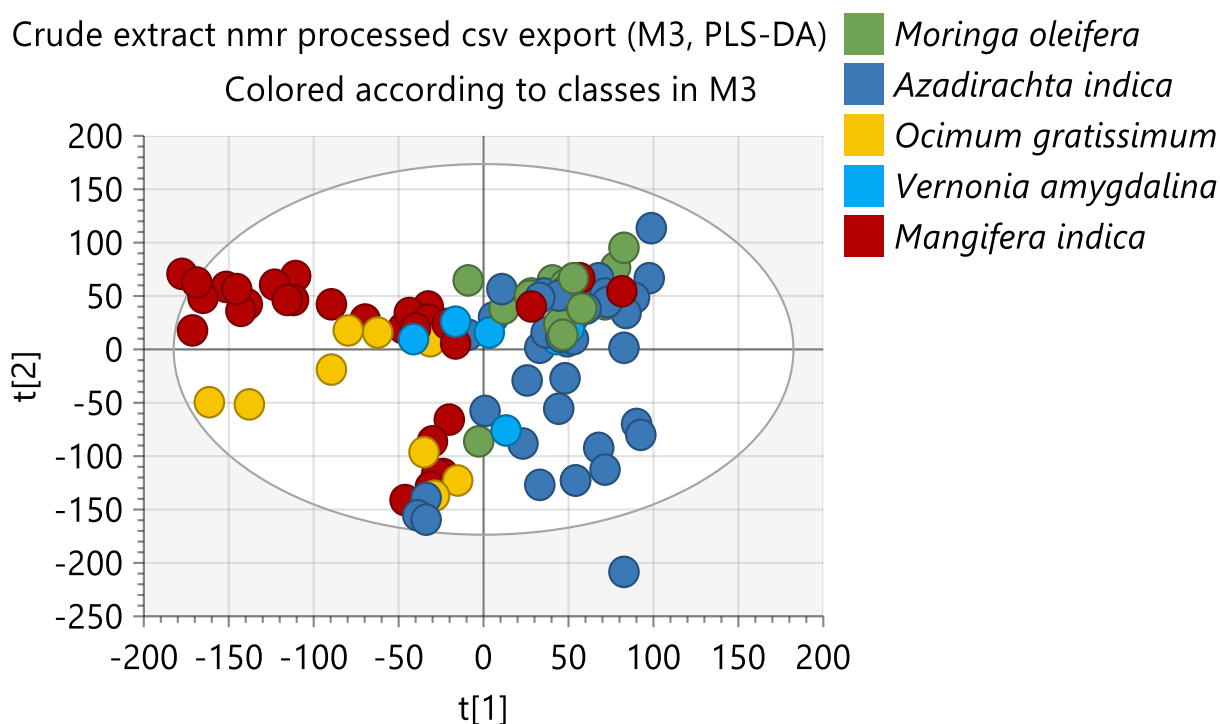


Figure 3.7: PLS-DA of the NMR spectra data of fungi crude extracts.

VIP scores for the 3 bioactive crude extracts were performed (Figure 3.8). VIP scores greater than 1 indicates important variables, while variables with VIP scores less than 1 are less important and can be excluded from the model. OPLS-DA indicated the top 20 VIP as they had VIP scores above 1. This confirmed the results of the loadings plot and heatmap obtained in Figure 3.6 and 3.9 respectively, which showed that the discriminatory metabolite consisted of aliphatics, sugars and aromatics ranging from 0.81 to 8.61 ppm. Discriminating metabolites observed on both VIP and heat map had common chemical shifts of 0.81, 0.85, 1.13, 1.21, 1.25, 1.29, 1.85, 3.37, 3.73, 6.09, 6.41, 6.53, 8.57, 8.61 ppm.

Spectra bins of the 3 active fungal isolates were analysed on MetaboAnalyst® in Figure 3.9B. The heatmap showed that BLS1-*F. proliferatum* had more metabolites around 0.81 to 3.37 ppm, which suggested the presence of aliphatic compounds and less sugar. This could be the predominant chemical functional group contributing to its bioactivity. DgS2-*A. alternata* had its predominate metabolites at the aromatic region (6.09 to 8.61 ppm). This explains the discriminatory nature of DgS2 in this study as compared to the other 2 active fungi.

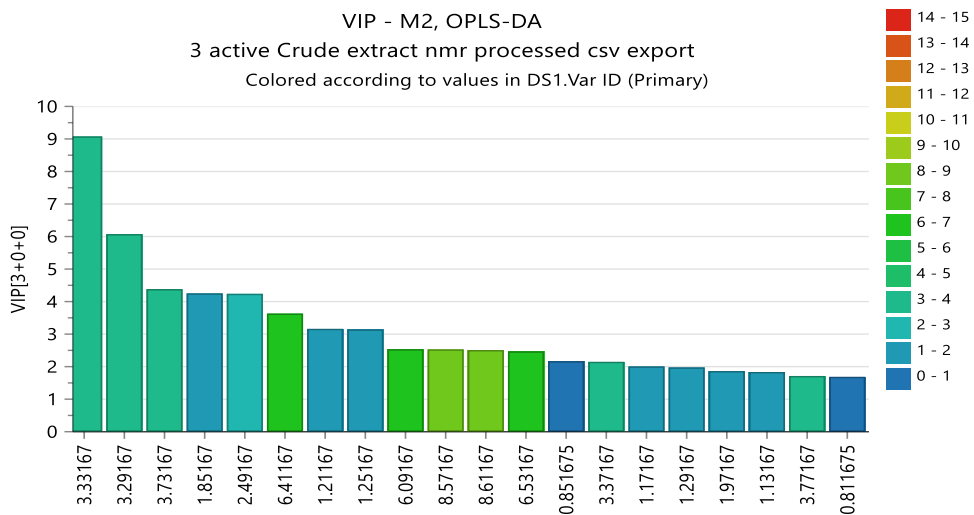


Figure 3.8 VIP scores of the 3 bioactive fungi extracts from Simca® showing the chemical shifts of 20 most discriminating metabolites with VIP scores above 1.

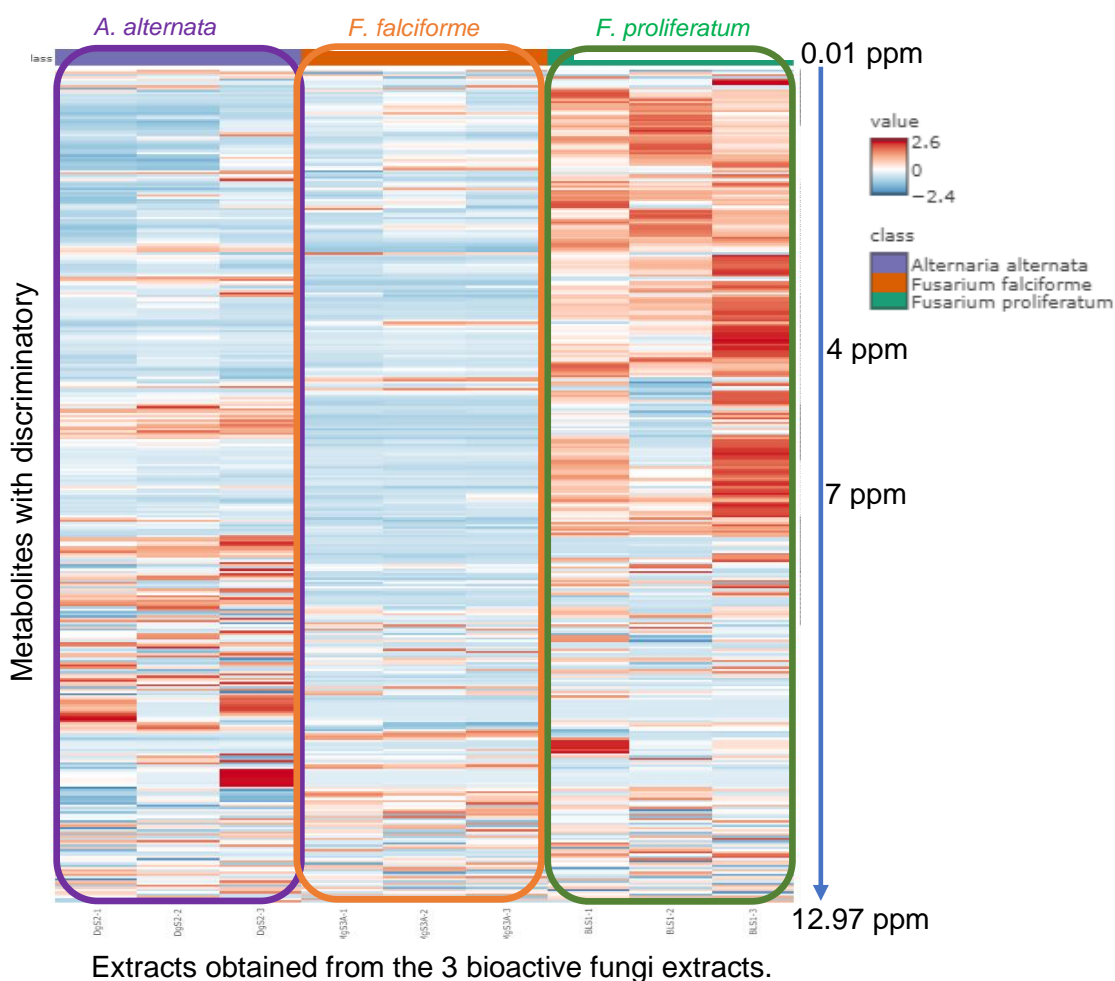


Figure 3.9A: Heatmap analysis of the NMR spectral data of the 3 bioactive fungal extracts generated by MetaboAnalyst®. The purple boxed extracts belong to *A. alternata*, orange boxed extracts belong to *F. falciforme*, while green box represents *F. proliferatum* extracts.

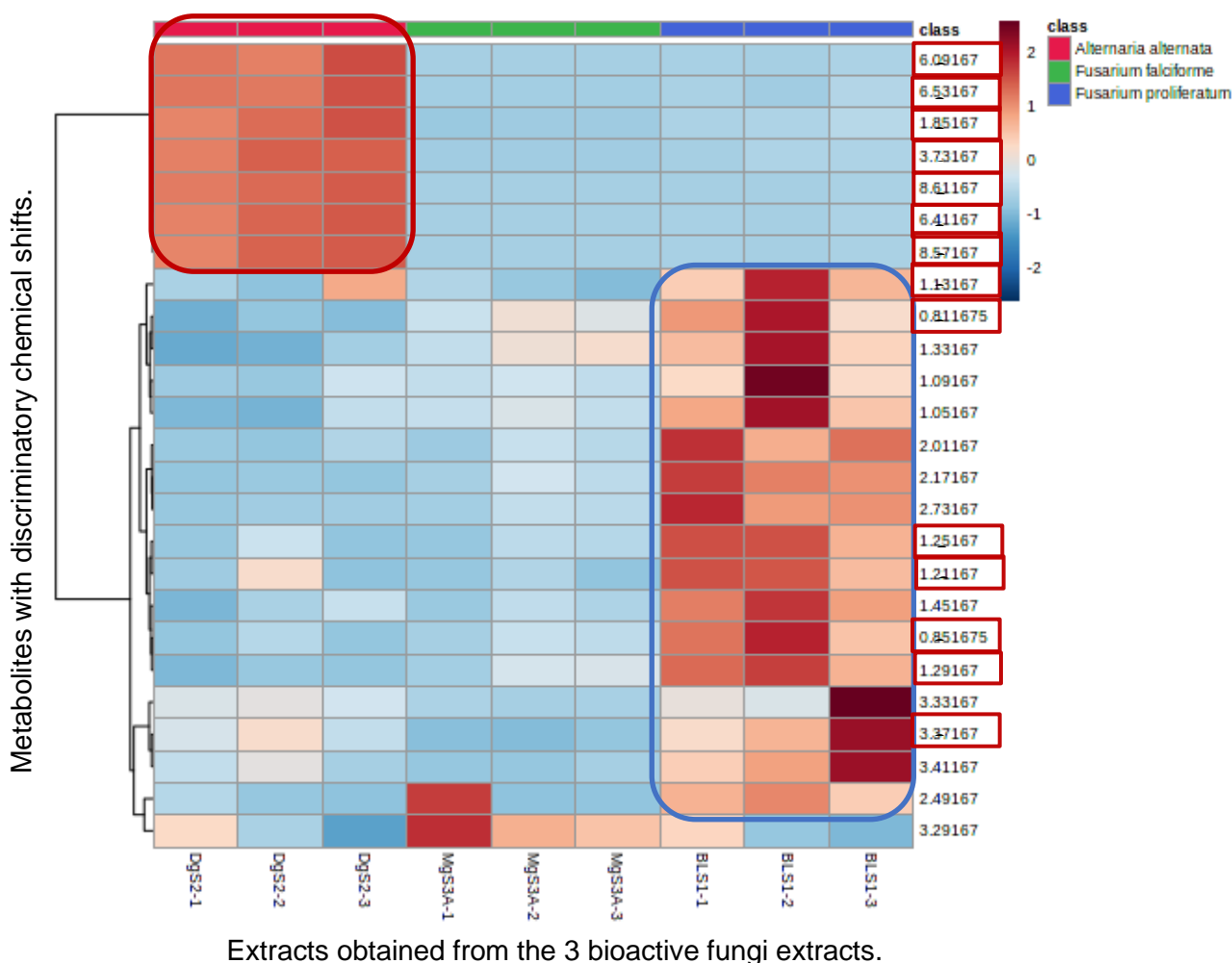


Figure 3.9B: Heatmap analysis of the NMR spectral data of the 3 bioactive fungal endophytes generated by MetaboAnalyst®. The boxed sections indicate areas with the discriminating chemical shifts. Highlighted chemical shifts on the Y-axis indicate common metabolites observed on the heatmap and VIP.

3.5 MVA of LC-HRMS data

For MVA, PCA scores and loadings plots were generated for the LC-MS data of the 34 fungi extracts. The extracts were grouped according to the different plants from which they were isolated. The unsupervised PCA scatter plot of the HR-LCMS data for the fungal extracts, as shown in Figure 3.10A, displayed metabolites of fungi isolated from *M. indica* and *A. indica* (DgS2 and DgS10) as outliers indicating their unique chemical profiles. The metabolites of fungi isolated from *O. gratissimum* showed a slight variation amongst themselves (red circles). The rest of the fungi extracts obtained from *V. amygdalina* and *M. oleifera* (yellow and purple)

clustered together denoting high similarity, with no huge difference in their chemical profiles. The loadings plot in Figure 3.10B displayed a similar pattern with the PCA scores plot. It demonstrated that discriminating metabolites from DgS2 and DgS10, afforded low molecular weight metabolites ranging from 200 to 300 Da (encircled in blue) at the upper right quadrant, while extracts from fungal isolates of *M. indica* afforded metabolites with higher molecular weight between 900 to 1000 Da, as circled in green.

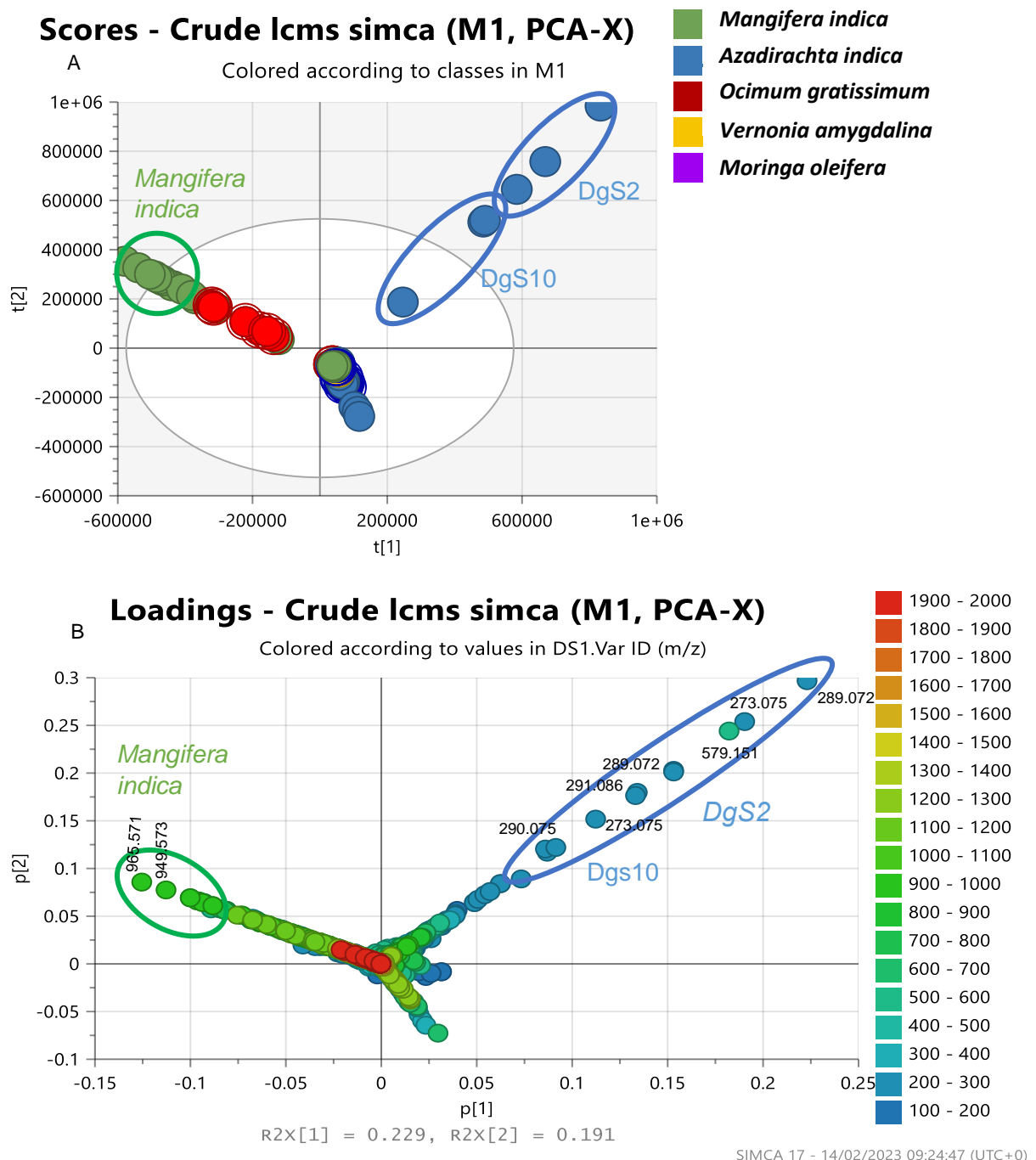


Figure 3.10: (A) PCA scores and (B) loadings plots of the LC-HRMS data of fungi crude extracts.

PCA scores and loadings plots were generated for the LC-MS data of the 3 active fungi extracts as shown in fig. 3.11. It showed a fitness (R_2) and predictability (Q_2) scores of 0.995 and 0.811 respectively, after seven components. The difference between R_2 and Q_2 values was less than 0.3. This proved to be a good fit, and a good model prediction. The variation between groups R_2X_0 [1] was 60.2% and within group R_2X [2] was 17.5%. From the scores plot, metabolites from MGS3A (yellow circles) were located at the upper left quadrant, metabolites for BLS1 (blue circles) were located at the lower left quadrant, while metabolites from DgS2 (red circles) were located in the upper right quadrant. The scores plot showed that the MGS3A and BLS1 were both located on the left quadrant separated from DgS2 which was in the right quadrant. It could be as result of BLS1 and MGS3A belonging to the same fungi genus (*Fusarium*). From the loadings plot, DgS2 contained metabolites with m/z ranging from 100-300 Da, and 500-600 Da. The compounds isolated from DgS2 and identified from the DNP database in Table 3.3 gave Mzmine IDs of P3002, P3843, N9859, P5845, P5925, N8460, N5739, N9609, N8808, represented by their respective m/z as 191.07, 235.096, 245.082, 261.076, 273.075, 277.072, 287.057, 289.072, and dereplicated as altechromone A, (ξ)-4-acetyl-5-hydroxy-3,6,7-trimethyl-2(3*H*)-benzofuranone, (S)-1-methylether-coniochaetone B, 5,8-dihydroxy-7-methyl-6-(2-oxopropyl)-1,4-naphthoquinone, 9-methylether alternariol, (R)-alternarienoic acid, dehydroaltenusin, altenusin and *N*-10-phenyl(3*H*,10*H*)-alloxazine, respectively and compounds with no hits. Altechromone A is a chromone derivative, which has been isolated from plant families such as Lamiaceae, Polygonaceae, Hypericaceae, and Fabaceae. Altechromone A, with an IUPAC name of 7-Hydroxy-2,5-dimethyl-4*H*-1-benzopyran-4-one, was first isolated from an *Alternaria* sp. in 1992. It has since been isolated from fungi species such as *Alternaria brassicicola*, *Hypoxium truncatum*, and *Ascomycota* sp. Researchers have concluded that altechromone A is a common fungal metabolite, having its origin in endophytic fungi (Königs *et al.*, 2010). Coniochaetone A and B is an antifungal cyclopentabenzopyran-4-ones, that was first isolated from cultures of *Coniochaeta saccardoi* (Wang *et al.*, 1995). The biological activities of alternariol 9-methyl ether, isolated from the endophytic fungus *Alternaria* sp. Samif01 and derived from *S. miltiorrhiza* Bunge, was first reported by (Lou *et al.*, 2016). The results proved the potential of *Alternaria* sp. Samif01 as a source of alternariol 9-methyl ether and also supported the fact that, alternariol 9-methyl ether is a natural compound with high potential bioactivity against microorganisms. Alternarienoic acid and altenusin have previously been isolated from solid rice culture media of *Alternaria* sp., an endophyte derived from the fresh leaves of three desert plants, *Lycium schweinfurthii* Dammer (Solanaceae), *Pancratium maritimum* L. (Amaryllidaceae), and *Cynanchum acutum* L. (Apocynaceae). The compounds

exhibited strong α -glucosidase and lipase inhibitory activities, indicating that they might act as naturally occurring anti-diabetic agents (Elbermawi *et al.*, 2022). Dehydroaltenusin, which was reported to have been isolated from the fungus *Alternaria tenuis* is an inhibitor of mammalian DNA polymerase α (Mizushina *et al.*, 2011).

MgS3A contained metabolites with m/z ranging from 300-400 Da and 600-700 Da, while BLS1 contained metabolites with m/z ranging from 300-500 Da and 784.417 Da. The compounds isolated from MgS3A and identified from the DNP database in Table 3.3 gave Mzmine IDs of P3977, P3975, and N427, represented by their respective m/z as 307.19, 325.2, 341.198 and dereplicated as ML 236A; 8-Deoxy, 3,5-dihydro, 3-oxo, hymeoglusin and phomolide C, and compounds with no hits. Hymeoglusin has been found to inhibit the replication of the dengue live virus (DEN-2 NGC virus) in K562 cells (Tomoda *et al.*, 2004). Phomolide C, a naphthoquinone anthraquinone derivative isolated from *Phomopsis* sp. B27, have been reported to have anti-HIV effect, cytotoxic against breast cancer, antibacterial against *S. aureus* and MRSA (Yang *et al.*, 2013, Lin *et al.*, 2008, Klaiklay *et al.*, 2012). The compounds isolated from BLS1 and identified from the DNP database in Table 3.3 gave Mzmine IDs of P6852, P1397, P6291, P6646, P1362, represented by their respective m/z as 347.116, 383.076, 416.207, 432.201, 784.417 and dereplicated as breynolide, bikaverin, fusarin A, fusarin F, and beauvericin. Bikaverin and Beauvericin has been isolated as a secondary metabolite from *Fusarium* sp. and was found to possess antibacterial effects (Sondergaard *et al.*, 2016). Fusarins, which are polyketides derived from amino acids are a class of mycotoxins produced mainly by the fungi *Fusarium*. It can infect agriculturally important crops such as oats, wheat, barley, corn, and rye. The discriminating features of the 3 active fungi were dereplicated in Table 3.3.

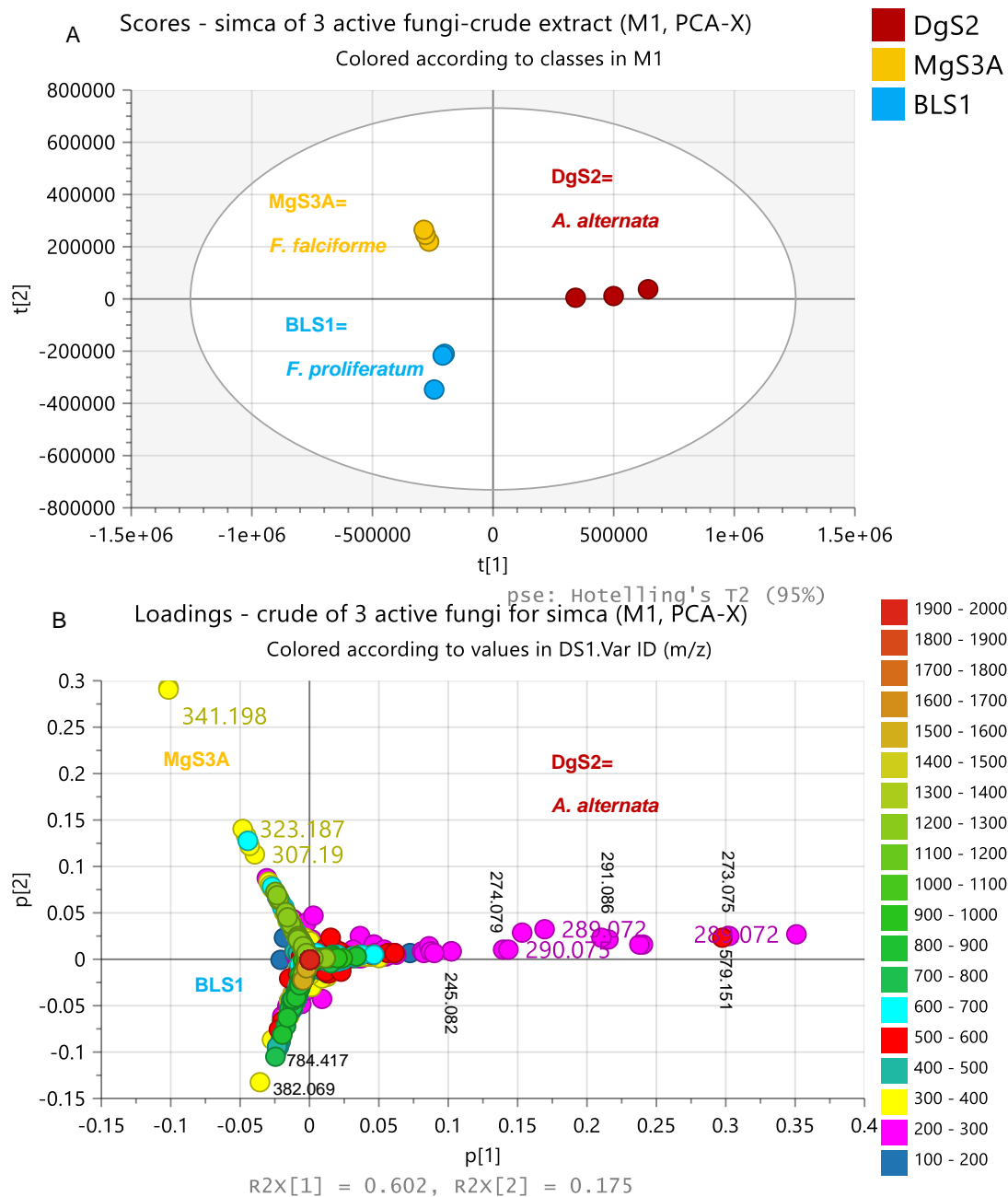


Figure 3.11: (A) PCA scores and (B) loadings plots of the LC-HRMS data of 3 active fungi crude extracts. $R_2X = 0.995$ and $Q_2X = 0.811$. The difference between group $R_2X_o [1]$ is equal to 60.2% and the difference within groups $R_2X [2]$ is 17.5%. The numbers on the loadings plot represents the m/z values of the metabolites.

Table 3.3: Compound hits for the discriminatory 3 active fungi metabolites isolated from 5 medicinal plants obtained from the loadings plot on Figure 3.11B.

Mzmine ID	<i>m/z</i>	Retention time	M. Wt	Molecular Formular (DBE)	Compound hits	Biological source
DgS2- <i>A. alternata</i>						
P3002	191.07	8.91	190.063	C ₁₁ H ₁₀ O ₃ (7)	Altechromone A (1)	<i>Alternaria</i> sp., <i>Papulaspora immersa</i> and <i>Talaromyces flavus</i> and a marine-derived fungal strain 222
P3843	235.096	7.60	234.089	C ₁₃ H ₁₄ O ₄ (7)	(ξ)-4-Acetyl-5-hydroxy-3,6,7-trimethyl-2(3 <i>H</i>)-benzofuranone (2)	Marine-derived <i>Alternaria</i> sp. HS-3
N9859	245.082	9.40	246.089	C ₁₄ H ₁₄ O ₄ (8)	(S)- 1-methylether coniochaetone B (3)	Marine-derived <i>Penicillium citrinum</i> PSU-F51
P5845	261.076	8.49	260.068	C ₁₄ H ₁₂ O ₅ (9)	5,8-dihydroxy-7-methyl-6-(2-oxopropyl)-1,4-naphthoquinone (4)	<i>Fusarium</i> sp.
P5925	273.075	8.95	272.068	C ₁₅ H ₁₄ O ₅ (10)	9-methylether alternariol (5)	<i>Alternaria</i> sp.
P4084	274.079	10.79	273.071		No hit	
N8460	277.072	5.90	278.079	C ₁₄ H ₁₄ O ₆ (8)	(<i>R</i>)-Alternarienoic acid (6)	<i>Alternaria</i> sp. strain No. II2L4, and a marine derived <i>Alternaria</i> sp NH-F6.
N5739	287.057	10.79	288.064	C ₁₅ H ₁₂ O ₆ (10)	Dehydroaltenusin (7)	<i>A. kikuchiana</i> , <i>A. tenuis</i> , <i>A. vermiculatum</i> , and <i>A. dauci</i> .
P5457	291.086	10.88	290.079		No hit	
P3719	291.086	10.68	290.079		No hit	

Mzmine ID	m/z	Retention time	M. Wt	Molecular Formular (DBE)	Compound hits	Biological source
N9609	289.072	9.94	290.079	C ₁₅ H ₁₄ O ₆ (9)	Altenusin (8)	<i>A. tenuis</i> , <i>Penicillium</i> sp. and <i>Talaromyces</i> sp.
N8808	289.072	10.61	290.08	C ₁₆ H ₁₀ N ₄ O ₂ (14)	<i>N</i> -10-phenyl-(3 <i>H</i> ,10 <i>H</i>)-alloxazine (9)	Parent residue present in riboflavin
P4085	292.09	10.63	291.082		No hit	
N10412	290.08	10.63	291.083		No hit	
N6931	579.151	10.54	580.158		No hit	
MgS3A- <i>F. falciforme</i>						
P3977	307.19	11.62	306.182	C ₁₈ H ₂₆ O ₄ (6)	8-Deoxy,3,5-dihydro, 3-oxo ML 236A (10)	<i>Eupenicillium javanicum</i> IFM 52670
P3975	325.2	11.66	324.193	C ₁₈ H ₂₈ O ₅ (5)	Hymeglusin (11)	<i>Cephalosporium</i> sp., <i>Scopulariopsis</i> sp. and <i>Fusarium</i> sp.
N427	341.198	11.47	342.205	C ₁₈ H ₃₀ O ₆ (4)	Phomolide C (12)	<i>Phomopsis</i> sp. B27
N10309	342.201	11.47	343.208		No hit	
P5819	602.429	25.01	601.422		No hit	
BLS1- <i>F. proliferatum</i>						
P6852	347.116	12.55	346.108	C ₁₅ H ₂₂ O ₇ S (5)	Breynolide (13)	<i>Breynia fruticosa</i>
P1397	383.076	16.77	382.069	C ₂₀ H ₁₄ O ₈ (14)	Bikaverin (14)	Pigment from <i>Fusarium oxysporum</i> , <i>F. solani</i> , <i>F. moniliforme</i> , <i>F. lycopersici</i> , <i>F. vasinfectum</i> , <i>F. bulbigenum-blasticola</i> , and <i>Gibberella fujikuroi</i> .
P6291	416.207	15.45	415.199	C ₂₃ H ₂₉ NO ₆ (10)	Fusarin A (15)	<i>Fusarium moniliforme</i>

Mzmine ID	m/z	Retention time	M. Wt	Molecular Formular (DBE)	Compound hits	Biological source
P6646	432.201	13.70	431.194	C ₂₃ H ₂₉ NO ₇ (10)	Fusarin F (16)	<i>Fusarium moniliforme</i>
P1362	784.417	25.29	783.41	C ₄₅ H ₅₇ N ₃ O ₉ (19)	Beauvericin (17)	Basidiomycetes and other fungi including, <i>Beauveria bassiana</i> , <i>Acremonium</i> sp. BCC28424, <i>Fusarium semitectum</i> , <i>F. moniliforme-subglutinans</i> , <i>Fusarium</i> sp. Fo740 and <i>F. proliferatum</i> M5991. Component of Bai Jiang Yang

LETTER before the number code indicates ionisation mode, P for positive and N for negative.

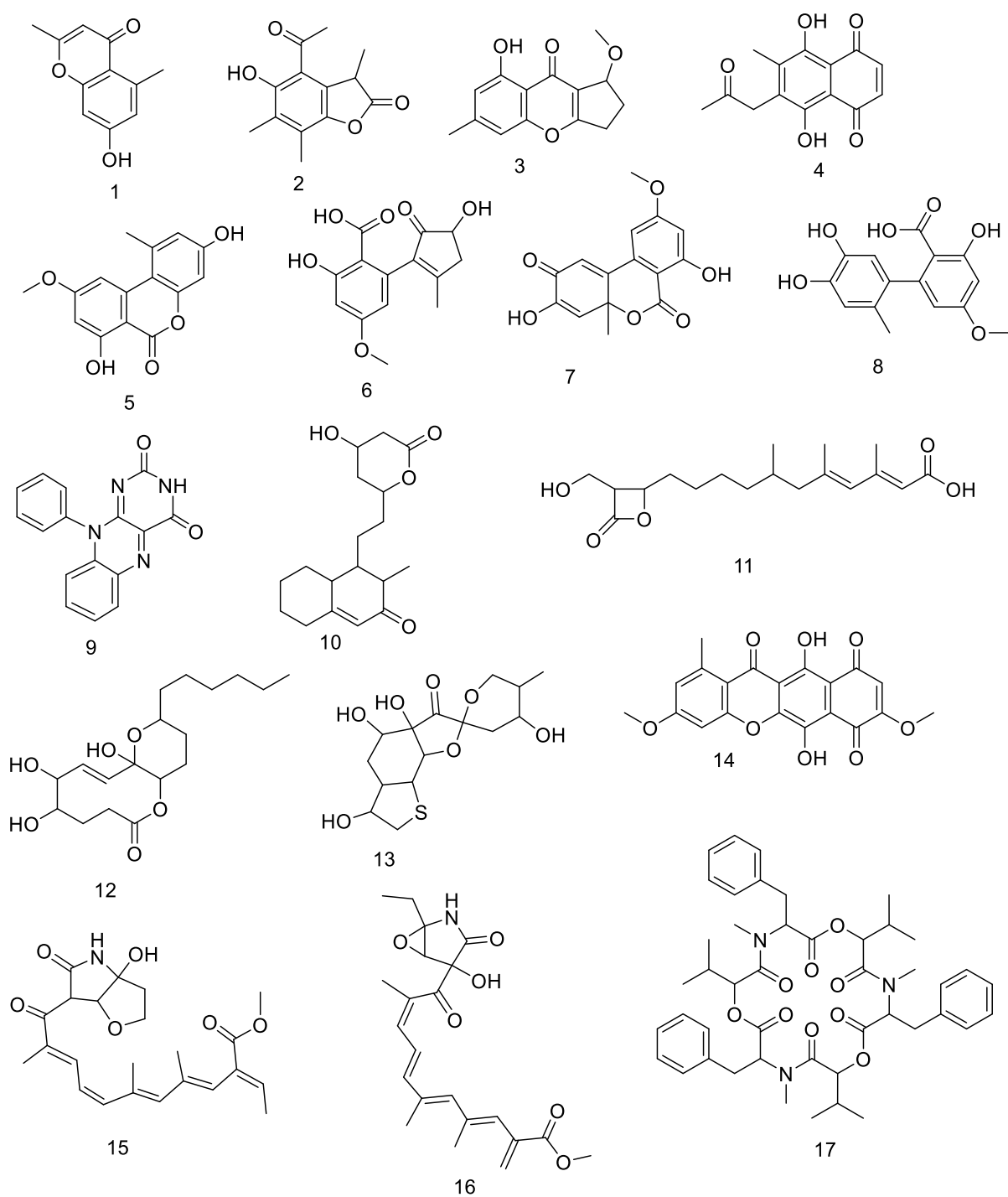


Figure 3.12: PCA Structures of compounds that were putatively identified through dereplication studies of 3 active fungi extracts listed in Table 3.3.

Base peak plot, MS1, m/s: 149.9984-1999.9817

Selected scan #901 (active fungi extract total ms/mL), RT: 10.61, base peak: 273.0750 m/s, IC: 7.5E8

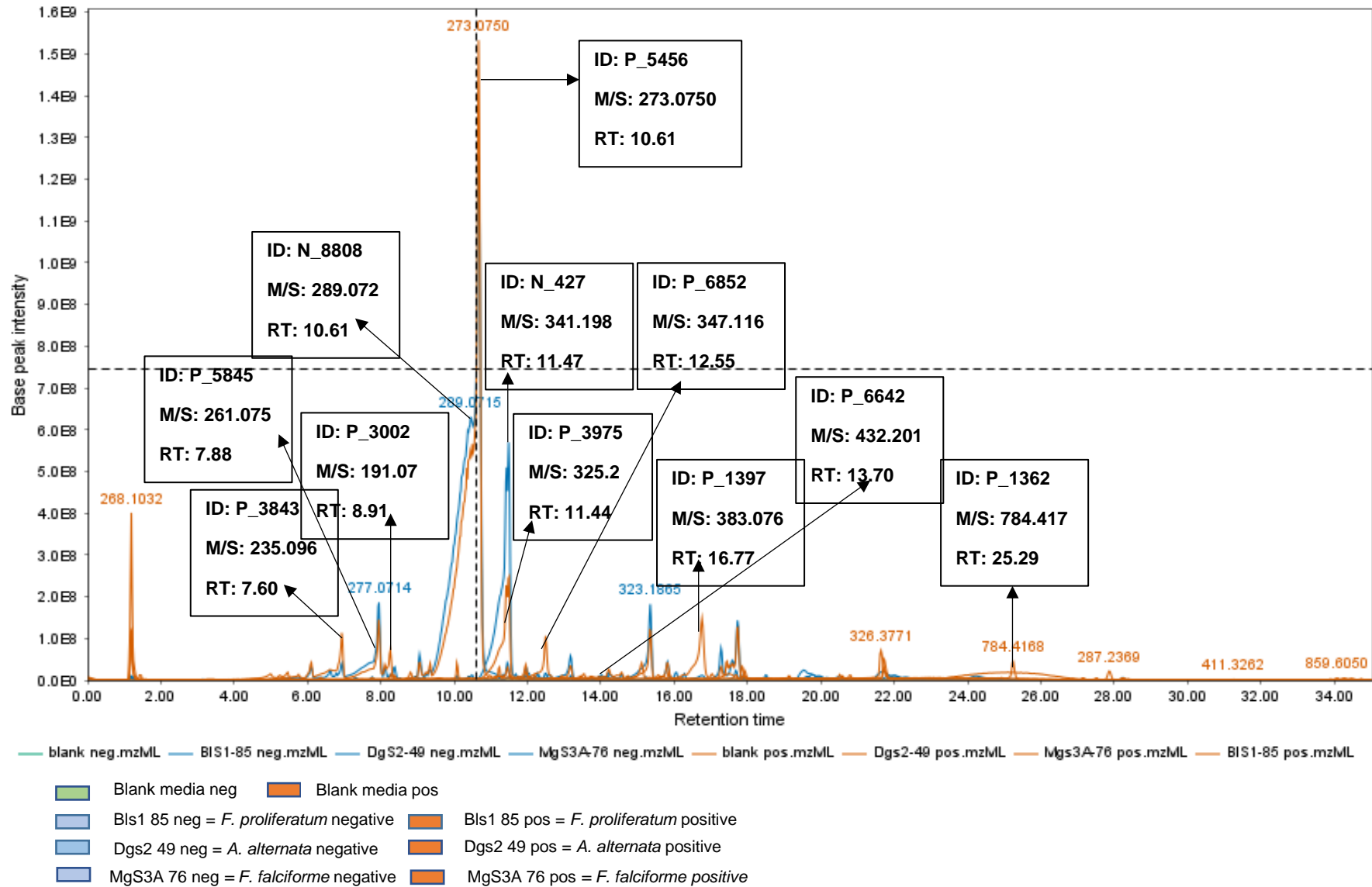


Figure 3.13: Total Ion Chromatogram (TIC) of both positive and negative modes produced from active and blank extracts. Red and blue line represents positive and negative ionisation modes respectively. The ion peaks that represent the discriminating features listed in table 3.3 have been labelled.

3.6 ITS gene sequencing

Based on the antibacterial antibiofilm results against MRSA, fungi Identification and molecular work was carried out for the 3 bioactive fungal endophytes. DNA was extracted from the active fungal strains and submitted for ITS gene sequencing to identify each of the isolated endophytic fungi. The ITS gene sequencing results were processed using Finch TV, then the gene sequences of each isolate obtained in this study was compared with the GenBank nucleotide database at the National Center for Biotechnology Information (NCBI), by using their Basic Local Alignment Search Tool (BLAST). Results of the BLAST sequence comparison is shown under the Appendix. Results of the ITS gene sequencing is shown below.

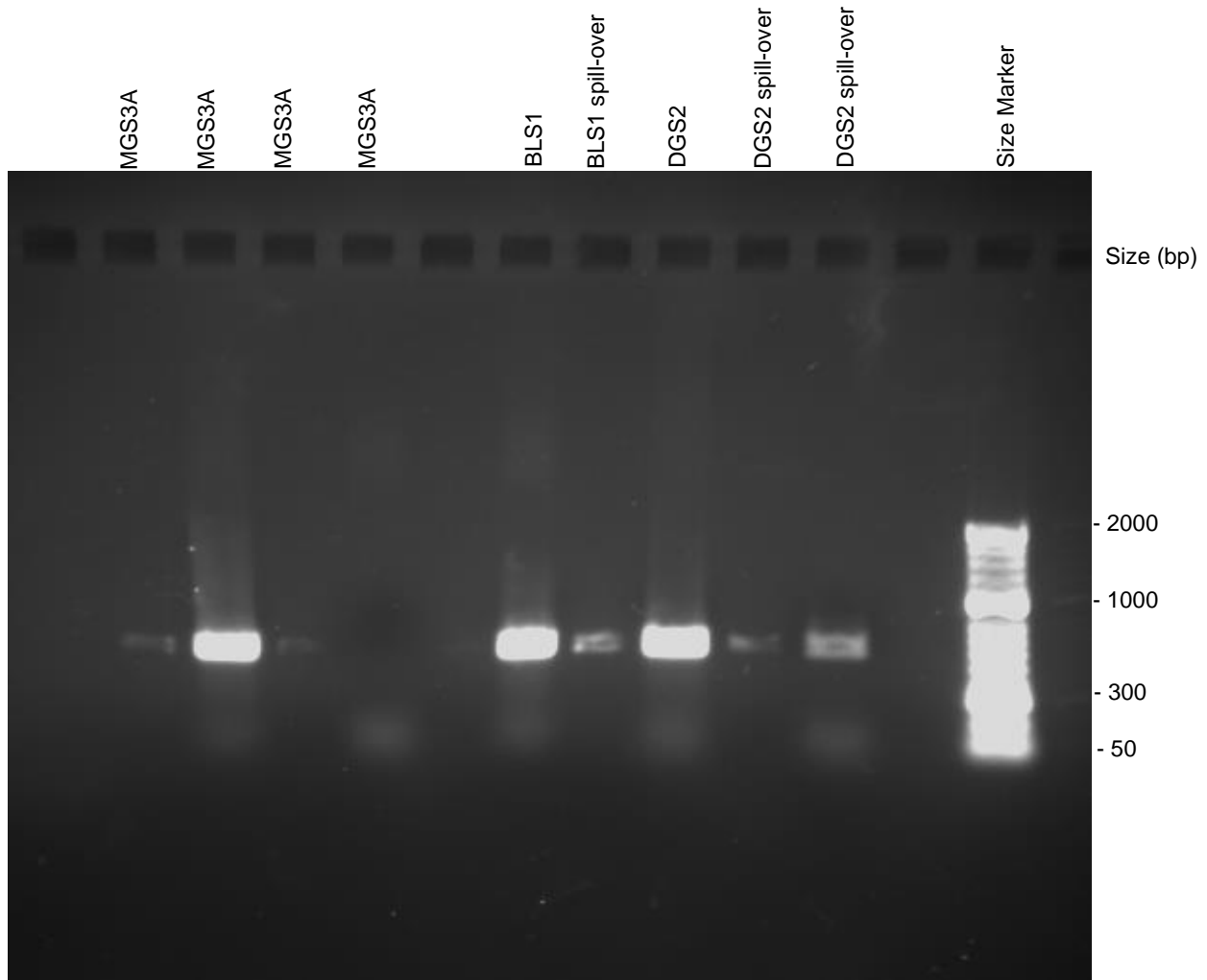


Figure 3.14: Electrophoresis gel image of the PCR products of three fungi samples. The ITS PCR products were resolved on a 1% (w/v) agarose gel and visualised by ethidium bromide staining. The size marker (measured in base pairs) was Hyperladder 50bp. The consequences of loading overspill of the ITS PCR product wells are evident as faint bands of the same size in adjacent lanes.

Identified active fungal endophytes.

Fungi Code	Plant Source	Identified name
BLS1	<i>V. amygdalina</i>	<i>F. proliferatum</i>
MgS3A	<i>M. oleifera</i>	<i>F. falciforme</i>
DgS2	<i>A. indica</i>	<i>A. alternata</i>

3.7 Review of the crude extract screening results

Five Nigerian medicinal plants were used for this work. Thirty-four fungi were isolated from the plants. Extracts from the 34 fungal isolates were tested against biofilm forming MRSA and *P. aeruginosa*. Three fungi extracts showed activity against MRSA, but none was active for *P. aeruginosa*. The active fungi extracts were obtained from and identified as *F. proliferatum*, *F. falciforme* and *A. alternata*. Their activity was in the order *F. proliferatum* > *F. falciforme* > *A. alternata* making *F. proliferatum* the most potent with an MIC and MBEC of 25 µg/mL. Although DgS2 extract was least active, it showed the presence of high intensity peaks and discriminatory metabolites as compared to the other 2 fungi extracts on the NMR spectroscopy, PCA scores and loadings plot.

CHAPTER 4

4 Secondary metabolites of *F. proliferatum* isolated from *V. amygdalina*.

4.1 Metabolites of *F. proliferatum*

F. proliferatum is a fungal species found on plants and in the soils under a wide range of environmental conditions (Stepien *et al.*, 2014). *F. proliferatum* was first identified as *C. proliferatum* in 1971 but has been known as a distinct species within *Fusarium* since 1976 (Nirenberg, 1976, Leslie and Summerell, 2006). Prior to this, it is likely that this fungus was among the *F. moniliforme* reported to be isolated from a variety of hosts. *F. proliferatum* produces a variety of biologically active metabolites, including the fumonisins, mycotoxins, fusaric acid, beauvericin, fusaproliferin, moniliformin, and fusarins, but fumonisin B toxins are the most prevalent among them. Its broad host range, amenability to meiotic and molecular genetic analyses, ability to produce diverse biologically active metabolites, makes *F. proliferatum* an excellent tool for fungal-plant interactions, and biological and chemical studies (Proctor *et al.*, 2009). It has also been found to produce ergosta-5, 7, 22-trien-3 β -ol, nectriafurone-8-methyl ether, 9-O-methyl fusarubin, and bostrycoidin (Dame *et al.*, 2016).

F. proliferatum is a recurrent hemi-biotrophic pathogen that infects a variety of host plants, such as vegetable crops, legumes, cereals, and fruits, which often leads to significant crop loss and yield reduction (Stepien *et al.*, 2015). It has a worldwide distribution and has been associated with a variety of diseases in important economical crops, such as banana and corn (Zhang *et al.*, 2013, Zakaria *et al.*, 2016). *F. proliferatum* is mainly transferred and spread by crop residues and seeds. Infection at preliminary seedling stages kills the plant and at later stages results in poor crop yield (Munkvold, 2003). During the infection, *F. proliferatum* synthesises secondary metabolites called mycotoxins, which weaken the host defence mechanisms. Previous studies indicate that fumonisin B₁ is a virulence factor causing FB₁-induced cell death, mediated by ROS activation, accumulation, phytoalexin, and PR gene overexpression (Berkey *et al.*, 2012, Lumsangkul *et al.*, 2019). By acting as specific effectors, they elicit host systemic acquired resistance (SAR), which involves the activation of salicylic acid (SA) signalling pathway (Glazebrook, 2005). A summary workflow for isolation, identification, and culture of *F. proliferatum* is shown in Figure 4.1.

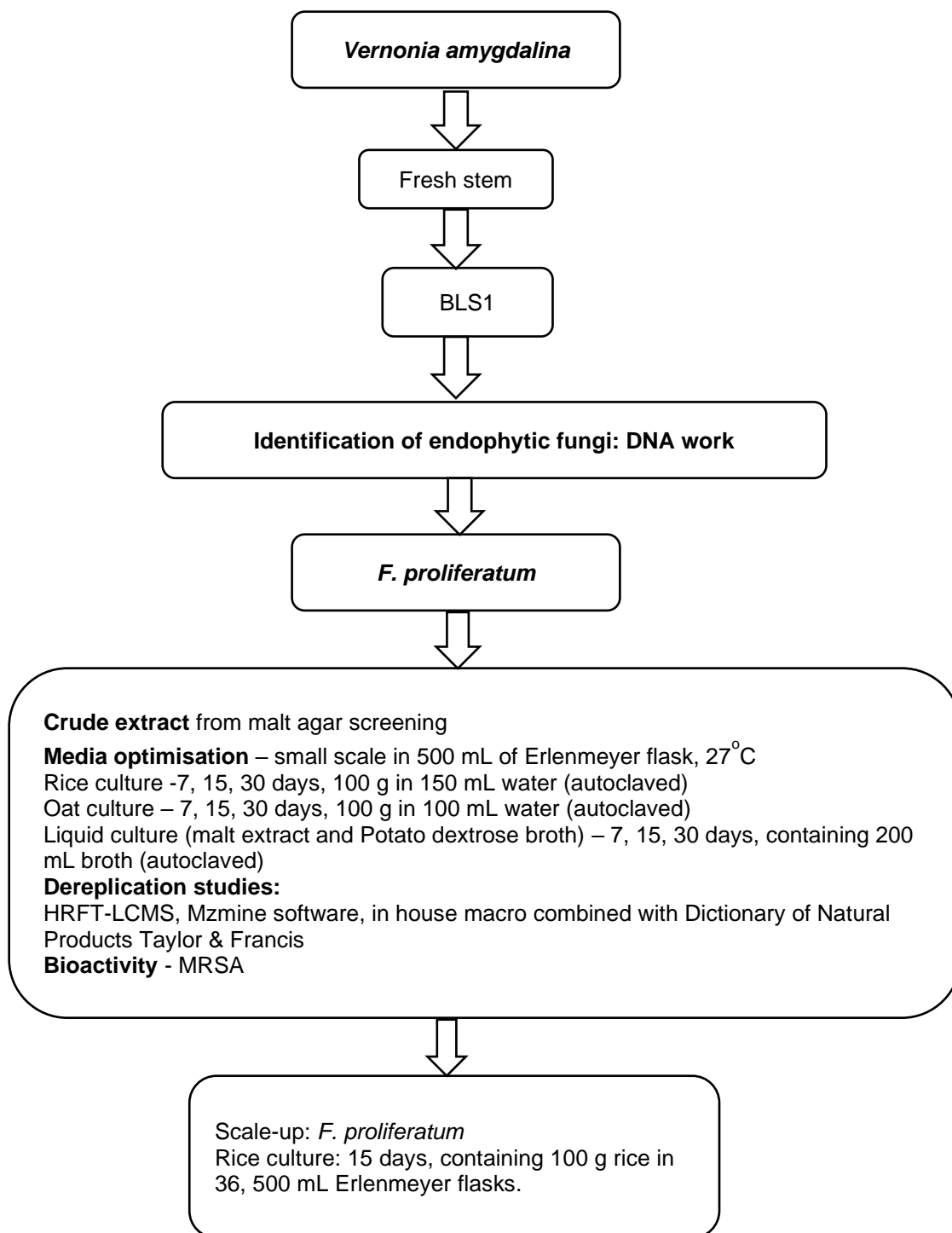


Figure 4.1: A summary workflow for isolation, identification, and culture of *F. proliferatum*

4.2 Results and Discussion

4.2.1 Media optimisation and identification of metabolite production from *F. proliferatum*.

Media optimisation and identification of metabolite production was carried out on the pure strain of *F. proliferatum* as described in Chapter 2.6. The metabolites produced from media optimisation extracts of *F. proliferatum* were analysed using NMR and HRESI-LCMS for dereplication studies and tested against MRSA.

4.2.2 *F. proliferatum* extract yields on 4 different media.

Solid media produced higher yields of extract than liquid media. As depicted in Table 4.1, the highest yield of *F. proliferatum* extract was gained from the oat medium. Meanwhile, the lowest extract yields were obtained from malt and potato broths. *F. proliferatum* obtained its highest yields on rice media incubated for 15 days and on oat for 15 days.

The histogram below in Figure 4.2 shows the extract yields for *F. proliferatum* at 7, 15, and 30 days of incubation on four different media. After 15 days of incubation in ME broth, potato dextrose broth, and rice media, *F. proliferatum* was seen to still be growing, and could be said to have attained its exponential growth phase at 30 days of incubation. On the other hand, the extract yields started to decline after 15 days of incubation on oat media, which indicated the end of its exponential phase and beginning of the decline phase. The decline phase on oat media was observed after 15 days of incubation, which could have occurred because of the endophytes inability to metabolise and process the media nutrient inherent in oat. This is evidenced by the inactivity observed on all extracts from oat media. The obtained yields of the extracts of *F. proliferatum* extract after 7, 15, and 30 days of incubation on four different media are listed in Table 4.1.

Table 4.1: Extract yields of *F. proliferatum*, grown on different media and incubated for 7, 15, and 30 days as illustrated in Figure 4.2. All cultures were incubated at 27°C.

7 days		15 days		30 days		Controls	
Solid media							
BLS1-R7-1	886.7	BLS1-R15-1	1584.4	BLS1-R30-1	1444.1	RC1	747.8
BLS1-R7-2	924.2	BLS1-R15-2	1535.0	BLS1-R30-2	3355.3	RC2	809.4
BLS1-R7-3	852.7	BLS1-R15-3	1567.7	BLS1-R30-3	1530.9	RC3	865.5
Average weight (mg)	887.9		1562.4		2110.1		807.6
BLS1-O7-1	5223.0	BLS1-O15-1	5863.0	BLS1-O30-1	5708.4	OC1	5963.4
BLS1-O7-2	5443.4	BLS1-O15-2	6518.1	BLS1-O30-2	5240.0	OC2	6291.9
BLS1-O7-3	6246.9	BLS1-O15-3	6229.1	BLS1-O30-3	4695.0	OC3	5822.3
Average weight (mg)	5637.8		6203.4		5214.5		6025.9
Liquid media							
BLS1-M7-1	22.6	BLS1-M15-1	39.2	BLS1-M30-1	61.0	MC1	7.1
BLS1-M7-2	28.3	BLS1-M15-2	53.3	BLS1-M30-2	58.0	MC2	6.7
BLS1-M7-3	16.2	BLS1-M15-3	42.1	BLS1-M30-3	30.5	MC3	6.2
Average weight (mg)	22.4		44.9		49.8		6.7
BLS1-P7-1	28.6	BLS1-P15-1	39.5	BLS1-P30-1	60.5	PC1	16.0
BLS1-P7-2	29.4	BLS1-P15-2	33.8	BLS1-P30-2	53.9	PC2	9.9
BLS1-P7-3	26.9	BLS1-P15-3	40.0	BLS1-P30-3	51.9	PC3	11.3
Average weight (mg)	28.3		37.8		55.4		12.2

Table 4.2: Types of media and incubation days

Code	Full name	Code	Full name
R7	Rice 7 days	M7	Malt 7 days
R15	Rice 15 days	M15	Malt 15 days
R30	Rice 30 days	M30	Malt 30 days
O7	Oat 7 days	P7	Potato 30 days
O15	Oat 15 days	P15	Potato 15 days
O30	Oat 30 days	P30	Potato 30 days

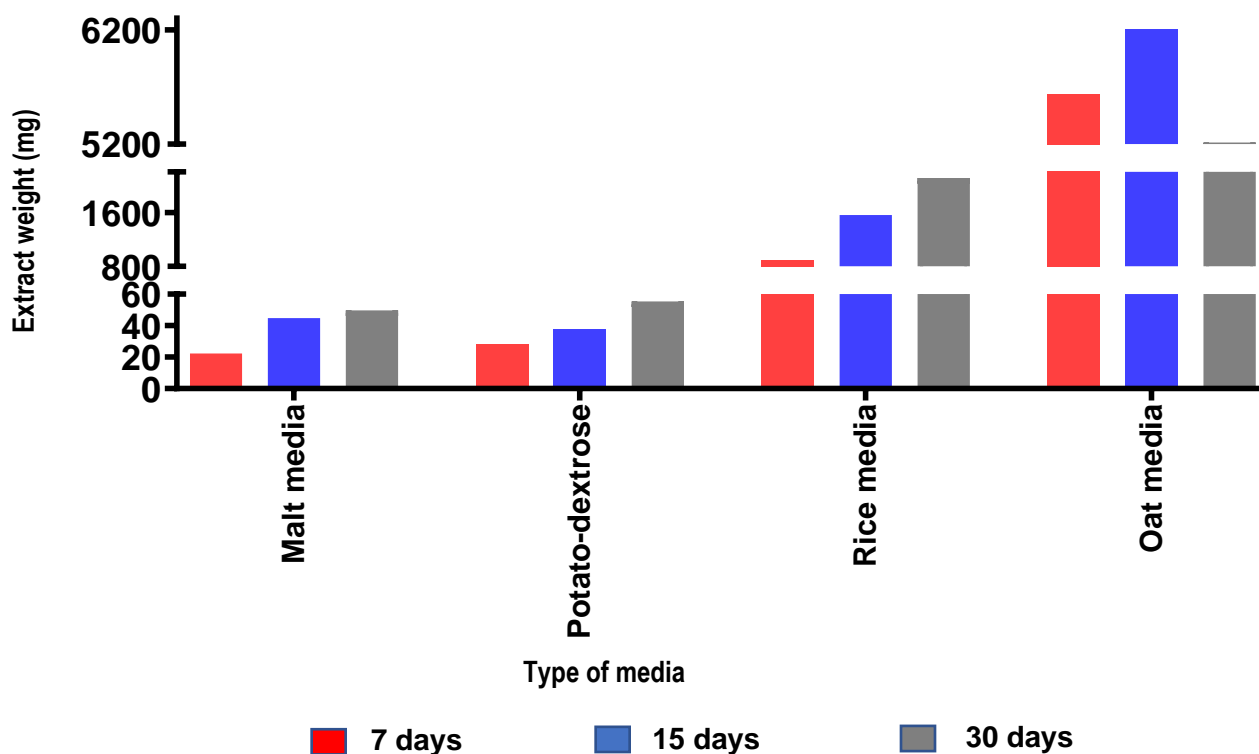


Figure 4.2: Histogram showing average weight of extracts from three respective replicates of *F. proliferatum* obtained from four different media and incubated at 7, 15, and 30 days.

4.2.3 Extracts test against MRSA

Before selecting the optimal medium for large-scale fermentation, the biological activity of *F. proliferatum* extracts obtained from various media were tested against MRSA cells. As depicted in Figure 4.3, incubation on malt for 7 and 30 days, on Potato for 30 days, and on rice for 7, 15, and 30 days afforded strongly active (77.5%-100% inhibition) fungal extracts against planktonic and prebiofilm MRSA, as bioactivity threshold was set at 40% cell viability (60% inhibition). All fungi extracts obtained from oat media were inactive. However, choosing the optimum fermentation conditions, parameters such as extract yield and incubation time were also considered. *F. proliferatum* incubated on rice for 7 days gave a lower yield while incubation on rice medium for 30 days needed longer incubation time, hence, the 15-days incubation period was found to be the most suitable for a scale up work. Both ^1H NMR and LC-HRMS data were used to investigate the chemical composition of the afforded extract.

Table 4.3: Summary activity of *F. proliferatum* extracts from different media against planktonic, prebiofilm, and postbiofilm MRSA at concentrations of 100 µg/ml.

Media	Incubation Period	Antimicrobial % inhibition	Stdev	Prebiofilm % inhibition	Stdev	Postbiofilm % inhibition	Stdev
Rice	7	93.50	3.32	99.30	1.39	84.40	8.43
Malt	7	90.90	2.38	99.60	0.42	67.20	13.24
Rice	15	89.49	0.84	100.00	0.24	79.30	7.24
Malt	15	72.80	27.16	83.50	28.38	91.20	3.92
Potato	15	65.50	21.96	72.42	16.41	71.30	3.48
Rice	30	91.10	3.52	100.00	0.46	78.30	25.70
Oat	30	38.80	4.15	<0.00	36.19	62.20	10.45
Malt	30	77.50	17.43	81.00	30.45	77.70	3.71
Potato	30	91.40	0.74	99.00	1.76	84.20	8.09

*Cells highlighted in blue colour indicates extracts with consistent bioactivity for all replicates, cells with white colour represents inactive fractions, while gold-coloured cells indicate active fractions with inconsistent bioactivity amongst replicates and therefore regarded as inactive. Fungal extracts not indicated were inactive for planktonic, prebiofilm and postbiofilm assays.

4.2.4 MVA analysis of LC-HRMS data

For MVA, PCA scores and loadings plot were generated for the LC-MS data. The extracts were grouped according to the different media, to which the endophyte was incubated for 7, 15 and 30 days. The PCA scores plot in Figure 4.3A of the LC-HRMS data of *F. proliferatum*, revealed that extracts obtained from malt media at 7, 15, and 30 days of incubation, were found on the right side of the plot, which implied a strong similarity in their metabolomic profiles (red circles). The fungal extract obtained from malt media on day 7 was separate from extracts obtained on days 15 and 30, which exhibited a difference in their chemical profiles. Discriminating metabolites in the malt media was observed on days 15, and 30. Rice media extracts incubated for 7, 15, and 30 days were clustered together on the lower right and left quadrants (green circles). The fungal extracts obtained from oat media (in blue circles) incubated for 7, 15, and 30 days, clustered together on the left lower quadrant. The extracts from rice and oat media did not produce any significant discriminating metabolites, and seemed to cluster together, indicating similarity in their chemical profiles. The fungal extracts obtained by incubation on the rice and oat media were far too rich in lipids masking the more interesting minor metabolites. While fungal extracts obtained

from potato media incubated at 7, 15, and 30 days were dispersed in the lower and upper left quadrant (yellow circles). The 7-, 15, and 30 days were dispersed in the lower and upper left quadrant (yellow circles). The 7 days extracts were clustered in the lower left quadrant, while 15- and 30-days extracts were seen at the upper left quadrant, with more distinct discriminating metabolites. This suggested that there was a strong likelihood that a more divergent profile was afforded with potato and malt medium between the three incubation periods when compared to extracts from other media. The loadings plot in Figure 4.3B, demonstrated that discriminating metabolites from extracts of culture from malt incubated at 15 and 30 days, produced low molecular weight metabolites ranging from 152 to 180 Da (encircled in red). While extracts from the oat media contained metabolites with higher molecular weight from 700 to 900 Da, as encircled in green. The discriminating metabolites for the outlying extracts obtained from the malt media incubated at 15 and 30 days were putatively identified as: Pulchellalactam **(1)** and 1,7a-dihydro, 7-hydroxy-abikoviromycin **(2)**. The outlying extracts obtained from potato media incubated at 15- and 30-days media yielded lower MW metabolites discriminated by ion peaks at m/z 227.127, and 347.115 Da. Discriminating metabolites of the extracts obtained from the PDA media incubated at 15 and 30 days gave no hits for m/z 227.127, while 347.115 Da was denoted as breynolide **(4)**. Abikoviromycin is an antiviral antibiotic piperidine alkaloid, produced by the bacteria *Streptomyces abikoensis* and *Streptomyces rubescens* (Wørmer and Poulsen, 2021). There are no studies on the antibacterial activities of abikoviromycin. The model gave goodness of fit (R_2) of 0.831 and a good predictability score (Q_2) of 0.611 after seven components. The difference between R_2 and Q_2 values was less than 0.3, which indicated an excellent fitted model and predictability.

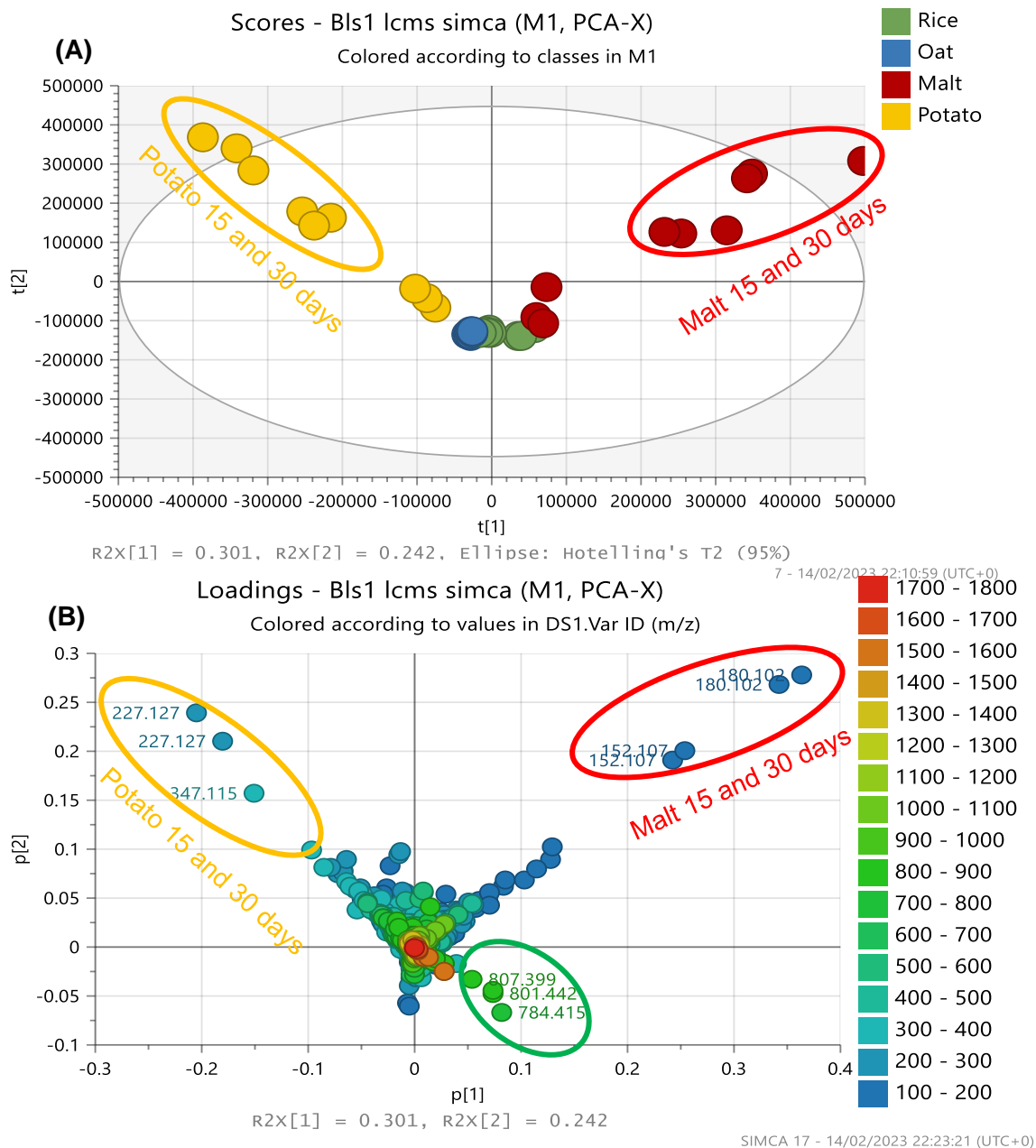


Figure 4.3: (A) PCA scores and (B) loading plots of LC-HRMS data of *F. proliferatum* extracts from four media incubated at 7, 15, and 30 days. $R_2X = 0.831$ and $Q_2X = 0.611$. Encircled features represent the discriminating ion peaks for the outlying extracts obtained from malt and potato media incubated for 15 and 30 days.

A PLS-DA was performed to show a clearer illustration of the differences in metabolic profiles between fungal extracts isolated from various media as shown in Figure 4.4. It showed fitness (R_2) and predictability (Q_2) scores of 0.965 and 0.895 respectively, after seven components. The difference between R_2 and Q_2 values was less than 0.3. This proved to be a good fit, and a good model prediction, which improved when compared to the PCA model above. The variation between groups R_2X_o [1] was 29.8 % and within group R_2X [2] was 23.5%. From the scores plot (Figure 4.4A), rice 7, 15 and 30 days was clustered together in the right upper quadrant (encircled in red), indicating similarity in the chemical profile of the extracts obtained at different days of incubation. Similarly, extracts obtained from oat media incubated for 7, 15 and 30 days (encircled in yellow), were clustered together in the left upper quadrant, indicating similarity in the chemical profile of the extracts obtained at different days of incubation. The rice and oat extracts were at close range on the PLS-DA plot, which could be because of the lipids produced in both media extracts. The fungal extracts obtained with the rice media contained metabolites with MW ranging from 100-300 Da, 700-900 Da, and m/z 1585.85 Da. There was no discriminating metabolites found on the oat media, but the metabolites therein had MW ranging from 100-400 Da, indicating the presence of lipids. Fungal extracts produced from the malt media after 7 days of incubation were separated from extracts obtained after incubating at 15- and 30-days (encircled in light blue). The metabolites were sparsely distributed between the upper and lower right quadrant, with MW between 100 and 300 Da. Similarly, fungal extracts obtained from the potato media incubated for 7 days were separated from those incubated at 15 and 30 days (encircled in purple). The metabolites were sparsely distributed on the left lower quadrant, with MW ranging between 100 and 400 Da (Figure 4.4B). The dereplicated discriminating features of *F. proliferatum* from each media were listed in Table 4.4.

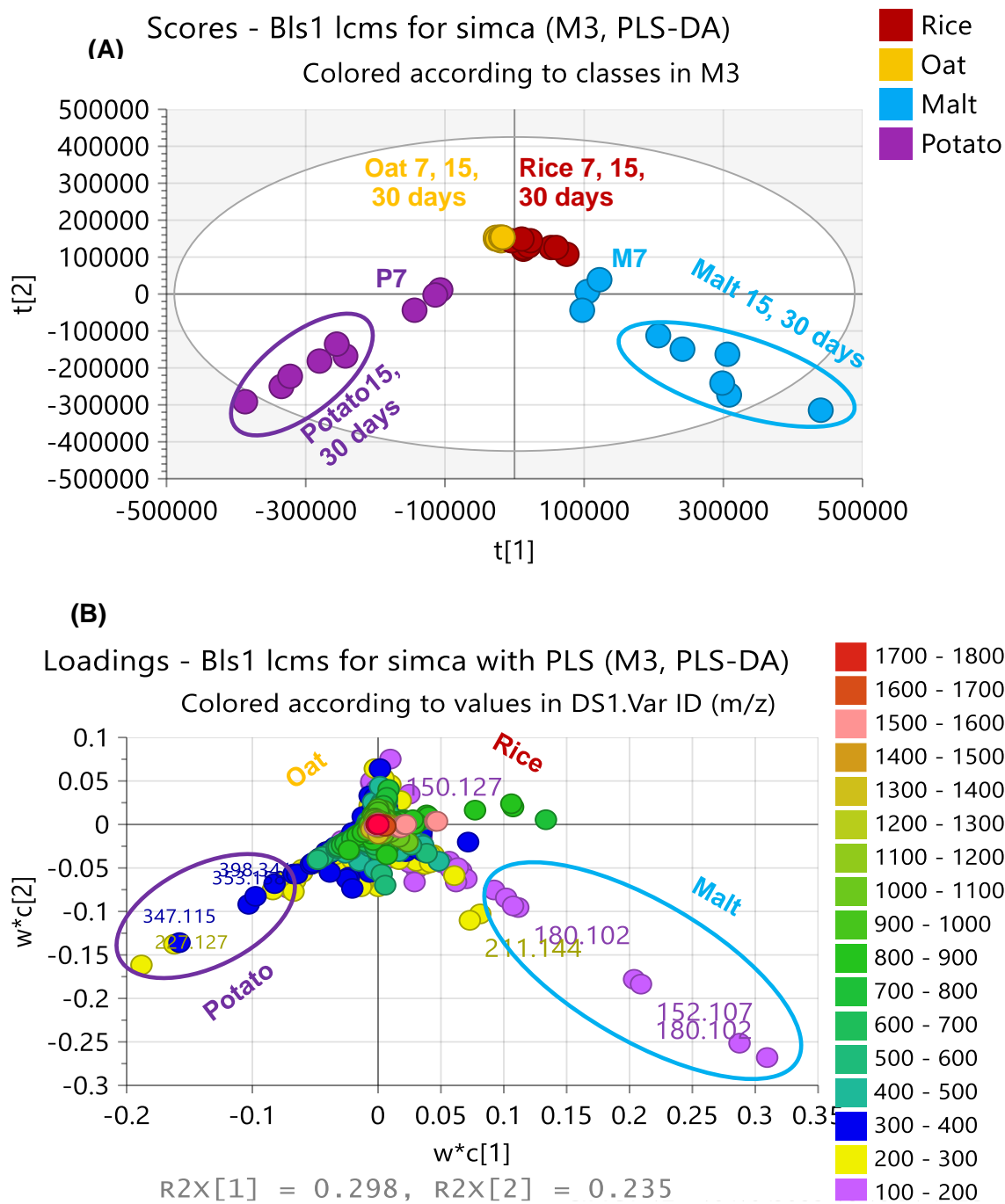


Figure 4.4: (A) PLS-DA scores and (B) loading plots of LC-HRMS of *F. proliferatum* extract obtained from different media. The encircled box indicated the discriminating feature for the respective fungal extracts from various media. $R_2 = 0.965$ and $Q_2 = 0.895$. The difference between group $R_2X_0 [1]$ is equal to 29.8% and the difference within groups $R_2X [2]$ is 23.5%.

Table 4.4: Dereplication data of the discriminating metabolites for (A) Malt, (B) Potato, (C) Rice, and (D) Oat obtained from PLS-DA loadings plot on Figure 4.4B. Structures are shown in Figure 4.5.

(A) Malt media extracts							
Mzmine ID	<i>m/z</i>	Rt	M. wt	<i>P</i> -value	Molecular Formular (DBE)	Compound hits	Biological source
P1566	152.107	5.98	151.1	0.001747	C ₉ H ₁₃ NO (4)	Pulchellalactam (1)	<i>Acrocarpospora sp.</i> FIRDI001 and the marine derived <i>Corollospora, pulchella, Monascus ruber</i> BB5, <i>Monascus pilosu</i>
P989	180.102	6.32	179.094	0.001010	C ₁₀ H ₁₃ NO ₂ (5)	1,7a-Dihydro, 7-hydroxy Abikoviromycin (2)	<i>Streptomyces sp.</i> SANK 65986
P1952	181.105	5.64	180.098	0.002414	C ₃ H ₁₂ N ₆ O ₃ (1)	No hit	-
P4171	211.144	5.49	210.136	4.40219e-05	C ₁₁ H ₁₈ N ₂ O ₂ (1)	Cyclo(isoleucylprolyl) (3)	Marine-derived <i>Pseudomonas aeruginosa</i> and <i>Vibrio parahaemolyticus</i>

(B) Potato media extracts							
P429	347.115	12.59	346.108	0.000460	C ₁₅ H ₂₂ O ₇ S (5)	Breynolide (4)	<i>Breynia fruticosa</i>
P630	353.158	14.55	352.151	0.000251	C ₁₈ H ₂₄ O ₇ (7)	Chlorajapolide E (5)	<i>Chloranthus japonicus</i>
P437	227.127	17.71	226.119	0.019340		No hit	

P89	227.127	17.20	226.12	0.031041		No hit	
N20	187.097	7.84	188.104	1.88503e-09		No hit	-
P417	225.112	17.65	224.105	0.000493	C ₁₂ H ₁₆ O ₄ (5)	Fujikurin A (6)	<i>Fusarium fujukuroi</i> IMI58289 and <i>Fusarium</i> sp. CR 377
P338	243.122	11.76	242.115	0.000184	C ₁₂ H ₁₈ O ₅ (4)	Agistatin A (7)	fungus FH-A 6239
N1785	329.233	13.12	330.241	1.19446e-07	C ₁₈ H ₃₄ O ₅ (2)	9,10,11-Trihydroxy-12- octadecenoic acid; (9ξ,10ξ,11ξ,12S)-form (8)	Roots of <i>Boehmeria nivea</i> , and the edible fungus <i>Tuber indicum</i>
P2679	398.341	11.19	397.33	0.000110	C ₂₇ H ₄₃ NO (7)	Solanidine (9)	Alkaloid from <i>Solanum</i> <i>tuberosum</i> , <i>Cestrum</i> <i>purpureum</i> , and <i>Rhinopetalum</i> <i>stenantherum</i> (<i>Solanaceae</i> , <i>Liliaceae</i>)

(C) Rice media extracts						
Mzmine ID	m/z	Rt	M. wt	Molecular Formular (DBE)	Compound hits	Biological source
P1155	150.127	33.70	149.12	C ₁₀ H ₁₅ N (4)	Antibiotic NA 337 (10)	<i>Streptomyces</i> sp. NA-337 and <i>actinomyces</i> strain MD736-C6
P4061	196.017	10.25	195.009	C ₉ H ₆ ClN O ₅ (7)	5-Chloro-1H-indole-3-carboxylic acid (11)	Produced by a marine-derived <i>Micromonospora</i> sp. FIM07-0019
N132	295.228	20.37	296.235	C ₁₈ H ₃₂ O ₃ (3)	Fusarisolin C (12)	Marine-derived <i>Fusarium solani</i> H918

P75	784.415	25.45	783.408	C ₄₅ H ₅₇ N ₃ O ₉ (19)	Beauvericin (13)	<i>Fusarium semitectum</i> , <i>Fusarium moniliforme</i> - <i>subglutinans</i> , <i>Fusarium</i> sp. Fo740 and <i>F. proliferatum</i> M5991.
P74	801.442	25.45	800.434	C ₄₄ H ₆₄ O ₁₃ (13)	Cynafoside C (14)	<i>Cynanchum africanum</i>
P3913	803.448	25.45	802.441		No hit	-
P73	806.396	25.46	805.389	C ₃₈ H ₅₁ N ₁₁ O ₉ (19)	Penaeustatin 19 (15)	-
P1954	807.399	25.46	806.392	C ₃₅ H ₅₄ N ₁₀ O ₁₂ (14)	<i>Hemicentrotus pulcherrimus</i> Sperm-activating peptide H2; 3-L-Serine, 4-L-isoleucine, 5-glycine analogue (16)	Egg jelly of <i>Tripneustes gratilla</i>
P1953	1584.85	25.39	1583.84		No hit	-
P418	1585.85	25.38	1584.84		No hit	-

(D) Oat media extracts							
P1135	150.127	34.92	149.12	0.004108	C ₁₀ H ₁₅ N (4)	Antibiotic NA 337 (10)	<i>Streptomyces</i> sp. NA-337 and actinomyces strain MD736-C6
P5862	161.107	17.64	160.1	0.077929	C ₁₀ H ₁₂ N ₂ (14)	Donaxamine (17)	Alkaloid from the aerial parts of <i>Arundo donax</i>
P2050	213.982	9.64	212.975	0.000306		No hit	-
P2491	379.335	25.29	378.328	0.0831924	C ₂₈ H ₄₂	28, 30-Dinor-17,19,21-gammaceratriene (18)	Messel shale

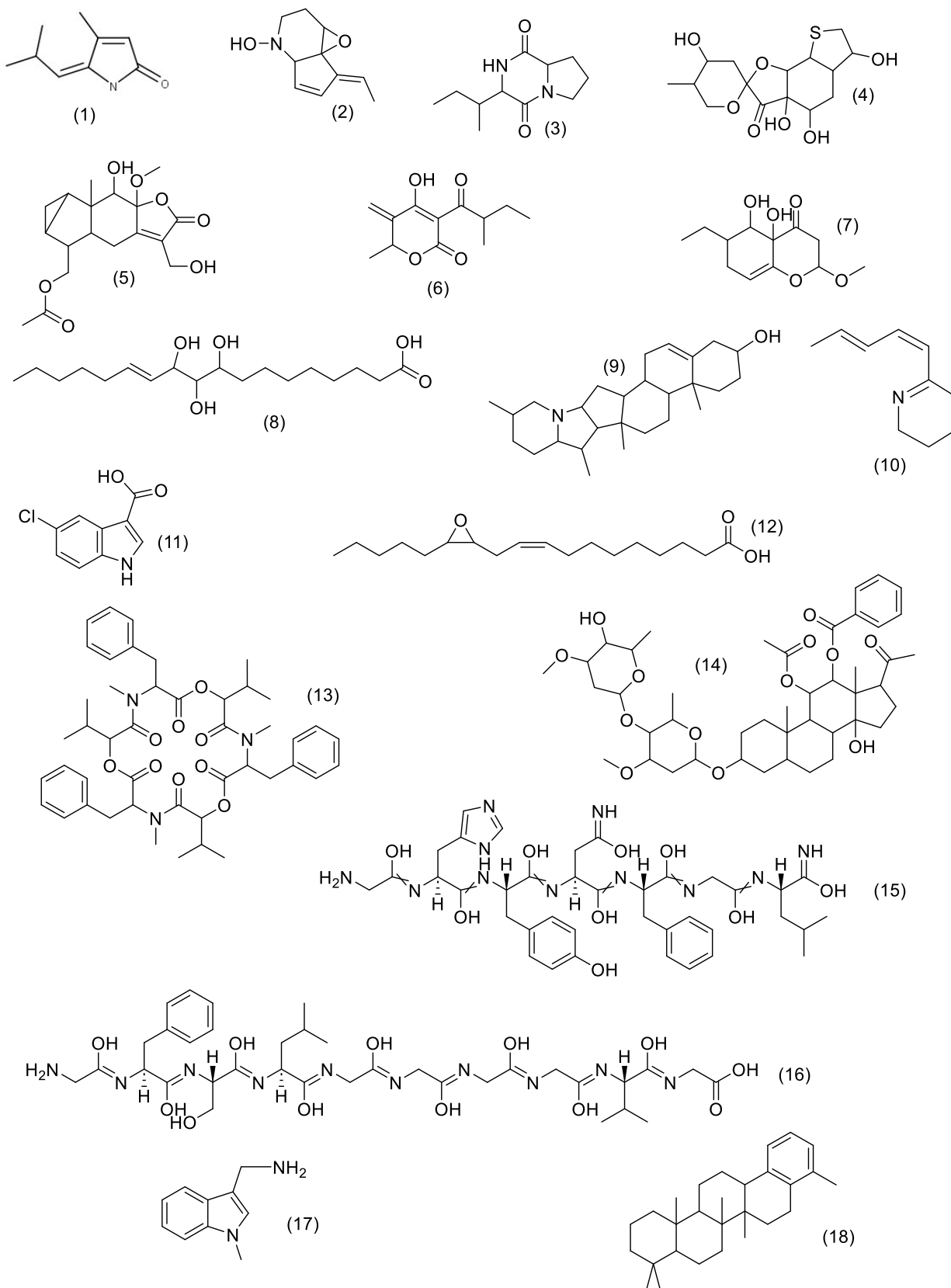


Figure 4.5: PLS-DA Structures of the discriminating metabolites from *F. proliferatum* extract obtained from different media and listed in Table 4.4.

An OPLS-DA was performed based on the anti-MRSA results to discriminate the metabolites between active and inactive extracts as shown in Figure 4.6. Active extracts were obtained by inoculation in malt media then incubated for 7 and 30 days, in potato dextrose for 30 days, and rice media extracts incubated for 7, 15, and 30 days, while those grown in malt for 15 days, and potato for 7 and 15 days and all those inoculated in oat media were found inactive. It showed fitness (R_2) and predictability (Q_2) scores of 0.912 and 0.759 respectively. This proved to be a good fit, and a good model prediction. The variation between groups R_2X_0 [1] was 67.4 % and within group R_2X [1] was 25.5 %. This showed that there was significant difference in the chemical profiles between the active and the inactive extracts, and a slight similarity within the extracts in their different classes.

The OPLS-DA scores plot in Figure 4.6A positioned the active extracts on the upper and lower left quadrants. Meanwhile, the inactive extracts were dispersed on the upper and lower right quadrant of the scores plot, as shown in Figure 4.6A. For the active extracts, the outliers were found on those inoculated on malt and incubated for 30 days (encircled in red), whereas, for the inactive extracts, the outliers were found for those on malt after 15 days of incubation (encircled in blue). The defined target metabolites afforded p -values < 0.05 , which indicated a strong model with a confidence interval of more than 95%. The bioactive metabolites gave an m/z range between 150 and 1600 Da. The rice culture media was therefore chosen for scale up of *F. proliferatum*, was active, but the extracts were not outliers as shown in Figure 4.6A and 4.6B.

Discriminating active metabolites with p -values less than 0.05 are listed in Table 4.5. Structures of putatively identified compound hits are shown in Figure 4.7. Five of the ion peaks gave no hits, which could indicate the presence of novel compounds.

Discriminating predicted bioactive compounds with molecular weight ranging between 150 and 300 Da, and DBE values of 1 to 4, indicated the presence of aliphatics, and olefinics. The compounds identified from the DNP database, as shown in Table 4.5 were, Mzmine IDs of P97, P95, P419, P294, N129, P80, and N737, represented by their respective m/z as 165.091, 203.179, 205.195, 209.153, 287.236, and 279.233, and dereplicated as fusalanipyrone (**19**), 1,3,5,10-bisabolatetraene; (R)-form (**20**), 8,11-daucadiene; (1 β ,4 β ,5 α)-form (**21**), 4-methyl-1-phenyl-2,3-hexanediol (**22**), araneosol (**23**), fusoxysporone (**24**), and 7-hydroxy-8,14-dimethyl-9-hexadecenoic acid (**25**), respectively. Fusalanipyrone, a monoterpene, was first isolated from the fungus *Fusarium solani* strain DSM 62416. Fusalanipyrone was found to be inactive against *S. aureus* and *E. coli*, but was a weak antibiotic against *Candida albicans*, *Mucor* and *Trichoderma koningii* (Wolf-Rainer and Hans-Adolf, 1988). Bisabolanes are sesquiterpenes found in the fragrances from familiar plants like lavender, as well as many coniferous species. They have been

evaluated in human tumour cell lines (HL-60, HCT-8, SF-295, and MDA-MB-435), and were found to be cytotoxic (Abreu *et al.*, 2015). Araneosol was previously isolated from *Anaphalis araneosa* (Ali, 1979), then later from the genus *Herissantia* (Silva *et al.*, 2005). There are no records of previous work on its antibacterial activity. Fusoxysporone is a diterpene, that was first isolated from liquid cultures of the fungus *Fusarium oxysporum* IMB FO 1/82, after it was cultivated for 7 weeks in a liquid biomalt medium (Abraham and Hanssen, 1992).

Discriminating compounds with Mzmine P121, P438, P74, and higher DBE values of 10 and 14, represented by ion peaks m/z 383.075, 384.079, and 801.442 Da respectively, indicated the presence of sugars. These metabolites were identified as bivakerin, glycyglycyglycine; 3, 5-dinitrobenzoyl, and cynafoside C. Bivakerin and beauvericin has been isolated as a secondary metabolite from *Fusarium* sp. and was found to possess antibacterial effects (Sondergaard *et al.*, 2016).

Discriminating metabolites with Mzmine IDs of P75, P73, and P1954, with higher DBE values ranging between 13 and 19, represented by ion peaks m/z 784.415, 806.396, 807.399 Da respectively, indicated the presence of aromatics. These metabolites were identified as beauvericin, penaeustatin 19, and *Hemicentrotus pulcherrimus* sperm-activating peptide H2; 3-L-serine, 5-glycine analogue, which is a decapeptide (GFDLNGGGVG) isolated from the solubilised jelly layer of the sea urchin *Hemicentrotus pulcherrimus*, known to stimulate the respiration and motility of *H. pulcherrimus* spermatozoa (Suzuki, 1995).

Fermentation conditions that yielded active extracts were then considered for scale-up. However, those incubated in Malt for 7 and 30 days, in potato for 30 days and in rice for 7 days were excluded due to their low yields. Rice culture 15 days (BLS1- R15) was selected as the optimum condition for the scale-up of *F. proliferatum*, in the production of bioactive metabolites.

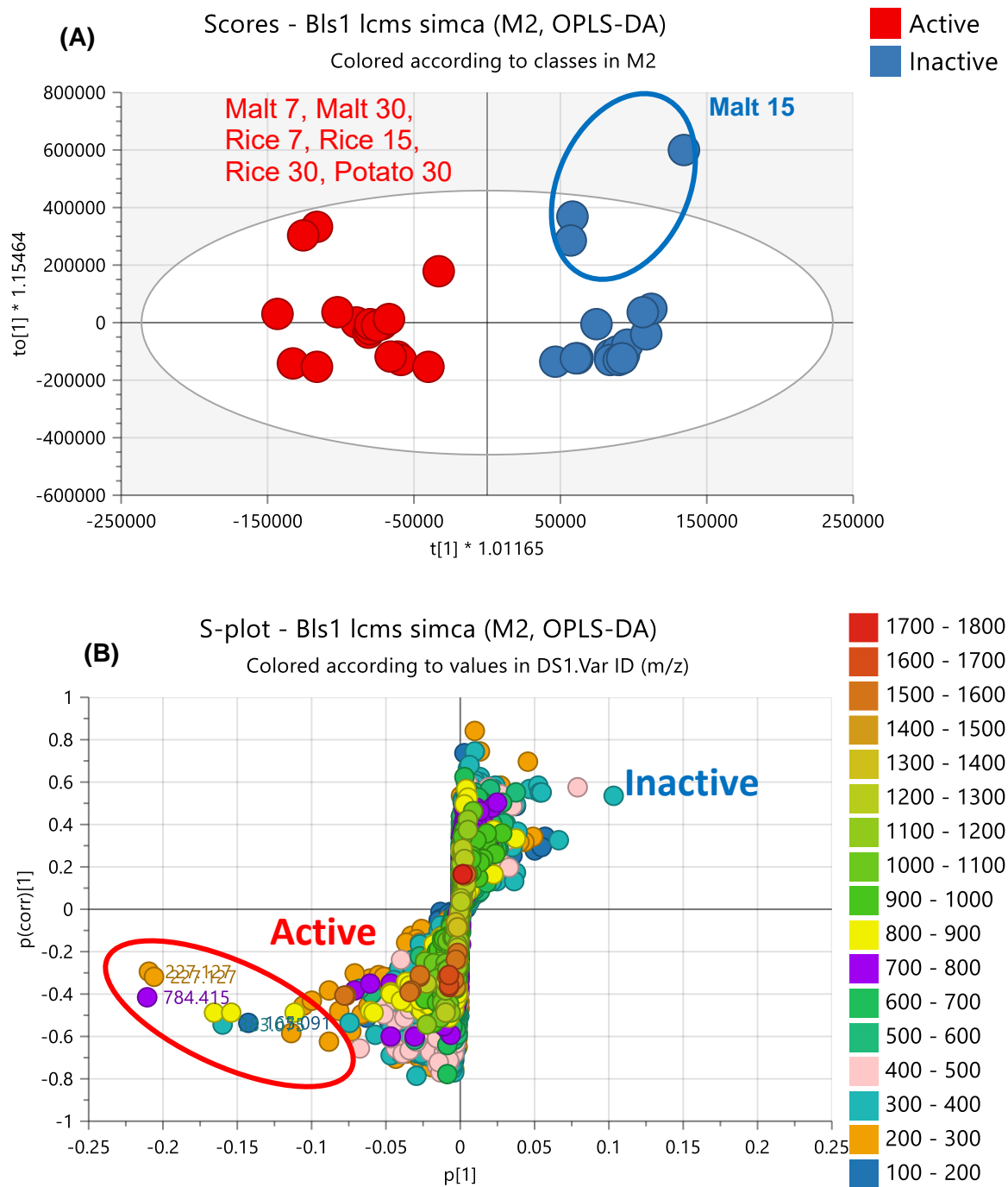


Figure 4.6: (A) OPLS-DA scores and (B) S- plots of LC-HRMS of *F. proliferatum* extracts obtained from different media. The encircled metabolites on S-plot indicated the discriminating feature for each media extracts. $R_2 = 0.912$ and $Q_2 = 0.759$. The difference between group $R_2X_0 [1]$ is equal to 67.4% and the difference within groups $R_2X [2]$ is 25.5%.

Table 4.5: Dereplication data of the discriminating bio-active metabolites of *F. proliferatum* from different media obtained from the OPLS-DA S-plot on Figure 4.6B. Structures are shown in figure 4.7.

Mzmine ID	m/z	Rt	M. Wt	P value	Molecular Formular (DBE)	Compound hits	Biological source
P97	165.091	12.97	164.083	0.007946	C ₁₀ H ₁₂ O ₂ (5)	Fusalanipyrone (19)	<i>Fusarium solani</i> DSM 62416 and <i>F. oxysporum</i> f. sp. <i>batatas</i> O-17
P95	203.179	16.76	202.172	0.055665	C ₁₅ H ₂₂ (5)	1,3,5,10-Bisabolatetraene; (R)-form (20)	Widespread occurrence in plants e.g. <i>Curcuma aromatica</i> , <i>Ambrosia</i> sp. and <i>Amorpha fruticosa</i> . Also, from the gorgonian <i>Muricea elongata</i>
P419	205.195	23.41	204.187	0.000329	C ₁₅ H ₂₄ (4)	8,11-Daucadiene; (1 β ,4 β ,5 α)-form (21)	<i>Vernonia galpinii</i>
P294	209.153	20.77	208.146	0.001777	C ₁₃ H ₂₀ O ₂ (4)	4-Methyl-1-phenyl-2,3-hexanediol (22)	<i>Acremonium</i> sp. PSU-MA70
P437	227.127	17.71	226.119	0.174633		No hit	
P89	227.127	17.20	226.12	0.145976		No hit	
N129	279.233	28.25	280.24	8.13986e-05	C ₁₈ H ₃₂ O ₂ (3)	Araneosol (23)	<i>Anaphalis araneosa</i> flowers
P80	287.236	27.86	286.229	0.000738	C ₂₀ H ₃₀ O (6)	Fusoxysporone (24)	<i>Fusarium oxysporum</i>
N737	297.243	21.16	298.251	0.020437	C ₁₈ H ₃₄ O ₃ (2)	7-Hydroxy-8,14-dimethyl-9-hexadecenoic acid (25)	Fungus <i>Pleurotus</i> sp.

P121	383.075	16.82	382.068	0.000256	C ₂₀ H ₁₄ O ₈ (14)	Bikaverin (26)	Pigment from <i>Fusarium oxysporum</i> , <i>F. solani</i> , <i>F. moniliforme</i> , <i>F. lycopersici</i> , <i>F. vasinfectum</i> , <i>F. bulbigenum-blasticola</i> , <i>Gibberella fujikuroi</i> .
P438	384.079	16.81	383.071	0.000318	C ₁₃ H ₁₃ N ₅ O ₉ (10)	Glycylglycylglycine; 3,5-Dinitrobenzoyl (27)	Various sources
P85	481.292	27.53	480.284	0.000797		No hit	-
P75	784.415	25.45	783.408	0.008088	C ₄₅ H ₅₇ N ₃ O ₉ (19)	Beauvericin (13)	<i>Fusarium semitectum</i> , <i>F. moniliforme-subglutinans</i> , <i>F. sp. Fo740</i> and <i>F. proliferatum M5991</i> .
P74	801.442	25.45	800.434	0.001383	C ₄₄ H ₆₄ O ₁₃ (13)	Cynafoside C (28)	<i>Cynanchum africanum</i>
P73	806.396	25.46	805.389	0.001571	C ₃₈ H ₅₁ N ₁₁ O ₉ (19)	Penaeustatin 19 (15)	<i>Penaeus monodon</i>
P1954	807.399	25.46	806.392	0.001465	C ₃₅ H ₅₄ N ₁₀ O ₁₂ (14)	<i>Hemicentrotus pulcherrimus</i> Sperm-activating peptide H2; 3-L-Serine, 5-glycine analogue (16)	Egg jelly of <i>Strongylocentrotus nudus</i> and <i>Tripneustes gratilla</i>
P1953	1584.85	25.40	1583.84	0.010516		No hit	-
P418	1585.85	25.38	1584.84	0.010551		No hit	-

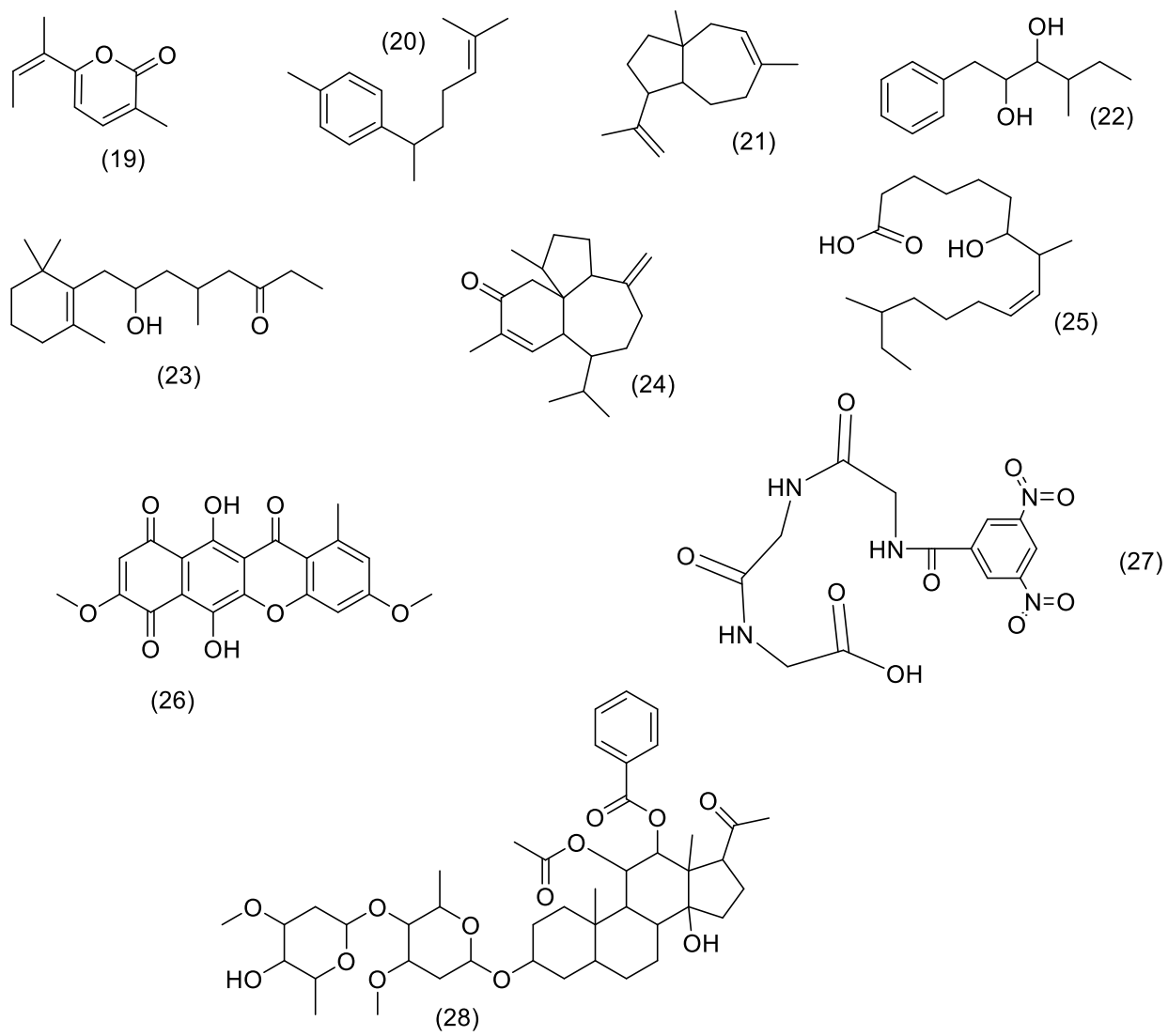


Figure 4.7: Structures of the discriminating active metabolites from *F. proliferatum* extract obtained from four different media and listed in Table 4.5.

Analysis on MetaboAnalyst® was also performed. The heatmap confirmed that bioactive extracts (red box) were obtained by incubation in malt for 7 and 30 days, in potato dextrose for 30 days, and in rice for 7, 15, and 30 days, yielded higher diversity, intensity, and concentration of metabolites observed in the active quadrant (Figure 4.6). The fungal extract obtained from malt media incubated for 15 days (small red box) showed metabolites of moderate intensity and concentration, which could explain its inactivity for inhibiting the growth of planktonic MRSA but did exhibit activity against biofilm formation in MRSA. The heatmap also showed that extracts obtained by incubation in potato for 7 and 15 days, those inoculated in oat media yielded a lower concentration of the secondary metabolites, which could have contributed to their inactivity.

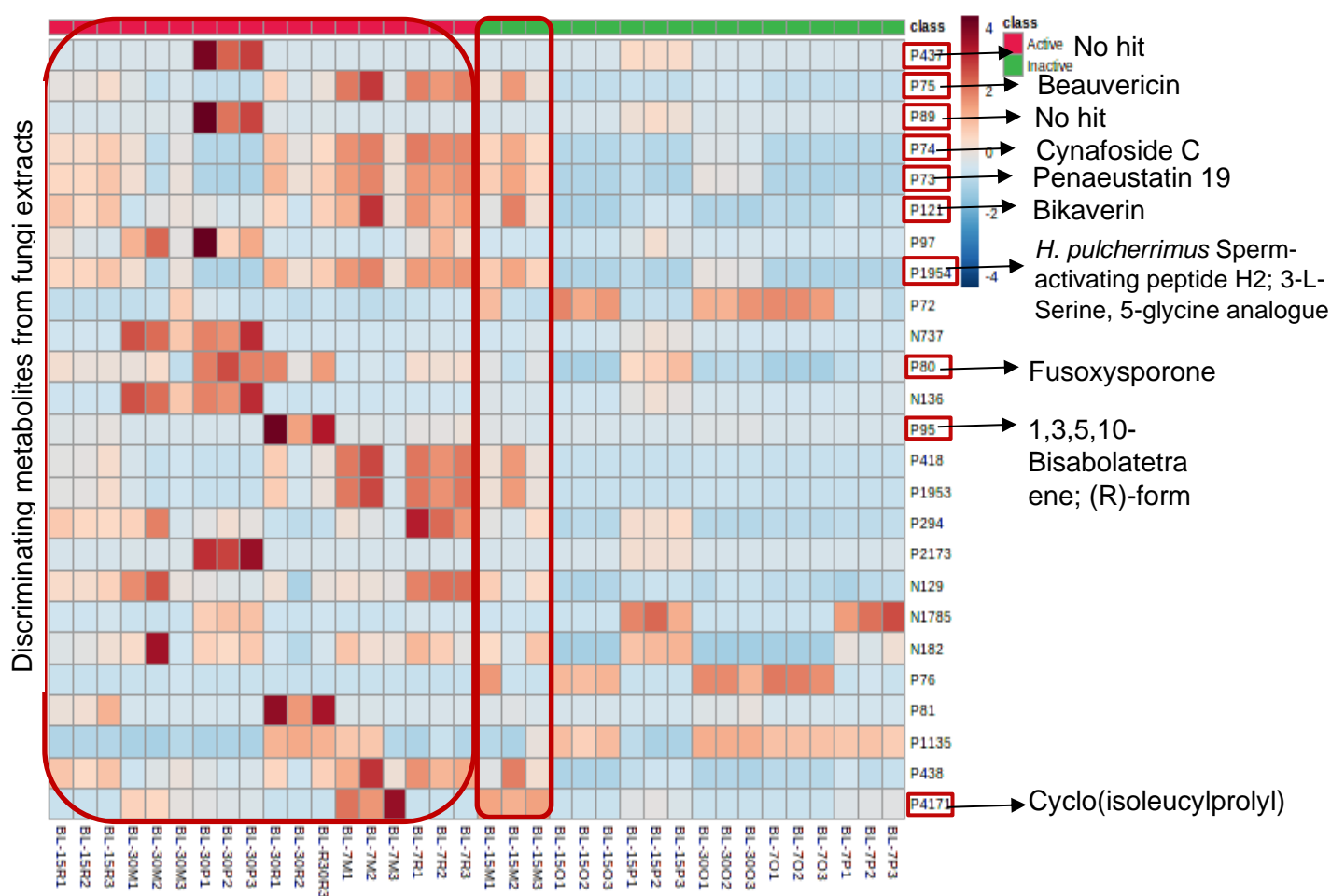
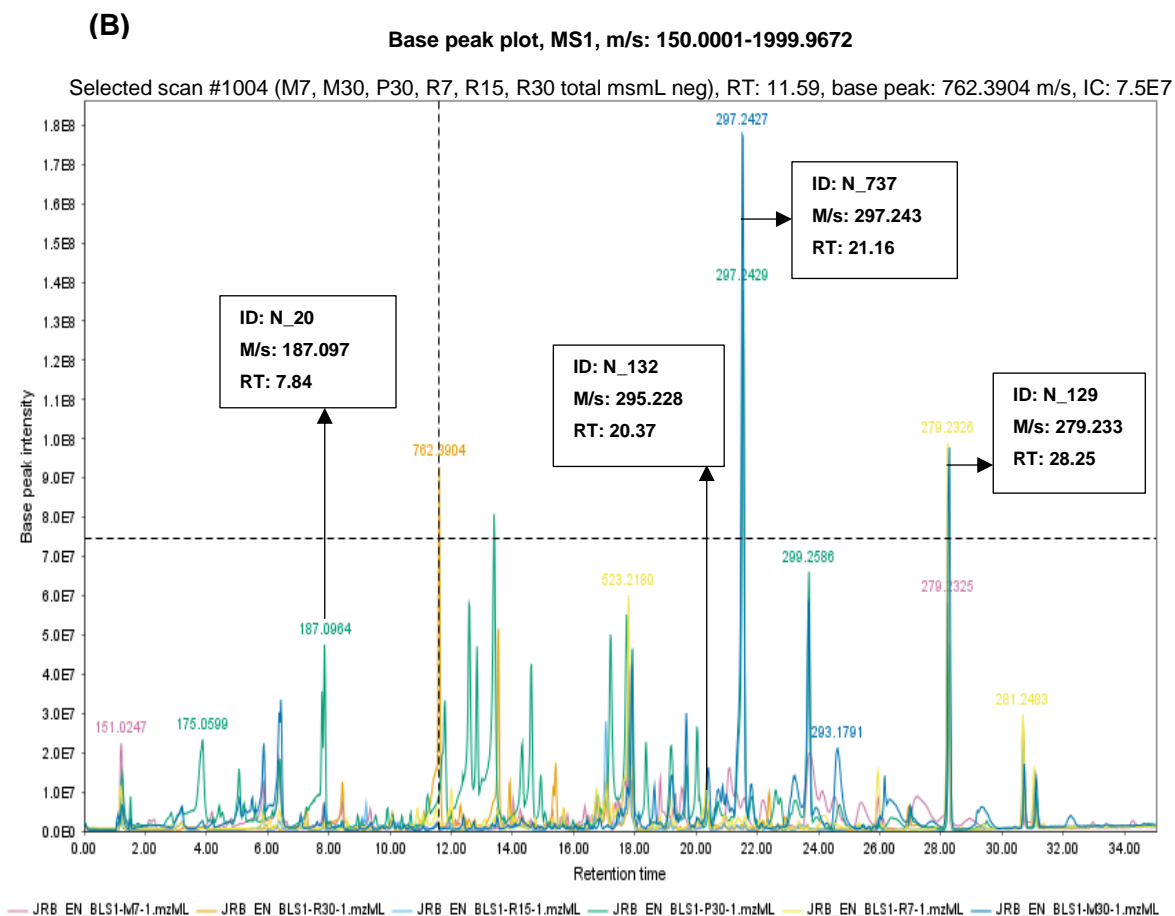


Figure 4.8: Heatmap analysis of the mass spectral data of *F. proliferatum* extracts with their Mzmine values, obtained from different media, generated by MetaboAnalyst®. The big red boxed are those discriminatory metabolites designated as biologically active against MRSA. Highlighted Mzmine values on the Y-axis indicate common metabolites observed on the heatmap and VIP.



- JRB_EN_BLS1-P30-1 = *F. proliferatum* incubated in potato media for 30 days
- JRB_EN_BLS1-M7-1 = *F. proliferatum* incubated in malt media for 7 days
- JRB_EN_BLS1-M30-3 = *F. proliferatum* incubated in malt media for 30 days
- JRB_EN_BLS1-R7-1 = *F. proliferatum* incubated in rice media for 7 days
- JRB_EN_BLS1-R15-1 = *F. proliferatum* incubated in rice media for 15 days
- JRB_EN_BLS1-R15-1 = *F. proliferatum* incubated in rice media for 30 days

Figure 4.9: Total ion chromatogram (TIC) (A= Positive, B= Negative) of the bioactive extracts of *F. proliferatum* from different media. The ion peaks that represent the discriminating features listed in Table 4.4 and 4.5 have been labelled (Schmid *et al.*, 2023).

4.2.5 Fractionation of *F. proliferatum* Scale-up crude extracts

Fractionation of *F. proliferatum* afforded F1-F14, W1-W4 (F15-F18) from EtOAc: MeOH wash, and W5-W7 from Acetone: MeOH wash. The fractions from the acetone wash were discarded as the TLC plate showed no trace of bands.

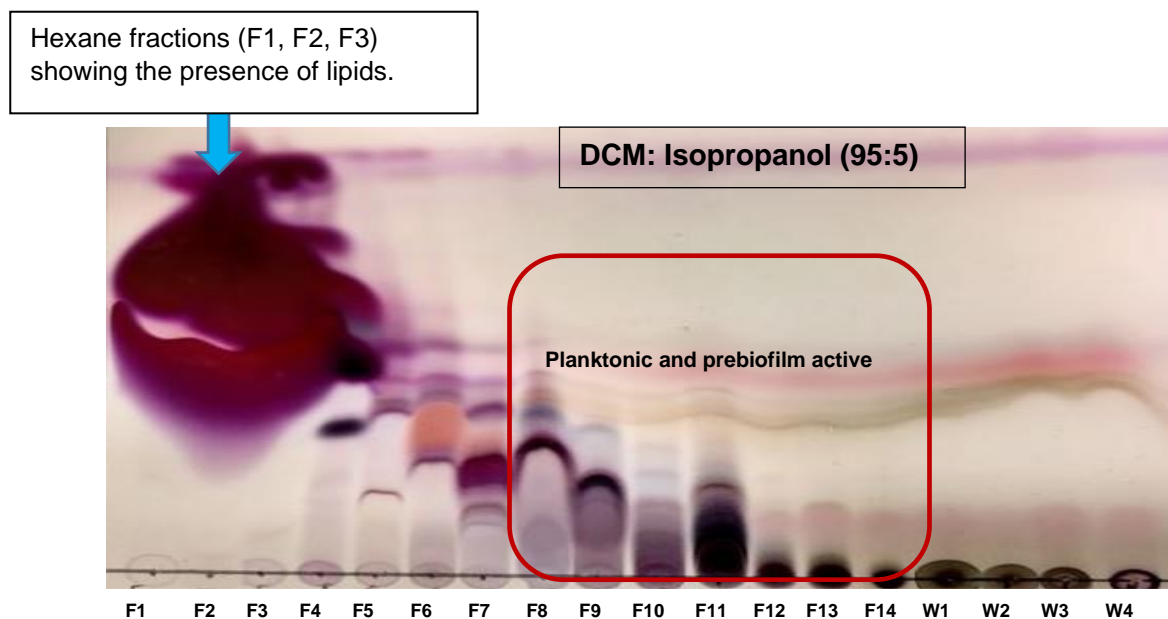


Figure 4.10: Summary TLC Plate of *F. proliferatum* pooled fractions after spraying with anisaldehyde-sulphuric acid. The TLC plate showed fractions from the non-polar solvent of hexane to the more polar solvent of ethylacetate (100% Hexane- 100% ethylacetate). Bioactive fractions are highlighted in red box.

Table 4.6: Extract weights of *F. proliferatum* fractions per vials

Fractions	Weight (mg)	Fractions	Weight (mg)
F6	509.1	W4	21.8
F7	472	W3	2221
F8	429.1	W2	6164
F9	275.8	W1	13235
F10	87.5	F14	33
F11	481.7	F13	11832
F12	95.5	F12	1441
F13	68.1	F11	4580
F14	58.6	F10	2089

4.2.6 Bioactivity test results of *F. proliferatum* fractions

The fractions obtained from fractionation of *Fusarium proliferatum* was subjected to antibacterial antibiofilm assay against MRSA. Fractions 8-14 showed antimicrobial (above 97.0 %) and prebiofilm activity (100.0 %), while fraction 1-5, 15-17 were inactive. Fraction 14 also showed postbiofilm activity. Fraction 6, 7 and 18 showed postbiofilm activity, but was inactive for planktonic and prebiofilm activity.

The bioactivity was in the decreasing order: F11 and F9> F12> F14> F13> F10> F8.

Table 4.7: Summary of bioactivity of *F. proliferatum* fractions against MRSA Planktonic, prebiofilm, and postbiofilm percentage viability.

Fractions	Antimicrobial % Inhibition	Prebiofilm % Inhibition	Postbiofilm % Inhibition
Fraction 6	18.6	<0	67.1
Fraction 7	49.5	<0	57.7
Fraction 8	98.1	100	<0
Fraction 9	100	100	19.2
Fraction 10	98.4	100	21.5
Fraction 11	100	100	<0
Fraction 12	99.7	100	<0
Fraction 13	98.6	100	49.6
Fraction 14	99.6	100	51.9
Fraction 18	22.3	<0	57.1

Cells with blue colour indicates active fractions against MRSA, while white cells indicate inactive fractions. Fractions not denoted were inactive for antibacterial and antibiofilm assays.

4.2.7 NMR spectroscopy for *F. proliferatum* fractions

After fractionation, the pooled fractions were subjected to proton NMR measurements to have an overview of the chemical profile and type of compounds expected to be found in each fraction. The ¹H NMR spectra of the bioactive fractions were stacked and presented in Figure 4.11. A high intensity of aliphatic peaks could be observed in the recorded ¹H NMR spectra of the fractions. Peaks between 3 and 5 ppm, 5 and 5.5 ppm, 6.0 and 9 ppm, as well as 11 and 12 ppm represented sugars, olefinics, aromatics, and carboxylic acids respectively.

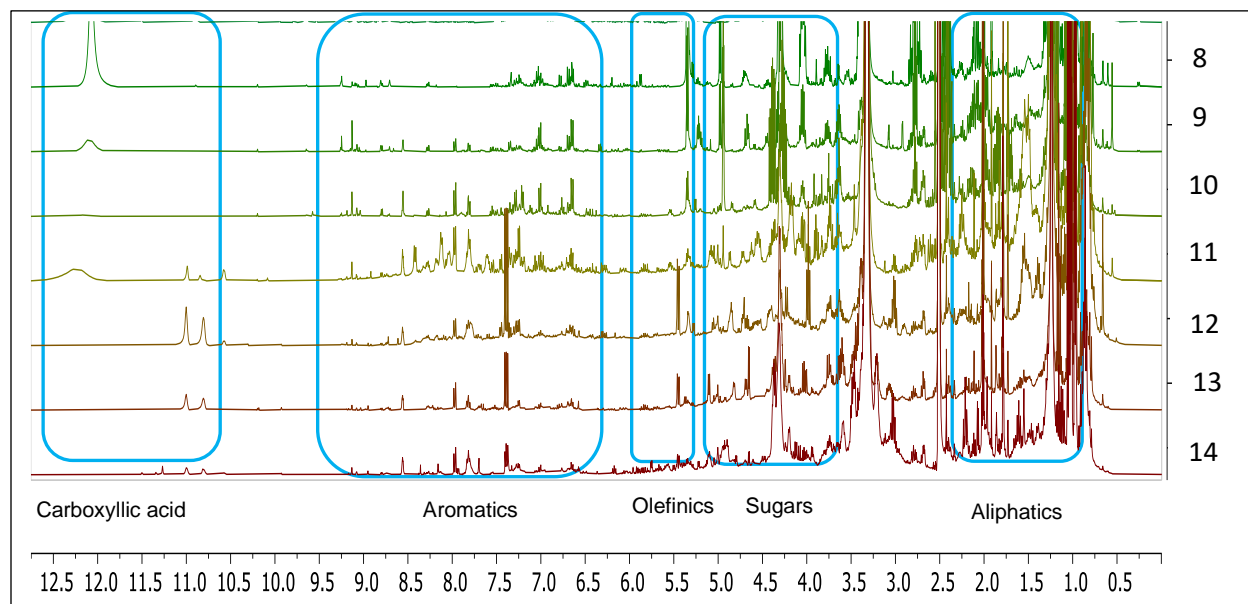


Figure 4.11: Stacked ¹H NMR spectra of the bioactive *F. proliferatum* fractions ranging from fraction 8 to 14.

The PCA scores scatter plot (Figure 4.12 A) shows F1 to be an outlier. All the active fractions were clustered together at the left quadrant, except F8, that was a bit dispersed from the active fractions. The loadings plot (Figure 4.12 B) indicated that the chemical shifts of the discriminating metabolites were within the range of 1 to 2 ppm and 3 to 4 ppm, which belongs to the aliphatics and sugars respectively. In the generated model at pareto scaling, the R_2 was 1.0 while Q_2 was 0.999 at seventeen components, which indicated a good fitted and predictability model.

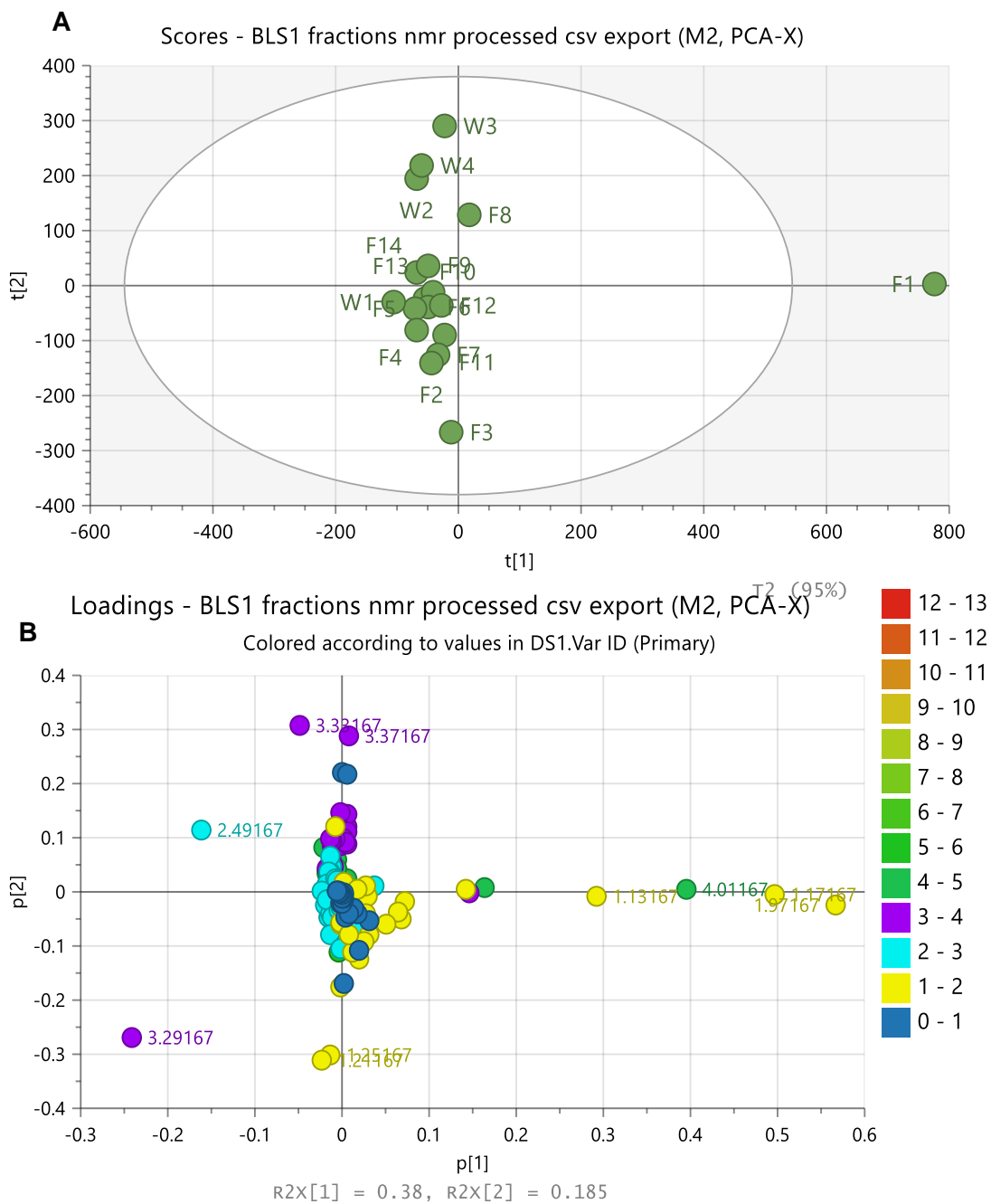


Figure 4.12: (A) PCA scatter and (B) loading plots of the NMR spectral data of the active fractions. The R_2X and Q_2X values were 1.00 and 0.99, respectively. The labelled numbers represent the chemical shifts of the extracts.

An OPLS-DA was also performed to indicate the discriminating signals for the active and inactive fractions. The active fractions were clustered together on the upper and lower left quadrants, while the inactive fractions were clustered on the upper right quadrant of the OPLS-DA scores plot, with F1 showing to be an outlier (Figure 4.13A). The loadings plot (Figure 4.13B) showed the occurrence of a range of resonance between 0.8 and 4.21 ppm for the discriminating active and inactive fractions, which indicated that the discriminating metabolites were mostly dominated with aliphatics and sugars. R_2 and Q_2 values were 0.996 and 0.915, respectively. The difference between group R_2X_0 [1] is equal to 36.9 %, and the difference within groups R_2X [2] is 6.0 %, which indicated low diversity of the samples within the respective groupings. There was an excellent separation between the active and inactive clusters, as the variation score between groups is greater than within groups. The proximity of active fractions 8 to 14, on the scores plot indicates they could have similar chemical profiles.

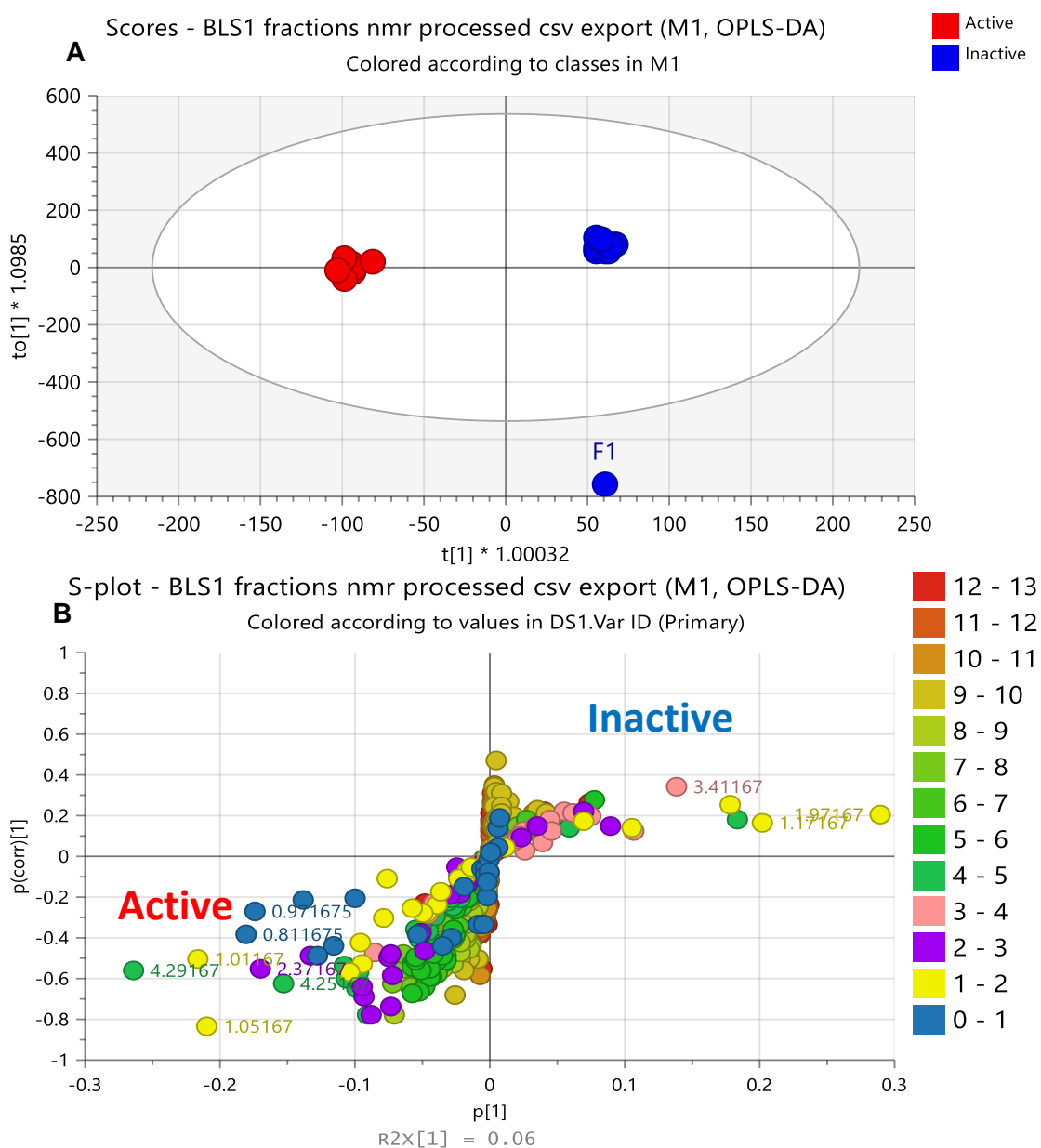


Figure 4.13: OPLS-DA scores (A) and loadings (B) plots of the NMR spectral data of *F. proliferatum* fractions grouped according to their bioactivity against MRSA. R_2 and Q_2 values were 0.996 and 0.915, respectively. The difference between group $R_2X_o [1]$ is equal to 36.9 % and the difference within groups $R_2X [2]$ is 6.0 %. The chemical shift of the discriminating features was labelled.

VIP scores greater than 1 indicates important variables, while variables with VIP scores less than 1 are less important and can be excluded from the model. OPLS-DA indicated the top 20 VIP. The VIP confirmed that the discriminatory metabolites mostly consisted of aliphatics and sugars ranging from 0.81 to 4.29 ppm. Discriminating metabolites observed on both VIP and heat map had common chemical shifts of 0.81, 0.85, 0.93, 0.97, 1.01, 1.05, 1.13, 1.17, 1.21, 1.97, 2.37, 2.77, 3.41, 4.01, 4.25 and 4.29 ppm.

The fractions were tested to see if fraction 1 was a true outlier using DModX, fraction 1 gave results of less than 0.05 which indicated that fraction 1 was not a true outlier. As shown by the DModX plot in Figure 4.15, variables above the red line are the true outliers that included only Fraction 7.

The spectra bins of each fraction were mechanically replicated, to have three replicates of each fraction, for analysis on MetaboAnalyst®. The heatmap confirmed that bioactive fractions F8 to F14 (red box) had metabolites with chemical shifts ranging from 0.77 to 4.29 ppm, which suggested the presence of aliphatic compounds, and sugars. This could be the metabolites contributing to their bioactivity. Results of the heatmap analysis was compatible to those found from the OPLS-DA loadings plot (fig. 4.13B), which confirmed that, the discriminatory bioactive metabolites mainly consisted of aliphatic systems and sugars. The heatmap showed that the active fractions exhibited high intensity and diversity of metabolites. F1 (green box) was more diverse and more intense compared to all the fractions but was inactive. The inactivity could have been because of the non-polar solvent (hexane) which was of a higher percentage at that fractionation point. The metabolites responsible for this discriminatory feature were also aliphatics and sugars as seen in the heatmap below (Fig. 4.16B).

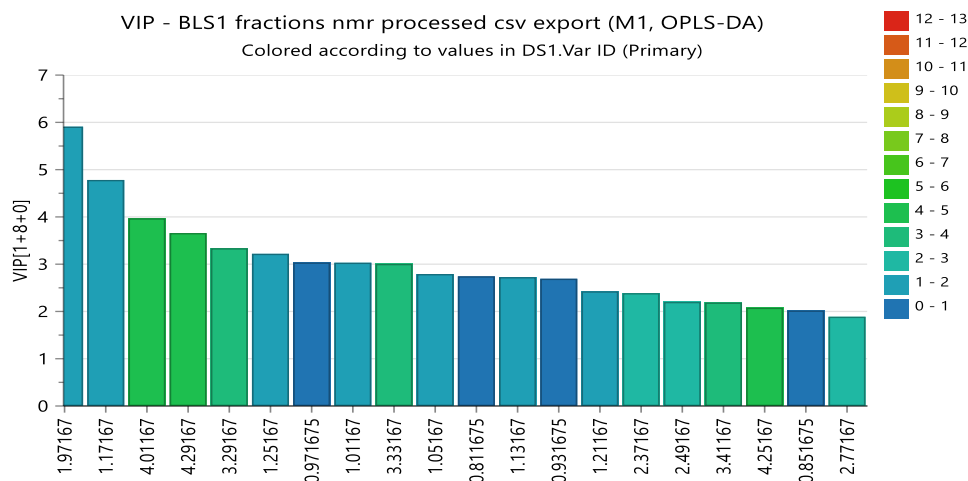


Figure 4.14: VIP scores of *F. proliferatum* fractions from Simca® showing the chemical shifts of 20 most discriminating metabolites with VIP scores above 1.

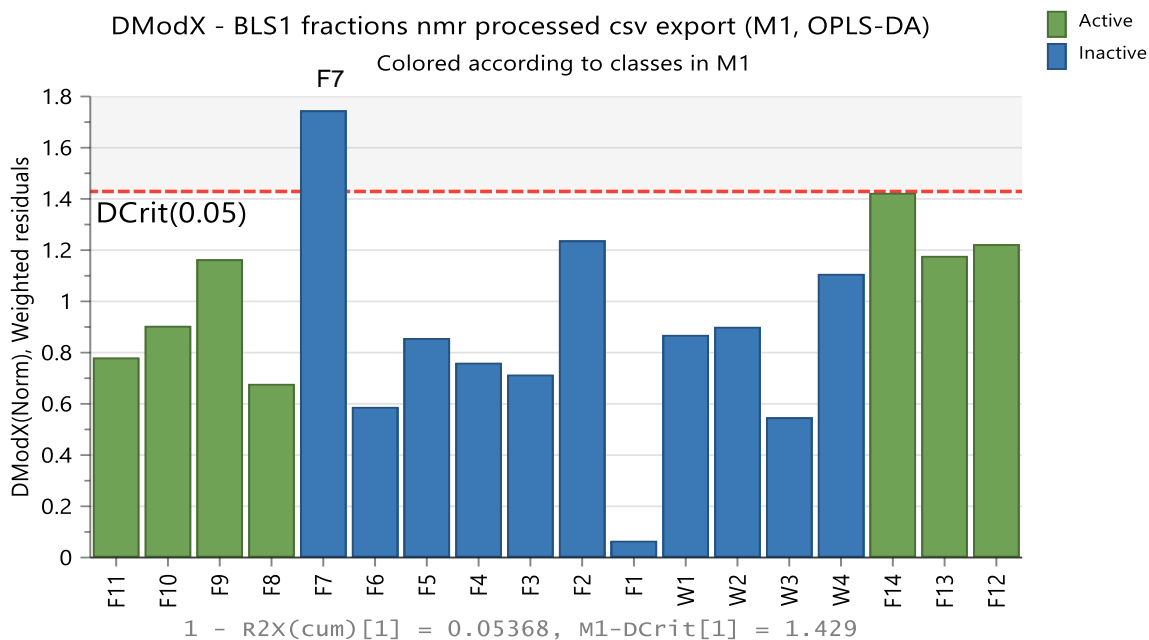
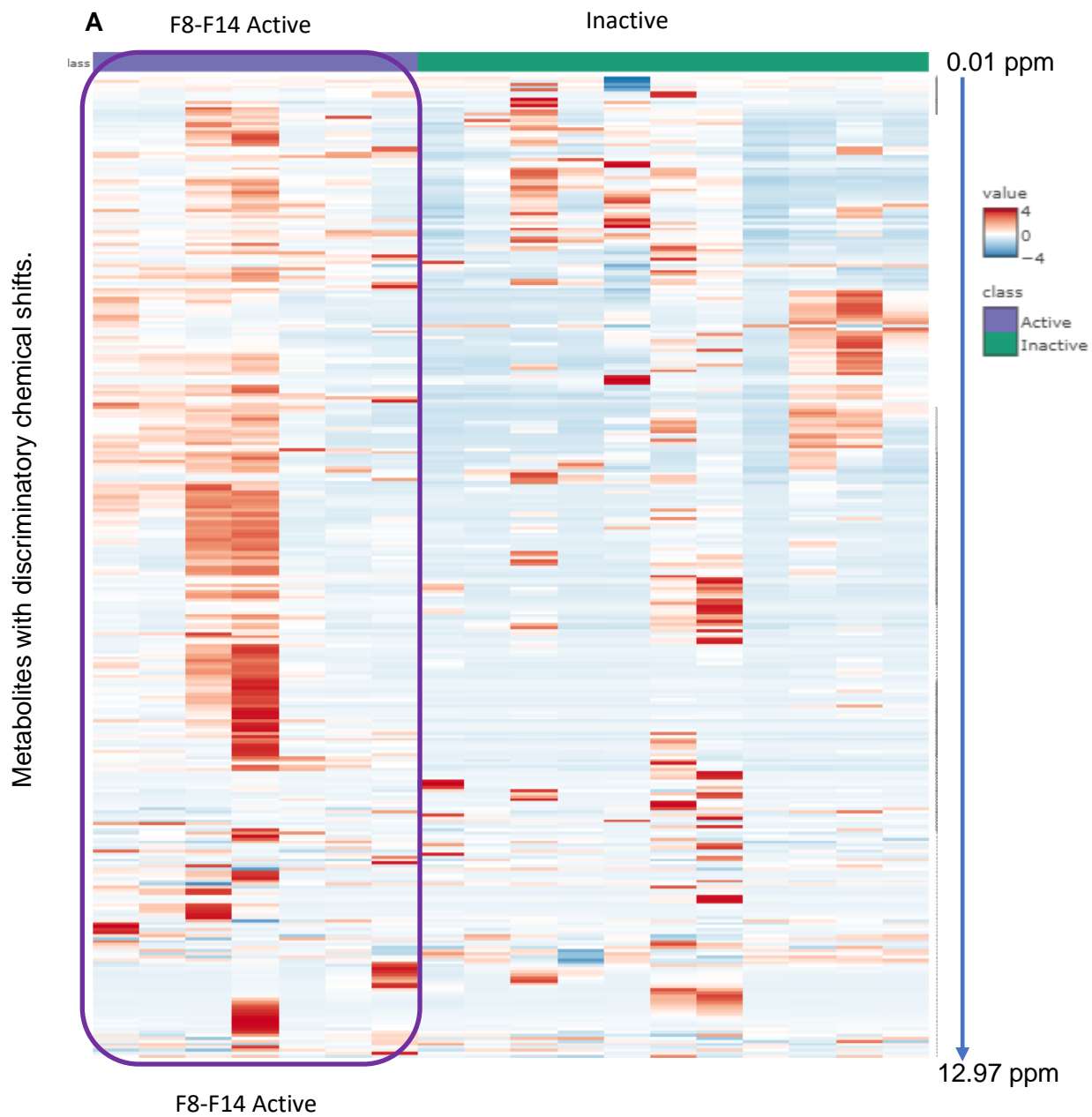
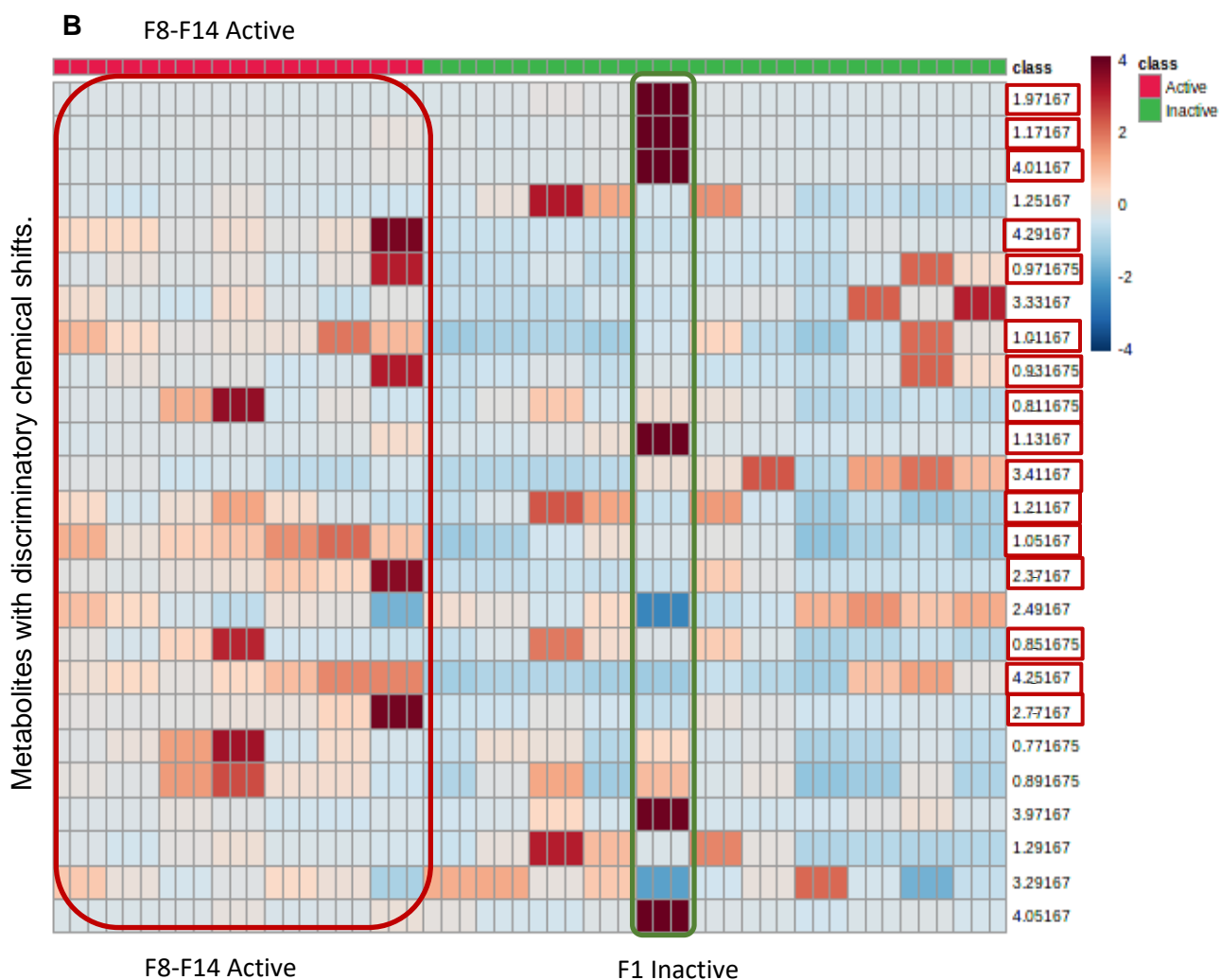


Figure 4.15: DMod X results to test the occurrence of true outliers. Variables above the red line are the true outliers that includes only fraction 8.



Extracts obtained from *F. proliferatum* fractions.

Figure 4.16A: Heatmap analysis of the NMR spectral data of *F. proliferatum* fractions generated by MetaboAnalyst®. The purple boxed fractions (F8-F14) are those biologically active against MRSA along with the discriminating chemical shifts.



Extracts obtained from 4 different media.

Figure 4.16B: Heatmap analysis of the NMR spectral data of *F. proliferatum* fractions generated by MetaboAnalyst®. The red boxed fractions (F8-F14) are those biologically active against MRSA along with the discriminating chemical shifts. The green boxed fraction (F1) was discriminatory but inactive. Highlighted chemical shifts on the Y-axis indicate common metabolites observed on the heatmap and VIP.

4.2.8 LC-HRMS analysis of *F. proliferatum* fractions

Multivariate analysis of the HR-LCMS spectral data was done, the unsupervised PCA scores plot showed the fractions to be at proximity with each other, and mostly clustered on the upper quadrant, except for F11 to F14 which showed to be an outlier (Figure 4.17A). The loadings plot (Figure 4.17B) indicated the presence of discriminating metabolites with low to high m/z values ranging between 388 to 1034 Da. The discriminating metabolites obtained from the outlying extracts with Mzmine IDs P4667 and P158, represented by m/z 388.142 (Rt 11.95) and 1022.67 (28.82) were putatively identified as 14-carboxyhexanorleukotriene E₃ (**29**) and *Bacillus amyloliquefaciens* Surfactin (**30**) respectively, while others gave no hits. Biosurfactants (BSs) are surface-active compounds produced by the genus *Bacillus* and diverse microorganisms. They possess biological activities such as antimicrobial, antibiofilm and antiadhesive effects that can lead to important applications in combating many infections (Englerová *et al.*, 2021), while 9-[(2-amino-2-carboxyethyl) thio]-10-hydroxy-3,5,7-tetradecatrienedioic acid is a human metabolite of leukotriene E₄ in humans. The model gave goodness of fit, (R_2) and predictability, Q_2 values as 1.0 and 0.997, respectively after 17 components. The dereplicated discriminating features of *F. proliferatum* fractions were shown in Table 4.8. Structures of the discriminating target bioactive metabolites against MRSA predicted by PCA loadings plots were presented in Figure 4.19.

The OPLS-DA of the active versus the inactive fractions gave fitness and predictability scores of 0.999 and 0.788 respectively. This indicated good fit and prediction of the generated OPLS-DA model. The difference between group R_2X_0 [1] is equal to 21.5 % and the difference within groups R_2X [2] is 14.1 %. The scores plot (fig. 4.18A) shows a very good separation between the active versus inactive fractions, and a decreased disparity within the active fractions. The active fractions (red circles) were on the left quadrant, while the inactive fractions (blue circles) were on the right quadrant. Fraction 11 was an outlier. The discriminating features for the active fractions were more diverse with ion peaks ranging between m/z 180 and 1020 Da. Discriminatory active fractions with Mzmine IDs of P1087, N3540, P905, P152, and P700, represented by m/z 180.102, 223.098, 347.115, 383.075, 416.206 Da, respectively were putatively identified by dereplication to be fusaric acid, fujikurin A, breynolide, bikaverin, and fusarin A. Fusaric acid is an antibiotic derived from picolinic acid, and was first isolated from the fungus *Fusarium heterosporium* (Yabuta, 1934). It is typically isolated from various *Fusarium* species and is a prospective metabolite for various therapeutic applications. Fusarins are polyketides that are derived from amino acids and belong to the class of mycotoxins produced mainly by the fungi *Fusarium*. It can infect agriculturally important crops such as oats, wheat, barley, corn, and rye. The discriminating

features of *F. proliferatum* fractions were dereplicated in Table 4.9. Structures of the discriminating target bioactive metabolites against MRSA predicted by OPLS-DA loadings S-plots were presented in Figure 4.19.

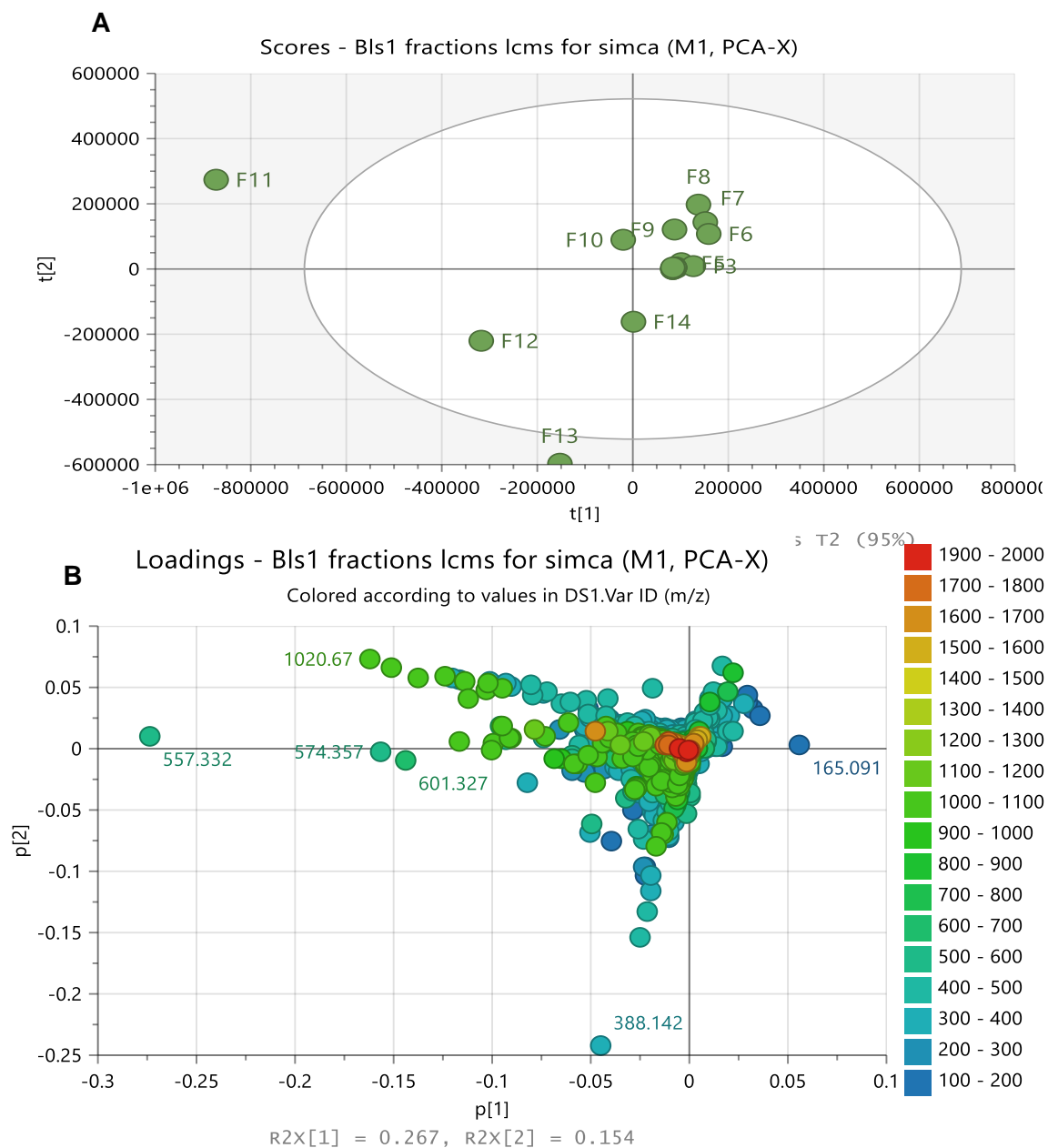


Figure 4.17: PCA scores (A) and loadings (B) plots of the LC-HRMS data of *F. proliferatum* fractions. Labelled features represent the discriminating ion peaks for the outlier F11 to F14. The R_2 and Q_2 values were 1.0 and 0.997 respectively.

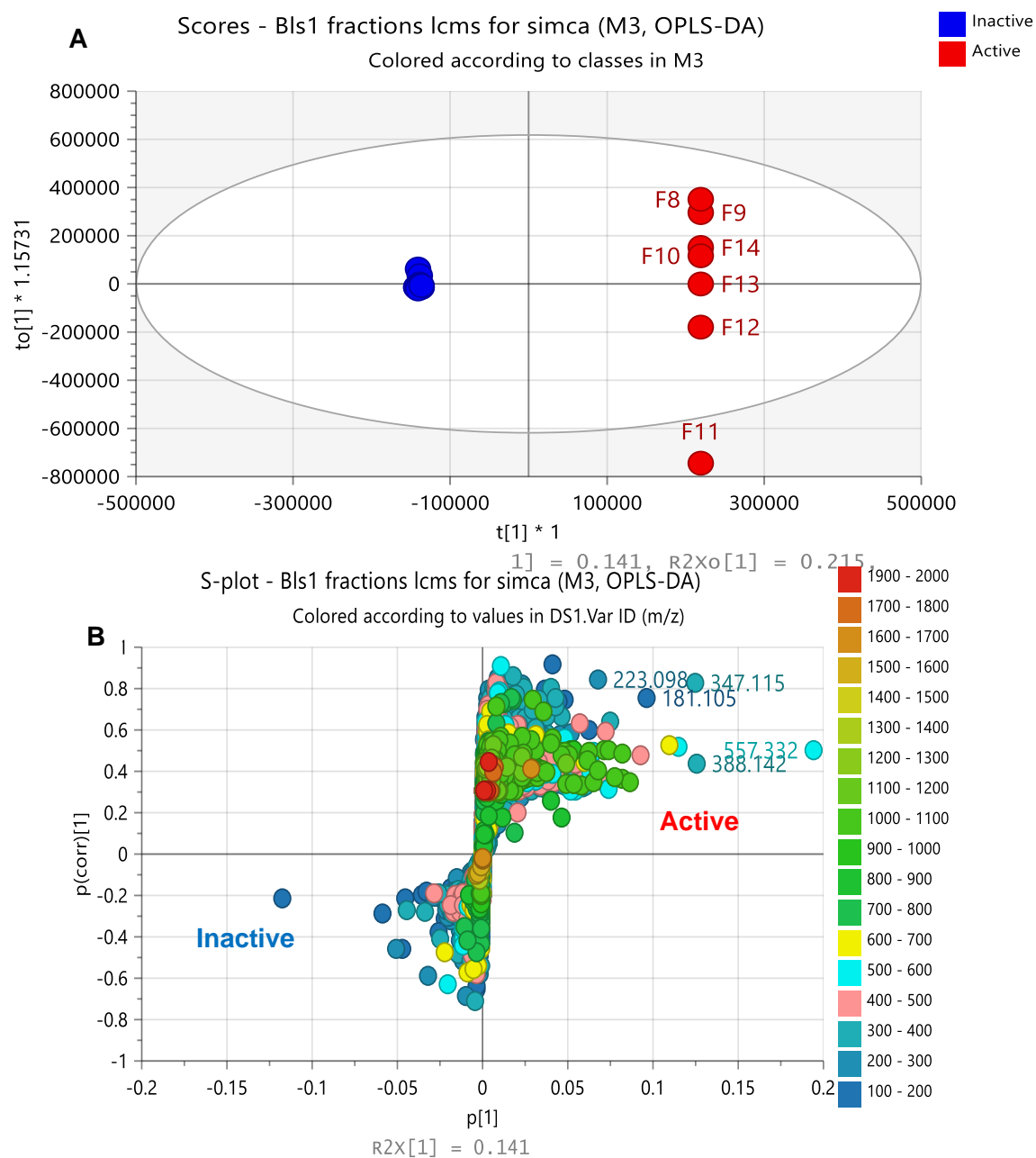


Figure 4.18: OPLS-DA scores (A) and S-plot (B) of the LC-HRMS data of *F. proliferatum* fractions. Labeled features represent the discriminating active fractions. The R_2 and Q_2 values were 0.999 and 0.788 respectively. The difference between group R_2Xo [1] is equal to 21.5 % and the difference within groups R_2X [2] is 14.1 %.

Table 4.8: Dereplication of the discriminating metabolites of *F. proliferatum* fractions obtained from the PCA loadings plot on Figure 4.17B.

Mzmine ID	<i>m/z</i>	Rt	M.wt	Molecular Formular (DBE)	Compound hits	Biological source
P4667	388.142	11.95	387.134	C ₁₇ H ₂₅ NO ₇ S (6)	14-carboxyhexanorleukotriene E ₃ (29)	Metabolite of Leukotriene E4
N3515	414.287	13.92	415.295	C ₂₃ H ₃₇ N ₅ O ₂ (8)	No hit	
P150	557.332	16.10	556.324	C ₂₉ H ₄₈ O ₁₀ (6)	No hit	
P155	574.357	16.16	573.35		[M+NH ₃] adduct of <i>m/z</i> 557.3316	
N3516	601.327	16.11	602.334	C ₃₃ H ₃₈ N ₁₂ (21)	No hit	
N3518	1006.65	29.3463	1007.66		No hit	
P158	1022.67	28.82	1021.67	C ₅₂ H ₉₁ N ₇ O ₁₃ (8)	Surfactin 2 (30)	<i>Bacillus amyloliquefaciens</i> BO5A
N2846	1020.67	28.82	1021.67		No hit	
N3526	1020.67	28.82	1021.67	C ₅₈ H ₈₇ N ₉ O ₇ (11)	No hit	
N2645	1034.68	30.09	1035.69		No hit	

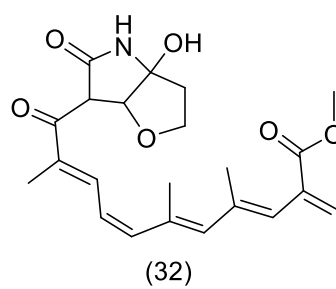
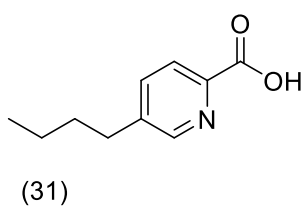
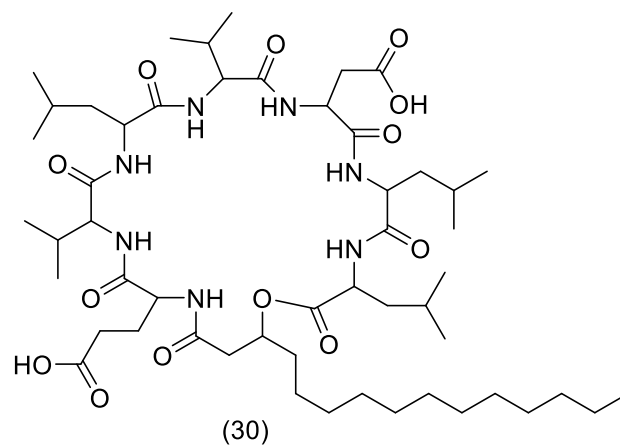
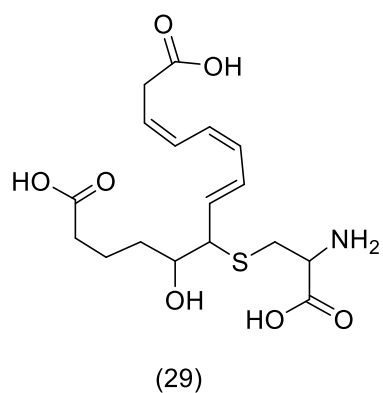


Figure 4.19: Structures of dereplicated compound hits showing PCA and OPLSDA active discriminating metabolites obtained from *F. proliferatum* fractions, as listed in table 4.8 and 4.9.

Table 4.9: Dereplication data of the discriminating antibacterial and antibiofilm-active metabolites of *F. proliferatum* fractions obtained from OPLS-DA S-Plot on Figure 4.18B. Structures are shown in Figure 4.19.

Mzmine ID	<i>m/z</i>	Rt	M.wt	<i>P-value</i>	Molecular Formular (DBE)	Compound hits	Biological source
P1087	180.102	37.67	179.094	9.67194e-08	C ₁₀ H ₁₃ NO ₂ (5)	Fusaric acid (31)	<i>Fusarium lycopersici</i> , <i>F. oxysporum</i> , <i>F. vasinfectum</i> and <i>Gibberella fujikuroi</i>
P1950	181.105	5.42	180.097	0.000316	C ₃ H ₁₂ N ₆ O ₃ (1)	No hit	
N3540	223.098	12.55	224.105	1.02606e-05	C ₁₂ H ₁₆ O ₄ (5)	Fujikurin A (6)	<i>Fusarium</i> sp. CR 377
P905	347.115	12.70	346.108	2.31868e-05	C ₇ H ₁₈ N ₆ O ₁₀ (2)	Breynolide (4)	
P152	383.075	16.99	382.068	0.003961	C ₂₀ H ₁₄ O ₈ (14)	Bikaverin (26)	Pigment from <i>F. oxysporum</i> , <i>F. solani</i> , <i>F. moniliforme</i> , <i>F. lycopersici</i> , <i>F. vasinfectum</i> , <i>F. bulbigenum-blasticola</i> , <i>Gibberella fujikuroi</i> .
P4667	388.142	11.95	387.134	0.067449	C ₉ H ₂₁ N ₇ O ₁₀ (3)	14-Carboxyhexanor-leukotriene E ₃ (29)	Metabolite of Leukotriene E4
P700	416.206	15.61	415.199	0.045673	C ₂₃ H ₂₉ NO ₆ (10)	Fusarin A (32)	<i>Fusarium moniliforme</i>
P150	557.332	16.10	556.324	0.034093		No hit	
P155	574.357	16.16	573.35	0.0276664		[M+NH ₃] adduct of <i>m/z</i> 557.3316	
N3516	601.327	16.11	602.334	0.0257685		No hit	
N3526	1020.67	30.67	1021.67	0.039743		No hit	

The fractions were re-tested to see if fraction 1 was a true outlier using DModX, and the data obtained from LCMS. Fraction 1 proved to be a true outlier, as it gave results above 0.05. As shown by the DModX plot in Figure 4.20, variables above the red line are the true outliers, which also included Fractions 4 and 2.

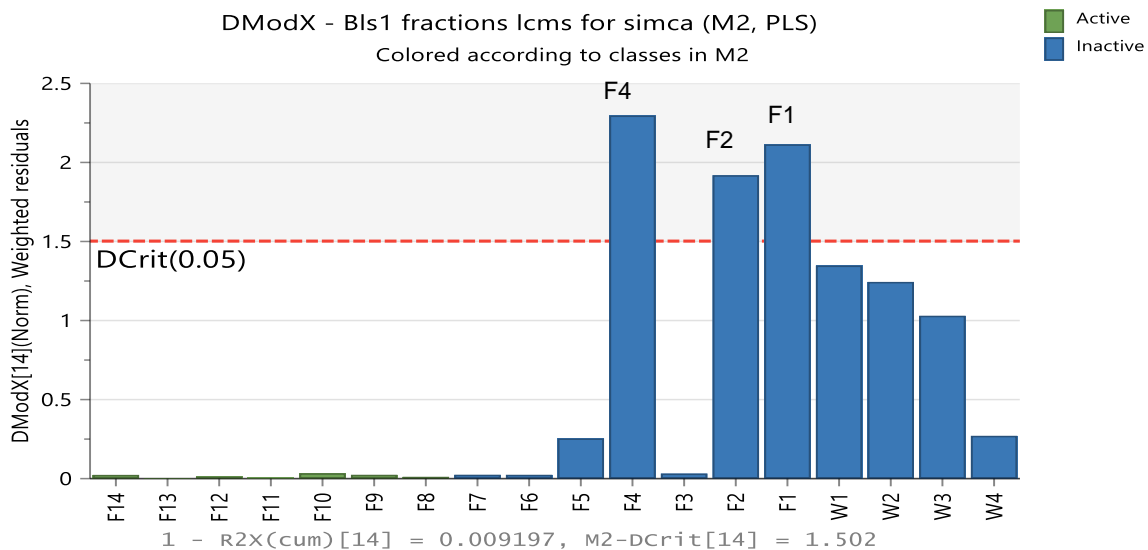
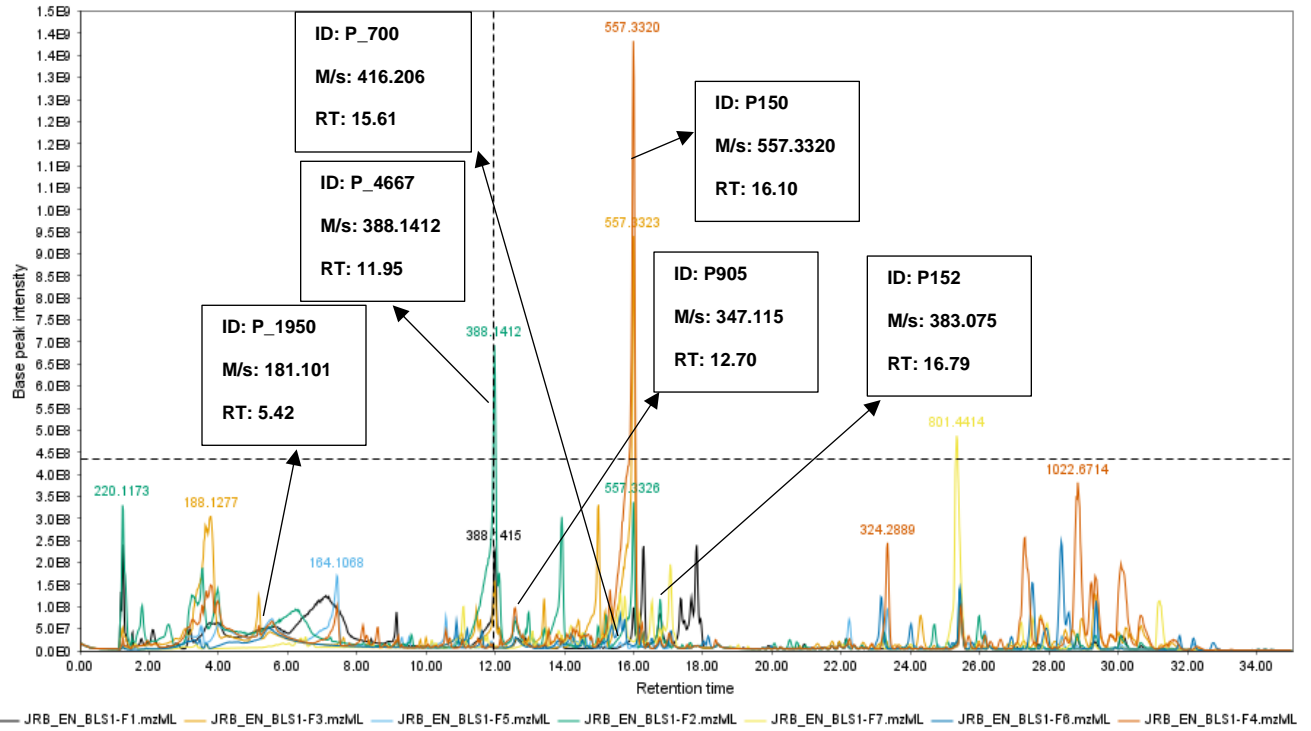


Figure 4.20: DMod X results to confirm the occurrence of true outliers. Variables above the red line are the true outliers, that includes extracts fraction 1, 2 and 4.

(A)

Base peak plot, MS1, m/s: 149.9970-1999.9546

Selected scan #1205 (F8-14 total msmL pos), RT: 11.94, base peak: 388.1413 m/s, IC: 4.3E8

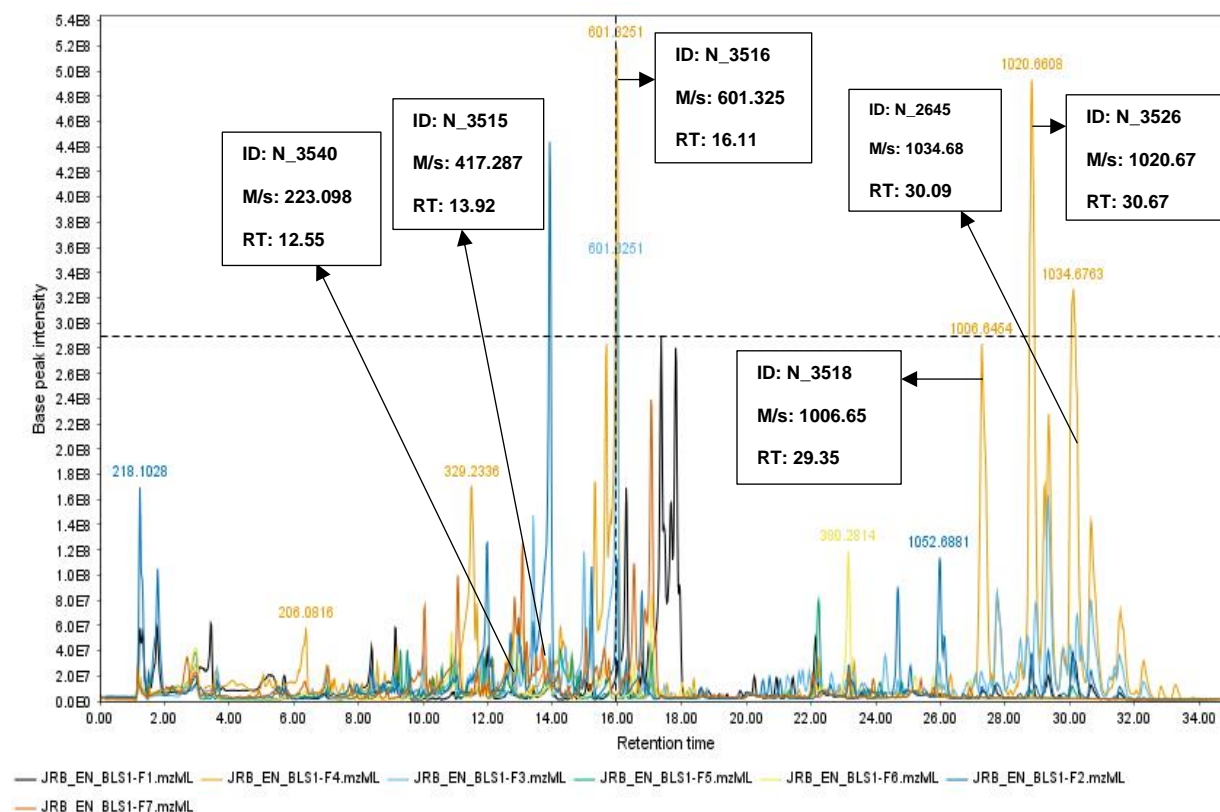


- JRB_EN_BLS1-F1 = *F. proliferatum* fraction 14
- JRB_EN_BLS1-F2 = *F. proliferatum* fraction 13
- JRB_EN_BLS1-F3 = *F. proliferatum* fraction 12
- JRB_EN_BLS1-F4 = *F. proliferatum* fraction 11
- JRB_EN_BLS1-F5 = *F. proliferatum* fraction 10
- JRB_EN_BLS1-F6 = *F. proliferatum* fraction 9
- JRB_EN_BLS1-F7 = *F. proliferatum* fraction 8

Base peak plot, MS1, m/s: 149.9998-1999.9496

(B)

Selected scan #1612 (F8-F14 total msmL neg), RT: 15.94, base peak: 601.3251 m/s, IC: 2.9E8



- JRB EN BLS1-F1 = *F. proliferatum* fraction 14
- JRB EN BLS1-F2 = *F. proliferatum* fraction 13
- JRB EN BLS1-F3 = *F. proliferatum* fraction 12
- JRB EN BLS1-F4 = *F. proliferatum* fraction 11
- JRB EN BLS1-F5 = *F. proliferatum* fraction 10
- JRB EN BLS1-F6 = *F. proliferatum* fraction 9
- JRB EN BLS1-F7 = *F. proliferatum* fraction 8

Figure 4.21: Total ion chromatogram (TIC) (A= Positive, B= Negative) of the bioactive fractions of *F. proliferatum*. The ion peaks that represent the discriminating features listed in Table 4.8 and 4.9 have been labelled.

4.2.9 Pure compound isolation

Fractions were selected for further purification work due to antimicrobial activity against MRSA. Planktonic and prebiofilm active fractions 8 to 14, and postbiofilm active fractions 6 and 7, and 18 were selected for purification work. Fractions 10, 12, 13, 14 and 18 were purified using prep TLC plates, while fractions 6, 7, 8, 9, and 11 were further fractionated. Sub-fraction F11-1 to F11-4, F8-4, and F6-9 were further purified with prep TLC plates.

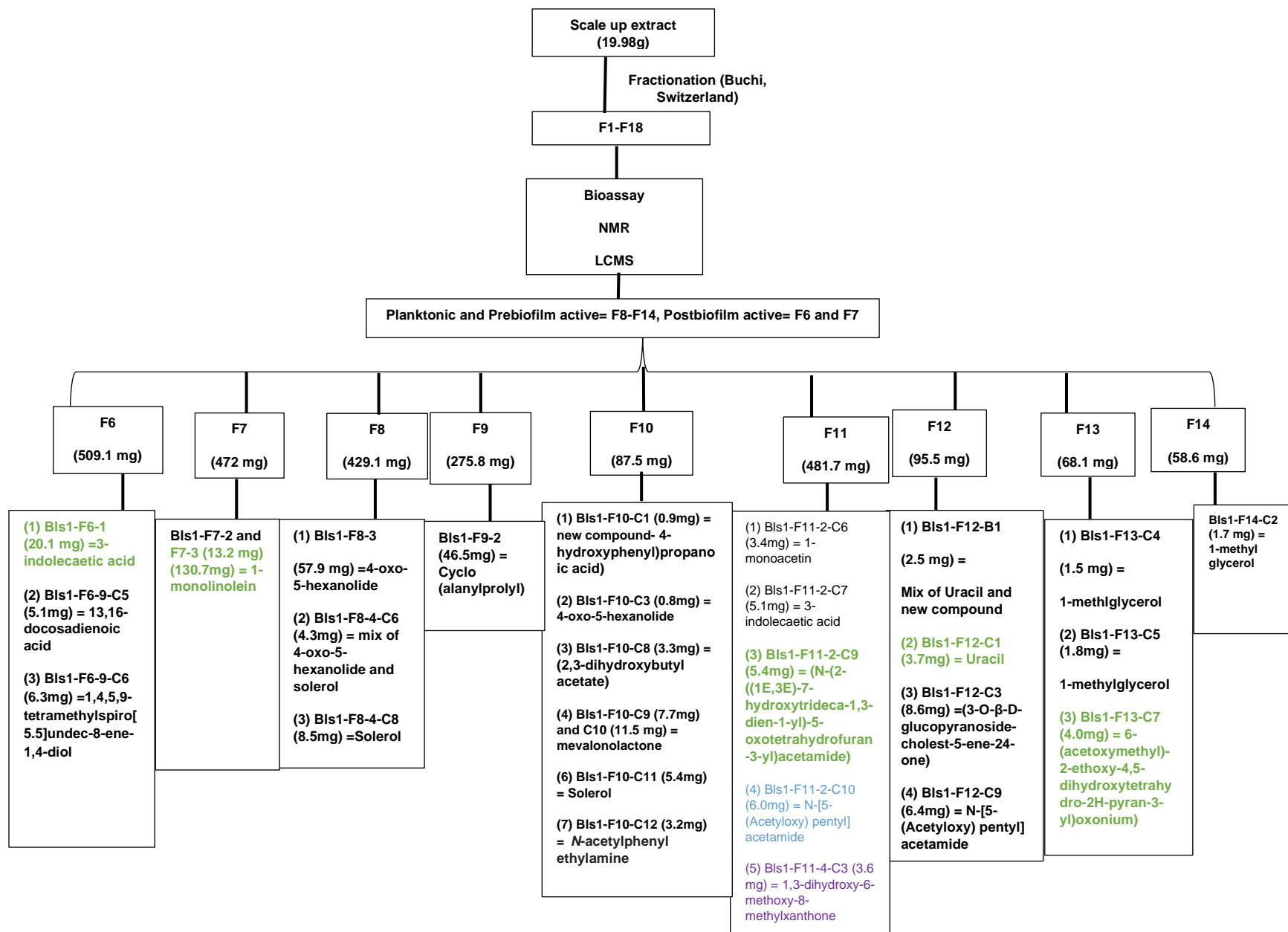


Figure 4.22: Summary workflow of *F. proliferatum* scale-up crude extract to isolated compounds. Compounds with 50% inhibition against MRSA are coloured blue, compounds with 50% inhibition against *Staphylococcus aureus* (S.A) are coloured green, while compound with 50% inhibition against both MRSA and SA was coloured purple.

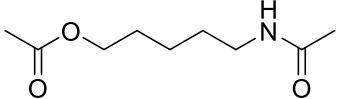
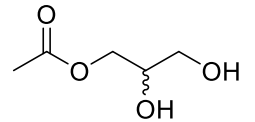
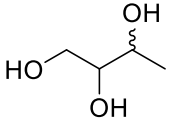
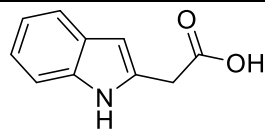
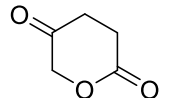
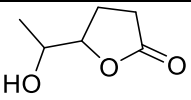
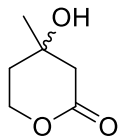
4.2.10 Structure elucidation and identification of isolated metabolites

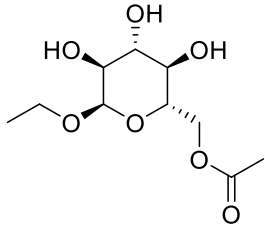
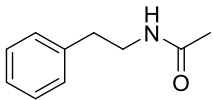
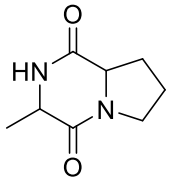
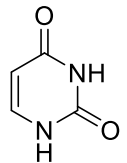
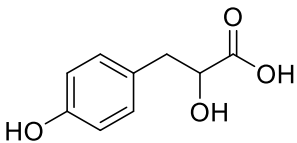
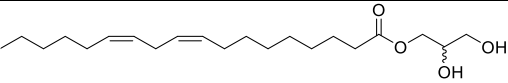
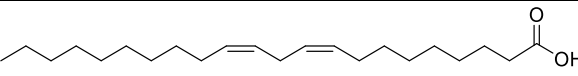
In the quest for bioactive novel compounds from *F. proliferatum*, nineteen compounds: 1-methylglycerol, uracil, N-[5-(acetyloxy) pentyl] acetamide, 1-monoacetin, 3-indoleacetic acid, 4-oxo-5-hexanolide, mevalonolactone, *N*-acetylphenylethylamine, cyclo(alanylprolyl), solerol, 1-monolinolein, 13,16-docosadienoic acid, 1,4,5,9-tetramethylspiro[5.5]undec-8-ene-1,4-diol, 2-hydroxy-3-(4-hydroxyphenyl)propanoic acid, 2,3-dihydroxybutyl acetate, *N*-(2-((1*E*,3*E*)-7-hydroxytrideca-1,3-dien-1-yl)-5-oxotetrahydrofuran-3-yl)acetamide, 1,3-dihydroxy-6-methoxy-8-methylxanthone, 3-O- β -D-glucopyranoside-cholest-5-ene-24-onec, 6-(acetoxymethyl)-2-ethoxy-4,5-dihydroxytetrahydro-2H-pyran-3-yl)oxonium were isolated.

Compounds that were active against *S.A* included 3-indoleacetic acid, 1-monolinolein, *N*-(2-((1*E*,3*E*)-7-hydroxytrideca-1,3-dien-1-yl)-5-oxotetrahydrofuran-3-yl)acetamide, uracil and 6-(acetoxymethyl)-2-ethoxy-4,5-dihydroxytetrahydro-2H-pyran-3-yl)oxonium, while *N*-[5-(acetyloxy) pentyl] acetamide was active against MRSA. Compound 1,3-dihydroxy-6-methoxy-8-methylxanthone was active against both *S.A* and MRSA.

The compounds were elucidated using ^1H NMR, 2D NMR and MS.

Table 4.10: Isolated pure compounds from *F. proliferatum*. For fraction source, underlined fractions were used for structural elucidation.

Drawn Structure	Name	Exact mass	Molecular Formula	Source Fraction	Yield (mg)	Purification method
	<i>N</i> -[5-(Acetyloxy)pentyl] acetamide New compound	187.12	C ₉ H ₁₇ NO ₃	<u>F12-C9</u> , F11-2-C10	12.4 (0.06%)	Preparative TLC
	1-monoacetin	134.06	C ₅ H ₁₀ O ₄	<u>F11-2-C6</u>	3.4 (0.02%)	Biotage and Preparative TLC
	1-methylglycerol (Coffinet <i>et al.</i> , 2020)	106.063	C ₄ H ₁₀ O ₃	<u>F13-C4</u> , F14-C2, F13-C5	5.0 (0.03%)	Preparative TLC
	3-indoleacetic acid (Singh <i>et al.</i> , 1978)	175.063	C ₁₀ H ₉ NO ₂	<u>F6-1</u> , F11-2-C7	25.2 (0.13%)	Biotage
	4-oxo-5-hexanolide	128.047	C ₆ H ₈ O ₃	<u>F8-3</u> , F10-C3, F8-4-C6	63.0 (0.32%)	Biotage
	solerol (Wishart lab in literature data-NP-MRD ID-NP0175096)	130.063	C ₆ H ₁₀ O ₃	<u>F8-4-C8</u> , F8-4-C6, F10-C11	13.9 (0.07%)	Biotage and Preparative TLC
	mevalonolactone (Amagata <i>et al.</i> , 1998)	130.063	C ₆ H ₁₀ O ₃	<u>F10-C9</u> , F10-C10	19.2 (0.10%)	Preparative TLC

Drawn Structure	Name	Exact mass	Molecular Formula	Source Fraction	Yield (mg)	Purification method
	6-(acetoxy methyl)-2-ethoxy-4,5-dihydroxy tetrahydro-2H-pyran-3-yl) oxonium New compound	250.105	C ₁₀ H ₁₈ O ₇	F13-C7	4.0 (0.02%)	Preparative TLC
	N-acetylphenyl ethylamine	163.100	C ₁₀ H ₁₃ NO	F10-C12	3.2 (0.02%)	Preparative TLC
	cyclo (alanyl prolyl)	168.090	C ₈ H ₁₂ N ₂ O ₂	F9-2	46.5 (0.23%)	Flash Chromatography-Grace
	uracil	112.027	C ₄ H ₄ N ₂ O ₂	F12-C1, F12-B1	3.7 (0.02%)	Preparative TLC
	2-hydroxy-3-(4-hydroxyphenyl) propanoic acid)	182.058	C ₉ H ₁₀ O ₄	F10-C1, F12-B1	0.9 (0.01%)	Preparative TLC
	1-monolinolein	410.340	C ₂₅ H ₄₆ O ₄	F7-3, F7-2	147.6 (0.74%)	Biotage
	13,16-docosadienoic acid	336.303	C ₂₂ H ₄₀ O ₂	F6-9-C5	5.1 (0.03%)	Preparative TLC

Drawn Structure	Name	Exact mass	Molecular Formula	Source Fraction	Yield (mg)	Purification method
A complex steroid molecule with a glucose moiety attached to the C-3 position and a ketone group at C-24.	(3-O-β-D-glucopyranoside-cholest-5-ene-24-one) New compound	562.387	C ₃₃ H ₅₄ O ₇	F12-C3	8.6 (0.04%)	Preparative TLC
A molecule consisting of a 5-oxotetrahydrofuran ring substituted with an acetamide group and a long chain containing two double bonds and a hydroxyl group.	(N-(2-((1E,3E)-7-hydroxytrideca-1,3-dien-1-yl)-5-oxotetrahydrofuran-3-yl)acetamide) New compound	337.2253	C ₁₉ H ₃₁ NO ₄	F11-2-C9	5.4 (0.03%)	Biotage and Preparative TLC
Two spirocyclic rings (a cyclohexene and a cyclohexane) sharing a single carbon atom, with four methyl groups and two hydroxyl groups attached.	1,4,5,9-tetramethyl spiro[5.5]undec-8-ene-1,4-diol (compared with 4-acorene-9,11-diol in (Jiang <i>et al.</i> , 2019). New compound	238.1993	C ₁₅ H ₂₆ O ₂	F6-9-C6	6.3 (0.03%)	Biotage and Preparative TLC
A four-carbon chain with hydroxyl groups at C-2 and C-3, and an acetate group at C-1.	2,3-dihydroxy butyl acetate New compound	148.07	C ₆ H ₁₂ O ₄	F10-C8	3.3 (0.02%)	Preparative TLC
A xanthone skeleton with hydroxyl groups at C-1 and C-3, a methoxy group at C-6, and a methyl group at C-8.	1,3-dihydroxy-6-methoxy-8-methylxanthone (Buitrago Díaz <i>et al.</i> , 2010)	272.0685	C ₁₅ H ₁₂ O ₅	F11-4-C3	3.6 (0.02%)	Preparative TLC

4.2.11 Bioactivity test results

The pure compounds obtained from purification of *F. proliferatum* were subjected to biological assay against MRSA ATCC 43300 and *S. aureus* (S.A) NCTC 8325. The bioassay protocol for S.A was similar to the one used for MRSA. It was observed that F11-4-C3 (6,1,3-dihydroxy-6-methoxy-8-methylxanthone) showed planktonic activity of 65.81%, while F11-2-C10 (*N*-[5-(acetyloxy) pentyl] acetamide) showed only postbiofilm activity of 52.73% against MRSA at 100µg/ml. Other pure compounds were inactive against MRSA.

It was also observed that F7-3 (1-monolinolein) and F11-4-C3 (1,3-dihydroxy-6-methoxy-8-methylxanthone) showed planktonic activity of 50.10% and 66.64%, while F6-1 (3-indoleacetic acid), F13-7 (6-(acetoxymethyl)-2-ethoxy-4,5-dihydroxytetrahydro-2H-pyran-3-yl)oxonium), F12-C1 (uracil) and F11-2-C9 (*N*-(2-((1*E*,3*E*)-7-hydroxytrideca-1,3-dien-1-yl)-5-oxotetrahydrofuran-3-yl)acetamide) showed prebiofilm activity of 63.09%, 53.60%, 56.81% and 69.97% respectively against SA-NCTC 8325 at 100µg/ml.

IC₅₀ (µM) for the isolated 19 compounds were not obtainable, as they did not exhibit bioactivity above the recommended 70% threshold.

Effect of pure compounds isolated from *F. proliferatum* on MRSA and SA-NCTC 8325

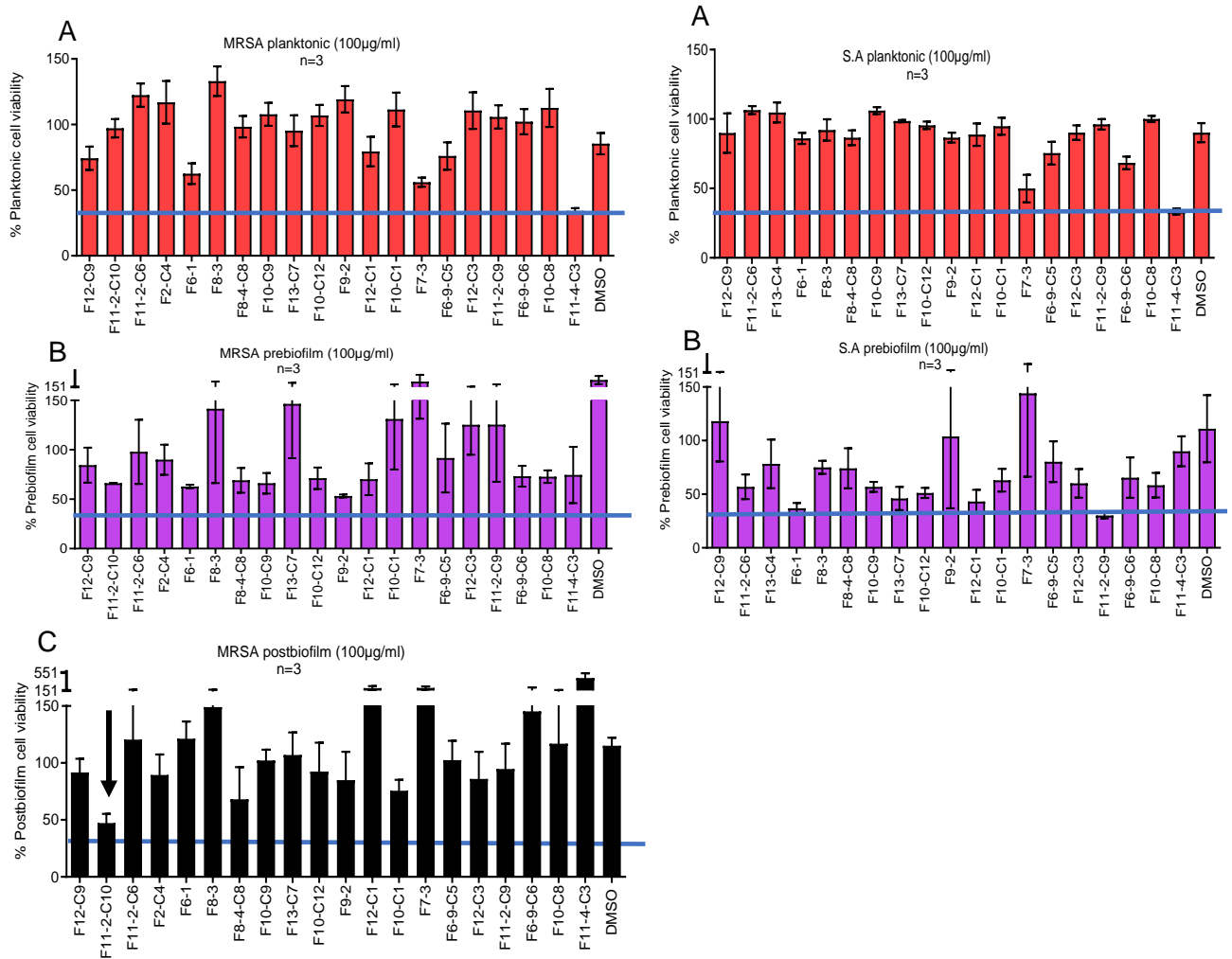


Figure 4.23: Effect of pure compounds isolated from *F. proliferatum*. Left-planktonic (A), prebiofilm (B), and postbiofilm (C) MRSA. Right- planktonic (A) and prebiofilm (B) SA-NCTC 8325 at 100µg/mL. The blue line indicates the bioactivity threshold which is 30% viability (70% inhibition).

Due to the poor or weak bioactivity of the isolated compounds, all the isolated compounds were revisited on their position on the OPLS-DA plot shown in Figures 4.13 and 4.6, using their MW as filters for the observable variables (Figures 4.24 and 4.25). It indicated that 10 of the isolated compounds namely 3-indolecaetic acid (175.063), 2-hydroxy-3-(4-hydroxyphenyl)propanoic acid) (182.058), *N*-[5-(acetyloxy) pentyl] acetamide (187.121), 1,4,5,9-tetramethylspiro[5.5]undec-8-ene-1,4-diol (238.193), 6-(acetoxymethyl)-2-ethoxy-4,5-dihydroxytetrahydro-2H-pyran-3-yl)oxonium (250.120), 1,3-dihydroxy-6-methoxy-8-methylxanthone (272.069), *N*-(2-((1*E*,3*E*)-7-hydroxytrideca-1,3-dien-1-yl)-5-oxotetrahydrofuran-3-yl)acetamide (337.226), *N*-acetylphenylethyl-amine (163.099), 1-monolinolein (354.276) and 3-*O*- β -D-glucopyranoside-cholest-5-ene-24-one (562.372) were found on the active right quadrant on the OPLS-DA plots. This signifies that, the earlier predicted isolated compounds were working in synergy to be active against MRSA, hence separating or isolating the compounds made them lose their synergistic property, resulting to the poor or weak bioactivity observed on the isolated compounds. Compound 272.069 (1,3-dihydroxy-6-methoxy-8-methylxanthone) was found in the active quadrant confirming its bioactivity at the crude and compound stage. The isolated compounds identified on the active quadrant by OPLS-DA with their corresponding MW are listed in Table 4.11.

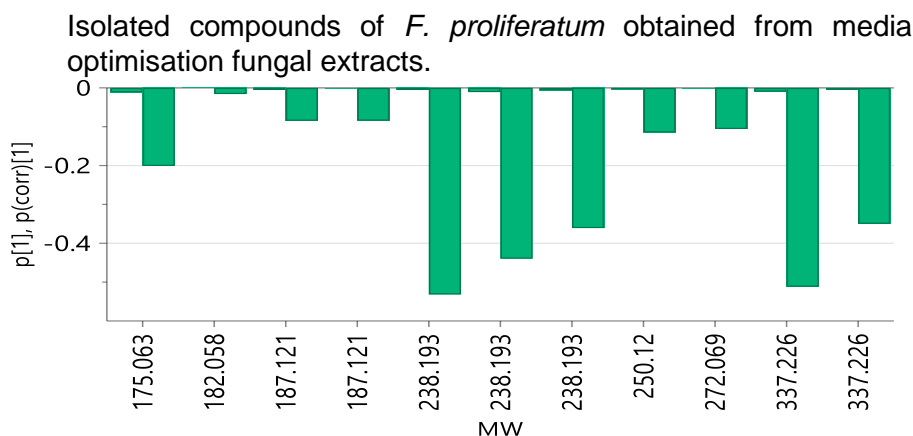


Figure 4.24: Distribution of the isolated compounds on the active quadrant by OPLS-DA showing predicted compounds with molecular weights 175.063 (3-indolecaetic acid), (182.058) (2-hydroxy-3-(4-hydroxyphenyl)propanoic acid), 187.121 (*N*-[5-(acetyloxy) pentyl] acetamide), 238.193 (1,4,5,9-tetramethylspiro[5.5]undec-8-ene-1,4-diol), 250.120 (6-(acetoxymethyl)-2-ethoxy-4,5-dihydroxytetrahydro-2H-pyran-3-yl)oxonium), 272.069 (1,3-dihydroxy-6-methoxy-8-methylxanthone), 337.226 (*N*-(2-((1*E*,3*E*)-7-hydroxytrideca-1,3-dien-1-yl)-5-oxotetrahydrofuran-3-yl)acetamide).

Isolated compounds of *F. proliferatum* fungal extract obtained from scale up fractions extract on rice media.

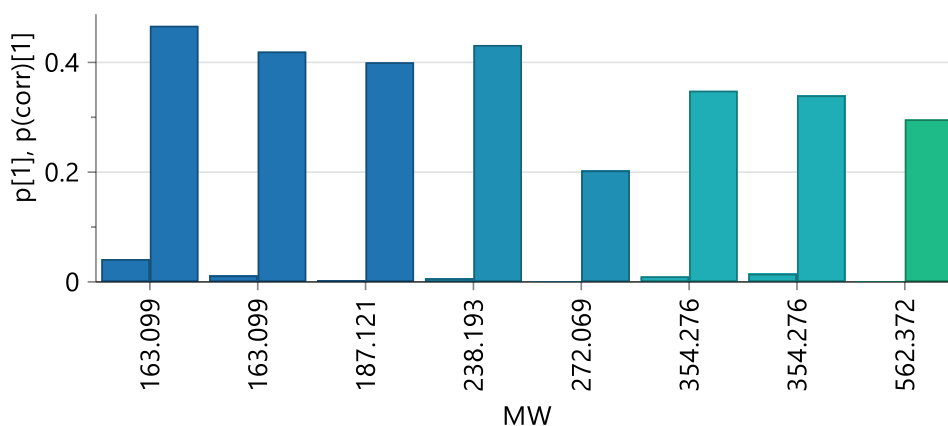


Figure 4.25: Distribution of the isolated compounds on the active quadrant by OPLS-DA showing predicted compounds with molecular weights 163.099 (*N*-acetylphenylethyl-amine), 187.121 (*N*-[5-(acetyloxy) pentyl] acetamide), 238.193 (1,4,5,9-tetramethylspiro[5.5]undec-8-ene-1,4-diol), 272.069 (1,3-dihydroxy-6-methoxy-8-methylxanthone), 354.276 (1-monolinolein) and 562.372 (3-O- β -D-glucopyranoside-cholest-5-ene-24-one).

Table 4.11: Isolated compounds observed on OPLS-DA active quadrants. Highlighted rows represent the bioactive metabolites.

Isolated compounds	Name	MW	Biofilm Stages of Observed Bioactivity	Observed / unobserved on OPLS-DA active quadrant from the fraction stage (MW, primary ID, rt)	Isolated compounds observed on OPLS-DA active quadrant as obtained from media optimisation stage (MW, primary ID, rt)
Bls1-F13-C4	1-methylglycerol	106.063	Inactive	Not detected*	Not detected*
Bls1-F12-C1	uracil	112.027	Inactive	Not detected*	Not detected*
Bls1-F11-2-C6	1-monoacetin	134.06	Inactive	Not detected*	Not detected*
Bls1-F6-1	3-indolecaetic acid	175.063	Inactive	Inactive quadrant (175.063)	Observed in active quadrant (175.063, P4923, rt= 8.26)
Bls1-F12-C9 New compound	<i>N</i> -[5-(acetyloxy)pentyl] acetamide	187.121	Postbiofilm (52.73%)	Observed in active quadrant (187.121, P3057, rt= 28.08)	Observed in active quadrant (187.121, P686, rt= 5.31)
Bls1-F8-3	4-oxo-5-hexanolide	128.047	Inactive	Not detected*	Not detected*
Bls1-F8-4-C8	solerol	130.063	Inactive	Not detected*	Not detected*
Bls1-F10-C9	mevalonolactone	130.063	Inactive	Not detected*	Not detected*
Bls1-F10-C12	<i>N</i> -acetylphenylethylamine	163.100	Inactive	Observed in active quadrant (163.099, P641, rt=7.59)	inactive quadrant (163.100)
Bls1-F9-2	cyclo(alanylprolyl)	168.090	Inactive	Not detected*	Not detected*
Bls1-F7-3	1-monolinolein	354.277	Inactive	Observed in active quadrant (354.276, P360, rt=20.13)	inactive quadrant (354.276)
Bls1-F6-9-C5	13,16-docosadienoic acid	336.303	Inactive	Not detected*	Not detected*
Bls1-F13-C7 New compound	6-(acetoxymethyl)-2-ethoxy-4,5-dihydroxytetrahydro-2H-pyran-3-yl)oxonium	250.105	Inactive	Inactive quadrant (250.103)	Observed in active quadrant (250.120, P3649, rt= 15.67)
Bls1-F10-C1	2-hydroxy-3-(4-hydroxyphenyl)propionic acid)	182.058	Inactive	Inactive quadrant (182.057)	Observed in active quadrant (182.058, P5314, rt= 16.80)

Isolated compounds	Name	MW	Biofilm Stages of Observed Bioactivity	Observed / unobserved on OPLS-DA active quadrant from the fraction stage (MW, primary ID, rt)	Isolated compounds observed on OPLS-DA active quadrant as obtained from media optimisation stage (MW, primary ID, rt)
Bls1-F11-2-C9 New compound	<i>N</i> -(2-((1 <i>E</i> ,3 <i>E</i>)-7-hydroxytrideca-1,3-dien-1-yl)-5-oxotetrahydrofuran-3-yl)acetamide	337.225	Inactive	Inactive quadrant (337.225)	Observed in active quadrant (337.226, N4326, rt= 15.66)
Bls1-F10-C8 New compound	2,3-dihydroxybutyl acetate	148.074	Inactive	Not detected*	Not detected*
Bls1-F12-C3 New compound	3-O-β-D-glucopyranoside-cholest-5-ene-24-one	562.387	Inactive	Observed in active quadrant (562.372, N16502, rt= 27.96)	Inactive quadrant (562.383)
Bls1-F6-9-C6 New compound	1,4,5,9-tetramethylspiro[5.5]undec-8-ene-1,4-diol	238.1933	Inactive	Observed in the inactive quadrant (238.1933, P6250, rt= 6.19)	Observed in the inactive quadrant (238.1933, P4625, rt= 16.84)
Bls1-F11-4-C3	1,3-dihydroxy-6-methoxy-8-methylxanthone	272.0685	Planktonic (65.81%)	Observed in active quadrant (272.069, N10512, rt= 9.96)	Observed in active quadrant (272.069, N4553, rt= 11.33)

*Compounds were not detected during the fraction and optimisation stage because their MWs were outside the measuring range of 150-1500 Da.

4.3 Summary and conclusion

4.3.1 Isolation of fungi and extraction

In this study, endophytic fungi *F. proliferatum* was isolated from the stem of *V. amygdalina*. *F. proliferatum* possess an extraordinary broad host range, and has been isolated from at least 25 plant species, including at least two conifer genera, multiple dicot genera, monocot crops such as maize, rice and wheat (Rim *et al.*, 2005, Ghiasian *et al.*, 2005, Galván *et al.*, 2008, Tsavkelova *et al.*, 2008) but there are no records of its isolation from *V. amygdalina*. Therefore, to the best of our knowledge, this will be the first time it will be isolated from *V. amygdalina*.

Crude extract of *F. proliferatum* proved to be very active (>80%) against MRSA but was inactive to *P. aeruginosa*.

4.3.2 Media optimisation and metabolomics bioassay guided isolation

Media optimisation showed *F. proliferatum* extracts from rice, malt, and potato media to be active against MRSA, with the fungal extract obtained from rice media cultivated for 15 days to be the optimum media for the scale up of *F. proliferatum*, as it gave an average weight of 1.56 g, 89.45% inhibition rate and completely inhibited biofilm formation. In terms of bioactivity, the optimum media in decreasing order was rice > malt > potato > oat. *F. proliferatum* extracts obtained from oat media were inactive. The oat media extracts were high in lipids, which could have prevented the fungi from metabolising sufficient nutrients from the media. The ¹H NMR data obtained from *F. proliferatum* extracts after incubation in oat media showed that the fungus may not be effectively metabolising media nutrients, resulting in poor secondary metabolite production.

The bioactivity of the fungal extract obtained from rice media could be because of the sugars present in rice, which it was probably utilising to produce the desired secondary metabolites. Previous literature has shown that *F. proliferatum* is attracted to sugars, which it uses to produce fumonisins as a source of carbon (Wu *et al.*, 2019). Furthermore, proton signals from the rice media extract at 0.50 to 2.20 ppm, 4.0 to 4.5 ppm, 5.0 to 5.5 ppm and 7.0 to 7.5 ppm indicated the presence of aliphatics, sugars, olefinics and aromatic compounds respectively. The huge intensity signals at 1.00 to 2.00 ppm were typical for methylene units of a long fatty acid chain. These compounds could have acted in synergy to bring about the bioactivity of the fungal extracts obtained from rice media by efficiently assisting in the absorbance of more bioactive metabolites through the microbial cell wall.

The dereplicated compound hits produced from rice, oat, malt, and potato media extract were quite different amongst the different media extracts (for example, the dereplicated compound

hits observed in rice media extract was different from the compound hits observed in malt media extract), except for *N*-Isopropyl-benzylamine, which was observed in both rice and oat media. It was found at the ion peak m/z 150.127 [M+H] for $C_{10}H_{15}N$, exhibited by P1155. Also, the dereplicated compound hits produced from media optimisation and scaled up fractions were different, except for bikaverin (m/z 383.075 [M+H], P121 for $C_{20}H_{14}O_8$), fujikurin A (m/z 225.112 [M+H, P417, $C_{12}H_{16}O_4$) and breynolide (m/z 347.115 [M+H], P905, $C_7H_{18}N_6O_{10}$), which were common metabolites produced in both stages. These compounds were not easy to isolate probably because the feasibility of isolating these compounds was highly dependent on their relative abundance. These compounds were easy to detect by ESI-mass spectrometry due to their excellent ionisation capability in such MS conditions but their low yields at microgram levels made these compounds impossible to isolate. The differences in metabolites produced from the different media could also have occurred due to changes in media composition and incubation time. This proves the OSMAC approach, where one fungus produces different metabolites due to its cultivation in different media. The different media used to cultivate *F. proliferatum* could have led to the variations in metabolites produced between the different media, and between the media optimisation and fraction stages.

Most of the dereplicated discriminatory compound hits observed at the crude extract stage were known fusarium chemotaxonomic markers with m/z 180.102, 225.112, 165.091, 287.236, 784.415, 383.075, 416.206 representing fusaric acid, fujikurin A, fusalanipyrone, fusoxysporone, beauvericin, bikaverin, and fusarin A respectively (Son *et al.*, 2008, von Bargen *et al.*, 2015, Abraham and Hanssen, 1992). These compounds could be responsible for the bioactivity observed at the crude extract stage as most fusarium compounds are known to be bioactive. However, these dereplicated compounds were not isolated in this study, as they might have low yields at microgram levels making these compounds impossible to isolate.

4.3.3 Pure compounds isolation

Scale-up of the fungus was carried out on rice media which was the optimum media. Fractionation was carried out on the scaled up crude extract using hexane and EtOAc as eluting solvents. Nineteen compounds were isolated from bioactive fractions of *F. proliferatum* as shown in Table 4.11 which includes; 1-methylglycerol, uracil, *N*-[5-(acetyloxy) pentyl] acetamide, 1-monoacetin, 3-indoleacetic acid, 4-oxo-5-hexanolide, mevalonolactone, *N*-acetylphenylethylamine, cyclo(alanylprolyl), solerol, 1-monolinolein, 13,16-docosadienoic acid, 1,4,5,9-tetramethylspiro[5.5]undec-8-ene-1,4-diol, 2-hydroxy-3-(4-hydroxyphenyl)propanoic acid, 2,3-dihydroxybutyl acetate, *N*-(2-((1*E*,3*E*)-7-hydroxytrideca-1,3-dien-1-yl)-5-oxotetrahydrofuran-3-yl)acetamide, 1,3-dihydroxy-6-methoxy-8-

methylxanthone, 3-O- β -D-glucopyranoside-cholest-5-ene-24-onec, 6-(acetoxymethyl)-2-ethoxy-4,5-dihydroxytetrahydro-2H-pyran-3-yl)oxonium.

The compounds were inactive against MRSA, except 1,3-dihydroxy-6-methoxy-8-methylxanthone which showed planktonic activity of 65.81%, while F11-2-C10 (*N*-[5-(acetyloxy) pentyl] acetamide showed post biofilm activity of 52.73%. Their MIC was not done as their rate of inhibition was not above the acceptable bioactivity threshold of 70.00% inhibition. The isolated pure compounds may have needed to work in synergy with themselves or with the dereplicated discriminatory compound hits to be active, as it was observed that the metabolites were active against MRSA at the crude extract stage but was inactive after the compounds were isolated or purified.

Synergism of compounds against a pathogenic bacterium refers to the effect caused by two or more compounds that are greater than the sum of the effects of the individual compounds. Extracts may contain hundreds or even thousands of individual constituents at varying abundance and identifying the compounds responsible for a given biological effect represents a significant challenge. Sometimes, it is assumed that the behaviour of a mixture can be described by the presence of just a few known constituents, nevertheless, a number of studies have shown that the overall activity of extracts can result from mixtures of compounds with synergistic, additive, or antagonistic activity (Wagner and Ulrich-Merzenich, 2009, Junio *et al.*, 2011, Ulrich-Merzenich *et al.*, 2010), and those who work in the field of NPs research will be quick to admit that it is very often the case that isolation efforts on an extract fail because activity is lost upon fractionation (Wagner and Ulrich-Merzenich, 2009, Junio *et al.*, 2011, Ulrich-Merzenich *et al.*, 2010). It is certainly true that in some cases loss of activity occurs because multiple constituents are required to observe the biological effect (Caesar and Cech, 2019).

4.3.4 Isolation of new compounds

Compounds 6-(acetoxymethyl)-2-ethoxy-4,5-dihydroxytetrahydro-2H-pyran-3-yl)oxonium ($C_{10}H_{18}O_7$), *N*-(2-((1*E*,3*E*)-7-hydroxytrideca-1,3-dien-1-yl)-5-oxotetrahydrofuran-3-yl)acetamide ($C_{19}H_{31}NO_4$), 3-O- β -D-glucopyranoside-cholest-5-ene-24-one ($C_{33}H_{54}O_7$), 11,4,5,9-tetramethylspiro[5.5]undec-8-ene-1,4-diol ($C_{15}H_{26}O_2$), 2,3-dihydroxybutyl acetate ($C_6H_{12}O_4$), and *N*-[5-(acetyloxy) pentyl] acetamide ($C_9H_{17}NO_3$) were not found in the DNP and in CAS SciFinder. They could be regarded as new NPs, although they were inactive. When these compounds were traced back to Table 4.11, it showed that, they were in the active quadrant either in the crude extract or as a fraction, but lost their activity after isolation, hence

these compounds might need to work in synergy to be active. It can be deduced that their activity could be restored back when they are in 2 or more components in mixtures.

Furthermore, it could be that these compounds needed to be isolated from a different media, such as malt extract broth to be active.

In conclusion, crude extracts of *F. proliferatum* was active against MRSA but lost most of its bioactivity upon isolation of the compounds. It could be that the compounds were working in synergy to be active and separating them made them lose their synergistic property. Compound 1,3-dihydroxy-6-methoxy-8-methylxanthone which has proven to be bioactive from previous literatures, showed MRSA planktonic activity of 65.81%.

CHAPTER 5

5 Secondary metabolites of *F. falciforme* isolated from *M. oleifera*

5.1 Metabolites of *F. falciforme*

F. falciforme belongs to the genus of *Fusarium*. It is a member of the *Fusarium solani* Species Complex (FSSC) and can appear as a white to cream-coloured aerial mycelium. A previous work by (Sooksai *et al.*, 2019) showed that among 23 isolates of cutinase-producing fungi from Thailand, one strain of *F. falciforme* PBURU-T5 exhibited the greatest cutinase activity (3.36 ± 0.12 U ml⁻¹) against *p*-nitrophenyl butyrate. There are reports on metabolites obtained from *fusarium* sp., but to the best of our knowledge, there are no records of any metabolites obtained from *F. falciforme*.

Fusarium is seen as a member of the most dominant endophytic fungal genus in the world, with the ability to grow on a wide range of substrates and possessing efficient mechanisms for dispersal, which affect their interaction and biology with their surrounding environments, characterised genetically with extraordinary discrepancy, together with secondary metabolism that makes *Fusarium* an important group of fungi (Singh *et al.*, 2021, Villavicencio *et al.*, 2021, Yadav and Meena, 2021, Ahmed *et al.*, 2023). *Fusarium* sp. includes a large number of strains associated with agricultural productions, such as toxin producers on edible parts of plants (Desjardins, 2006), and plant pathogens (Kistler, 1997, Leslie and Summerell, 2006).

Many *Fusarium* species have been reported as plant endophytes, and this endophytic routine could have added further to their chemical diversity (Kaul *et al.*, 2016). *Fusarium* species can be found in palm plants as endophytic fungi (Song *et al.*, 2016). They are known as opportunistic pathogens, belonging to tropical fungi that grow in high rainfall conditions (Irawati *et al.*, 2014). They are pathogens to humans and can cause several diseases, such as infection of the eye and keratinocytes' cornea, as they can produce the enzyme keratinase (Mangiaterra *et al.*, 2001).

Over 100 structurally unique chemical compounds with various bioactivities such as antimicrobial, antiviral, antiparasitic, antioxidant, anticancer, and immunomodulators have been reported from *Fusarium* species. The members of this genus are also important from agricultural point of view as they have been found to produce fungicidal and nematocidal compounds and may act as biocontrol agents (Toghueo, 2020). This genus holds vast potential as reservoir of natural biochemicals which could contribute positively to human welfare (Singh *et al.*, 2021). Furthermore, plenty of evidence also indicate

that *Fusarium* possesses potential capability to produce a great number of secondary metabolites with significant biological activities, such as antimicrobial (Jayasinghe *et al.*, 2006, Wang *et al.*, 2011).

5.2 Results and Discussion

5.2.1 Media optimisation and identification of metabolite production from *F. falciforme*

Media optimisation and identification of metabolite production was carried out on the pure strain of *F. falciforme*, and the extracts were tested against MRSA. The bioactivity test results on the media optimisation of *F. falciforme* extracts (Table 5.2) showed that the extract from the rice culture media on day 7 and 15 (MgS3A R7 and MgS3A R15), malt extract broth day 7 (M7), and Potato dextrose broth 30 days (P30) showed intense activity.

5.2.2 *F. falciforme* extract yields on 4 different media.

Solid media produced higher yields of extract than liquid media. As depicted in Table 5.1, the highest yield of *F. falciforme* extract was gained from oat medium. Meanwhile, the lowest extract yields were obtained from malt broth media. *F. falciforme* obtained its highest yields on oat media incubated for 30 days.

The histogram below (Figure 5.1) shows the extract yields for *F. falciforme* at 7, 15, and 30 days of incubation on four different media. After 15 days of incubation in rice media, *F. falciforme* was seen to still be growing and metabolising the nutrients therein till 30 days, as shown from the huge difference observed between the rice media control and the rice extracts obtained from day 7, 15, and 30. For the oat media, *F. falciforme* showed a slight increase in its growth between day 7 and day 15. An exponential growth was observed on day 30 extract yield. On the other hand, for liquid media, malt extract yields started to decline after 15 days of incubation, which indicated the end of its exponential phase and beginning of the decline phase, as the extract yield was reduced at day 30. The potato dextrose broth showed an increase in extract yield from day 7 till day 30, which could be because of the endophytes ability to metabolise and use up the nutrient inherent in potato dextrose media.

The obtained weights of *F. falciforme* extracts after 7, 15, and 30 days of incubation on four different media are listed in Table 5.1.

Table 5.1: Extract weights of *F. falciforme*, grown on different media and incubated for 7, 15, and 30 days. All cultures were incubated at 27°C.

7 days		15 days		30 days		Controls	
Solid media							
MGS3A-R7-1	1254.0	MGS3A-R15-1	2419.4	MGS3A-R30-1	4510.0	RC1	747.8
MGS3A-R7-2	1295.5	MGS3A-R15-2	2519.7	MGS3A-R30-2	4686.5	RC2	809.4
MGS3A-R7-3	1347.0	MGS3A-R15-3	2435.7	MGS3A-R30-3	3706.0	RC3	865.5
Average weight (mg)	1268.8		2458.3		4300.8		807.6
MGS3A-O7-1	6427.5	MGS3A-O15-1	6956.8	MGS3A-O30-1	10810.9	OC1	5963.4
MGS3A-O7-2	6351.5	MGS3A-O15-2	6945.8	MGS3A-O30-2	7475.9	OC2	6291.9
MGS3A-O7-3	6301.2	MGS3A-O15-3	6581.4	MGS3A-O30-3	6765.7	OC3	5822.3
Average weight (mg)	6360.1		6828.0		8350.8		6025.9
Liquid media							
MGS3A-M7-1	46.3	MGS3A-M15-1	112.2	MGS3A-M30-1	85.3	MC1	7.1
MGS3A-M7-2	47.0	MGS3A-M15-2	121.0	MGS3A-M30-2	90.2	MC2	6.7
MGS3A-M7-3	41.0	MGS3A-M15-3	125.0	MGS3A-M30-3	90.0	MC3	6.2
Average weight (mg)	44.8		119.5		88.5		6.7
MGS3A-P7-1	80.6	MGS3A-P7-1	169.1	MGS3A-P30-1	268.3	PC1	15.5
MGS3A-P7-2	54.5	MGS3A-P7-2	169.0	MGS3A-P30-2	252.8	PC2	9.9
MGS3A-P7-3	86.1	MGS3A-P7-3	130.8	MGS3A-P30-3	275.3	PC3	11.3
Average weight (mg)	73.7		156.3		265.5		12.2

*Media code and full names are listed in Table 4.2

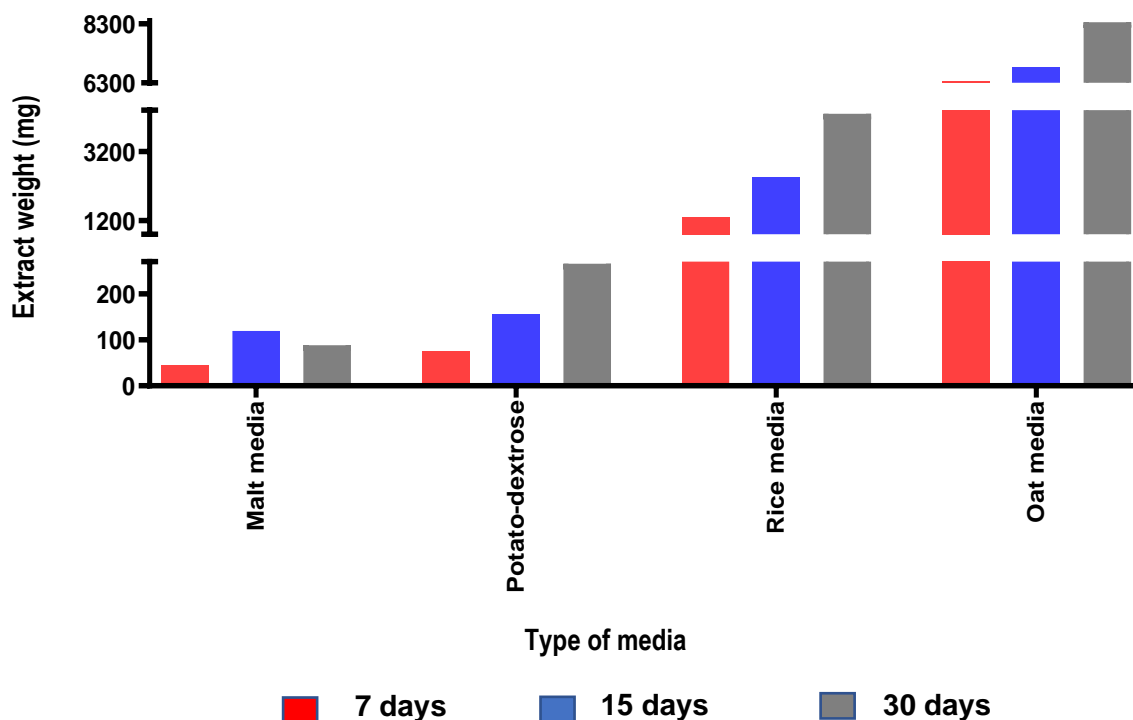


Figure 5.1: Histogram of extract average weights of *F. falciforme* obtained from four different media and incubated at 7, 15, and 30 days.

5.2.3 Extract test against MRSA

Before selecting the optimal medium for large-scale fermentation, the biological activity of *F. falciforme* extracts obtained from various media were tested against MRSA cells. Fungal extracts obtained by incubation in rice and malt for 7 and 30 days, respectively, were active (59.9%-61.6% activity) only against the planktonic MRSA. On the other hand, fungal extracts obtained from malt media incubated at 7 and 15 days; rice at 15 days; and potato dextrose at 15 days were active (72.2%- 99.4%) against planktonic MRSA and inhibited its biofilm formation while all extracts from the oat media were found inactive. The bioactivity threshold was set at 30% cell viability (or 70% inhibition) for extracts that were both planktonic and prebiofilm active. Both ¹H NMR and LC-HRMS data were used to investigate the chemical composition of the afforded extracts.

Table 5.2: Summary activity of *F. falciforme* extracts from different media against planktonic, prebiofilm, and postbiofilm MRSA at concentrations of 100 µg/ml.

Media	Incubation Period	Antimicrobial % inhibition	Stdev	Prebiofilm % inhibition	Stdev	Postbiofilm % inhibition	Stdev
Rice	7	61.7	3.23	67.7	31.47	26.4	36.40
Malt	7	90.0	0.35	98.4	1.21	79.6	2.93
Potato	7	58.5	14.83	19.9	38.35	58.8	17.15
Rice	15	72.4	18.00	72.2	24.39	59.61	10.73
Malt	15	90.3	1.14	99.4	0.08	49.0	27.50
Potato	15	92.2	1.41	99.4	0.23	48.7	4.96
Malt	30	59.9	3.03	<0	21.64	26.0	8.44

*Cells highlighted in blue colour indicates fractions with consistent bioactivity for all replicates, cells with white colour represents inactive fractions, while gold-coloured cells indicate active fractions with inconsistent bioactivity amongst replicates and therefore regarded as inactive.

5.2.4 MVA of LC-HRMS data

For multivariate analysis, PCA scores, and loadings plot were generated for the LC-MS data. The extracts were grouped according to the different media, to which the endophyte was incubated for 7, 15 and 30 days. The PCA scores plot in Figure 5.2A of the LC-HRMS data of *F. falciforme*, revealed that extracts obtained from malt media at 7, 15, and 30 days of incubation, were found in the upper and lower right side of the plot, which implied a strong similarity in their metabolomic profiles (red circles). The fungal extracts obtained from the malt media incubated for 7 and 15 days were separate from extracts obtained from 30 days incubation, which exhibited a slight difference in their chemical profiles due to the longer incubation period. Outlying metabolites from the malt media were observed on day 7 and 30. Rice media extracts incubated for 7, 15 and 30 days were clustered together on the upper and lower left quadrant (green circles). Potato media extracts incubated for 7, 15 and 30 days were slightly clustered on the upper and lower left quadrant (yellow circles). The oat media extracts (in blue circles) incubated for 7, 15, and 30 days, were clustered together on the lower left quadrant. The rice, oat, and potato media extracts were not producing discriminating metabolites, and were close together on the left quadrant, indicating slight similarity in their chemical profiles. This suggested that there was a strong likelihood that a more divergent profile was afforded with malt medium extracts in the three incubation periods when compared to the other media extracts. The loadings plot in Figure 5.2B, demonstrated that discriminating

metabolites from malt media extracts produced low and high molecular weight metabolites ranging from 181 to 1225 Da. The discriminatory metabolites obtained from malt media incubated for 7, 15 and 30 days were putatively identified as 3-propylgentisylquinone **(1)**, Tanzawaic acid A **(2)**, restrictinol **(3)**, colletorin B **(4)**, albocycline K1 **(5)**, hymeglusins **(6)**, fusaridionic acid A **(7)**, albocycline M8 **(8)**, Phomopoxide A **(9)**, and cyclosporin A **(10)**, represented by ion peaks at m/z 181.086, 271.169, 279.197, 289.179, 307.19, 323.186, 343.211, 341.197, 343.213, and 1202.85 respectively. There were no compound hits for 15 ion peaks indicating that they could be novel compounds. Compound 3-Propylgentisylquinone **(1)** is a benzenediol. Benzenediols have proven to have broad spectrum antimicrobial activity, including resistant and multidrug-resistant species of dermatophytes (*Trichophyton mentagrophytes*), *Candida* sp. and the ESKAPE panel of bacteria (Dalla Lana *et al.*, 2019). Tanzawaic acid A **(2)** is a derivative of Tanzawaic acid. Tanzawaic acids are conjugation inhibitors which can be isolated as natural compounds. They have the potential to specially inhibit IncW and IncFII conjugative systems, including plasmids, thus reducing antibiotic resistance (Getino *et al.*, 2016). They are an inhibitor of superoxide anion production, PTB1B inhibitor and Bacterial conjugation inhibitor. It shows anti-inflammatory property and exhibits antifungal activity.

Colletorin B **(4)** have previously been isolated from *Fusarium* sp. and displayed moderate herbicidal, antifungal, and antibacterial activities towards *Ustilago*, *Chlorella fusca*, *violacea*, and *Bacillus megaterium* and *Fusarium oxysporum* (Hussain *et al.*, 2015). Albocycline K1 **(5)** and M8 **(8)** are derivatives of albocycline. Albocycline have been reported to show selective antibiotic activity against *S. aureus* by inhibiting the peptidoglycan biosynthesis (Koyama *et al.*, 2013). It is weakly active against gram-positive bacteria. Hymeglusins **(6)**, as a fungal β -lactone antibiotic, is an HMG-CoA synthase inhibitor with IC_{50} of 0.12 μ M. It covalently modifies the active Cys¹²⁹ residue of the enzyme. Hymeglusins inhibit dengue type 2 (DEN-2) new guinea C (NGC) live virus replication in K562 cells (Greenspan *et al.*, 1987, Tomoda *et al.*, 1988). It also has antimicrobial activity against a few species including *S. aureus* (MIC 50 μ g/ml) and *Candida albicans* (MIC 12.5 μ g/mL) (Tomoda *et al.*, 1988). Hymeglusins are active against Gram-positive bacteria and fungi. It is a specific inhibitor of cholesterol biosynthesis and HMG-CoA synthetase. It circumvents β -lactam drug resistance in MRSA. Cyclosporin A **(10)** is a derivative of cyclosporin. Cyclosporin has been found to inhibit certain fungi, viruses, protozoa, and helminths, but their bioactivities are insignificant in practical terms (Kim and Perfect, 1989). The model gave goodness of fit (R_2) of 0.935 and a good predictability score (Q_2) of 0.824 after nine components. The difference between R_2 and Q_2 values was less than 0.3, which indicated an excellent fitted model and predictability. The discriminating features of

F. falciforme from each media were dereplicated in Table 5.3, while the structures are shown in Figure 5.3.

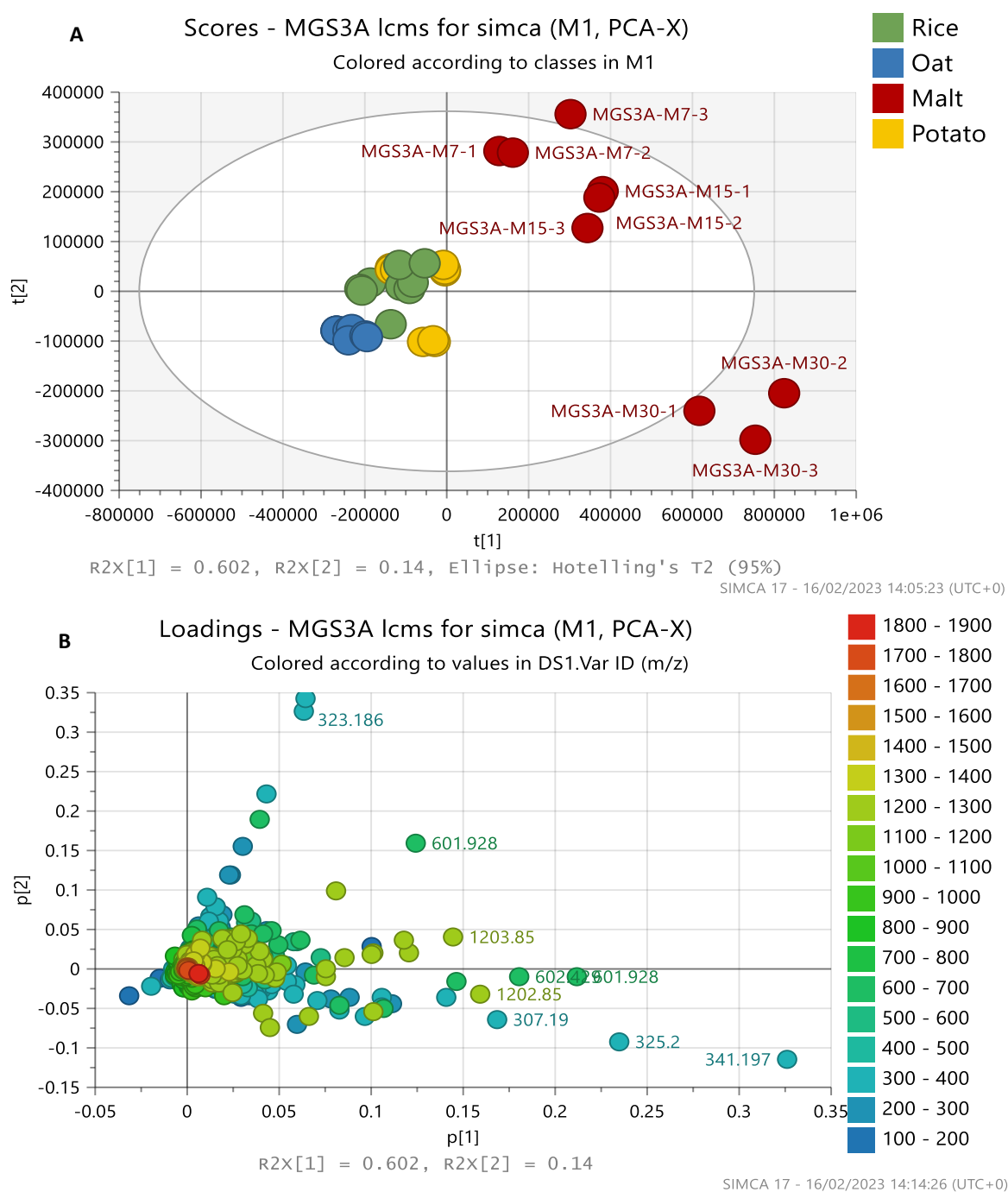


Figure 5.2: (A) PCA scores (B) loading plots of LC-HRMS data of *F. falciforme* extracts from four media incubated at 7, 15, and 30 days. $R_2X = 0.935$ and $Q_2X = 0.824$. Labelled features on the loadings plot represent the discriminating ion peaks for the outlying extracts obtained from malt media incubated for 7, 15 and 30 days.

Table 5.3: PCA loadings plot – Dereplicated compound hits from bioactive discriminatory and active metabolites from Malt media. Numbered structures are shown in Figure 5.3.

Mzmine ID	m/z	Rt	M.wt	Molecular Formular (DBE)	Compound hits	Biological source
P605	181.086	8.89	180.078	C ₁₀ H ₁₂ O ₃ (5)	3-Propylgentisylquinone (1)	Produced by fungal isolate CR1223-D
P553	271.169	15.40	270.161	C ₁₈ H ₂₂ O ₂ (8)	Tanzawaic acid A (2)	A marine-derived <i>Penicillium citrinum</i> and <i>Penicillium</i> sp. strains IBWF104-06 and SF-6013.
N752	279.197	15.44	280.204	C ₁₇ H ₂₈ O ₃ (4)	Restrictinol (3)	<i>Penicillium</i> sp. NR6564 and <i>Aspergillus sclerotiorum</i>
P558	289.179	11.60	288.172	C ₁₈ H ₂₄ O ₃ (7)	Colletorin B (4)	<i>Cephalosporium diospyri</i> and <i>Nectria galligena</i> .
P552	307.19	11.60	306.182	C ₁₈ H ₂₆ O ₄ (6)	Albocycline K1 (5)	<i>Streptomyces</i> sp. OH-3984
N79	323.186	15.44	324.194	C ₁₈ H ₂₈ O ₅ (5)	Hymeglusin (6)	<i>Cephalosporium</i> sp., <i>Scopulariopsis</i> sp. and <i>Fusarium</i> sp.
P1096	326.203	11.59	325.196		No hit	
P564	343.211	11.59	342.203	C ₁₈ H ₃₀ O ₆ (4)	Fusaridioic acid A (7)	<i>Cephalosporium</i> sp. and the marine derived <i>Scopulariopsis candida</i> .
N26	341.197	11.59	342.204	C ₁₈ H ₃₀ O ₆ (4)	Albocycline M8 (8)	<i>Streptomyces bruneogriseus</i>
N1291	342.2	11.59	343.207		No hit	
N564	343.213	12.42	344.22	C ₁₈ H ₃₂ O ₆ (3)	Phomopoxide A (9)	<i>Phomopsis</i> sp. YE3250
P1956	601.928	25.13	600.92		No hit	
P551	601.928	17.26	600.92		No hit	

Mzmine ID	m/z	Rt	M.wt	Molecular Formular (DBE)	Compound hits	Biological source
P2345	602.429	25.22	601.421		No hit	
P591	602.93	25.19	601.922		No hit	
N751	647.38	15.43	648.387		No hit	
N763	683.4	11.60	684.408		Complex of 341.1968 and 341.1968 m/z No hit	
P2349	1202.85	25.50	1201.84	C ₆₂ H ₁₁₁ N ₁₁ O ₁₂ (13)	Cyclosporin A (10)	<i>Trichoderma inflatum</i> NRRL 8044 (previously <i>T. polysporum</i>). <i>Fusarium solani</i> and <i>Tolypocladium sinense</i> .
P563	1202.85	17.28	1201.84	C ₆₂ H ₁₁₁ N ₁₁ O ₁₂ (13)	Cyclosporin A (10)	<i>Trichoderma inflatum</i> NRRL 8044 (previously <i>T. polysporum</i>). <i>Fusarium solani</i> and <i>Tolypocladium sinense</i> .
P587	1203.85	25.48	1202.84		No hit	
P1634	1204.85	25.35	1203.85		No hit	
P1986	1219.87	25.64	1218.87		No hit	
P1633	1219.87	25.78	1218.87		No hit	
P575	1220.88	25.71	1219.87		No hit	
P1966	1224.83	26.01	1223.82		No hit	
P2946	1225.83	26.02	1224.82		No hit	

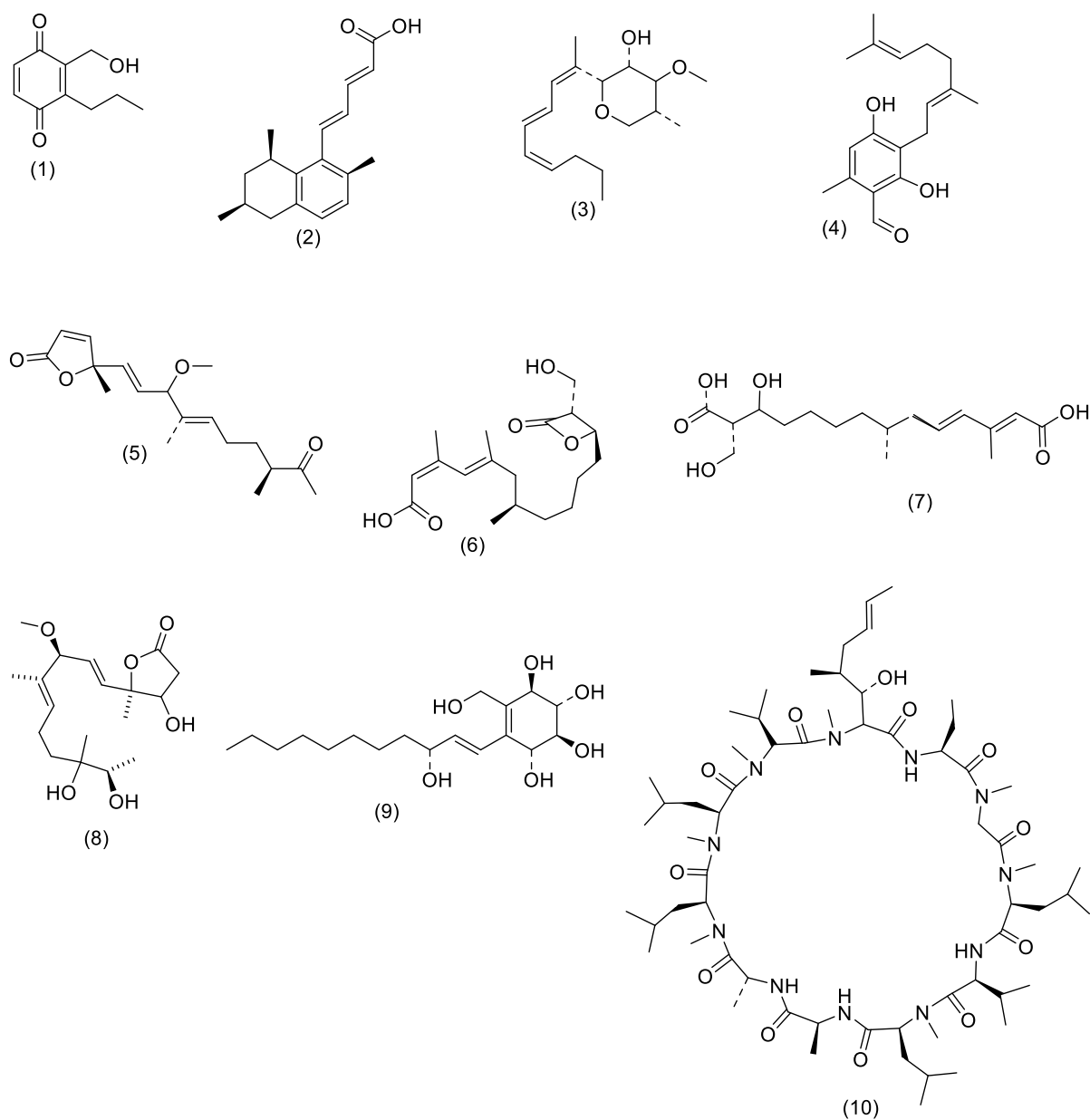


Figure 5.3: PCA Structures of the discriminating metabolites from *F. falciforme* extract obtained from malt media and listed in Table 5.3.

A PLS-DA analysis was performed to show a clearer illustration of the differences in metabolic profiles between fungal extracts isolated from various media as shown in Figure 5.4. It gave a clearer illustration by distinguishing the potato, rice and oat media metabolites on scores and loadings as compared to the PCA, which only illustrated the malt media discriminatory metabolites on the loadings plot. It showed fitness (R_2) and predictability (Q_2) scores of 0.923 and 0.973 respectively, after six components. The difference between R_2 and Q_2 values was less than 0.3. This proved to be a good fit, and a good model prediction, which improved when compared to the PCA model above. The variation between groups R_2X_0 [1] was 59.8 % and within group R_2X [2] was 4.5. From the scores plot (Figure 5.4A), extracts obtained from rice media incubated for 7, 15 and 30 days was clustered together in the lower right quadrant (encircled in green), indicating similarity in the chemical profile of the extracts obtained at different days of incubation. Similarly, oat media extracts incubated for 7, 15 and 30 days (encircled in blue), were clustered together in the lower right quadrant, indicating similarity in the chemical profiles of the extracts obtained at different days of incubation. The rice and oat media extracts were at close range on the PLS-DA plot, which could be because of the lipids produced by both media extracts. The rice media extracts contained metabolites with m/z values of 211.097 and 665.392 Da. The oat media contained metabolites with m/z values of 299.109, 324.289 and 431.315 Da, while potato media extracts contained metabolites with m/z values ranging from 329 to 635 Da. Extracts obtained from malt media incubated for 15 days were clustered together while malt 7- and 30-days extracts (red circles) were sparsely distributed within close range, although they were all located on the left quadrant. This indicates strong similarity in the chemical profiles of malt 15 days extracts. It can be observed that extracts obtained from malt media incubated for 7, 15 and 30 days were separated from other extracts on the scores plot. This indicated that the extracts were producing metabolites with divergent chemical profiles, hence malt media was considered for scale up of *F. falciforme*. The discriminatory metabolites obtained from potato, rice and oat media were putatively identified as peniciltide B (**11**), 12,13-Epoxy-9,10,18-trihydroxyoctadecanoic acid (**12**), solanidine (**13**), rabdophyllin H (**14**), antibiotic MR 387A (**15**) and N-(2-Hydroxyethyl) linoleamide (**16**) represented by m/z ion peaks 329.233, 345.228, 398.341, 469.242, 503.25, 324.289. There were no compound hits for 6 ion peaks, indicating the presence of novel compounds. Solanidine (**13**) are alkaloids produced by *Solanaceae* family plants. Previous reports have shown that solanidine has no inhibitory properties at the studied concentrations of 125–2000 $\mu\text{g/mL}$ (Noori *et al.*, 2023). The discriminating features of *F. falciforme* from each media were dereplicated in Table 5.4 and the structures are shown in Figure 5.5.

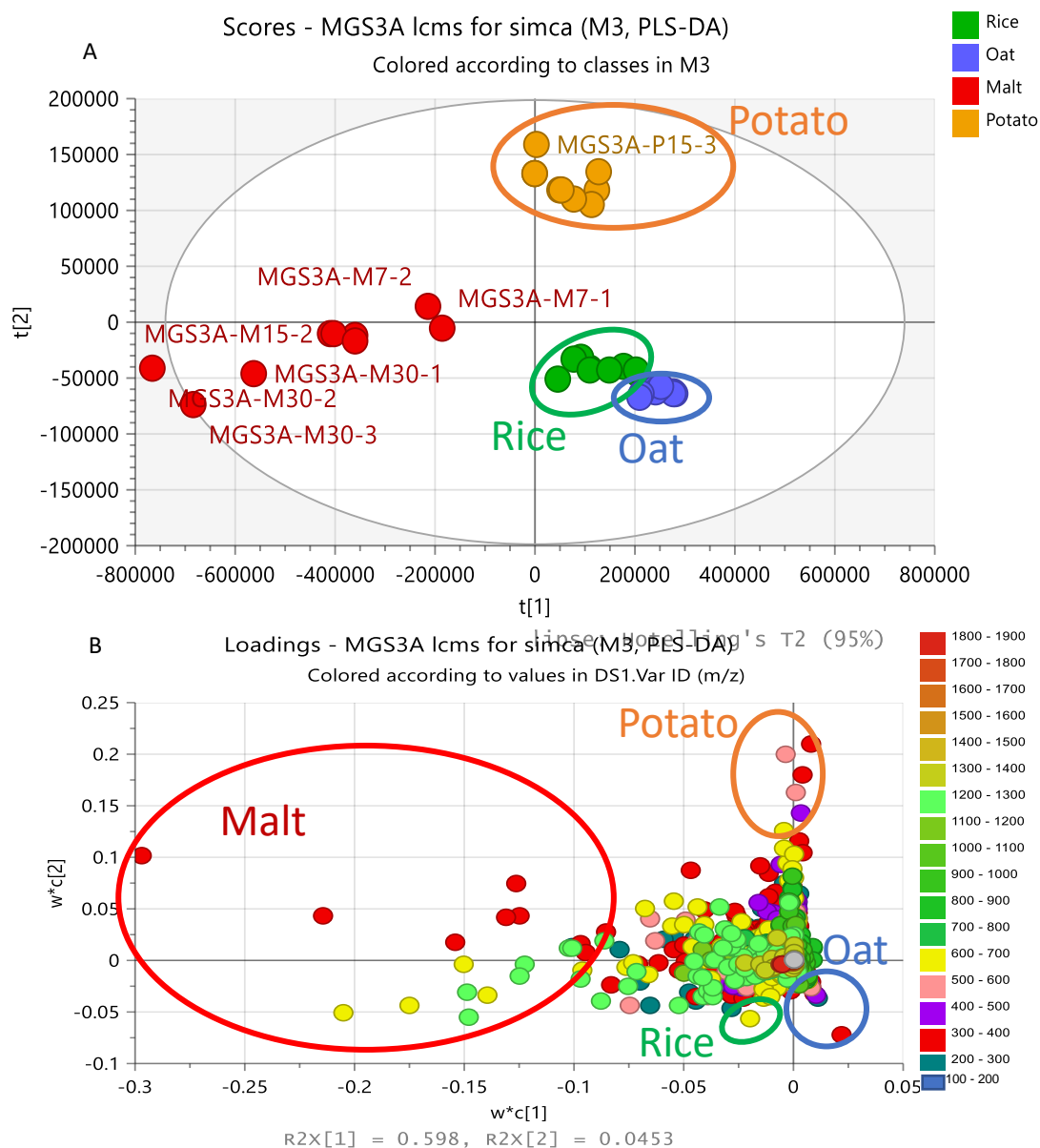


Figure 5.4: (A) PLS-DA scores and (B) loading plots of LC-HRMS of *F. falciforme* extract obtained from different media. The encircled box indicated the discriminating feature for each media extracts. $R_2 = 0.923$ and $Q_2 = 0.973$. The difference between group $R_2Xo [1]$ is equal to 59.8% and the difference within groups $R_2X [2]$ is 4.5%.

Table 5.4: PLS-DA- Scores plot – Dereplicated compound hits from bioactive discriminating metabolites for potato, rice, and oat media. Numbered structures are shown in Figure 5.5.

Mzmine ID	m/z	Rt	M. wt	P-value	Molecular Formular (DBE)	Compound hits	Biological source
Potato media extracts							
N334	329.233	13.03	330.241	2.24354e-07	C ₁₈ H ₃₄ O ₅ (2)	Penicitide B (11)	Marine-derived <i>Penicillium chrysogenum</i> QEN24-S
N5000	345.228	8.44	346.235	2.24354e-07	C ₁₈ H ₃₄ O ₆ (2)	12,13-Epoxy-9,10,18-trihydroxyoctadecanoic acid (12)	-
P3572	398.341	11.23	397.334	2.24354e-07	C ₂₇ H ₄₃ NO (7)	Solanidine (13)	<i>Solanum tuberosum</i> , <i>Cestrum purpureum</i> , <i>Fritillaria camtschatcensis</i> , <i>Rhinopetalum bucharicum</i> and <i>R. stenanthum</i> (Solanaceae, Liliaceae)
P3915	399.344	11.24	398.337	4.61102e-07		No hit	
P3573	469.242	10.13	468.235	3.17742e-05	C ₂₄ H ₃₆ O ₉ (7)	Rabdophyllin H (14)	<i>Rabdosia macrophylla</i> , <i>Isodon macrocalyx</i> and <i>I. macrophyllus</i>
N6750	503.25	10.06	504.257	4.32339e-05	C ₂₅ H ₃₆ N ₄ O ₇ (10)	Antibiotic MR387A (15)	<i>Streptomyces neyagawaensis</i> SL-387
P569	607.381	13.88	606.374	0.000350		No hit	
P578	629.363	13.88	628.355	0.000234		No hit	
P1128	635.412	15.60	634.404	0.000514		No hit	
Rice media extracts							
N812	211.097	9.49	212.104			No hit	
N104	665.392	16.17	666.399			No hit	
Oat media extracts							
P90	324.289	23.37	323.282	3.3304e-06	C ₂₀ H ₃₇ NO ₂ (3)	N-(2-Hydroxyethyl) linoleamide (16)	Alkaloid from <i>Vaccaria segetalis</i>

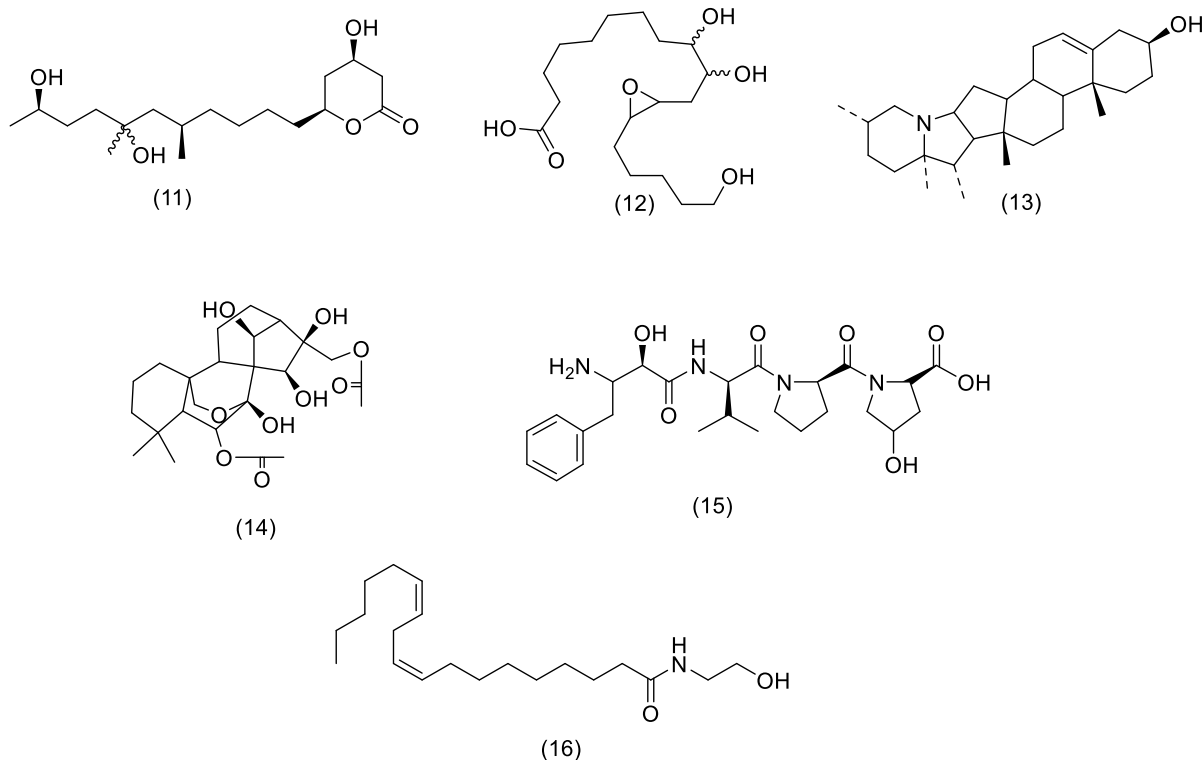


Figure 5.5: PLS-DA Structures of the discriminating metabolites from *F. falciforme* extract obtained from potato, rice, and oat media as listed in Table 5.4.

An OPLS-DA analysis was performed based on the anti-MRSA results, which gave an illustration of the active versus inactive extracts as shown in Figure 5.6. Malt media extracts obtained after 7 and 15 days of incubation, potato media extract incubated for 15 days, and rice media extracts obtained after 15 days of incubation were active, while malt extract obtained after 30 days of incubation, potato extract obtained after 7 and 30 days of incubation and rice media extracts obtained after 7 and 30 days of incubation were inactive. All the oat media extracts were inactive. The OPLS-DA scores plot in Figure 5.6A positioned the active extracts on the upper and lower left quadrants, while the inactive extracts were dispersed on the upper and lower right quadrant of the scores plot. It showed fitness (R_2) and predictability (Q_2) scores of 0.978 and 0.907 respectively. This proved to be a good fit, and a good model prediction. The variation between groups R_2X_0 [1] was 54.6 % and within group R_2X [1] was 12.3 %. This showed that there was significant difference in the chemical profiles between the active versus the inactive extracts, and a slight similarity within the extracts in their different classes.

Active extracts from malt media (encircled in red) incubated for 7 and 15 were clustered at the upper left quadrant indicating similarity in the chemical profiles, while active extracts obtained from rice and potato media (encircled in red) incubated for 15 days were clustered at the lower left quadrant indicating similarity in their chemical profile. For the inactive extracts, the outliers were found on malt media extracts with 30 days of incubation (encircled in blue), while the other inactive extracts (encircled in blue) were clustered together at the lower right quadrant with p-values < 0.05, which indicated a strong model with a confidence interval of more than 95%. The inactive extracts were mostly obtained from the oat media which consisted more of lipids. The discriminatory bioactive metabolites gave an m/z value range between 181.086 to 1219.87 Da.

Discriminating active metabolites with p-values less than 0.05 are listed in Table 5.5. Structures of putatively identified compound hits are shown in Figure 5.7. Seven of the ion peaks gave no hits, which could indicate the presence of novel compounds.

The compounds identified from the DNP database, as shown in Table 5.5 were, Mzmine IDs P605, P553, N752, P550, P547, P548, N79, N753, N26, P563 with DBE values ranging between 4 to 13, represented by ion peaks m/z 181.086, 271.169, 279.197, 289.179, 307.19, 325.200, 323.186, 325.202, 341.197, and 1202.85 Da respectively indicate the presence of aliphatics, sugars, olefinics and aromatics. These metabolites were identified as 6,7-dihydro-3-(hydroxymethyl)-6-methyl-4(5*H*)-benzofuranone (**17**), tanzawaic acid A (**2**), 5(1→10)-dbeo-1,8-patchoulanediol; 8β-form, 8-Ac (**18**), 5-dcetyl-2,3-dihydro-2-(1-hydroxy-1-methylethyl)-7-(3-methyl-2-butenyl)benzofuran (**19**), albocycline K1 (**5**), albocycline M1 (**20**), hymeglusin (**6**), penisporolide A (**21**), albocycline M8 (**8**), cyclosporin X (**22**). Compound 6,7-Dihydro-3-(hydroxymethyl)-6-methyl-4(5*H*)-benzofuranone (**17**) belongs to the class of benzofuran. Benzofurans are ubiquitous in nature. Numerous studies have shown that most benzofuran compounds have strong biological activities such as antibacterial, anti-tumour, anti-viral and anti-oxidative activities. Benzofuran compounds have attracted more attention of pharmaceutical and chemical researchers worldwide, making these compounds potential natural drug lead compounds, due to their biological activities and potential applications. An example is the recently discovered novel macrocyclic Benzofuran compound, which has anti-hepatitis C virus activity and has the prospect to be an effective therapeutic drug for hepatitis C disease (Miao *et al.*, 2019).

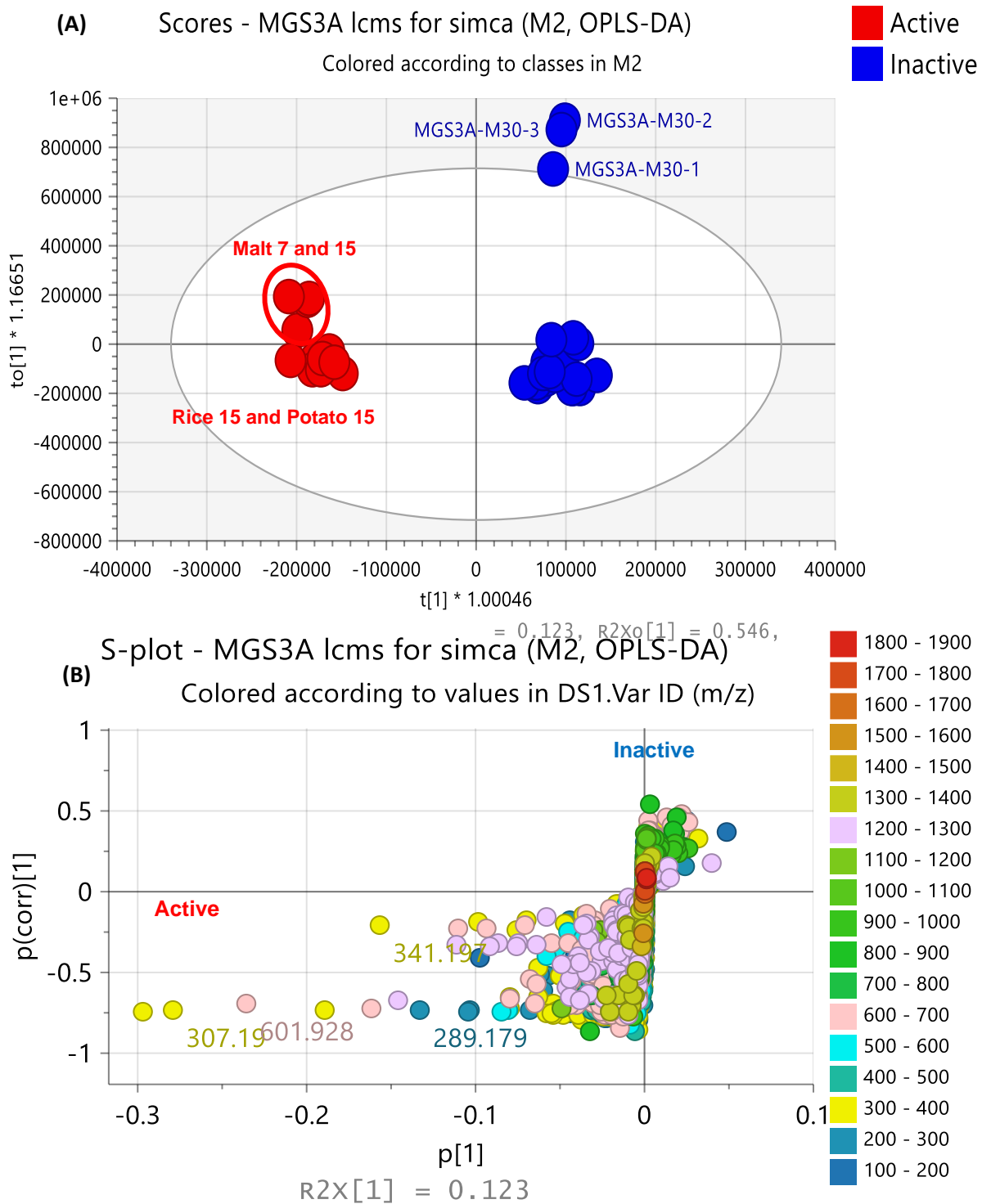


Figure 5.6: (A) OPLS-DA scores and (B) S- plots of LC-HRMS of *F. falciforme* extracts obtained from different media. $R_2 = 0.978$ and $Q_2 = 0.907$. The difference between group R_2Xo [1] is equal to 54.6% and the difference within groups R_2X [2] is 12.3%.

Table 5.5: Dereplicated compound hits for the discriminating planktonic and prebiofim active metabolites of *F. falciforme* obtained from the OPLS-DA S-Plot on Figure 5.6B.

Mzmine ID	<i>m/z</i>	Rt	M. wt	<i>P value</i>	Molecular Formular (DBE)	Compound hits	Biological source
P605	181.086	8.89	180.078	0.016868	C ₁₀ H ₁₂ O ₃ (5)	6,7-Dihydro-3-(hydroxymethyl)-6-methyl-4(5 <i>H</i>)-benzofuranone (17)	<i>Phomopsis</i> sp. hsla01-1
P553	271.169	15.40	270.161	4.78786e-07	C ₁₈ H ₂₂ O ₂ (8)	Tanzawaic acid A (2)	<i>Securinega suffruticosa</i>
N752	279.197	15.44	280.204	3.52471e-07	C ₁₇ H ₂₈ O ₃ (4)	5(1→10)-Abeo-1,8-patchoulanediol; 8β-form, 8-Ac (18)	<i>Valeriana fauriei</i>
P550	289.179	15.40	288.172	5.10715e-07	C ₁₈ H ₂₄ O ₃ (7)	5-Acetyl-2,3-dihydro-2-(1-hydroxy-1-methylethyl)-7-(3-methyl-2-butenyl) Benzofuran (19)	No hit
P547	307.190	15.44	306.182	4.78451e-07	C ₁₈ H ₂₆ O ₄ (6)	Albocycline K1 (5)	<i>Streptomyces</i> sp. OH-3984
P548	325.200	15.42	324.193	5.17256e-07	C ₁₈ H ₂₈ O ₅ (5)	Albocycline M1 (20)	<i>Streptomyces bruneogriseus</i>
N79	323.186	15.44	324.194	3.7291e-07	C ₁₈ H ₂₈ O ₅ (5)	Hymeglusin (6)	<i>Cephalosporium</i> sp., <i>Scopulariopsis</i> sp. and <i>Fusarium</i> sp.
N753	325.202	14.38	326.209	2.45818e-05	C ₁₈ H ₃₀ O ₅ (4)	Penisporolide A (21)	Marine derived <i>Penicillium</i> sp. (HK1 strain GT20022605)
N26	341.197	11.59	342.204	0.226744	C ₁₈ H ₃₀ O ₆ (4)	Albocycline M8 (8)	<i>Streptomyces bruneogriseus</i>
P554	347.182	15.43	346.175	9.26243e-07	Related to [M+Na-H] adduct of <i>m/z</i> 325.2003.	Albocycline M1 (20)	<i>Streptomyces bruneogriseus</i>
P783	594.92	16.80	593.913	5.29004e-07		No hit	
P551	601.928	17.26	600.92	6.01513e-06		No hit	

Mzmine ID	m/z	Rt	M. wt	P value	Molecular Formular (DBE)	Compound hits	Biological source
P2345	602.429	25.21	601.421	0.189063		No hit	
P583	609.925	16.60	608.917	1.09663e-05		No hit	
N751	647.38	15.43	648.387	1.44457e-06		No hit	
P563	1202.85	17.28	1201.84	1.4711e-05	C ₆₂ H ₁₁₁ N ₁₁ O ₁₂ (13)	Cyclosporin X (22)	<i>Tolypocladium inflatum</i> NRRL 8044, DSM 63544
P587	1203.85	25.48	1202.84	0.052185		No hit	
P1986	1219.87	25.64	1218.87	0.0626812		No hit	

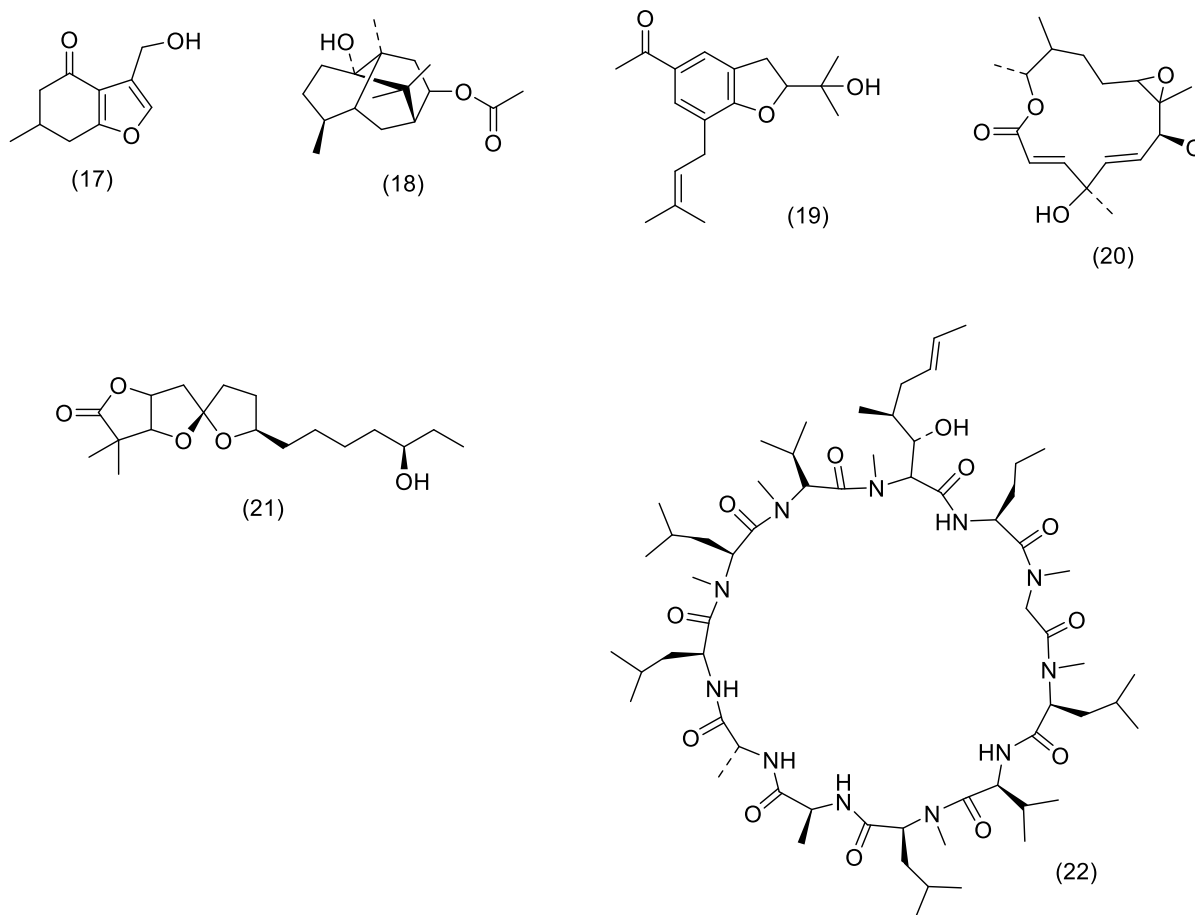
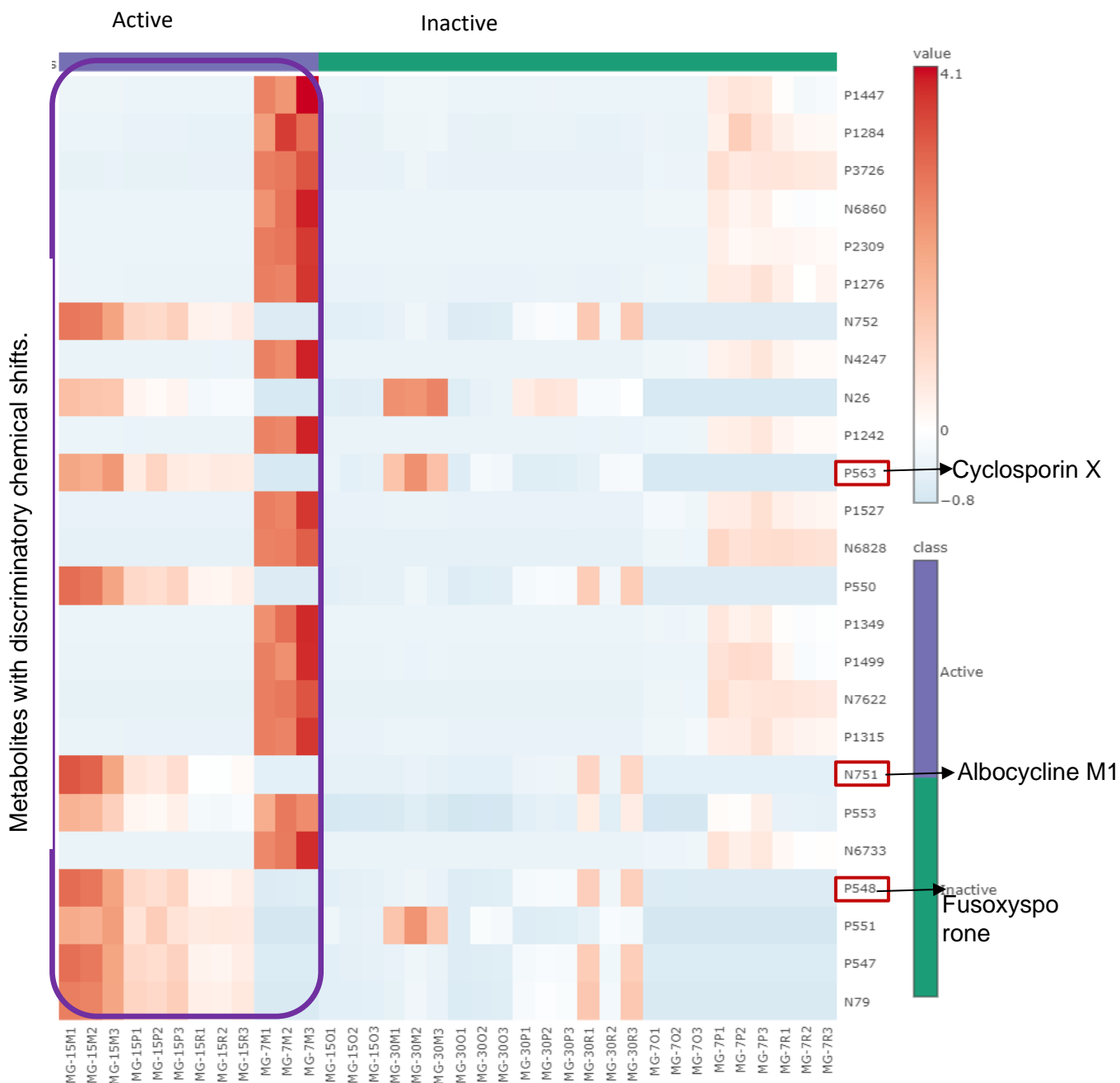


Figure 5.7: Structures of the discriminating bioactive metabolites of *F. falciforme* extracts from different media and listed in Table 5.5.

Analysis on MetaboAnalyst® was performed. The heatmap confirmed that bioactive fungal extracts (purple box) were observed in malt media after 7 and 15 days of incubation, with potato dextrose at 15 days, and rice media at 15 days, due to more diverse, high intensity, and concentration of metabolites observed in the active section (Figure 5.8), with malt 7 being more discriminatory. The heatmap also showed that all fungal extracts from the oat culture media had less intensity and lesser concentration of metabolites, which could have contributed to their inactivity.

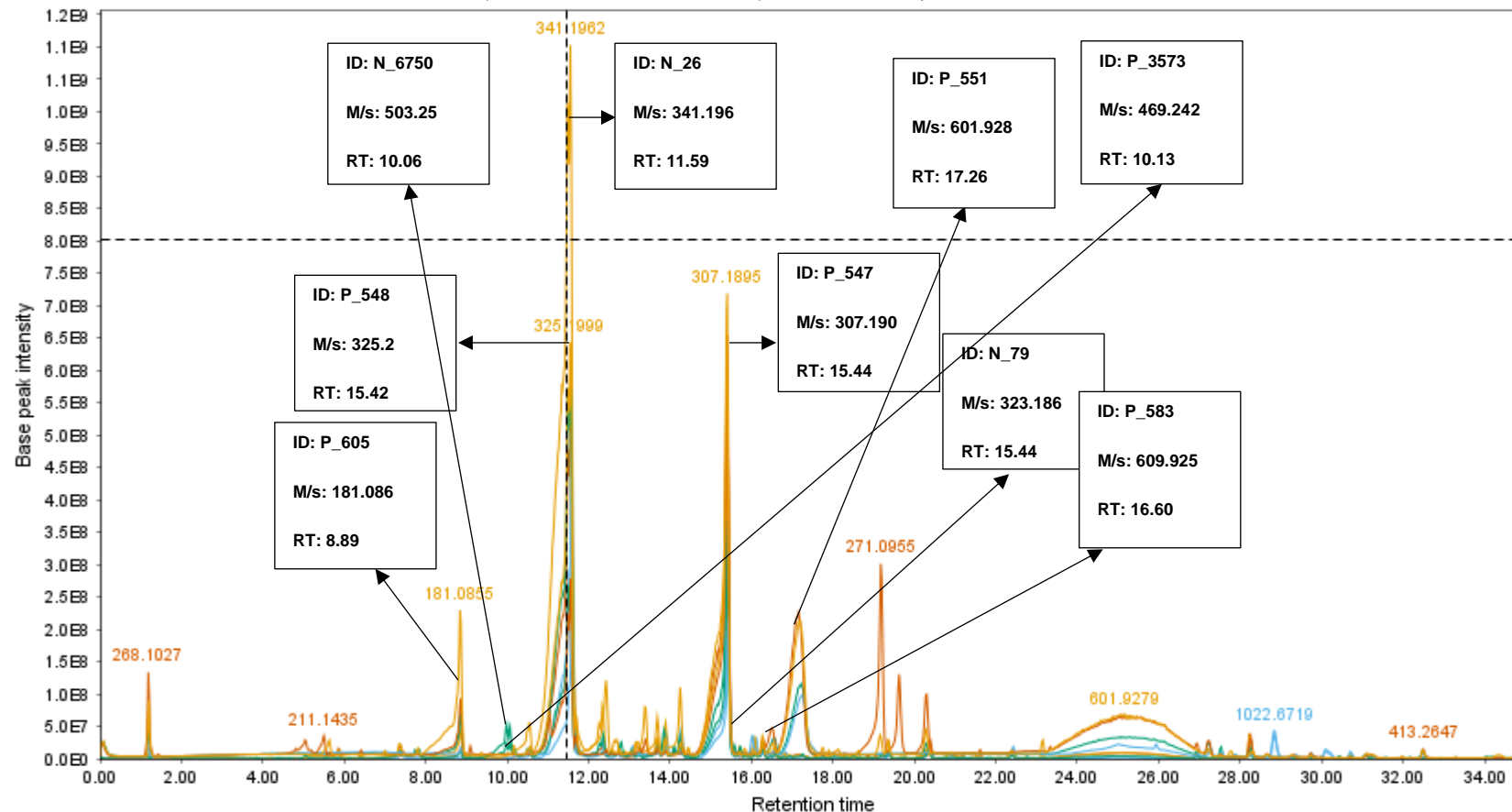


Extracts obtained from 4 different media.

Figure 5.8: Heatmap analysis of the mass spectral data of *F. falciforme* extracts with their Mzmine values, obtained from different media, generated by MetaboAnalyst®. The purple boxed extracts are biologically active against MRSA and producing discriminatory metabolites, which includes malt extract 7 and 15 days, rice extract 15 days and potato 15 days. Highlighted Mzmine values on the Y-axis indicate common metabolites observed on the heatmap and VIP, while MzmineID's N752, N26, P563, P550, N751, P553, P548, P551, P547, N79 observed on the heatmap were dereplicated in Table 5.5.

Base peak plot, MS1, m/s: 149.9987-1999.8989

Selected scan #1032 (M7, M15, P15, R15 total ms/mL), RT: 11.46, base peak: 341.1941 m/s, IC: 8.0E8



— JRB_EN_MGS3A-M7-1.mzML — JRB_EN_MGS3A-R15-1.mzML — JRB_EN_MGS3A-M15-1.mzML — JRB_EN_MGS3A-P15-1.mzML — JRB_EN_MGS3A-P15-1pos.mzML
 — JRB_EN_MGS3A-R15-1pos.mzML — JRB_EN_MGS3A-M7-1pos.mzML — JRB_EN_MGS3A-M15-1pos.mzML

- JRB_EN_MGS3A-M7-1 = *F. falciforme* incubated in malt media for 7 days negative and positive
- JRB_EN_MGS3A-M7-1 = *F. falciforme* incubated in malt media for 15 days negative and positive
- JRB_EN_MGS3A-R15-1 = *F. falciforme* incubated in rice media for 15 days negative and positive
- JRB_EN_MGS3A-P15 = *F. falciforme* incubated in potato media for 15 days negative and positive

Figure 5.9: Total ion chromatogram (TIC) of the bioactive extracts of *F. falciforme* from different media. The ion peaks that represent the discriminating features listed in Table 5.4 and 5.5 have been labelled.

5.2.5 Scale up fermentation and extraction of *F. falciforme* in the production of bioactive metabolites.

During the media optimisation, bioactive fungal extracts were afforded from malt culture media at 7 and 15 days of incubation, while with rice, and potato dextrose media, bioactive fungal extracts were obtained only with 15 days. Extracts from the malt media culture at 30 days of incubation was weakly active (59.9% inhibition), which was lower than the bioactivity threshold of 70.0% inhibition set against planktonic and prebiofilm MRSA. Extracts from the 15 days rice culture media exhibited 72.4% inhibition was not selected because its activity against MRSA was below 90% inhibition. However, extracts obtained from malt culture media incubated for 7- and 15-days and those in potato dextrose culture media for 15 days incubation exhibited $\geq 90\%$ bioactivity against planktonic and prebiofilm MRSA. Fungal extracts from the malt culture media incubated for 7 days were excluded due to its low average extract weight of only 44.8 mg. *F. falciforme* extracts obtained from the 3 incubation periods (7, 15, and 30 days) in malt media were active against MRSA (above 50% growth inhibition), proving the growth stability of *F. falciforme* on malt media.

In potato dextrose media, bioactivity of the fungal extracts was only observed after 15 days of incubation, while found inactive for the other incubation periods, showing its instability on potato media. Furthermore, on the PLSDA scores plots in Figures 5.4 along with the OPLS-DA scores plot (Figure 5.6), it can be observed that extracts from malt media were separated from other media extracts, showing that the metabolites inherent could be divergent and novel. Therefore, in the quest for novel compounds, malt media at 15 days of incubation with an average extract weight of 119.5 mg was selected as the optimum media for the scale up of *F. falciforme*.

5.2.6 Results obtained from Solvent – Solvent partitioning of *F. falciforme*.

Scaled-up crude extract for *F. falciforme* weighed 15.18 g. The Solvent – Solvent partitioning of *F. falciforme* afforded MeOH and Hexane fractions at almost equal ratios.

Table 5.6: Weight of fractions after solvent-solvent partitioning

Fraction	Extract weight
Methanol extract	4.1 g
Hexane extract	4.13 g

5.2.7 Bioactivity test results of *F. falciforme* fractions

The fractions obtained from solvent-solvent partition were subjected to biological assay against MRSA. MeOH fraction showed weak activity against prebiofilm MRSA but was inactive to planktonic and postbiofilm assays. The hexane fraction was inactive to planktonic, prebiofilm and postbiofilm assays against MRSA. The bioactivity was in the decreasing order: MeOH fraction > hexane fraction.

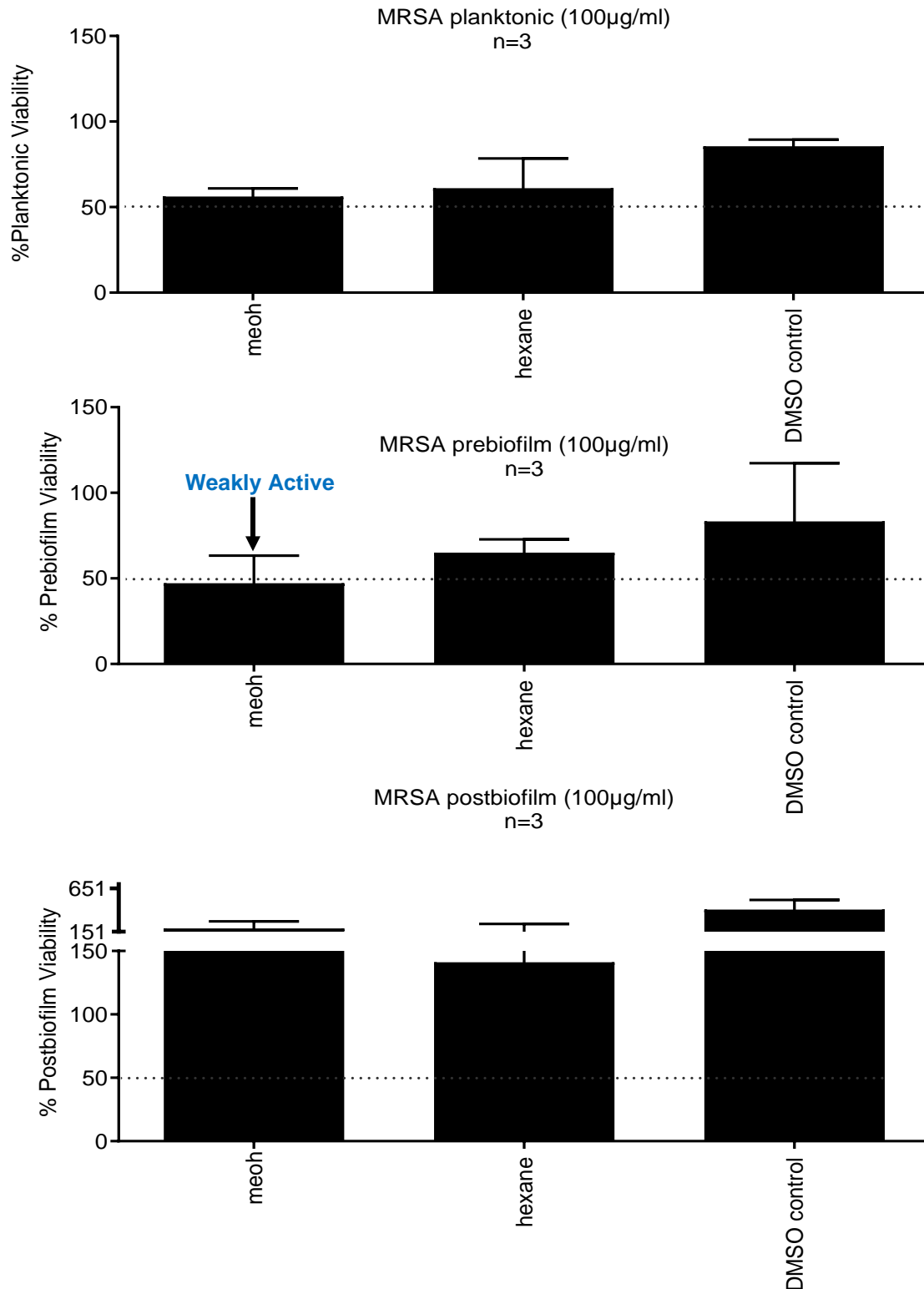


Figure 5.10: Effect of *F. falciforme* MeOH and Hexane fractions against MRSA.

Table 5.7: Summary of bioactivity of *F. falciforme* fractions against MRSA Planktonic, prebiofilm, and postbiofilm percentage viability.

Media	Antimicrobial % Viability	Prebiofilm % Viability	Postbiofilm % Viability
Methanol	56.20	47.16	189.63
Hexane	61.05	65.07	141.12

Cells with blue colour indicates active fractions against MRSA, while white cells indicate inactive fractions.

5.2.8 NMR spectroscopy for *F. falciforme* fractions

Due to the loss of bioactivity observed in the MeOH and hexane fractions of *F. falciforme* extracts after solvent-solvent partition, the MeOH and hexane fractions were subjected to proton NMR measurements to have an overview of their change in chemical profiles responsible for the loss in bioactivity. The ¹H NMR spectra of the fractions were presented in Figure 5.11. Their chemical profiles were compared with extracts obtained from the small-scale malt culture media incubated at 15 days.

Common peaks were observed for the 3 extracts (blue boxes) between 0.8 to 2.8 ppm and 5 to 5.5 ppm representing aliphatics and olefinics respectively with a higher intensity on the hexane extracts indicating a high level of fatty acids. Similar peaks were observed on malt extract 15 days and MeOH fraction (red boxes) between 3.5 to 4.5 ppm and 6.0 to 7.5 ppm denoting the presence of sugars and aromatics. Peaks were observed at 9.0 to 10.0 ppm for only malt extract 15 days (green box), while common peaks were observed at 12.0 ppm in malt extract 15 days and hexane extract (red box), indicating the presence of carboxylic acid.

Malt 15 days was extracted using EtOAc, hexane fraction was extracted with hexane while MeOH fraction was extracted with MeOH. The stacked ¹H NMR spectra in Figure 5.11 shows that after solvent-to-solvent partition, the metabolites inherent the fungal extract obtained from malt media after 15 days of incubation, were partitioned between the MeOH and hexane fractions. Their bioactivity was in the decreasing order: Malt extract 15 days > MeOH fraction > hexane fraction.

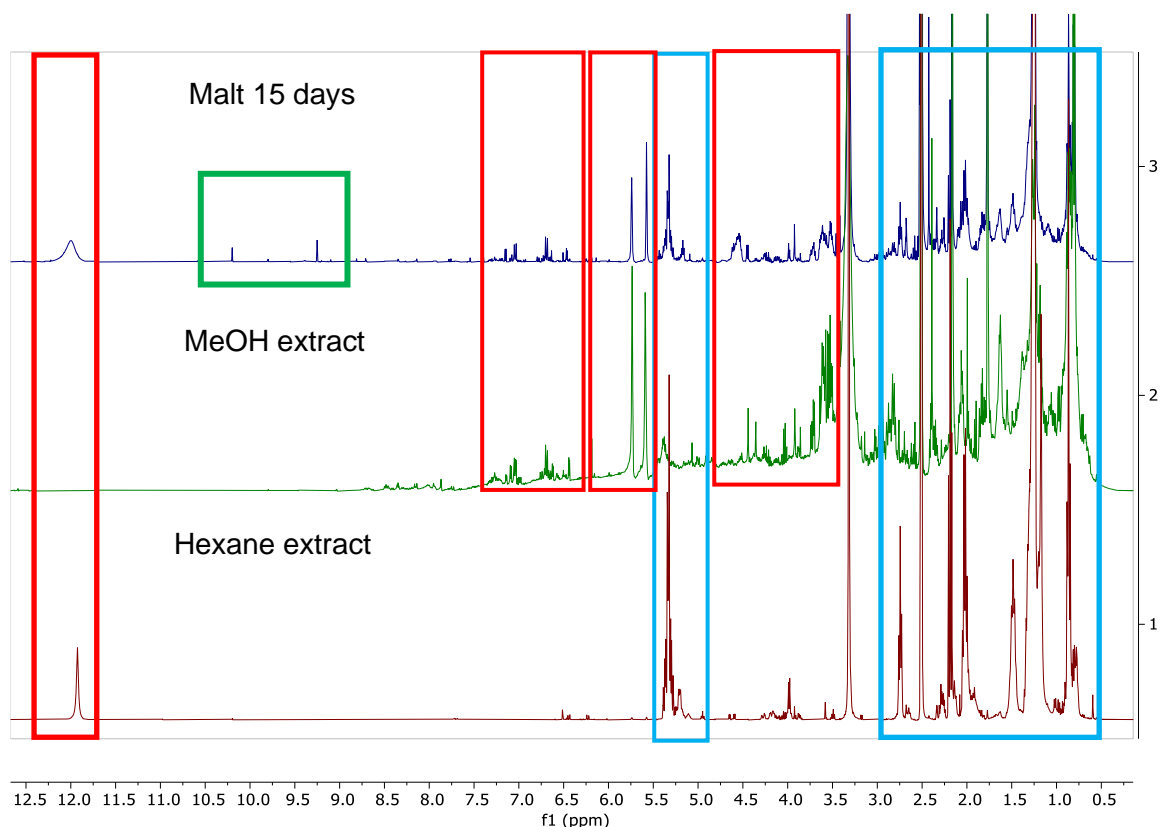


Figure 5.11: Stacked ^1H NMR spectra of *F. falciforme* malt 15 days crude extract, MeOH and hexane fractions.

The PCA scores scatter plot (Figure 5.12 A) confirmed the ^1H NMR analysis of the 3 extracts as shown above in Figure 5.11 to be more similar than different. It showed that extracts from Malt 15 days, MeOH fraction and hexane fraction were located at close proximity confirming that their chemical profiles were similar. However, the loadings plot indicated malt 15 days extract and hexane fraction to be close to each other. This could be because of the presence of carboxylic acids (11.0 to 12.0 ppm), aliphatic acids (0.8 to 2.8 ppm) and olefinics (5.0 to 5.5 ppm) observed on both extracts in Figure 5.26. The presence of carboxylic acids (11.93 and 11.97 ppm) in malt 15 days and hexane fraction is shown on the loadings plot (Figure 5.12B). In the generated model at pareto scaling, the R_2 was 1.0 while Q_2 was 0.997 after 2 components, which indicates a good fitted and predictability model.

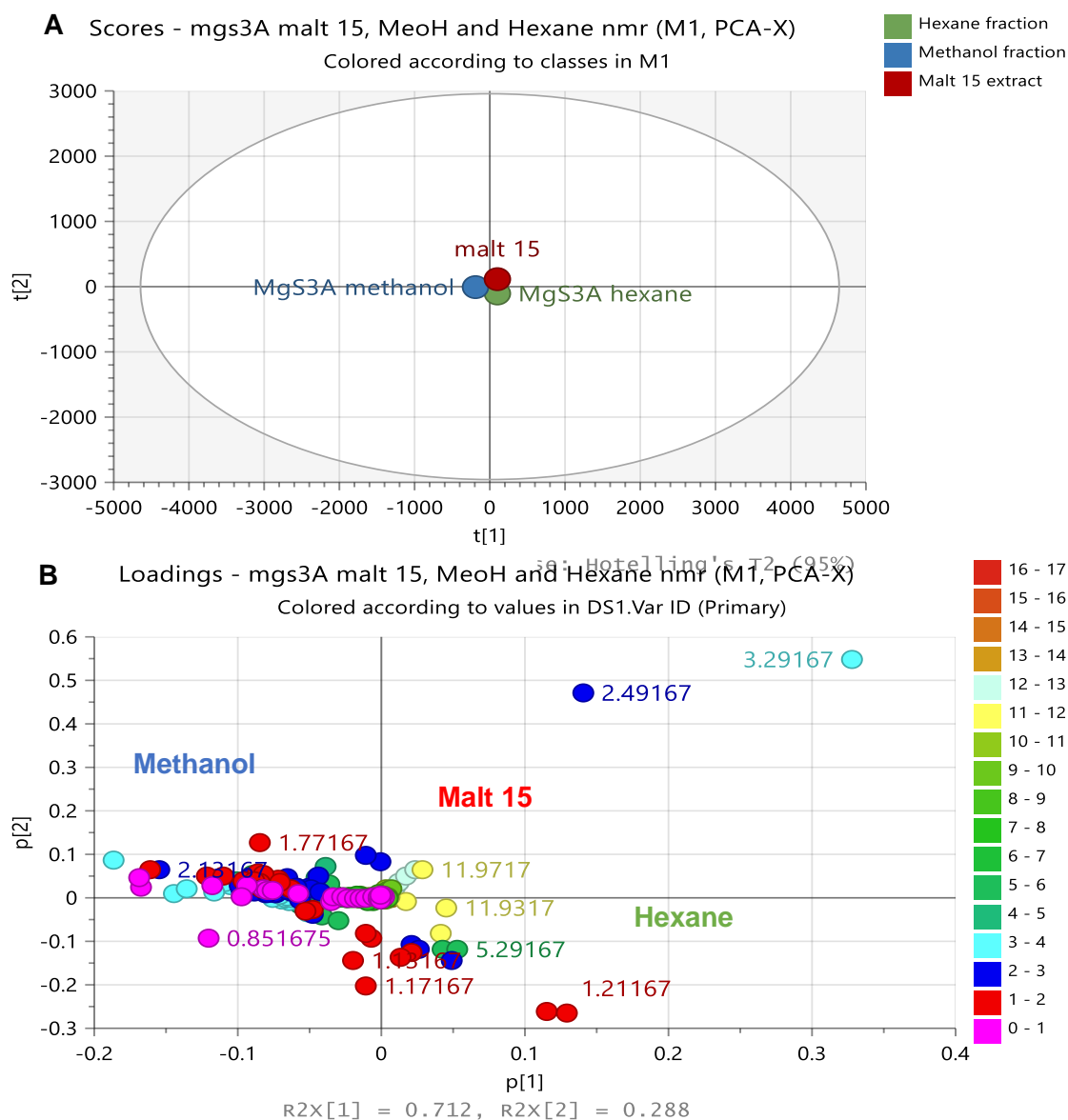


Figure 5.12: (A) PCA scatter and (B) loading plots of the NMR spectral data of *F. falciforme* malt 15 days crude extract, MeOH and hexane fractions. The R^2X and Q^2X values were 1.00 and 0.997, respectively.

An OPLS-DA was also performed to give a better illustration of the differences in chemical profiles between the active extract (malt 15 days) and inactive fractions (MeOH and hexane) in Figure 5.13. The inactive fractions were clustered together on the upper and lower left quadrants, while the active extract was located between the upper and lower right quadrant of the OPLS-DA scores plot (Figure 5.13A). The extracts were close to each other on the scores plot but were located on different quadrants. This could be because the extracts were obtained

from the same fungi but were extracted with different solvents. The difference in the extraction solvents used could be the major factor contributing to their different chemical profiles. The loadings plot (Figure 5.13B) showed the occurrence of a range of resonance for the metabolites. The difference between group R_2X_0 [1] is equal to 38.6 %, and the difference within groups R_2X [2] is 61.4 % showing the difference in chemical profiles between and within the active and inactive extracts.

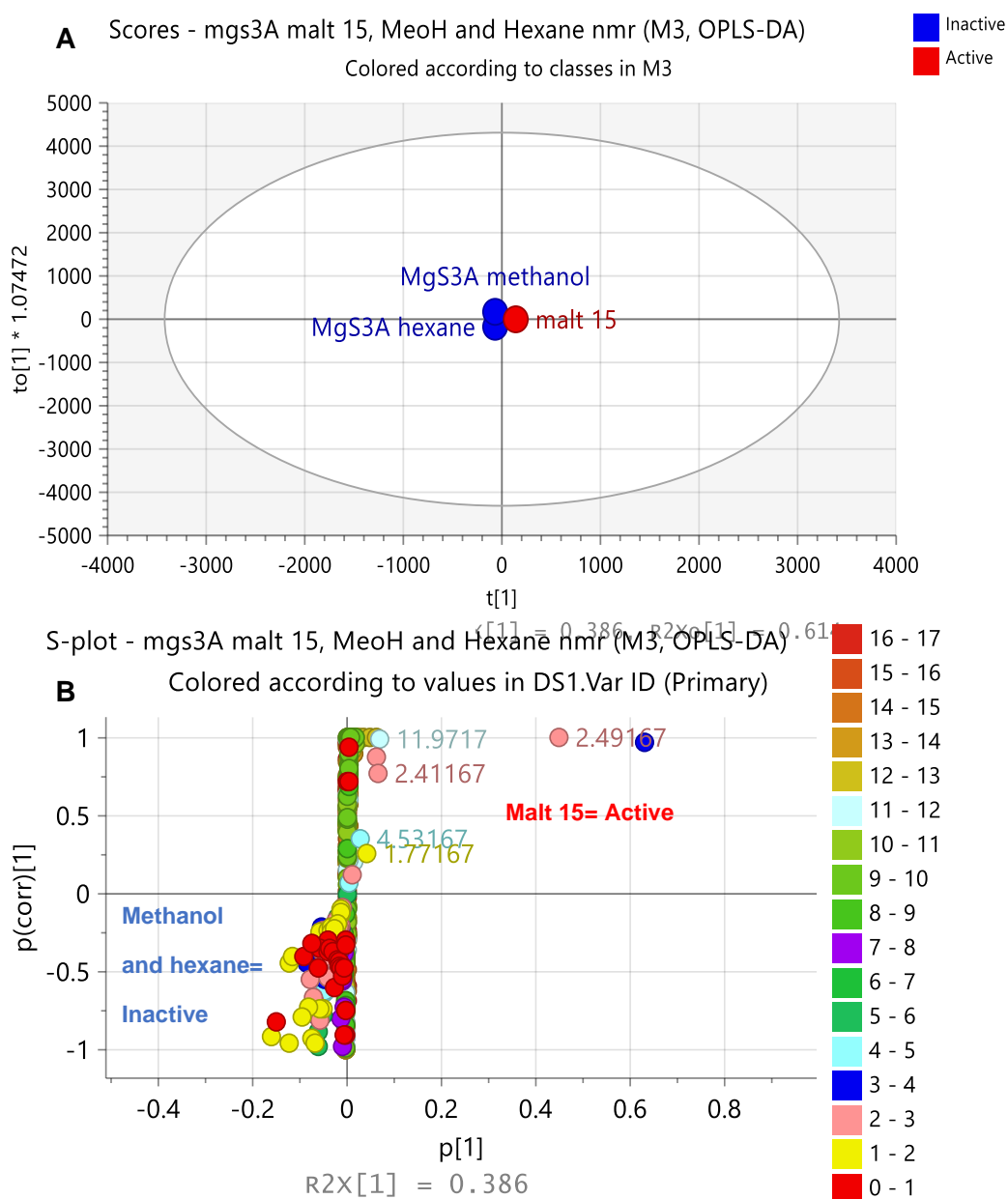


Figure 5.13: OPLS-DA scores (A) and S (B) plots of the NMR spectral data of *F. falciforme* extracts grouped according to their bioactivity against MRSA. R_2 and Q_2 values were both 1. The difference between group R_2X_0 [1] is equal to 61.4 % and the difference within groups R_2X [2] is 38.6 %. The chemical shift of the discriminating features were labelled.

OPLS-DA indicated the top 20 VIP in Figure 5.14. This showed that the discriminatory metabolites from malt 15 extract, MeOH and hexane fractions mostly consisted of aliphatics and sugars ranging from 0.77 to 3.57 ppm.

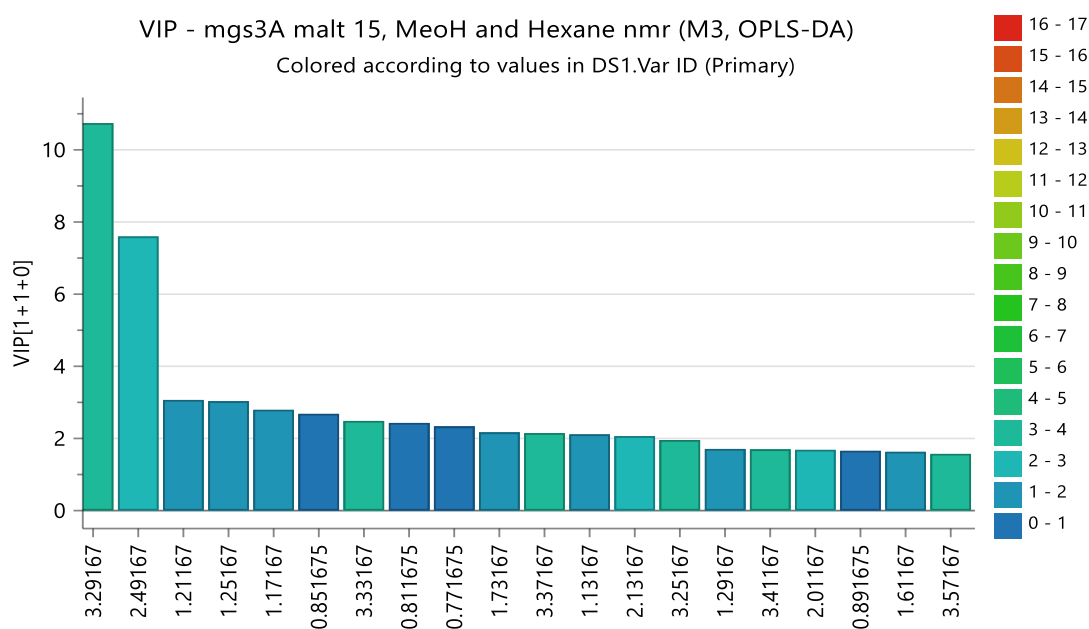
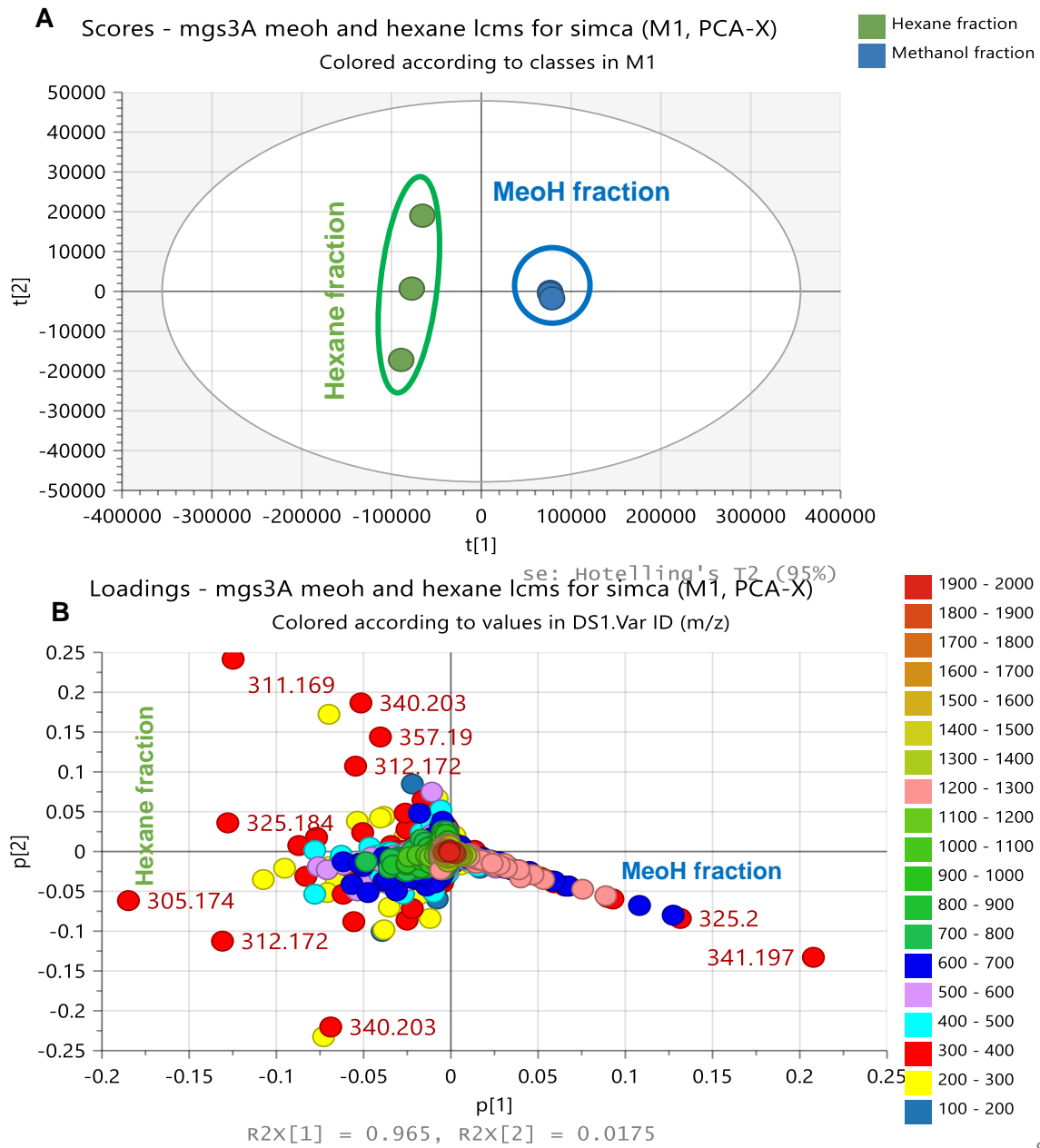


Figure 5.14: VIP scores of *F. falciforme* malt 15 extract, MeOH and hexane fractions from Simca® showing the chemical shifts of 20 most discriminating metabolites with VIP scores above 1.

5.2.9 LC-HRMS analysis of *F. falciforme* fractions

The MeOH and hexane fractions were further subjected to multivariate analysis of the HR-LCMS data to further understand the discrepancies in the chemical profiles of MeOH and hexane fractions which lead to the loss in bioactivity after solvent-solvent partition. The fractions were analysed, and their metabolites compared with malt 15 days extract to understand the differences in metabolites. The unsupervised PCA scores plot showed the MeOH fractions to be at proximity with each other on the right quadrant, while the hexane fractions were located at the upper and lower left quadrant indicating differences in their chemical profiles (5.15A). The loadings plot (Figure 5.15B) indicated the presence of discriminating metabolites from MeOH with low to high m/z values ranging between 271.169 to 1204.85 Da and low m/z values ranging between 197.117 to 506.295 for the hexane fractions. The model gave goodness of fit, (R_2) and predictability, Q_2 values as 0.990 and 0.950, respectively after 3 components. The dereplicated discriminating features of *F. falciforme* MeOH and hexane fractions were shown in Table 5.8. Structures of the discriminating target inactive metabolites predicted by PCA loadings plots were presented in Figure 5.16.



S

Figure 5.15: PCA scores (A) and loadings (B) plots of the LC-HRMS data of *F. falciforme* MeoH and hexane fractions. Labeled features represent the discriminating ion peaks. The R_2 and Q_2 values were 0.990 and 0.950 respectively.

Table 5.8: PCA scores plot dereplicated compound hits for the discriminating metabolites of *F. falciforme* MeOH and hexane fractions. Highlighted rows in green are those earlier defined biomarkers for bioactivity during the optimisation stage.

Mzmine ID	m/z	Rt	M. wt	Molecular Formular (DBE)	Compound hits	Biological source
MeOH fractions						
P2432	271.169	11.56	270.161	C ₁₈ H ₂₂ O ₂ (8)	Tanzawaic acid A (2)	Produced by a marine-derived <i>Penicillium citrinum</i> and <i>Penicillium</i> sp. strains IBWF104-06 and SF-6013
P3113	275.091	12.38	274.084	C ₁₅ H ₁₄ O ₅ (9)	Citrinolactone C (23)	<i>Penicillium citrinum</i>
P2451	289.179	11.56	288.172	C ₁₈ H ₂₄ O ₃ (7)	5-Acetyl-2,3-dihydro-2-(1-hydroxy-1-methylethyl)-7-(3-methyl-2-butenyl) benzofuran (19)	No hit
P4045	291.086	13.34	290.079	C ₁₅ H ₁₄ O ₆ (9)	Javanicin (24)	<i>Fusarium javanicum</i> , <i>F. martici-pisi</i> , <i>F. solani</i> , <i>Nectria haematococca</i> , <i>Neocosmospora vasinflecta</i> and a <i>Cloridium</i> sp.
P2452	307.190	11.63	306.182	C ₁₈ H ₂₆ O ₄ (6)	Albocycline K1 (5)	<i>Streptomyces</i> sp. OH-3984
P2454	325.200	11.61	324.193	C ₁₈ H ₂₈ O ₅ (5)	Albocycline M1 (20)	<i>Streptomyces bruneogriseus</i>
P2455	326.203	11.56	325.196		No hit	
P2384	343.211	11.50	342.203	C ₁₈ H ₃₀ O ₆ (4)	Phomolide C (25)	<i>Phomopsis</i> sp. B27
N1335	341.197	11.56	342.204	C ₁₈ H ₃₀ O ₆ (4)	Albocycline M8 (8)	<i>Streptomyces bruneogriseus</i>
N1336	342.199	11.56	343.207		No hit	
N1638	343.212	12.36	344.22	C ₁₈ H ₃₂ O ₆ (3)	Phomopoxide A (9)	<i>Phomopsis</i> sp. YE3250
N2261	383.208	13.68	384.215	C ₂₀ H ₃₂ O ₇ (5)	Botcinin E (26)	<i>Botrytis cinerea</i> AEM 211

Mzmine ID	m/z	Rt	M. wt	Molecular Formular (DBE)	Compound hits	Biological source
P9000	601.927	18.87	600.92		No hit	
P13688	601.928	24.91	600.921		No hit	
P9014	602.429	18.88	601.421		No hit	
P9001	602.93	18.87	601.923		No hit	
P11733	609.925	22.60	608.917		No hit	
N1338	683.401	11.56	684.408	C ₃₇ H ₅₆ N ₄ O ₈ (12)	3,14-Dihydroxybufa-20,22-dienolide; (3β,5β,14β)-form, 3-(Argininylpimeloyl) (27)	<i>Bufo vulgaris formosus</i> venom
P9037	1202.85	18.90	1201.84	C ₆₂ H ₁₁₁ N ₁₁ O ₁₂ (13)	Cyclosporin X (22)	<i>Tolypocladium inflatum</i> NRRL 8044, DSM 63544
P9017	1203.85	18.88	1202.84		No hit	
P9002	1204.85	18.87	1203.85		No hit	
Hexane fractions						
P5378	197.117	15.01	196.11	C ₁₁ H ₁₆ O ₃ (4)	4-Acetyl-2,4-octadienoic acid; (2E,4S)-form, Me ester (28)	<i>Xylaria</i> sp. NCY2
P11858	233.193	22.74	232.186		No hit	
P9925	241.122	20.19	240.115	C ₁₆ H ₁₆ O ₂ (9)	Menaquinone 1 (29)	<i>Tabebuia avellanedae</i> heartwood; tissue cultures of <i>Catalpa ovata</i>
N2786	249.153	14.62	250.16		No hit	
P5198	255.123	14.50	254.115	C ₁₃ H ₁₈ O ₅ (9)	Phomalone (30)	Metabolite of <i>Phoma etheridgei</i>
P9927	273.148	20.22	272.141	C ₁₇ H ₂₀ O ₃ (8)	1,8,13,16-Heptadecatetraene-4,6-diyne-3,11,12-triol (31)	-

Mzmine ID	m/z	Rt	M. wt	Molecular Formular (DBE)	Compound hits	Biological source
N3197	298.156	15.81	299.163	C ₁₇ H ₂₁ N ₃ O ₂ (9)	Cyclo(isoleucyltryptophyl) (32)	-
P10008	305.174	20.25	304.167	C ₁₈ H ₂₄ O ₄ (7)	Fusamarin (33)	A strain of <i>Fusarium</i> sp.
N4027	311.169	17.78	312.176	C ₁₇ H ₂₈ O ₃ S (4)	3,7-Dimethyl-1-octanol; (R)-form, 4-Methylbensenesulfonyl (34)	-
N4032	312.172	17.77	313.179	C ₁₈ H ₂₃ N ₃ O ₂ (9)	Martensine B (35)	Alkaloid from <i>Martensia fragilis</i>
N3664	313.164	16.89	314.172		No hit	
N4134	327.18	18.51	328.187		No hit	
N4879	340.203	21.41	341.21	C ₂₀ H ₂₇ N ₃ O ₂ (9)	Iboluteine (36)	
P7619	357.19	17.03	356.183	C ₁₈ H ₂₈ O ₇ (5)	Antibiotic SEN 366D1 (37)	<i>Streptomyces</i> sp. SEN366-BP577
P11447	405.226	21.95	404.219	C ₂₃ H ₃₂ O ₆ (7)	Atranone J (38)	<i>Stachybotrys chartarum</i>
P7632	406.243	16.90	405.236		No hit	
P8913	506.295	18.64	505.288		No hit	

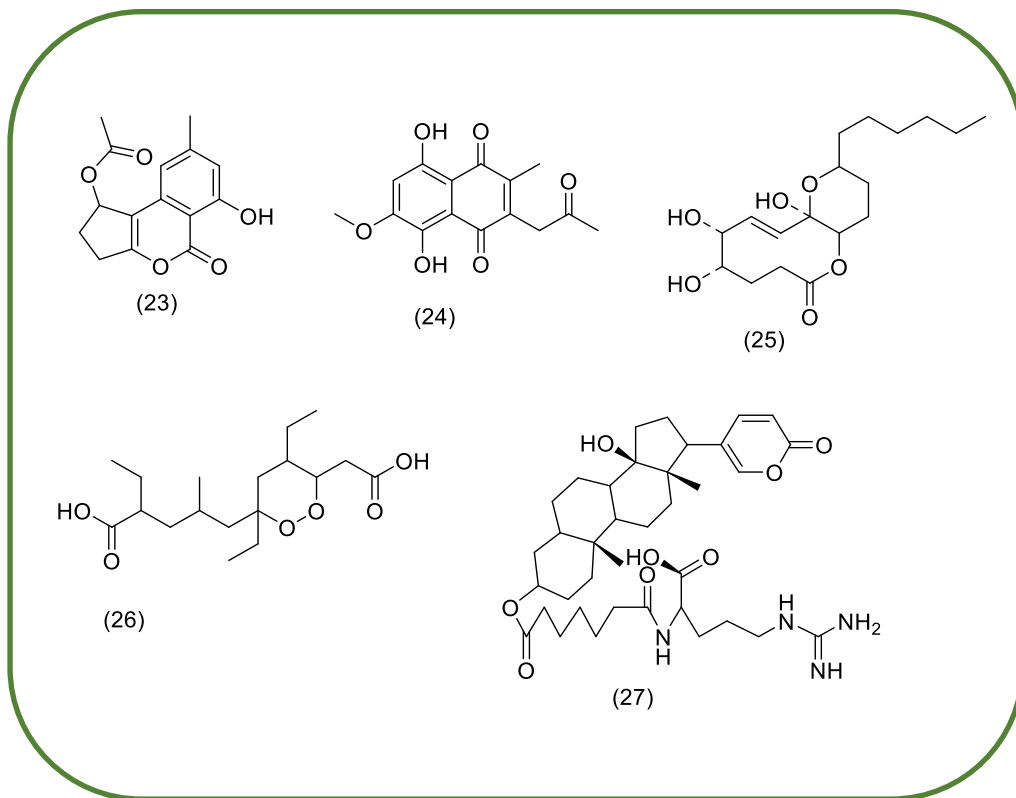


Figure 5.16: Structures of dereplicated compound hits showing PCA discriminating metabolites obtained from *F. falciforme* MeOH (green box) and Hexane (purple box) fractions, as listed in table 5.8 and 5.9.

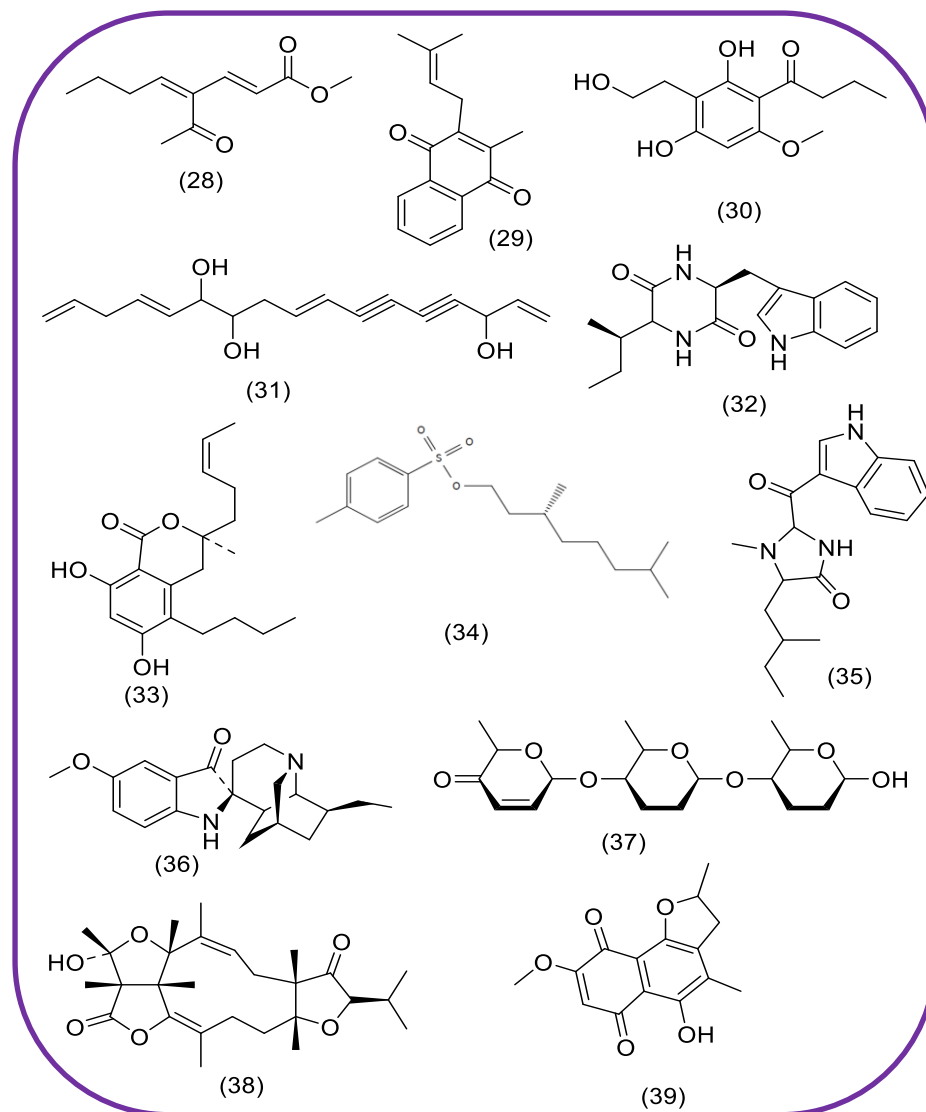


Figure 5.16: Structures of dereplicated compound hits showing PCA discriminating metabolites obtained from *F. falciforme* MeOH (green box) and Hexane (purple box) fractions, as listed in table 5.8 and 5.9.

A PCA scores, and loadings plot were also generated for the LC-MS data, this time including malt 15 days extract. It showed fitness (R_2) and predictability (Q_2) scores of 0.984 and 0.937 respectively, after 3 components. The difference between R_2 and Q_2 values was less than 0.3. This proved to be a good fit, and a good model prediction, which improved when compared to the PCA model. The PCA scores plot in Figure 5.17A of the LC-HRMS data of *F. falciforme*, revealed that extracts obtained from malt 15 days were found in the upper and lower right quadrant (red circles). The methanol fractions were clustered in the upper left quadrant (blue circles), while the hexane fractions (green circles) were clustered in the lower left quadrant of the scores plot, indicating differences in their chemical profiles. This suggested that there was a strong likelihood that a more divergent profile was afforded with malt medium 15 days extracts when compared to the MeOH and hexane fractions.

A PLS-DA analysis was further performed to show a clearer illustration of the differences in metabolic profiles between malt 15 extracts, MeOH and Hexane fractions of *F. falciforme* as shown in Figure 5.18. It gave a clearer illustration by distinguishing the malt 15, Methanol and hexane metabolites on scores and loadings as compared to the PCA. It showed fitness (R_2) and predictability (Q_2) scores of 0.995 and 0.992 respectively, after two components. The difference between R_2 and Q_2 values was less than 0.3. This proved to be a good fit, and a good model prediction, which improved when compared to the PCA model. The variation between groups R_2X_0 [1] was 92.6 % and within group R_2X [2] was 3.5, indicating a high level of percentage similarity within groups and a wide discrepancy in the chemical profiles between groups, and this further explains the differences in their bioactivity. From the scores plot (Figure 5.18A), extracts obtained from malt 15 media were clustered in the middle-left quadrant (red circles). The methanol fractions were clustered in the upper right quadrant (blue circles), while the hexane fractions (green circles) were clustered in the lower right quadrant on the PLS-DA plot.

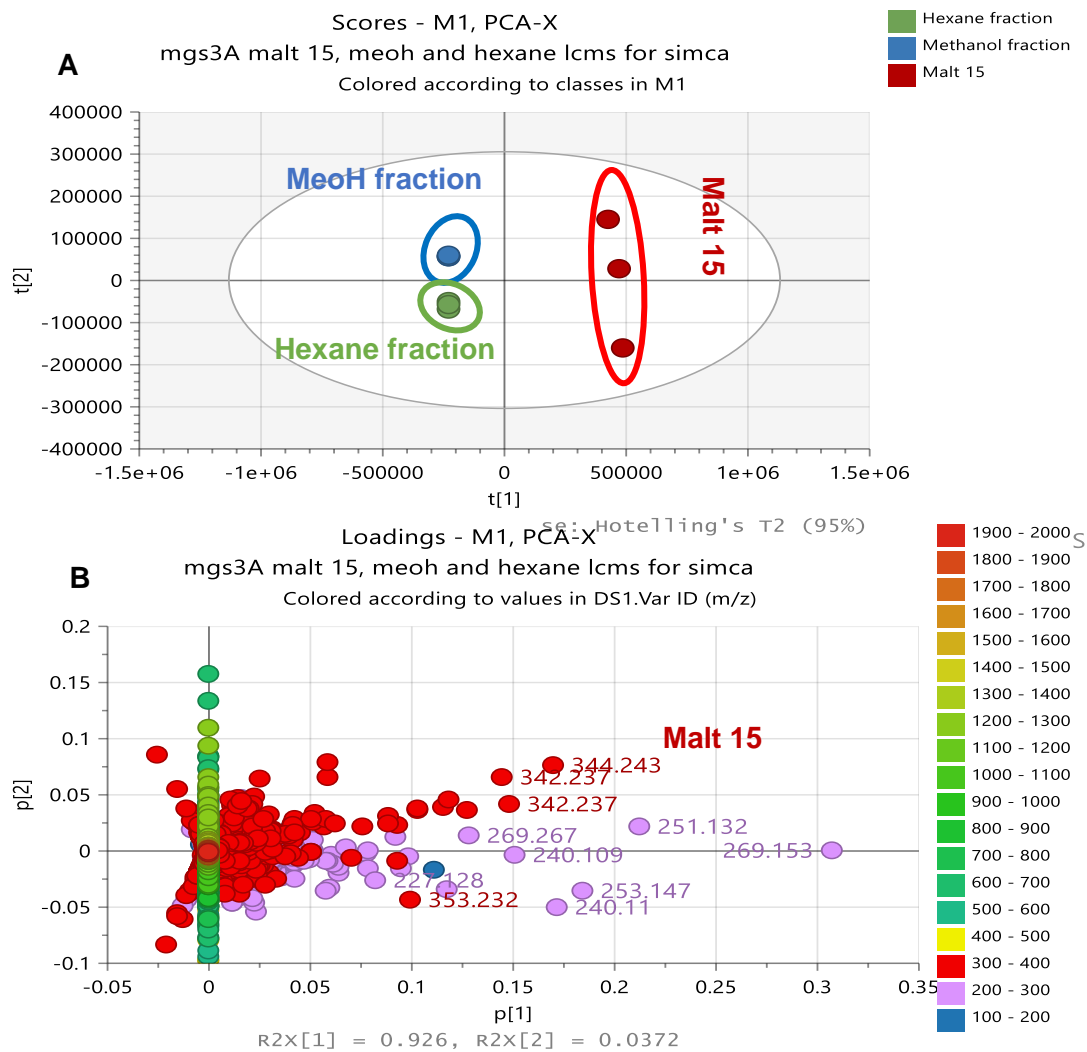


Figure 5.17: PCA scores (A) and loadings (B) plots of the LC-HRMS data of *F. falciforme* Malt 15 days extracts, MeOH and hexane fractions. Labelled features represent the discriminating ion peaks. The R_2 and Q_2 values were 0.984 and 0.937 respectively.

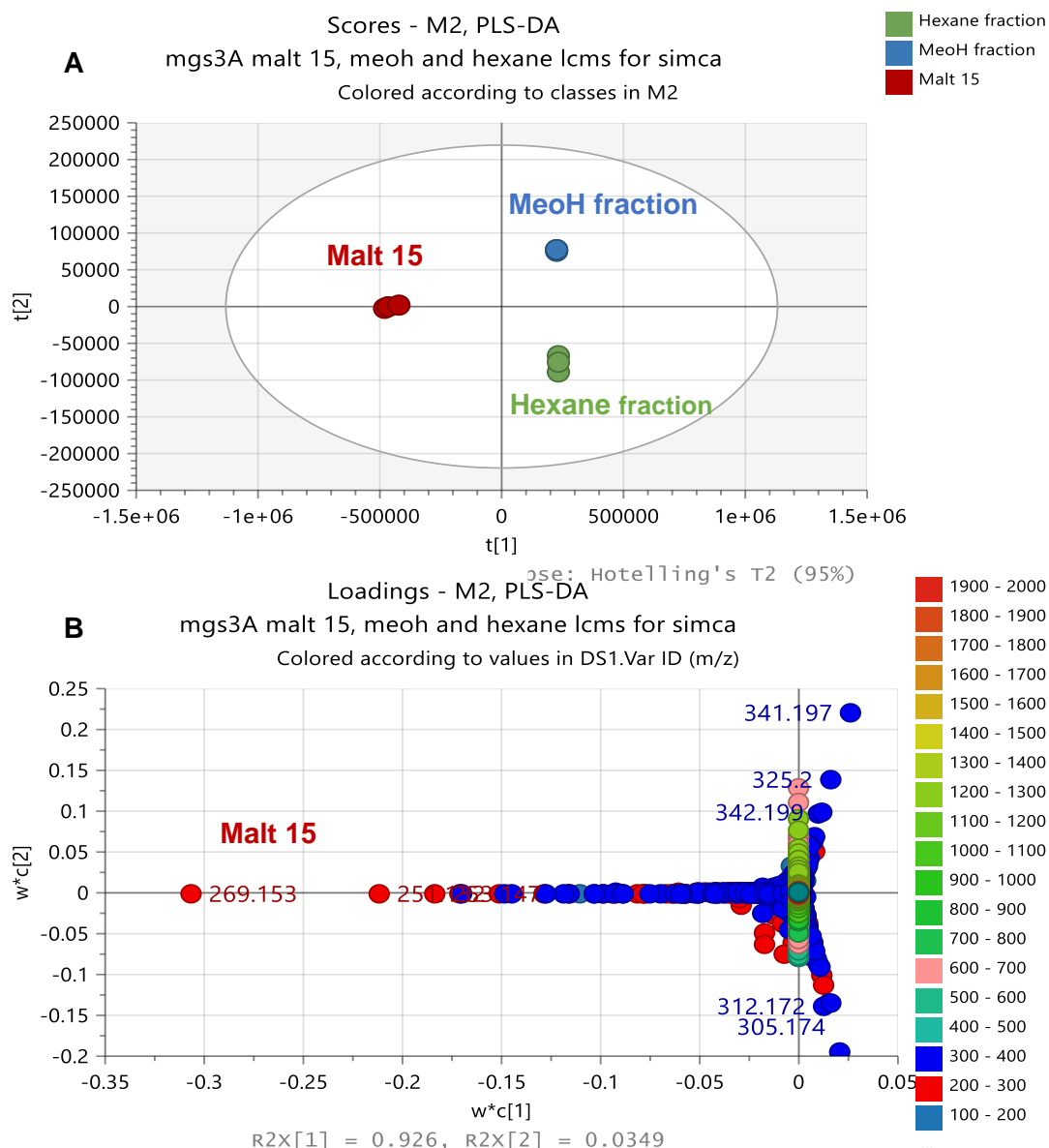


Figure 5.18: PLS-DA scores (A) and loadings (B) plots of the LC-HRMS data of *F. falciforme* Malt 15 days extracts, MeOH and hexane fractions. Labeled features represent the discriminating ion peaks. The R_2 and Q_2 values were 0.995 and 0.992 respectively.

Table 5.9: Dereplicated compound hits for the discriminating metabolites of *F. falciforme* malt 15 days extract obtained from the PLS-DA loadings plot on Figure 5.18B. Compound structure (39) is shown in figure 5.16.

Mzmine ID	m/z	Rt	M. wt	P value	Molecular Formular (DBE)	Compound hits	Biological source
P605	181.086	8.89	180.078	1.33266e-05	C ₁₀ H ₁₂ O ₃ (5)	3-Propylgentisylquinone (1)	Fungal isolate CR1223-D
P553	271.169	15.40	270.161	4.78786e-07	C ₁₈ H ₂₂ O ₂ (8)	Tanzawaic acid A (2)	<i>Securinega suffruticosa</i>
P1107	275.091	12.45	274.084	1.61312e-06	C ₁₅ H ₁₄ O ₅ (9)	Dihydroanhydrojavanicin (39)	<i>Fusarium solani</i>
N752	279.197	15.44	280.204	3.52471e-07	C ₁₇ H ₂₈ O ₃ (4)	5(1→10)-Abeo-1,8-patchoulanediol; 8β-form, 8-Ac (18)	<i>Valeriana fauriei</i>
P558	289.179	11.60	288.172	0.0231184	C ₁₈ H ₂₄ O ₃ (7)	Colletorin B (4)	<i>Cephalosporium diospyri</i> and <i>Nectria galligena</i> .
P1097	291.086	13.41	290.079	6.82377e-12	C ₁₅ H ₁₄ O ₆ (9)	Javanicin (24)	<i>Fusarium javanicum</i> , <i>Fusarium martici-pisi</i> , <i>F. solani</i> , <i>Nectria haematococca</i> , <i>Neocosmospora vasinfecta</i> and a <i>Chloridium</i> sp.
P547	307.190	15.44	306.182	4.78451e-07	C ₁₈ H ₂₆ O ₄ (6)	Albocycline K1 (5)	<i>Streptomyces</i> sp. OH-3984
P548	325.200	15.42	324.193	5.17256e-07	C ₁₈ H ₂₈ O ₅ (5)	Albocycline M1 (20)	<i>Streptomyces bruneogriseus</i>
N79	323.186	15.44	324.194	3.7291e-07	C ₁₈ H ₂₈ O ₅ (5)	Hymeglusin (6)	<i>Cephalosporium</i> sp., <i>Scopulariopsis</i> sp. and <i>Fusarium</i> sp.
P1096	326.203	11.59	325.196	0.0175882		No hit	
N753	325.202	14.38	326.209	2.45818e-05	C ₁₈ H ₃₀ O ₅ (4)	Penisporolide A (21)	Marine derived <i>Penicillium</i> sp. (HKI strain GT20022605)
N26	341.197	11.59	342.204	0.226744	C ₁₈ H ₃₀ O ₆ (4)	Albocycline M8 (8)	<i>Streptomyces bruneogriseus</i>
N1291	342.2	11.59	343.207	0.0267748		No hit	

Mzmine ID	<i>m/z</i>	Rt	M. wt	<i>P value</i>	Molecular Formular (DBE)	Compound hits	Biological source
P1956	601.928	25.13	600.92	0.123156		No hit	
P2345	602.429	25.22	601.421	0.123534		No hit	
N751	647.38	15.43	648.387	0.000127556		No hit	
N763	683.4	11.60	684.408	0.0174762		Complex of <i>m/z</i> 341.197	
P563	1202.85	17.28	1201.84	1.4711e-05	C ₆₂ H ₁₁₁ N ₁₁ O ₁₂ (13)	Cyclosporin X (22)	<i>Tolypocladium inflatum</i> NRRL 8044, DSM 63544
P587	1203.85	25.48	1202.84	0.052185		No hit	

Table 5.10: Comparison of dereplicated compound hits for the discriminatory metabolites of *F. faliforme* extracts obtained from malt broth 15 days, MeOH and hexane fractions.

	Malt 15 days	MeOH fractions	Hexane fractions
1	2-(Hydroxymethyl)-3-propyl-1,4-benzenediol; 1,4-Quinone	Phomolide C	4-Acetyl-2,4-octadienoic acid; (2E,4S)-form, Me ester (1)
2	Tanzawaic acid A	Tanzawaic acid A	Iboluteine
3	2,3-Dihydro-5-hydroxy-8-methoxy-2,4-dimethylnaphtho[1,2-b] furan-6,9-dione	5-Acetyl-2,3-dihydro-2-(1-hydroxy-1-methylethyl)-7-(3-methyl-2-butenyl) Benzofuran	2-Methyl-3-prenyl-1,4-naphthoquinone
4	5(1→10)-Abeo-1,8-patchoulanediol; 8β-form, 8-Ac	Citrinolactone B; 1-Ac	Antibiotic SEN 366D1
5	Colletorin B	Phomopoxide A	Phomalone
6	Javanicin	Javanicin	1,8,13,16-Heptadecatetraene-4,6-diyne-3,11,12-triol
7	Albocycline K1	Albocycline K1	Cyclo(isoleucyltryptophyl)
8	Albocycline M1	Albocycline M1	3,7-Dimethyl-1-octanol; (R)-form, 4-Methylbenzenesulfonyl
9	Hymeglusin	Botcinin A; O-De-Ac	Martensine A; 10-Ketone
10	Penisporolide A	3,14-Dihydroxybufa-20,22-dienolide; (3β,5β,14β)-form, 3-(Argininylpimeloyl)	Fusamarin
11	Albocycline M8	Albocycline M8	Atranone J
12	Cyclosporin X	Cyclosporin X	
13	No hits	No hits	No hits

Highlighted metabolites (blue box) indicate common metabolites observed on malt 15 days extracts, MeOH and hexane fractions.

Six common metabolites were observed in malt 15 days extracts and MeOH fractions as shown in Table 5.10, but no common metabolites were observed for the hexane fractions. This could explain why the MeOH fraction was partially active only against prebiofilm MRSA, but the hexane fraction was completely inactive.

It can be deduced that the bioactivity observed from malt 15 days extract was dependent on the extract remaining in its crude form together with the fatty acids inherent in the crude. The solvent-solvent partition removed the lipids using hexane solvent, and this could have contributed to the

loss in bioactivity. The bioactivity of *F. falciforme* depended on the synergistic effects between the lipids and the metabolites, hence separating them could have resulted in the loss of its bioactivity. This can be confirmed by the fact that; the bioactivity was restored after the methanol extract (0.5 mg/ mL) and hexane extract (0.5 mg/ mL) were merged. The combination was able to inhibit planktonic MRSA by 54.51% and eradicate preformed biofilm by 59.65 % as shown in Figure 5.19 below. The fatty acids inherent in the extract could have contributed to its postbiofilm activity, as it has been observed during this study, that fatty acid metabolites could permeate the cell wall of the pathogenic MRSA, hence eradicating or reducing already formed biofilm.

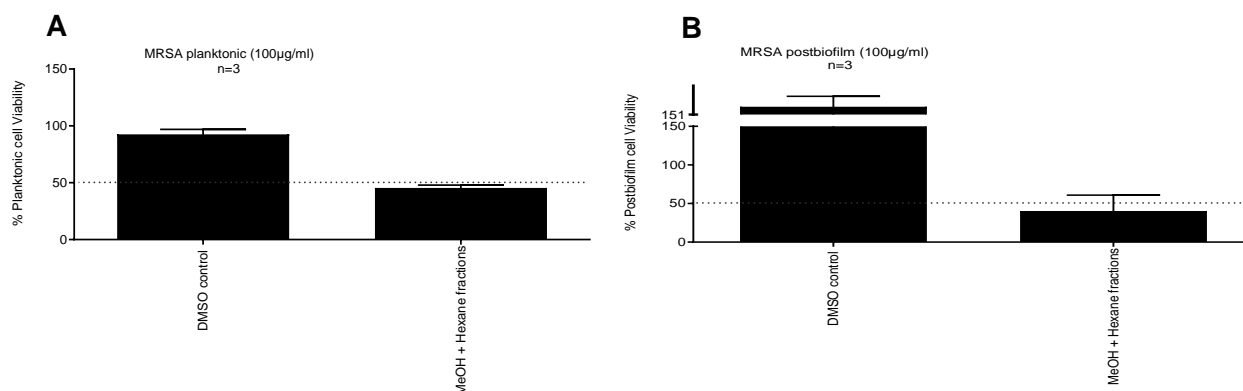


Figure 5.19: Effect of *F. falciforme* fractions (MeOH + Hexane) on (A) Planktonic and (B) Post biofilm MRSA. The combination of 50% MeOH and 50% hexane fractions restored *F. falciforme* bioactivity.

5.3 Summary and conclusion

5.3.1 Isolation of fungi and extraction

The endophytic fungi *F. falciforme* was isolated from the stem of *M. oleifera* in this study. There are previous reports on the isolation of *F. falciforme* from other plants such as cassava tubers, *Boehmeria nivea*, chrysanthemum, and chickpea, but there are no records of its isolation from *M. oleifera*, hence this will be the first report. Crude extract of *F. falciforme* proved to be active (>80%) against MRSA but was inactive to *P. aeruginosa*.

5.3.2 Media optimisation and metabolomics guided fractionation

Media optimisation showed *F. falciforme* extracts from rice, malt, and potato media to be active against MRSA, but the extract from oat media was inactive. *F. falciforme* proved to be stable on all the malt media at 7-, 15-, and 30-days of incubation period, with the best were the extracts from malt media incubated for 15 days, hence was selected as the optimum media for scaling up, with an average extract weight of 119.4 mg, antimicrobial inhibition of 90.28%, and biofilm prevention at 99.36%. Also, when processed on Simca, metabolites from the other media were clustered together indicating that those metabolites were not unique, while metabolites from malt media were discriminatory. Furthermore, proton NMR spectra for malt media showed differences between the blank media and fungal extracts at δ_H 5.5 to 6.0 ppm, 9.0 to 9.5 ppm and 13.00 to 13.5 ppm indicating the presence of aromatics and carboxylic acids. The huge intensity signals at 1.00 to 2.00 ppm represent aliphatic acids, while the olefinic protons present in unsaturated fatty acids were found at around 5.00 to 5.50 ppm, indicating diversity of metabolites inherent in the extract when incubated in the malt media. Therefore, malt media was selected as the optimum media for the scale up cultivation of *F. falciforme*, with the understanding that the secondary metabolites that will be isolated from this fungus using this media, would be active and could be novel or unique. The effect on the production of the bioactive metabolites in the various media used in this study was in decreasing order: Malt > potato > rice > oat.

5.3.3 Scale up and loss of bioactivity

The scaled up crude extract of *F. falciforme* showed two layers of fatty acids on the TLC plate. Solvent to solvent partition using hexane and aqueous methanol was done to separate the fatty acids from the secondary metabolites. Bioassay was performed on the methanol and hexane fractions to select the active extract for further purification work, and it was observed that there was a loss in bioactivity. The dereplicated compound hits showed that there were six common metabolites found in both the MeOH fraction and the crude extract obtained from the malt media incubated for 15 days, while none of these metabolites were found to be common in the hexane fraction. The common metabolites were tanzawaic acid A, javanicin, albocycline K1, albocycline M1, albocycline M8 and cyclosporin X. The loss in bioactivity could be attributed to the solvents used for the partitioning. The change of solvents from EtOAc to methanol and hexane, could have contributed to the loss of activity. A previous study demonstrated that EtOAc crude extract presented high broad-spectrum activity as compared to hexane extract. This means that ethyl acetate likely contained the maximum concentration of bioactive compounds which directly or

indirectly influenced inhibition (Elghaffar *et al.*, 2022). It can also be deduced that the bioactivity observed from malt 15 days crude extract was dependent on the extract remaining in its crude form together with the fatty acids inherent in the crude extract. Thus, the bioactivity of *F. falciforme* depended on the synergistic or complementary effect between the lipids and the predicted bioactive metabolites, therefore separating them could have resulted in the loss of its bioactivity. The lipids would have been necessary to permeate the bacterial cell wall and/or the biofilm. This can be confirmed by the fact that; the bioactivity was restored after the methanol extract (0.5 mg/mL) and hexane extract (0.5 mg/mL) were merged. The combination was able to inhibit planktonic MRSA by 54.51% and eradicate preformed biofilm by 59.65 %.

In conclusion, crude extract of *F. falciforme* was active against MRSA. PCA Simca plot showed the metabolites inherent to the crude extract to be discriminatory and unique. After scaling up and solvent to solvent partition using hexane and aqueous MeOH to separate the lipids, *F. falciforme* lost its bioactivity, hence MeOH and hexane fractions of *F. falciforme* did not go to further purification work. It can therefore be deduced that the lipids played an active role in making the crude extract bioactive, as it worked in synergy with the other predicted bioactive metabolites inherent in the crude extract to be active against MRSA.

CHAPTER 6

6 Secondary metabolites of *A. alternata* isolated from *A. indica*

6.1 Metabolites of *A. alternata*

Alternaria fungi are widely spread in nature and have been reported to act as phytopathogens, plant pathogens, parasites, saprophytes, and endophytes (Thomma, 2003). Endophytic isolates of *A. alternata* have been shown to exist as asymptomatic symbionts with no ability to cause disease (Spurr Jr and Welty, 1975).

A. alternata was among the first reported endophytic fungi isolated from *Viola rotundifoliarhisomes*. It is found widely in nature (Aly *et al.*, 2008). Previous chemical investigations of *A. alternata* identified terpenoids, phenolics, pyranones, steroids, quinones, and nitrogen-containing metabolites, some of which exhibited cytotoxic, phytotoxic, antimicrobial, and antifungal activities (Abbas and Riley, 1996, Lou *et al.*, 2013, Sabbagh *et al.*, 2019, Musetti *et al.*, 2007).

Toxic metabolites secreted by *Alternaria* species can be categorised into three major structural categories (i) dibenzo- α -pyrone derivatives which are exemplified by alternariol (AOH), alternariol monomethyl ether (AME) and altenuene (ALT); (ii) perylene derivatives like altertoxins I, II and III, (iii) tetramic acid derivative, and tenuasonic acid (TeA). The chemical composition of three mycotoxins commonly produced by *Alternaria sp.* are (i) AOH (C₁₄H₁₀O₅): 3, 7, 9-trihydroxy-1-methyl-6H-dibenzo (b, d) pyran-6-one; M.W. 258; (ii) AME (C₁₅H₁₂O₅): 3, 7-dihydroxy-9-methoxy-1-methyl-6H-dibenzo (b, d) pyran-6-one; M.W. 272; (iii) TeA (C₁₀H₁₅O₃N): 3-acetyl-5-sec-butyl-4-hydroxy-3-pyrrolin-2-one; M.W. 197 (Meena *et al.*, 2017, Ostry, 2008, Logrieco *et al.*, 2009).

6.2 Results and Discussion

6.2.1 Media optimisation and identification of metabolite production from *A. alternata*.

Media optimisation and identification of metabolite production was carried out on the pure strain of *A. alternata*. The metabolites produced from media optimisation extracts of *A. alternata* were analysed using NMR and HRESI-LCMS for dereplication studies and tested against MRSA activity. Media optimisation of *A. alternata* extracts showed that the extract obtained from the rice

culture media incubated for 15 days (DgS2 R15), malt extract broth on 7 and 15 days (DgS2 M7 and M15), and potato dextrose broth on 30 days (P30) showed bioactivity against MRSA with at least 60% planktonic and antibiofilm inhibition (Table 6.2).

6.2.2 A. *alternata* extract yields on 4 different media.

Solid media produced higher yields of extract than liquid media. As depicted in Table 6.1, the highest yield of *A. alternata* extract was gained from the oat medium while the lowest extract yield was obtained from malt broth.

The histogram below (Figure 6.1) shows the extract yields for *A. alternata* at 7, 15, and 30 days of incubation on four different media. After 15 days of incubation in malt extract (ME) broth, potato dextrose broth, and rice media, *A. alternata* was seen to still be exponentially growing, and could be said to have attained the stationary growth phase on the 30th day of incubation. This indicates that the fungi culminated to metabolise the nutrients inherent in the media. Huge differences were observed in the extract yield between the liquid media and their controls indicating that the liquid media were more utilised by the fungi than the solid media. On the other hand, the extract yields started to decline after 15 days of incubation on oat media, which implied the end of its stationary phase and beginning of the death phase. The stationary and death phase experienced on oat media, after 15 days of incubation could also be signified by the endophytes inability to metabolise and process the media nutrient inherent in oat. The obtained yield of the extracts of *A. alternata* extract after 7, 15, and 30 days of incubation on four different media are listed in Table 6.1.

Table 6.1: Extract weights of *A. alternata* grown on different media and incubated for 7, 15, and 30 days as illustrated in Figure 6.1. All cultures were incubated at 27°C.

7 days		15 days		30 days		Controls	
Solid media							
DgS2-R7-1	812.4	DgS2-R15-1	2743.5	DgS2-R30-1	2780.8	RC1	747.8
DgS2-R7-2	907.1	DgS2-R15-2	2992.1	DgS2-R30-2	3157.6	RC2	809.4
DgS2-R7-3	866.0	DgS2-R15-3	2869.2	DgS2-R30-3	3174.3	RC3	865.5
Average weight (mg)	861.8		2868.3		3037.6		807.6
DgS2-O7-1	5904.7	DgS2-O15-1	5571.3	DgS2-O30-1	4117.5	OC1	5963.4
DgS2-O7-2	5969.2	DgS2-O15-2	5053.3	DgS2-O30-2	3683.1	OC2	6291.9
DgS2-O7-3	5773.0	DgS2-O15-3	5248.8	DgS2-O30-3	3951.8	OC3	5822.3
Average weight (mg)	5882.3		5291.1		3917.5		6025.9
Liquid media							
DgS2-M7-1	69.7	DgS2-M15-1	117.6	DgS2-M30-1	135.8	MC1	7.1
DgS2-M7-2	66.0	DgS2-M15-2	113.1	DgS2-M30-2	112.3	MC2	6.7
DgS2-M7-3	65.4	DgS2-M15-3	114.1	DgS2-M30-3	113.4	MC3	6.2
Average weight (mg)	67.0		114.9		120.5		6.7
DgS2-P7-1	40.9	DgS2-P15-1	316.8	DgS2-P30-1	344.8	PC1	15.5
DgS2-P7-2	41.0	DgS2-P15-2	213.1	DgS2-P30-2	355.6	PC2	9.9
DgS2-P7-3	54.7	DgS2-P15-3	490.2	DgS2-P30-3	395.5	PC3	11.3
Average weight (mg)	45.5		340.0		365.3		12.2

*Media code and full names are listed in Table 4.2

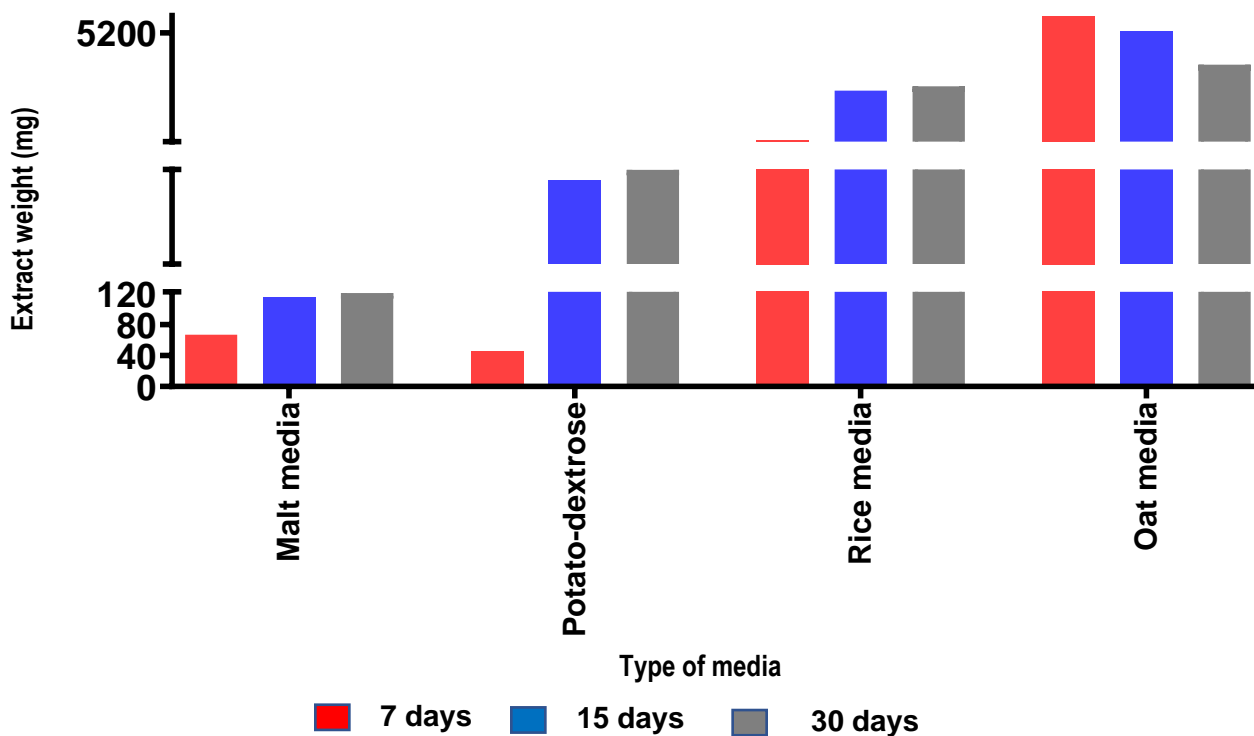


Figure 6.1: Histogram showing average weight of extracts from three respective replicates of *A. alternata* obtained from four different media and incubated at 7, 15, and 30 days.

6.2.3 Extract test against MRSA

The biological activity of *A. alternata* extracts obtained from various media were tested against MRSA cells before selecting the optimal medium for large-scale fermentation. Incubation of the fungus on malt for 7 and 15 days, on rice for 15 days, and on potato dextrose for 30 days afforded 69.16% to 100% inhibition of planktonic and prebiofilm MRSA but all the extracts from oat media were found to be inactive. Bioactivity threshold was set at 40% cell viability (60% inhibition) for both planktonic and prebiofilm activity. Both ¹H NMR and LC-HRMS data were used to investigate the chemical composition of the afforded extracts.

Table 6.2: Summary activity of *A. alternata* extracts from different media against Planktonic, prebiofilm, and postbiofilm MRSA at concentrations of 100 µg/ml.

Media	Incubation Period	Antimicrobial % inhibition	Stdev	Prebiofilm % inhibition	Stdev	Postbiofilm % inhibition	Stdev
Malt	7	69.16	4.15	93.07	2.06	<0.00	17.86
Rice	15	80.64	11.33	98.17	13.80	14.26	7.69
Malt	15	60.70	11.23	100.00	4.75	<0.00	2.46
Potato	15	41.69	15.15	84.03	24.07	48.10	12.07
Malt	30	56.63	36.92	95.09	5.23	<0.00	>100.00
Potato	30	91.69	2.30	100.00	2.02	20.64	17.16

*Cells highlighted in blue colour indicates extracts with consistent bioactivity for all replicates, cells with white colour represents inactive fractions, while gold-coloured cells indicate active fractions with inconsistent bioactivity amongst replicates and therefore regarded as inactive.

6.2.4 MVA of LC-HRMS data

For multivariate analysis, a PCA scores and loadings plot were generated for the LC-MS data. The extracts were grouped according to the different media on which the endophyte was incubated for 7, 15 and 30 days. The PCA scores plot in Figure 6.2A of the LC-HRMS data of *A. alternata* revealed that extracts obtained from malt media after 30 days of incubation, were found on the upper right side of the plot, while extracts from 7 and 15 days incubation were on the left quadrant which implied a strong similarity in their metabolomic profiles (red dots), as extracts obtained by incubation from malt for 7 and 15 days were active against MRSA but the fungal extract from malt incubated for 30 days was inactive. Fungal extracts from rice media incubated for 7 and 15 days were clustered in the middle of the plot and in the lower left quadrant, while extracts from rice 30 days were discriminatory in the lower right quadrant (green dots). Extracts obtained from rice after 30 days of incubation afforded unique discriminatory metabolites but were inactive. The fungal extracts from the oat media were clustered at the lower left quadrant (blue dots) close to extracts obtained from rice incubated for 7 and 15 days. Their proximity in the plot could be because of the presence of high lipid content inherent in both media. Extracts obtained from potato media at 7 and 15 days were in the lower and upper left quadrant (yellow dots). On

the scores plot, fungal extracts from potato dextrose incubated for 30 days were clustered on the upper quadrant (yellow dots), which were separated from those incubated for 7 and 15 days indicating the differences in their chemical profiles which could have contributed to the bioactivity observed in potato 30 days. The loadings plot in Figure 6.2B, demonstrated that discriminating metabolites from extracts of culture grown on rice for 30 days produced low molecular weight metabolites ranging from 191 to 338 Da (encircled in green). While extracts from the potato and malt media incubated for 30 days contained discriminatory metabolites with molecular weight from 245 to 579 Da, as encircled in yellow and red. The discriminating metabolites obtained from the malt and potato media incubated at 30 days were represented by ion peaks at m/z 273.075, 273.041, 273.041, 287.057, 329.046, 347.057, 349.072, 579.151, 245.082, 274.079, 289.072, 290.075 were putatively identified as: 9-O-methylalternariol, altenuisol, 2-hydroxyalternariolc, dehydroaltenusin, 2-deoxybulgarhodin, altertoxin III, altechin, and gambiriin A1, respectively, along with no compound hits for four ion peaks indicating the presence of novel compounds. The discriminating metabolites of the extracts obtained from the rice media incubated for 30 days were represented by ion peaks at m/z 191.07, 257.08, 274.091, 277.072, 291.088, 337.093, 338.096 was denoted as 2-acetyl-7-methoxyBenzofuran, resveratrodehyde, citrinolactone C, alternarienoic acid, altenuene, and exserolide J. Dereplicated compound hits for the discriminating metabolites are listed in Table 6.3. Compound 9-O-methylalternariol have previously showed antinematodal activity against *Caenorhabditis elegans* and *Bursaphelenchus xylophilus* with IC_{50} values of 74.62 $\mu\text{g/mL}$ and 98.17 $\mu\text{g/mL}$ respectively (Lou *et al.*, 2016). It is also a mycotoxin and a glycogen-synthase-kinase 3 β (GSK-3) inhibitor. Alternariol (AOH) is a mycotoxin formed in *A. alternata*, and has been reported to possess genotoxic properties (Fehr *et al.*, 2009). Dehydroaltenusin is an antifungal agent. It possesses anti-tumor activity against human adenocarcinoma tumor in vivo and serves as an inhibitor of mammalian DNA polymerase α . Previous report on altertoxins suggested that the epoxyperylene structural scaffold inherent in them may be manipulated to produce potent anti-HIV therapeutics (Bashyal *et al.*, 2014). Gambiriin A1 could serve as a potential biomarker for the consumption of foods. This is because it has been detected but not quantified in several different foods, such as green tea, red tea, herbal tea, teas (*Camellia sinensis*), and herbs and spices. Altenuene exhibited moderate to weak inhibition against *Bacillus subtilis* (Wang *et al.*, 2014). 2-Acetyl-7-methoxyBenzofuran is an α -glucosidase inhibitor. 1-O-caffeoylquinic acid; 4- Deoxy (CQAs) possess anti-inflammatory and antioxidant properties, hence have been considered beneficial for human health (Alcázar Magaña *et al.*, 2021).

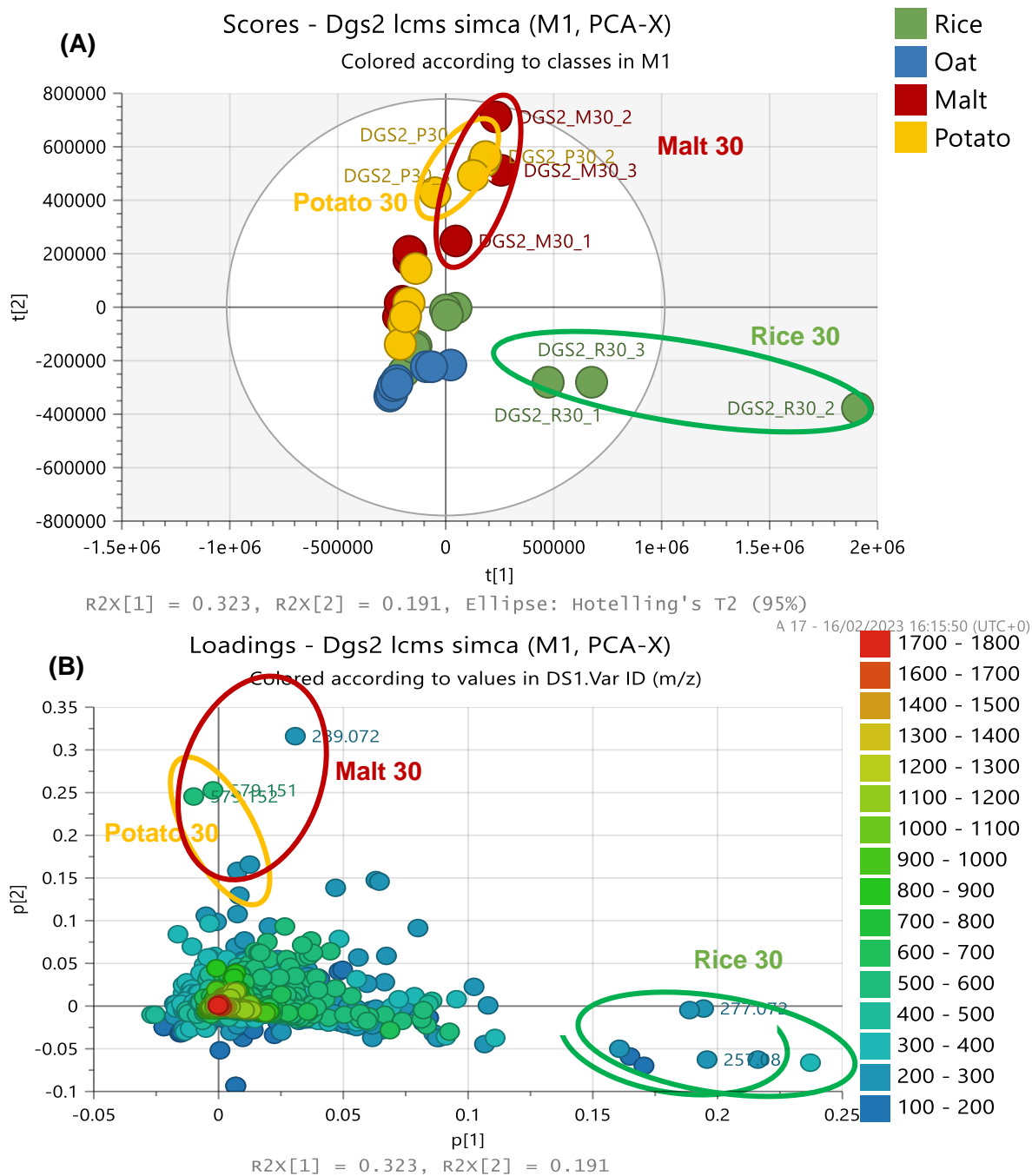


Figure 6.2: (A) PCA scores and (B) loading plots of LC-HRMS data of *A. alternata* extracts from four media incubated at 7, 15, and 30 days. $R_2X = 0.727$ and $Q_2X = 0.374$. Encircled features represent the discriminating ion peaks for the outlying extracts obtained from malt 30, potato 30 and rice 30 days. Annotations for discriminating metabolites are listed under Table 6.3.

Table 6.3: Dereplication data of the discriminating metabolites of *A. alternata* from potato, malt, and rice media 30 days acquired from the PCA loadings plot on Figure 6.2B. Structures of compound hits are shown under Figure 6.3.

Mzmine ID	<i>m/z</i>	Rt (min)	M.wt	Molecular formular (DBE)	Compound HITS	Reported Biological Source
Malt 30 days and potato 30 days						
N15965	245.082	10.60	246.0891		No hit	
P2	273.075	15.86	272.068	C ₁₅ H ₁₂ O ₅ (10)	9-O-methylalternariol (1)	<i>Alternaria</i> sp. including marine sp. <i>Anthocleista djalensis</i> , <i>Penicillium diversum</i> and <i>Lachnum palmae</i> .
P377	274.079	18.91	273.071		No hit	
N15024	273.041	12.22	274.048	C ₁₄ H ₁₀ O ₆ (10)	Altenuisol (2)	<i>Alternaria tenuis</i> and <i>Penicillium verruculosum</i> F375.
N373	273.041	12.55	274.048	C ₁₄ H ₁₀ O ₆ (10)	2-hydroxyalternariol (3)	Mangrove derived <i>Alternaria</i> sp. SK6YW3L
N1362	287.057	10.71	288.064	C ₁₅ H ₁₂ O ₆ (10)	Dehydroaltenusin (4)	<i>Alternaria kikuchiana</i> , <i>A. tenuis</i> , <i>A. vermiculatum</i> , <i>A. dauci</i> , <i>Talaromyces flavus</i> , <i>Penicillium</i> sp. and <i>Acremonium</i> sp. 98H02B04-1
N49	289.072	10.75	290.079	C ₁₅ H ₁₄ O ₆ (9)	Altenusin (5)	<i>Alternaria tenuis</i> , <i>Penicillium</i> sp. and <i>Talaromyces</i> sp.
N8157	290.075	10.72	291.082		No hit	
N30	329.046	14.45	330.054	C ₂₀ H ₁₀ O ₅ (16)	2-deoxybulgarhodin (6)	<i>Bulgaria inquinans</i> and <i>Heteroconium</i> sp.
N33	347.057	14.47	348.064	C ₂₀ H ₁₂ O ₆ (15)	Altertoxin III (7)	<i>Alternaria alternata</i>

Mzmine ID	m/z	Rt (min)	M.wt	Molecular formular (DBE)	Compound HITS	Reported Biological Source
N116	349.072	14.06	350.080	C ₂₀ H ₁₄ O ₆ (14)	Altechin (8)	Pigment from <i>Alternaria</i> sp., including a marine sp.
N2202	579.151	10.72	580.159	C ₃₀ H ₂₈ O ₁₂ (17)	Gambiriin A1 (9)	Isolated from <i>Uncaria gambir</i> and <i>Sanguisorba officinalis</i>
Rice 30 days						
P2278	191.07	8.35	190.063	C ₁₁ H ₁₀ O ₃ (7)	2-acetyl-7-methoxybenzofuran (10)	Mangrove-derived <i>Sporothrix</i> sp. No.4335
P517	257.08	9.36	256.073	C ₁₅ H ₁₂ O ₄ (10)	Resveratrodehyde A (11)	Mangrove-derived <i>Alternaria</i> sp. R6
P518	275.091	9.48	274.084	C ₁₅ H ₁₄ O ₅ (9)	Citrinolactone C (12)	<i>Penicillium citrinum</i>
N6457	277.072	7.97	278.079	C ₁₄ H ₁₄ O ₆ (8)	Alternarienoic acid (13)	<i>Alternaria</i> sp. strain No. II2L4, <i>Cercospora lagenariae</i> MT-45 and a marine-derived <i>Alternaria</i> sp. NH-F6
N86	291.088	9.37	292.095	C ₁₅ H ₁₆ O ₆ (8)	Altenuene (14)	<i>Alternaria tenuis</i> , <i>A. alternata</i>
N98	337.093	9.34	338.101	C ₁₆ H ₁₈ O ₈ (8)	Exserolide J (15)	Marine-derived <i>Setosphaeria</i> sp. SCSIO41009
N8159	338.096	9.39	339.104		No hit	

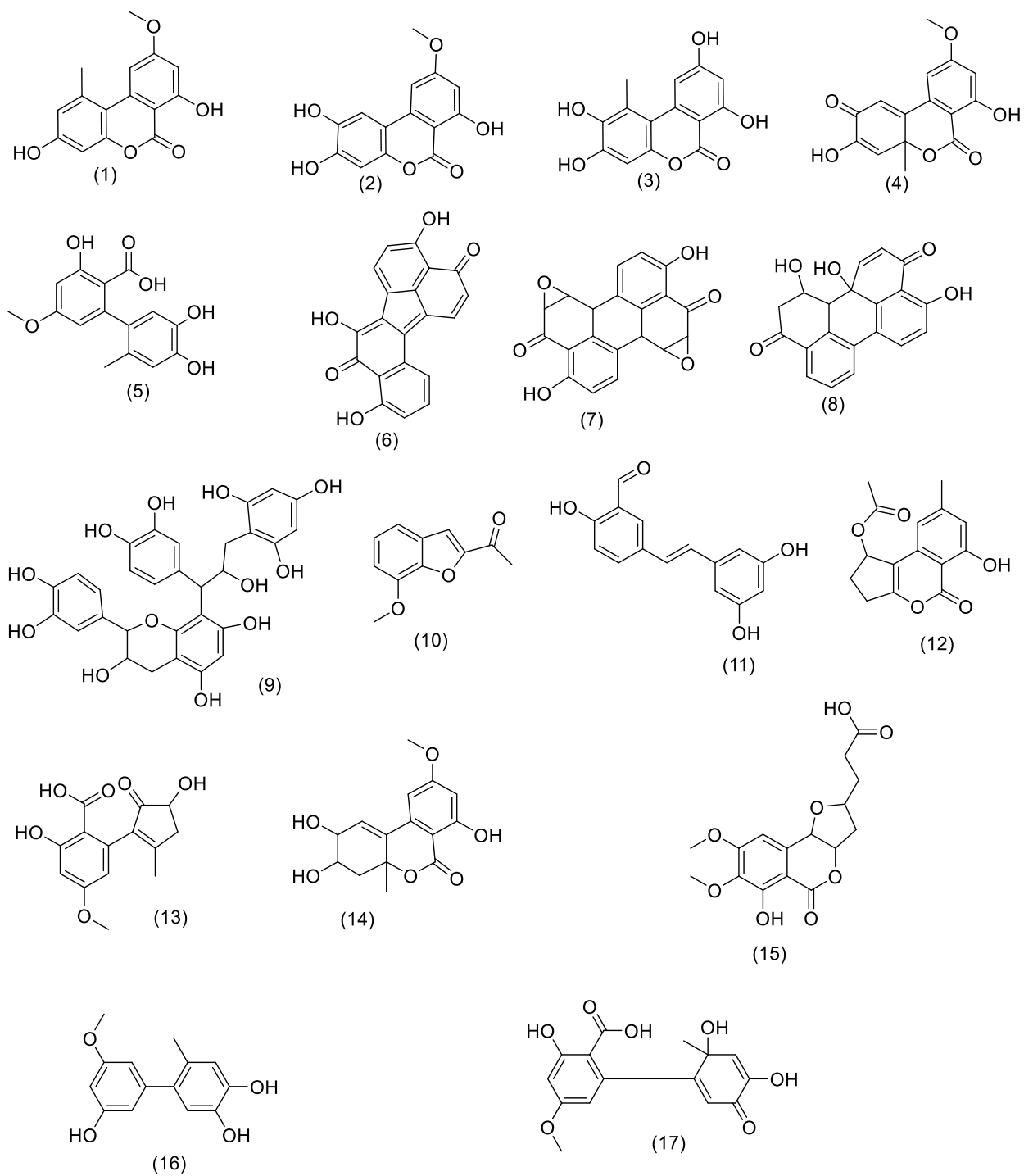


Figure 6.3: PCA Structures of the discriminating metabolites from *A. alternata* extract obtained from different media and listed in Table 6.3.

An OPLS-DA was performed based on the anti-MRSA results, to discriminate the metabolites between active and inactive extracts as shown in Figure 6.4. Active extracts obtained by inoculation in malt media then incubated for 7 and 15 days, in potato dextrose for 30 days and in rice media incubated for 15 days were active, while those grown in malt media incubated for 30 days, potato dextrose for 7 and 15 days, rice media for 7 and 30 days and all oat media extracts were found inactive. The fitness (R_2) and predictability (Q_2) scores were 0.998 and 0.869 respectively, which is a good fit, and a good model prediction. The variation between groups R_2X_0 [1] was 60.8 % and within group R_2X [1] was 24.1%. This showed that there was significant difference in the chemical profiles between the active and the inactive extracts, and a slight similarity within the extracts in their different classes, hence the excellent separation observed between the active and inactive extracts.

The OPLS-DA scores plot in Figure 6.4A positioned the active extracts on the upper and lower left quadrants (red dots), while the inactive extracts were dispersed on the upper and lower right quadrant of the scores plot. The active metabolites were clustered together on the scores plot indicating similarity in their chemical profiles. Outliers were found on those inoculated on rice media and incubated for 30 days (blue dots). The defined target metabolites afforded p-values < 0.05, which indicated a strong model with a confidence interval of more than 95%. The bioactive metabolites gave an m/z value range between 150 and 1600 Da.

Discriminating active metabolites with p-values less than 0.05 are listed in Table 6.4. Structures of putatively identified compound hits are shown in Figure 6.3. Two of the ion peaks gave no hits, which could indicate the presence of novel compounds.

Discriminating metabolites with Mzmine N4024, N5, N15024, N10335, P516, P111, N4132, N30, N33, N116, N2202, N15965 and N8157 with moderate to high DBE values ranging between 8 and 17, represented by ion peaks m/z 245.082, 271.062, 273.041, 287.057, 291.086, 293.101, 305.067, 329.046, 347.057, 349.072, 579.151, 245.082, and 290.075 Da respectively, indicated the presence of sugars and aromatics. This is evidenced by the ^1H NMR spectral data in Figure 6.7 to 6.10 (potato, malt, rice, and oat media extracts), which showed signals resonating between 3.5 to 4.8 ppm and 6.0 to 8.50 ppm. These metabolites were identified as decarboxyaltenuisin, 9-O-methylalternariol, 2-hydroxy; alternariol, dehydroaltenuisin, altenuisin, altenuene, dehydroaltenuisic acid, 2-deoxy; bulgarhodin, altertoxin 111, altechin, gambiriin A1, respectively, while 2 peak ions gave no compound hits. Previous reports proved that altenuisin has antibacterial properties and has shown strong activity against *P. brasiliensis* with MIC values ranging between 1.9 and 31.2 $\mu\text{g/ml}$, and 62.5 $\mu\text{g/ml}$ for *S. pombe* (Johann *et al.*, 2012). Dehydroaltenuisic acid

has been reported to exhibit significant inhibitory activity against a number of both gram-positive and gram-negative bacteria (Jabbar *et al.*, 1998).

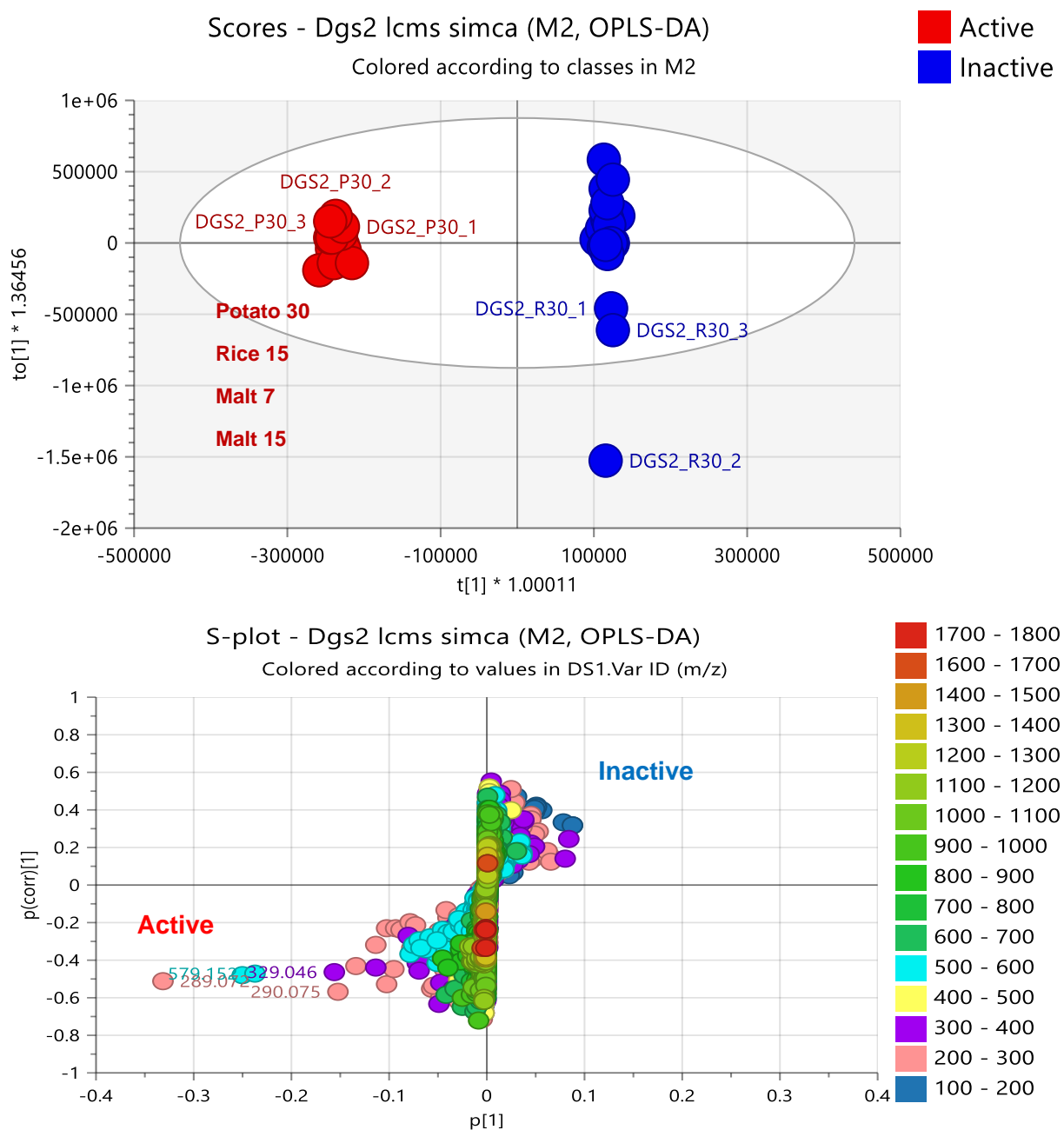
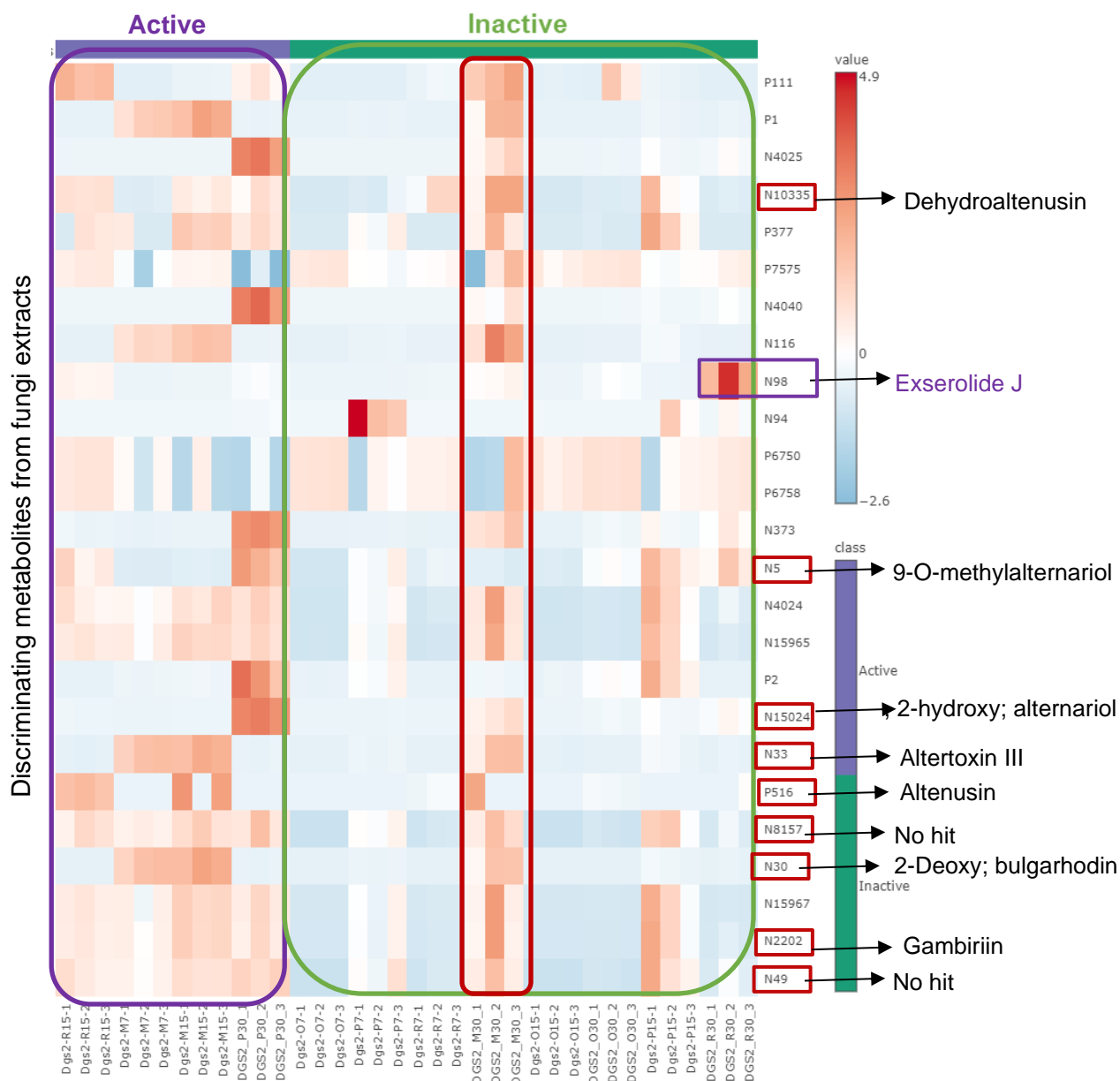


Figure 6.4: (A) OPLS-DA scores and (B) S- plots of LC-HRMS of *A. alternata* extracts obtained from different media. The labelled metabolites on S-plot indicated the discriminating active extracts as listed under table 6.4. $R_2 = 0.998$ and $Q_2 = 0.869$. The difference between group $R_2X_0 [1]$ is equal to 60.8% and the difference within groups $R_2X [2]$ is 24.1%.

Table 6.4: Dereplication data of discriminating bio-active metabolites of *A. alternata* from different media acquired from the OPLSDA S-plot on Figure 6.4B. Structures of compound hits are shown under Figure 6.3.

Mzmine ID	<i>m/z</i>	Rt	M.wt	<i>P value</i>	Molecular Formula (DBE)	Compound HITS	Reported Biological Source
N15965	245.082	10.60	246.089	0.001087		No hit	
N4024	245.082	10.77	246.089	0.00700	C ₁₄ H ₁₄ O ₄ (8)	Decarboxyaltenusin (16)	<i>Ulocladium</i> sp., <i>Nigrospora sphaerica</i> No. 83-1-1-2, marine-derived <i>Alternaria</i> sp. strains SCSIO41014 and SCSIOS02F49
N5	271.062	15.87	272.070	0.17756	C ₁₅ H ₁₂ O ₅ (10)	9- <i>O</i> -methylalternariol (1)	<i>Alternaria</i> spp. incl. marine spp., <i>Anthocleista djalonensis</i> , <i>Penicillium diversum</i> and <i>Lachnum palmae</i>
N15024	273.041	12.22	274.048	0.060964	C ₁₄ H ₁₀ O ₆ (10)	2-hydroxyalternariol (3)	<i>Alternaria tenuis</i> and <i>Penicillium verruculosum</i> F375
N10335	287.057	10.98	288.064	0.250012	C ₁₅ H ₁₂ O ₆ (10)	Dehydroaltenusin (4)	<i>Alternaria kikuchiana</i> , <i>A. tenuis</i> , <i>A. vermiculatum</i> , <i>A. dauci</i> , <i>Talaromyces flavus</i> , <i>Penicillium</i> sp. and <i>Acremonium</i> sp. 98H02B04-1.
P516	291.086	10.73	290.079	0.010096	C ₁₅ H ₁₄ O ₆ (9)	Altenuisin (5)	<i>Alternaria tenuis</i> , <i>Penicillium</i> sp. and <i>Talaromyces</i> sp.
N8157	290.075	10.72	291.0823	0.000290		No hit	
P111	293.101	9.40	292.094	0.222652	C ₁₅ H ₁₆ O ₆ (8)	Altenuene (13)	<i>Alternaria tenuis</i> , <i>A. alternata</i>
N4132	305.067	9.50	306.074	3.93699e-05	C ₁₅ H ₁₄ O ₇ (9)	Dehydroaltenusinic acid (17)	<i>Streptomyces</i> sp.
N30	329.046	14.45	330.054	0.004385	C ₂₀ H ₁₀ O ₅ (16)	2-deoxybulgarhodin (5)	<i>Bulgaria inquinans</i> and <i>Heteroconium</i> sp.
N33	347.057	14.47	348.064	0.006855	C ₂₀ H ₁₂ O ₆ (15)	Altertoxin III (6)	<i>Alternaria alternata</i>
N116	349.072	14.06	350.080	0.105806	C ₂₀ H ₁₄ O ₆ (14)	Altechin (7)	Pigment from <i>Alternaria</i> sp., including a marine sp.
N2202	579.151	10.72	580.159	0.003626	C ₃₀ H ₂₈ O ₁₂ (17)	Gambiriin A1 (8)	Isolated from <i>Uncaria gambir</i> and <i>Sanguisorba officinalis</i>

Analysis on MetaboAnalyst® was performed. The heatmap confirmed that bioactive extracts (purple box) were observed in malt media incubated for 7 and 15 days, potato dextrose media incubated for 30 days, and rice media incubated for 15 days due to the higher intensity and concentration of metabolites observed in the active section (Figure 6.5). The fungal extract obtained from malt media incubated for 30 days (small red box) showed moderate metabolites intensity although it was inactive. Metabolites from rice media incubated for 30 days (small black box) were inactive but discriminatory, with high intensity concentrated at N98 (m/z 337.093). The metabolite responsible for that discriminatory feature was exserolide J and it only occurred on the inactive group. Even though exserolide J is known for its anti-inflammatory property, it can also inhibit the development of *Spodoptera litura* larvae. Hence, the heatmap indicated it to be amongst the top significant metabolites, even though it was inactive to MRSA. It could be that the rice media were far too rich in lipids, masking the antimicrobial property of the interesting and discriminatory property of exserolide J.



Extracts obtained from 4 different media.

Figure 6.5: Heatmap analysis of the mass spectral data of *A. alternata* extracts with their Mzmine values, obtained from different media, generated by MetaboAnalyst®. The big purple boxed extracts are those discriminatory metabolites designated as biologically active against MRSA. Highlighted Mzmine values on the Y-axis indicate common metabolites observed on the heatmap and VIP.

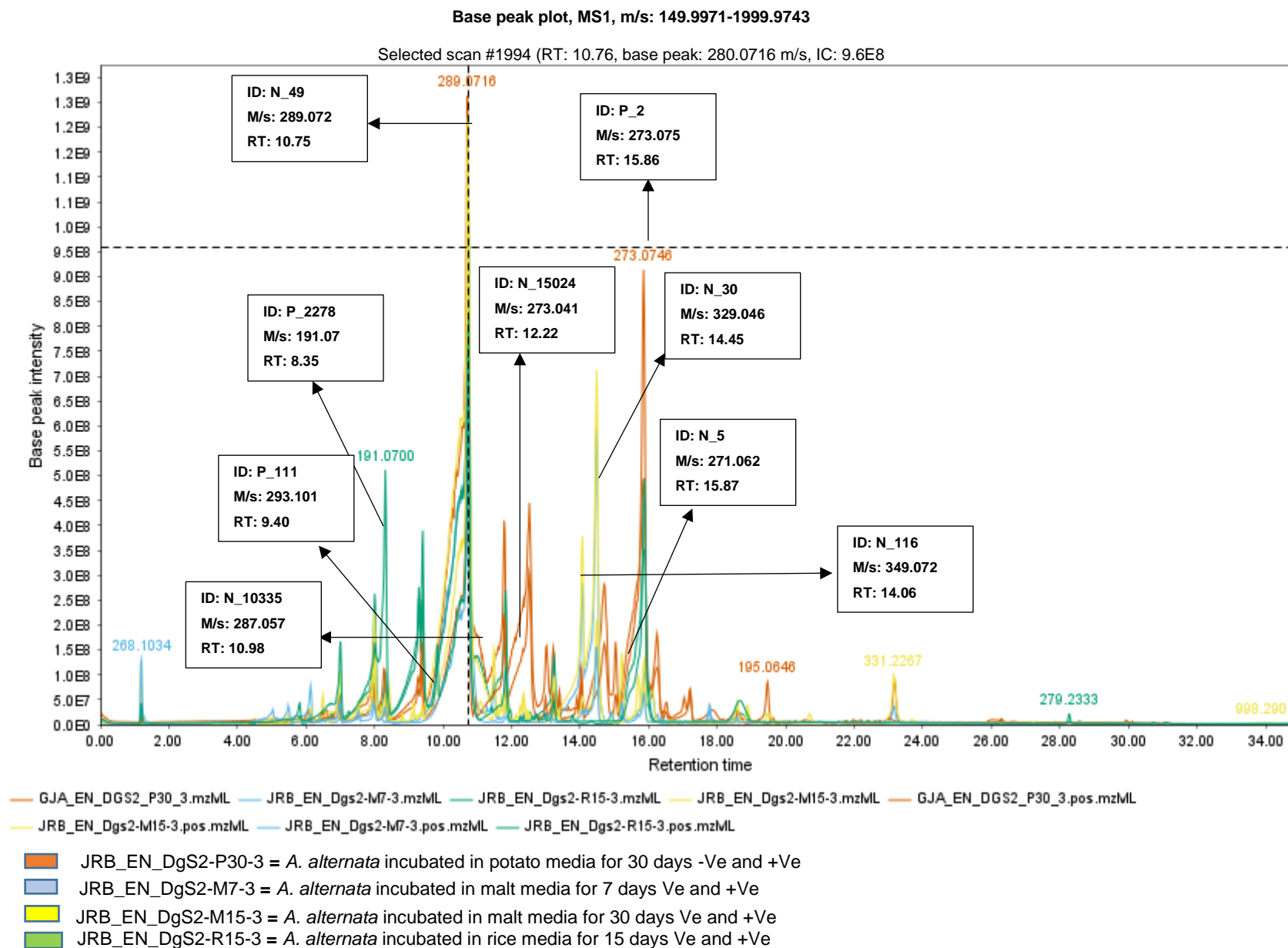


Figure 6.6: Total ion chromatogram (TIC) of the bioactive extracts of *A. alternata* from different media. The ion peaks that represent the discriminating features listed in table 6.4 have been labelled.

6.2.5 Fractionation of *A. alternata* Scale-up crude extracts

Fractionation of *A. alternata* afforded F1-F10, 2 precipitates coded as Dgs2- 30P, Dgs2- 31P and W1 from Acetone: MeOH wash (70:30) as shown in Figure 6.7.

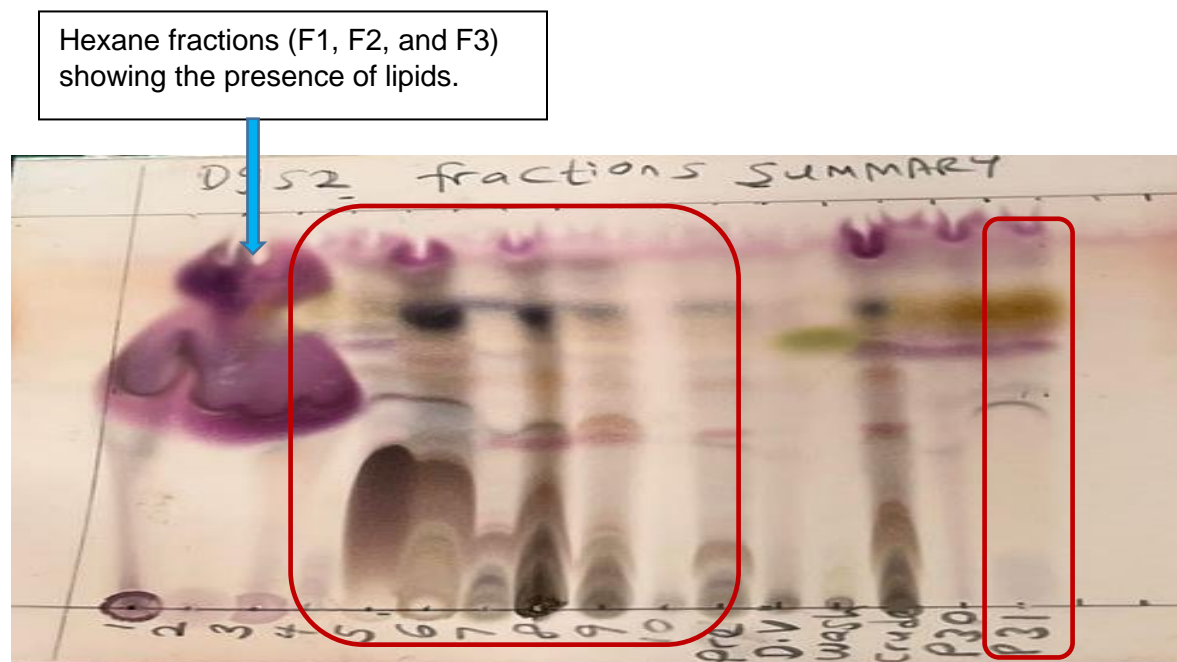


Figure 6.7: Summary TLC Plate of *A. alternata* pooled fractions after spraying with anisaldehyde-sulphuric acid. The TLC plate showed fractions from the non-polar solvent of hexane to the more polar solvent of ethylacetate (100% Hexane- 100% ethylacetate). Bioactive fractions are highlighted in red box.

Table 6.5: Extract weights of *A. alternata* fractions

Fractions	Weight (mg)	Fractions	Weight (mg)
F1	29.5	F10	7.7
F2	1425.9	F30-P	22.0
F3	572.9	F31-P	64.0
F4	186.2	Wash	8.1
F5	962.6		
F6	2156.8		
F7	7009.1		
F8	14103.0		
F9	1242.5		

6.2.6 Bioactivity test results of *A. alternata* fractions

The fractions obtained from fractionation of *A. alternata* were subjected to biological assay against MRSA. Fractions 4-9 and F31-P showed antimicrobial (81.8% and above) and prebiofilm activity (86.4% and above), fraction 10 showed only weak planktonic activity but was inactive for prebiofilm. The bioactivity was in this order: F5 > F8 > F7 > F9 > F4 > 31-P > F6 > F10.

Table 6.6: Summary of bioactivity of *A. alternata* fractions against MRSA Planktonic, prebiofilm, and postbiofilm percentage viability.

Fractions	Antimicrobial % inhibition	Prebiofilm % inhibition	Postbiofilm % inhibition
Fraction 4	92.35	96.73	59.80
Fraction 5	95.95	87.95	72.96
Fraction 6	81.75	88.21	63.11
Fraction 7	92.93	87.40	51.57
Fraction 8	95.80	85.35	56.44
Fraction 9	92.86	86.36	32.38
Fraction 10	53.14	11.35	<0
P31	91.84	99.46	18.67
Wash	14.66	74.47	<0

*Cells with blue colour indicates active fractions against MRSA, while white cells indicate inactive fractions

6.2.7 NMR spectroscopy for *A. alternata* fractions

After fractionation, the pooled fractions were subjected to proton NMR measurements to have an overview of the chemical profile and type of compounds expected to be found in each fraction. The ¹H NMR spectra of the bioactive fractions were stacked and presented in Figure 6.8. A high intensity of aliphatic peaks could be observed in the recorded ¹H NMR spectra of the fractions. Peaks between 3.7 and 4 ppm, 6.0 and 7.5 ppm, 10 and 11 ppm as well as 12 ppm represented

sugars, aromatics, carboxylic acids and exchangeable protons (OH and NH) respectively with more intense and diverse peaks observed in F31-P. Olefinics (5.0 to 5.5 ppm) were found in little quantities from F6 to F10.

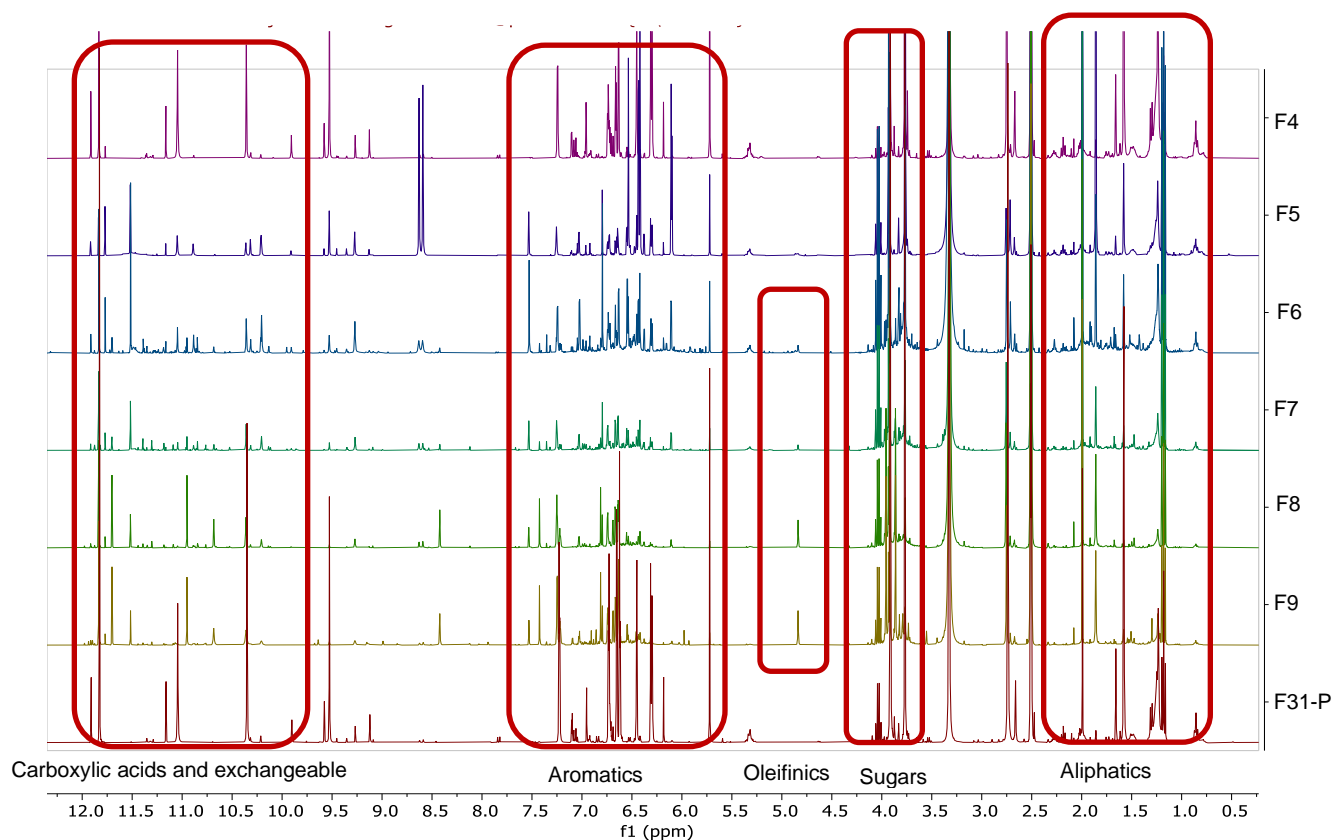


Figure 6.8: Stacked ¹H NMR spectra of the bioactive *A. alternata* fractions ranging from fraction F4 to F9 and F31-P.

The PCA scores scatter plot (Figure 6.9 A) shows F3 to be an outlier. The active fractions were distributed in the upper and lower quadrant. The loadings plot (Figure 6.9 B) indicated that the chemical shifts of the discriminating metabolites were within the range of 0.85 to 2 ppm, 3 to 4 ppm and 6.61 ppm which belongs to the aliphatic, sugars and aromatics, respectively. In the generated model at pareto scaling, the R_2 was 0.997 while Q_2 was 0.686 at eleven components, which indicated a good fitted and predictability model.

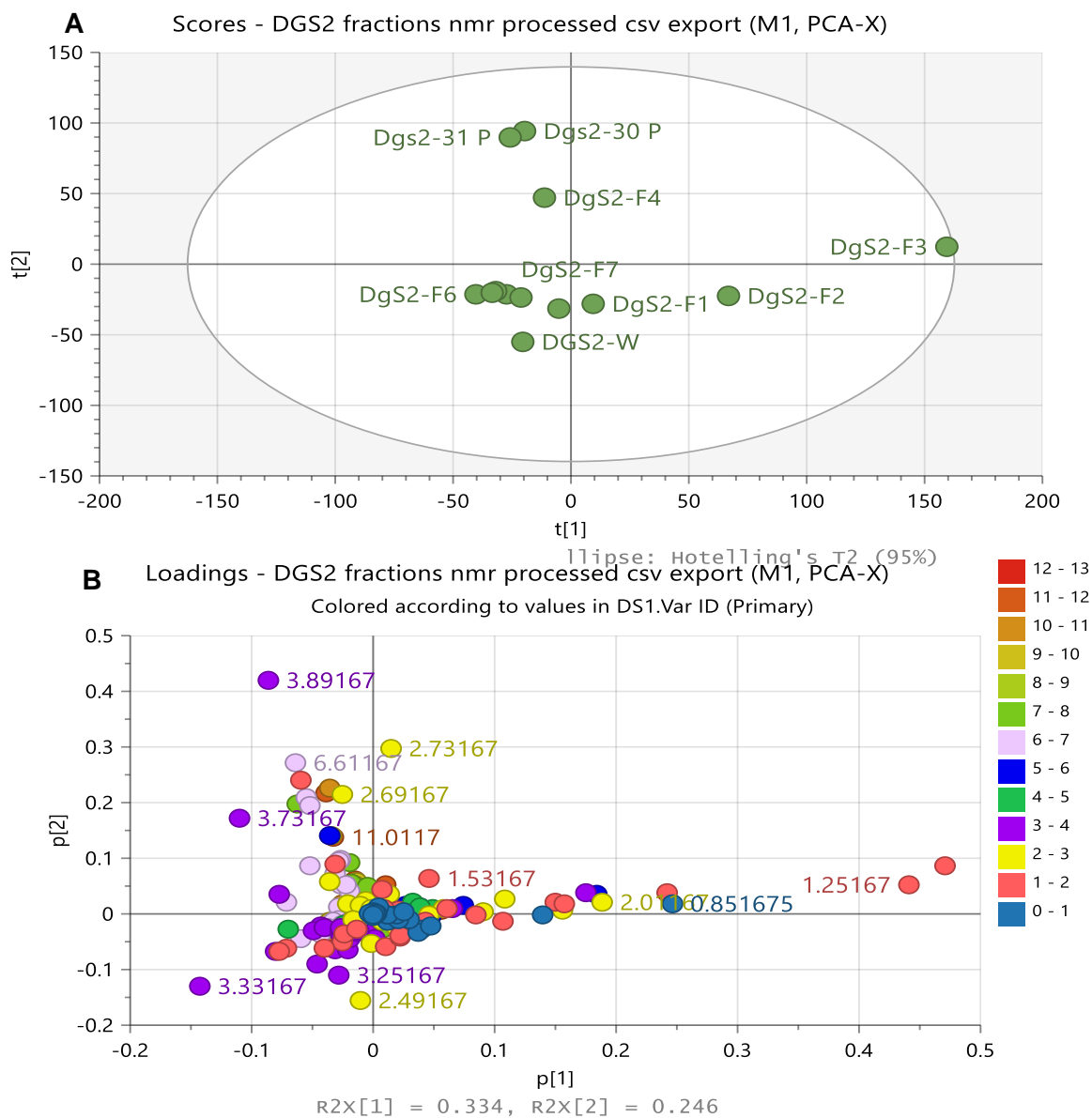


Figure 6.9: (A) PCA scatter and (B) loading plots of the NMR spectral data of the active fractions. The R_2X and Q_2X values were 0.997 and 0.686 respectively.

An OPLS-DA was also performed to indicate the discriminating chemical shifts for the active and inactive fractions. The active fractions were clustered together on the upper and lower left quadrants (red dots), while the inactive fractions were clustered on the upper and lower right quadrant of the OPLS-DA scores plot, with F3 showing to be an outlier (Figure 6.10A). The loadings plot (Figure 6.10B) showed the occurrence of a range of resonance between 0.81 and 6.89 ppm for the discriminating active and inactive fractions, which indicated that the discriminating metabolites consisted of aliphatic, sugars and aromatics. R_2 and Q_2 values were 0.970 and 0.670, respectively. The difference between group R_2X_o [1] is equal to 25.8 %, and the difference within groups R_2X [2] is 16.9 %. There was an excellent separation between the active and inactive clusters, as the variation score between groups was greater than within groups. The close proximity of active fractions F4 to F9 and F31-P on the scores plot indicates they could have similar chemical profiles.

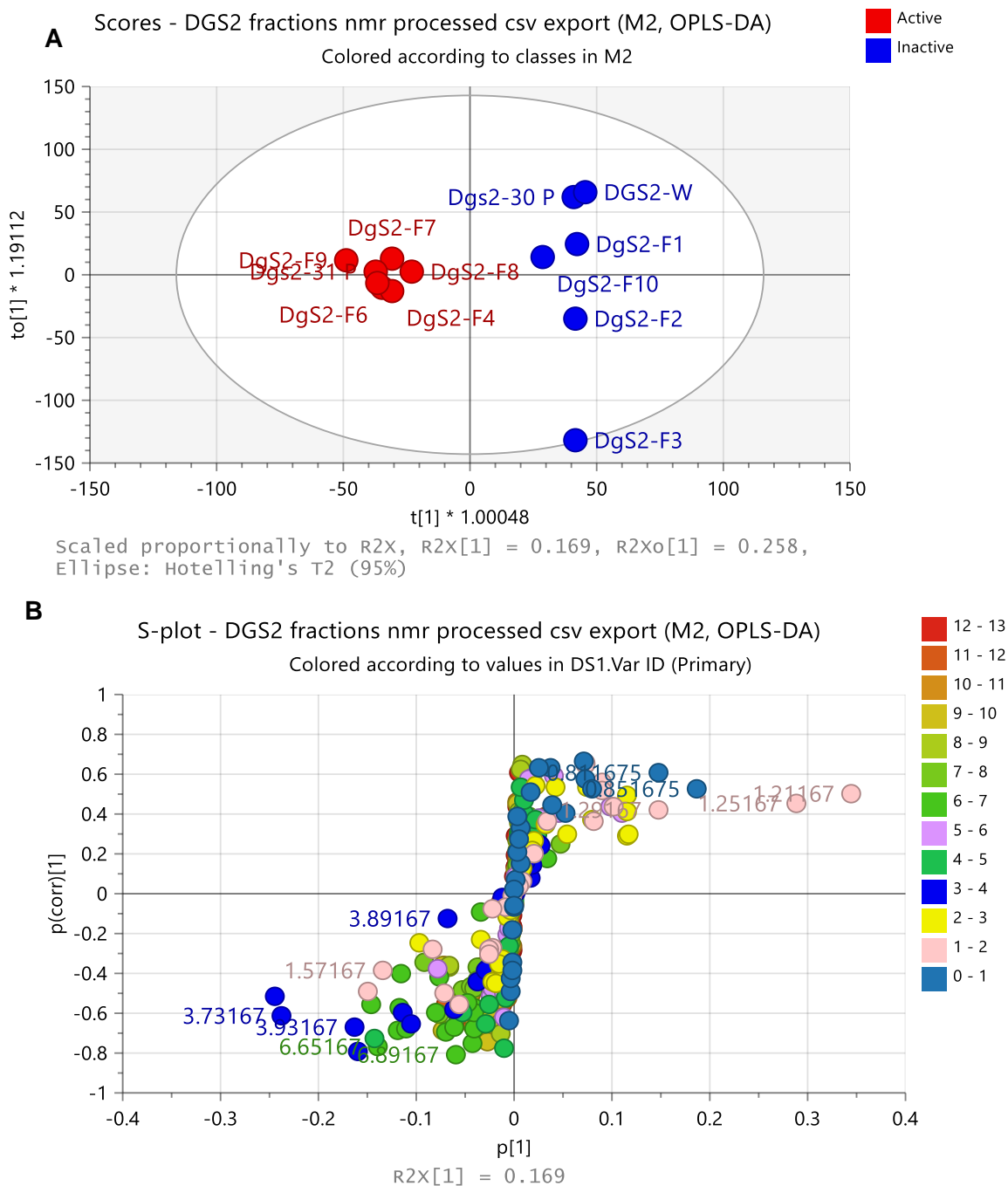


Figure 6.10: OPLS-DA scores (A) and loadings (B) S-plots of the NMR spectral data of *A. alternata* fractions grouped according to their bioactivity against MRSA. R_2 and Q_2 values were 0.970 and 0.670 respectively. The difference between group R_2X_o [1] is equal to 25.8 % and the difference within groups R_2X [2] is 16.9 %. The chemical shift of the discriminating features was labelled.

The fractions were tested for true outliers using DModX, fraction 3 gave results of less than 0.05 which indicated that fraction 3 was not a true outlier as shown in Figure 6.9A and 6.10A. As shown by the DModX plot in Figure 6.11, variables above the red line are the true outliers that included only Fraction 5 which was active.

VIP scores greater than 1 indicates important variables, while variables with VIP scores less than 1 are less important and can be excluded from the model. OPLS-DA indicated the top 20 VIP in Figure 6.12. This confirmed the results of the loadings plot and heatmap obtained in Figure 6.10B and 6.13B respectively, which showed that the discriminatory metabolites mostly consisted of aliphatics and sugars ranging from 0.81 to 6.41 ppm. Discriminating metabolites observed on both VIP and heat map had common chemical shifts of 0.81, 0.85, 1.21, 1.25, 1.29, 1.57, 1.85, 2.01, 2.69, 3.73, 3.77, 3.93, 4.01, 6.29, 6.41.

The spectra bins of each fraction were mechanically replicated, to have three replicates of each fraction, for analysis on MetaboAnalyst®. The heatmap confirmed that bioactive fractions F4 to F9 and F31-P (purple box) had metabolites with chemical shifts ranging from 0.81 to 6.41 ppm, which suggested the presence of aliphatic compounds, sugars, and aromatics. This could be the metabolites contributing to their bioactivity. The heatmap showed that the active fractions exhibited high intensity and diversity of metabolites. F3 (green box) was more diverse and more intense compared to all the fractions but was inactive. The inactivity could have been because of the non-polar solvent (hexane) which was of a higher percentage at that fractionation point. The metabolites responsible for this discriminatory feature were also aliphatic compounds and sugars as seen in the heatmap below (Figure 6.13).

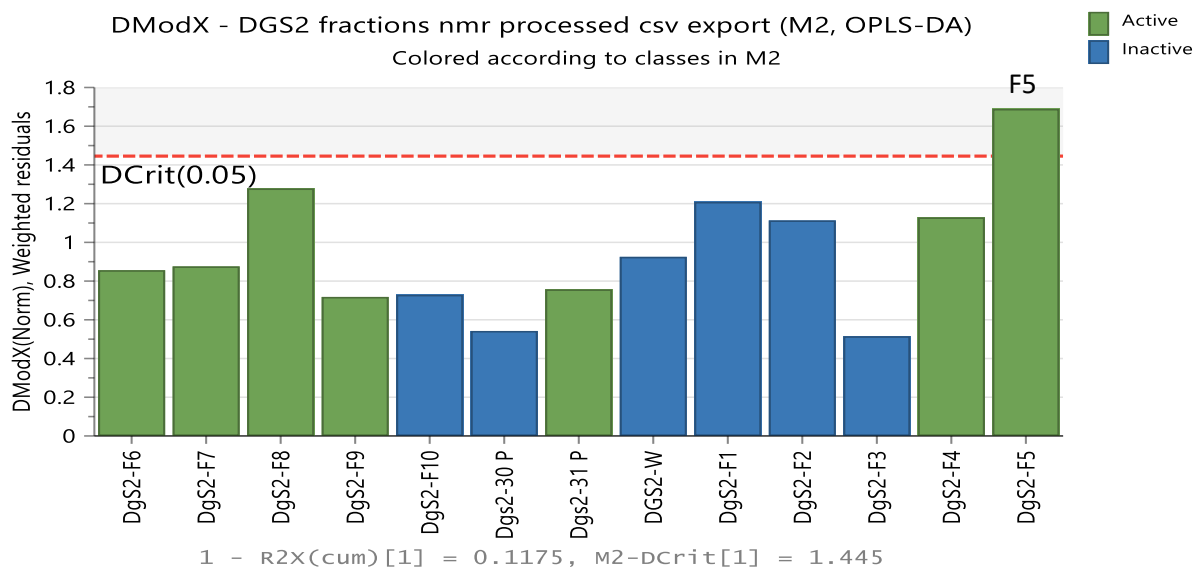


Figure 6.11: DMod X results to test the occurrence of true outliers. Variables above the red line are the true outliers that includes only fraction 5.

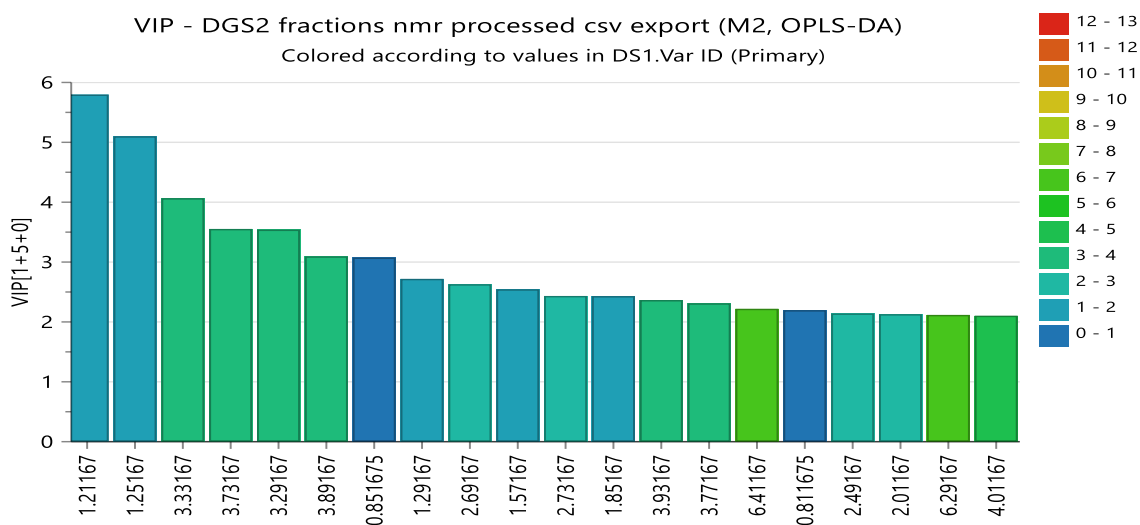
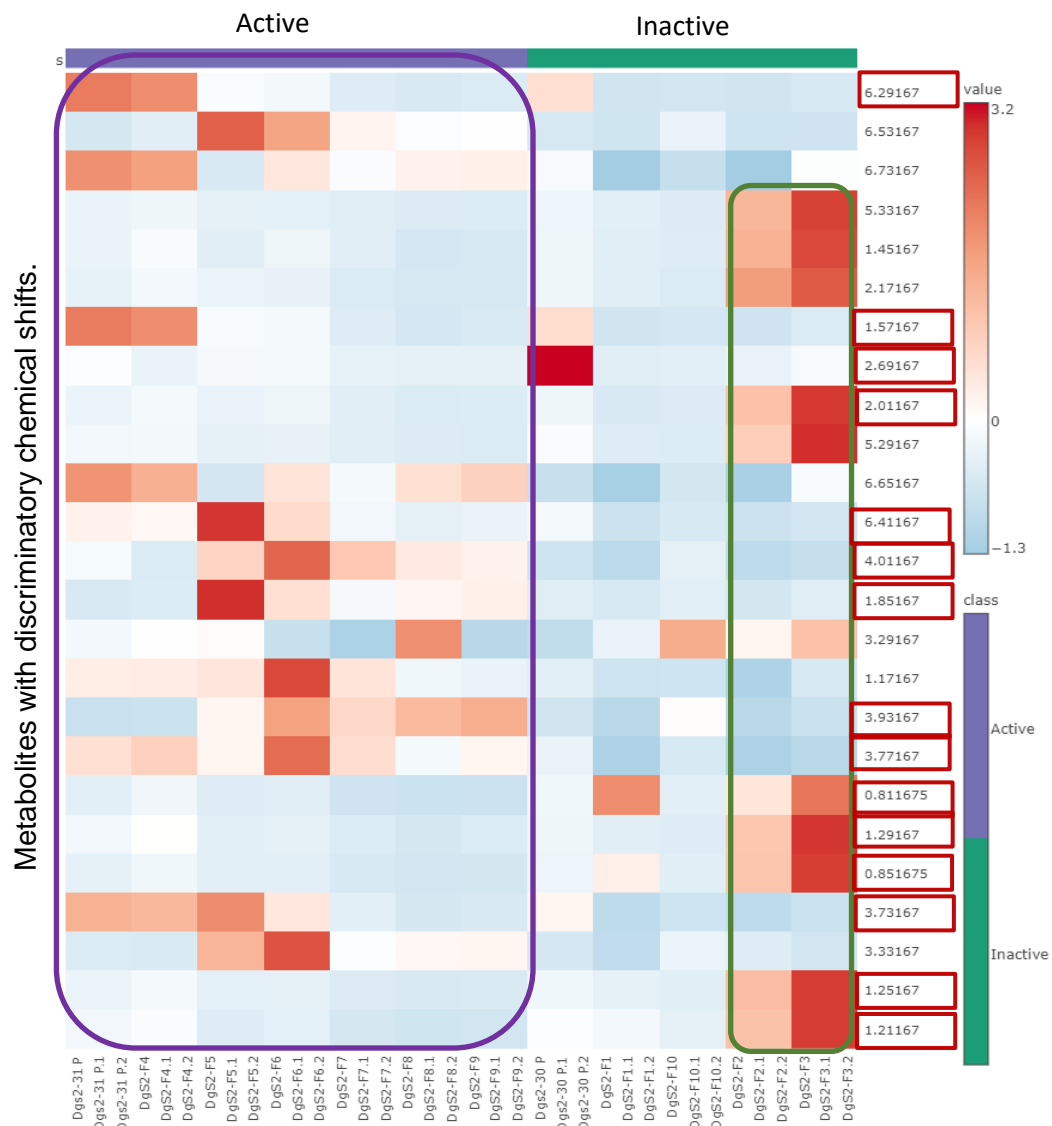


Figure 6.12: VIP scores of *A. alternata* fractions from Simca® showing the chemical shifts of 20 most discriminating metabolites with VIP scores above 1.



A. alternata fractions

Figure 6.13: Heatmap analysis of the NMR spectral data of *A. alternata* fractions generated by MetaboAnalyst®. The purple boxed fractions (F4-F9, F31-P) are those biologically active against MRSA along with the discriminating chemical shifts. The green boxed fractions were F2 and F3 which was discriminatory but inactive. Highlighted chemical shifts on the Y-axis indicate common metabolites observed on the heatmap and VIP.

6.2.8 LC-HRMS analysis of *A. alternata* fractions

Multivariate analysis of the HR-LCMS spectral data was done, the unsupervised PCA scores plot showed the fractions to be at proximity with each other on the upper and lower left quadrant, except for F4, F5, F30-P and F31-P which showed to be an outlier (Figure 6.14A). The loadings plot (Figure 6.14B) indicated the presence of discriminating metabolites with low to high m/z values ranging between 259 to 580 Da. The discriminating metabolites were putatively identified alternariol, 8-dihydroxy-1-(hydroxymethyl)anthraquinone, 9-O-methylalternariol, altenuisol, 2-hydroxyalternariol, O-de-methyl-altenusin, altenusin, dehydroaltenusin, 2-ketone-altenuene, alternethanoxin A, dehydroaltenusinic acid, fusarubin, 4-deoxyaltersolanol A, and mumbaistatin, while 4 ions peaks gave no hits. The results were compatible to those detected during the media optimisation stage indicating the stability of the production of the bioactive metabolites from screening stage to scale-up. The common metabolites observed during the media optimisation stage and fraction stage were altenusin, dehydroaltenusin, 2-hydroxyalternariol, dehydroaltenusinic acid and 9-O-methylalternariol.

Alternariol and altenusin have shown previous antibacterial properties against *S. aureus* and *B. subtilis* (Qader *et al.*, 2021). Anthraquinone 8-Dihydroxy-1-(hydroxymethyl) is a derivative of anthraquinone and anthraquinones are bioactive NPs often found in medicinal herbs. They exert antioxidant-related pharmacological actions including anticancer, anti-inflammation, neuroprotective effects, hepatoprotective effects and anti-aging (Zhao and Zheng, 2023). Altenuene and its derivatives have shown antibiotic activity against gram positive bacteria (Jiao *et al.*, 2006). Alvertoxin, altenuene, and alternariol are dibenzopyrone derivatives which have been reported to show antimicrobial activity and phytotoxicity (Jiao *et al.*, 2006). Alternethanoxins A, which was reported in *A. sonchi* earlier, was later re-identified as moniliphenone. The isolated compound was tested for phytotoxic, antimicrobial, insecticidal, cytotoxic, and esterase-inhibition activities. They demonstrated low phytotoxicity when tested on leaf segments of perennial sow thistle (*Sonchus arvensis*) and couch grass (*Elytrigia repens*). They did not show acute toxicity against *Paramecium caudatum* but showed moderate to low cytotoxicity ($IC_{50} > 25 \mu\text{g/mL}$) for U937 and K562 tumour cell lines (Dalinova *et al.*, 2020). Fusarubin have proven to repress proliferation and increase apoptosis in cell lines obtained from haematological cancers (Adorisio *et al.*, 2019). Altersolanol A is a tetrahydroanthraquinone and have shown cytostatic, cytotoxic, anti-inflammatory, and anti-migrative activity against A549 lung cancer cells and human chronic myeloid K562 leukaemia cells in a dose dependent manner without affecting the viability of non-cancerous cells (Teiten *et al.*, 2013). Mumbaistatin is a new anthraquinone natural product and one of the most potent known inhibitors of hepatic glucose-6-

phosphate translocase, an important target for the treatment of type II diabetes. However, its availability has been limited due to its extremely low yield from the natural source (Lee *et al.*, 2007).

The model gave goodness of fit, (R_2) and predictability, Q_2 values as 0.995 and 0.787, respectively after 10 components. The dereplicated discriminating features of *A. alternata* fractions were shown in Table 6.7. Structures of the discriminating target bioactive metabolites against MRSA predicted by PCA loadings plots were presented in Figure 6.16.

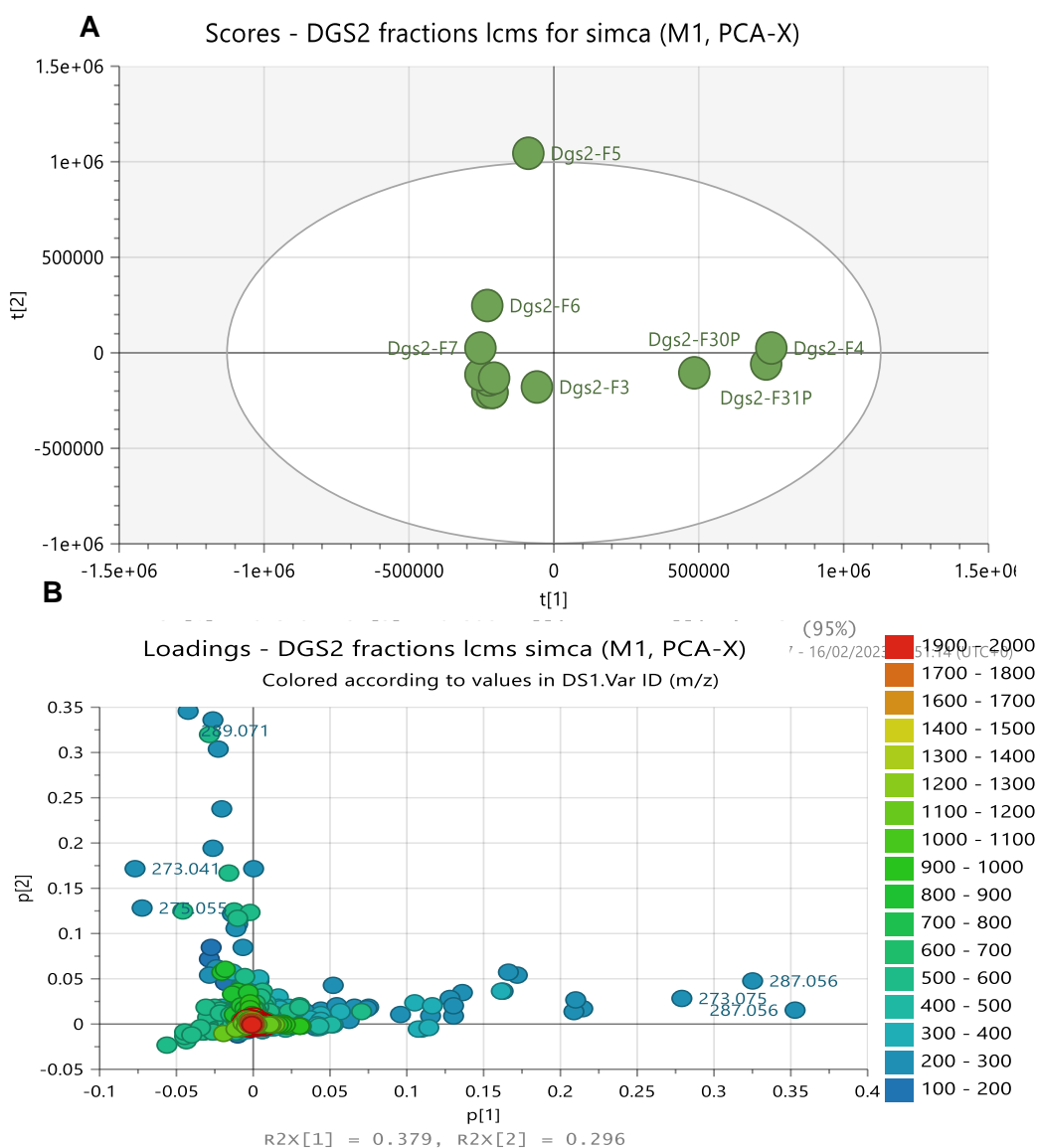


Figure 6.14: PCA scores (A) and loadings (B) plots of the LC-HRMS data of *A. alternata* fractions. Labeled features represent the discriminating ion peaks for the outlier F4, F5, F30P and F31P. The R_2 and Q_2 values were 0.995 and 0.787, respectively.

The OPLS-DA of the active versus the inactive fractions gave fitness and predictability scores of 0.866 and 0.599 respectively. This indicated good fit and prediction of the generated OPLS-DA model. The difference between group R_2X_0 [1] is equal to 27.4 % and the difference within groups R_2X [2] is 16.2 % which shows that the active fractions were related. The scores plot (Figure 6.15A) shows a very good separation between the active versus inactive fractions except for F8 which was in the right quadrant. The active fractions (red circles) were on the left quadrant, while the inactive fractions (blue circles) were on the right quadrant. The discriminating features for the active fractions were more diverse with ion peaks ranging between m/z 180 and 1020.67 Da. Discriminatory active fractions with Mzmine IDs of P3749, N651, P397, P493, P3101, P351, N353, P6560, P5493, P522, P473, N1164, N96, and N2096, represented by m/z 191.07, 217.086, 259.06, 271.06, 273.075, 275.055, 273.041, 289.07 (Rt-10.58), 289.07 (Rt-10.64), 291.086, 321.097, 547.089, 559.089, 579.151 Da, respectively, were putatively identified by dereplication to be 2-acetyl-7-methoxybenzofuran, 2-acetyl-3,8-dihydroxy-1-methylnaphthalene, alternariol, 2,8-dihydroxy-1-(hydroxymethyl) anthraquinone, alternariol; 9-Me ether, 2-hydroxyalternariol, 9-Me ether-2,3,7,9-tetrahydroxy-6H-dibenzo[*b,d*]pyran-6-one, 11-deoxy-graphis lactone D, 4,9-O-di-de-Me-alterlactone), dehydroaltenusin, altenusin, 4-deoxy-altersolanol A, mumbaistatin, sirodesmin A; trisulfide homologue, 2a-Ac. Graphis lactone being an antioxidant, demonstrated efficacy in preventing and protecting against oxidative injury, it can be predicted that this metabolite could serve as a potential agent in the management of oxidative damage-initiated diseases. The discriminating features of *A. alternata* fractions were dereplicated in Table 6.8. Structures of the discriminating target bioactive metabolites against MRSA predicted by OPLS-DA loadings S-plots were presented in Figure 6.16.

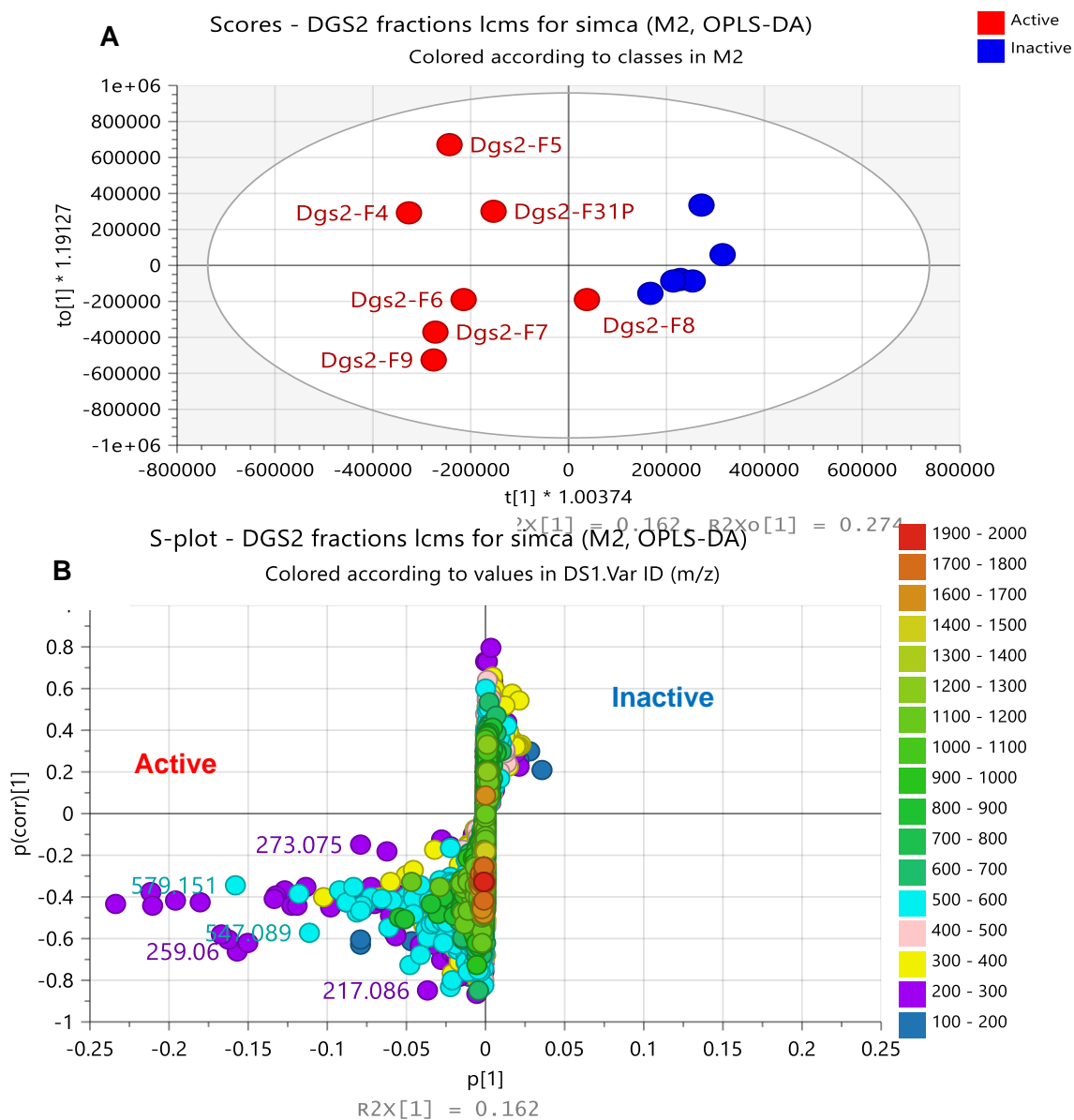


Figure 6.15: OPLSDA scores (A) and S (B) plots of the LC-HRMS data of *A. alternata* fractions. Labeled features represent the discriminating bioactive metabolites listed under table 6.8. The R_2 and Q_2 values were 0.866 and 0.599 respectively. The difference between group R_2Xo [1] is equal to 27.4 % and the difference within groups R_2X [2] is 16.2 %.

Table 6.7: Dereplication data of the discriminating metabolites of *A. alternata* fractions obtained from the PCA loadings plot on Figure 6.14B.

Mzmine ID	<i>m/z</i>	Rt	M.wt	Molecular Formular (DBE)	Compound hits	Biological source
F4, F5, F30P, F31P						
P397	259.06	11.87	258.053	C ₁₄ H ₁₀ O ₅ (10)	Alternariol (18)	Occurs in mycelium of <i>Alternaria tenuis</i> responsible for <i>Alternaria</i> cone disorder in hops and fruit spot on papaya (<i>Carica papaya</i>) and <i>Passiflora</i> sp. Also, from marine <i>Alternaria</i> sp.
P5496	271.06	11.63	270.053	C ₁₅ H ₁₀ O ₅ (11)	2,8-dihydroxy-1-(hydroxymethyl) anthraquinone (19)	<i>Alternaria kikuchiana</i>
N353	273.041	12.48	274.048	C ₁₄ H ₁₀ O ₆ (10)	Altenuisol (2)	<i>Alternaria tenuis</i> and <i>Penicillium verruculosum</i> F375
P3101	273.075	10.68	272.068	C ₁₅ H ₁₂ O ₅ (10)	9-O-methylalternariol (1)	<i>Alternaria</i> sp.
P468	274.079	15.81	273.071		No hit	
P351	275.055	12.47	274.047	C ₁₄ H ₁₀ O ₆ (10)	2-hydroxyalternariol (3)	Mangrove derived <i>Alternaria</i> sp. SK6YW3L
N315	275.056	12.29	276.063	C ₁₄ H ₁₂ O ₆ (9)	O-demethylaltenusin (20)	<i>Alternaria</i> sp. strain No. II2L4
N109	287.056	10.50	288.064	C ₁₅ H ₁₂ O ₆ (10)	9-Me ether-3,4,7,9-tetrahydroxy-1-methyl-6H-dibenzo[<i>b,d</i>]pyran-6-one (21)	<i>Alternaria</i> sp. strain No. II2L4
N4090	288.059	10.66	289.067		No hit	
N318	289.071	10.68	290.079	C ₁₅ H ₁₄ O ₆ (9)	Altenuisin (16)	<i>Alternaria tenuis</i> , <i>Penicillium</i> sp. and <i>Talaromyces</i> sp.

P5493	289.07	10.64	288.063	C ₁₅ H ₁₂ O ₆ (10)	Dehydroaltenusin (4)	<i>Alternaria kikuchiana</i> , <i>A. tenuis</i> , <i>A. vermiculatum</i> , <i>A. dauci</i> , <i>Talaromyces flavus</i> , <i>Penicillium</i> sp. and <i>Acremonium</i> sp. 98H02B04-1
P522	291.086	10.71	290.078	C ₁₅ H ₁₄ O ₆ (9)	2-ketone-altenuene stereoisomer (22)	An unidentified freshwater fungus
P476	303.086	13.51	302.079	C ₁₆ H ₁₄ O ₆ (10)	Alternethanoxin A (23)	<i>Alternaria sonchi</i> S-102
N729	305.066	10.34	306.074	C ₁₅ H ₁₄ O ₇ (10)	Dehydroaltenusinic acid (17)	<i>Streptomyces</i> sp.
P492	307.081	10.32	306.073	C ₁₅ H ₁₄ O ₇ (10)	Fusarubin (24)	<i>Fusarium solani</i> , <i>F. martici-pisi</i> , <i>F. javanicum</i> , <i>F. martii</i> , other <i>Fusarium</i> sp., <i>Neocosmospora vasinfecta</i> , <i>Alternaria solani</i> and <i>Nectria haematococca</i> . Isolated from a marine-derived <i>Fusarium</i> sp. PSU-F135
P473	321.097	13.50	320.089	C ₁₆ H ₁₆ O ₇ (9)	4-deoxyaltersolanol A (25)	<i>Alternaria porri</i> and <i>Dactylaria lutea</i> , marine-derived <i>Alternaria</i> sp. SJ-2008003 and <i>Pleospora</i> sp. IFB-E006.
N1164	547.089	12.4778	548.096	C ₂₈ H ₂₀ O ₁₂ (19)	Mumbaistatin (26)	<i>Streptomyces</i> sp. DSM 11641
N2096	579.151	10.6801	580.158		No hit	
N2425	580.154	10.68	581.161		No hit	

Table 6.8: Dereplication data for the discriminating antibacterial- and antibiofilm-active metabolites of *A. alternata* fractions obtained from the OPLS-DA S-Plot on Figure 6.15B.

Mzmine ID	<i>m/z</i>	Rt	M.wt	<i>P-value</i>	Molecular Formular (DBE)	Compound hits	Biological source
P3749	191.07	8.20	190.063	0.033685	C ₁₁ H ₁₀ O ₃ (7)	2-acetyl-7-methoxybenzofuran (9)	A mangrove-derived <i>Sporothrix</i> sp. No.4335
P651	217.086	8.13	216.078	0.002328	C ₁₃ H ₁₂ O ₃ (8)	2-acetyl-3,8-dihydroxy-1-methylnaphthalene (27)	<i>Streptomyces</i> sp. MBT76
P397	259.06	11.87	258.053	0.030646	C ₁₄ H ₁₀ O ₅ (10)	Alternariol (18)	<i>Alternaria tenuis</i> , marine <i>Alternaria</i> sp.
P493	271.06	10.50	270.053	0.170644	C ₁₅ H ₁₀ O ₅ (11)	2,8-dihydroxy-1-(hydroxymethyl) anthraquinone (19)	<i>Alternaria kikuchiana</i>
P3101	273.075	10.68	272.068	0.192104	C ₁₅ H ₁₂ O ₅ (10)	9-O-methylalternariol (1)	<i>Alternaria</i> sp.
P351	275.055	12.47	274.047	0.036186	C ₁₄ H ₁₀ O ₆ (10)	2-hydroxyalternariol (3)	Mangrove derived <i>Alternaria</i> sp. SK6YW3L
N353	273.041	12.48	274.048	0.049977	C ₁₄ H ₁₀ O ₆ (10)	Altenuisol (2)	<i>Alternaria tenuis</i> and <i>Penicillium verruculosum</i> F375
P6560	289.07	10.58	288.063	0.23442	C ₁₅ H ₁₂ O ₆ (10)	11-deoxy-4,9-O-di-de-Me graphislactone D (alterlactone) (28)	<i>Alternaria</i> sp. strain No. II2L4
P5493	289.07	10.64	288.063	0.20094	C ₁₅ H ₁₂ O ₆ (10)	Dehydroaltenusin (4)	<i>Alternaria kikuchiana</i> , <i>A. tenuis</i> , <i>A. vermiculatum</i> , <i>A. dauci</i> , <i>Talaromyces flavus</i> , <i>Penicillium</i> sp. and <i>Acremonium</i> sp. 98H02B04-1
P522	291.086	10.71	290.078	0.208645	C ₁₅ H ₁₄ O ₆ (9)	Altenusin (16)	<i>Alternaria tenuis</i> , <i>Penicillium</i> sp. and <i>Talaromyces</i> sp.

P473	321.097	13.50	320.089	0.218606	C ₁₆ H ₁₆ O ₇ (9)	4-deoxyaltersolanol A (25)	<i>Alternaria porri</i> and <i>Dactylaria lutea</i> , marine-derived <i>Alternaria</i> sp. SJ-2008003 and <i>Pleospora</i> sp. IFB-E006.
N1164	547.089	12.48	548.096	0.062322	C ₁₅ H ₁₄ O ₆ (9)	Mumbaistatin (26)	<i>Streptomyces</i> sp. DSM 11641
N96	559.089	13.1174	560.096	0.245034	C ₂₂ H ₂₈ N ₂ O ₉ S ₃ (10)	Trisulfide homologue, 2a-acetysirodesmin A (29)	<i>Microsphaeropsis</i> sp.
N2096	579.151	10.6801	580.158	0.288946		No hit	

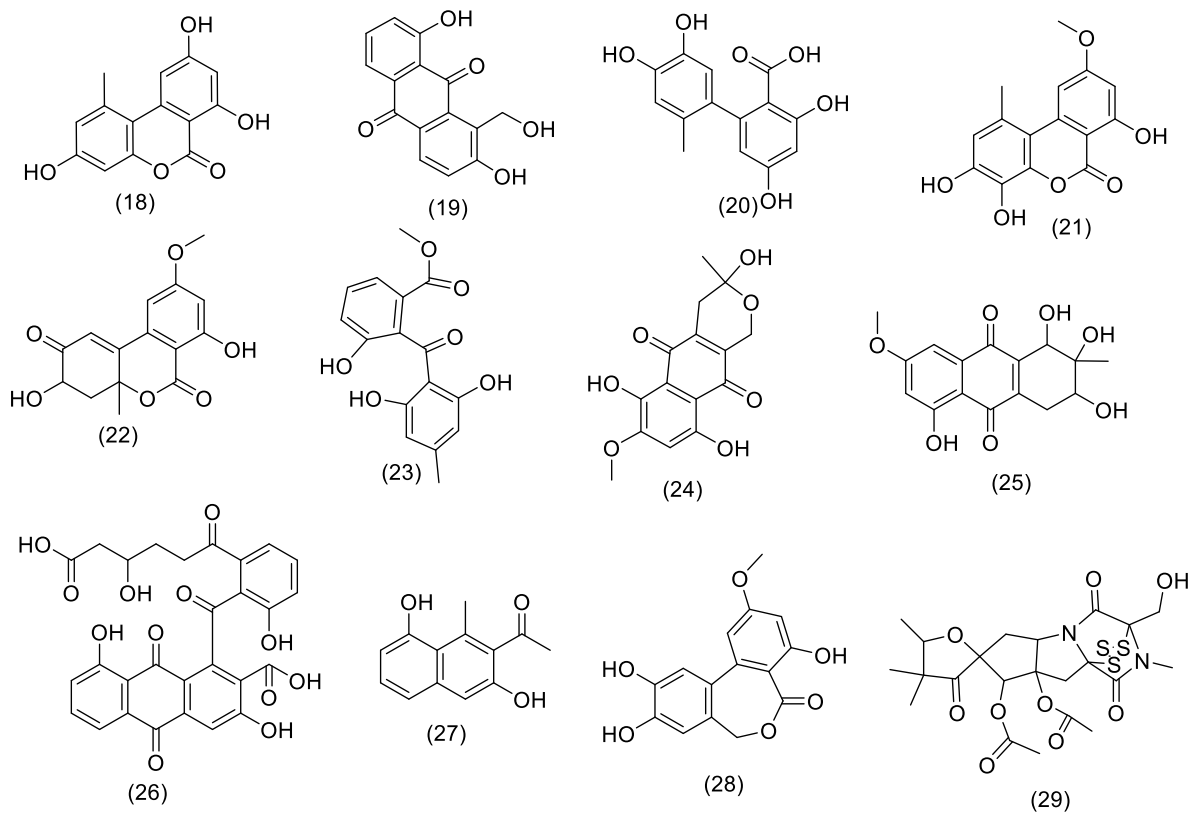


Figure 6.16: Structures of dereplicated compound hits showing MVA discriminating metabolites obtained from *A. alternata* fractions, as listed in Tables 6.7 and 6.8.

Base peak plot, MS1, m/s: 149.9971-1999.9743

Selected scan #1473, RT: 15.81, base peak: 273.0750 m/s, IC: 1.7E9

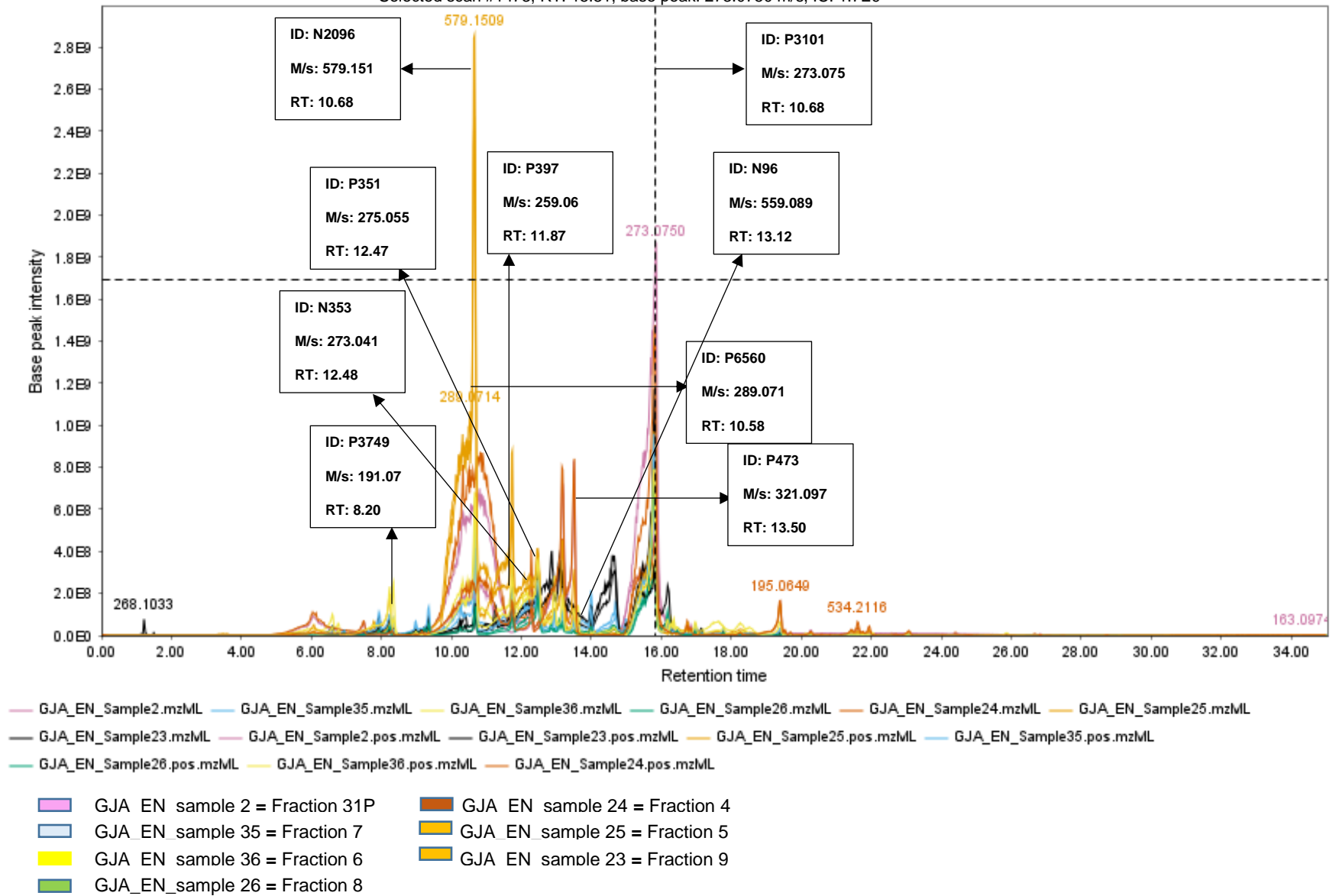


Figure 6.17: Total ion chromatogram (TIC) of the bioactive fractions of *A. alternata*. The ion peaks that represent the discriminating features listed in table 6.8 have been labelled.

6.2.9 Pure compound isolation

Fractions were selected for further purification work due to antimicrobial activity against MRSA. Planktonic and Prebiofilm active fractions 4 to 9 and 31P were selected for purification work. Eleven known compounds were isolated from *A. alternaria* namely: 3,7-dihydroxy-9-methoxy-1-methyl-6H-benzo[c]chromen-6-one, (9-O-methylalternariol), alternariol, 3,9-di-O-acetyalternariol, 9-O-acetyalternariol, altenusin, 7-O-methyldehydroaltenusin tautomer, 3,4,7-tri-O-acetyaltenusin, altenuisol, altenuene, 4'-epialtenuene and linoleic acid. Compounds were structurally elucidated and identified by ¹H NMR and 2D NMR experiments.

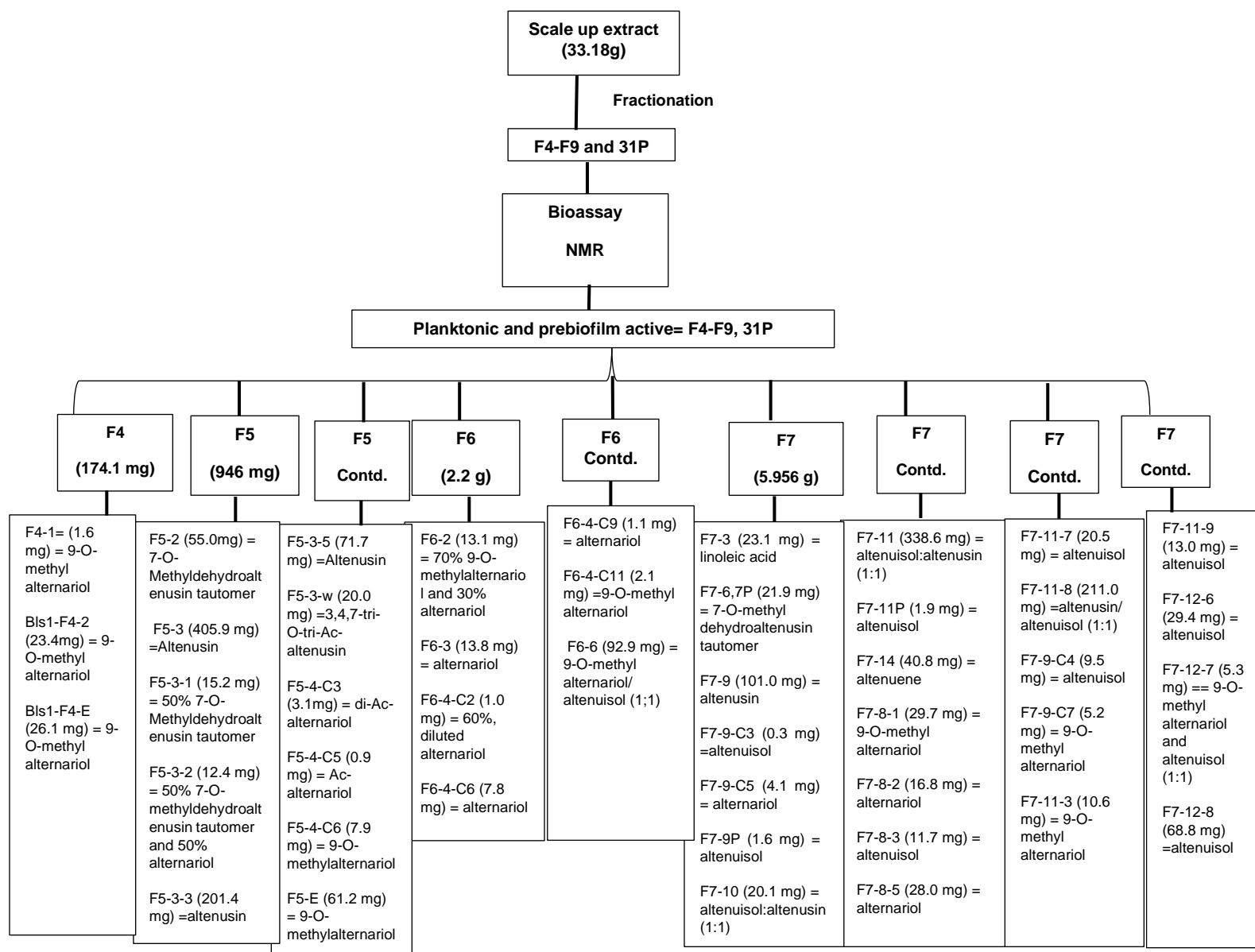


Figure 6.18: Summary workflow of *A. alternata* scale-up crude extract showing isolated and re-isolated compounds.

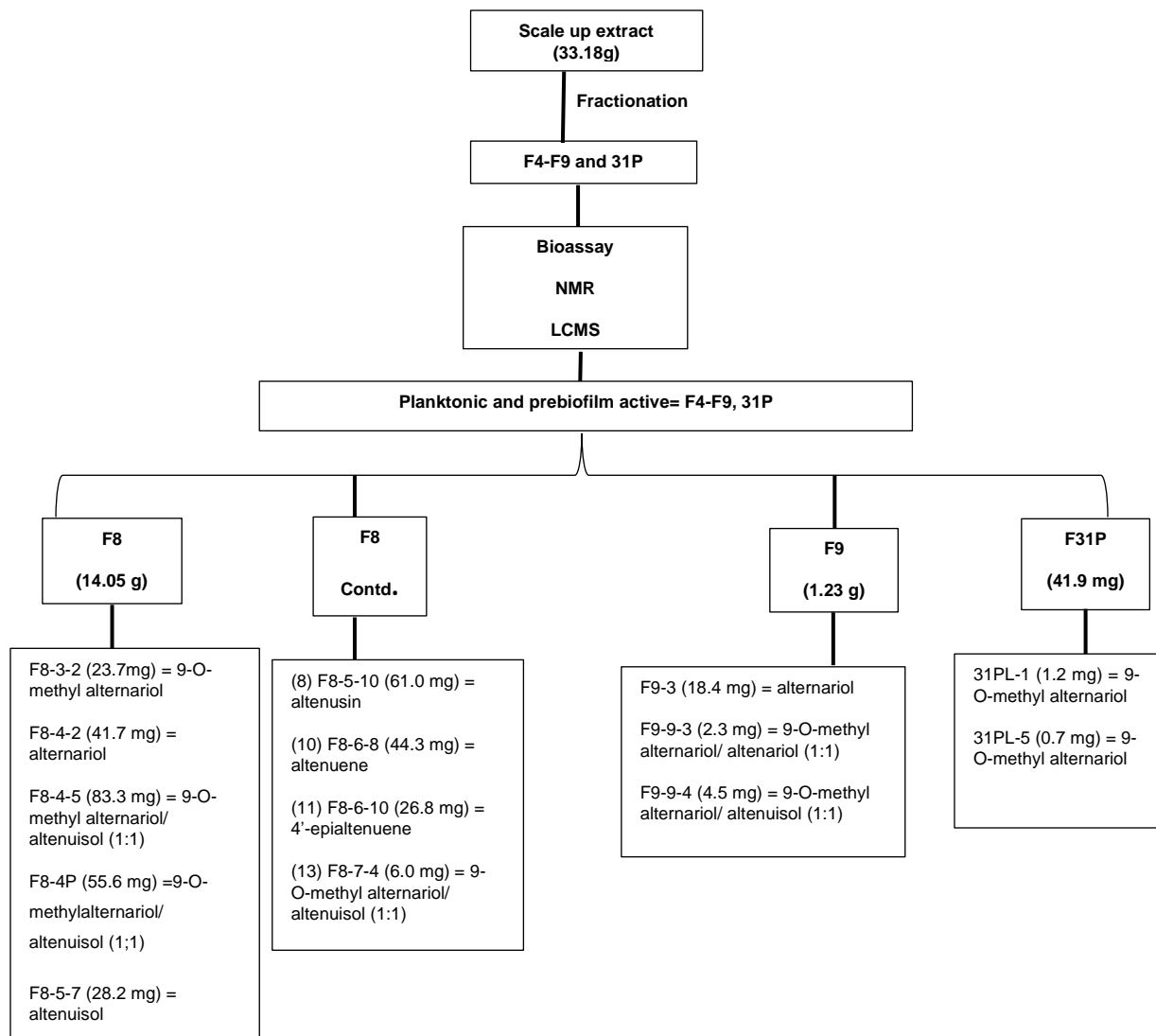
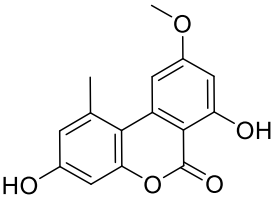
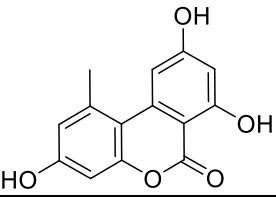
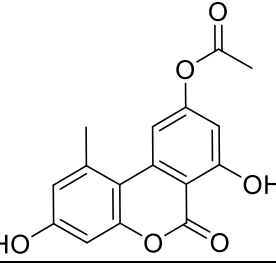
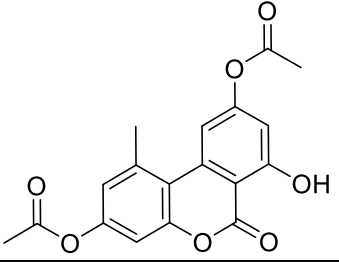
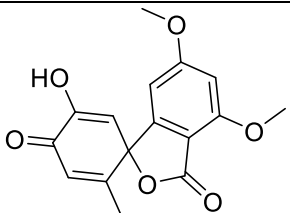
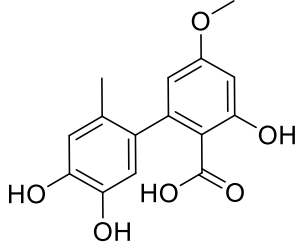
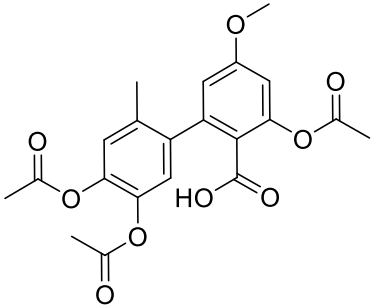
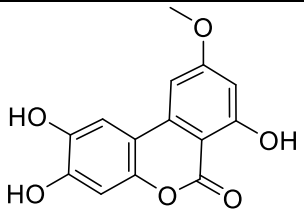
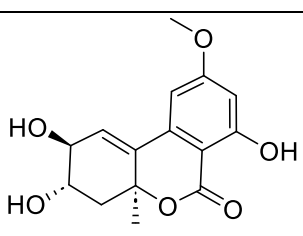
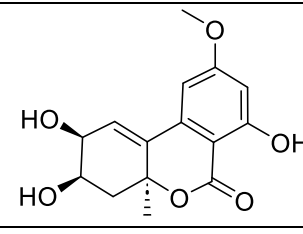
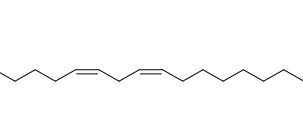


Figure 6.18 contd.: Summary workflow of *A. alternata* scale-up crude extract showing isolated and re-isolated compounds.

Table 6.9: Isolated pure compounds from *A. alternata*. For fraction source, underlined fractions were used for structural elucidation.

Drawn Structure	Name	Exact mass	Molecular Formula	Fraction source	Weight (mg)	Purification method
	9-O-methyl alternariol (Lou <i>et al.</i> , 2016)	272.0685	C ₁₅ H ₁₂ O ₅	<u>F4-1</u> , F4-2, F4-eq, F5-4-C6, F5-Eq, F6-2 (70%), F6-4-C11, F7-8-1, F7-9-C7, F7-11-3, F8-3-2	200.7 (0.60%)	Biotage
	Alternariol (Abdou and Dawoud, 2020)	258.0528	C ₁₄ H ₁₀ O ₅	<u>F6-4-C6</u> , F5-3-2 (50%), F6-2 (30%), F6-4-2 (60%, diluted), F6-4-C9, F7-8-2, F7-9-C5, F8-4-2, F9-3, F7-8-5	128.6 (0.39%)	Biotage and Preparative TLC
	9-O-acetylalternariol (compared with alternariol in Abdou and Dawoud, 2020)	300.0634	C ₁₆ H ₁₂ O ₆	<u>F5-4-C5</u>	0.9 (0.003%)	Biotage and Preparative TLC
	3,9-di-O-acetylalternariol (compared with alternariol in Abdou and Dawoud, 2020)	342.0740	C ₁₈ H ₁₄ O ₇	<u>F5-4-C3</u>	3.1 (0.009%)	Biotage and Preparative TLC

	7-O-methyldehydroaltenusin tautomer	302.0790	C ₁₆ H ₁₄ O ₆	F5-2 , F5-3-1 (50%), F5-3-2 (50%), F7-6,7P	90.7 (0.27%)	Biotage
	Altenusin (Ayer and Racok, 1990)	290.0790	C ₁₅ H ₁₄ O ₆	F5-3-5 , F5-3, F5-3-3, F7-9, F8-5-10	841.0 (2.53%)	Biotage
	3,4,7-tri-O-acetylaltenusin (compared with altenusin in (Ayer and Racok, 1990)	416.1107	C ₂₁ H ₂₀ O ₉	F5-3-W	20.0 (0.06%)	Biotage
	Altenuisol (Cole and Cox, 1981)	274.0477	C ₁₄ H ₁₀ O ₆	F7-9P , F7-9-C3, F7-11P, F7-8-3, F7-9-C4, F7-11-C7, F7-11-9, F7-12-8, F8-5-7	155.5 (0.47%)	Biotage

	<p>Alenuene (Bhagat <i>et al.</i>, 2016)</p>	292.0947	C ₁₅ H ₁₆ O ₆	F7-14 , F8-6-8	85.1 (0.26%)	Grace
	<p>4'-epialenuene (Aly <i>et al.</i>, 2008)</p>	292.0947	C ₁₅ H ₁₆ O ₆	F8-6-10	26.8 (0.08%)	Grace
	<p>linoleic acid (Wishart <i>et al.</i>, 2009)</p>	280.2402	C ₁₈ H ₃₂ O ₂	F7-3	23.1 (0.07%)	Grace

6.2.10 Bioactivity test results

The pure compounds obtained from purification of *A. alternata* were subjected to biological assay against MRSA ATCC 43300 exhibiting selective bioactivity. It was observed that 9-*O*-methylalternariol, alternariol, 9-*O*-acetylalternariol, 3,9-di-*O*-acetylalternariol, 7-*O*-methyldehydroaltenusin tautomer, altenusin, 3,4,7-tri-*O*-acetylaltenusin, altenuisol, altenuene, 4'-epialtenuene and linoleic acid inhibited planktonic MRSA by 35.32%, 73.39%, 28.19%, 16.41%, 51.98%, 67.34%, 65.91%, 70.80%, 38.06%, 26.08, 0.00% and prebiofilm MRSA by 51.96%, 49.85%, 70.45%, 65.20%, 55.94%, 24.54%, 47.26%, 54.99, 0.00%, 0.00%, 0.00% respectively at 100µg/ml. Above the bioactivity threshold of 70%, only alternariol and altenuisol indicated antibacterial activity. On the other hand, alternariol was the only compound that showed postbiofilm activity against MRSA by 58.95%.

However, it was observed that 9-*O*-methylalternariol, alternariol, 9-*O*-acetylalternariol, 3,9-di-*O*-acetylalternariol, 7-*O*-methyldehydroaltenusin tautomer, altenusin, 3,4,7-tri-*O*-acetylaltenusin, altenuisol, altenuene, 4'-epialtenuene and linoleic acid inhibited planktonic SA (NCTC 8325) by 95.51%, 91.22%, 95.63%, 94.93%, 89.97%, 91.77%, 97.03%, 87.54%, 43.27%, 32.00%, 38.63% while for prebiofilm inhibition against SA-NCTC 8325, the compounds indicated activity between 75% and 100% (Figure 6.19). The bioassay against planktonic SA-NCTC 8325 was less selective resulting in a general planktonic antibacterial activity for almost all isolated compounds except for altenuene, 4'-epialtenuene and linoleic acid that indicated inhibition bioactivity below the 70% threshold, while all the compounds inhibited biofilm formation in SA-NCTC 8325.

The MIC and MBEC values were calculated for compounds which exhibited 70% and above MRSA planktonic and prebiofilm activity. MIC values were obtained for alternariol and altenuisol to be 25 µg/mL and 50 µg/mL respectively, while MBEC value for 9-*O*-acetylalternariol gave 25 µg/mL.

Effect of pure compounds isolated from *A. Alternaria* on MRSA and SA-NCTC 8325

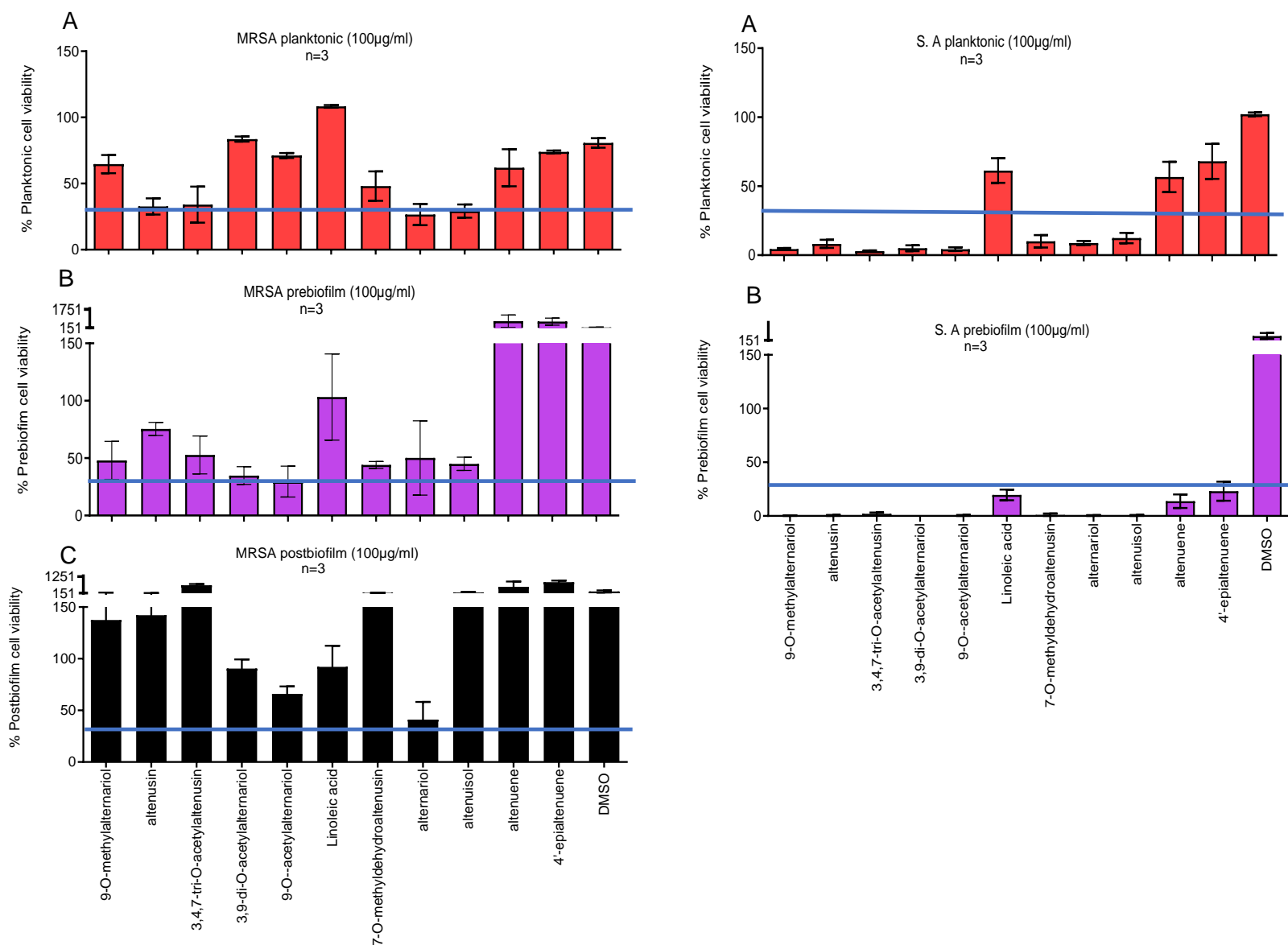


Figure 6.19: Effect of pure compounds isolated from *A. alternata*. Left-planktonic (A), prebiofilm (B), and postbiofilm (C) MRSA. Right-planktonic (A) and prebiofilm (B) SA-NCTC 8325 at 100µg/mL. The blue line indicates the bioactivity threshold which is 30% viability (70.0% inhibition).

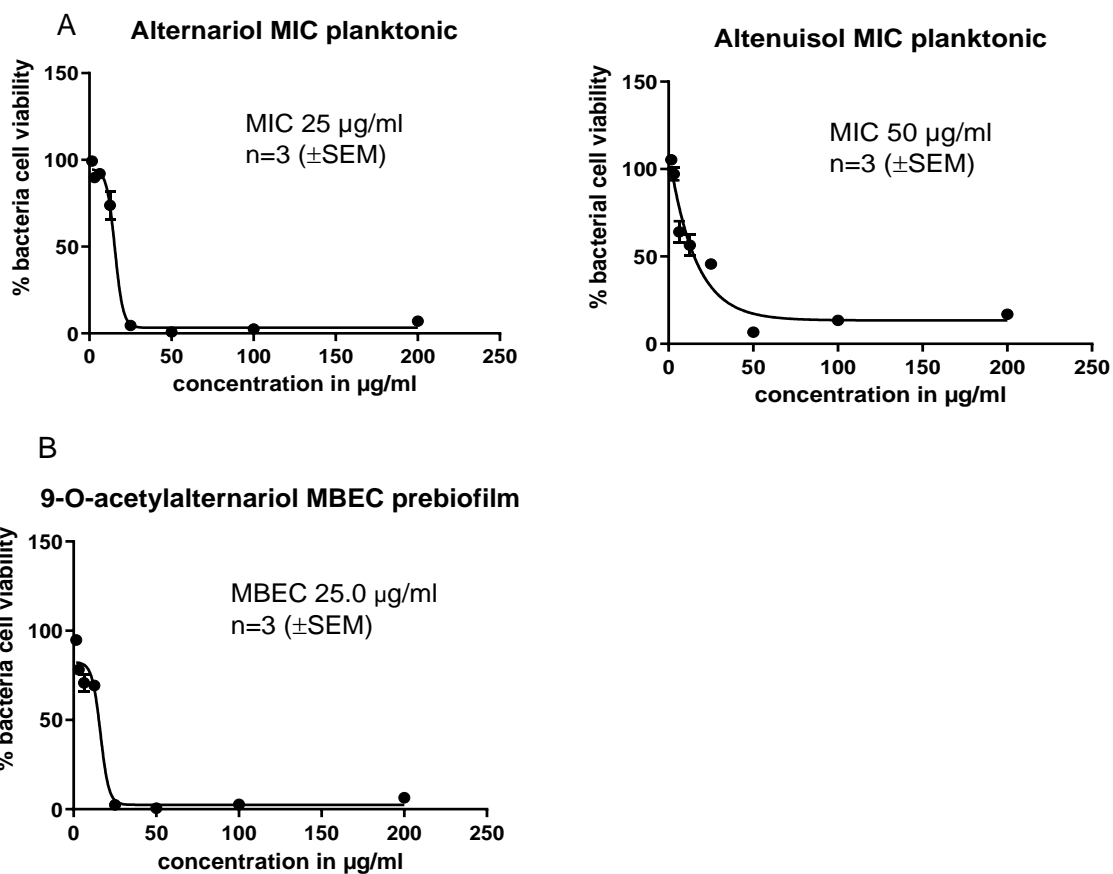


Figure 6.20: (A) MIC of alternariol and altenuisol, (B) MBEC results 9-O-acetylalternariol.

IC₅₀ (µM) were obtained only for compounds which exhibited above the recommended 70% bioactivity threshold using graph pad prism 10.3.1.

Table 6.10: IC₅₀ (µM) for the bioactive isolated compounds against MRSA

Compound name	MRSA planktonic	MRSA prebiofilm	IC ₅₀ (µg/ml)	IC ₅₀ (µM)	R ²
Alternariol	Active	-	14.94	57.90	0.98
Altenuisol	Active	-	12.11	44.19	0.92
9-O-acetylalternariol	-	Active	14.82	49.39	0.92

The isolated compounds were revisited on their position on the OPLS-DA plot shown in Figure 6.15 (fractions) and Figure 6.4 (media optimisation) using their MW features (Figures 6.21 and 6.22). It was observed that ten of the isolated compounds were found on the active right quadrant on the OPLS-DA plots. This confirms the bioactivity of the isolated compounds against MRSA, and further proves that the isolated compounds can be active both in their pure forms and in synergy with other metabolites, hence separating or isolating some compounds did not make them lose their activity as observed at the fraction or media optimisation stage, except for 292.094 (altenuene, 4'-epialtenuene) and 280.240 (linoleic acid), which lost their bioactivity after separation from the other metabolites. These three latter compounds needed to act in synergy with the other compounds to be active. It also confirms the stability of the identified active compounds, which were biologically stable both in the crude extracts, fractions and as in the pure compound stage. The isolated compounds identified on the active quadrant by OPLSDA with their corresponding MW are listed in Table 6.11.

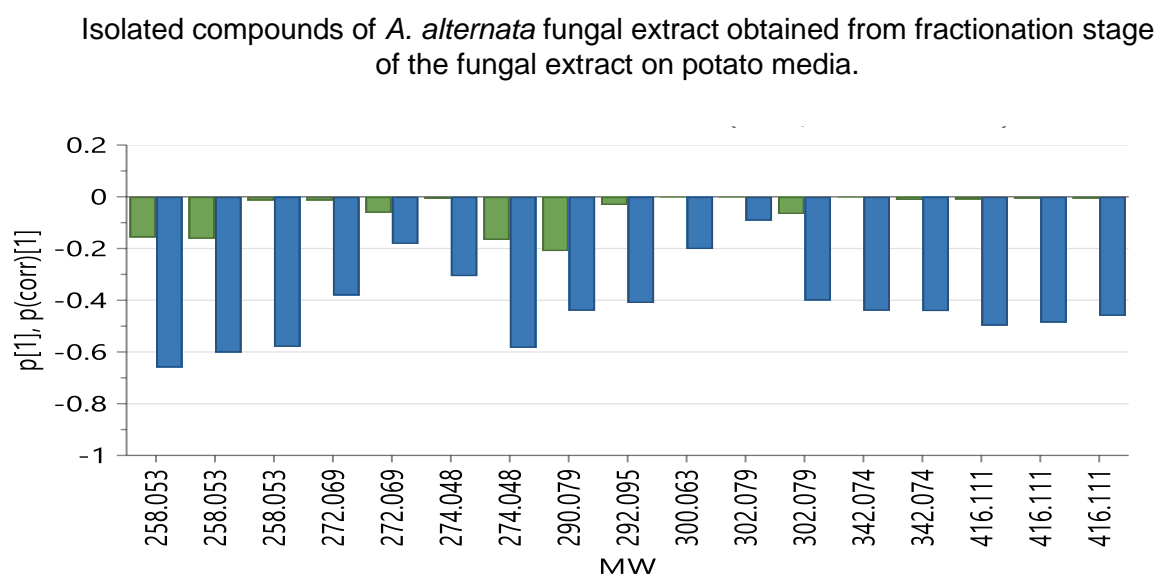


Figure 6.21: Distribution of the isolated compounds on the active quadrant by OPLS-DA S-plot for the fractionation stage. Isolated compounds with molecular weights 258.053 (alternariol), 272.069 (9-O-methylalternariol), 274.048 (altenuisol), 290.079 (altenusin), 292.095 (altenuene and 4'-epialtenuene), 300.063 (9-O-acetylalternariol), 302.079 (7-O-methyldehydro altenusin tautomer), 342.074 (3,9-di-O-acetylalternariol), 416.111 (3,4,7-tri-O-acetylaltenusin) showing projections correlating to the left S-plot quadrant of for the active fractions confirming activity of the bioactive compounds against MRSA.

Isolated compounds of *A. alternata* obtained from the crude extracts during the media optimisation stage.

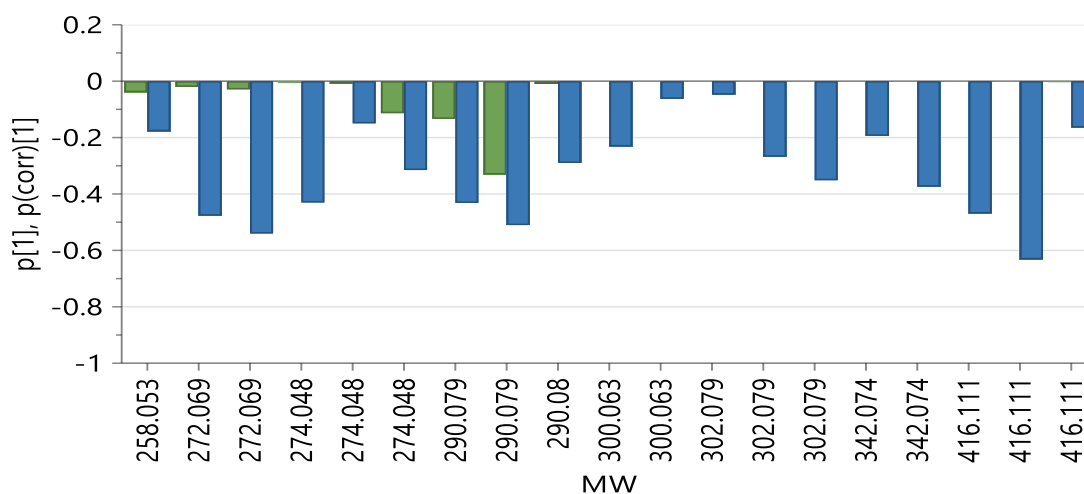


Figure 6.22: Distribution of the isolated compounds on the active quadrant by OPLS-DA S-plot during the media optimisation stage. Isolated compounds with molecular weights 258.053 (alternariol), 274.048 (altenuisol), 290.079 (altenusin), 300.063 (9-O-acetylalternariol), 302.079 (7-O-methyldehydro altenusin tautomer), 342.074 (3,9-di-O-acetylalternariol) and 416.111 (3,4,7-tri-O-acetylaltenusin) were observed confirming the bioactivity of the active compounds against MRSA.

Table 6.11: Isolated compounds observed on OPLS-DA active quadrant (fig. 6.15 and 6.4). Highlighted rows represent the bioactive metabolites.

Isolated compounds	Name	MW	Biofilm Stages of Observed Bioactivity	Observed / unobserved on OPLS-DA active quadrant from the fraction stage (MW, primary ID, rt)	Isolated compounds observed on OPLS-DA active quadrant as obtained from media optimisation stage (MW, primary ID, rt)
Dgs2-F4-1	9-O-methylalternariol	272.0685	Prebiofilm (51.96%)	Observed in active quadrant (272.069, N3145, rt= 10.75)	Observed in active quadrant (272.069, N2226, rt= 10.78)
Dgs2-F6-4-C6	Alternariol	258.0528	Planktonic (73.39%) and postbiofilm (58.95%)	Observed in active quadrant (258.053, P397, rt= 11.87)	Observed in active quadrant (258.053, P23, rt= 11.81)
Dgs2-F5-4-C5	9-O-acetylalternariol	300.0634	Prebiofilm (70.45%)	Observed in active quadrant (300.063, P2518, rt= 9.46)	Observed in active quadrant (300.063, P2184, rt= 12.18)
Dgs2-F5-4-C3	3,9-di-O-acetylalternariol	342.0740	Prebiofilm (65.20%)	Observed in active quadrant (342.074, P2801, rt= 13.50)	Observed in active quadrant (342.074, N13408, rt= 14.51)
Dgs2-F5-2	7-O-methyldehydroaltenusin tautomer	302.0790	Planktonic (51.98%) and prebiofilm (55.94%)	Observed in active quadrant (302.078, P476, rt= 13.50)	Observed in active quadrant (302.079, N3605, rt= 7.29)
Dgs2-F5-3-5	altenusin	290.0790	Planktonic (67.34%)	Observed in active quadrant (290.079, N318, rt= 10.68)	Observed in active quadrant (290.079, N49, rt= 10.75)
Dgs2-F5-3w	3,4,7-tri-O-acetylaltenusin	416.1107	Planktonic (65.91%)	Observed in active quadrant (416.111, P1047, rt= 12.88)	Observed in active quadrant (416.111, N10659, rt= 7.48)
Dgs2-F7-9P	altenuisol	274.0477	Planktonic (70.80%) and prebiofilm (54.99%)	Observed in active quadrant (274.048, N353, rt= 12.48)	Observed in active quadrant (274.048, P2377, rt= 9.42)
Dgs2-F7-14	altenuene	292.0947	Inactive	Observed in active quadrant (292.094, N1172, rt= 9.33)	Inactive quadrant
Dgs2-F8-6-10	4'-epialtenuene	292.0947	Inactive	Observed in active quadrant (292.094, N1172, rt= 9.33)	Inactive quadrant
Dgs2-F7-3	linoleic acid	280.2402	Inactive	Inactive quadrant	Inactive quadrant

6.3 Summary and conclusion

6.3.1 Isolation of fungi and extraction

In this study, endophytic fungi *A. alternata* was isolated from the stem of *A. indica*. Crude extract of *A. alternata* proved to be slightly active (>50%) against MRSA but was inactive to *P. aeruginosa*. In 2021, Techaoei and co-workers found out that the EtOAc crude extract of endophytic *A. alternata* isolated from lotus displayed more potential bioactivity against both *S. epidermidis*, and MRSA (Techaoei *et al.*, 2021). Chatterjee and co-workers also revealed that the EtOAc extract of endophytic fungus *A. alternata* AE1 isolated from *A. indica*, was also effective against both gram-positive and gram-negative bacteria (Chatterjee *et al.*, 2019).

6.3.2 Media optimisation and metabolomics bioassay guided isolation

Media optimisation showed *A. alternata* extracts from rice, malt, and potato media to be active against MRSA, but extracts from oat media were inactive. Potato media with 30 days of incubation proved to be the optimum media for *A. alternata*, with an average extract weight of 365.3 mg per 200 mL media, 91.69% inhibition, and was able to completely prevent biofilm formation. The most effective media in terms of yielding biologically active metabolites is in decreasing order as follows: Potato > malt > rice > oat. Previous study has shown that *Alternaria* grows well in potato dextrose agar or broth (Wei *et al.*, 1985, Koley and Mahapatra, 2015, Jaggal *et al.*, 2013).

There were differences in the dereplicated compounds from potato and rice media extracts, proving the OSMAC approach would afford different metabolites produced by a fungus if the media composition is altered. The common metabolites observed during the media optimisation stage and fraction stage were altenusin, dehydroaltenusin, 2-hydroxyalternariol, dehydroaltenusinic acid and 9-O-methylalternariol showing the stability of the compounds at both stages.

Dereplication of the LC-HRMS data on OPLS-DA S-plot showed that, the antimicrobial and antibiofilm active extracts afforded known *Alternaria* metabolites amongst which 9-O-methylalternariol, alternariol, altenusin, altenuisol, and altenuene with m/z 273.075 [M+H], 259.060 [M+H], 291.086 [M+H], 273.043 [M+H], and 293.101 [M+H] were successfully isolated in this study.

6.3.3 Pure compounds isolation

Scale-up of the fungus was carried out on potato dextrose media which was the optimum media to produce the antibiotic compounds. Fractionation was carried out on the scaled up crude extract using hexane and EtOAc as solvents. Eleven known compounds were isolated from *A. alternata* as shown in Table 6.31 which includes 9-O-methylalternariol, alternariol, 9-O-acetylalternariol, 3,9-di-O-acetylalternariol, 7-O-methyldehydroaltenusin tautomer, altenusin, 3,4,7-tri-O-acetylaltenusin, altenuisol, altenuene, 4'-epialtenuene and linoleic acid. Eight of the compounds exhibited either planktonic, prebiofilm or postbiofilm activity as shown in Table 6.11, but altenuene, 4'-epialtenuene and linoleic acid were inactive. This was proven by the fact that their molecular weights were observed on the inactive quadrant at the crude extract stage as shown in Table 6.11, while other active compounds were observed on the active quadrant, confirming their bioactivity.

Compound 9-O-methylalternariol was not as active as alternariol. The demethylation in the structure of alternariol to form an OH at position 9 could be responsible for its improved bioactivity against MRSA in this study, as the difference in the structure between alternariol and 9-O-methylalternariol was in the methylation of the latter compound at C9. Altenuene and 4'-epialtenuene which are isomers were also inactive. When compared with the structure of alternariol, there is an observed chiral centre at positions C-2', C-4' and C-5', alternariol was hydroxylated at C5' to form altenuene and 4'-epialtenuene and the hydroxy group (OH) in alternariol on position 9 is substituted for a methoxy group in altenuene and 4'-epialtenuene. These substitution and elimination in the functional groups of alternariol to form altenuene and 4'-epialtenuene could have led to their inactivity against MRSA, whilst enhancing alternariol bioactivity.

The structure of altenuisol with altenuene and 4'-epialtenuene were similar with slight variations, as the latter two compounds possess chiral centres at positions C-2', C-4' and C-5' unlike altenuisol. This slight variation could be responsible for the observed bioactivity in altenuisol and the observed inactivity in altenuene and 4'-epialtenuene.

Altenuisol and alternariol have been isolated as the major phytotoxins produced by an *Alternaria* sp., a pathogenic fungus of the invasive weed *Xanthium italicum* (Tang *et al.*, 2020), while in this study, altenuisol and alternariol have been isolated as the major bioactive compounds of *A. alternata*, an endophytic fungus of *A. indica*.

CHAPTER 7

7.1 Secondary metabolites from co-culture of isolated fungal endophytes and MRSA

Currently, the healthcare system is being challenged by the emergence and re-emergence of multidrug-resistant (MDR) pathogens. Infections caused by MDR pathogens are difficult to cure, hence the patient must undergo multiple treatments regimen with broad-spectrum antibiotics, which are more expensive, less efficient, and more toxic (Lara *et al.*, 2010). Biofilms significantly contribute to the development and spreading of nosocomial infections by allowing microorganisms to colonise not only tissues and organs but also various medical instruments and equipment. Characteristic features of biofilm-producing microorganisms involve the ability to resist the immune system of the host and increased resistance against antimicrobials and disinfectants. Antibiotic (ATB) therapy of biofilm infections is very demanding and often insufficient and, therefore, these infections may become frequently regressive and long-lasting (Englerová *et al.*, 2021, Sharma *et al.*, 2019, Khan *et al.*, 2021).

S. aureus belongs to the group of pathogenic microorganisms that are the most frequent agents of communal infections and health care related infections. It is an important opportunistic pathogen responsible for a broad spectrum of infections due to its variable genome (Tong *et al.*, 2015). *S. aureus* colonises mostly the nasal mucosa and infections are frequently induced by impairment of mucosal barrier and penetration of bacterial cells into the bloodstream or tissues. It is a causative agent of a great number of infections such as bacteraemia, acute skin abscesses, endocarditis, and infections of chronic wounds. *S. aureus* infections are mostly complicated; hence they are difficult to eradicate, especially those caused by MRSA (Sakr *et al.*, 2018). Production of biofilm by *S. aureus* was most frequently observed on medical implants and host tissues, hence, it is among the most common agents of chronic infections associated with biofilm formation.

To tackle this issue in this modern era, new antimicrobial compounds are urgently needed to fill the drug development pipeline. Several studies have indicated the possible prospect of endophytes from *Fusarium* and *Alternaria* genus, as a promising resource of antimicrobial compounds (Toghueo, 2020).

Microbial interactions are often characterised by competition of space or limited resources and antagonism, which trigger the activation of silent gene clusters, leading to the production of special bioactive metabolites as defence mechanisms. Co-culturing represents an attempt to imitate this highly interactive setting in the laboratory, in which competition is purposely provoked between two or more growing organisms with expectation that cryptic biosynthetic

gene clusters (BGCs) are activated and transcribed under stressed co-culture conditions (Bertrand *et al.*, 2014). An example of co-culture was performed between the fungus *Aspergillus nidulans* and the soil-dwelling bacterium *Streptomyces rapamycinicus*. The association induced the expression of a silent fungal gene cluster to yield the archetypal polyketide orsellinic acid and its analogues (Nützmann *et al.*, 2011).

In this study, extracts were prepared from three fungal isolates co-cultured with MRSA, respectively and were tested for their efficacy against MRSA to determine their prospects of producing new metabolites. Scale-up was accomplished on the co-culture between *Fusarium proliferatum* and MRSA that afforded the extract with the best bioactivity against MRSA.

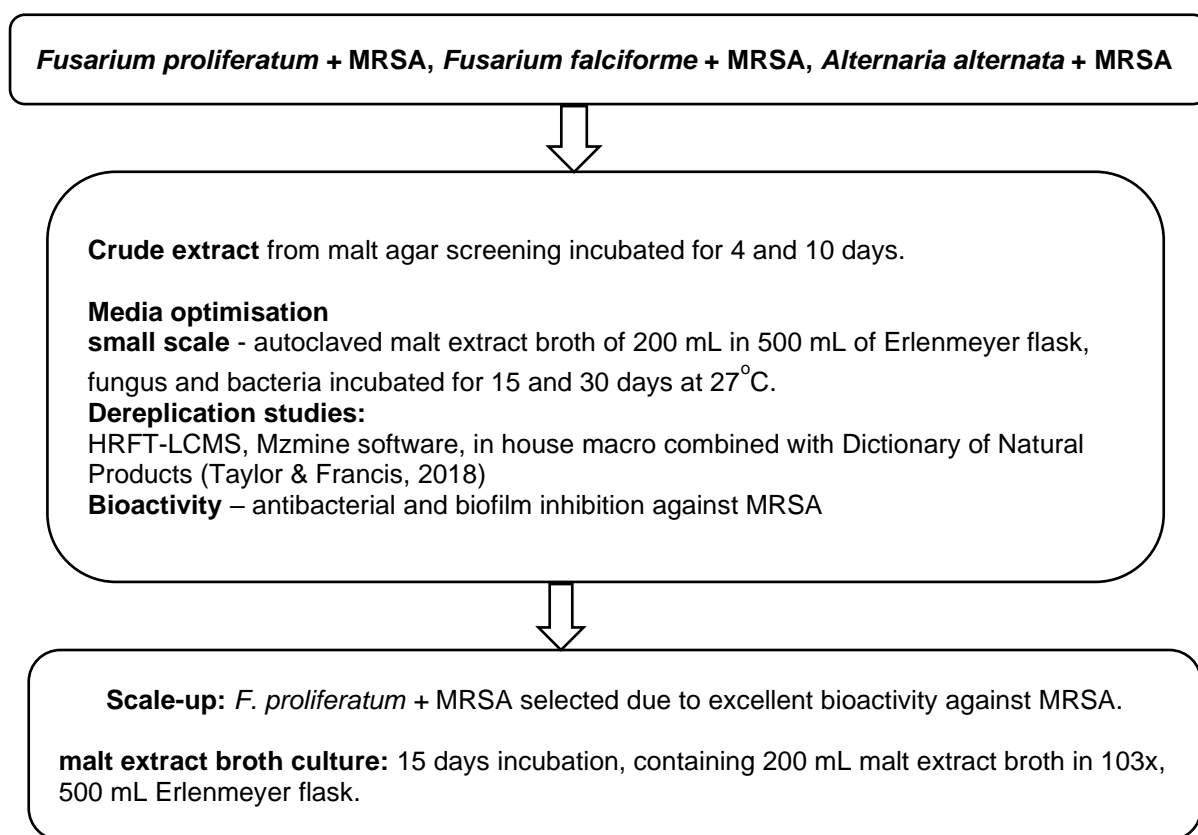


Figure 7.1: A summary workflow for crude extract screening, media optimisation and scaling up of three fungal isolates co-cultured with MRSA. The bacterial and fungal isolates were added the same day on malt extract agar. The growing temperature of the fungus was chosen for inoculation rather than that of the bacteria to slow down the growth of bacteria, which only has a 24h growth cycle at 37°C, which will compensate the fungal growth cycle of 15 to 30 days.

7.2. Results and Discussion

7.2.1 Co-culture extract yields on solid malt extract agar media

As depicted in Table 7.1, the highest yield of *F. proliferatum* and MRSA co-culture (CoBIS1) was gained at day 4 with an extract weight of 37.1 mg. *F. falciforme* and MRSA co-culture (CoMgs3A) gained its highest yield at day 10 with an extract weight of 59.8 mg, while *A. alternata* and MRSA co-culture (CoDgS2) gained its highest yield at day 4 with an extract weight of 61.5 mg. The histogram below in Figure 7.4 shows that *F. proliferatum*-MRSA co-culture and *A. alternata*-MRSA co-culture attained its exponential phase at day 4 and has started to decline at day 10, while *F. falciforme*-MRSA co-culture was still growing at day 4 and could have attained its exponential phase after 10 days of incubation. The obtained weights of the co-culture extracts are listed in Table 7.1.

Table 7.1: Co-culture extracts weights incubated for 4 and 10 days as illustrated in Figure 7.2. All cultures were incubated at 27°C.

Sample	Weights (mg)	Sample	Weights (mg)
	4 days		10 days
Co-Control	46.3	Co2-Control	13.9
CoBIs1 -1	44.6	Co2 BIs1- 1	35.6
CoBIs1 -2	36.6	Co2 BIs1- 2	30.8
CoBIs1 -3	30.2	Co2 BIs1- 3	28.3
Average weight	37.1		31.6
Comgs3A-1	51.2	Co2Mgs3A-1	58.1
Comgs3A-2	50.9	Co2Mgs3A-2	60.8
Comgs3A-3	47.7	Co2Mgs3A-3	60.6
Average weight	49.9		59.8
CoDgS2-1	77.9	Co2Dgs2-1	31.9
CoDgS2-2	55.2	Co2Dgs2-2	52.7
CoDgS2-3	51.4	Co2Dgs2-3	33.6
Average weight	61.5		39.4

Table 7.2: Sample codes

Code	Full name
CoBlS1	<i>F. proliferatum</i> and MRSA co-culture 4 days
Comgs3A	<i>F. falciforme</i> and MRSA co-culture 4 days
CoDgS2	<i>A. alternata</i> and MRSA co-culture 4 days
Co2BlS1	<i>F. proliferatum</i> and MRSA co-culture 10 days
Co2Mgs3A	<i>F. falciforme</i> and MRSA co-culture 10 days
Co2Dgs2	<i>A. alternata</i> and MRSA co-culture 10 days

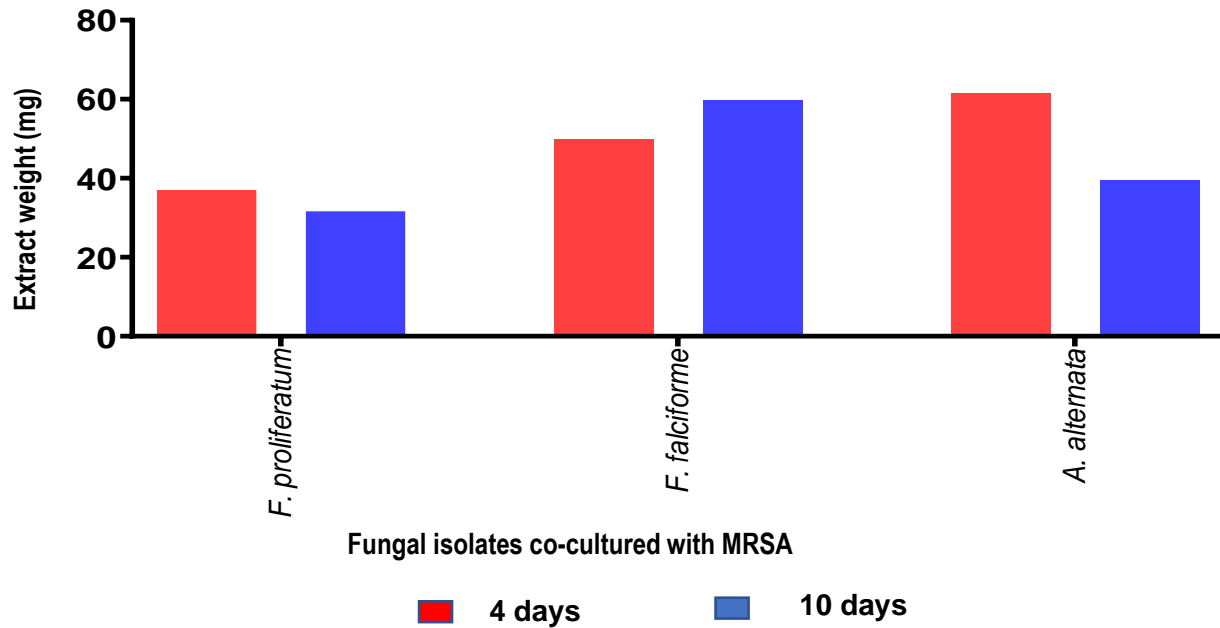


Figure 7.2: Histogram showing average weight of extracts from three respective replicates of *F. proliferatum* + MRSA, *F. falciforme* + MRSA and *A. alternata* + MRSA co-cultures obtained from malt extract media and incubated for 4 and 10 days.

7.2.2 Crude extract biological assay screening

F. proliferatum + MRSA, *F. falciforme* + MRSA and *A. alternata* + MRSA were co-cultured on malt agar plates as explained in 2.6.2.7. The metabolites produced from the co-culture extracts were analysed using NMR and HRESI-LCMS for dereplication studies and tested for MRSA activity.

The results showed that *F. proliferatum* and MRSA (BLS1-MRSA) incubated for 10 days showed planktonic activity (92.23%) and prebiofilm activity (83.43%), while the other extracts were inactive. Bioactivity threshold was set at 20.0% cell viability (80.0% inhibition).

7.2.3 MVA of LC-HRMS data

For multivariate analysis, PCA scores and loadings plot were generated for the LC-MS data. The extracts were grouped according to the 3 different fungal co-cultures. The PCA scores plot in Figure 7.3A of the LC-HRMS data of the co-cultures revealed that extracts obtained from *F. falciforme*-MRSA after 4 and 10 days of incubation were found on the right side of the plot (red circles), with slight variation between extracts obtained from 4 and 10 days of incubation. On the other side, extracts obtained from *A. alternata*-MRSA co-culture after 4 and 10 days of incubation were found clustered together on the left side of the plot (green circles) indicating similarity between extracts. The fungal extract obtained from *F. proliferatum*-MRSA co-culture (blue circles) was in the upper (4 days extract) and lower left quadrant (10 days). Variation was observed in the extracts obtained from day 4 and extracts obtained from day 10, indicating differences in the chemical profile between both days. The differences in the chemical profile could be the cause of bioactivity observed in day 10 extract. The loadings plot in Figure 7.3B demonstrated that discriminating metabolites from co-culture extracts of *F. falciforme* and MRSA produced low to moderate molecular weight metabolites ranging from 279 to 602 Da and were putatively identified as 2-acetyl-5-dodecylfuran, 10,15-cyclo-11,14-dihydroxy-1,2-dinor-6-phyten-3-one, 8,13-dihydroxy-9,11-octadecadienoic acid, albocycline M8 and phomenoic acid. *F. proliferatum*-MRSA co-culture produced low molecular weight discriminatory metabolites ranging from 152 to 353 Da (extracts in blue circles) and putatively identified as pulchellalactam, fusalanipyrone, fusaric acid, 2,4,6-trimethyl-1-nonanol-O-sulfate, and 1-tetradecanol-hydrogen sulfate while extracts from *A. alternata*-MRSA co-culture produced discriminatory metabolites ranging from 273 to 289 Da and putatively identified as 9-O-methylalternariol and altenusin. Slight variations were observed in the compound hits obtained from the monocultures as compared with the co-cultures, but most of the discriminatory compounds hits putatively identified in the co-cultures were previously observed in the fungal monocultures indicating their dominance over the pathogenic MRSA. As some of the compounds reported in the biologically active monocultures were still present

in the inactive co-culture extracts (except for *F. proliferatum*-MRSA co-culture), it can be deduced that the presence of MRSA could have weakened the antibiotic activity of the compounds, hence the inactivity observed from these respective co-culture extracts. For example, 9-O-methylalternariol and altenusin were present in both the monocultures of *A. alternata* and the co-culture of *A. alternata* with MRSA as active compound hits but the extracts obtained from the co-cultures slightly lost their bioactivity. The weakening of the bioactivity of the compounds could be attributed to the co-occurrence of the pathogenic MRSA. However, the model gave a poor goodness of fit (R_2) of 0.481 and a low predictability score (Q_2) of 0.274 due to the undefinable overlapping features between *A. alternata*-MRSA and 4-days culture of *F. proliferatum*-MRSA.

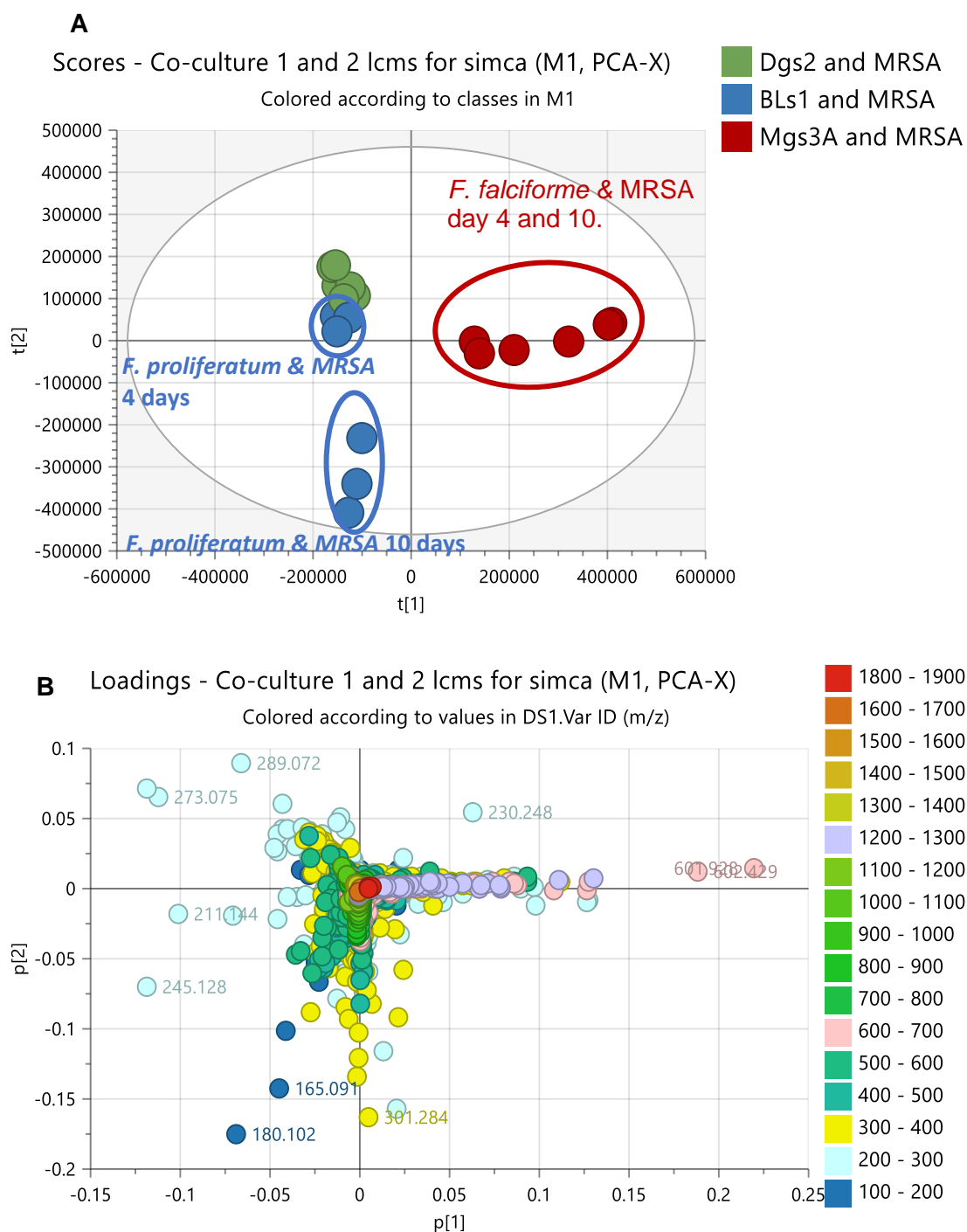


Figure 7.3: (A) PCA scores and (B) loadings plots of LC-HRMS data of co-culture extracts from malt extract media incubated at 4 and 10 days. $R_2X = 0.481$ and $Q_2X = 0.274$. Labelled features represent the discriminating ion peaks for the outlying extracts obtained from co-cultures of *F. proliferatum*-MRSA, *F. falciforme*-MRSA and *A. alternata*-MRSA.

Table 7.3: Dereplicated compound hits from discriminating metabolites from co-culture of fungus and MRSA incubated for 4 and 10 days obtained from the PCA loadings plot on Figure 7.3B. **Hits were filtered according to their microbial source except when no other compound hits were found under this filter.** Structures are shown in figure 7.4.

Mzmine ID	m/z	Rt	M.wt	Molecular Formular (DBE)	Compound hits	Biological source
<i>F. falciforme</i>-MRSA 4 and 10 days						
P943	279.232	20.31	278.224	C ₁₈ H ₃₀ O ₂ (4)	Coriolide (1)	<i>Stagonospora</i>
N154	295.228	20.32	296.235	C ₁₈ H ₃₂ O ₃ (4)	Piliferolide A (2)	<i>Pseudomonas brassicacearum</i> MA250
N2227	311.223	18.59	312.23	C ₁₈ H ₃₂ O ₄ (4)	6,8-Dihydroxy-9,12-octadecadienoic acid (3)	A mangrove-derived <i>Penicillium javanicum</i> HK1-22
N256	341.197	11.53	342.205	C ₁₈ H ₃₀ O ₆ (4)	Albocycline M8	<i>Streptomyces bruneogriseus</i>
P6034	594.92	21.04	593.913		No hit	
P6037	595.422	21.01	594.414	C ₃₄ H ₅₈ O ₈ (6)	Phomenoic acid (4)	<i>Phoma lingam</i>
P6051	601.928	20.56	600.921		No hit	
P13552	602.429	24.85	601.422		No hit	
BLS1 and MRSA 10 days						
P2796	152.107	5.67	151.1	C ₉ H ₁₃ NO (4)	Pulchellalactam	<i>Acrocarpospora</i> sp. FIRDI001 and the marine derived <i>Corollospora pulchella</i> , <i>Monascus ruber</i> BB5, <i>Monascus pilosu</i>
P2835	165.091	12.88	164.084	C ₁₀ H ₁₂ O ₂ (5)	Fusalanipyrone	<i>Fusarium solani</i> DSM 62416 and <i>F. oxysporum</i> f. sp. <i>batatas</i> O-17
P441	180.102	5.85	179.095	C ₁₀ H ₁₃ NO ₂ (5)	Fusaric acid	<i>Fusarium lycopersici</i> , <i>F. oxysporum</i> , <i>F. vasinfectum</i> and <i>Gibberella fujikuroi</i>

Mzmine ID	m/z	Rt	M.wt	Molecular Formular (DBE)	Compound hits	Biological source
N13	265.148	15.61	266.155	C ₁₂ H ₂₆ O ₄ S (0)	2,4,6-Trimethyl-1-nonanol-O-Sulfate (5)	Isolated from the sea cucumber <i>Cucumaria frondosa</i>
N103	293.18	18.38	294.187	C ₁₄ H ₃₀ O ₄ S (0)	1-Tetradecanol-hydrogen sulfate (6)	Natural waxes
P1082	301.284	15.24	300.277		No hit	
N104	309.174	17.02	310.182		No hit	
N50	353.201	17.61	354.208		No hit	
DgS2 and MRSA 10 days						
P890	273.075	15.79	272.068	C ₁₅ H ₁₂ O ₅ (10)	9-O-methylalternariol	<i>Alternaria</i> sp. including marine sp., <i>Anthocleista djalonensis</i> , <i>Penicillium diversum</i> and <i>Lachnum palmae</i>
N91	289.072	10.69	290.079	C ₁₅ H ₁₄ O ₆ (9)	Altenusin	<i>Alternaria tenuis</i> , <i>Penicillium</i> sp. and <i>Talaromyces</i> sp.

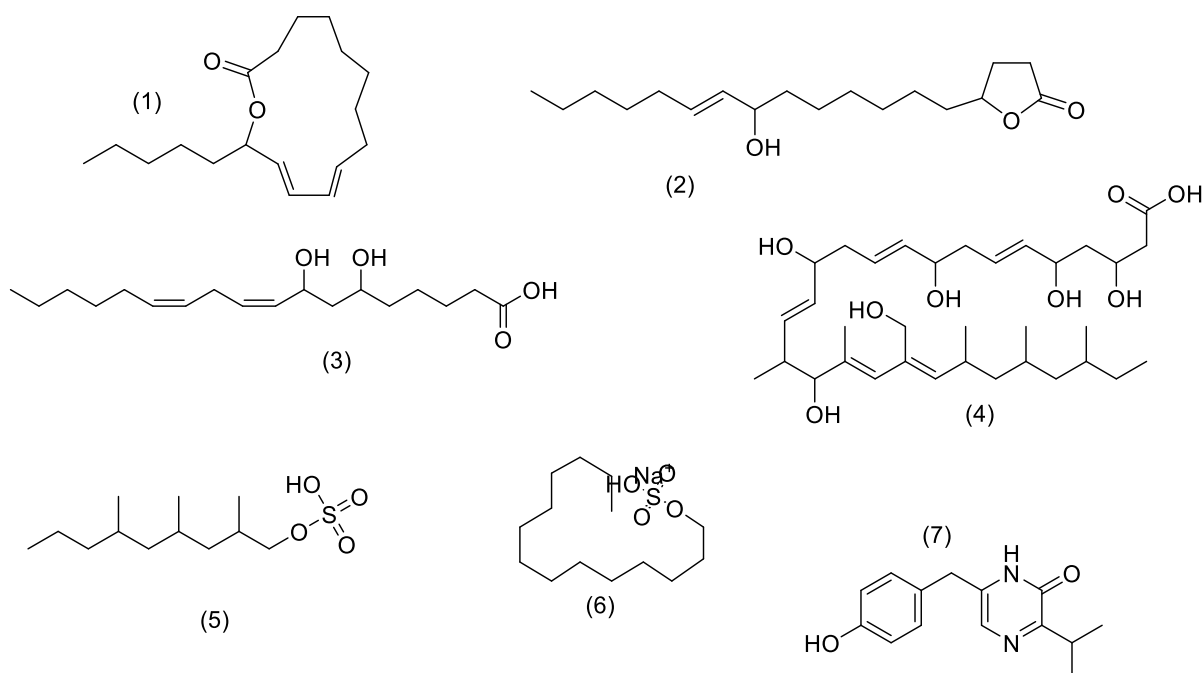


Figure 7.4: Structures of dereplicated compound hits showing PCA discriminating metabolites obtained from co-culture extracts, as listed in Table 7.3.

A PLS-DA was performed to show a clearer illustration of the differences in metabolic profiles between the co-culture extracts from malt extract broth in Figure 7.5. It showed fitness (R_2) and predictability (Q_2) scores of 0.992 and 0.911 respectively, after five components. The difference between R_2 and Q_2 values was less than 0.3. This proved to be a good fit, and a good model prediction, which improved when compared to the PCA model above. The variation between groups R_2X_0 [1] was 29.3 % and within group R_2X [2] was 17.3%. From the scores plot, extracts from *F. proliferatum*-MRSA co-cultures were positioned in the upper right quadrant (blue circles), extracts from *A. alternata*-MRSA co-cultures were positioned in the lower right quadrant (green circles), while extracts from *F. falciforme*-MRSA co-cultures were found in the upper and lower left quadrant (red circles). The plot showed that although there were slight variations between the different incubation periods of 4 and 10 days amongst the co-culture extracts, extracts obtained at 4 and 10 days were still at proximity with each other, indicating similarity in the metabolites obtained from the different incubation periods. Furthermore, the three co-culture extracts were in different quadrants defining the differences in their chemical profile.

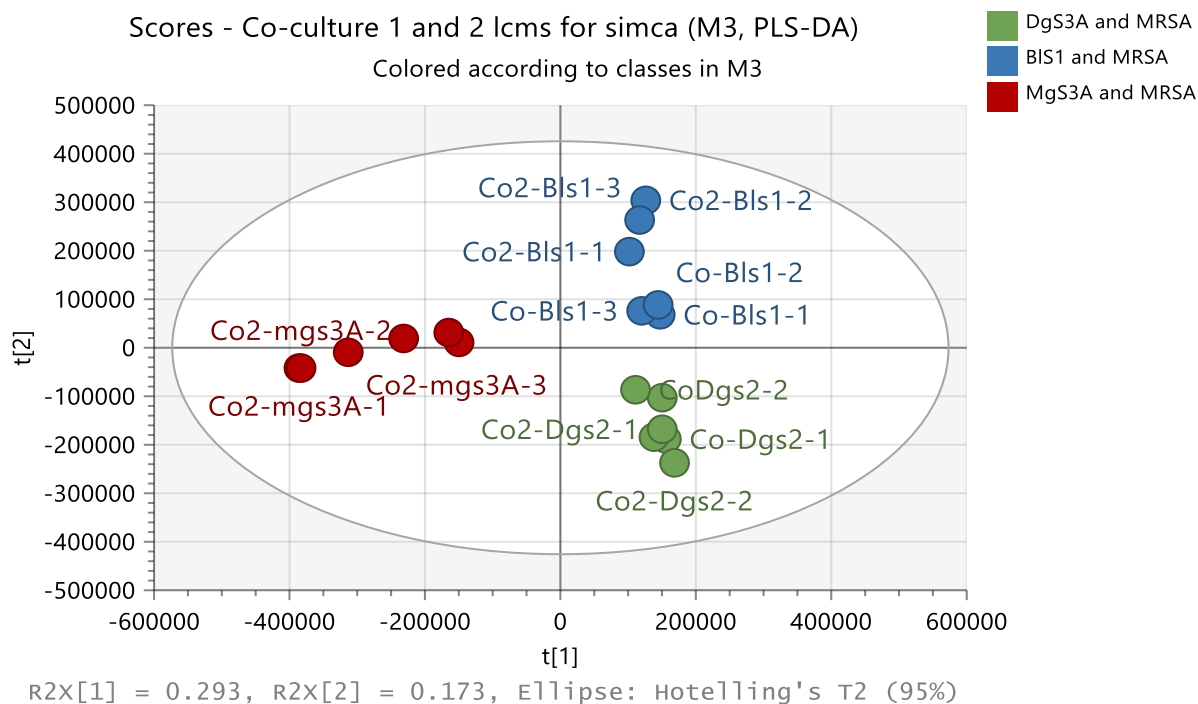


Figure 7.5: PLSDA scores of LC-HRMS data of co-culture extracts from malt extract media incubated at 4 and 10 days. $R^2X = 0.992$ and $Q^2X = 0.911$. The variation between groups $R^2X_o [1]$ was 29.3 % and within group $R^2X [2]$ was 17.3%.

An OPLS-DA was performed based on the anti-MRSA results to discriminate the metabolites between active and inactive extracts as shown in Figure 7.6. Active extracts were obtained by inoculation of *F. proliferatum*-MRSA co-culture in malt extracts media then incubated for 10 days while the other co-culture extracts were found inactive. It showed fitness (R^2) and predictability (Q^2) scores of 0.987 and 0.889 respectively. This proved to be a good fit, and a good prediction model. The variation between groups $R^2X_o [1]$ was 27.2 % and within group $R^2X [1]$ was 18.3 %. This showed that there was a slight similarity within the extracts in their different classes.

The OPLS-DA scores plot in Figure 7.6A positioned the active extracts on the upper and lower right quadrants (red circles), while the inactive extracts were found on the upper and lower left quadrant of the scores plot (blue circles). The defined target metabolites afforded p -values < 0.05 , which indicated a strong model with a confidence interval of more than 95%. The bioactive metabolites gave an m/z range between 152 and 397 Da. Discriminating active metabolites with p -values less than 0.05 are listed in Table 7.4. Structures of putatively

identified compound hits are shown in Figure 7.4. Six of the ion peaks gave no hits, which could indicate the presence of novel compounds.

The compounds identified from the DNP database, as shown in Table 7.4 were, Mzmine IDs of P2796, P2835, P441, P17610, P17631, N13, N103, P3916, P1082, N104, N2051, P1242, N50, N116 represented by their respective *m/z* as 152.107, 165.091, 180.102, 211.144, 245.128, 265.148, 293.18, 383.076, 301.284, 309.174, 325.184, 329.316, 353.201 and 397.227 respectively and dereplicated as pulchellalactam, fusalanipyrone, fusaric acid, cyclo(isoleucylprolyl), 5-benzyl-3-hydroxy-2-isopropylpyrasine; 4'-hydroxy-2,4,6-trimethyl-1-nonanol-O-sulfate, 1-tetradecanol hydrogen sulfate, and bikaverin while six ion peaks found no hits, respectively.

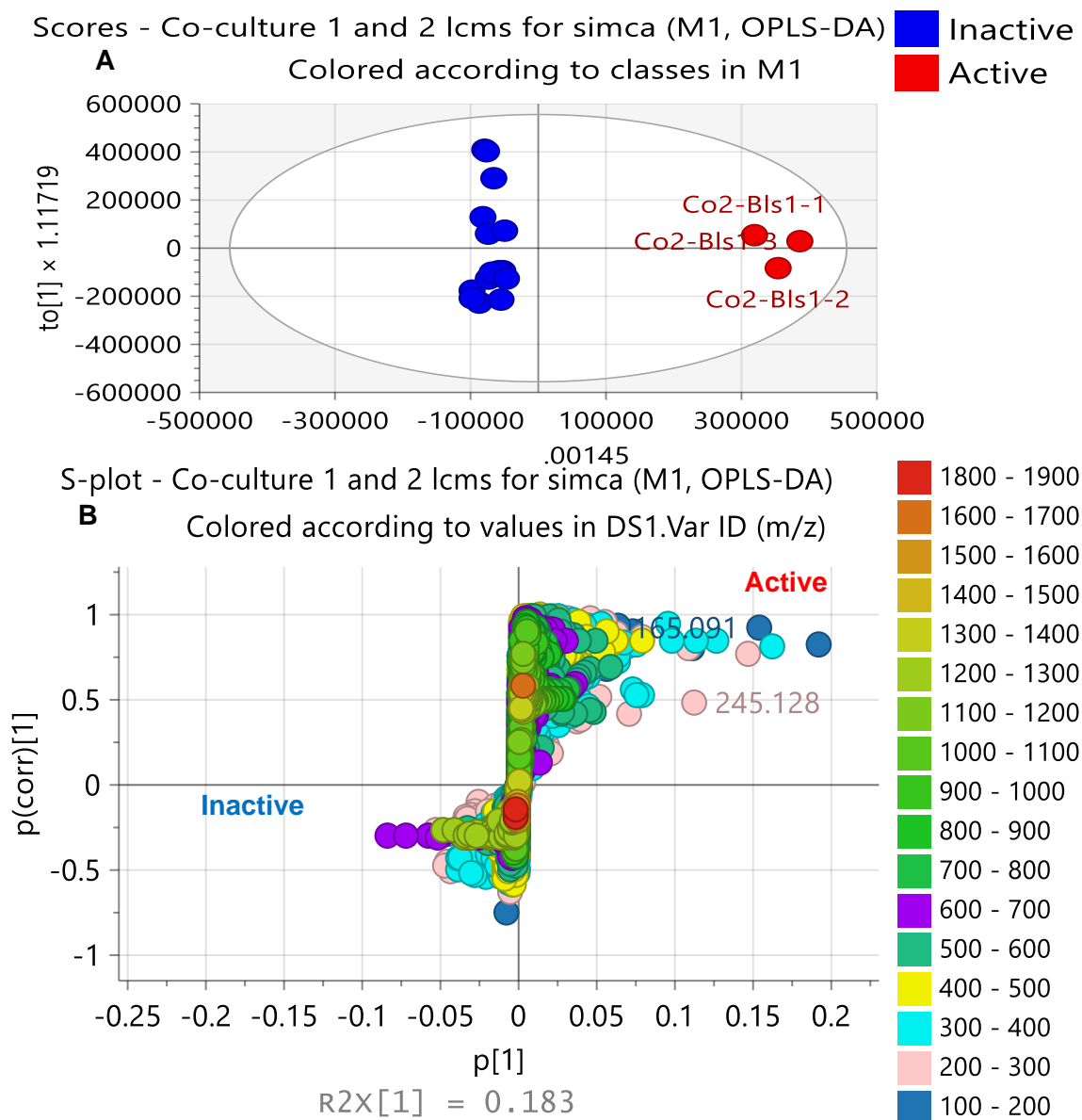


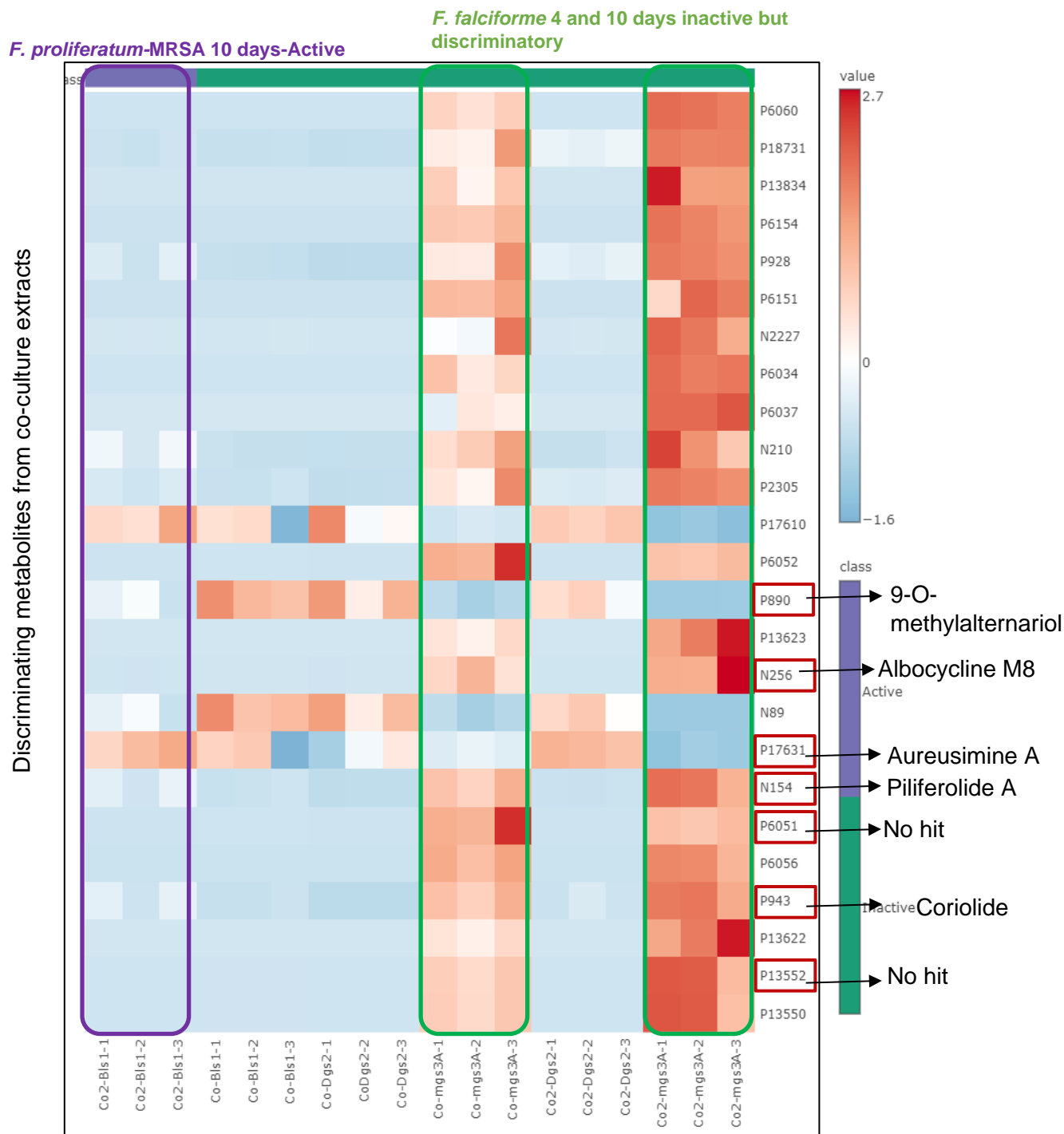
Figure 7.6: (A) OPLS-DA scores and (B) S- plots of LC-HRMS of co-culture extracts obtained from malt extract media. The labelled metabolites on S-plot indicated the discriminating feature for each media extracts. $R_2 = 0.987$ and $Q_2 = 0.889$. The difference between group R_2X_0 [1] is equal to 27.2% and the difference within groups R_2X [2] is 18.3%.

Table 7.4: Dereplicated compound hits from discriminating metabolites from co-culture of fungi and MRSA incubated for 4 and 10 days obtained from the OPLS-DA S-plot on Figure 7.6B. **Hits were filtered according to their microbial source except when no other compound hits were found under this filter.** Structures are shown in figure 7.4.

Mzmine ID	m/z	Rt	M. wt	p-value	Molecular Formular (DBE)	Compound hits	Biological source
P2796	152.107	5.68	151.1	7.00733e-05	C ₉ H ₁₃ NO (4)	Pulchellalactam	<i>Acrocarpospora</i> sp. FIRDI001 and the marine derived <i>Corollospora pulchella</i> , <i>Monascus ruber</i> BB5, <i>Monascus pilosus</i>
P2835	165.091	12.88	164.084	3.04224e-08	C ₁₀ H ₁₂ O ₂ (5)	Fusalanipyrone	<i>Fusarium solani</i> DSM 62416 and <i>F. oxysporum</i> f. sp. <i>batatas</i> O-17
P441	180.102	5.85	179.095	2.83638e-05	C ₁₀ H ₁₃ NO ₂ (5)	Fusaric acid	<i>Fusarium lycopersici</i> , <i>F. oxysporum</i> , <i>F. vasinfectum</i> and <i>Gibberella fujikuroi</i>
P17610	211.144	5.05	210.136	0.129933	C ₁₁ H ₁₈ N ₂ O ₂ (4)	Cyclo(isoleucylprolyl	Marine-derived <i>P. aeruginosa</i> and <i>Vibrio parahaemolyticus</i>
P17631	245.128	6.16	244.121	0.059871	C ₁₄ H ₁₆ N ₂ O ₂ (8)	4'-Hydroxy-5-Benzyl-3-hydroxy-2-isopropylpyrasine; (Aureusimine A) (7)	<i>S. aureus</i>
N13	265.148	15.61	266.155	0.000538	C ₁₂ H ₂₆ O ₄ S (0)	2,4,6-Trimethyl-1-nonanol-O-Sulfate	Isolated from the sea cucumber <i>Cucumaria frondosa</i>
N103	293.18	18.38	294.187	0.000129	C ₁₄ H ₃₀ O ₄ S	1-Tetradecanol hydrogen sulfate	From various plant waxes
P1082	301.284	15.24	300.277	7.79886e-05		No hit	
N104	309.174	17.02	310.182	2.16095e-05		No hit	
N2051	325.184	17.77	326.192	0.024936		No hit	
P1242	329.316	18.86	328.309	0.040266		No hit	
N50	353.201	17.61	354.208	2.41538e-05		No hit	

Mzmine ID	<i>m/z</i>	Rt	M. wt	<i>p-value</i>	Molecular Formular (DBE)	Compound hits	Biological source
P3916	383.076	16.78	382.069	1.63272e-08	C ₂₀ H ₁₄ O ₈ (18)	Bikaverin	Pigment from <i>Fusarium oxysporum</i> , <i>F. solani</i> , <i>F. moniliforme</i> , <i>F. lycopersici</i> , <i>F. vasinfectum</i> , <i>F. bulbigenum-blasticola</i> , <i>Gibberella fujikuroi</i> .
N116	397.227	17.97	398.234	2.36965e-05		No hit	

Analysis on MetaboAnalyst® was performed. The heatmap showed that the bioactive co-culture extract of *F. proliferatum* and MRSA (purple box) incubated for 10 days were not discriminatory (Figure 7.7). The co-culture extracts of *F. falciforme* incubated for 4 and 10 days were inactive but discriminatory as denoted by the high intensity and concentration of metabolites observed on both incubation periods (green boxes). It can be deduced that, the pathogenic bacteria (MRSA), which was inoculated with *F. falciforme*, weakened the fungal endophyte, leading to a loss in bioactivity, even though it was producing high intensity and concentration of metabolites.



Co-culture extracts obtained from malt extract agar media.

Figure 7.7: Heatmap analysis of the mass spectral data of co-culture crude extracts with their Mzmine values, obtained from malt extract media, generated by MetaboAnalyst®. The purple box represents active extracts from *F. proliferatum*-MRSA co-culture, while the green boxes represent the inactive but discriminatory metabolites from *F. falciforme*-MRSA co-culture. Highlighted Mzmine values on the Y-axis indicate common metabolites observed on the heatmap and VIP.

Base peak plot, MS1, m/s: 149.9997-1999.9756

Selected scan #1387, RT: 15.19, base peak: 301.2842 m/s, IC: 2.9E8

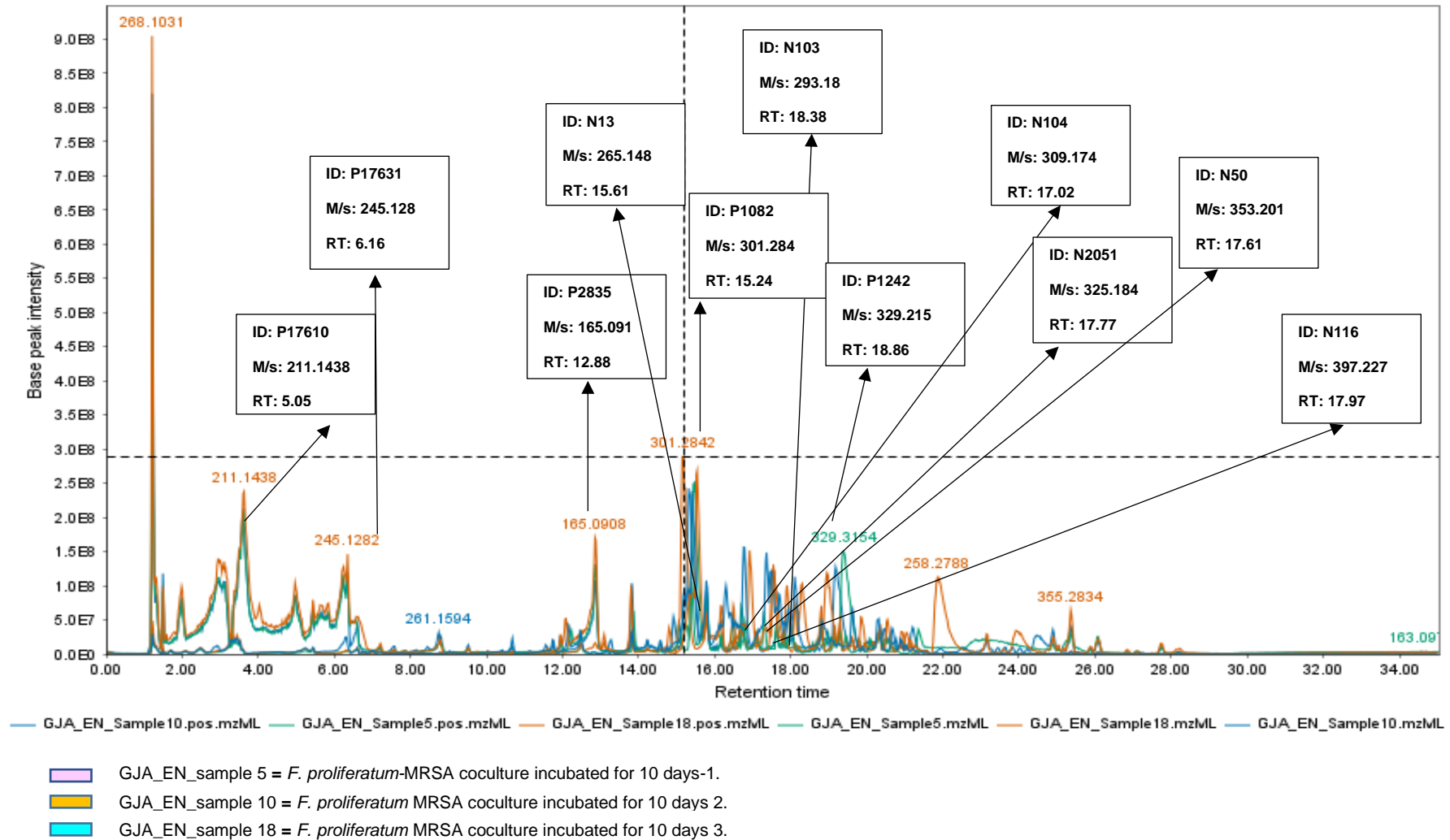


Figure 7.8: Total ion chromatogram (TIC) of the bioactive extracts of *F. proliferatum*-MRSA co-culture from malt extract media. The ion peaks that represent the discriminating features listed in table 7.4 have been labelled.

7.2.4 Co-culture extract yields on liquid malt extract media

As depicted in Table 7.5, the highest extract weight of *F. proliferatum* and MRSA co-culture (CoBIS1) was gained at day 30 with an extract weight of 108.4 mg. *F. falciforme* and MRSA co-culture (CoMgs3A) gained its highest yield at day 15 with an extract weight of 84.4 mg, while *A. alternata* and MRSA co-culture (CoDgs2) gained its highest yield at day 15 with an extract weight of 135.6 mg. The histogram below in Figure 7.9 shows that *F. proliferatum*-MRSA co-culture attained its exponential phase at day 30, while *F. falciforme*-MRSA and *A. alternata*-MRSA co-culture attained exponential phase at day 15 and death phase at 30 days of incubation.

Table 7.5: Co-culture extract weights incubated for 15 and 30 days as illustrated in Figure 7.9. All cultures were incubated at 27°C.

Sample	Weights (mg)	Sample	Weights (mg)
	15 days		30 days
Control 15	22.3	Control 30	38
Co15BlS1 -1	83.1	Co30 bls1- 1	109.8
Co15BlS1 -2	88.3	Co30bls1- 2	107.4
Co15BlS1 -3	107.5	Co30 bls1- 3	108.1
Average weight	93.0		108.4
Co15mgs3A-1	68.6	Co30Mgs3A-1	84.4
Co15mgs3A-2	91.8	Co30Mgs3A-2	76.5
Co15mgs3A-3	92.8	Co30Mgs3A-3	67.5
Average weight	84.4		76.1
Co15DgS2-1	150.4	Co30Dgs2-1	75.9
Co15DgS2-2	131.0	Co30Dgs2-2	75.3
Co15DgS2-3	125.5	Co30Dgs2-3	78.7
Average weight	135.6		76.6

Table 7.6: Sample codes

Code	Full name
Co15BlS1	<i>F. proliferatum</i> and MRSA co-culture 15 days
Co15mgs3A	<i>F. falciforme</i> and MRSA co-culture 15 days
Co15DgS2	<i>A. alternata</i> and MRSA co-culture 15 days
Co30BlS1	<i>F. proliferatum</i> and MRSA co-culture 30 days
Co30Mgs3A	<i>F. falciforme</i> and MRSA co-culture 30 days
Co30Dgs2	<i>A. alternata</i> and MRSA co-culture 30 days

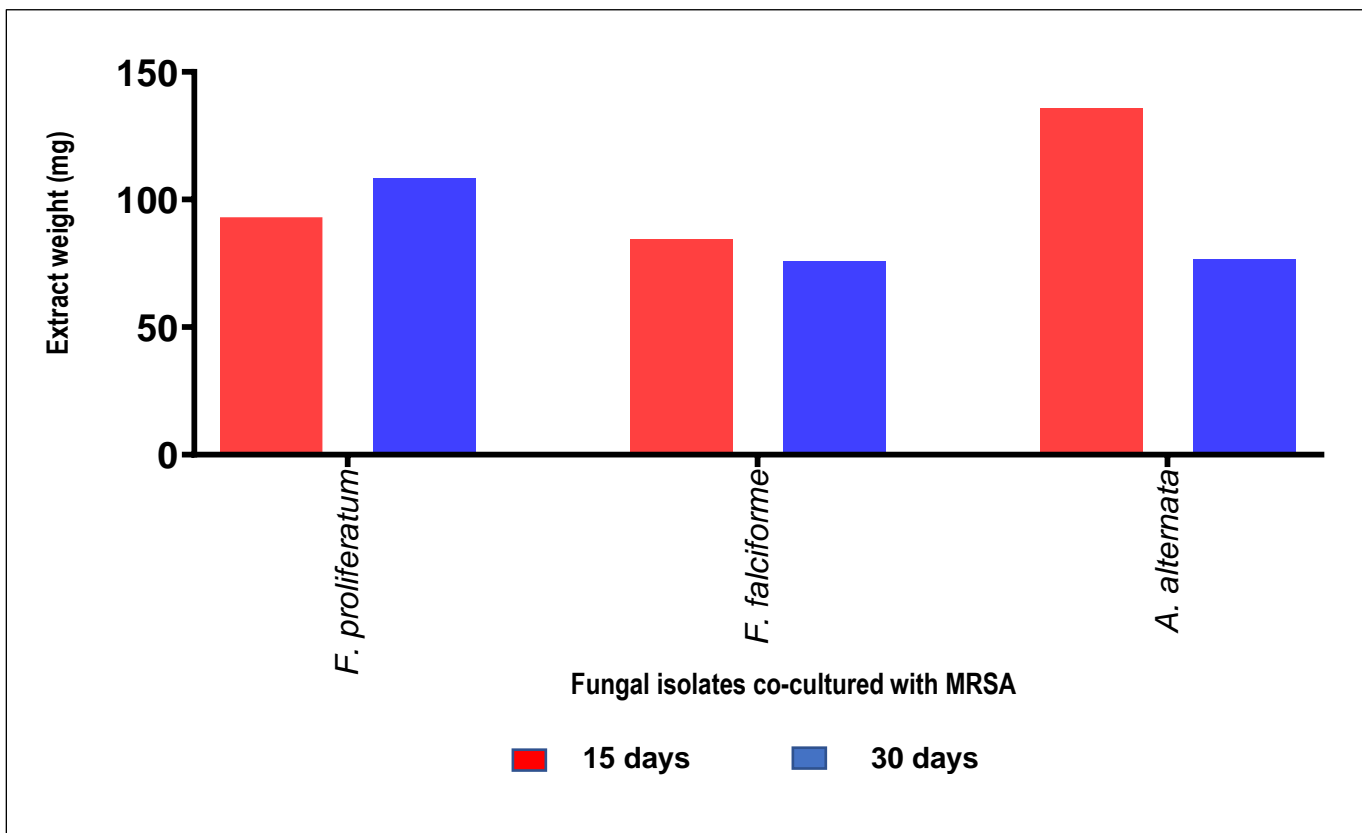


Figure 7.9: Histogram showing average weight of extracts from three respective replicates of *F. proliferatum* + MRSA, *F. falciforme* + MRSA and *A. alternata* + MRSA co-cultures obtained from malt extract media and incubated for 15 and 30 days.

7.2.5 Crude extract biological assay screening

F. proliferatum + MRSA, *F. falciforme* + MRSA and *A. alternata* + MRSA was co-cultured on malt extract broth as explained in 2.6.2.7. The metabolites produced from the co-culture extracts were analysed using NMR and HRESI-LCMS for dereplication studies and tested for MRSA activity.

The results show that *F. proliferatum* and MRSA (BLS1-MRSA) incubated for 15 days were active against MRSA, while the other extracts were inactive. Bioactivity threshold was set at 5.0% cell viability (95.0% inhibition).

Table 7.7: Summary activity of active co-culture extract against MRSA at concentrations of 100 µg/ml.

Media	Incubation period (days)	Antimicrobial % inhibition	Prebiofilm % inhibition	Postbiofilm % inhibition
C015BLS1	15	98.84	98.15	<0
Co15DgS2	15	45.32	92.16	<0
Co30BLS1	30	41.00	60.43	<0

*Cells highlighted in blue colour indicates active extracts while white cells indicate inactive extracts. *F. proliferatum*-MRSA was active against planktonic and prebiofilm MRSA, *F. falciforme* + MRSA and *A. alternata* + MRSA co-cultures exhibited only prebiofilm activity (above 50% inhibition), hence regarded as inactive.

7.2.6 MVA of LC-HRMS data

For multivariate analysis, PCA scores and loadings plot were generated for the LC-MS data. The extracts were grouped according to the 3 different fungi co-cultures. The PCA scores plot in Figure 7.10A of the LC-HRMS data of the co-cultures revealed that extracts obtained from *A. alternata*- MRSA after 15 and 30 days of incubation were found on the upper right side of the plot (red circles). Extracts obtained from *F. falciforme*-MRSA co-culture were found on the lower right quadrant of the plot (blue circles). The fungal extract obtained from *F. proliferatum*-MRSA co-culture (green circles) was in the upper and lower left quadrant. The variation observed in the extracts from their location in different quadrants, indicates differences in their chemical profiles, but within the extracts, the 15- and 30-days extracts were at proximity

indicating similarities in their chemical profiles. The loadings plot in Figure 7.10B demonstrated that discriminating metabolites from extracts of *F. falciforme*-MRSA produced moderate to high molecular weight metabolites ranging from 307 to 1204 Da and were putatively identified as 9'-ketoalbocycline K2; hymeclusin, albocycline M8 and 4 ion peaks gave no hits. *F. proliferatum*-MRSA co-culture produced low to moderate molecular weight discriminatory metabolites ranging from 241 to 405 Da (extracts in blue circles) and putatively identified as bushrin, Peniphenylane D, cyclo(isoleucyltryptophyl), (R)-3,7-dimethyl-1-octanol, 4-methylbenzenesulfonyl, N1-Me-(3S,6R)-cyclo(leucyltryptophyl), sophasrine, iboluteine oxime, and 7'-alcohol antibiotic K 76; while 3 ion peaks gave no hits. Extracts from *A. alternata*-MRSA co-culture produced low molecular weight discriminatory metabolites ranging from 273 to 289 Da and again putatively identified as 9-O-methylalternariol and altenusin. Sophazrine and 7'-alcohol iboluteine oxime are however plant metabolites but were the only compound hits found from the database indicating that the respective ion peaks could be new microbial metabolites with possibly novel structures. The challenge remains though whether it would be feasible to isolate these novel compounds when they are only present in micro- or nanogram yields.

Slight variations were observed in the compound hits obtained from the monocultures as compared with the co-cultures, but most of the discriminatory compounds hits putatively identified in the co-cultures were previously observed in their respective fungal monocultures indicating their dominance over the pathogenic MRSA co-cultured with them. As the compounds were still present but inactive, it can be deduced that the MRSA weakened them (except in *F. proliferatum*-MRSA co-culture), hence the inactivity observed from other co-culture extracts. The model gave goodness of fit (R_2) of 0.939 and a predictability score (Q_2) of 0.647 which is an excellent fitted model.

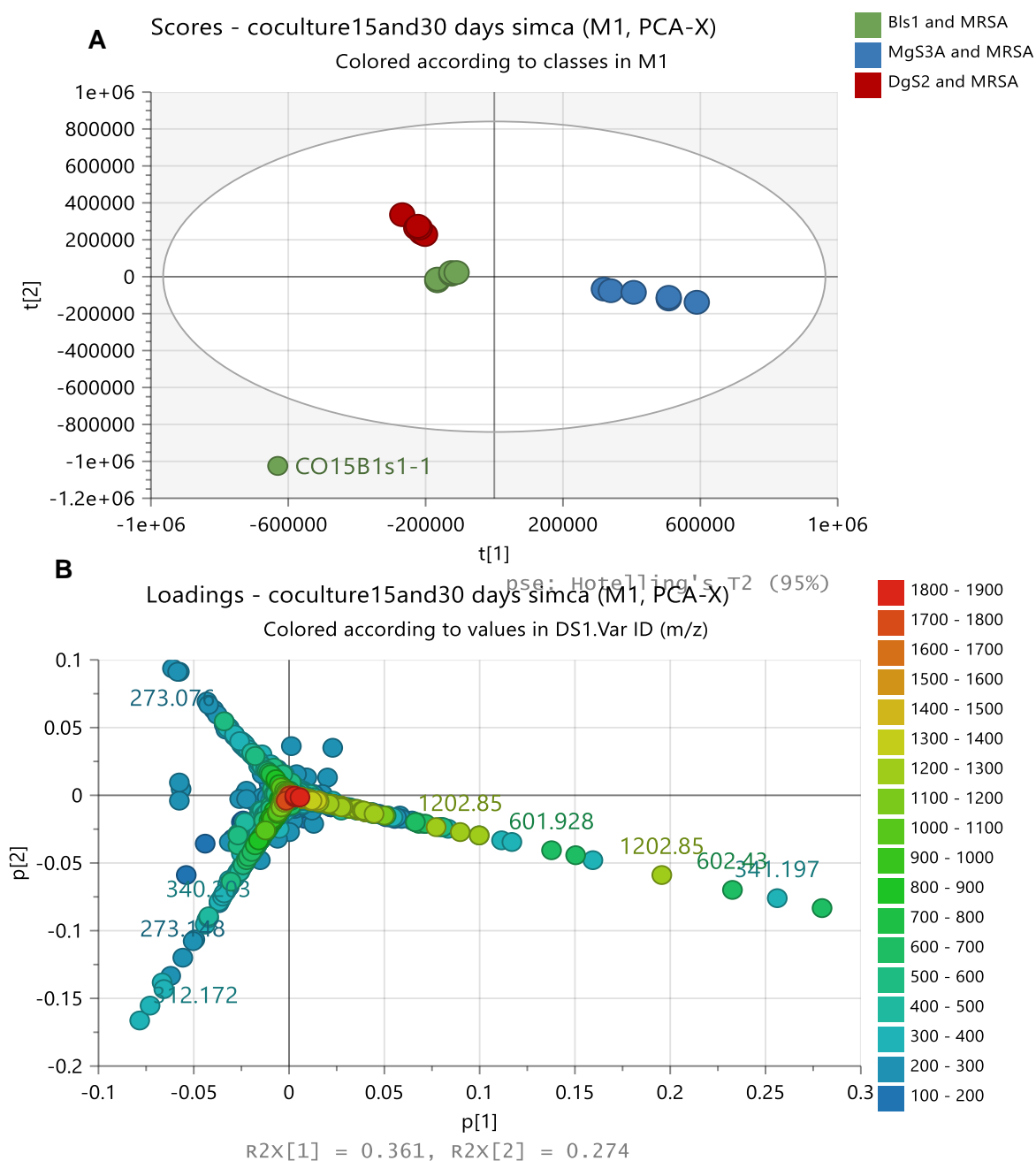


Figure 7.10: (A) PCA scores and (B) loadings plots of LC-HRMS data of co-culture extracts from malt extract media incubated at 15 and 30 days. $R_2X = 0.939$ and $Q_2X = 0.647$. Labelled features represent the discriminating ion peaks for the outlying extracts obtained from co-cultures of *F. proliferatum*-MRSA, *F. falciforme*-MRSA and *A. alternata*-MRSA.

Table 7.8: Dereplicated compound hits from discriminating metabolites from co-culture of fungi and MRSA incubated for 15 and 30 days obtained from the PCA loadings plot on Figure 7.10B. **Hits were filtered according to their microbial source except when no other compound hits were found under this filter.** Structures are shown in figure 7.11.

Mzmine ID	m/z	Rt	M.wt	Molecular Formular (DBE)	Compound hits	Biological source
<i>F. falciforme</i>-MRSA 15 and 30 days						
P6028	307.19	11.64	306.183	C ₁₈ H ₂₆ O ₄ (6)	Albocycline K1	Streptomyces sp. OH-3984
P3750	325.201	11.59	324.193	C ₁₈ H ₂₈ O ₅ (5)	Hymeglusin	<i>Cephalosporium</i> sp., <i>Scopulariopsis</i> sp. and <i>Fusarium</i> sp.
N1198	341.197	11.57	342.204	C ₁₈ H ₃₀ O ₆ (4)	Albocycline M8	<i>Streptomyces bruneogriseus</i>
N6447	342.2	11.45	343.208		No hit	
P5445	601.928	18.72	600.921		No hit	
P17515	1202.85	25.24	1201.84		2[P5445+H] ⁺	
P18957	1204.86	18.69	1203.85		No hit	
<i>F. proliferatum</i>- MRSA 15 and 30 days						
P19233	241.122	20.55	240.115	C ₁₆ H ₁₆ O ₂ (4)	Bushrin (8)	Marine-derived <i>Penicillium stutzeri</i> CMG 1030
P1068	273.148	19.76	272.141	C ₁₇ H ₂₀ O ₃ (5)	Peniphenylane D (9)	Marine-derived <i>Penicillium fellutanum</i> HDN14-32
N433	297.153	16.53	298.161		No hit	
N1452	298.157	16.49	299.164	C ₁₇ H ₂₁ N ₃ O ₂ (9)	Cyclo(isoleucyltryptophyl) (10)	<i>Penicillium brevi-compactum</i>
P19235	306.178	20.37	305.17		No hit	

Mzmine ID	m/z	Rt	M.wt	Molecular Formula (DBE)	Compound hits	Biological source
N1450	312.172	17.40	313.18	C ₁₈ H ₂₃ N ₃ O ₂ (9)	(3S,6R)-N1-Me-Cyclo(leucyltryptophyl), (11)	<i>Aspergillus flavus</i>
N7523	325.185	19.88	326.192		No hit	
N1451	326.188	19.33	327.195	C ₁₉ H ₂₅ N ₃ O ₂ (9)	Sophazrine (12)	Alkaloid from <i>Sophora griffithii</i> (Leguminosae).
N1454	340.203	21.26	341.211	C ₂₀ H ₂₇ N ₃ O ₂ (9)	Iboluteine oxime	Alkaloid from genus <i>Tabernaemontana</i>
P19234	405.227	22.12	404.219	C ₂₃ H ₃₂ O ₆ (8)	Antibiotic K 76; 7'-Alcohol (13)	Produced by <i>Stachybotrys</i> sp. Mer-NF5003
A. alternata-MRSA 15 and 30 days						
P298	273.076	15.82	272.068	C ₁₅ H ₁₂ O ₅ (10)	9-O-methylalternariol	<i>Alternaria</i> sp. including marine sp, <i>Anthocleista djalonensis</i> , <i>Penicillium diversum</i> and <i>Lachnum palmae</i>
N127	289.072	10.72	290.079	C ₁₅ H ₁₄ O ₆ (9)	Altenusin	<i>Alternaria tenuis</i> , <i>Penicillium</i> sp. and <i>Talaromyces</i> sp.

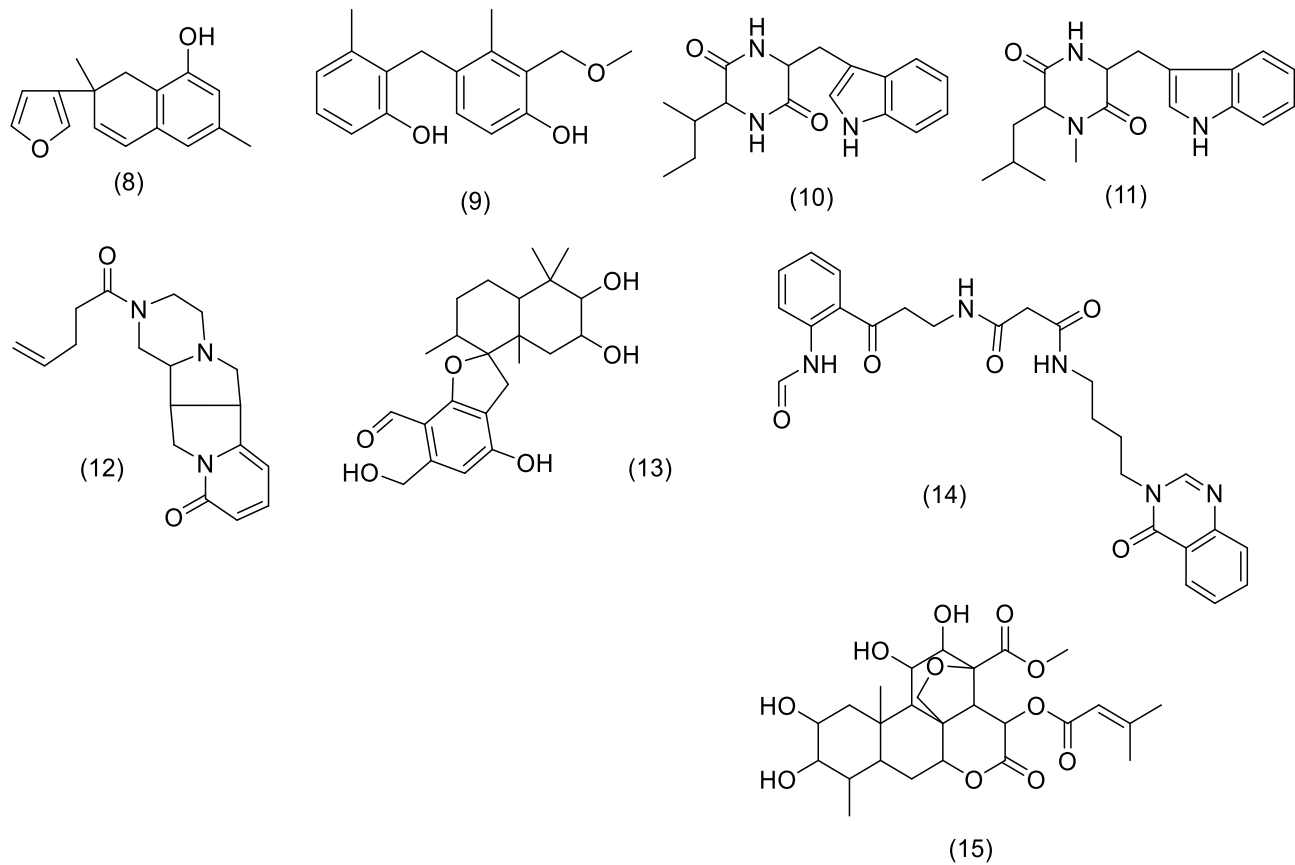


Figure 7.11: Structures of dereplicated compound hits showing PCA discriminating metabolite obtained from 15- and 30-days co-culture extracts, as listed in Table 7.8 and 7.9.

The OPLS-DA scores plot in Figure 7.12A positioned the active extracts on the upper and lower left quadrants (green circles), while the inactive extracts were found on the upper and lower right quadrant of the scores plot (blue circles). The defined target metabolites afforded p -values < 0.05 , which indicated a strong model with a confidence interval of more than 95%. The bioactive metabolites gave an m/z range between 165 and 525 Da. Discriminating active metabolites with p -values less than 0.05 are listed in Table 7.9. Structures of putatively identified compound hits are shown in Figure 7.11. Four of the ion peaks gave no hits, which could indicate the presence of novel compounds.

The compounds identified from the DNP database, as shown in Table 7.9 were, Mzmine IDs of P1184, P6582, P19233, P1068, N1452, N1450, N1451, N1454, P19234, N2325, P2942, N433, P19235, N7523, N370 represented by their respective m/z as 165.091, 180.102, 241.122, 273.148, 298.157, 312.172, 326.188, 340.203, 405.227, 476.193, 525.232, and 4 ion peaks which gave no hits respectively. The dereplicated ion peaks were similar to the discriminatory metabolites for the respective cluster except monodontamide F and javanicolide C. However, the respective sources of these two NPs are not microbial therefore could as well be considered as probably new NPs. Comparing the bioactive compounds putatively identified from the solid malt agar media and from the liquid malt extract broth, only two compounds were similar (fusalanipyrone and fusaric acid), while other compounds were different. This shows that the co-culture can affect the type of metabolites produced by an organism.

It showed fitness (R_2) and predictability (Q_2) scores of 0.989 and 0.943 respectively. This proved to be a good fit, and a good model prediction. The variation between groups R_2X_0 [1] was 28.3 % and within group R_2X [1] was 17.5 %. This showed that there was slight similarity within the extracts in their different classes.

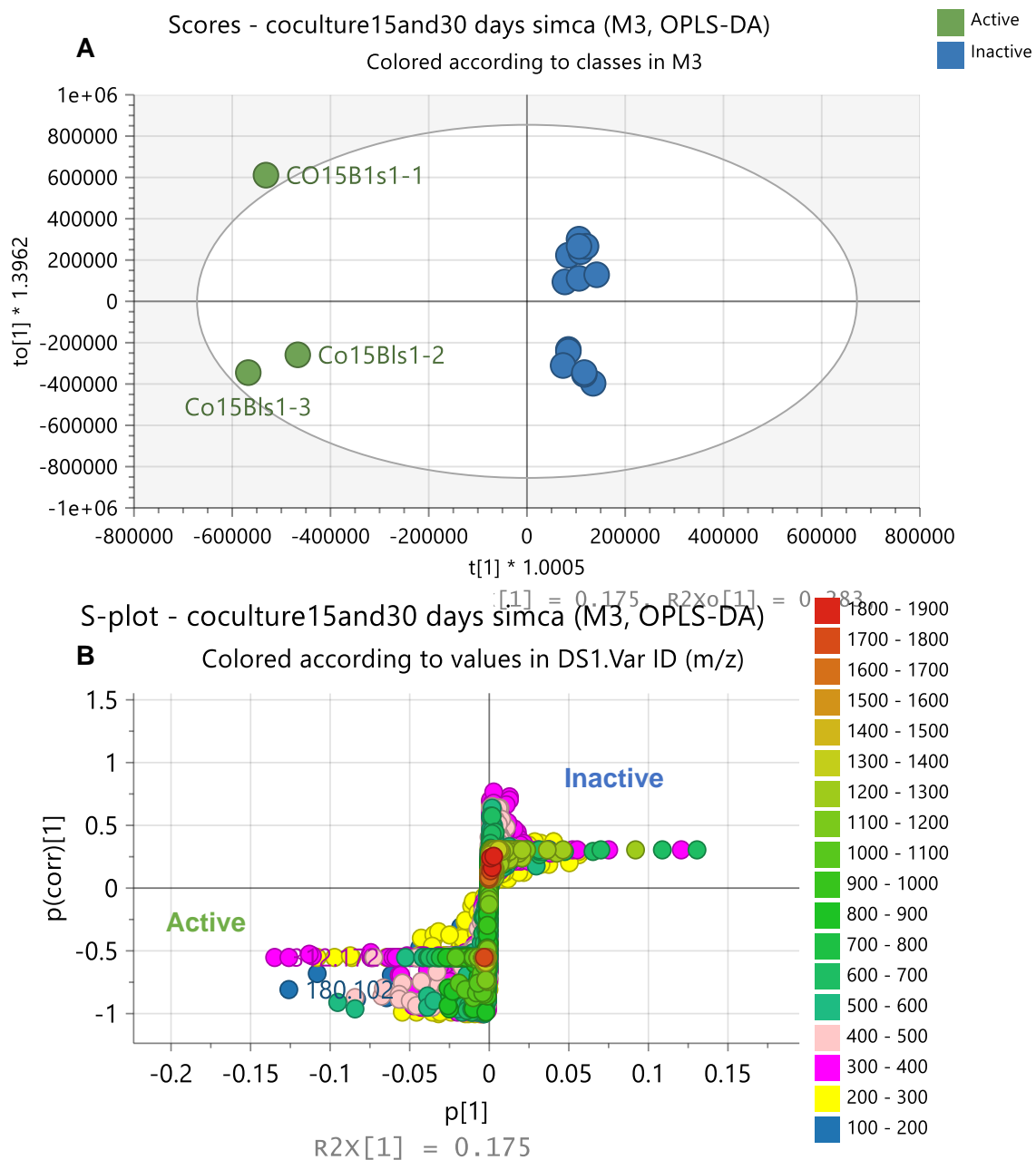


Figure 7.12: (A) OPLS-DA scores and (B) S-plots of LC-HRMS of co-culture extracts obtained from malt extract media. The labelled metabolites on S-plot indicated the discriminating feature for each media extracts. $R_2 = 0.989$ and $Q_2 = 0.943$. The difference between group $R_2Xo[1]$ is equal to 28.3% and the difference within groups $R_2X[2]$ is 17.5%.

Table 7.9: Dereplicated compound hits from discriminating metabolites from co-culture of fungi and MRSA incubated for 15 and 30 days obtained from the OPLS-DA S-plot on Figure 7.12B. **Hits were filtered according to their microbial source except when no other compound hits were found under this filter.** Structures are shown in Figure 7.11.

Mzmine ID	m/z	Rt	M. wt	p-value	Molecular Formula (DBE)	Compound hits	Biological source
P1184	165.091	13.01	164.084	8.01501e-07	C ₁₀ H ₁₂ O ₂ (5)	Fusalanipyrone	<i>F. solani</i> DSM 62416 and <i>F. oxysporum</i> f. sp. <i>batatas</i> O-17
P6582	180.102	5.85	179.095	0.001348	C ₁₀ H ₁₃ NO ₂ (5)	Fusaric acid	<i>Fusarium lycopersici</i> , <i>F. oxysporum</i> , <i>F. vasinfectum</i> and <i>Gibberella fujikuroi</i>
P19233	241.122	20.55	240.115	0.020047	C ₁₆ H ₁₆ O ₂ (4)	Bushrin	Marine derived <i>Penicillium stutzeri</i> CMG 1030
P1068	273.148	19.76	272.141	0.020081	C ₁₇ H ₂₀ O ₃ (5)	Peniphenylane D	Marine-derived <i>Penicillium fellutanum</i> HDN14-32
N433	297.153	16.53	298.161	0.020240		No hit	
N1452	298.157	16.45	299.164	0.020657	C ₁₇ H ₂₁ N ₃ O ₂ (9)	Cyclo(isoleucyltryptophyl)	<i>Penicillium brevi-compactum</i>
P19235	306.178	20.37	305.17	0.020060		No hit	
N1450	312.172	17.40	313.18	0.020067	C ₁₈ H ₂₃ N ₃ O ₂ (9)	(3 <i>S</i> ,6 <i>R</i>)- <i>N</i> 1-Me-Cyclo(leucyltryptophyl)	<i>Aspergillus flavus</i>
N7523	325.185	19.88	326.192	0.030553		No hit	
N1451	326.188	19.33	327.195	0.020333	C ₁₉ H ₂₅ N ₃ O ₂ (9)	Sophasrine	Alkaloid from <i>Sophora griffithii</i> (Leguminosae).

N1454	340.203	21.26	341.211	0.020313	$C_{20}H_{27}N_3O_2$ (9)	Iboluteine oxime	Alkaloid from genus <i>Tabernaemontana</i>
P19234	405.227	22.12	404.219	0.020079	$C_{23}H_{32}O_6$ (8)	7'-Alcohol-Antibiotic K 76;	Produced by <i>Stachybotrys</i> sp. Mer-NF5003
N2325	476.193	14.26	477.201	1.82055e-06	$C_{25}H_{27}N_5O_5$ (15)	Monodontamide F (14)	Alkaloid from the marine gastropod mollusc <i>Monodonta</i> <i>labio</i>
P2942	525.232	17.88	524.225	4.47383e-12	$C_{26}H_{36}O_{11}$ (9)	Javanicolide C (15)	<i>Brucea javanica</i>
N370	523.219	17.69	524.227	1.26808e-08		No hit	

Analysis on MetaboAnalyst® was performed. The heatmap showed that the bioactive co-culture extract of *F. proliferatum* and MRSA (purple box) incubated for 15 days were more discriminatory with more metabolite concentration than the inactive extracts (green box).

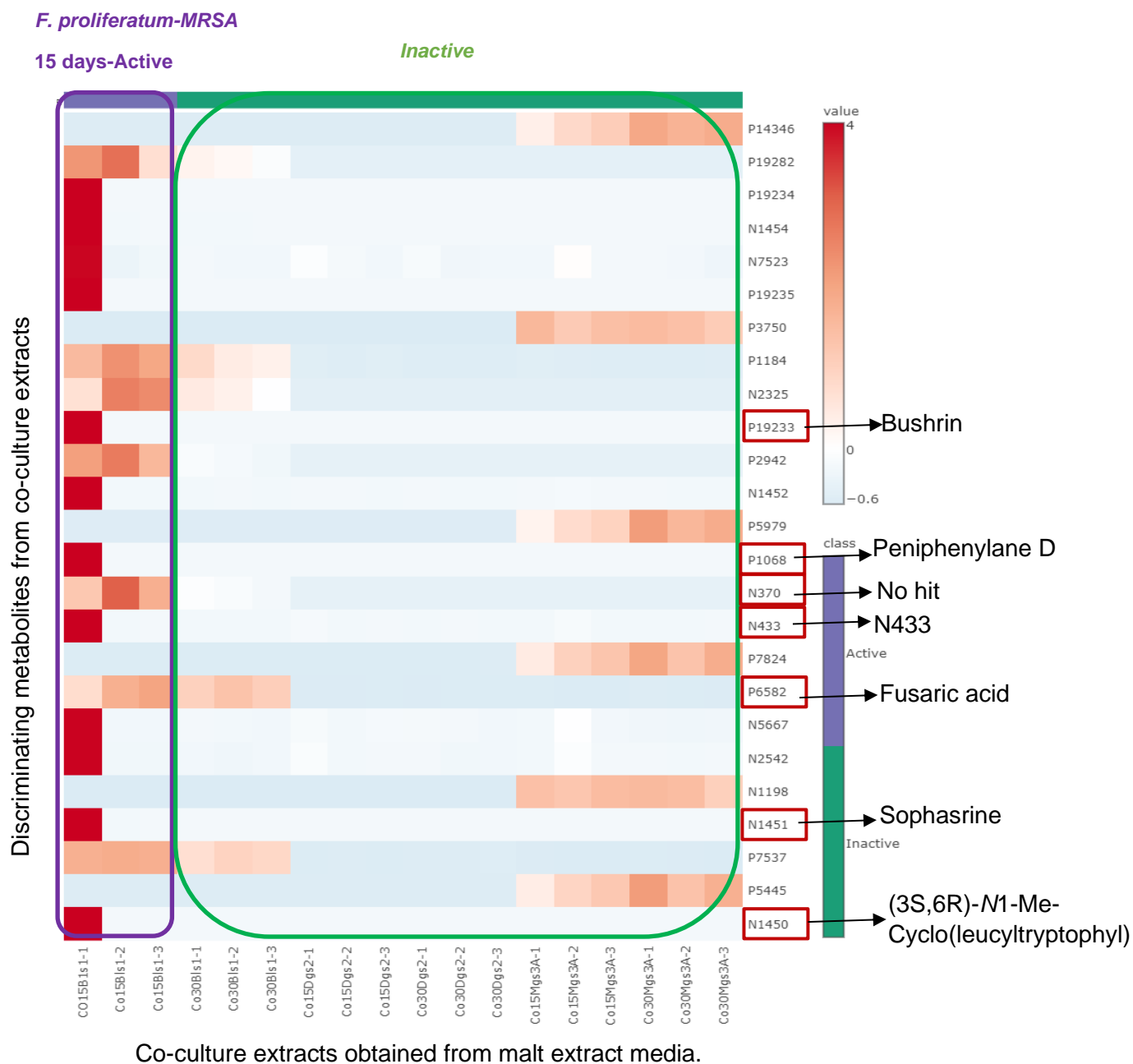


Figure 7.13: Heatmap analysis of the mass spectral data of co-culture crude extracts with their Mzmine values, obtained from malt extract media, generated by MetaboAnalyst®. The purple box represents active extracts from *F. proliferatum*-MRSA co-culture, while the green box represents the inactive extracts. Highlighted Mzmine values on the Y-axis indicate common metabolites observed on the heatmap and VIP.

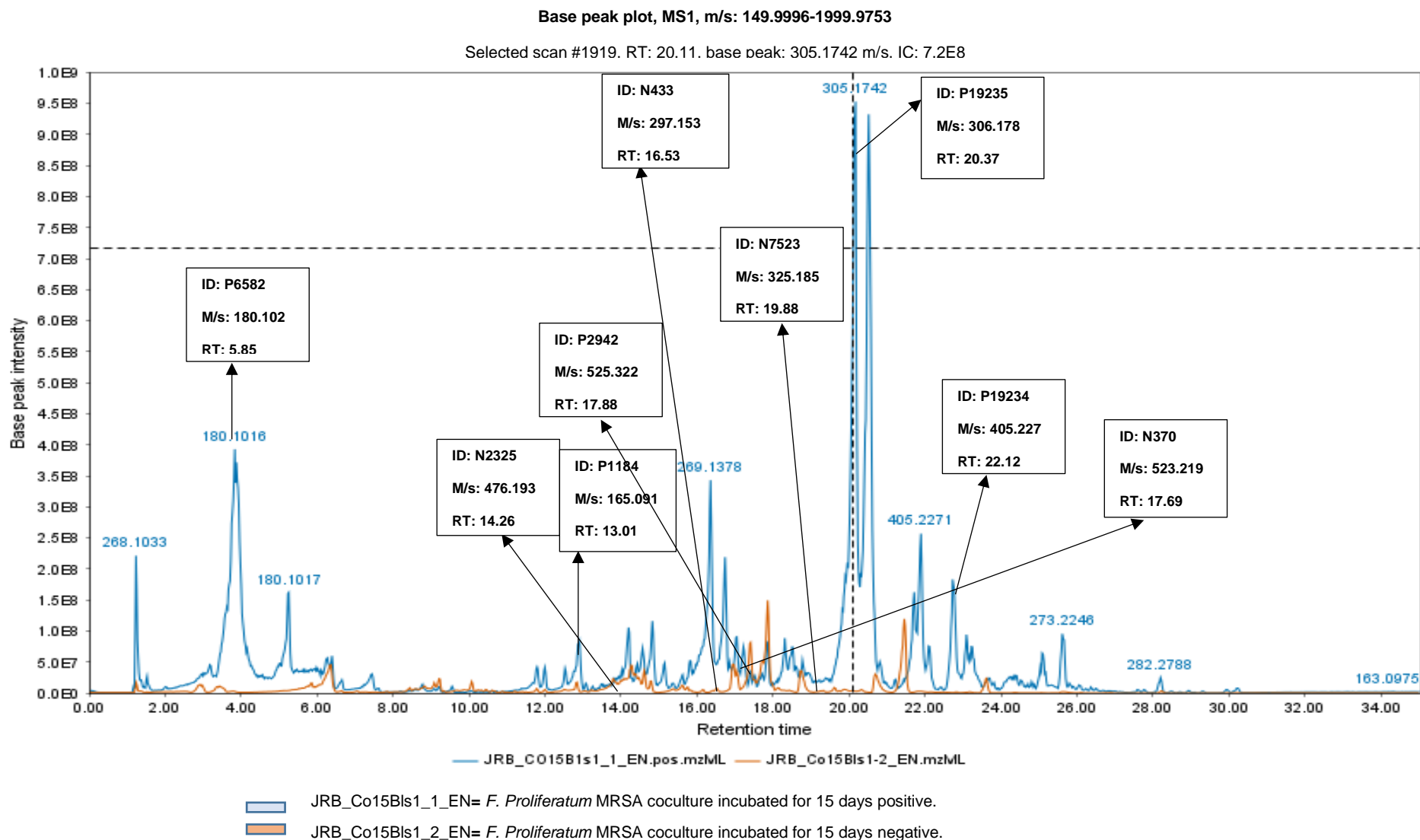


Figure 7.14: Total ion chromatogram (TIC) of the bioactive extracts of *F. proliferatum*-MRSA co-culture from malt extract media. The ion peaks that represent the bioactive discriminating features listed in Table 7.9 have been labelled.

7.2.7 Fractionation of *F. proliferatum*-MRSA Scale-up crude extracts

Fractionation of *F. proliferatum*-MRSA afforded F1-F8.

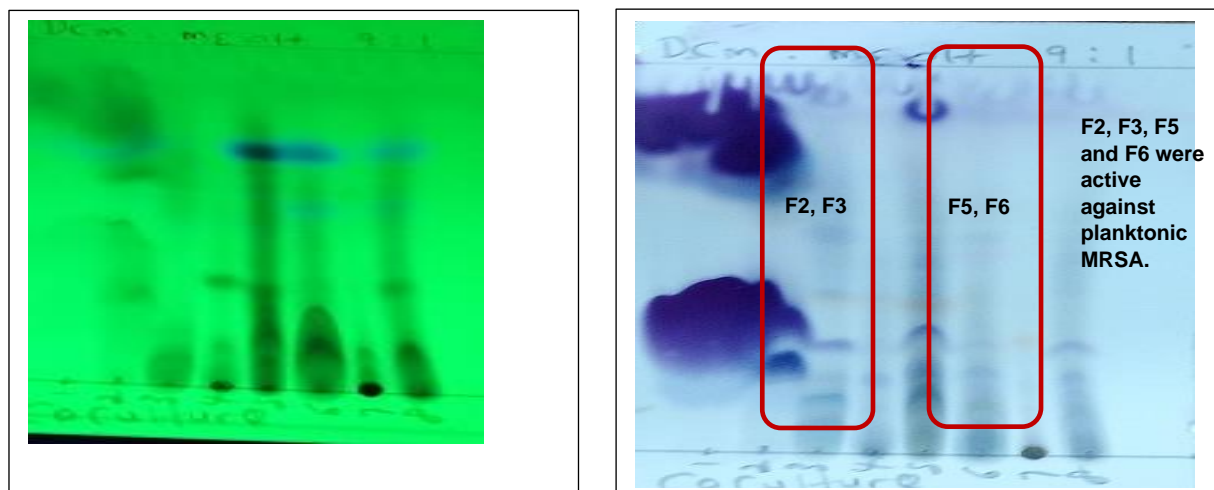


Figure 7.15: Summary TLC Plate of *F. proliferatum*-MRSA pooled fractions before (UV bands) and after spraying with anisaldehyde-sulphuric acid. The TLC plate showed fractions from the non-polar solvent of hexane to the more polar solvent of ethylacetate (100% Hexane- 100% ethylacetate). Bioactive fractions are highlighted in red box.

Table 7.10: Extract weights of *F. proliferatum*-MRSA co-culture fractions

Fractions	Weight (mg)
F1	1177
F2	201.1
F3	684.3
F4	1121
F5	59.5
F6	34.7
F7	2.9
F8	51

7.2.8 Bioactivity test results of *F. proliferatum*-MRSA fractions

The pooled chromatographic fractions from co-cultures of *Fusarium proliferatum*-MRSA were subjected to biological assay against MRSA. Fractions 2, 3, 5 and 6 showed weak antimicrobial activity while fractions 1, 4, 7 and 8 were inactive. Bioactivity threshold was set at 50.78% cell viability (49.22% inhibition). Only fraction 5 was prebiofilm active. Fractions 1, 2, 3, 5, 7, and 8 were postbiofilm active, while other fractions were inactive. Active fractions for further isolation work were selected based on their planktonic activity. Except for fraction 5, other active fractions were weakly active. This could have occurred because of the inoculation of MRSA with *F. proliferatum*. The pathogenic MRSA could have weakened the extract leading to reduced bioactivity or could have required the occurrence of other metabolites to assist the bioactivity expression by improvement of the extracts' physico-chemical properties such as improved absorption or solubility.

The bioactivity was in decreasing order: F5> F2> F6> F3.

Table 7.11: Summary of bioactivity of fractions obtained from *Fusarium proliferatum*-MRSA co-cultures against Planktonic MRSA, along with their prebiofilm, and postbiofilm stages indicated by their percentage viability.

Fractions	Antimicrobial % Inhibition	Prebiofilm % Inhibition	Postbiofilm % Inhibition
Fraction 2	59.2	<0	78.8
Fraction 3	49.2	<0	69.5
Fraction 5	98.3	100	50.7
Fraction 6	56.6	<0	39.5

^aCells with blue colour indicates active fractions against MRSA.

7.2.9 NMR spectroscopy for *F. proliferatum*-MRSA fractions

After fractionation, the pooled fractions were subjected to proton NMR measurements to have an overview of the chemical profile and type of compounds expected to be found in each fraction. The ¹H NMR spectra of the bioactive fractions were stacked and presented in Figure 7.16. A high intensity of aliphatic peaks could be observed in the recorded ¹H NMR spectra of the fractions. Peaks between 4 and 4.5 ppm, 5 and 5.5 ppm, 6.5 and 8.5 ppm, as well as 12.0 and 12.5 ppm represented sugars, olefinics, aromatics, and carboxylic acids respectively,

although the incidences and intensities of these chemical functions differ amongst the fractions.

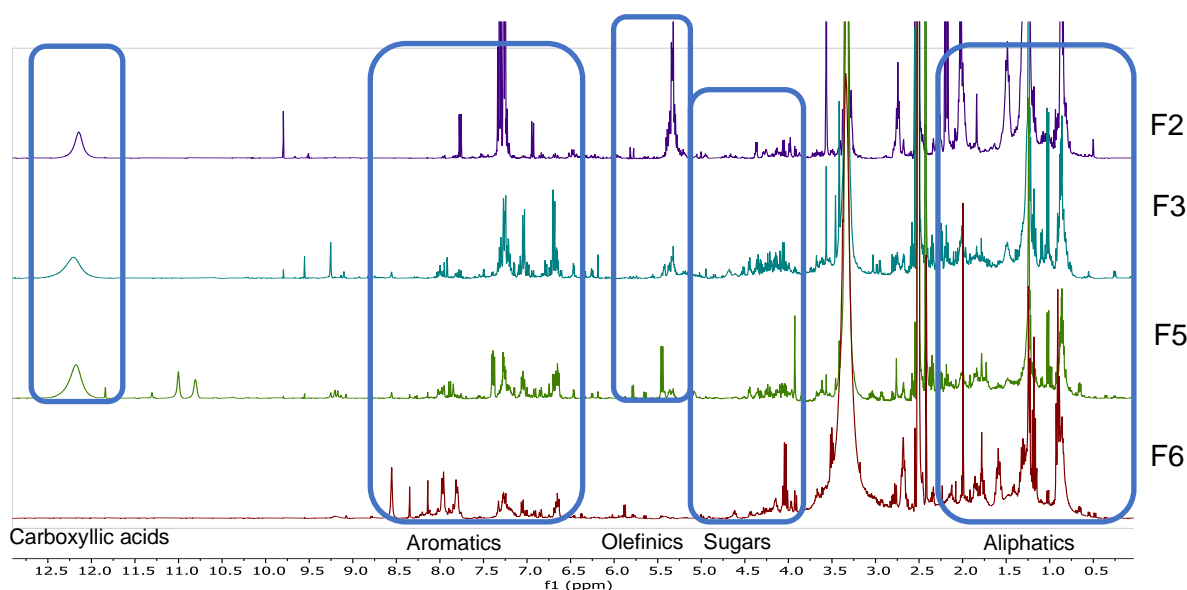


Figure 7.16: Stacked ^1H NMR spectra of the bioactive *F. proliferatum*-MRSA fractions consisting of F2, F3, F5, F6.

The PCA scores scatter plot (Figure 7.17A) showed the inactive F7 to be an outlier. All the active fractions were clustered together at the lower left quadrant, except F2, that was a bit dispersed from the active fractions. The loadings plot (Figure 7.17 B) indicated that the chemical shifts of the discriminating metabolites were within the range of 1 to 2 ppm, 2 to 3 ppm and 3 to 4 ppm, which belongs to the acetylated aliphatics and sugars or amines, respectively. In the generated model at pareto scaling, the R_2 was 0.982 while Q_2 was 0888 at four components which indicated a model with good fit and predictability.

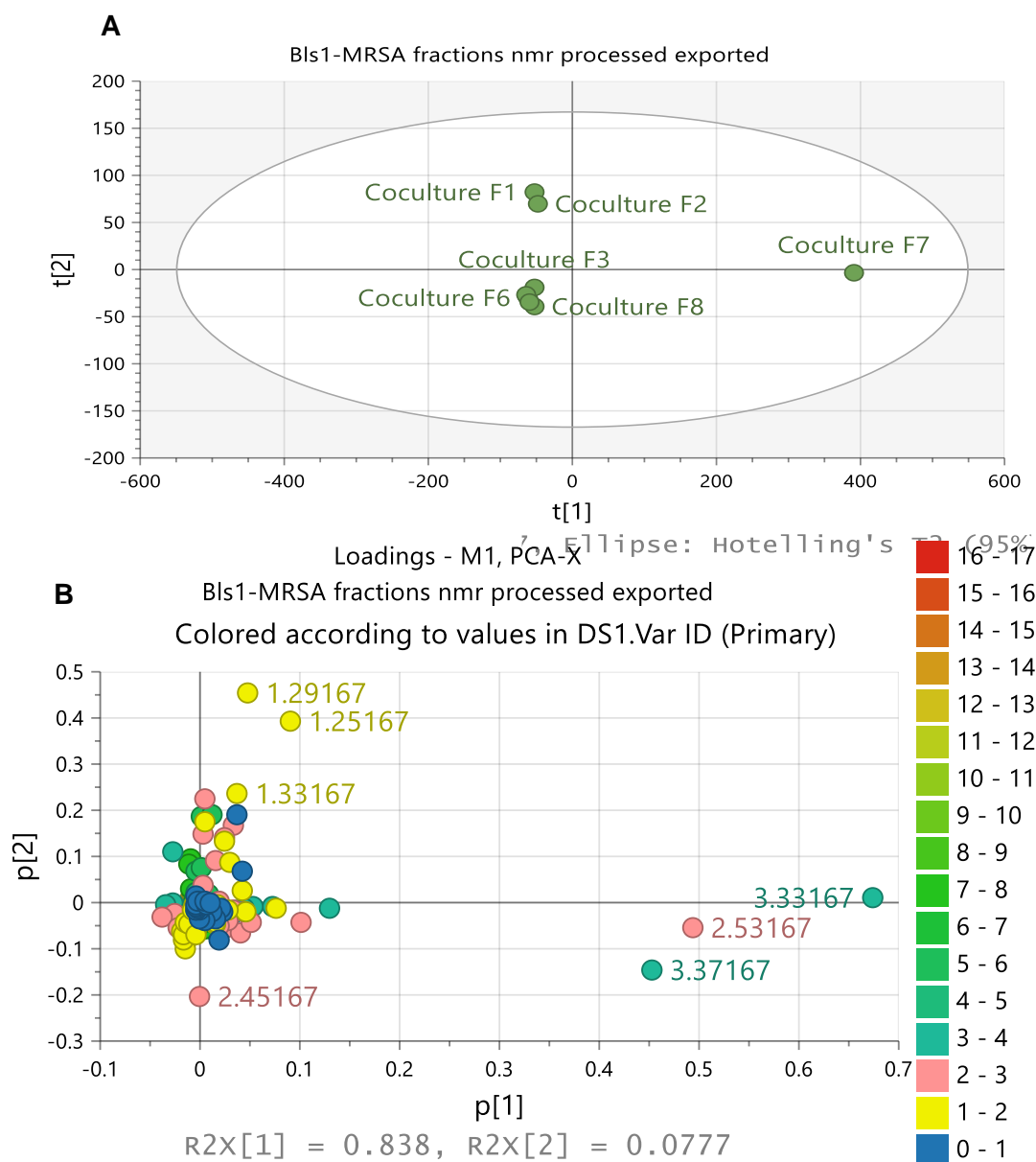


Figure 7.17: (A) PCA scatter and (B) loadings plots of the NMR spectral data of the active fractions. The R_2X and Q_2X values were 0.982 and 0.888, respectively.

An OPLS-DA was also performed to indicate the discriminating resonances for the active and inactive fractions. The active fractions (blue circles) were clustered at the upper and lower right quadrants, while the inactive fractions were clustered on the upper and lower left quadrant of the OPLS-DA scores plot, with F7 showing to be an outlier (Figure 7.18A). The loadings plot (Figure 7.18B) showed the occurrence of resonances at 2.45, 7.29 and 12.17 for the active fractions, although they were not discriminatory. R_2 and Q_2 values were 1.000 and 0.779, respectively. The difference between group R_2X_o [1] is equal to 26.6%, and the

difference within groups $R_2X [2]$ is 16.7%. There was an excellent separation between the active and inactive clusters, as the variation score between groups is greater than within groups. The proximity of active fractions 2, 3, 5 and 6 on the scores plot indicates they could have similar chemical profiles.

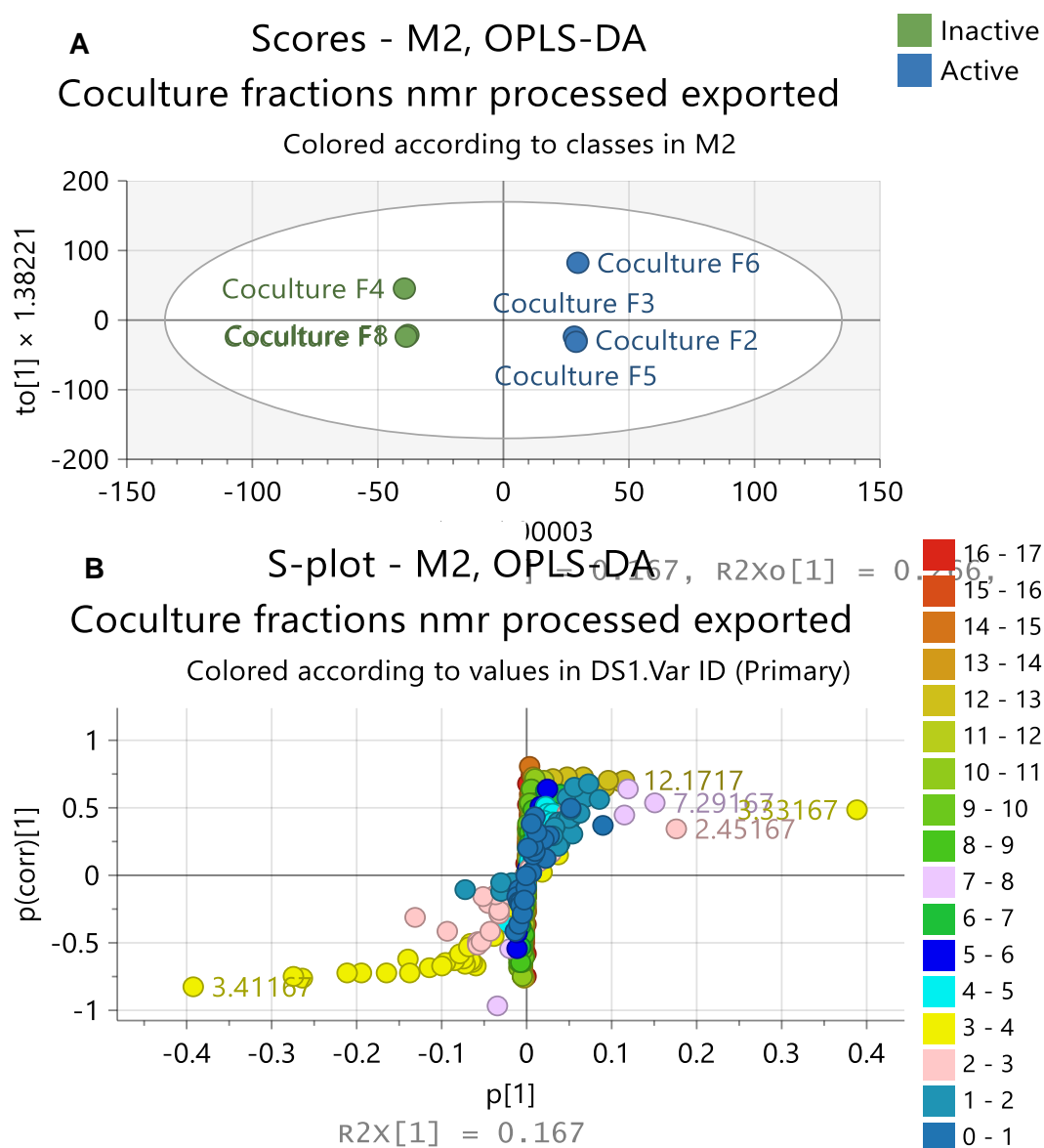


Figure 7.18: OPLS-DA scores (A) and loadings (B) plots of the NMR spectral data of *F. proliferatum*-MRSA fractions grouped according to their bioactivity against MRSA. R_2 and Q_2 values were 1.000 and 0.779, respectively. The difference between group $R_2X_o [1]$ is equal to 26.6 % and the difference within groups $R_2X [2]$ is 16.7 %.

The fractions were tested to see the true outlier using DModX, fraction 3 gave results of less than 0.05 which indicated that fraction 3 was the true outlier as shown in Figure 7.19. However, fraction 3 cannot be excluded from the model because this is an active fraction, so it is essential to further investigate its unique discriminatory metabolites for the active fractions.

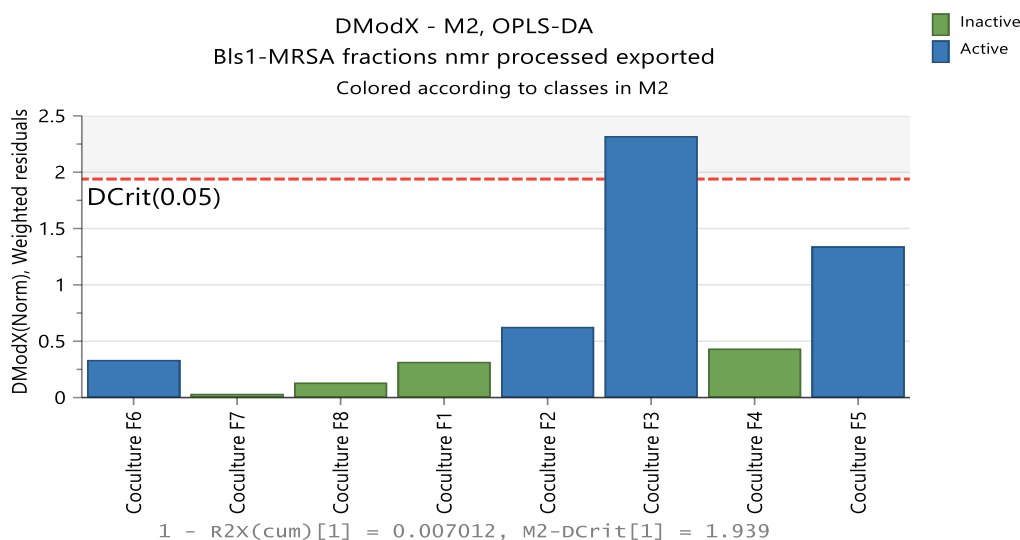


Figure 7.19: DMod X results to test the occurrence of true outliers. Variables above the red line are the true outliers that includes only fraction 3.

OPLS-DA indicated the top 20 VIP which showed that the discriminatory metabolites mostly consisted of aliphatics, sugars and aromatics ranging from 1.13 to 7.29 ppm, although most of the metabolites were in little concentrations. Discriminating metabolites observed on both VIP and heat map had common chemical shifts of 1.13, 1.25, 1.29, 2.29, 2.45, 2.53, 3.13, 3.17, 3.21, 3.25, 3.29, 3.37, 3.41, 3.45, 3.49, 7.29 and 7.33 ppm representing aliphatics and aromatics.

The spectra bins of each fraction were mechanically replicated, to have three replicates of each fraction, for analysis on MetaboAnalyst®. The heatmap showed that the active fractions (purple box) exhibited high concentration of metabolites. Fraction 7 (green box) was more diverse and more intense compared to all the fractions but was inactive. Fraction 7 was obtained from 50% acetone: 50% isopropanol which was the wash. Most of the remaining metabolites in the column were washed off at this point leading to a high concentration of metabolites inherent in F7 and the inactivity could have been because of the solvent (acetone) used at this fractionation point which could have masked the activity of the metabolites or

because the interesting active metabolites have been earlier fractionated and inherent in F2, F3, F5 and F6.

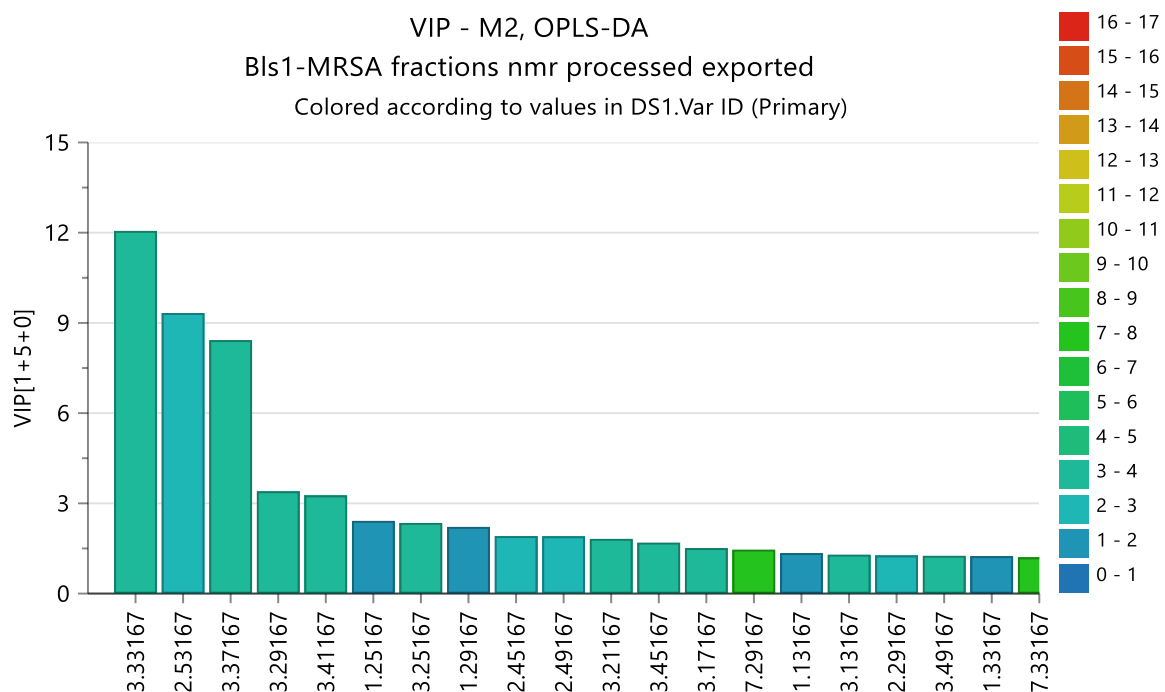


Figure 7.20: VIP scores of *F. proliferatum*-MRSA fractions from Simca® showing the chemical shifts of 20 most discriminating metabolites with VIP scores above 1.

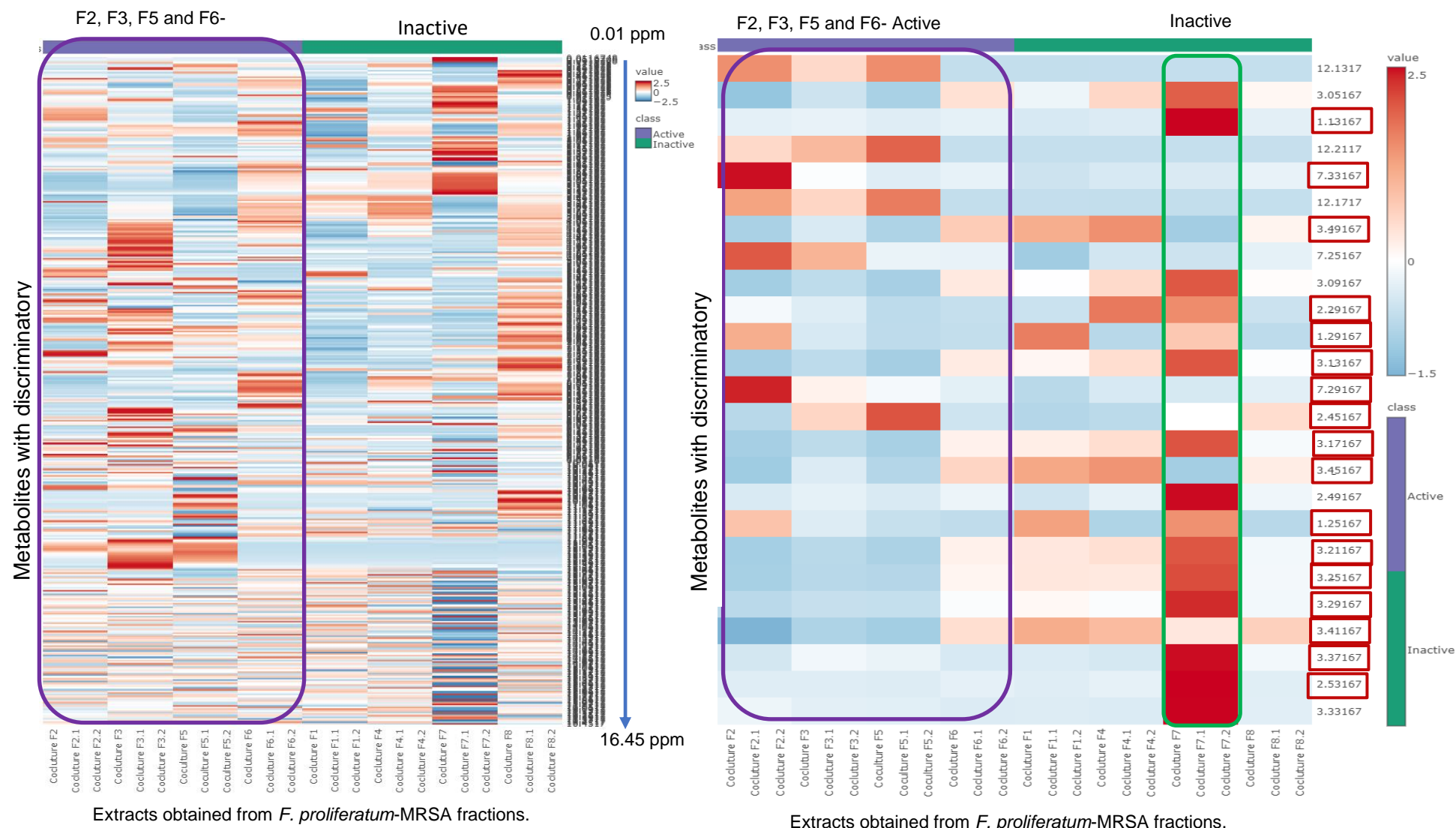


Figure 7.21: Heatmap analysis of the NMR spectral data of *F. proliferatum*-MRSA fractions generated by MetaboAnalyst®. The purple boxed fractions are those biologically active against MRSA along with the discriminating chemical shifts. The green boxed fraction (F7) was discriminatory but inactive. Highlighted chemical shifts on the Y-axis indicate common metabolites observed on the heatmap and VIP.

7.2.10 LC-HRMS analysis of *F. proliferatum*-MRSA fractions

Multivariate analysis of the HR-LCMS spectral data was done, the unsupervised PCA scores plot showed the fractions to spread across the quadrant (Figure 7.22A). The loadings plot (Figure 7.22B) indicated the presence of discriminating metabolites with low m/z values ranging between 121 to 297 Da. The discriminating metabolites with Mzmine IDs of P24177, P25479, N11083, P749, P359, P360, P428 represented by m/z 279.232, 295.227, 297.244, 211.144, 134.097, 152.107, 180.102 were putatively identified as (6*E*,10*E*,14*R*)-14-hydroxy-1,2-dinor-6,10,15-phytatrien-3-one, (*E,E*)-11-oxo-9,12-octadecadienoic acid, (*R*)-11-cycloheptyl-2-hydroxyundecanoic acid, cyclo(isoleucylprolyl), noractinidine, pulchellalactam, and 5-butyl-2-pyridinecarboxylic acid, respectively. Metabolites with Mzmine IDs N1271, P420 represented by ion peaks 165.055, 181.105 gave no hits. The model gave goodness of fit, (R_2) and predictability, Q_2 values as 1.0 and 0.999, respectively after 7 components. The dereplicated discriminating features of *F. proliferatum*-MRSA fractions were shown in Table 7.12. Structures of the discriminating target bioactive metabolites against MRSA predicted by PCA loadings plots were presented in Figure 7.23.

The OPLS-DA of the active versus the inactive fractions gave fitness and predictability scores of 1.00 and 0.953 respectively. This indicated good fit and prediction of the generated OPLS-DA model. The difference between group R_2X_0 [1] is equal to 39.9 % and the difference within groups R_2X [2a] is 16.2 %. The scores plot (Figure 7.24A) shows a very good separation between the active versus inactive fractions. The active fractions (blue circles) were on the right quadrant, while the inactive fractions (green circles) were on the left quadrant. The loadings plot shows the discriminating features for the active fractions to be low molecular weight values with ion peaks ranging between m/z 121 and 297 Da. Discriminatory active fractions with Mzmine IDs of P360, P428, P17843, P749, P19630, P25692, P25515, P24177, P25971, N1085, N11083, represented by m/z 123.044, 152.107, 180.102, 182.131, 211.144, 227.128, 263.237, 277.216, 279.232, 281.247, 295.247 and 297.244 Da, respectively were putatively identified by dereplication to be pulchellalactam, 5-butyl-2-pyridinecarboxylic acid, 10-undecynoic acid, cyclo(isoleucylprolyl), 3-(1-hydroxy-2,4-dimethylpentyl)-4-methyl-2,5-furandione, ent-11,12-dihydro 14,15-dinor-3,11-clerodadien-13-one, plakolide A, (6*E*,10*E*,14*R*)-14-hydroxy-1,2-dinor-6,10,15-phytatrien-3-one, (6*S*,9*S*)-octadecadienoic acid, (9*S*,12*R*,13*S*)-12,13-epoxy-9-octadecenoic acid, (*R*)-11-cycloheptyl-2-hydroxyundecanoic acid, while 3 ion peaks gave no hits. Dereplicated compounds cyclo(isoleucylprolyl) and pulchellalactam have been earlier detected during the media optimisation stage. The discriminating features of *F. proliferatum*-MRSA fractions were dereplicated in Table 7.12.

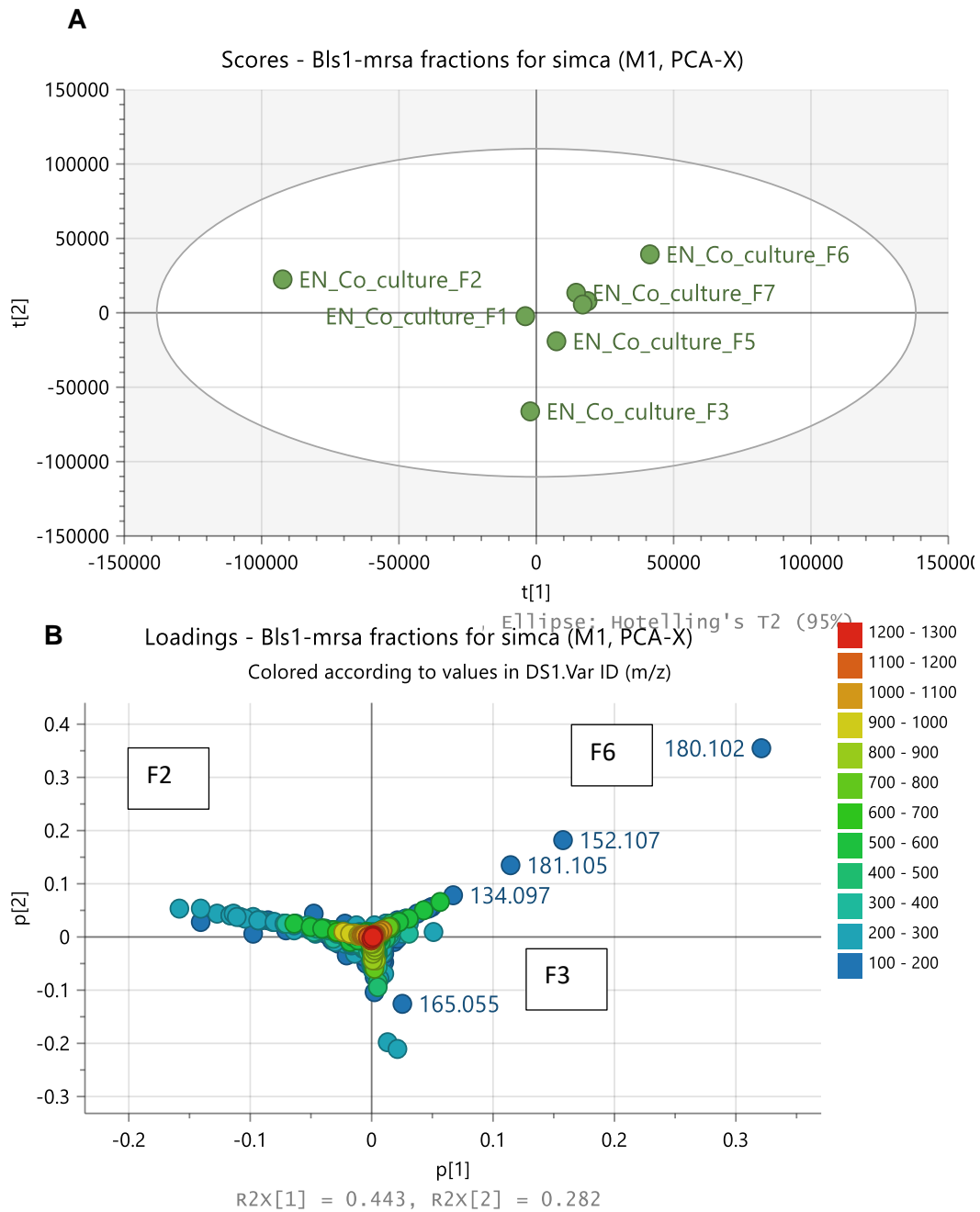


Figure 7.22: PCA scores (A) and loadings (B) plots of the LC-HRMS data of *F. proliferatum*-MRSA fractions. Labelled features represent the discriminating ion peaks. The R_2 and Q_2 values were 1.0 and 0.999 respectively.

Table 7.12: Dereplicated compound hits for the discriminating metabolites of *F. proliferatum*-MRSA fractions obtained from the PCA loadings Plot on Figure 7.22B. Compound hits were filtered using microbial sources except if there are no other hits found.

Mzmine ID	m/z	Rt	M.wt	Molecular Formular (DBE)	Compound hits	Biological source
F2						
P24177	279.232	20.46	278.225	C ₁₈ H ₃₀ O ₂ (4)	Coriolide	<i>Stagonospora</i>
P25479	295.227	21.45	294.22	C ₁₈ H ₃₀ O ₃ (4)	(<i>E, E</i>)-11-Oxo-9,12-octadecadienoic acid (16)	<i>Trichoderma</i> sp. F5594
N11083	297.244	21.48	298.251	C ₁₈ H ₃₄ O ₃ (2)	(<i>R</i>)-11-Cycloheptyl-2-hydroxyundecanoic acid (17)	Fatty acids of <i>Alicyclobacillus cycloheptanicus</i> and <i>Alicyclobacillus acidocaldarius</i>
F3						
N1271	165.055	6.35	166.062		No hit	
P749	211.144	5.36	210.137	C ₁₁ H ₁₈ N ₂ O ₂ (4)	Cyclo(isoleucylprolyl)	Marine-derived <i>P. aeruginosa</i> and <i>Vibrio parahaemolyticus</i>
F6						
P359	134.097	5.24	133.089	C ₉ H ₁₁ N (5)	Noractinidine (18)	<i>Pedicularis macrochila</i> and <i>Tecoma stans</i>
P360	152.107	5.29	151.1	C ₉ H ₁₃ NO ₁ (4)	Pulchellalactam	<i>Acrocarpospora</i> sp. FIRDI001, marine derived <i>Corollospora pulchella</i> , <i>Monascus ruber</i> BB5, <i>M. pilosus</i>
P428	180.102	5.24	179.095	C ₁₀ H ₁₃ NO ₂ (5)	5-Butyl-2-pyridinecarboxylic acid (19)	<i>Fusarium lycopersici</i> , <i>F. oxysporum</i> , <i>F. vasinfectum</i> and <i>Gibberella fujikuroi</i>
P420	181.105	5.24	180.098		No hit	

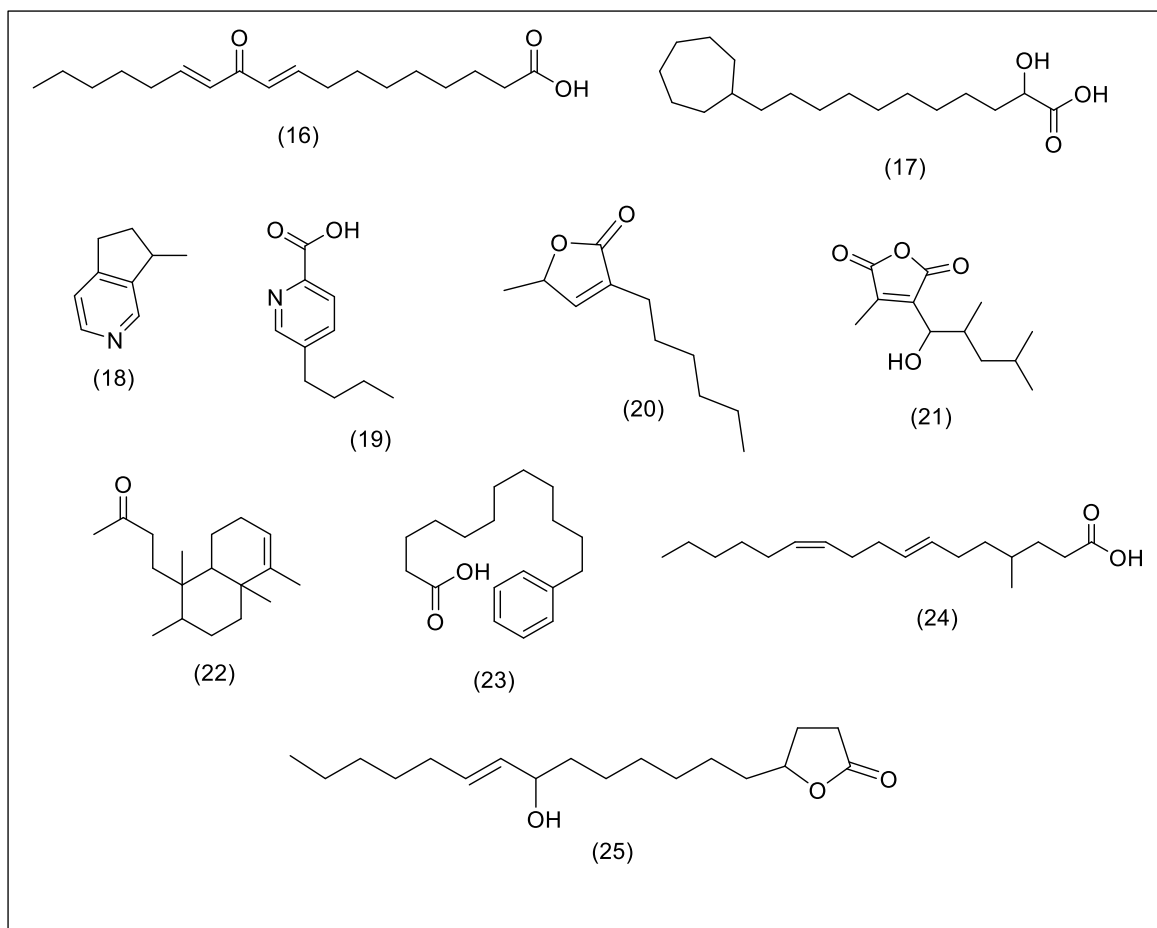


Figure 7.23: Structures of dereplicated compound hits showing PCA discriminating metabolites obtained from fractions of *F. proliferatum*-MRSA co-culture extract, as listed in table 7.12 and 7.13.

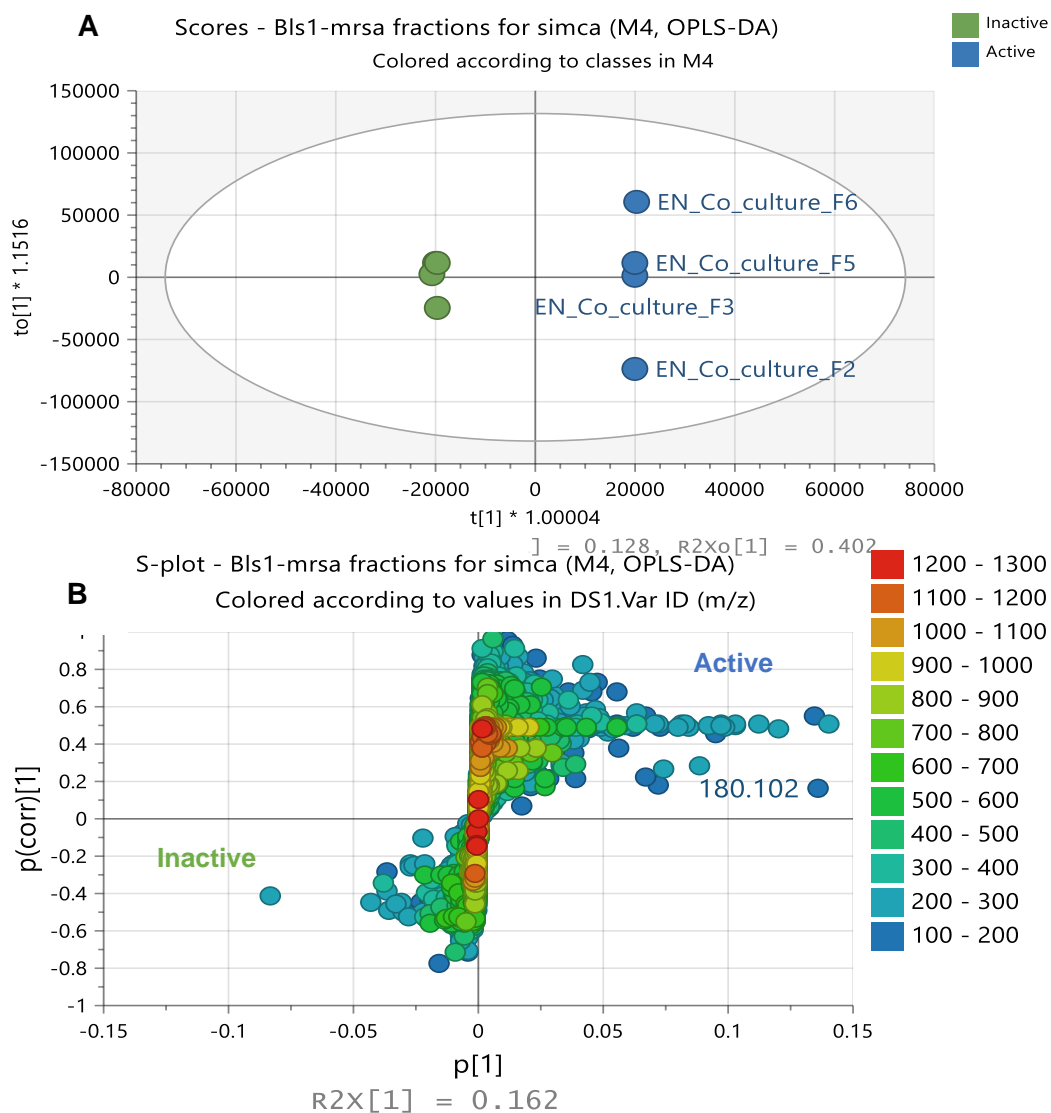


Figure 7.24: OPLS-DA scores (A) and S-plot (B) of the LC-HRMS data of *F. proliferatum*-MRSA fractions. Labeled features represent the discriminating active fractions. The R^2 and Q^2 values were 1 and 0.953 respectively. The difference between group $R^2_{Xo}[1]$ is equal to 39.9 % and the difference within groups $R^2X[2]$ is 16.2 %.

Table 7.13: Dereplicated compound hits for the discriminating active metabolites of *F. proliferatum*-MRSA fractions detected from the OPLS-DA loadings plot on Figure 7.24B. Structures of dereplicated compound hits are presented in Figure 7.23.

Mzmine ID	m/z	Rt	M.wt	Molecular Formular (DBE)	Compound hits	Biological source
P360	152.107	5.29	151.1	C ₉ H ₁₃ NO (4)	Pulchellalactam	<i>Acrocarpospora</i> sp. FIRD1001, marine derived <i>Corollospora pulchella</i> , <i>Monascus ruber</i> BB5, <i>M. pilosus</i>
N1271	165.055	6.35	166.062		No hit	
P428	180.102	5.24	179.095	C ₁₀ H ₁₃ NO ₂ (5)	5-Butyl-2-pyridinecarboxylic acid	<i>Fusarium lycopersici</i> , <i>F. oxysporum</i> , <i>F. vasinfectum</i> and <i>Gibberella fujikuroi</i>
P420	181.105	5.24	180.098		No hit	
P17843	183.138	16.47	182.131	C ₁₁ H ₁₈ O ₂ (3)	(S)-3-Hexyl-5-methyl-2(5H)-furanone-10-undecynoic acid (20)	<i>Streptomyces griseus</i> and <i>S. odorifer</i>
P749	211.144	5.36	210.137	C ₁₁ H ₁₈ N ₂ O ₂ (4)	Cyclo(isoleucylprolyl)	Marine-derived <i>P. aeruginosa</i> and <i>Vibrio parahaemolyticus</i>
P19630	227.128	17.58	226.121	C ₁₂ H ₁₈ O ₄ (4)	3-(1-Hydroxy-2,4-dimethylpentyl)-4-methyl-2,5-furandione (21)	<i>Streptomyces</i> sp. FH 317
P25692	263.237	21.48	262.23	C ₁₈ H ₃₀ O (4)	14,15-Dinor-3,11-clerodadien-13-one; ent-form, 11,12-Dihydro (22)	<i>Parentucellia latifolia</i> and a <i>Mycale</i> sp.
P25515	277.216	21.41	276.209	C ₁₈ H ₂₈ O ₂ (5)	12-Phenyldodecanoic acid (23)	Marine-derived <i>Bacillus</i> and <i>Vibrio</i>
P24177	279.232	20.46	278.225	C ₁₈ H ₃₀ O ₂ (4)	Coriolide	Fungus <i>Stagonospora</i>
P25971	281.247	21.59	280.24	C ₁₈ H ₃₂ O ₂ (3)	Sporothricenoic acid (24)	Fungus <i>Sporothrix</i>
N10845	295.228	20.81	296.235	C ₁₈ H ₃₂ O ₃ (4)	Piliferolide A (25)	<i>Ophiostoma piliferum</i> and <i>Pseudomonas brassicacearum</i> MA250
N11083	297.244	21.48	298.251	C ₁₈ H ₃₄ O ₃ (2)	(R)-11-Cycloheptyl-2-hydroxyundecanoic acid	Fatty acids of <i>Alicyclobacillus Cycloheptanicus</i> and <i>A. acidocaldarius</i>

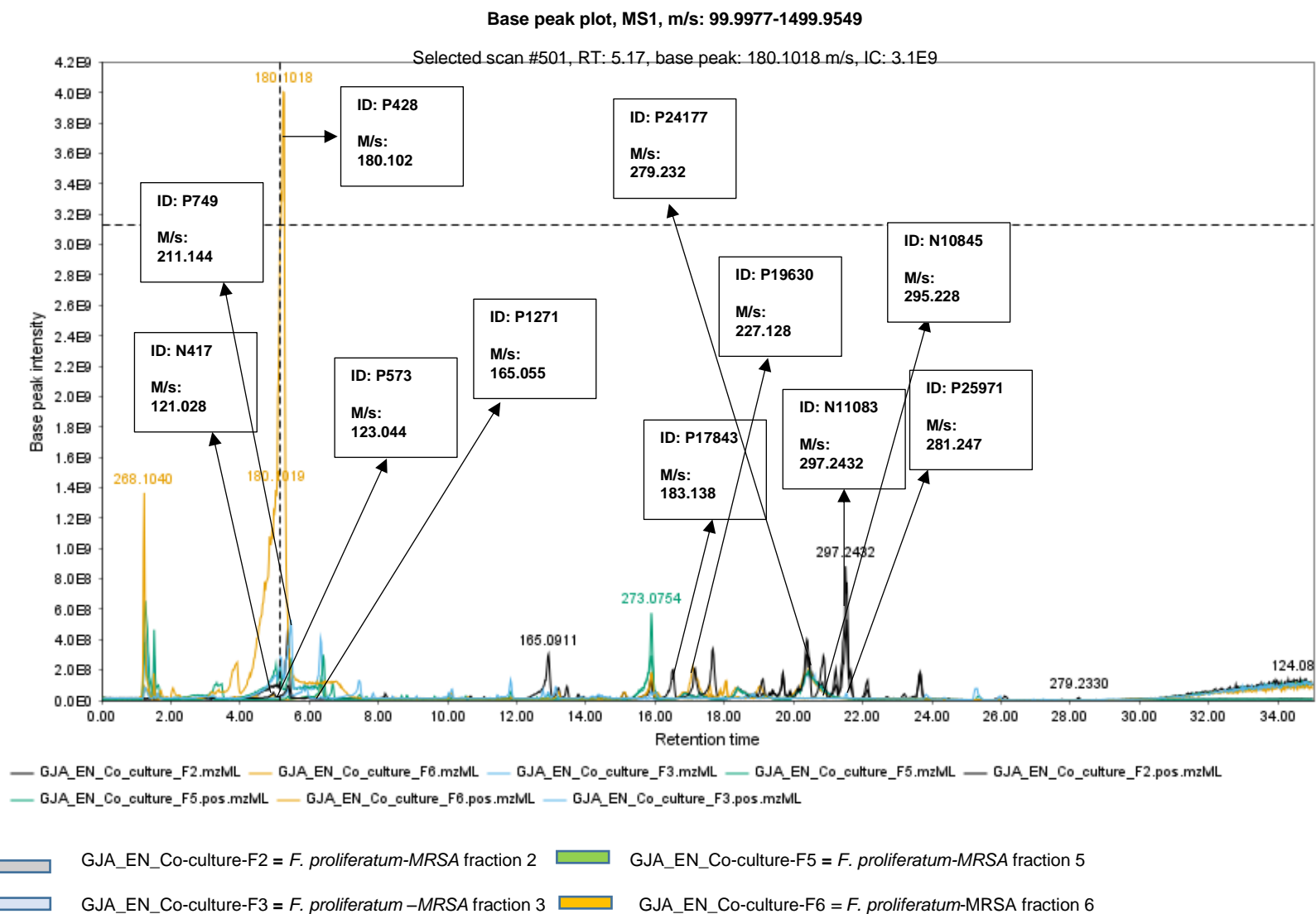


Figure 7.25: Total ion chromatogram (TIC) of the bioactive fractions of *F. proliferatum*-MRSA. The ion peaks that represent the discriminating features listed in Table 7.13 have been labelled.

7.2.11 Pure compound isolation

Fractions were selected for further purification work due to antimicrobial activity against MRSA. Planktonic active fractions F2, F3, F5 and F6 were selected for purification work.

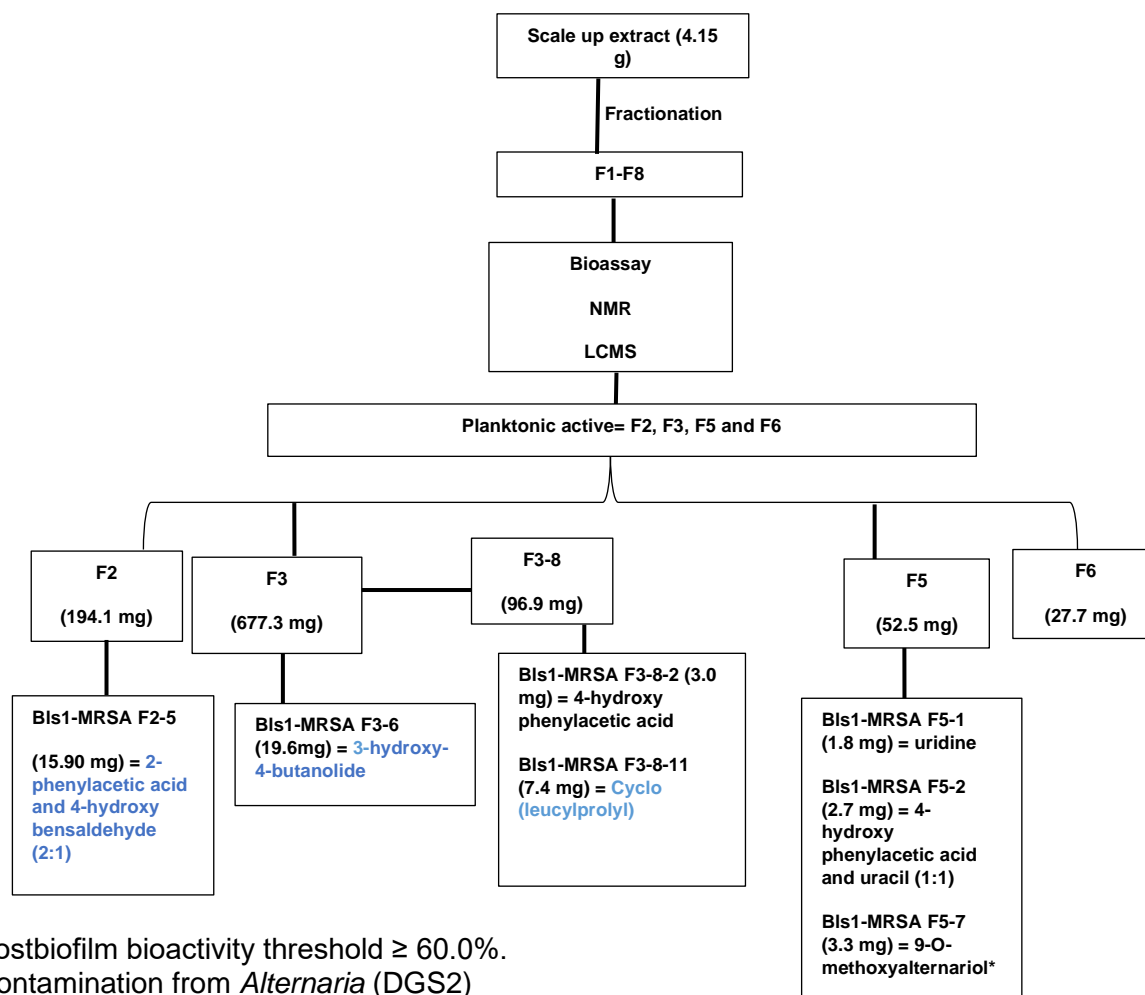
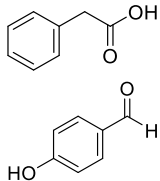
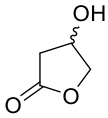
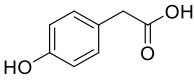
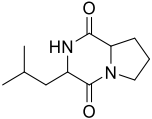
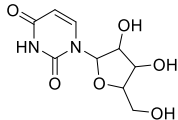


Figure 7.26: Summary workflow of *F. proliferatum*-MRSA scale-up crude extract to isolated compounds. Compounds with above 60.0% postbiofilm bioactivity are highlighted in blue. Other subfractions obtained from F2, F3 and F5 were mixtures but none of them exhibited planktonic MRSA activity at 60% or above, hence further purification was not performed on them reflecting only low yield of the active subfractions.

Fractions 2 and 3 were purified using flash chromatography (Biotage), which resulted in the isolation of 2-phenylacetic acid and *p*-hydroxybenzaldehyde at 2:1 (F2-5, 15.90 mg, 0.38%) and 3-hydroxy-4-butanolide (F3-6, 19.6 mg, 0.47%). Further purification of F3-8 using prep

TLC afforded 4-hydroxyphenylacetic acid (F3-8-2, 3.0 mg, 0.07%) and cyclo(leucylprolyl) (F3-8-11, 7.4 mg, 0.18%), fraction 5 afforded uridine (F5-1, 1.8 mg, 0.04%) by Prep TLC.

Table 7.14: Isolated pure compounds from co-culture of *F. proliferatum*-MRSA.

Drawn Structure	Name	Exact mass	Molecular Formula	Fraction from	Yield (mg)	Purification method
	2-phenylacetic acid <i>p</i> -hydroxybenzaldehyde at 2:1	136.0524 122.0368	C ₈ H ₈ O ₂ C ₇ H ₆ O ₂	F2-5	15.9	Biotage
	3-hydroxy-4-butanolide (compared to γ -butyrolactone unit of honaucin A (Choi <i>et al.</i> , 2012))	100.052	C ₅ H ₈ O ₂	F3-6	19.6	Biotage
	4-hydroxyphenylacetic acid (compared to parahydroxyphenylacetic acid (Wishart <i>et al.</i> , 2009))	152.047	C ₈ H ₈ O ₃	F3-8-2	3.0	Biotage and Preparative TLC
	cyclo(leucylprolyl) (Yannai, 2003)	210.137	C ₁₁ H ₁₈ N ₂ O ₂	F3-8-11	7.4	Biotage and Preparative TLC
	Uridine (Wishart <i>et al.</i> , 2009)	244.070	C ₉ H ₁₂ N ₂ O ₆	F5-1	1.8	Preparative TLC

7.2.12: Bioactivity test results

The pure compounds obtained from purification of *F. proliferatum*-MRSA co-culture were subjected to biological assay against MRSA ATCC 43300 and *S. aureus* (S.A) NCTC 8325. It was observed that only 2-phenylacetic acid and *p*-hydroxybenzaldehyde showed MRSA planktonic inhibition of 50.01%, while the other compounds were inactive. None of the isolated compounds were prebiofilm active or inhibited biofilm formation. For postbiofilm or the capability of the compounds to disrupt the biofilm, 2-phenylacetic acid and *p*-hydroxybenzaldehyde, 3-hydroxy-4-butanolide and cyclo(leucylprolyl) exhibited 60.20%, 69.23% and 63.76% MRSA inhibition respectively, while 4-hydroxy phenylacetic acid was inactive. However, none of the isolated compounds were able to exhibit pronounced bioactivity that is above the 70% inhibition threshold requirement.

Effect of pure compounds isolated from *F. proliferatum*-MRSA on MRSA and SA-NCTC 8325

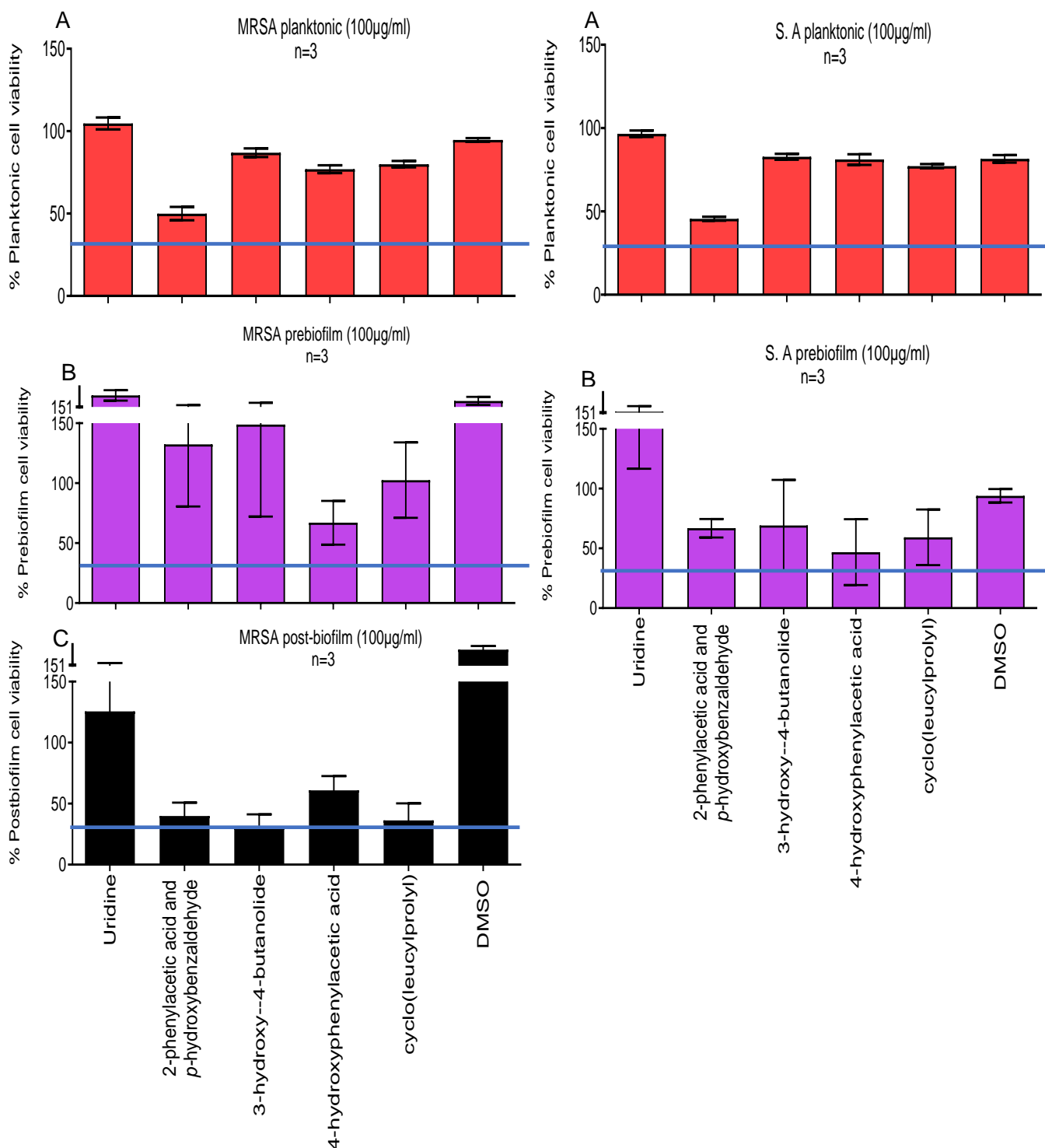


Figure 7.27: Effect of pure compounds isolated from *F. proliferatum*-MRSA. Left plots are the planktonic (A), prebiofilm (B), and postbiofilm (C) activity against MRSA. Right plots are the planktonic (A) and prebiofilm (B) activity on SA-NCTC 8325 at 100µg/mL. The blue line indicates the bioactivity threshold which is 30% viability (70.0% inhibition).

When the isolated compounds were tested against SA-NCTC 8325, 2-phenylacetic acid and *p*-hydroxybenzaldehyde showed MRSA planktonic inhibition of 54.40%, while the other compounds were inactive. For prebiofilm activity, 4-hydroxy phenylacetic acid showed 53.19% inhibition against SA-NCTC 8325 at 100µg/ml, while the other compounds were inactive (Figure 7.27). IC₅₀ (µM) for the isolated compounds were not obtainable, as they did not exhibit bioactivity above the recommended 70% threshold.

Due to the poor or weak bioactivities of the isolated compounds, all compounds were revisited on their position on the OPLS-DA S-plot shown in Figure 7.24 and Figure 7.12, by using their MW features (Figure 7.28 and Figure 7.29). It was observed that three of the isolated compounds were found on the active quadrant on the OPLS-DA plot. The compounds with their MW features included 4-hydroxy phenylacetic acid (152.047 Da), cyclo(leucylprolyl) (210.137 Da) and uridine (244.070 Da). However, the positions of 2-phenylacetic acid (136.0524 Da) and *p*-hydroxybenzaldehyde (122.0368 Da) and 3-hydroxy-4-butanolide (100.052 Da) in the active quadrant of the OPLS-DA S-plot were not possible to validate because they were below the measuring range. This indicates that, the isolated compounds that were inactive, were working in synergy or complementary to each other with their respective roles in the bioactivity of the fraction or the extract against MRSA, Hence, separating or isolating the compounds made them lose their synergistic property, resulting to the poor bioactivity observed on the isolated compounds. The isolated compounds identified on the active quadrant by OPLS-DA with their corresponding MW are listed in Table 7.15.

Isolated compounds of *F. proliferatum*-MRSA obtained from 15- and 30-days media optimisation fungal extracts.

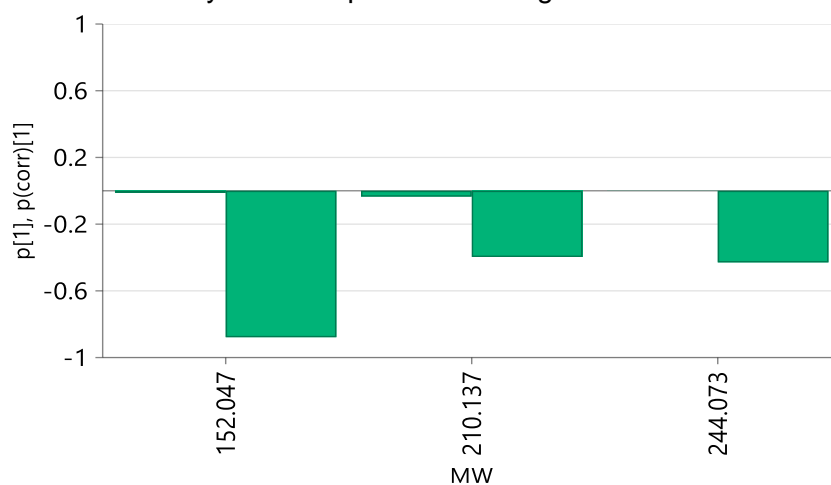


Figure 7.28: Distribution of the isolated compounds detected on the left active quadrant of the OPLS-DA loadings plot of the co-culture extracts generated during the media optimisation stage, indicating the predicted bioactive compounds to be (152.047 Da) 4-hydroxyphenylacetic acid, (210.137 Da) cyclo(leucylprolyl), and (244.070 Da) uridine.

Isolated compounds of *F. proliferatum*-MRSA fungal extract obtained from scaled up fractions extract on malt extract media.

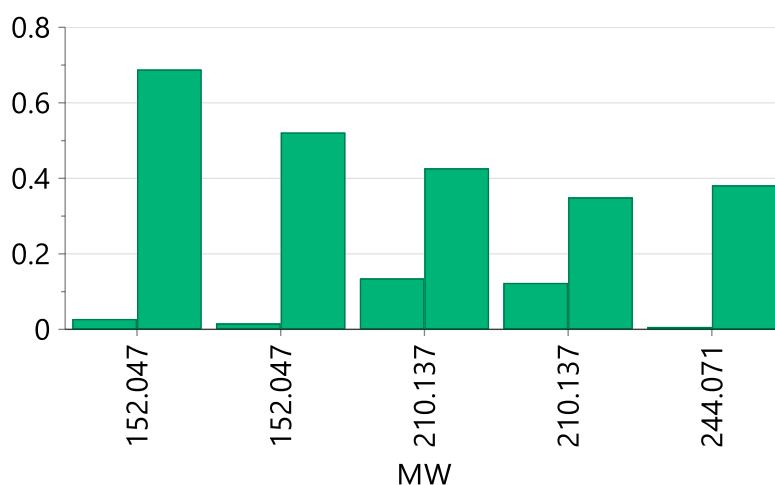


Figure 7.29: Distribution of the isolated compounds on the right active quadrant of the OPLS-DA loadings plot of the chromatographic fractions indicating the predicted bioactive compounds to be (152.047 Da), 4-hydroxy phenylacetic acid, (210.137 Da) cyclo(leucyl prolyl) and (244.070Da) uridine.

Table 7.15: Isolated compounds observed on OPLS-DA active quadrant (fig. 7.24 and 7.12).

Highlighted rows represent relatively weak antibiofilm metabolites that exhibited at least greater than a 60% bioactivity threshold.

Isolated compounds	Name	MW	Biofilm Stages of Observed Bioactivity	Observed / unobserved on OPLS-DA active quadrant from the fraction stage (MW, primary ID, rt)	Isolated compounds observed on OPLS-DA active quadrant as obtained from media optimisation stage (MW, primary ID, rt)
F2-5	2-phenylacetic acid <i>p</i> -hydroxy benzaldehyde at 2:1	136.0524 122.0368	postbiofilm (60.20%)	Not detected*	Not detected*
F3-6	3-hydroxy-4-butanolide	100.052	postbiofilm (69.23%)	Not detected*	Not detected*
F3-8-2	4-hydroxy phenylacetic acid	152.047	inactive	Observed in active quadrant (152.047, P1174, rt= 5.73)	Observed in active quadrant (152.047, P3261, rt= 5.91)
F3-8-11	cyclo(leucyl prolyl)	210.137	postbiofilm (63.76%)	Observed in active quadrant (210.137, P749, rt= 5.36)	Observed in active quadrant (210.137, P17569, rt= 5.01)
F5-1	uridine	244.070	inactive	Observed in active quadrant (244.071, P9284, rt= 10.98)	Observed in active quadrant (244.073, N195, rt= 7.75)

*MW is outside the measuring range of m/z 150 to 2000 Da.

7.3 Summary and conclusion

7.3.1 Media optimisation and metabolomics bioassay guided isolation

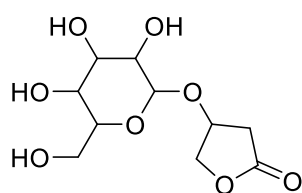
Endophytic fungi *F. proliferatum*, *F. falciforme* and *A. alternata* isolated in this study were co-cultured with the pathogenic MRSA and tested against MRSA to elicit the production of new compounds. Even though NMR spectra of *F. falciforme*-MRSA and *A. alternata*-MRSA showed to be more discriminatory than *F. proliferatum*-MRSA, when co-cultured on malt extract agar and malt extract broth, *F. proliferatum*-MRSA emerged the best with bioactivity of 92.23% and 98.98% respectively. It can be deduced that the pathogenic MRSA weakened *F. falciforme* and *A. alternata* at the crude co-culture stage, hence the weak bioactivity observed. Therefore, co-culture of *F. proliferatum*-MRSA was selected for scale up and purification works. This will be the first report on the co-culture of *F. proliferatum*-MRSA.

Dereplicated compound hits afforded some Fusarium metabolites observed in the monoculture such as fusalanipyrone, fusaric acid and bikaverin with m/z 165.091, 180.102 and 383.076 Da, respectively. The feasibility of isolating these compounds was highly dependent on their relative abundance. These compounds were easy to detect by ESI-mass spectrometry due to their excellent ionisation capability in such MS conditions but their low yields at microgram levels made these compounds impossible to isolate. The same was encountered with non-dereplicated ion peaks, which indicated the presence of novel compounds. The ion peak at m/z 211.144 eluting between 5 and 6 min which was dereplicated as cyclo(isoleucylprolyl), was then isolated in this study and structurally elucidated as cyclo(leucylprolyl). The occurrence of cyclo(leucylprolyl) was consistently observed as a discriminatory metabolite for the bioactivity of the co-culture of *F. proliferatum*-MRSA from the screening to media optimisation to the fractionation of the scaled-up extracts. Cyclo(leucylprolyl) disrupted MRSA biofilm at 63.76%.

7.3.2 Pure compounds isolation

Scale-up of the fungus was carried out on malt extract media which was the optimum media to produce the antibiotic compounds. Fractionation was carried out on the scaled up crude extract using hexane and EtOAc as solvents. Five known compounds, which includes, 2-phenylacetic acid, *p*-hydroxybenzaldehyde, 3-hydroxy-4-butanolide, 4-hydroxy phenylacetic acid, cyclo(leucylprolyl), and uridine were isolated from the co-culture as shown in Table 7.15. All the isolated compounds were inactive to MRSA at the bioactivity threshold of 70.0% inhibition for strong reliable bioactivity. Compounds 4-hydroxy phenylacetic acid and uridine were found in the active quadrant at the crude stage, indicating that they could function better

against MRSA when they work in synergy with other compounds but would be weakened and inactive when isolated. Compound 3-hydroxy-4-butanolide, a butyrolactone, was inactive to planktonic and pre-biofilm MRSA, but was able to disrupt postbiofilm by 69.23%, indicating that it could interrupt quorum sensing ability after biofilm formation. Its inactivity to planktonic and prebiofilm MRSA could be because of the position of hydroxyl group at C-5. Its derivative goodyeroside A, isolated from *Crocus sativus* and *Goodyera* spp have shown significant hepatoprotectant activity (Zhang *et al.*, 2009). Another derivative named honaucin A (4-chloro-2E-butenoyl), isolated from *Leptolyngbya crossbyana* is an Inhibitor of bacterial quorum sensing and an anti-inflammatory agent (Choi *et al.*, 2012).



goodyeroside A

In conclusion, crude extract of *F. proliferatum*-MRSA co-culture was very active against MRSA but lost most of its bioactivity upon isolation of the compounds. It could be that the compounds were working complementarily to each other to be active and separating them made them lose their bioactive property.

CHAPTER 8

8.1 Secondary metabolites from the co-culture of two fungal endophytes

Co-cultures between two fungal strains can be a major source of new secondary metabolites (SMs) and consists of two types including solid state fermentation (SSF) and liquid state fermentation (LSF). Rice media and potato dextrose broth (PDB) are the most common co-culture media for fungal SSF and LSF respectively. LSF can facilitate metabolite exchange and transportation and has the ability to trigger new SMs biosynthesis (Zhuang and Zhang, 2021). A total of 75 new SMs was obtained from LSF co-culture by the end of 2022, such as polyketides, macrolides, terpenes, etc. (Xu *et al.*, 2023). Furthermore, fungal co-culture has important roles in increasing activity of valuable enzymes such as pectinase and laccase (Rehman *et al.*, 2014, Stoilova *et al.*, 2005), and improving yield of important products (such as oleanolic acid, ursolic acid, and betulinic acid (Ola *et al.*, 2013, Ross *et al.*, 2014).

The main aim for this coculture study is to retain back the antibacterial capability of *F. falciforme* (MGS3A) and *F. proliferatum* (BLS1) that was lost during fermentation scale-up and high throughput isolation work. The running hypothesis is that the coculture condition will induce the biosynthesis of potent antibiofilm metabolites.

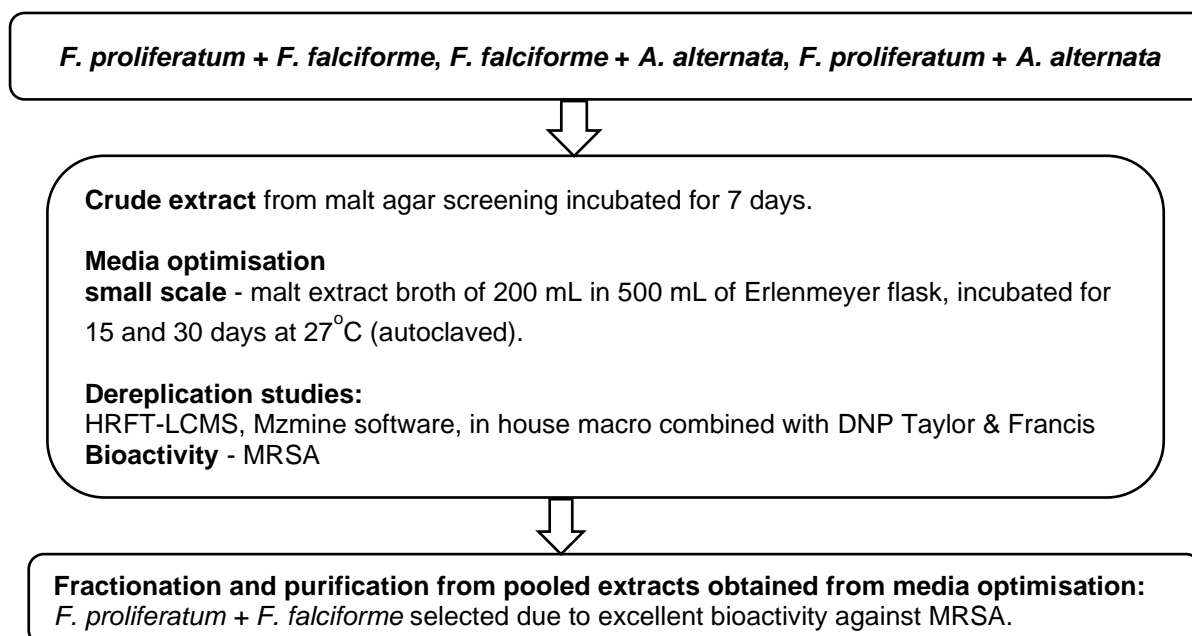


Fig 8.1: A summary workflow for crude extract screening, media optimisation and scale-up of co-cultures of two fungal strains.

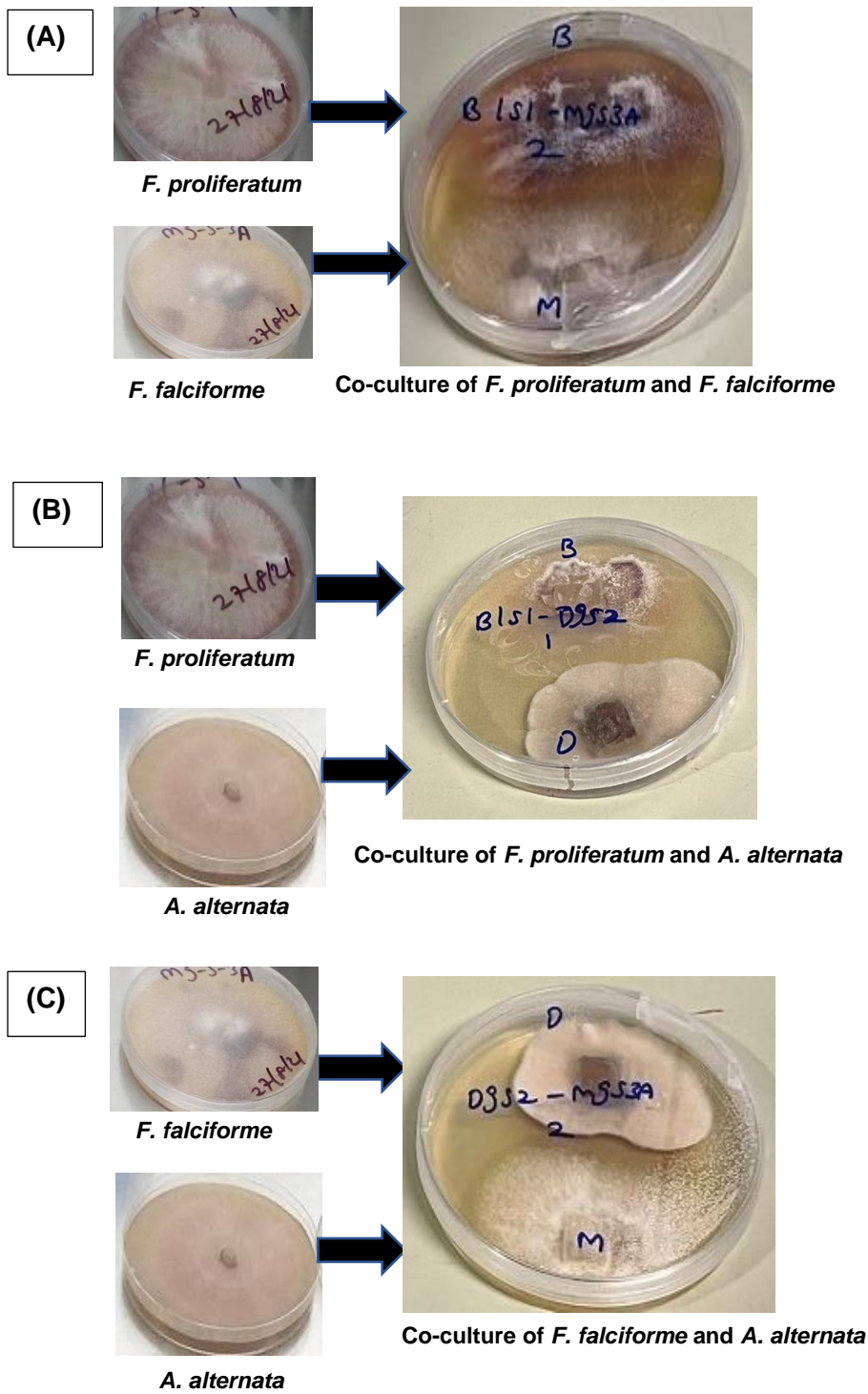


Fig 8.2: Source and co-cultures of *F. proliferatum* + *F. falciforme*, *F. falciforme* + *A. alternata*, *F. proliferatum* + *A. alternata* on solid malt extract agar.

8.2 Results and Discussion

8.2.1 Co-culture extract weights on solid malt extract agar media

As depicted in Table 8.1, the highest weight was obtained by *A. alternata* and *F. falciforme* co-culture with 55.0 mg at 7 days of incubation. The average yields were in the decreasing order *A. alternata* and *F. falciforme* (55.0 mg) > *F. proliferatum* + *F. falciforme* (49.5 mg) > *F. proliferatum* + *A. alternata* (35.9).

Table 8.1: Co-culture extracts weights incubated for 7 days as illustrated in Figure 8.3. All cultures were incubated at 27°C.

Sample	Weights (mg)
F-F Control	9.5
BM -1	56.9
BM -2	48.7
BM -3	42.8
Average weight	49.5
BD -1	34.3
BD -2	36.6
BD -3	36.7
Average weight	35.9
DM -1	51.9
DM -2	56.5
DM -3	56.6
Average weight	55.0

Table 8.2: Sample codes

Code	Full name
BM	<i>F. proliferatum</i> + <i>F. falciforme</i>
BD	<i>F. proliferatum</i> + <i>A. alternata</i>
DM	<i>A. alternata</i> + <i>F. falciforme</i>

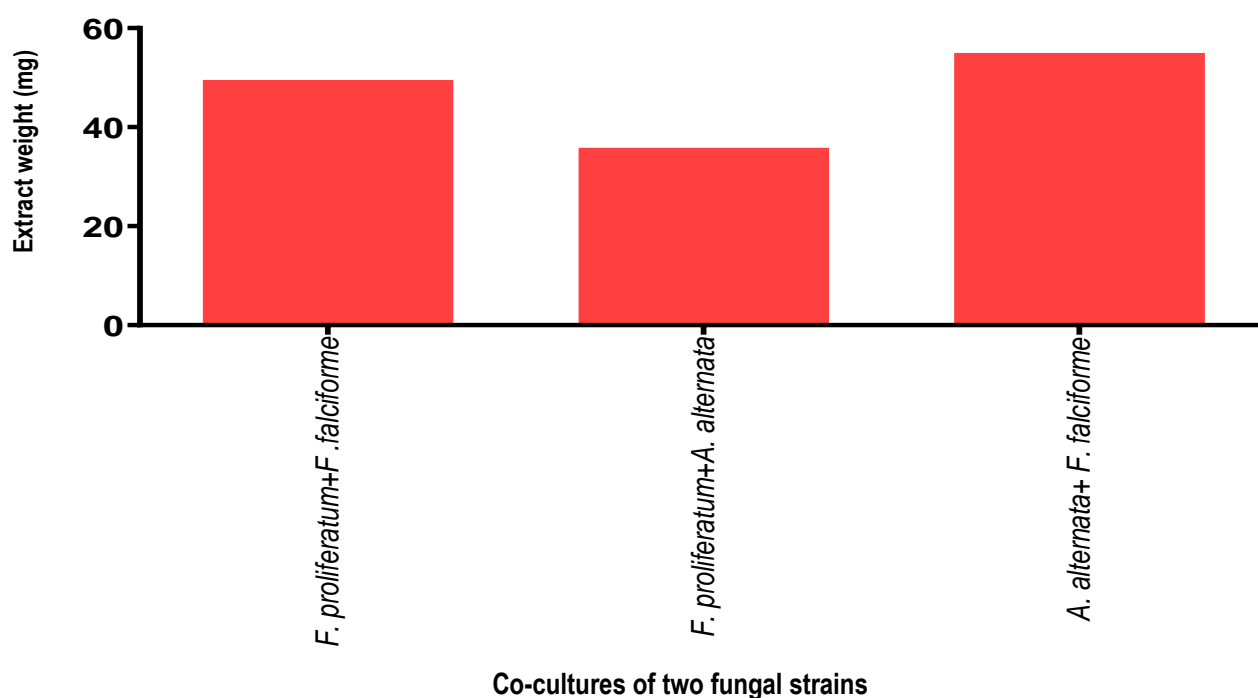


Figure 8.3: Histogram showing average weight of extracts from three respective replicates of *F. proliferatum* + *F. falciforme*, *F. proliferatum* + *A. alternata*, *A. alternata* + *F. falciforme* co-cultures obtained from malt extract media and incubated for 7 days.

8.2.2 Crude extract biological assay screening

F. proliferatum + *F. falciforme*, *F. proliferatum* + *A. alternata*, *A. alternata* + *F. falciforme* was co-cultured on malt agar plates as explained in 2.6.2.7. The metabolites produced from the co-culture extracts were tested against MRSA.

The results show that *F. proliferatum* + *F. falciforme* (BM) and *F. proliferatum* + *A. alternata* (BD) incubated for 7 days were active while *A. alternata* + *F. falciforme* (DM) was inactive. Bioactivity threshold was set at 10.0% cell viability (90.0% inhibition) for planktonic and prebiofilm assays. Hence, BM and BD were selected for liquid media (malt extract broth) optimisation.

Table 8.3: Summary activity of active co-culture extract against MRSA at concentrations of 100 µg/ml.

Media	Incubation period	Antimicrobial % inhibition	Prebiofilm % inhibition	Postbiofilm % inhibition
BM	7 days	97.53	99.54	41.54
BD	7 days	94.70	100%	<0

*Cells highlighted in blue colour indicates active extracts while white cell with indicate inactive extracts.

8.2.3 MVA of LC-HRMS data

For multivariate analysis, PLS-DA scores and loadings plot were generated for the LC-MS data. The extracts were grouped according to the 3 different fungal co-cultures. The PLS-DA scores plot in Figure 8.4A of the LC-HRMS data of the co-cultures revealed that fungal extracts obtained from *A. alternata* and *F. falciforme* were found on the upper right side of the plot (red circles), extracts obtained from *F. proliferatum* and *F. falciforme* (green circles) were on the lower right side of the plot (green circles) while *F. proliferatum* and *A. alternata* were found on the lower left plot (blue circles). Their different locations in the plot indicates different chemical profiles between the fungal co-cultures. The loadings plot in Figure 8.4B demonstrated that discriminating metabolites from extracts of *F. proliferatum* and *F. falciforme* produced low to high molecular weight metabolites ranging from 307 to 1202 Da and were putatively identified as phomolide C, spiculisporic acid D (**1**), fusamarin, ML263A (**2**), hyme-gluslin, while four ion peaks gave no hits indicating that they could be novel compounds. *F. proliferatum* and *A. alternata* co-culture produced low to moderate molecular weight discriminatory metabolites ranging from 273 to 579 Da and were putatively identified as 9-O-methylalternariol, and altenusin, while two ion peaks gave no hits. Dereplication of the discriminating metabolites indicated by the loadings plot indicated the dominance of the biosynthesis of *Alternaria* metabolites when co-cultured with *F. proliferatum*, such as alternariol and altenusin as found in the monocultures as described in chapter 6. On the other hand, interestingly the coculture of two *Fusarium* strains, *F. proliferatum* and *F. falciforme* were able to yield metabolites that have never been described for *Fusarium* (except for the *F. falciforme* monoculture used in this work) while some discriminatory metabolites did not find any match in our database. Hence, dereplication of the discriminating metabolites indicated by the loadings plot also indicated the dominance of the biosynthesis of *F. falciforme* when co-cultured with *F. proliferatum*, such as hyme-gluslin, fusamarin and phomolide C as found with the monocultures in chapter 5. The model gave goodness of fit (R_2) of 0.994 and a predictability score (Q_2) of 0.888. R_2X_0 [1] gave a variation score of 45.1%, while the difference within groups R_2X [2] was 21.4%.

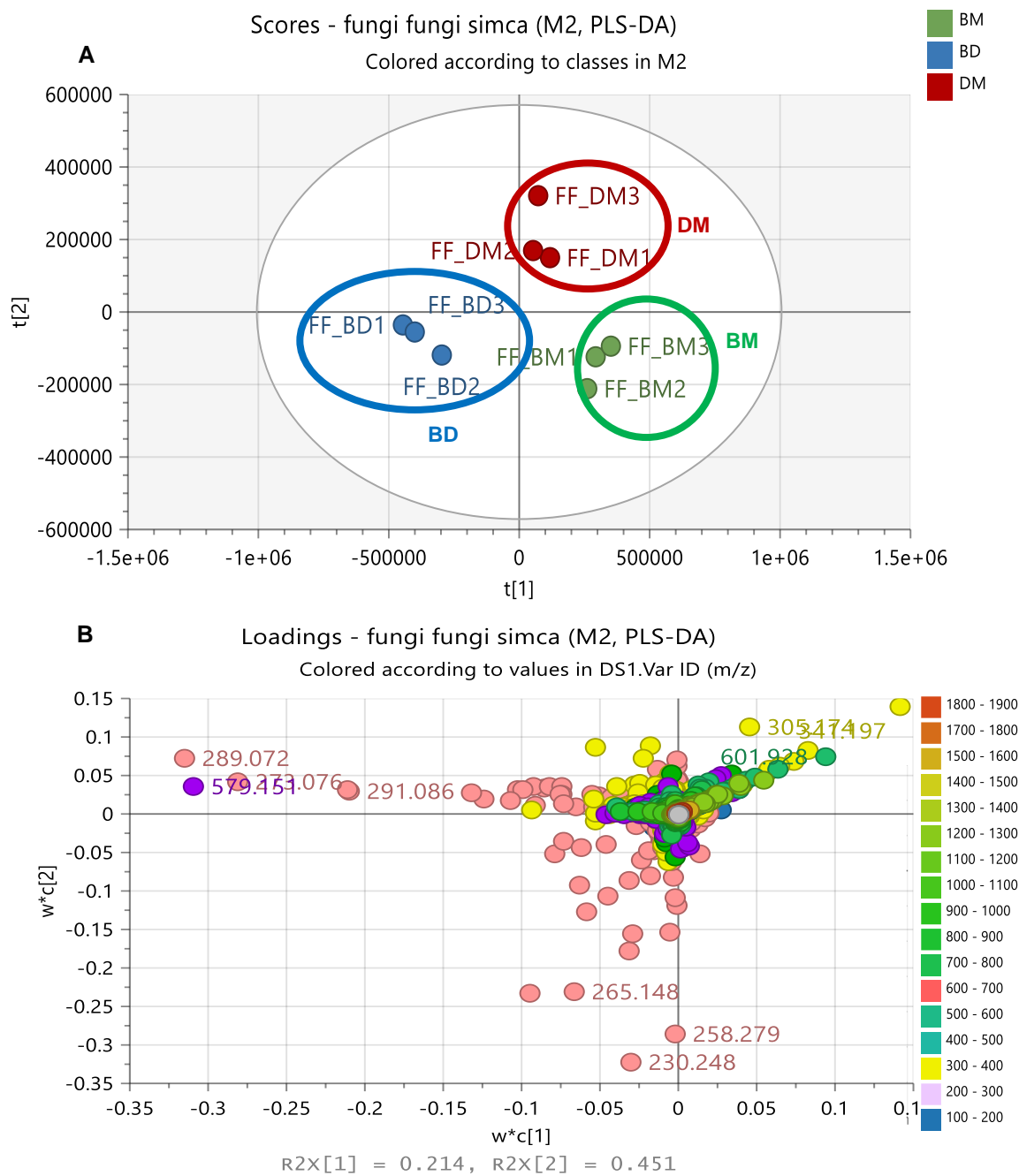


Figure 8.4: (A) PLS-DA scores and (B) loading plots of LC-HRMS data of co-cultured fungal extracts from malt extract media incubated at 7 days. $R^2X = 0.994$ and $Q^2X = 0.888$. The difference between groups $R^2X_o[1]$ is equal to 45.1 % and the difference within groups $R^2X[2]$ is 21.4%. Labelled features represent the discriminating ion peaks obtained from the respective co-cultures.

Table 8.4: Dereplicated compound hits from discriminating metabolites from co-cultured of fungal endophytes incubated for 7 days obtained from the PLS-DA loadings plot on Figure 8.4B. Structures are shown in Figure 8.5.

Mzmine ID	m/z	Rt	M.wt	P-value	Molecular Formular (DBE)	Compound hits	Biological source
<i>F. proliferatum</i> and <i>F. falciforme</i>							
P2506	601.928	24.81	600.921	7.49E-07		No hits	
P283	601.928	18.93	600.921	2.69E-04		No hits	
P297	1202.85	18.93	1201.84	6.87E-04		2[M+H] of P283	
N318	341.197	11.56	342.204	7.97E-04	C ₁₈ H ₃₀ O ₆ (4)	phomolide C	<i>Phomopsis</i> sp. B27
						spiculisporic acid D (1)	Marine-derived <i>Aspergillus</i> sp.
P338	609.925	22.65	608.918	1.02E-03		No hits	
N885	342.200	11.56	343.208	1.34E-03		No hits	
P7182	305.174	19.83	304.167	8.93E-05	C ₁₈ H ₂₄ O ₄ (7)	Fusamarin	Metabolite of a strain of <i>Fusarium</i> sp.
P284	307.190	11.54	306.183	1.53E-03	C ₁₈ H ₂₆ O ₄ (6)	ML263A (2)	<i>Eupenicillium javanicum</i> IFM 52670 and <i>Penicillium citrinum</i> Sank 18767
P3014	325.201	11.56	324.193	2.33E-03	C ₁₈ H ₂₈ O ₅ (5)	Hymeglusin	Metabolite of a <i>Cephalosporium</i> sp., <i>Scopulariopsis</i> sp. and <i>Fusarium</i> sp.
<i>F. proliferatum</i> and <i>A. alternata</i>							
P823	273.076	10.71	272.068	2.74E-06	C ₁₅ H ₁₂ O ₅ (10)	9-O-Methylalternariol	<i>Alternaria</i> sp. including marine sp. <i>Anthocleista djalonensis</i> , <i>Penicillium diversum</i> and <i>Lachnum palmae</i>
N97	279.164	17.13	280.171	6.18E-04		No hits	

Mzmine ID	<i>m/z</i>	Rt	M.wt	<i>P-value</i>	Molecular Formula (DBE)	Compound hits	Biological source
N118	289.072	10.71	290.079	1.35E-06	C ₁₅ H ₁₄ O ₆ (9)	Altenusin	<i>Alternaria alternata</i> , <i>A. tenuis</i> , and the marine derived <i>Alternaria</i> sp. strains SCSIO41014
N883	290.075	10.71	291.08	1.90E-06		No hits	
P1817	291.086	10.40	290.079	1.94E-06	C ₁₅ H ₁₄ O ₆ (9)	Same as N118	
N882	579.151	10.71	580.158	2.95E-09	C ₃₀ H ₂₈ O ₁₂ (17)	[2M-H] of N118	

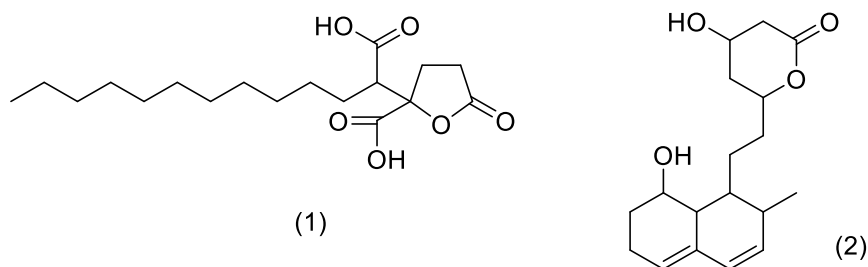


Figure 8.5: Structures of dereplicated compound hits showing PLS-DA discriminating metabolites obtained from co-culture extracts, as listed in Table 8.4.

An OPLS-DA was performed based on the anti-MRSA results to discriminate the metabolites between active and inactive extracts as shown in Figure 8.6. Active fungal extracts were obtained by inoculation of co-cultures of *F. proliferatum*-*F. falciforme* and *F. proliferatum*-*A. alternata* in malt extracts media then incubated for 7 days while the other co-culture extracts were found inactive. It showed fitness (R_2) and predictability (Q_2) scores of 0.983 and 0.886 respectively. This proved to be a good fit, and a good model prediction. The variation between groups R_2X_0 [1] was 47.9 % and within group R_2X [1] was 7.6 %. The slight difference within groups showed that the two active co-cultures may have some similarity in their chemical profiles, while the high variation between groups explains the disparity in the chemical profile between the active and inactive extracts.

The OPLS-DA scores plot positioned the active extracts on the upper and lower left quadrants (red circles), while the inactive extracts were found on the upper and lower right quadrant of the scores plot (blue circles). The bioactive metabolites gave an m/z range between 165 and 579 Da. Discriminating active metabolites with p-values less than 0.05 are listed in Table 8.5. Structures of putatively identified compound hits are shown in Figure 8.7. Two of the ion peaks gave no hits, which could indicate the presence of novel compounds.

The compounds identified from the DNP database, as shown in Table 8.5 were, Mzmine IDs of P2221, P279, P295, N2154, P12352, N2156, N2157, P289, N3537, P4483, P314, P7210, P287, N882 represented by their respective m/z as 165.091, 200.237, 207.102, 223.097, 227.128, 241.108, 265.148, 289.143, 326.188, 347.116, 351.143, 383.076, 388.142, and 579.151 respectively were putatively identified as (*E*)-1',2'-didehydro-5-butyl-6-methyl-2*H*-pyran-2-one (**3**), 6-tridecylamine (**4**), acremine D (**5**), phomopsinone A (**6**), phomolide B (**7**), phomolide E (**8**), 2,4,6-trimethyl-1-nonanol-*O*-sulfate (**fig 7.12**), *N*-chloromethylhectorinium (**9**), sophasrine, breynolide, tetrahydroaltersolanol F (**10**), bikaverin, 9-[(2-amino-2-carboxyethyl)-thio]-10-hydroxy-3,5,7-tetradecatrienedioic acid, and gambiriin A1. Two ion peaks with Mzmine IDs of P305 and P4787 represented by m/z 226.116 and 227.124 respectively gave no hits.

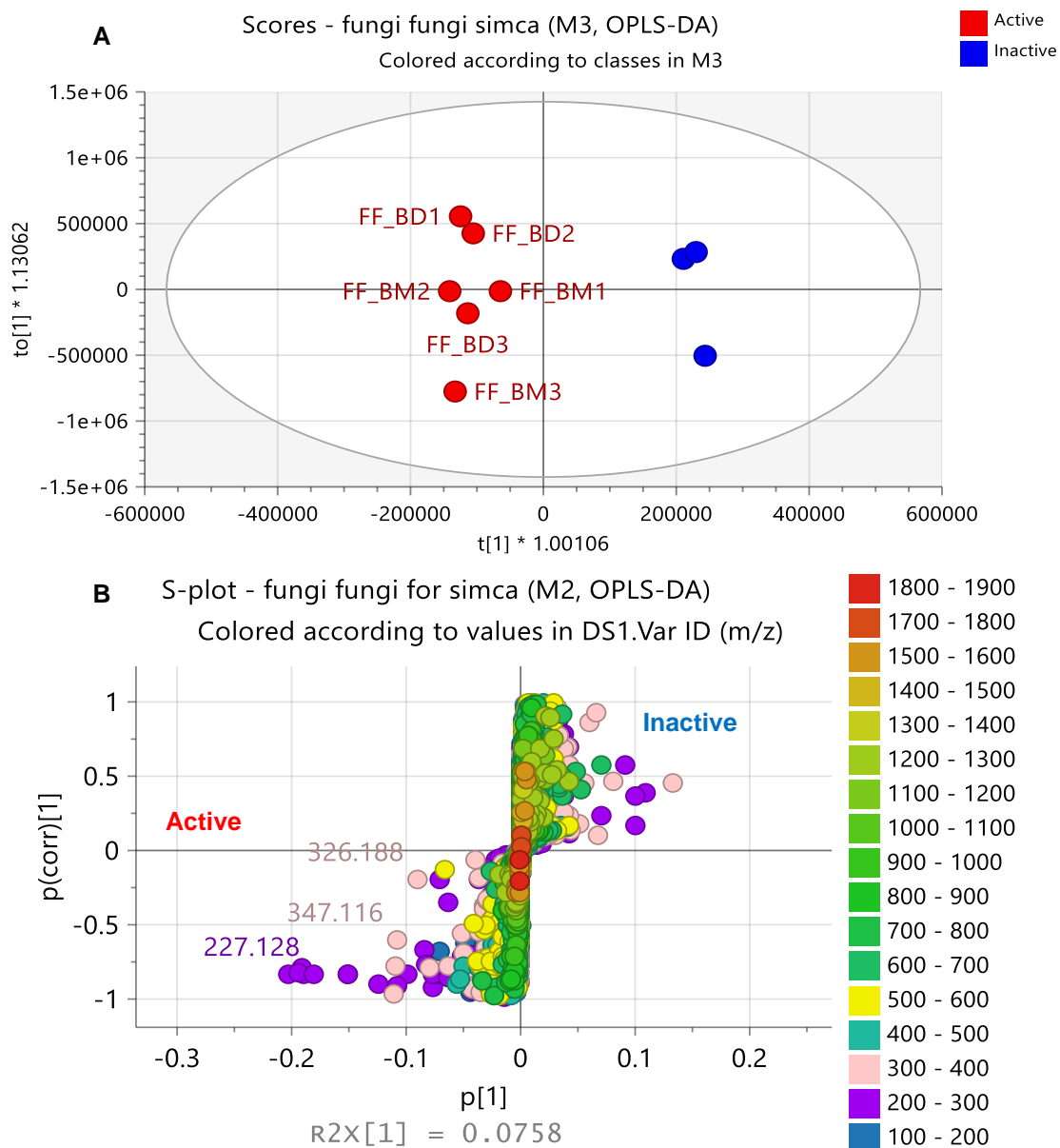


Figure 8.6: (A) OPLS-DA scores and (B) S-plots of LC-HRMS of co-cultured extracts obtained from malt extract media. The labelled metabolites on S-plot indicated the discriminating feature for the active extracts. $R_2 = 0.983$ and $Q_2 = 0.886$. The difference between group $R_2X_0 [1]$ is equal to 47.9% and the difference within groups $R_2X [2]$ is 7.6%.

Table 8.5: Dereplicated compound hits from discriminating metabolites from co-cultured of fungal endophytes incubated for 7 days obtained from the OPLS-DA S-plot on Figure 8.6B. Structures are shown in Figure 8.7.

Mzmine ID	m/z	Rt	M.wt	P-value	Molecular Formular (DBE)	Compound hits	Biological source
<i>F. proliferatum</i> and <i>F. falciforme</i>							
P2221	165.091	13.12	164.084	0.050602	C ₁₀ H ₁₂ O ₂ (5)	(<i>E</i>)-1',2'-Didehydro-5-butyl-6-methyl-2 <i>H</i> -pyran-2-one (3)	Fungal culture LL-11G219
P279	200.237	15.31	199.23	0.341046	C ₁₃ H ₂₉ N (0)	6-Tridecylamine (4)	Cyanobacterium <i>Microcoleus lyngbyaceus</i>
P295	207.102	17.54	206.094	0.007432	C ₁₂ H ₁₄ O ₃ (6)	Acremine D (5)	<i>Acremonium byssoides</i> strain A20
N2154	223.097	12.50	224.104	0.000413	C ₁₂ H ₁₆ O ₄ (5)	Phomopsinone A (6)	<i>Phomopsis</i> sp.
P305	226.116	17.55	225.108	0.006609		No hit	
P12352	227.128	16.98	226.120	0.012009	C ₁₂ H ₁₈ O ₄ (4)	Phomolide B (7)	<i>Phomopsis</i> sp. hsla01-1
P4787	228.131	17.66	227.124	0.009329		No hit	
N2156	241.108	11.65	242.115	0.017118	C ₁₂ H ₁₈ O ₅ (4)	Phomolide E (8)	<i>Phomopsis</i> sp. A123
N2157	265.148	16.20	266.155	0.643856	C ₁₂ H ₂₆ O ₄ S (0)	2,4,6-Trimethyl-1-nonanol-O-sulfate	Sea cucumber <i>Cucumaria frondosa</i>
P289	289.143	15.21	288.136	0.000630	C ₁₄ H ₂₃ ClNO ₃	N-Chloromethylhectorinium (9)	Alkaloid from <i>Senecio nemorensis</i>
N3537	326.188	18.73	327.195	0.649398	C ₁₉ H ₂₅ N ₃ O ₂ (9)	Sophasrine	Alkaloid from <i>Sophora griffithii</i> (Leguminosae).
P4483	347.116	12.52	346.109	0.096417	C ₁₅ H ₂₂ O ₇ S (5)	Breynolide	<i>Breynia fruticosa</i>
P314	351.143	13.43	350.136	0.015660	C ₁₈ H ₂₂ O ₇ (8)	Tetrahydroaltersolanol F (10)	Marine-derived <i>Alternaria</i> sp. SJ-2008003

P7210	383.076	16.75	382.069	0.015353	C ₂₀ H ₁₄ O ₈ (14)	Bikaverin	Pigment from <i>Fusarium oxysporum</i> , <i>F. solani</i> , <i>F. moniliforme</i> , <i>F. lycopersici</i> , <i>F. vasinfectum</i> , <i>F. bulbigenum-blasticola</i> , <i>Gibberella fujikuroi</i> .
P287	388.142	11.98	387.135	9.04326e-05	C ₁₇ H ₂₅ NO ₇ S (6)	14-Carboxyhexanorleukotriene E ₃	Urinary metabolite
N882	579.151	10.71	580.158	0.742295	C ₃₀ H ₂₈ O ₁₂ (17)	Gambiriin A1	<i>Uncaria gambir</i> and <i>Sanguisorba officinalis</i>

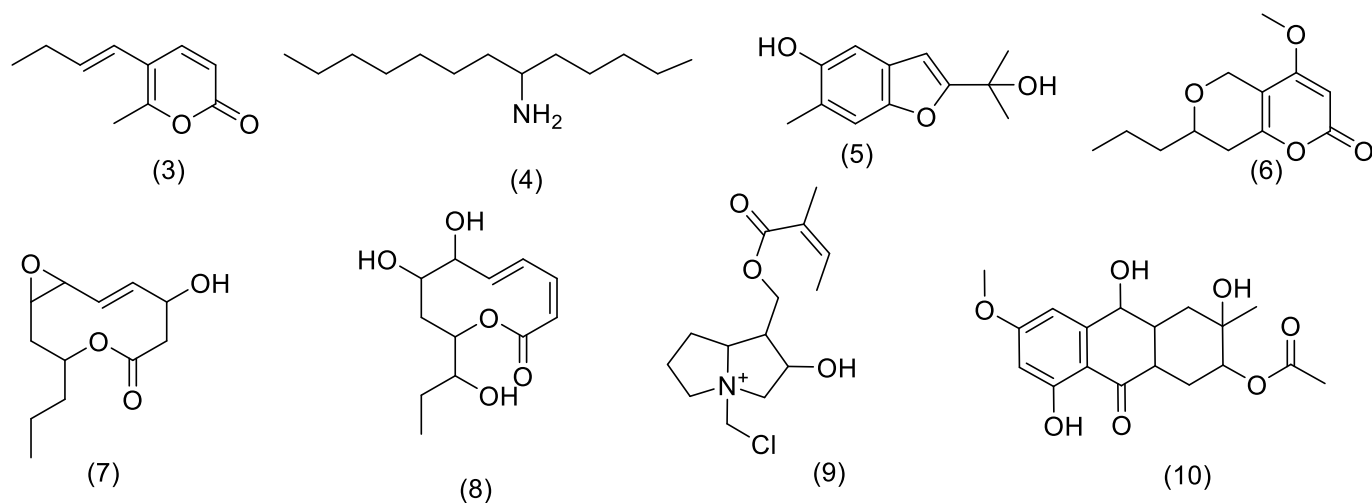


Figure 8.7: Structure of dereplicated compound hit showing OPLS-DA discriminating metabolite obtained from bioactive co-culture extracts, as listed in table 8.5.

Analysis on MetaboAnalyst® was performed. The heatmap showed that the bioactive co-culture extract of *F. proliferatum* and *F. falciforme* (purple box) incubated for 7 days were discriminatory (Figure 8.8) which explains the bioactivity observed. The co-culture extracts of *A. alternata* and *F. falciforme* were less concentrated with discriminatory metabolites which explains the inactivity observed (green box).

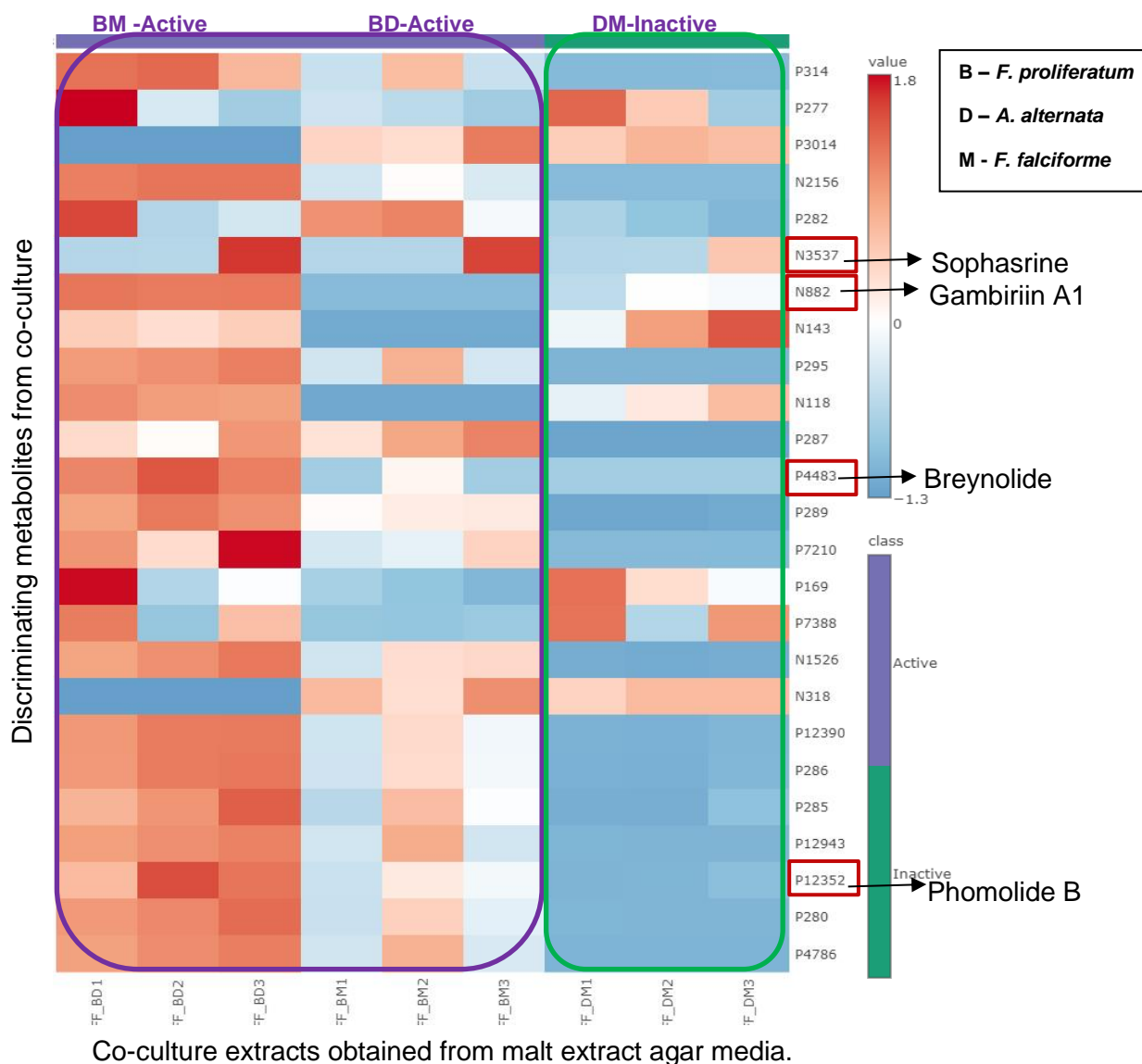


Figure 8.8: Heatmap analysis of the mass spectral data of co-culture crude extracts with their Mzmine values, obtained from malt extract media, generated by MetaboAnalyst®. The purple box represents active extracts from *F. proliferatum*-*F. falciforme* co-culture and *F. proliferatum*-*A. alternata*, while the green boxes represent the inactive but discriminatory metabolites from *A. alternata*-*F. falciforme* co-culture. Highlighted Mzmine values on the Y-axis N3537, N882, P4483, and P12352 indicate common metabolites observed on the heatmap and dereplicated in Table 8.5.

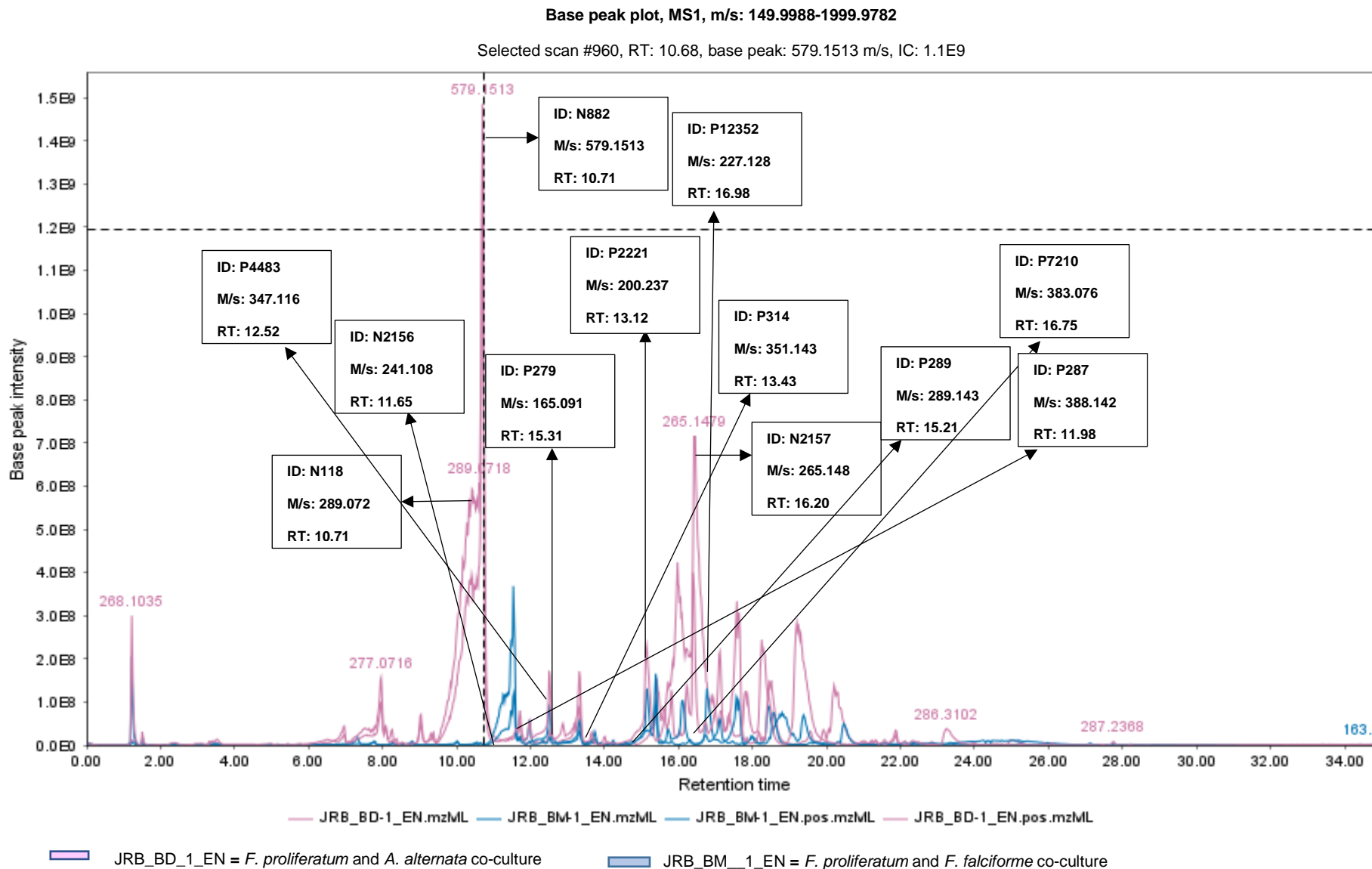


Figure 8.9: Total ion chromatogram (TIC) of the bioactive co-culture extracts from malt extract agar media. The ion peaks that represent the discriminating features listed in table 8.5 have been labelled.

8.2.4 Co-culture extract yields on liquid malt extract media

Further work on co-cultures of *F. falciforme* and *A. alternata* was not carried out due to the inactivity observed on the fungal extract, which was obtained after 7 days of incubation on malt extract agar. The highest extract weight of *F. proliferatum* and *F. falciforme* (BM) was gained at day 15 with an extract weight of 162.1 mg. The co-culture gained its exponential phase at 15 days incubation and started to decline at 30 days incubation. *F. proliferatum* and *A. alternata* (BD) co-culture was still growing at day 15 and gained its highest weight (exponential phase) at day 30 with an extract weight of 133.4 mg. The obtained weights of the co-culture extracts are listed in Table 8.6.

Table 8.6: Weights of crude extracts of Fungal co-cultures after 15- and 30-days incubation on malt extract broth media.

Sample	Weights (mg)	Sample	Weights (mg)
15 days extracts		30 days extracts	
		F-FB Control 30	21.2
BM15-1	161.7	BM30-1	132.3
BM15-2	158.5	BM30-2	100.6
BM15-3	166.1	BM30-3	136.8
Average weight	162.1		123.2
BD15-1	121.7	BD30-1	132.8
BD15-2	113.5	BD30-2	139.8
BD15-3	99.2	BD30-3	127.5
Average weight	111.5		133.4

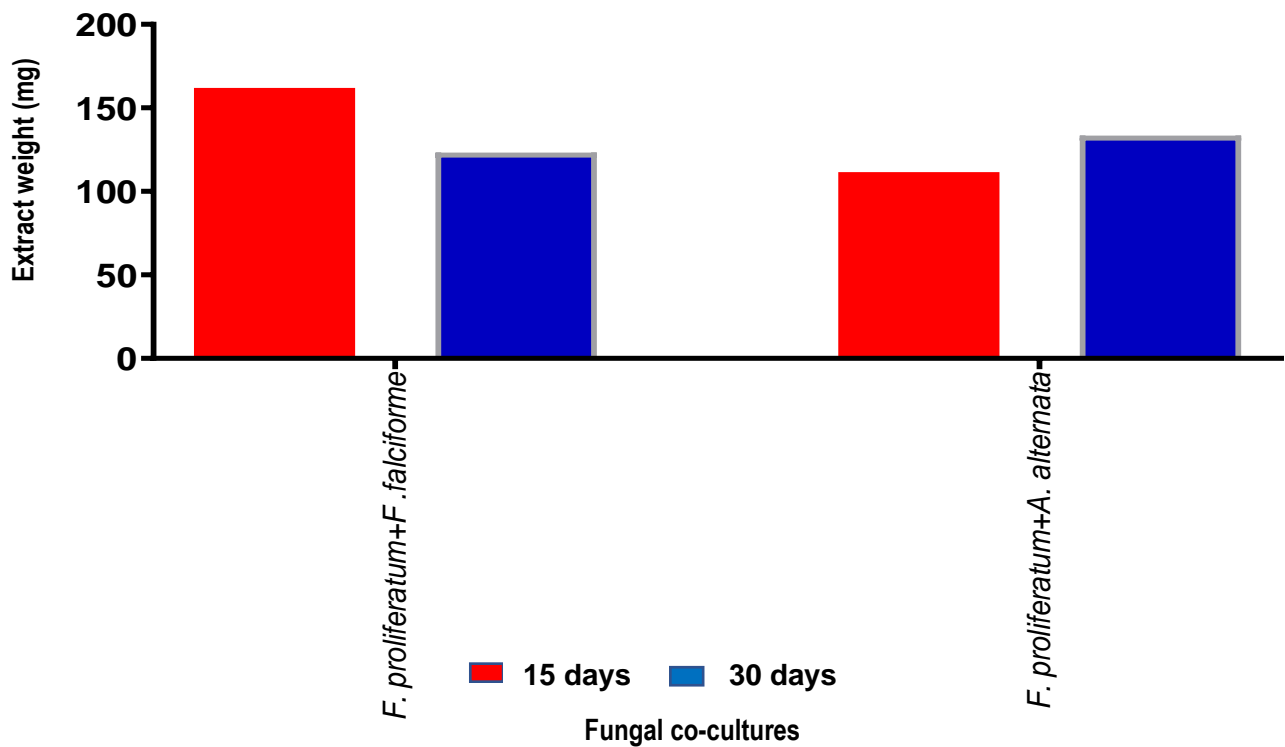


Figure 8.10: Histogram showing average weight of extracts from two respective replicates of co-cultures of *F. proliferatum* + *F. falciforme* and *F. proliferatum* + *A. alternata* obtained from malt extract media and incubated for 15 and 30 days.

8.2.5 Crude extract biological assay screening

F. proliferatum-*F. falciforme* and *F. proliferatum*-*A. alternata* were co-cultured on malt extract broth. The metabolites produced from the co-culture extracts were tested for MRSA activity.

The results show that *F. proliferatum* and *F. falciforme* (BM) incubated for 15 and 30 days was active against MRSA, while *F. proliferatum*-*A. alternata* showed inconsistent activity or inactive. Bioactivity threshold was set at 10.0% cell viability (90.0% planktonic and prebiofilm inhibition).

Table 8.7: Summary activity of active fungi to fungi co-culture extract against MRSA at concentrations of 100 µg/ml.

Media	Incubation period	Antimicrobial % inhibition	Prebiofilm % inhibition	Postbiofilm % inhibition
BM	15 days	91.6	99.6	<0
BM	30 days	94.4	99.7	<0

*Cells highlighted in blue colour indicates active extracts while white cells indicate inactive extracts.

8.2.6 Multivariate analysis of LC-HRMS data

For multivariate analysis, PCA scores and loadings plot were generated for the LC-MS data. The PCA scores plot in Figure 8.11A of the LC-HRMS data of the fungal extracts from the co-culture revealed that extracts obtained from *F. proliferatum*-*F. falciforme* after 15 and 30 days of incubation were found on the right side of the plot (encircled in red). Fungal extracts obtained from *F. proliferatum*-*A. alternata* co-culture were found on the upper and lower left quadrant of the plot (encircled in blue). The 15- and 30-days fungal extracts from *F. proliferatum*-*F. falciforme* were clustered indicating similarities in their chemical profiles. The loadings plot in Figure 8.11B demonstrated that discriminating metabolites from extracts of *F. proliferatum*-*F. falciforme* produced low to moderate molecular weight metabolites ranging from 289 to 683 Da and were putatively identified colletoxin B, ML263A, hymeglusin, fusaridic acid A, phomolide C, and 10-carboxy-11,12,13,14-tetranorplakortide Q, while three ion peaks gave no hits. Co-cultures of *F. proliferatum* and *A. alternata* produced low to moderate molecular weight discriminatory metabolites ranging from 230 to 579 Da and were putatively identified as 9-O-methylalternariol, altenusin, (3*H*,10*H*)-*N*10-phenylalloxasine, gambiriin A1, 2-amino-3-tetradecanol (**11**) and 2,4,6-trimethyl-1-nonanol-*O*-sulfate, while two ion peaks gave no hit indicating the presence of a novel compound. Slight variations were observed in the compound hits obtained from the monocultures as compared with the co-cultures. Most of the discriminatory compounds hits putatively identified in the co-cultures were previously observed in the fungi monocultures although new compound hits not previously identified emerged, while the ion peaks with no hits indicates the presence of novel compounds. Most of the putatively identified hits observed from the co-culture of *F. proliferatum* and *F. falciforme* were also identified in the monoculture of *F. falciforme* showing its dominance over *F. proliferatum*, even though fungal crude extracts from the monoculture of *F. proliferatum* displayed better bioactivity. In parallel, most of the putatively identified hits observed from the

fungal extracts of co-cultures of *F. proliferatum* and *A. alternata* were also identified in the monoculture of *A. alternata* showing its dominance over *F. proliferatum*, even though similarly, the crude extract from the monoculture of the latter fungus displayed better bioactivity. In both co-culture conditions, the bioactivity of the weaker antibacterial monoculture extracts from *F. falciforme* and *A. alternata* have shown their dominance and improved their bioactivities in the presence of *F. proliferatum*. However, co-culturing *F. falciforme* and *A. alternata* resulted to a loss in bioactivity. The model gave goodness of fit (R_2) of 0.898 and a predictability score (Q_2) of 0.651 which is an excellent fitted model. Dereplicated compound hits are listed in Table 8.8, while the structures are shown in Figure 8.12.

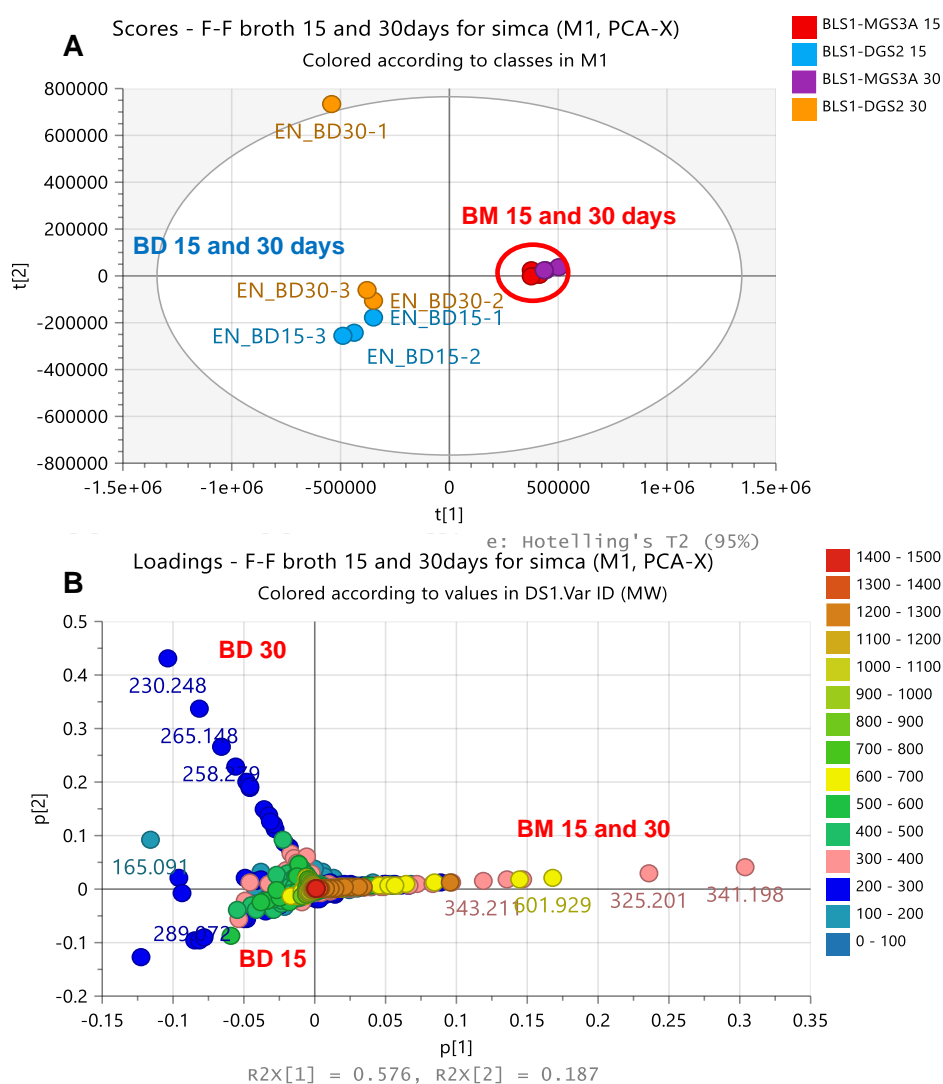


Figure 8:11: (A) PCA scores and (B) loading plots of LC-HRMS data of co-culture fungal extracts from malt extract media incubated at 15 and 30 days. $R_2X = 0.898$ and $Q_2X = 0.651$. Labelled features represent the discriminating ion peaks for the outlying extracts.

Table 8.8: Dereplicated compound hits from discriminating metabolites from co-culture of fungi to fungi incubated for 15 and 30 days obtained from the PCA loadings plot on Figure 8:11B. Structures are shown in Figure 8.12.

Mzmine ID	m/z	Rt	M.wt	Molecular Formular (DBE)	Compound hits	Biological source
<i>F. proliferatum</i> and <i>F. falciforme</i> 15 and 30 days						
P2927	289.18	12.05	288.172	C ₁₈ H ₂₄ O ₃ (7)	Colletorin B	<i>Cephalosporium diospyri</i> and <i>Nectria galligena</i>
P2068	307.190	12.07	306.183	C ₁₈ H ₂₆ O ₄ (6)	ML263A	<i>Eupenicillium javanicum</i> IFM 52670 and <i>Penicillium citrinum</i> Sank 18767
P1791	325.201	12.05	324.194	C ₁₈ H ₂₈ O ₅ (5)	Hymeglusin	<i>Cephalosporium</i> sp., <i>Scopulariopsis</i> sp. and <i>Fusarium</i> sp.
P2572	343.211	12.04	342.204	C ₁₈ H ₃₀ O ₆ (4)	Fusaridioic acid A	<i>Cephalosporium</i> sp. and the marine derived <i>Scopulariopsis candida</i>
N183	341.198	12.05	342.205	C ₁₈ H ₃₀ O ₆ (4)	phomolide C	<i>Phomopsis</i> sp. B27
N4590	342.201	12.05	343.208		No hits	
N4591	343.213	12.86	344.22	C ₁₈ H ₃₂ O ₆ (3)	10-Carboxy-11,12,13,14-tetranorplakortide Q	<i>Plakortis</i> sp.
N4273	383.208	14.39	384.216		No hit	
P1803	601.929	18.82	600.921		No hits	
P12894	602.43	18.82	601.423		No hits	
N4592	683.402	12.02	684.409		Complex of m/z 341.1976	
<i>F. proliferatum</i> and <i>A. alternata</i> 15 days						
P8674	273.076	11.45	272.068	C ₁₅ H ₁₂ O ₅ (10)	9-O-methylalternariol	<i>Alternaria</i> spp. incl. marine spp. <i>Anthocleista djalonsensis</i> , <i>Penicillium diversum</i> and <i>Lachnum palmae</i>
P1591	291.086	11.23	290.079	C ₁₅ H ₁₄ O ₆ (9)	Altenusin	<i>Alternaria tenuis</i> , <i>Penicillium</i> sp. and <i>Talaromyces</i> sp.

N4	289.072	11.22	290.08	C ₁₆ H ₁₀ N ₄ O ₂ (14)	(3 <i>H</i> ,10 <i>H</i>)- <i>N</i> 10-phenylalloxasine	
N16	579.152	11.36	580.159	C ₃₀ H ₂₈ O ₁₂ (17)	Gambiriin A1	<i>Uncaria gambir</i> and <i>Sanguisorba officinalis</i>
<i>F. proliferatum</i> and <i>A. alternata</i> 30 days						
P24	230.248	16.32	229.241	C ₁₄ H ₃₁ NO (0)	2-Amino-3-tetradecanol (11)	No hit
P62	258.279	19.39	257.272		No hit	
P2328	265.148	18.10	266.156	C ₁₂ H ₂₆ O ₄ S (0)	2,4,6-Trimethyl-1-nonanol; O-Sulfate	Sea cucumber <i>Cucumaria frondosa</i>
N5	279.164	18.33	280.171		No hit	

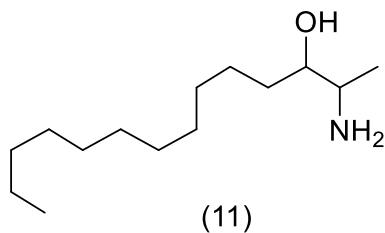


Figure 8.12: Structures of dereplicated compound hits showing PCA discriminating metabolites obtained from fungi-to-fungi co-culture extracts, as listed in table 8.8.

An OPLS-DA was performed based on the anti-MRSA results to discriminate the metabolites between active and inactive extracts as shown in Figure 8.13. While the other co-culture extracts were found inactive, active extracts were obtained by co-culturing *F. proliferatum* and *F. falciforme* in malt extract media then incubated for 15 and 30 days. It showed fitness (R_2) and predictability (Q_2) scores of 0.996 and 0.989 respectively. This proved to be a good fit, and a good model prediction. The variation between groups R_2X_o [1] was 57.0 % and within group R_2X [1] was 15.6 %. This showed that there was slight similarity within the extracts in their different classes.

The OPLS-DA scores plot positioned the active extracts on the upper and lower left quadrants (red circles), while the inactive extracts were found on the upper and lower right quadrant of the scores plot (blue circles). The defined target metabolites afforded p -values < 0.05 , which indicated a strong model with a confidence interval of more than 95%. The bioactive metabolites gave an m/z range between 275 and 1202 Da. Discriminating active metabolites with p -values less than 0.05 are listed in Table 8.9. Five of the ion peaks gave no hits, which could indicate the presence of novel compounds.

The compounds identified from the DNP database, as shown in Table 8.9 were, Mzmine IDs of P3327, P2927, P2068, P1791, P2572, N183, N459 represented by their respective m/z as 275.091, 289.18, 307.190, 325.201, 343.211, 341.198 and 343.213 respectively and dereplicated as dihydroanhydrojavanicin, colletorin B, ML263A, hymeglusin, fusaridioic acid A, phomolide C, and phomopoxide A respectively, all of which are earlier reported fungal metabolites (Table 8.9). Five ion peaks with Mzmine IDs of N4590, N4273, P1803, P12894, P2591 represented by their respective m/z as 342.201, 383.203, 601.929, 602.43 and 1202.85 gave no hits.

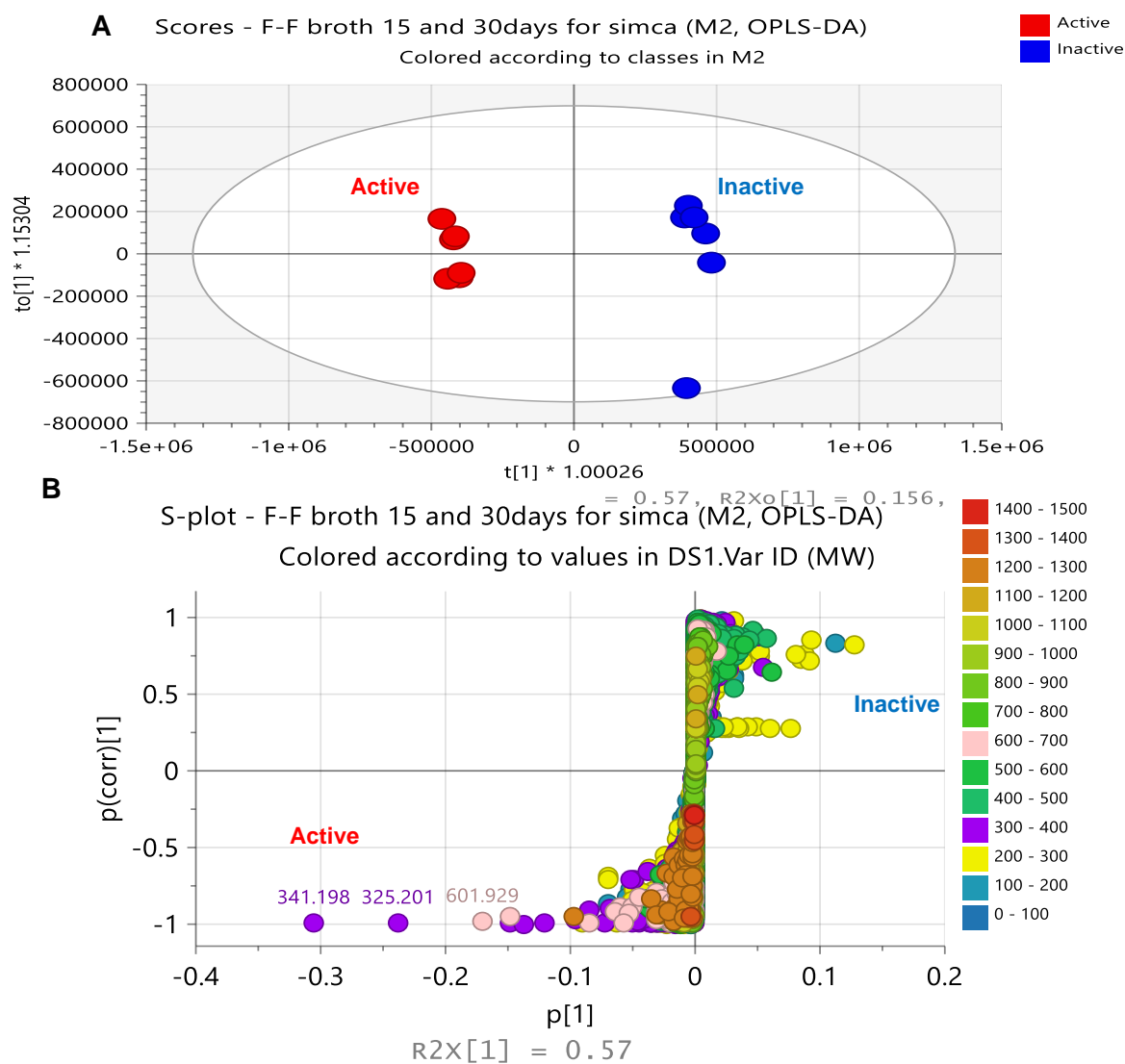
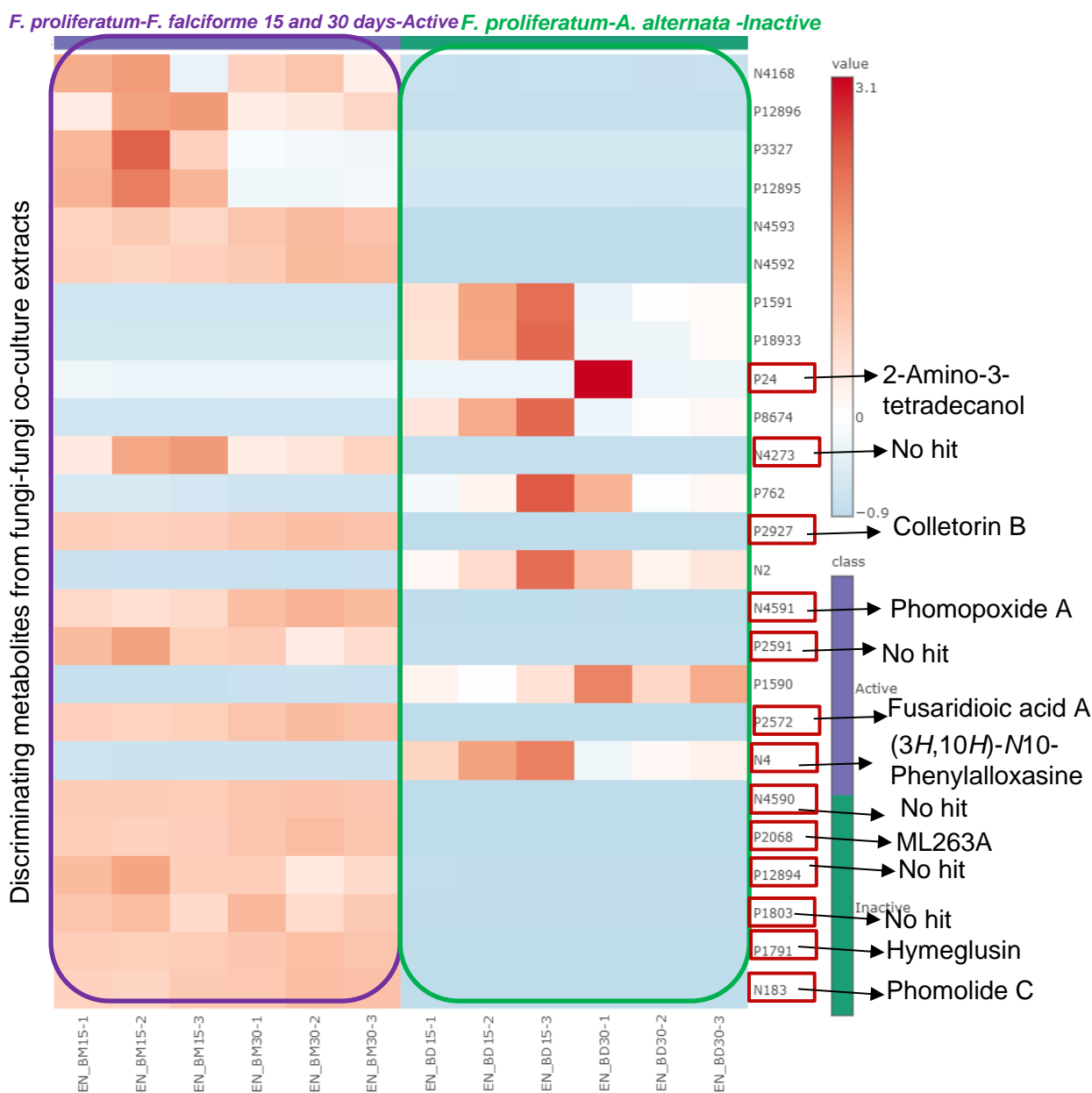


Figure 8.13: (A) OPLS-DA scores and (B) S-plots of LC-HRMS of co-culture extracts obtained from malt extract media. The labelled metabolites on S-plot indicated the discriminating feature for each media extracts. $R_2 = 0.996$ and $Q_2 = 0.989$. The difference between group $R_2X_0[1]$ is equal to 57.0% and the difference within groups $R_2X[2]$ is 15.6%.

Table 8.9: Dereplicated compound hits from discriminating active metabolites from co-culture of two *Fusarium* endophytes incubated for 15 and 30 days obtained from the OPLS-DA S-plot on Figure 8.13B.

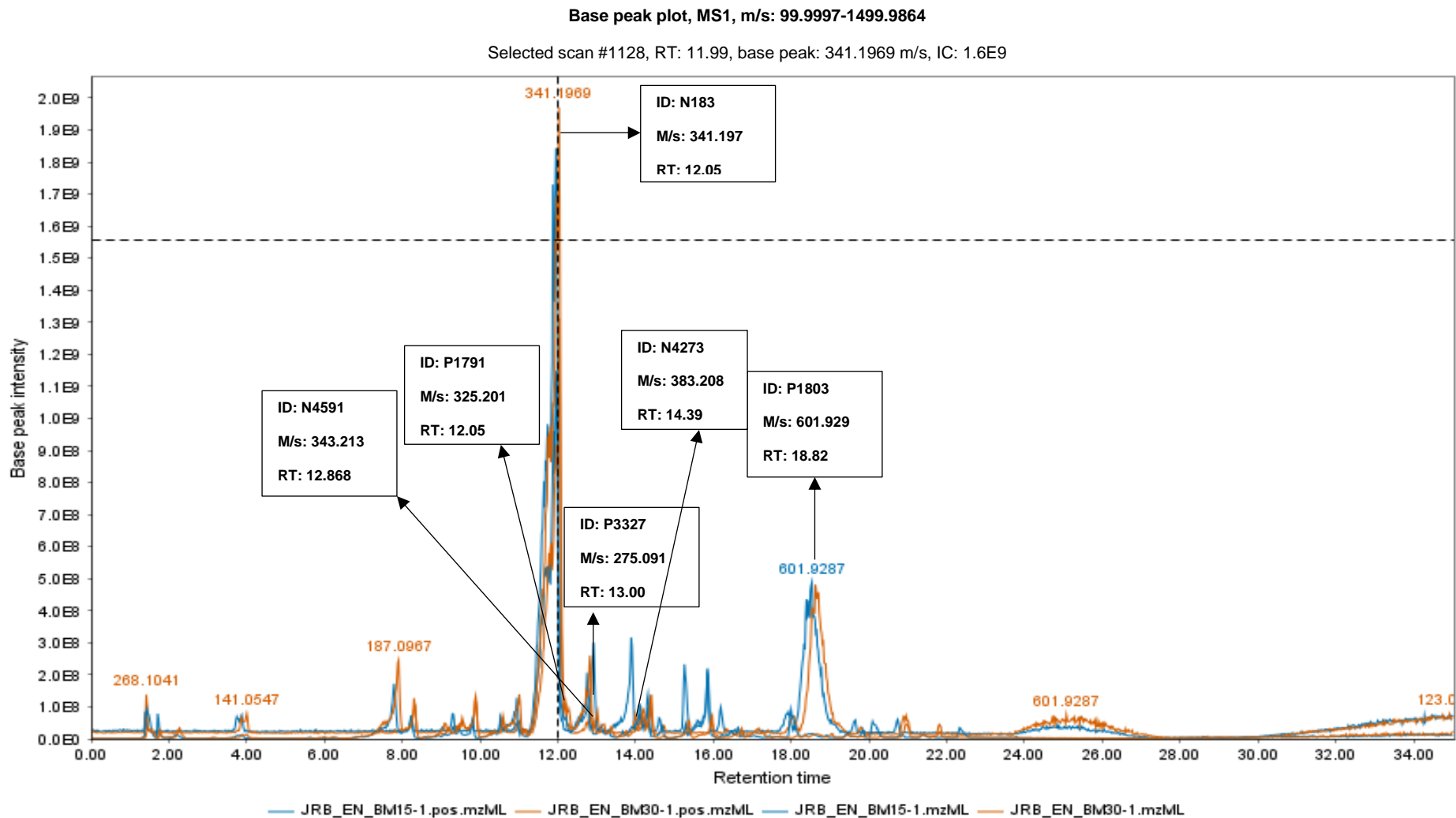
Mzmine ID	m/z	Rt	M.wt	P-value	Molecular Formular (DBE)	Compound hits	Biological source
<i>F. proliferatum</i> and <i>F. falciforme</i> 15 and 30 days							
P3327	275.091	13.00	274.084	0.0128271	C ₁₅ H ₁₄ O ₅ (9)	Dihydroanhydrojavanicin	<i>Fusarium solani</i>
P2927	289.18	12.05	288.172	8.52533e-12	C ₁₈ H ₂₄ O ₃ (7)	Colletorin B	<i>Cephalosporium diospyri</i> and <i>Nectria galligena</i>
P2068	307.190	12.07	306.183	9.86488e-12	C ₁₈ H ₂₆ O ₄ (6)	ML263A	<i>Eupenicillium javanicum</i> IFM 52670 and <i>Penicillium citrinum</i> Sank 18767
P1791	325.201	12.05	324.194	1.98009e-12	C ₁₈ H ₂₈ O ₅ (5)	Hymeglusin	<i>Cephalosporium</i> sp., <i>Scopulariopsis</i> sp. and <i>Fusarium</i> sp.
P2572	343.211	12.04	342.204	6.38372e-11	C ₁₈ H ₃₀ O ₆ (4)	Fusaridioic acid A	<i>Cephalosporium</i> sp. and the marine derived <i>Scopulariopsis candida</i>
N183	341.198	12.05	342.205	6.42952e-11	C ₁₈ H ₃₀ O ₆ (4)	Phomolide C	<i>Phomopsis</i> sp. B27
N4590	342.201	12.05	343.208	5.21608e-14		No hits	
N4591	343.213	12.86	344.22	1.17874e-07	C ₁₈ H ₃₂ O ₆ (3)	Phomopoxide A	<i>Phomopsis</i> sp. YE3250
N4273	383.208	14.39	384.216	4.27252e-05		No hit	
P1803	601.929	18.82	600.921	6.84323e-09		No hits	
P12894	602.43	18.82	601.423	8.65577e-07		No hits	
N4592	683.402	12.02	684.409	4.41899e-11		Complex of 341.1976 and 341.1976 m/z	
P2591	1202.85	18.82	1201.84	1.64447e-06		No hits	

Analysis on MetaboAnalyst® was also performed. The heatmap showed that the bioactive co-culture extract of *F. proliferatum* and *F. falciforme* (purple box) incubated for 15 and 30 days had more metabolite concentration than the inactive extracts (green box).



Fungi to fungi o-culture extracts obtained from malt extract media.

Figure 8.14: Heatmap analysis of the mass spectral data of fungi-to-fungi co-culture crude extracts with their Mzmine values, obtained from malt extract media, generated by MetaboAnalyst®. The purple box represents active extracts from *F. proliferatum-F. falciforme* co-culture, while the green box represents the inactive extracts. Highlighted Mzmine values on the Y-axis P24, N4273, P2927, N4591, P2591, P2572, N4, N4590, P2068, P12894, P1803, P1791 and N183 indicate common metabolites observed on the heatmap and VIP and were also dereplicated in Table 8.9.



▭ JRB_EN_BM15= *F. Proliferatum-F. falciforme* coculture incubated for 15 days. ▭ JRB_EN_BM15= *F. Proliferatum-F. falciforme* coculture incubated for 30 days.

Figure 8.15: Total ion chromatogram (TIC) of the bioactive extracts of *F. proliferatum-F. falciforme* co-culture from malt extract media. The ion peaks that represent the bioactive discriminating features listed in table 8.9 have been labelled.

8.2.7: Fractionation of *F. proliferatum*-*F. falciforme* crude extracts

The study shows that the of ^1H NMR spectral data and LC-HRMS data of the fungal extracts obtained from media optimisation of the co-cultures, using malt extract media incubated at 15 and 30 days had similar chemical profile. Hence, the replicates for the two incubation periods were merged to give a total weight of 770 mg and fractionated.

Fractionation of *F. proliferatum*-*F. falciforme* afforded F1-F8, W1, W2 and W3.

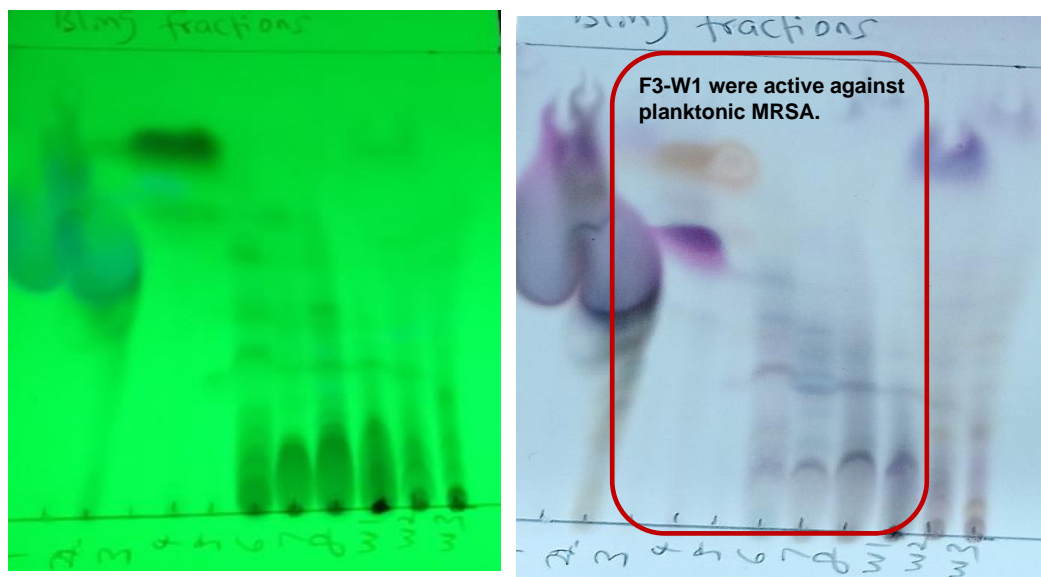


Figure 8.16: Summary TLC Plate of *F. proliferatum*-*F. falciforme* pooled fractions before (UV bands) and after spraying with anisaldehyde-sulphuric acid. The TLC plate showed fractions from the non-polar solvent of hexane to the more polar solvent of ethylacetate (100% Hexane-100% ethylacetate). Bioactive fractions are highlighted in red box.

Table 8.10: Extract yields of *F. proliferatum*-*F. falciforme* co-culture fractions

Sample	Weight (mg)
F1	179.9
F2	36.3
F3	20.9
F4	15.6
F5	45.7
F6	132.5
F7	102.7
F8	41.7
W1	97.6
W2	10.4
W3	19.7

8.2.8 Bioactivity test results of *F. proliferatum*-*F. falciforme* fractions

The fractions obtained from fractionation of the co-culture extracts of *F. proliferatum* and *F. falciforme* was subjected to biological assay against MRSA. Fractions 3 to 8 and W1 showed antimicrobial activity while fractions 1, 2, W2 and W3 were inactive. Bioactivity threshold was set at 50.0% cell viability (50.0% inhibition). Fraction 2, 4 to 8 and W1 to W3 were prebiofilm active. None of the fractions was postbiofilm active. Active fractions for further work were selected based on planktonic activity. Except for fraction 3, other active fractions exhibited strong activity.

The bioactivity was in the decreasing order: W1> F8> F6> F7>F5>F4>F3.

Table 8.11: Summary of bioactivity of *F. proliferatum*-*F. falciforme* fractions against MRSA Planktonic, prebiofilm, and postbiofilm percentage viability.

Fractions	Antimicrobial % Inhibition	Prebiofilm % Inhibition	Postbiofilm % Inhibition
Fraction 3	51.1	19.7	35.9
Fraction 4	91.8	98.4	<0
Fraction 5	92.5	98.1	<0
Fraction 6	96.0	98.9	<0
Fraction 7	94.0	97.7	<0
Fraction 8	97.2	98.1	<0
Fraction W1	97.5	99.1	<0

Cells with blue colour indicates active fractions against MRSA, while white cells indicate inactive fractions.

8.2.9 NMR spectroscopy for *F. proliferatum*-*F. falciforme* co-culture fractions

The ¹H NMR spectra of the bioactive fractions were stacked and presented in Figure 8.17. A high intensity of aliphatic peaks could be observed in the recorded ¹H NMR spectra of the fractions. Peaks between 4 and 4.5 ppm, 5 and 5.5 ppm, 5.5 and 7.2 ppm, as well as 12.0 to 13.0 ppm represented sugars, olefinics, aromatics, carboxylic acids and the exchangeable protons respectively, although the incidences and intensities of these chemical functions differ amongst the fractions, with F5 having more peak incidences at the downfield region.

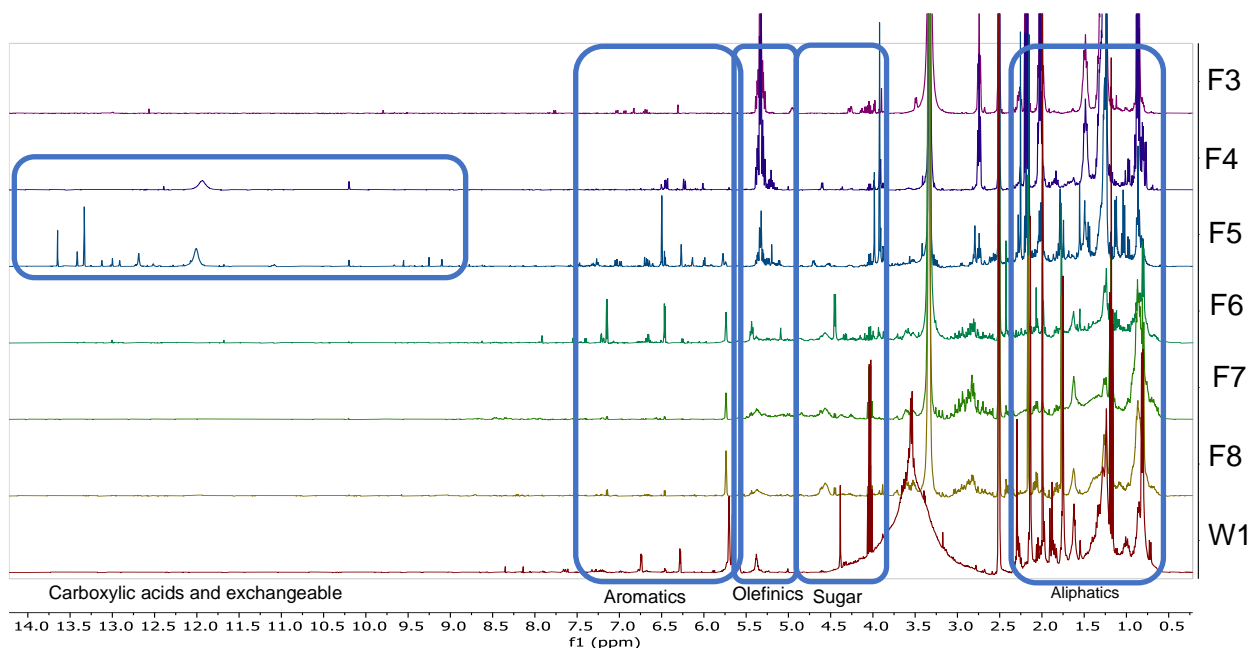


Figure 8.17: Stacked ¹H NMR spectra of the bioactive *F. proliferatum*-*F. falciforme* fractions consisting of F3, F4, F5, F6, F7, F8, W1.

The PCA scores scatter plot (Figure 8.18A) showed that fractions 1 to 5 were at proximity to each other, likewise, fractions 6 to 8 and wash 1 to 3, indicating similarity in their chemical profile, which follows the polarity trend for chromatographic separation. The loadings plot (Figure 8.18B) indicated that the chemical shifts of the discriminating metabolites were within the range of 1.0 to 4.0 ppm, which belongs to the aliphatics and sugars, respectively. In the generated model at pareto scaling, the R_2 was 0.972 while Q_2 was 0.514 at seven components which indicated a good fitted and predictability model.

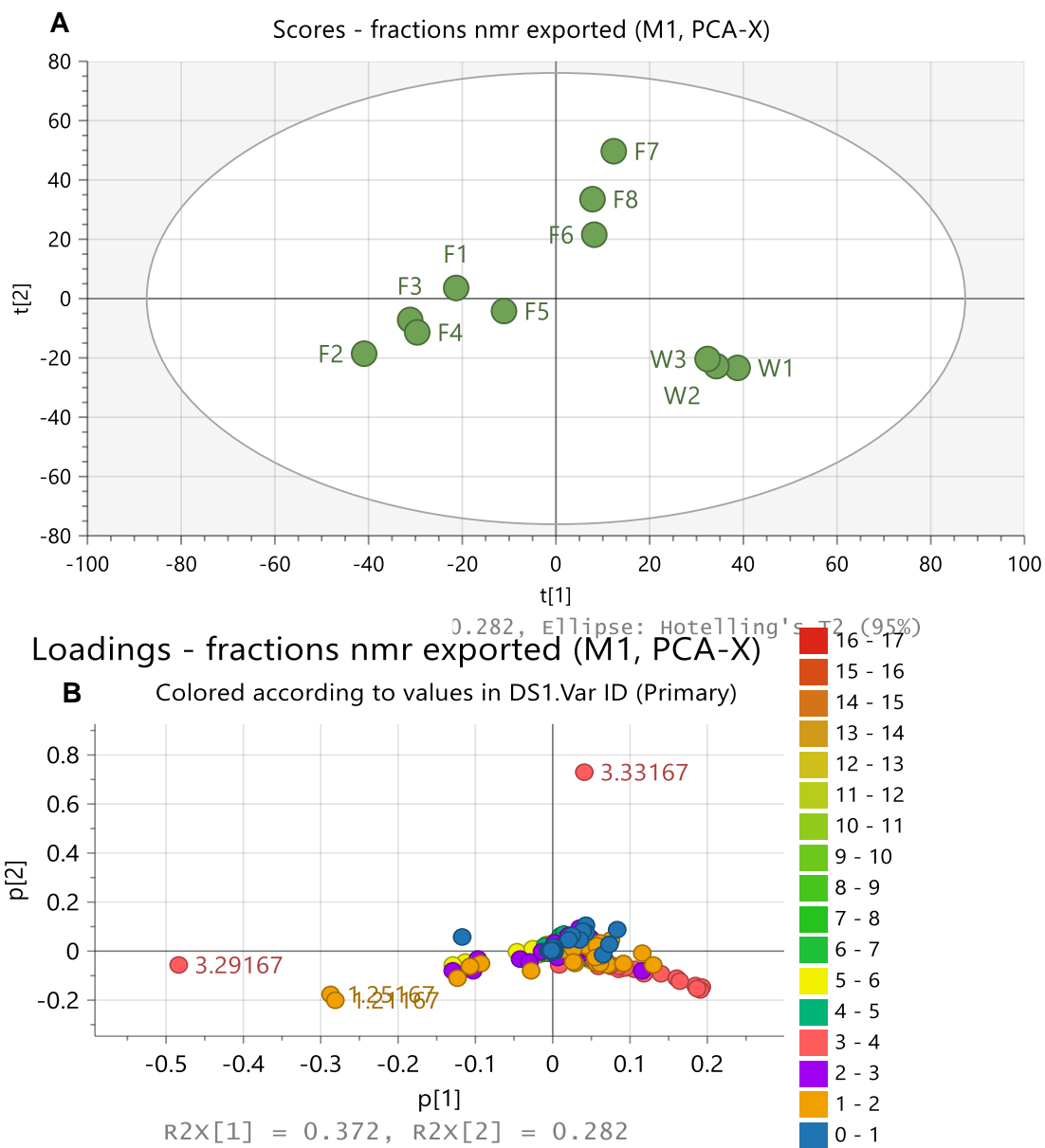


Figure 8.18: (A) PCA scatter and (B) loading plots of the NMR spectral data of the active fractions. The R_2X and Q_2X values were 0.972 and 0.514, respectively.

An OPLS-DA (Figure 8.19) was also performed to indicate the discriminating signals for the active and inactive fractions. The active fractions (red circles) were clustered at the upper and lower left quadrants, while the inactive fractions were clustered on the upper and lower right quadrant of the OPLS-DA scores plot. R_2 and Q_2 values were 0.999 and 0.662, respectively. The difference between group R_2X_0 [1] is equal to 68.2%, and the difference within groups R_2X [2] is 14.3%. There was an excellent separation between the active and inactive clusters, as the variation score between groups is greater than within groups. The proximity of active fractions 2, 3, 5 and 6 on the scores plot indicates they could have similar chemical profiles.

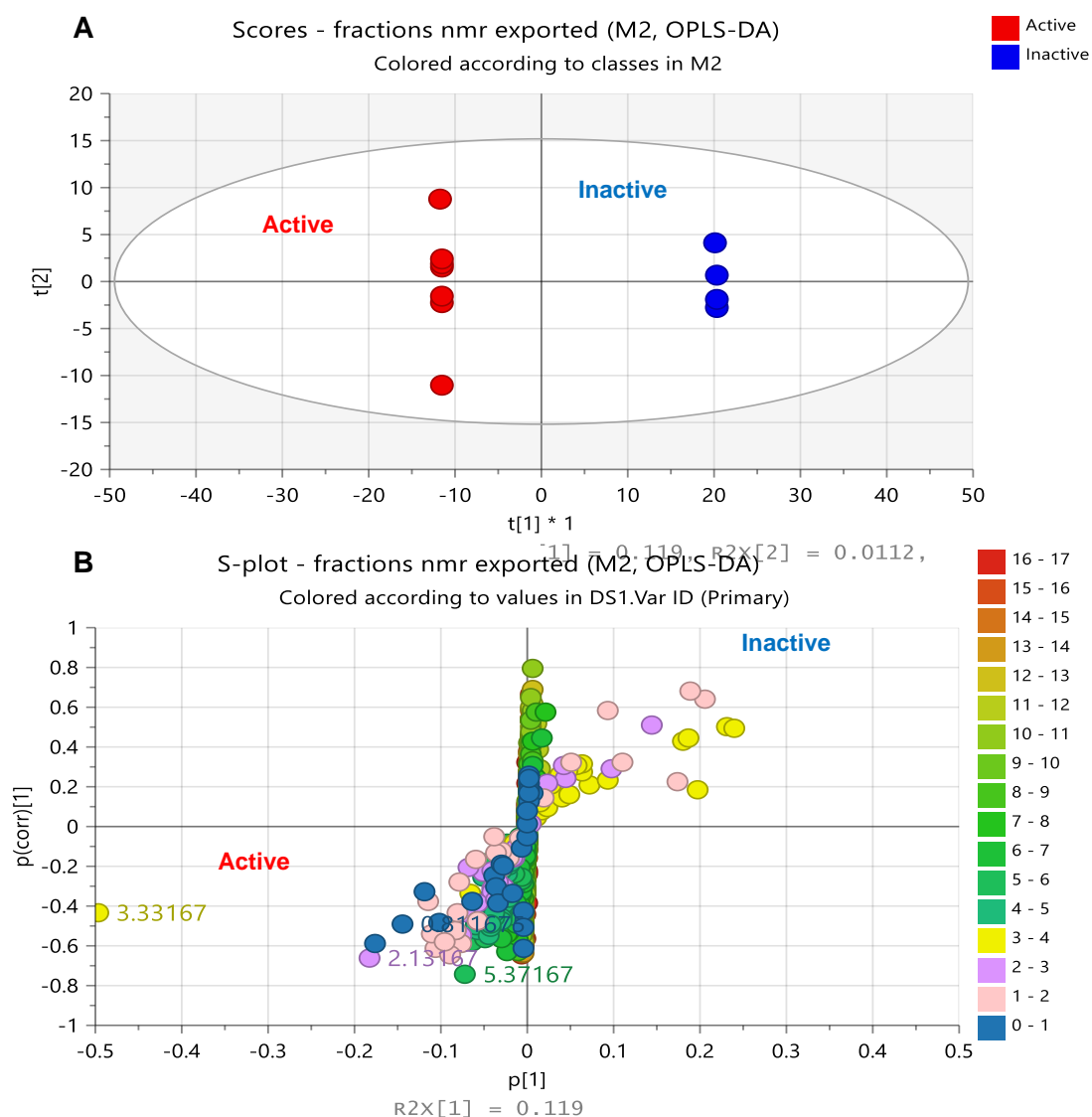


Figure 8.19: OPLS-DA scores (A) and (B) S plots of the NMR spectral data of *F. proliferatum*-*F. falciforme* fractions grouped according to their bioactivity against MRSA. R_2 and Q_2 values were 1.0 and 0.318, respectively. The difference between group R_2X_0 [1] is equal to 11.9 % and the difference within groups R_2X [2] is 1.1 %.

OPLS-DA indicated the top 20 VIP which showed that the discriminatory metabolites mostly consisted of aliphatics and sugars ranging from 0.81 to 3.53 ppm. Discriminating metabolites observed on both VIP and heat map had common chemical shifts of 1.21, 3.41, 3.45, 3.37, 1.13, 3.49, 1.09, 2.13, 0.81, 0.85 and 2.09 ppm representing aliphatics and sugars.

The spectral bins of each fraction have three replicates of each fraction, for analysis on MetaboAnalyst®. The heatmap showed that the active fractions (purple box) exhibited high concentration of metabolites. The wash (green box) also showed a high concentration of extracts but was inactive. These extracts could be active or inactive depending on the concentration of metabolites obtained and the solvent used for the wash.

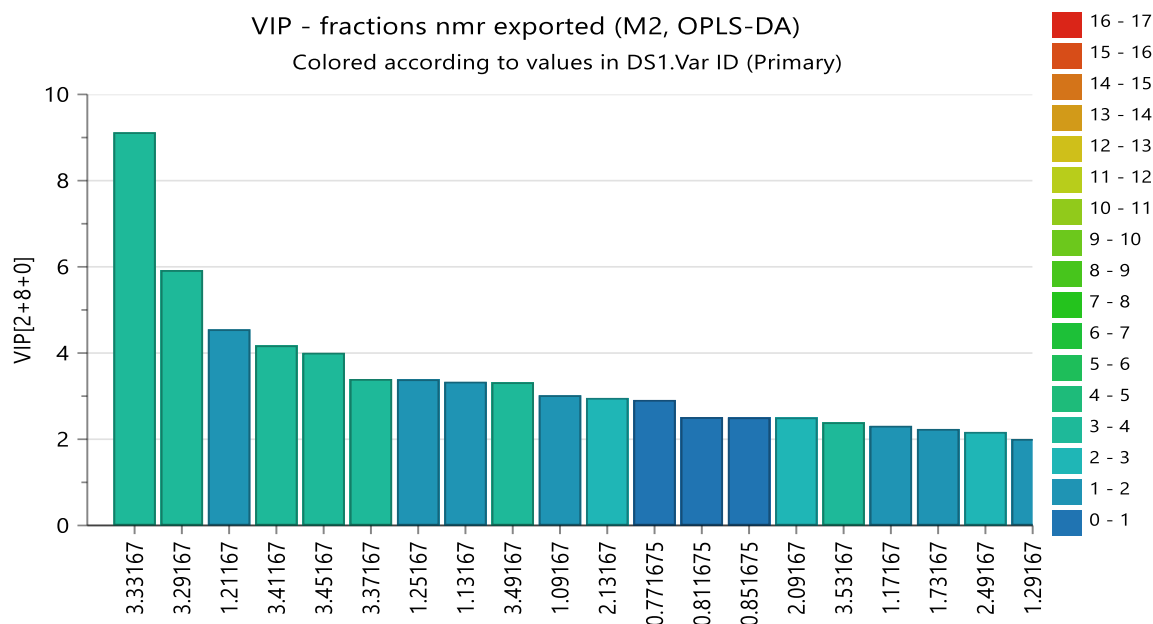


Figure 8.20: VIP scores of *F. proliferatum*-*F. falciforme* fractions from Simca® showing the chemical shifts of 20 most discriminating metabolites with VIP scores above 1. The top 20 VIP showed that the discriminatory metabolites mostly consisted of aliphatics and sugars ranging between 0.81 to 3.53 ppm.

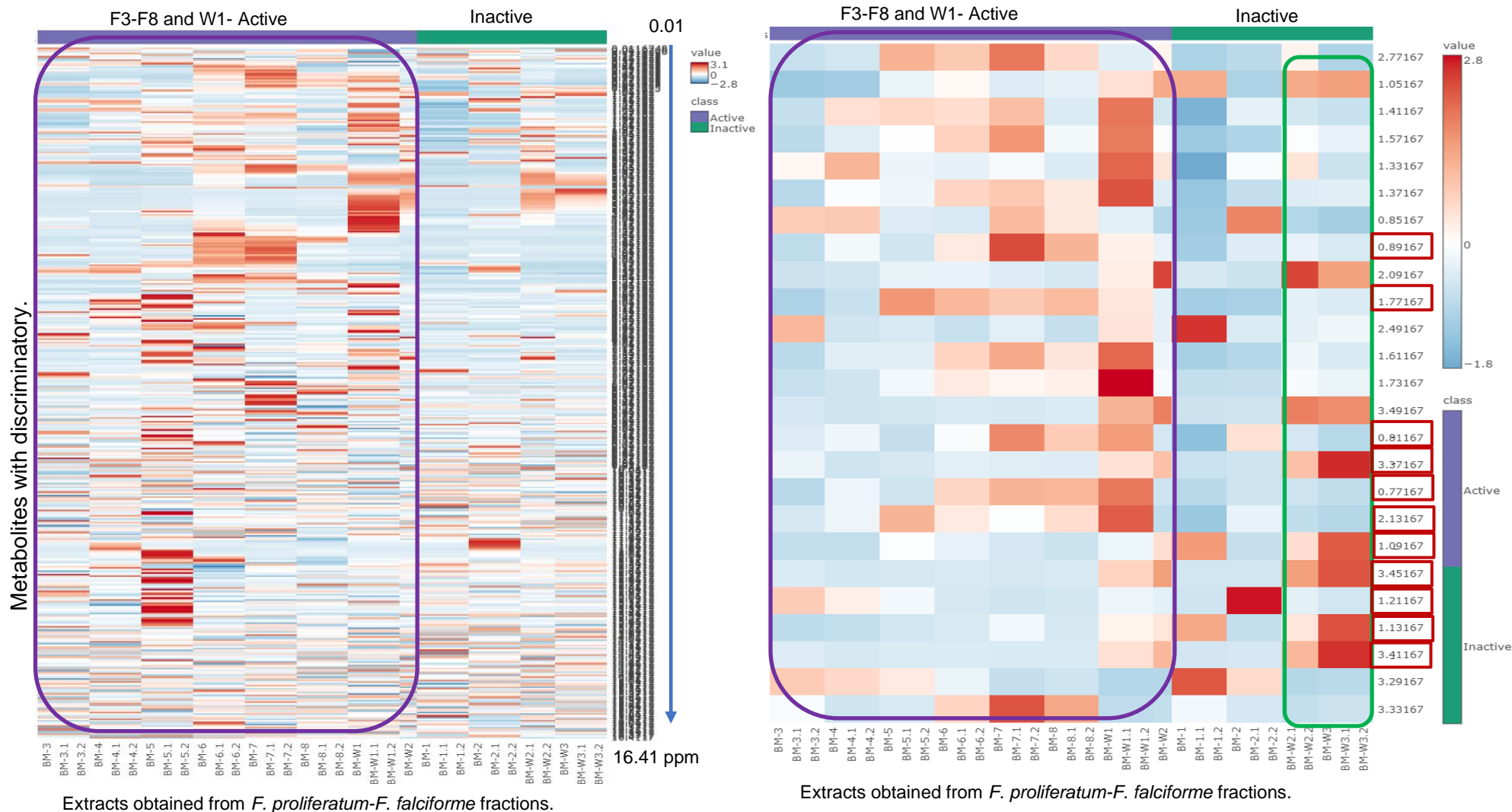


Figure 8.21: Heatmap analysis of the NMR spectral data of *F. proliferatum*-*F. falciforme* fractions generated by MetaboAnalyst®. The purple boxed fractions are those biologically active against MRSA along with the discriminating chemical shifts. The green boxed fraction (wash) was discriminatory but inactive. Highlighted chemical shifts on the Y-axis indicate common metabolites observed on the heatmap and VIP.

8.2.10 LC-HRMS analysis of *Fusarium* fractions

MVA of the HR-LCMS spectral data was done, the unsupervised PCA scores plot showed the fractions to spread across the quadrant (Figure 8.22A). The loadings plot (Figure 8.22B) indicated the presence of discriminating metabolites with low m/z values ranging between 181 to 1202.85 Da. The discriminating metabolites with Mzmine IDs of P13165, P15544, P5625, P11362, P1239, P11328 represented by m/z 275.091, 291.086, 181.088, 307.19, 325.2 and 343.211 were putatively identified as dihydroanhydrojavanicin, javanicin, 3-propylgentisylquinone, ML263A, hymeglusin, phomolide C respectively, all of which are fungal metabolites and have been identified from the early stages of the chemical screening work. Five ion peaks gave no hits. Most of these compounds were previously putatively identified from the monoculture of *F. falciforme* as shown in chapter 5, signifying its dominance over *F. proliferatum*. The model gave goodness of fit, (R_2) and predictability, Q_2 values as 0.920 and 0.488, respectively after 5 components. The dereplicated discriminating features of *F. proliferatum-F. falciforme* fractions were shown in Table 8.12.

The OPLS-DA of the active versus the inactive fractions gave fitness and predictability scores of 1.00 and 0.604 respectively. The difference between group R_2X_0 [1] is equal to 32.3 % and the difference within groups R_2X [2] is 11.5%. The scores plot (Figure 8.23A) shows a very good separation between the active versus inactive fractions. The active fractions (red circles) were on the right quadrant, while the inactive fractions (blue circles) were on the left quadrant. The loadings plot shows the discriminating features for the active fractions to be low to high molecular weight values with ion peaks ranging between m/z 275 and 1203 Da. Discriminatory active metabolites dereplicated in Table 8.13 and putatively identified from the OPLSDA S-plot, were also identified in the dereplicated PCA loadings plot, while 8 ion peaks gave no hits.

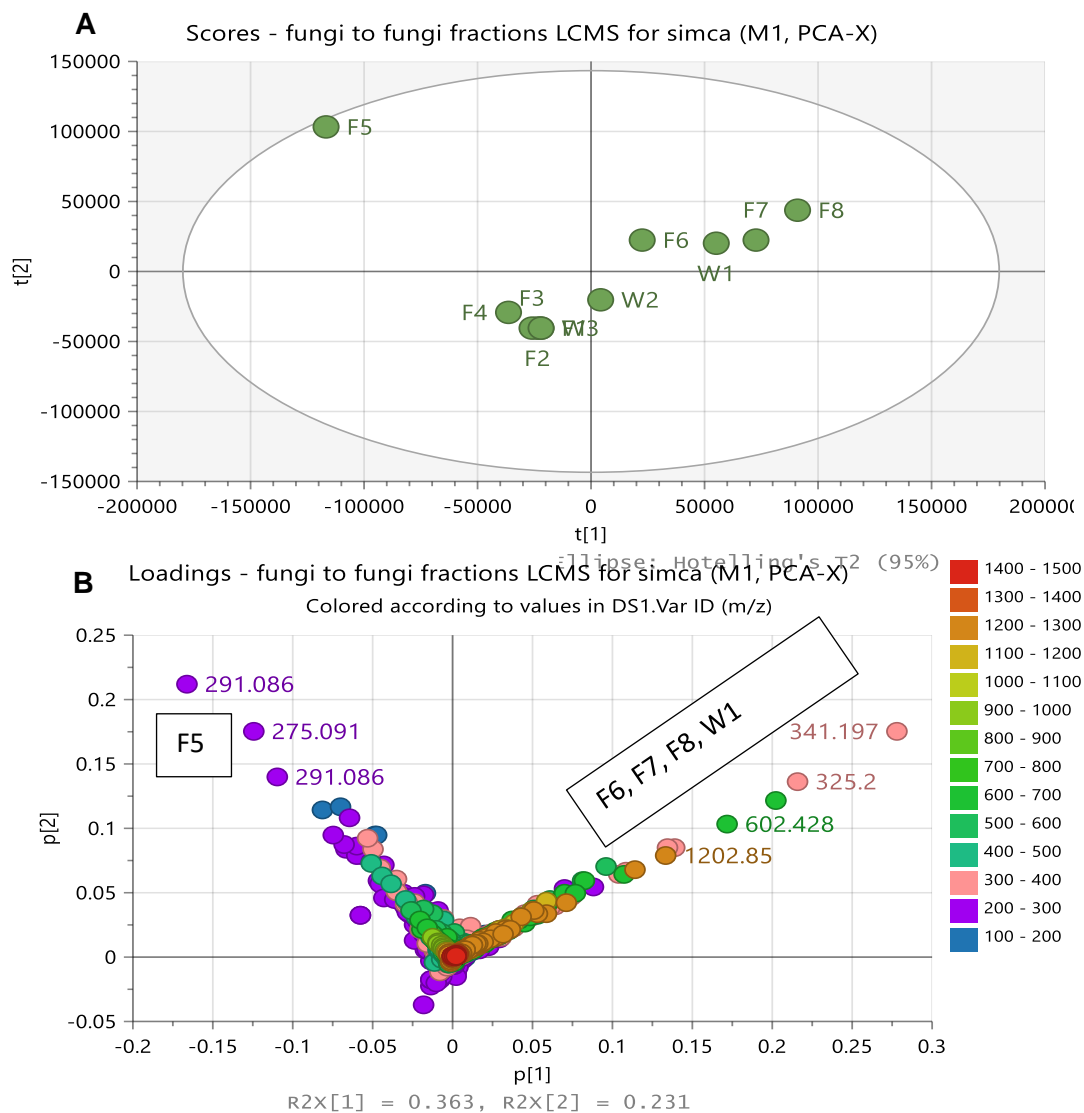


Figure 8.22: PCA scores (A) and loadings (B) plots of the LC-HRMS data of co-cultured *F. proliferatum*-*F. falciforme* fractions. Labelled features represent the discriminating ion peaks. The R_2 and Q_2 values were 0.920 and 0.488 respectively.

Table 8.12: Dereplicated compound hits for the discriminating metabolites from respective fractions of co-cultured *Fusarium* endophytes obtained from the PCA loadings plot on Figure 8.22B. Highlighted in green were the isolated compounds.

Mzmine ID	m/z	Rt	M.wt	Molecular Formular (DBE)	Compound hits	Biological source
F5						
P13165	275.091	12.39	274.084	C ₁₅ H ₁₄ O ₅ (9)	Dihydroanhydrojavanicin	<i>Fusarium solani</i>
P15544	291.086	13.40	290.079	C ₁₅ H ₁₄ O ₆ (9)	Javanicin	<i>Fusarium javanicum</i> , <i>F martici-pisi</i> , <i>F solani</i> , <i>Nectria haematococca</i> , <i>Neocosmospora vasinfecta</i> and a <i>Chloridium</i> sp.
F4						
P5625	181.086	8.73	180.079	C ₁₀ H ₁₂ O ₃ (5)	3-Propylgentisylquinone	Fungal isolate CR1223-D
F6, F7, F8, W1						
P11362	307.19	11.72	306.183	C ₁₈ H ₂₆ O ₄ (6)	ML263A	<i>Eupenicillium javanicum</i> IFM 52670 and <i>Penicillium citrinum</i> Sank 18767
P11239	325.2	11.62	324.193	C ₁₈ H ₂₈ O ₅ (5)	Hymeglusin	<i>Cephalosporium</i> sp., <i>Scopulariopsis</i> sp. and <i>Fusarium</i> sp.
P11347	326.204	11.63	325.196		No hit	
P11328	343.211	11.62	342.204	C ₁₈ H ₃₀ O ₆ (4)	Phomolide C	<i>Phomopsis</i> sp. B27
N4896	342.2	11.62	343.207		No hit	
P25887	594.92	17.90	593.913		No hit	
P26406	601.927	18.24	600.92		No hit	
P26363	602.428	18.11	601.421		No hit	
P26376	602.931	18.10	601.923		No hit	
P26456	1202.85	18.17	1201.84		No hit	

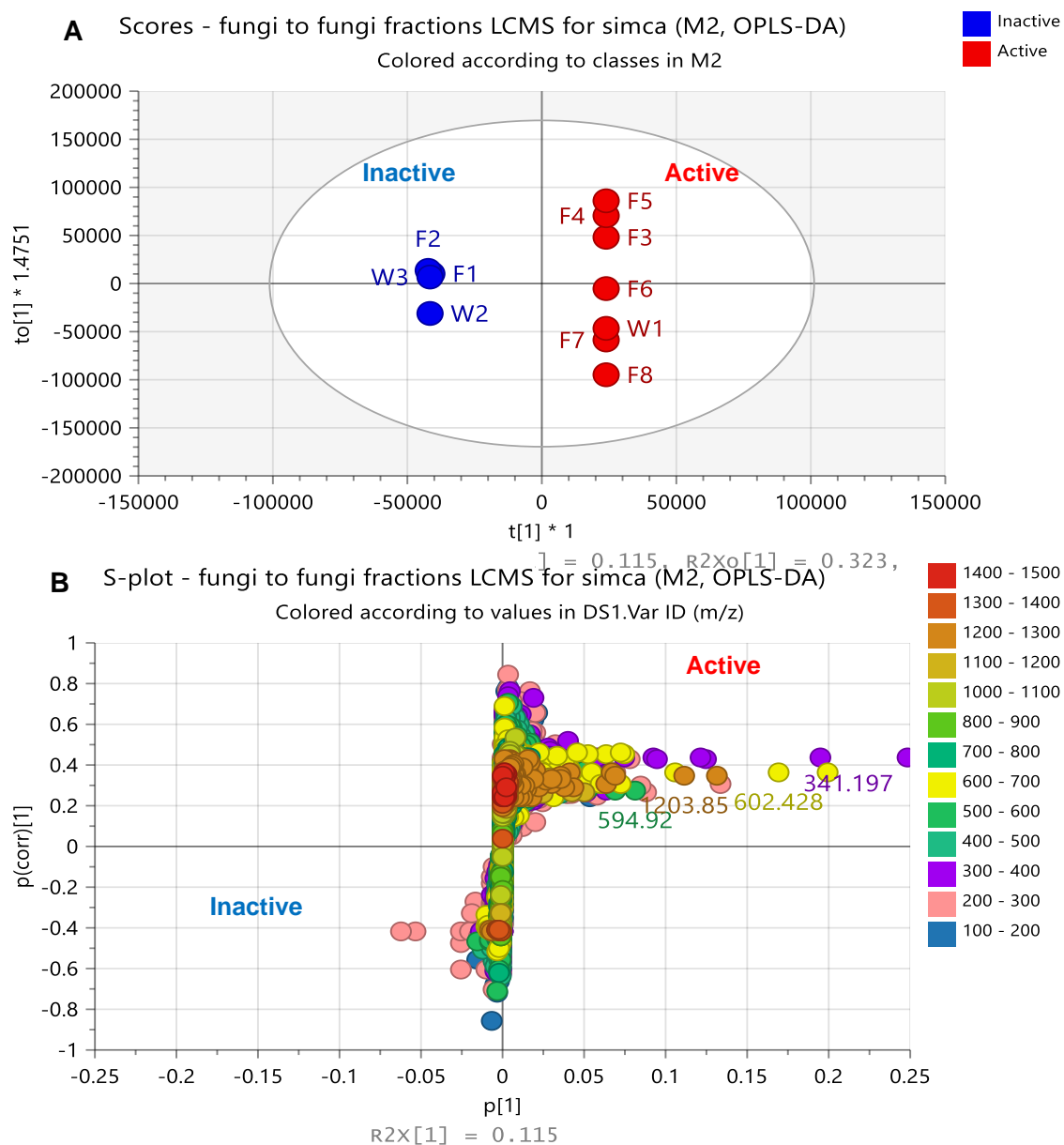


Figure 8.23: OPLS-DA scores (A) and S-plot (B) of the LC-HRMS data of *F. proliferatum*-*F. falciforme* fractions. Labeled features represent the discriminating active fractions. The R^2 and Q^2 values were 1 and 0.604 respectively. The difference between group R^2_{Xo} [1] is equal to 32.3 % and the difference within groups R^2_X [2] is 11.5 %.

Table 8.13: Dereplicated compound hits for the antibacterial-active discriminating active metabolites of fractions from co-cultured *Fusarium* endophytes obtained from the OPLS-DA S-Plot on Figure 8.23B. Highlighted in green were the isolated compounds.

Mzmine ID	m/z	Rt	M.wt	P-value	Molecular Formular (DBE)	Compound hits	Biological source
P13165	275.091	12.39	274.084	0.435067	C ₁₅ H ₁₄ O ₅ (9)	Dihydroanhydrojavanicin	<i>Fusarium solani</i>
P15544	291.086	13.40	290.079	0.352837	C ₁₅ H ₁₄ O ₆ (9)	Javanicin	<i>Fusarium javanicum</i> , <i>F. martici-pisi</i> , <i>F. solani</i> , <i>Nectria haematococca</i> , <i>Neocosmospora vasinfecta</i> and a <i>Chloridium</i> sp.
P11362	307.19	11.72	306.183	0.187131	C ₁₈ H ₂₆ O ₄ (6)	ML263A	<i>Eupenicillium javanicum</i> IFM 52670 and <i>Penicillium citrinum</i> Sank 18767
P11239	325.2	11.62	324.193	0.176739	C ₁₈ H ₂₈ O ₅ (5)	Hymeglusin	<i>Cephalosporium</i> sp., <i>Scopulariopsis</i> sp. and <i>Fusarium</i> sp.
P11347	326.204	11.63	325.196	0.181697		No hit	
P11328	343.211	11.62	342.204	0.188561	C ₁₈ H ₃₀ O ₆ (4)	Phomolide C	<i>Phomopsis</i> sp. B27
N4896	342.2	11.62	343.207	0.175649		No hit	
P25887	594.92	17.90	593.913	0.409679		No hit	
P26406	601.927	18.24	600.92	0.269804		No hit	
P26363	602.428	18.11	601.421	0.269465		No hit	
P26376	602.931	18.10	601.923	0.271343		No hit	
P26456	1202.85	18.17	1201.84	0.295628		No hit	
P26475	1203.85	18.14	1202.84	0.29590		No hit	

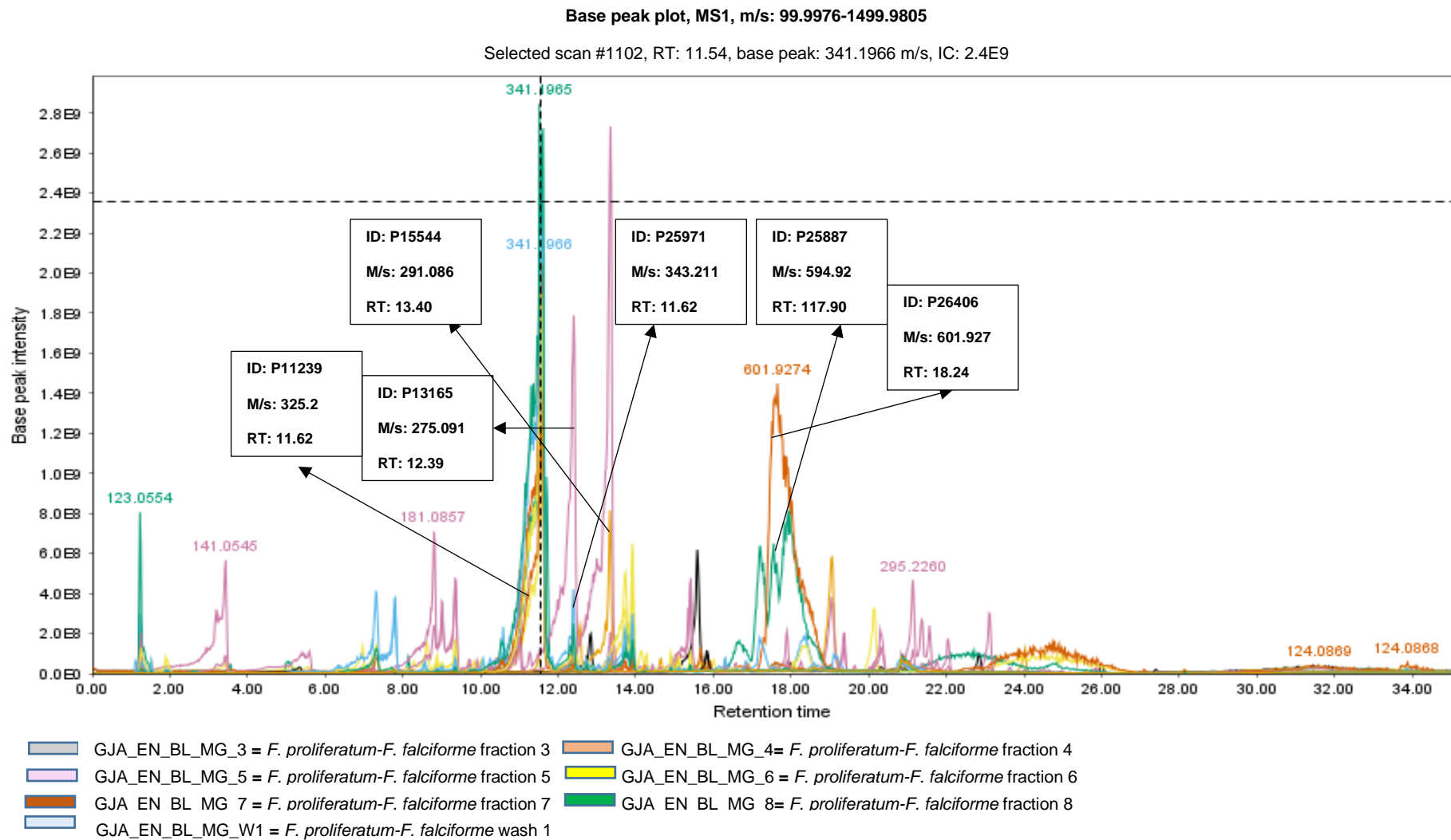


Figure 8.24: Total ion chromatogram (TIC) of the bioactive fractions of *F. proliferatum-F. falciforme*. The ion peaks that represent the discriminating features listed in table 8.13 have been labelled.

8.2.11 Pure compound isolation

Fractions were selected for further purification work due to antimicrobial activity against MRSA. Planktonic active fractions F3 to F8 and W1 (wash 1) were selected for purification work.

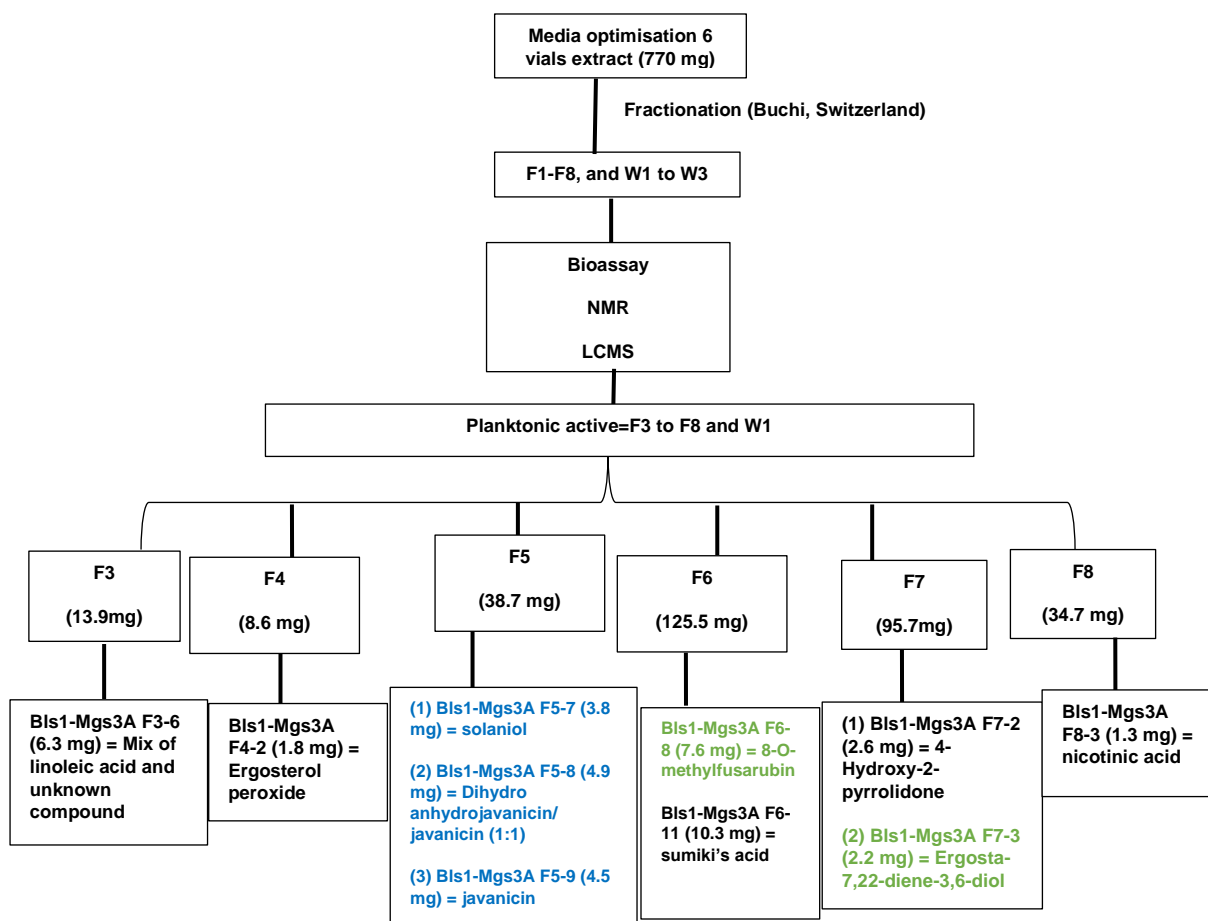
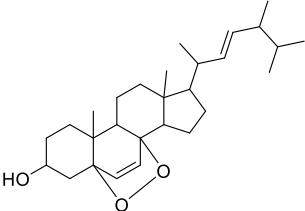
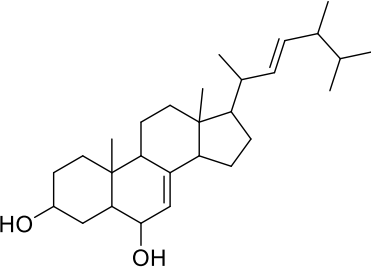
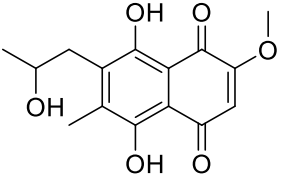
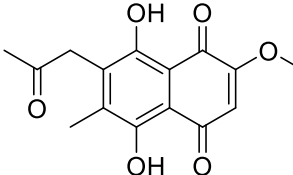
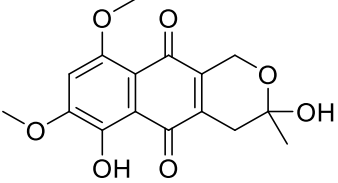
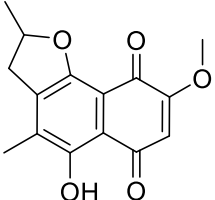
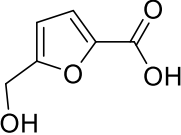
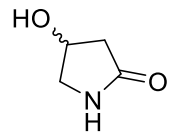
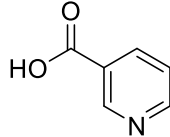
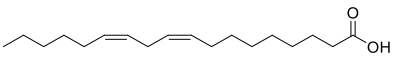


Figure 8.25: Summary workflow of *F. proliferatum*-*F. falciforme* co-culture crude extract to isolated compounds. Compounds with above 70% planktonic activity against MRSA are coloured blue, while compounds within the range of 60%-69% bioactivity are coloured green. Inactive subfractions were not considered for further purification work.

Table 8.14: Isolated pure compounds from co-culture of *F. proliferatum*-*F. falciforme*.

Drawn Structure	Name	Exact mass	Molecular Formula	Source Fraction	Weight (mg)	Purification method
	ergosterol peroxide (Shin <i>et al.</i> , 2001)	428.329	C ₂₈ H ₄₄ O ₃	F4-2	1.8	Preparative TLC
	ergosta-7,22-diene-3,6-diol (Compared with ergosterol peroxide (Shin <i>et al.</i> , 2001)	414.350	C ₂₈ H ₄₆ O ₂	F7-3	2.2	Preparative TLC
	solaniol (Kehelpannala <i>et al.</i> , 2021)	292.095	C ₁₅ H ₁₆ O ₆	F5-7	3.8	Preparative TLC
	javanicin (Moni <i>et al.</i> , 2022).	290.079	C ₁₅ H ₁₄ O ₆	F5-9	4.5	Preparative TLC

Drawn Structure	Name	Exact mass	Molecular Formula	Source Fraction	Weight (mg)	Purification method
	8-O-methylfusarubin (Tatum and Baker, 1983)	320.090	C ₁₆ H ₁₆ O ₇	F6-8	7.6	Biotage
	Dihydroanhydrojavanicin (Compared with javanicin (Moni <i>et al.</i> , 2022).	274.084	C ₁₅ H ₁₄ O ₅	F5-8	4.9	Preparative TLC
	Sumiki's acid (Jadulco, 2002)	142.027	C ₆ H ₆ O ₄	F6-11	10.3	Biotage
	4-Hydroxy-2-pyrrolidone (Huang <i>et al.</i> , 1999)	101.048	C ₄ H ₇ NO ₂	F7-2	2.6	Preparative TLC
	Nicotinic acid (Wishart <i>et al.</i> , 2009)	123.032	C ₆ H ₅ NO ₂	F8-3	1.3	Preparative TLC
	Mix linoleic acid and unknown compound	280.240	C ₁₈ H ₃₂ O ₂	F3-6	6.3	Preparative TLC

8.2.12: Bioactivity test results

The pure compounds obtained from the extracts of co-cultures of *Fusarium proliferatum* and *F. falciforme* were subjected to a biological assay against MRSA ATCC 43300 at concentrations of 100 µg/ml. MRSA planktonic inhibitions were observed in solaniol (F5-7, 86.34%), dihydroanhydrojavanicin (F5-8, 85.05%) and javanicin (F5-9, 91.21%), while the other compounds were inactive, as they exhibited activity below the 70% inhibition threshold at 8-O-methylfusarubin (F6-8, 65.38%), ergosta-7,22-diene-3,6-diol (F7-3, 67.61%), Sumiki's acid (F6-11, 13.27%), 4-hydroxy-2-pyrrolidone (F7-2, 15.74%) and nicotinic acid (F8-3, 19.04%). Ergosterol peroxide (F4-2) did not show any activity at all. Unusually, F3-6 containing linoleic acid as the main component was found active exhibiting 81.56% inhibition of planktonic MRSA. Comparing this result with the inactivity of linoleic acid isolated from the *Alternaria* (DGS2) extract, the bioactivity of F3-6 can be assigned to a second component that remains unidentified. The presence of another compound can be observed in the ¹H-NMR data when the two purified fractions (DGS2-F7-3 and BLS1-MgS3A-F3-6) were compared as shown in Figure 8.26.

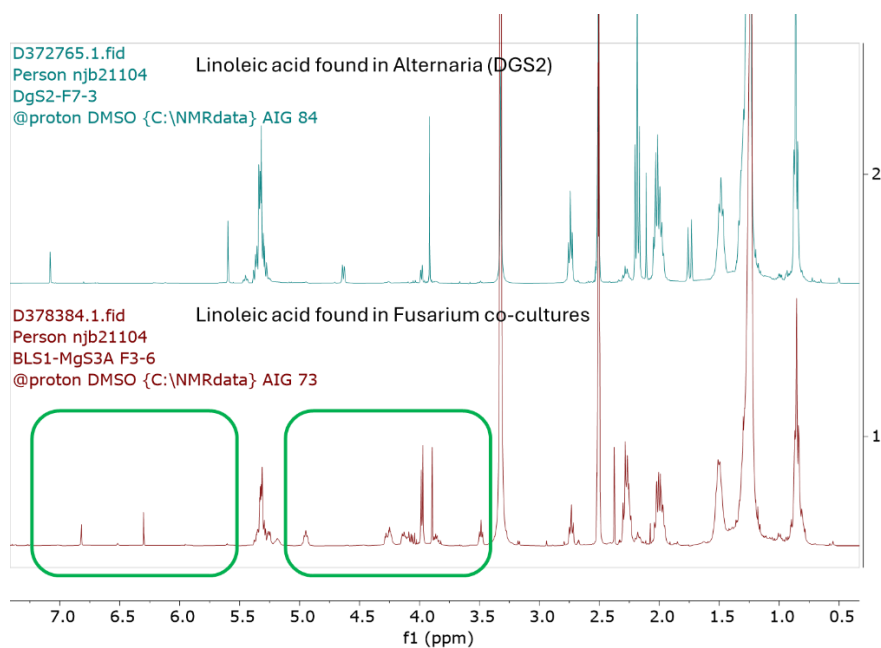


Figure 8.26 Comparison of the ¹H-NMR data of linoleic acid isolated from *Alternaria* (DGS2) and the *Fusarium* co-culture. Green boxes show the occurrence of a second and third components that have not been identified in this study.

The mass spectral data F3-6 did exhibit an ion peak at m/z 305.101 [M+H]⁺ for C₁₆H₁₇O₆ (Figures 8.27A, B, and C), which was dereplicated as bostrycin and methoxylated congener javanicin. The ¹H NMR spectrum (Figure 8.27D) did show resonances for a methyl-ether

derivative of javanicin. However, the methoxylation will need to be proven by HMBC after another needed purification step, which was no longer feasible with the remaining amount of fraction available. The red band observed on the preparative TLC plate exemplified the occurrence of the said naphthoquinone congener as well (Figure 8.27B). Only this naphthoquinone congener could be possibly responsible for the bioactivity of F3-6.

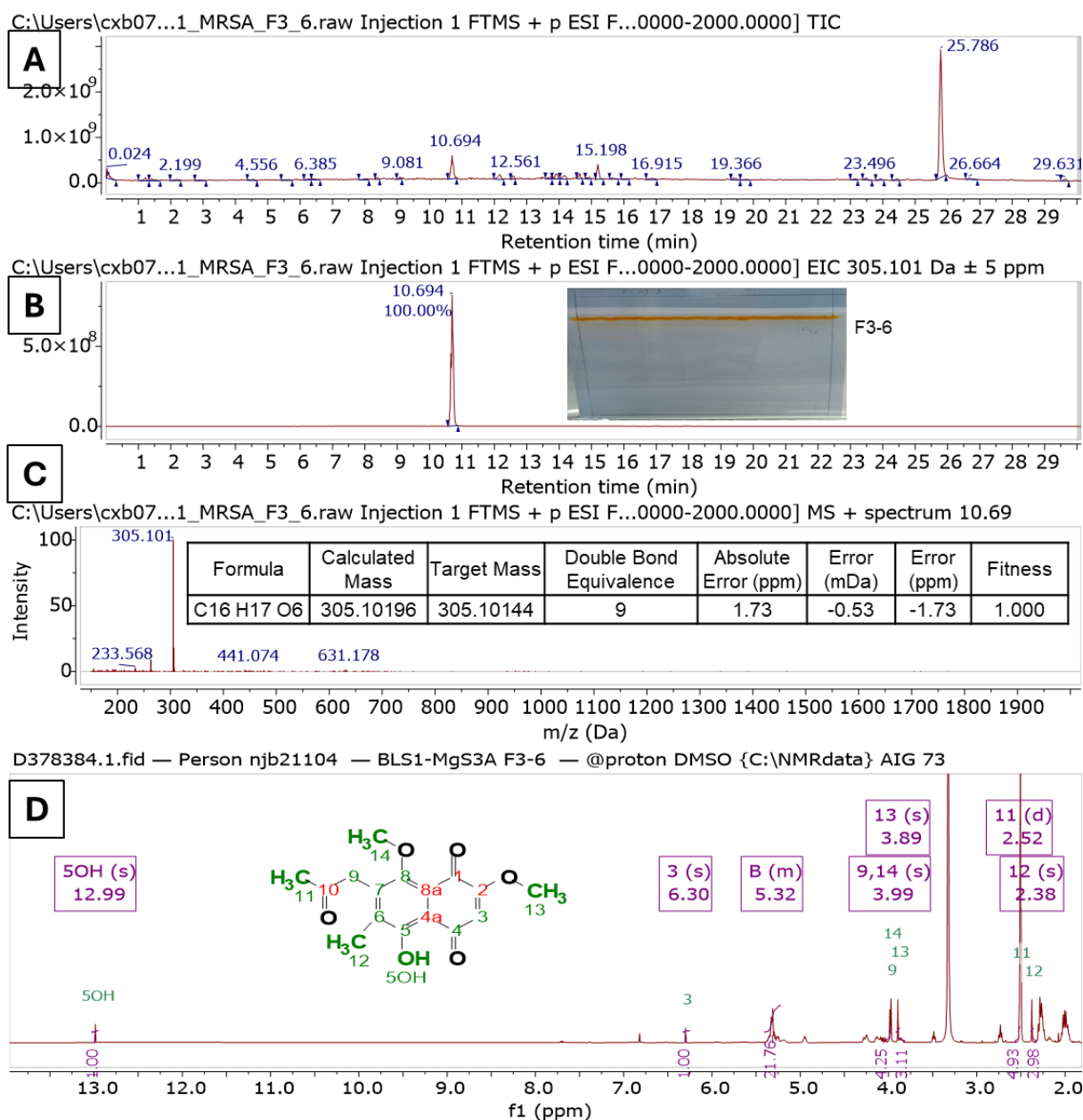


Figure 8.27. Mass and NMR spectral data of F3-6 indicating the occurrence of a methyl-ether derivative of javanicin. A) TIC of F3-6, B) EIC for ion peak at m/z 305.101 $[M+H]^+$ and TLC band for F3-6. C) Mass spectrum for ion peak at m/z 305.101 $[M+H]^+$ for C₁₆H₁₇O₆. D) ¹H NMR spectrum of F3-6 showing the proton assignments for a methyl-ether derivative of javanicin in DMSO-d₆.

Prebiofilm inhibition against MRSA ATCC 43300 was observed only amongst the naphthoquinones namely solaniol (96.57%), dihydroanhydrojavanicin (98.06%), javanicin (97.80%) and 8-*O*-methylfusarubin (77.46%). For postbiofilm, disruption of biofilm in MRSA was observed in ergosta-7,22-diene-3,6-diol (84.33%), 4-hydroxy-2-pyrrolidone (83.28%) and nicotinic acid (79.92%), while the other compounds were inactive. It can be deduced that seven of the isolated compounds were able to exhibit pronounced bioactivity that is above the 70% bioactivity threshold requirement against MRSA either at the planktonic, prebiofilm or postbiofilm stages.

The isolated compounds were also tested against SA-NCTC 8325 at concentrations of 100µg/ml. MRSA planktonic inhibitions were observed in solaniol (88.60%), dihydroanhydrojavanicin (88.27%), javanicin (92.12%) and 8-*O*-methylfusarubin (89.48%). In contrast, F3-6 (67.13%), ergosterol peroxide (4.74%), ergosta-7,22-diene-3,6-diol (24.21%), sumiki's acid (41.67%), 4-hydroxy-2-pyrrolidone (18.60%) and nicotinic acid (16.41%) were inactive.

For prebiofilm activity against SA-NCTC 8325, activity was observed on solaniol (100.00%), dihydroanhydrojavanicin (96.45%), javanicin (100.00%) and 8-*O*-methylfusarubin (99.74%). In parallel, structurally unrelated compounds to naphthoquinones showed inhibitions at F3-6 (93.16%), ergosterol peroxide (88.47%), ergosta-7,22-diene-3,6-diol (95.24%), 4-hydroxy-2-pyrrolidone (86.07%) and nicotinic acid (81.88%), while Sumiki's acid inhibited at only 64.89% (Figures 8.28).

The MIC and MBEC values (Figure 8.29) were calculated for compounds which exhibited inhibition activity against planktonic and prebiofilm MRSA at 80% and above. An MIC value of 12.5 µg/mL was obtained for solaniol, dihydroanhydrojavanicin and javanicin. MBEC values for solaniol gave 6.5 µg/mL and 25 µg/mL for both dihydroanhydrojavanicin and javanicin.

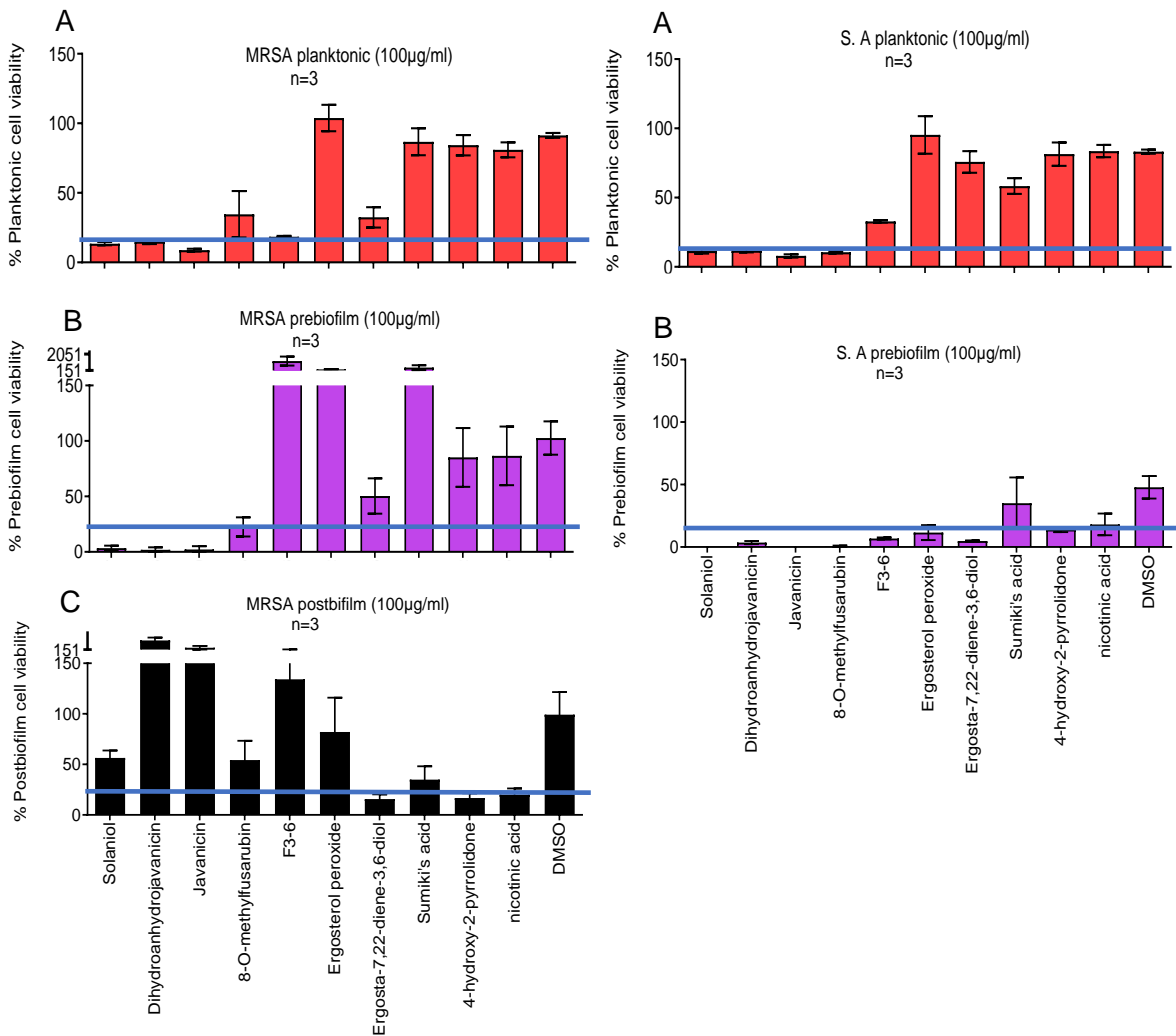


Figure 8.28: Effect of pure compounds isolated from *F. proliferatum*-*F. falciforme*. Left plots are the planktonic (A), prebiofilm (B), and postbiofilm (C) activity against MRSA. Right plots are the planktonic (A) and prebiofilm (B) activity on SA-NCTC 8325 at 100µg/mL. The blue line indicates the bioactivity threshold which is 20% viability (80.0% inhibition).

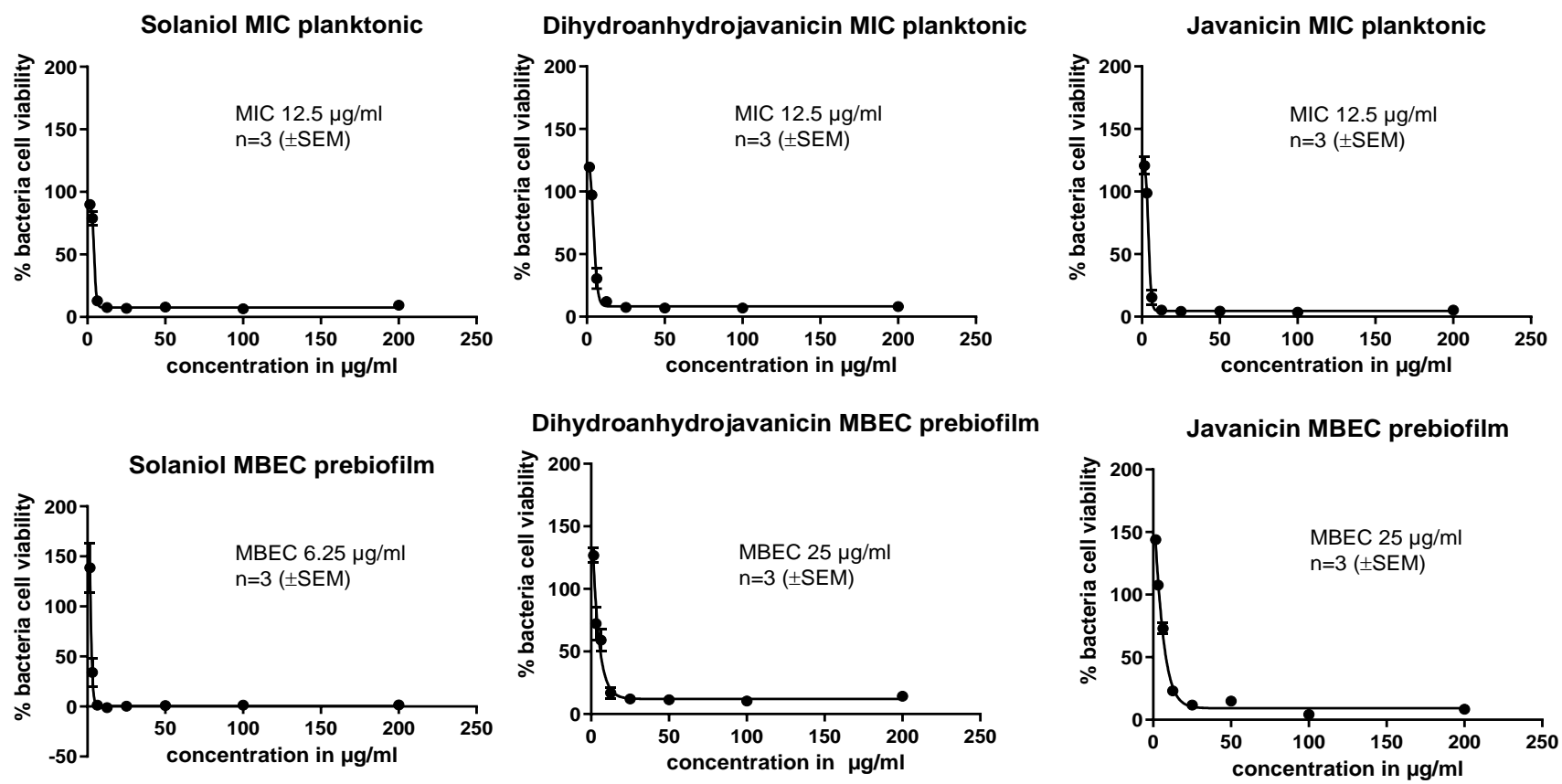


Figure 8.29: (Top) MIC and (Down) MBEC results of compounds with bioactivity above 80.00%.

IC₅₀ (μM) were obtained only for compounds which exhibited above 80% bioactivity threshold using graph pad prism 10.3.1.

Table 8.15: IC₅₀ (μM) for the bioactive isolated compounds against MRSA

Compound name	MRSA planktonic	IC ₅₀ (μg/ml)	IC ₅₀ (μM)	R ²
Solaniol	Active	4.21	14.42	0.99
Dihydrojavanicin	Active	4.47	16.32	0.99
Javanicin	Active	4.13	14.24	0.99
Compound name	MRSA prebiofilm	IC ₅₀ (μg/ml)	IC ₅₀ (μM)	R ²
Solaniol	Active	2.82	9.65	0.92
Dihydrojavanicin	Active	4.30	15.69	0.91
Javanicin	Active	5.81	20.02	0.98

Due to the poor or weak bioactivities of some of the isolated compounds, their positions were revisited on the OPLS-DA plot (Figures 8.23 and 8.13) by using their MW features as shown in Figures 8.30 and 8.31. It was observed that the isolated compounds namely 4-hydroxy-2-pyrrolidone (101.048), nicotinic acid (123.031), sumiki's acid (142.027), dihydroanhydrojavanicin (274.084), javanicin (290.079), solaniol (292.095), 8-O-methylfusarubin (320.090) and ergosterol peroxide (428.329) were found on the active quadrant of the OPLS-DA plots. This confirms the bioactivity of the isolated naphthoquinones, while indicating that the decreased activity of 4-hydroxy-2-pyrrolidone, nicotinic acid, ergosterol peroxide and sumiki's acid, needed to work in synergy with other compounds to be active. The isolated compounds identified on the active quadrant by OPLS-DA with their corresponding MW are listed in Table 8.16.

Isolated compounds of *F. proliferatum*-*F. falciforme* co-culture fungal extract obtained from scaled up fractions extract on malt extract media.

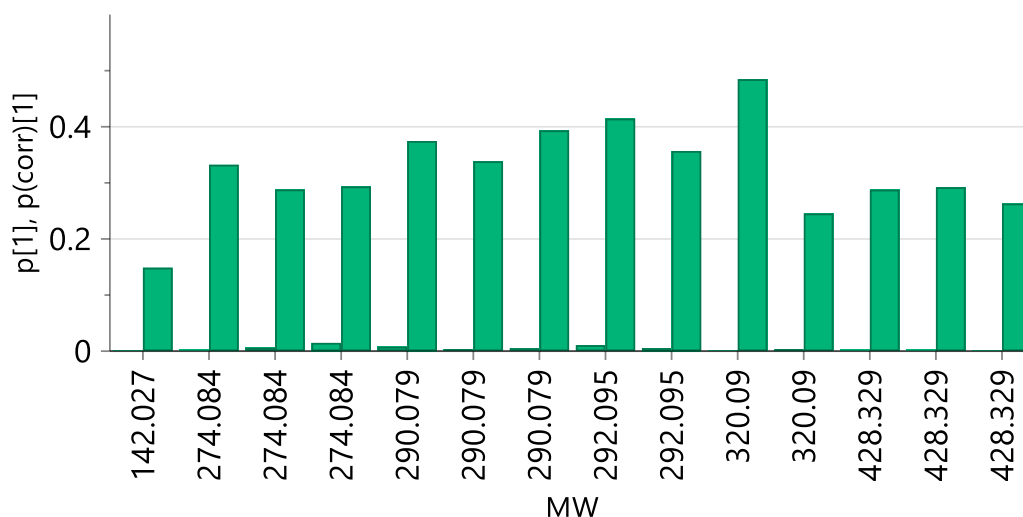


Figure 8.30: Distribution of the isolated compounds on the right active quadrant of the OPLS-DA loadings plot of the chromatographic fractions indicating the predicted bioactive compounds with molecular weights of 142.027 (sumiki's acid), 274.084 (dihydroanhydrojavanicin), 290.079 (javanicin), 292.095 (solaniol), 320.090 (8-O-methylfusarubin), 428.329 (ergosterol peroxide).

Isolated compounds *F. proliferatum*-*F. falciforme* co-culture fungal extract obtained from 15- and 30-days media optimisation fungal extracts.

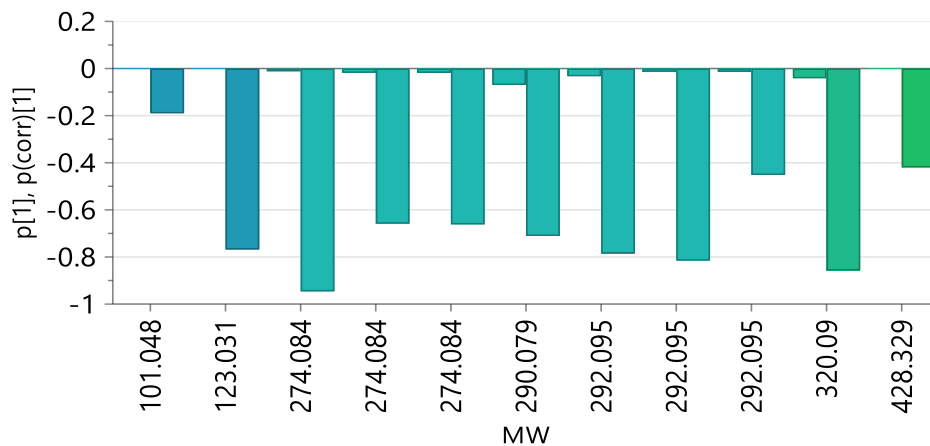


Figure 8.31: Distribution of the isolated compounds on the right active quadrant of the OPLS-DA loadings plot of the crude extracts indicating the predicted bioactive compounds with molecular weights of 101.048 (4-hydroxy-2-pyrrolidone), 123.031 (nicotinic acid), 274.084 (dihydroanhydrojavanicin), 290.079 (javanicin), 292.095 (solaniol), 320.090 (8-O-methylfusarubin), 428.329 (ergosterol peroxide).

Table 8.16: Isolated compounds observed on OPLS-DA active quadrant (fig. 8.23 and 8.13).

Highlighted rows represent active planktonic and prebiofilm metabolites that exhibited greater than 80% bioactivity threshold.

Isolated compounds	Name	MW	Biofilm Stages of Observed Bioactivity	Observed / unobserved on OPLS-DA active quadrant from the fraction stage (MW, primary ID, rt)	Isolated compounds observed on OPLS-DA active quadrant as obtained from media optimisation stage (MW, primary ID, rt)
F4-2	Ergosterol peroxide	428.329	Inactive	Observed in active quadrant (428.329, P38.221, rt= 28.95)	Observed in active quadrant (428.329, P11668, rt= 29.75)
F7-3	Ergosta-7,22-diene-3,6-diol	414.350	Planktonic (67.61%) and postbiofilm (84.33%)	Inactive quadrant (414.369)	Inactive quadrant (414.324)
F5-7	Solaninol	292.095	Planktonic and prebiofilm (>80.00%)	Observed in active quadrant (292.095, N1835, rt= 8.35)	Observed in active quadrant (292.095, P12971, rt= 11.75)
F5-9	Javanicin	290.079	Planktonic and prebiofilm (>80.00%)	Observed in active quadrant (290.079, P22910, rt= 16.43)	Observed in active quadrant (290.079, P12895, rt= 14.03)
F6-8	8-O-methylfusarubin	320.090	Planktonic (65.38%) and prebiofilm (77.46%)	Observed in active quadrant (320.090, P13089, rt= 12.35)	Observed in active quadrant (320.090, P5593, rt= 9.09)
F5-8	Dihydroanhydrojavanicin	274.084	Planktonic and prebiofilm (>80.00%)	Observed in active quadrant (274.084, N13448, rt= 19.19)	Observed in active quadrant (274.084, P18898, rt= 15.83)
F6-11	Sumiki's acid	142.027	Inactive	Observed in active quadrant (142.027, N16100, rt= 37.73)	Not detected*
F7-2	4-Hydroxy-2-pyrrolidone	101.048	Postbiofilm (83.28%)	Not detected*	Observed in active quadrant (101.048, P18898, rt= 24.46)
F8-3	Nicotinic acid	123.032	Postbiofilm (79.92%)	Inactive quadrant	Observed in active quadrant (123.031, N5957, rt= 11.19)

*MW is outside the measuring range of m/z 150 to 2000 Da.

8.3 Summary and conclusion

8.3.1 Media optimisation and metabolomics bioassay guided isolation

Endophytic fungi *F. proliferatum*, *F. falciforme* and *A. alternata* isolated in this study were co-cultured amongst themselves and tested against MRSA. Their co-cultures on malt extract agar at 7 days of incubation and malt extract broth incubated at 15 and 30 days showed co-cultures of *F. proliferatum* and *F. falciforme* to be the best exhibiting bioactivities of 97.53%, 91.60% and 94.40% inhibitions, respectively. It was observed that the NMR and LC-HRMS spectra of 15- and 30-days fungal extract of *F. proliferatum*- *F. falciforme* were similar, therefore the extracts from both incubation days were merged for purification works. This will be the first report on the co-culture of *F. proliferatum* and *F. falciforme*.

Extracts of the monoculture of *F. proliferatum* showed higher bioactivity than those from monocultures of *F. falciforme* and *A. alternata*. However, when *F. proliferatum* was co-cultured with *F. falciforme*, it showed that the metabolites from *F. falciforme* were more dominant, as the co-culture gave dereplicated compound hits previously observed in the monoculture of *F. falciforme* such as phomolide C (m/z 343.211), hymeglusin (m/z 325.2), javanicin (m/z 292.086), dihydroanhydrojavanicin (m/z 275.091), 3-propylgentsylquinone (m/z 181.086), fusaridioic acid (m/z 343.211) and colletorin (m/z 298.18), out of which dihydroanhydrojavanicin and javanicin was isolated from their co-culture. The metabolites of *A. alternata* also showed dominance when co-cultured with *F. proliferatum*, as the co-culture gave dereplicated compound hits previously observed in the monoculture of *A. alternata* such as altenusin (m/z 291.086) and 9-O-methylalternariol (m/z 273.076). The non-dereplicated ion peaks indicated the presence of novel compounds, although no novel compound was isolated from the co-culture of *F. proliferatum* and *F. falciforme*.

8.3.2 Pure compounds isolation

Fractionation was carried out on the merged crude extract using hexane and EtOAc as solvents, followed by isolation work which afforded ten known compounds namely solaniol (F5-7), dihydroanhydrojavanicin (F5-8), javanicin (F5-9) and 8-O-methylfusarubin (F6-8) linoleic acid (F3-6), ergosterol peroxide (F4-2), ergosta-7,22-diene-3,6-diol (F7-3), sumiki's acid (F6-11), 4-hydroxy-2-pyrrolidone (F7-2), nicotinic acid (F8-3), with the first four compounds (naphthoquinones) proving to be the most bioactive. These four compounds were also found in the active quadrant of the OPLSDA confirming their bioactivity and stability both at crude extract and compound stage. The bioactivity observed with solaniol and javanicin

could be because of the hydroxyl group at C-5 and C-8 and the methoxy group at C-2. Whereas for 8-O-methylfusarubin, the hydroxyl group at C-5 and the methoxy group at C-6 and C-8 could be responsible for the bioactivity. While for dihydroanhydrojavanicin, the hydroxyl group at C-5 and methoxy group at C-2 do play a role in the bioactivity of the compounds. All four naphthoquinone derivatives have a quinoidal core at C-1 and C-4, with a hydroxyl attached to the benzene ring at C-5, and a substituted methoxy group at C-2, except for 8-O-methylfusarubin whose methoxy group was substituted at C-6 and C-8. The difference in position of the methoxy group in 8-O-methylfusarubin when compared to the other three naphthoquinone derivatives, could explain why it exhibited lesser potency than the other naphthoquinones in this study.

Naphthoquinones are natural organic compounds derived from naphthalene. Oxidation of two atoms in the α -position of the naphthalene nucleus of the benzene ring leads to 1,4-naphthoquinone. The quinone ring is easily susceptible to reduction, oxidation, and addition of O-, N-, and S-nucleophiles and contains a system of double bonds conjugated with carbonyl groups. 1,4-Naphthoquinones are common metabolites of bacteria, fungi, plants, animals, and (Aminin and Polonik, 2020). The range of biological effects of natural and synthetic 1,4-naphthoquinones is diverse and includes antimicrobial, antiviral, antifungal, antiprotozoal, cytotoxic, antitumor, wound healing, hepatoprotective properties, anti-inflammatory and analgesic properties and some other properties (Sánchez-Calvo *et al.*, 2016, Zhang *et al.*, 2006, Aminin and Polonik, 2020).

8.3.3 Proposed biosynthetic pathway of 1,4-Naphthoquinones.

The biosynthetic pathway for naphthoquinones produced by the fungi genus *Fusarium* have been proposed to start with an aromatic acid, the primary metabolite in pigment synthesis by Gatenbeck and Bentley (Gatenbeck and Bentley, 1965) and later Arsenault (Arsenault, 1968). Aromatic acid is later methylated to fusarubinic acid. Fusarubinic acid was not found for over 20 years and was later isolated from the culture medium of *N. haematococca* and characterised (Parisot *et al.*, 1988). It then underwent successive reduction and was subsequently transformed to the aromatic aldehyde, then to the primary alcohol fusarubin and then to javanicin, solaniol and bostricoidin (Arsenault, 1968). Fusarubin and javanicin underwent dehydration to form anhydrofusarubin and anhydrojavanicin respectively. Also, fusarubinic acid can be directly converted into anhydrofusarubin lactone which then undergoes reduction to form anhydrofusarubin lactol (Parisot *et al.*, 1990, Medentsev and Akimenko, 1998).

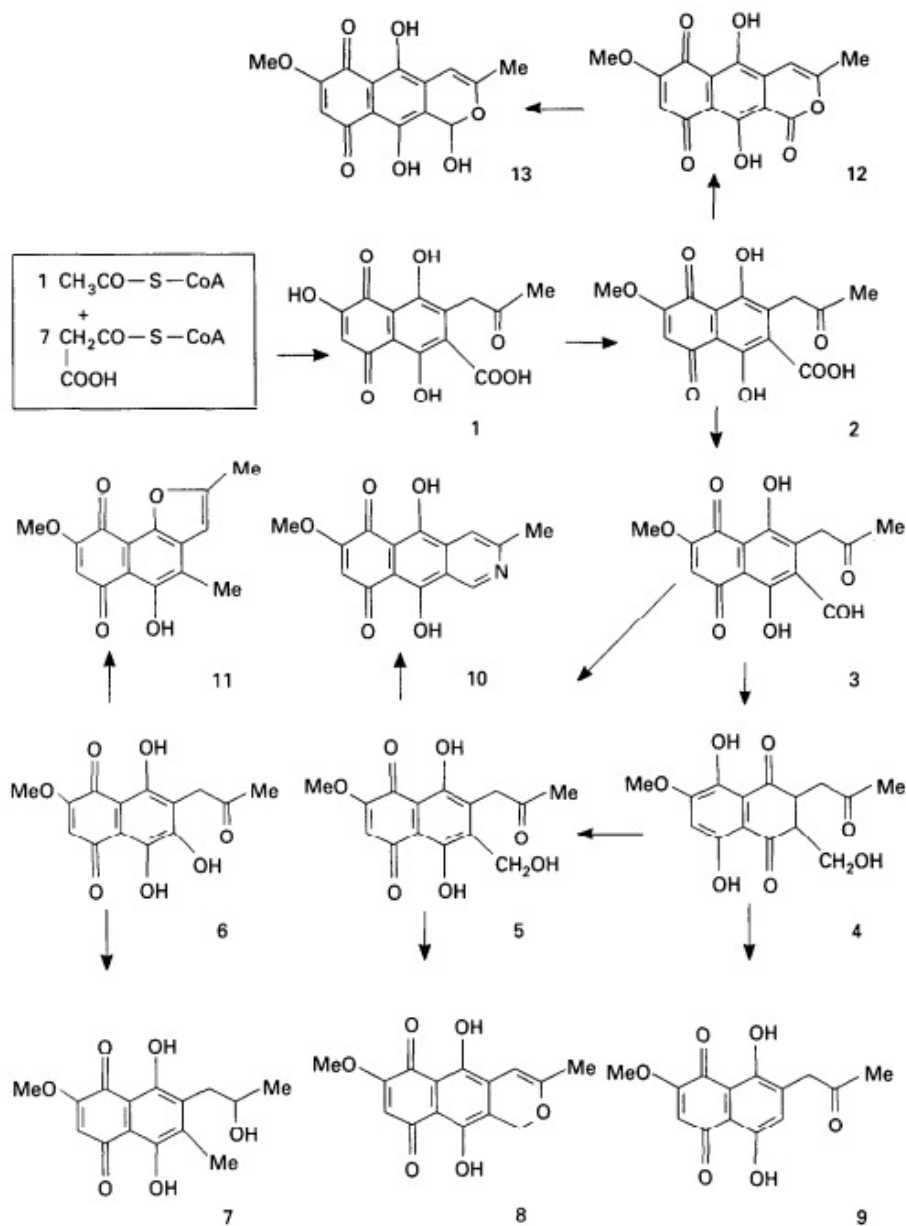


Figure 8.32: Schematic diagram of proposed naphthoquinone biosynthetic pathway in the fungi genus *Fusarium*. 1-aromatic acid; 2- fusarubinic acid; 3-aromatic aldehyde; 4- dihydrofusarubin; 5-fusarubin; 6-javanicin; 7-solaniol; 8-anhydrofusarubin; 9-norjavanicin; 10- bostricoidin; 11-anhydrojavanicin; 12-anhydrofusarubin lactone; 13-anhydrofusarubin lactol (Medentsev and Akimenko, 1998).

In conclusion, when comparing the bioactivity of *F. proliferatum* monoculture and its co-culture with *F. falciforme* on malt extract broth, the antimicrobial and antibiofilm activities were improved by 19.2% and 17.4% respectively. Also, from the dereplication Table, we can deduce that mixed cultures of *F. proliferatum* and *F. falciforme* possess the tendency to elicit the production of novel metabolites, although no new compound was isolated from this co-culture. Furthermore, co-culture of *F. proliferatum* and *F. falciforme* brought about an increase in extract weight from 44.9 mg obtained in the monoculture to 162.1 mg obtained in the co-culture. Finally, the naphthoquinones isolated in this study exhibited excellent antimicrobial and antibiofilm properties.

CHAPTER 9

Overall summary and future recommendations

The main aim of this research was to isolate antimicrobial and antibiofilm active metabolites against biofilm forming MRSA bacteria from endophytic fungi obtained from Kaduna, Nigeria. This section summarised the result chapters: 3, 4, 5, 6, 7 and 8. The objective of this study was to determine the antimicrobial activity of fungal extracts against both biofilm-forming MRSA via prebiofilm and planktonic assays. The bioactive discriminating metabolites were determined through a metabolomics approach and the predicted metabolites were identified through a dereplication HRFT-LCMS, Mzmine software, in house macro combined with Dictionary of NPs (Taylor & Francis, 2018 with annual update support). Bioactive fungi extracts were taxonomically identified by ITS gene sequencing as *F. proliferatum*, *F. falciforme* and *A. alternata*. *F. proliferatum* afforded MIC and MBEC of 25 µg/mL. The three antimicrobial-active fungi; *F. proliferatum*, *F. falciforme*, and *A. alternata* were further optimised on four different media namely, malt extract (ME) broth, potato dextrose broth (PD broth), rice solid media and oat solid media. Based on the planktonic and prebiofilm assay results, in addition to the unique chemical profiles of the various fungal extracts determined by multivariate analysis; *F. proliferatum* incubated for 15 days at 27°C on rice solid media, *F. falciforme* incubated for 15 days at 27°C on malt extract broth and *A. alternata* incubated for 30 days at 27°C on potato dextrose broth were chosen for the scale-up experiments.

Co-cultures were performed amongst the three fungi (*F. proliferatum*-*F. falciforme*, *F. proliferatum*-*A. alternata*, *F. falciforme*-*A. alternata*) for 7 days on malt extract agar, then for 15 and 30 days on malt extract broth, and the best co-culture extract which was obtained from *F. proliferatum*-*F. falciforme*, with bioactivity above 90.0%, was fractionated using the crude extracts obtained from media optimisation on malt extract broth incubated for 15 and 30 days, as it was observed that the fungi extracts obtained from both incubation days had similar bioactivity and chemical profile. Co-cultures were also performed between the fungi monocultures and MRSA (*F. proliferatum*-MRSA, *F. falciforme*-MRSA and *A. alternata*-MRSA) for 4 and 10 days on malt extract agar, and for 15 and 30 days on malt extract broth, and the best co-culture extract which was obtained from *F. proliferatum*-MRSA with bioactivity above 90.0% was chosen for further scale-up experiments. Hence, fractionation using hexane and EtOAc were performed on the scale-up crude extracts of *F. proliferatum* and *A. alternata* monocultures, co-culture of *F. proliferatum*-MRSA and media optimisation crude extracts of *F.*

proliferatum- *F. falciforme*. The scaled-up crude extracts of *F. falciforme* monoculture were subjected to solvent partitioning with n-hexane and EtOAc to remove lipids and two layers of fatty acids from the extract. The hexane and EtOAc extracts were assayed to determine which fraction will undergo further fractionation and purification, it was observed that *F. falciforme* had lost its bioactivity and further isolation work on its monoculture was discontinued. Lipids do play a role in the absorption of the antimicrobial components through the microbial cell wall. Hence, separating the fraction from its lipid component, resulted to a loss of the fraction's antimicrobial activity.

The MPLC fractions were assayed, and the antimicrobial-active fractions were chosen for further purification. The fractions were also analysed using ¹H NMR and HR-LCMS. HR-LCMS data was processed using Mzmine followed by dereplication using an in-house macro excel. The data were exported to SIMCA for analysis using PCA and OPLSDA.

Chromatographic isolation work on the crude extract of monocultures of *F. proliferatum*, afforded 19 compounds as listed in Table 4.10 with 6 compounds being new. The new compounds included 6-(acetoxymethyl)-2-ethoxy-4,5-dihydroxytetrahydro-2H-pyran-3-yl)oxonium (C₁₀H₁₈O₇), *N*-(2-((1*E*,3*E*)-7-hydroxytrideca-1,3-dien-1-yl)-5-oxotetrahydrofuran-3-yl)acetamide (C₁₉H₃₁NO₄), 3-*O*-β-D-glucopyranoside-cholest-5-ene-24-one (C₃₃H₅₄O₇), 11,4,5,9-tetramethylspiro[5.5]undec-8-ene-1,4-diol (C₁₅H₂₆O₂), 2,3-dihydroxybutyl acetate (C₆H₁₂O₄), and *N*-[5-(acetyloxy) pentyl] acetamide (C₉H₁₇NO₃). Out of the 19 compounds, only 2 showed rather weak bioactivity against planktonic MRSA (1,3-dihydroxy-6-methoxy-8-methylxanthone, 65.81%,) and postbiofilm MRSA (*N*-[5-(acetyloxy) pentyl] acetamide, 52.73%), while the others were inactive.

Chromatographic isolation work on the crude extract of monocultures of *A. alternata* afforded 11 known compounds as listed in Table 6.9, out of which 5 discriminatory compounds namely 9-*O*-methylalternariol, alternariol, altenusin, altenuisol and altenuene were dereplicated in this study. Eight of the compounds exhibited either planktonic, prebiofilm or postbiofilm activity as shown in Table 6.11, but altenuene, 4'-epialtenuene and linoleic acid were inactive. Compound 9-*O*-methylalternariol, alternariol, altenusin and altenuisol were re-isolated many times during purification showing their discriminatory and dominance property for the active fractions, although only alternariol and altenuisol gave exceptional bioactivity above 70.0% with an MIC of 25 µg/mL and 50 µg/mL respectively.

Chromatographic isolation work on the crude extract of co-cultures of *F. proliferatum* and MRSA afforded 6 compounds as listed in Table 7.14 namely 2-phenylacetic acid, p-hydroxybenzaldehyde, 3-hydroxy-4-butanolide, 4-hydroxy phenylacetic acid,

cyclo(leucylprolyl) and uridine. The molecular isomer of the isolated cyclo(leucylprolyl), namely cyclo(isoleucylprolyl) was dereplicated in this study with ion peak at m/z 211.144. The 2:1 mixture of 2-phenylacetic acid, *p*-hydroxybenzaldehyde showed 50.01% inhibition of planktonic bacterial and 60.20% postbiofilm disruption, 3-hydroxy-4-butanolide and cyclo(leucylprolyl) showed 69.23% and 63.76% postbiofilm disruption. None of the isolated compounds attained the bioactivity threshold of 70.0% inhibition for strong reliable bioactivity. The compounds being observed in the active quadrant of OPLS-DA plot at crude extract stage, is an indication that the compounds were working complementarily to each other to be active and separating them made them lose their bioactive property.

Chromatographic isolation work on the crude extract of co-cultures *F. proliferatum* and *F. falciforme* afforded 10 compounds as listed in Table 8.14 out of which isolated compounds dihydroanhydrojavanicin and javanicin were dereplicated during the earlier chemical-profiling stages of the study. The dereplicated compound hits obtained from the co-culture proved the dominance of *F. falciforme* over *F. proliferatum* as the compound hits obtained from the co-culture consisted mostly of those observed in the monoculture of *F. falciforme*. The compound hits observed in both the monoculture and co-culture are phomolide C (m/z 343.211), hymeclusin (m/z 325.2), javanicin (m/z 292.086), dihydroanhydrojavanicin (m/z 275.091), 3-propylgentisylquinone (m/z 181.086), fusaridioic acid (m/z 343.211) and colletorin (m/z 298.18). Assay of the pure compounds proved three of the isolated naphthoquinones to have the best bioactivity in terms of planktonic and prebiofilm, while the fourth naphthoquinone (8-O-methylfusarubin) was moderately active inhibiting planktonic and prebiofilm MRSA by 65.38% and 77.46%, respectively. The three isolated bioactive naphthoquinones namely solaniol, dihydroanhydrojavanicin and javanicin had MIC values of 12.5 $\mu\text{g/mL}$. Solaniol afforded an MBEC value of 6.5 $\mu\text{g/mL}$ while the two javanicin congeners only gave 25 $\mu\text{g/mL}$. The four isolated naphthoquinones compounds were also found in the active quadrant of the OPLS-DA validating their bioactivity and stability both at the crude extract and pure compound stages. Naphthoquinones are secondary metabolites universal in nature, consisting of an extensive variety of chemical structures based on the naphthalene skeleton. They exhibit several substituents and may group together forming dimers and trimers. Their potential therapeutic activity and toxicity depend on their ability to act as oxidising agents or bind nucleophilic molecules. These abilities allow them to influence gene transcription, cellular signalling pathways and the activity of multiple enzymes (Pinho *et al.*, 2012).

Also, comparing the monoculture of *F. falciforme* with its co-culture to *F. proliferatum*, the problem with the monoculture was that it was producing more fatty acids (FA), which led to the decision to perform liquid-liquid partitioning. However, the mixture of the bioactive

naphthoquinones was still too low in comparison to the occurrence of other components which explains the loss in bioactivity after getting rid of the fatty acids, hence losing the complementary effect of the FA on the biofilm cell matrix to absorb the bioactive compounds. Purification of these compounds will lead to a return in the bioactivity, but it will be inefficient or impossible to isolate them if the active compounds are only present at micro- or nanogram concentrations which was exactly the case in the monoculture. Dihydrojavanicin and javanicin were detected in the monocultures, but they were probably present in minute amounts. The coculture was an advantage because it increased their yield in addition to the production of other naphthoquinone derivatives, that they were able to be isolated, although no new compounds were isolated from it.

When *F. proliferatum* was co-cultured with the pathogenic MRSA, the isolated compounds had weak or no bioactivity, as the MRSA could have weakened the fungi while competing for nutrients or survival, but when *F. proliferatum* was co-cultured with *F. falciforme*, the antimicrobial and antibiofilm activities were improved by 19.2% and 17.4% respectively. Also, co-culture of *F. proliferatum* and *F. falciforme* brought about an increase in extract weight from 44.9 mg obtained in the monoculture to 162.1 mg obtained in the co-culture. It can therefore be deduced that, manipulating culture conditions such as monoculture or co-culture of organisms can positively or negatively affect the biological activity of the isolated compounds.

Future Recommendations

First question: Would the isolated compounds from monoculture of *A. alternata* and co-culture of *F. proliferatum* and *F. falciforme* be safe to use to obtain the desired biological activity?

Different concentrations of the isolated antimicrobial-active compounds should be tested on L929 mouse fibroblast according to ISO 10993-5 standards. The concentration range should be parallel to the antimicrobial activity based on their MIC and MBEC values. Toxic concentrations should be calculated to determine the safety of the compounds *in vitro*.

Second question: Could the most bioactive co-culture (*F. proliferatum* and *F. falciforme*) be subjected to a biotechnological industrial scale-up to target the production of the isolated antimicrobial compounds from this work, as potential new drugs?

The co-culture of *F. proliferatum* and *F. falciforme* was performed to elicit the production of novel metabolites against MRSA. No new compound was isolated during this study, although dereplication of the HR-LCMS data pinpointed the potential of this co-culture to elicit novel

metabolites. Co-cultures of *F. proliferatum* and *F. falciforme* were not scaled up due to time factor, but the six extracts obtained from media optimisation were merged and used for isolation work. This brought about the isolation of compounds with good inhibition rates against MRSA and improved extract yield. I will therefore suggest that *F. proliferatum* and *F. falciforme* be scaled-up for the first time as there are no previous reports on its scale-up, and the sole purpose of this scale-up would be to target novel compounds using metabolomics, which were already detected during the chemical profiling stage.

A pilot industrial scale-up of 400-500 litres should be subjected to the same procedure of bioassay guided fractionation and purification. Similar chromatographic fractionation using the procedure previously performed in the lab should be done at a larger scale with a larger silica column and a proportional flowrate. As a quality control protocol to confirm the production of the targeted antimicrobial compounds, crude extracts and fractions should then be assayed against biofilm-forming MRSA using a standardised HR-LCMS SOP.

Co-culture is a biological system in which two or more different strains of microorganisms are cultivated together. Although the number of reported compounds is increasing, there is still a great potential for producing novel compounds if silent gene clusters can be activated. Co-culture is one of the techniques used to activate these silent gene clusters. It can also lead to increased yield of bioactive compounds and production of known compounds that were not present in pure strain cultures. With reference to this study, co-culture has an advantage over their pure culture counterparts if the right strains are chosen. The results obtained in this study suggest that co-culture cannot be universally applied to generate new compounds, as the outcome of the co-culture system is often specific to each study. As was observed from this study, co-cultures of *F. proliferatum*-MRSA and of *F. proliferatum*-*F. falciforme* did not produce any new compound but the isolated known compounds such as the naphthoquinones exhibited excellent bioactivity.

In conclusion, the original research question was answered, as the study showed that endophytic fungi derived from Nigerian medicinal plants are good sources of new bioactive compounds, with antibacterial antibiofilm activity against MRSA. Co-culture of *F. proliferatum*-*F. falciforme* produced compounds with excellent bioactivity. The hypothesis was also correct, as implementing metabolomics processes such as dereplication, PCA, PLS-DA, OPLS-DA, to search for antibacterial and anti-biofilm bioactive compounds from endophytic fungi associated with Nigerian plants, helped to putatively identify bioactive compounds.

10 References

- ABBAS, H. K. & RILEY, R. T. 1996. The presence and phytotoxicity of fumonisins and AAL-toxin in *Alternaria alternata*. *Toxicon*, 34, 133-136.
- ABD EL-GHANI, M. 2016. Traditional medicinal plants of Nigeria: an overview. *Agric Biol J North America*, 7, 220-247.
- ABDOU, R. & DAWOUD, M. 2020. Cytotoxic metabolites of *Alternaria alternata*, an endophyte of the medicinal plant *Bidens bipinnata*. *Int J Pharm Pharm Sci*, 12, 42-48.
- ABRAHAM, W.-R. & HANSSSEN, H.-P. 1992. Fusoxysporone - a new type of diterpene from *Fusarium oxysporum*. *Tetrahedron*, 48, 10559-10562.
- ABREU, P. A., WILKE, D. V., ARAUJO, A. J., MARINHO-FILHO, J. D. B., FERREIRA, E. G., RIBEIRO, C. M. R., PINHEIRO, L. S., AMORIM, J. W., VALVERDE, A. L., EPIFANIO, R. A., COSTA-LOTUFO, L. V. & JIMENEZ, P. C. 2015. Perezone, from the gorgonian *Pseudopterogorgia rigida*, induces oxidative stress in human leukemia cells. *Rev Brasil Farmacog*, 25, 634-640.
- ADEBOLU, T. & SALAU, A. 2005. Antimicrobial activity of leaf extracts of *Ocimum gratissimum* on selected diarrhoea causing bacteria in southwestern Nigeria. *Afr J Biotech*, 4, 682-684.
- ADORISIO, S., FIERABRACCI, A., MUSCARI, I., LIBERATI, A. M., CANNARILE, L., THUY, T. T., SUNG, T. V., SOHRAB, H., HASAN, C. M., AYROLDI, E., RICCARDI, C., MAZID, A. & DELFINO, D. V. 2019. Fusarubin and anhydrofusarubin isolated from a *Cladosporium* species inhibit cell growth in human cancer cell lines. *Toxins (Basel)*, 11, 503.
- AHMED, A. M., MAHMOUD, B. K., MILLÁN-AGUIÑAGA, N., ABDELMOHSEN, U. R. & FOUAD, M. A. 2023. The endophytic *Fusarium* strains: a treasure trove of natural products. *RSC Advances*, 13, 1339-1369.
- AIYELAAGBE, O. & OSAMUDIAMEN, P. M. 2009. Phytochemical screening for active compounds in *Mangifera indica* leaves from Ibadan, Oyo State. *Plant Sci Res*, 2, 11-13.
- AKINPELU, D. A. 1999. Antimicrobial activity of *Vernonia amygdalina* leaves. *Fitoterapia*, 70, 432-434.
- AKINYEMI, K. O., OLADAPO, O., OKWARA, C. E., IBE, C. C. & FASURE, K. A. 2005. Screening of crude extracts of six medicinal plants used in South-West Nigerian unorthodox medicine for anti-methicillin resistant *Staphylococcus aureus* activity. *BMC Complement Altern Med*, 5, 6.
- ALARA, O. R., ABDURAHMAN, N. H., UKAEGBU, C. I., HASSAN, Z. & KABBASHI, N. A. 2018. Dataset on LC-Q-TOF/MS tentative identification of phytochemicals in the extract of *Vernonia amygdalina* leaf through positive ionization. *Data Brief*, 21, 1686-1689.
- ALCÁZAR MAGAÑA, A., KAMIMURA, N., SOUMYANATH, A., STEVENS, J. F. & MAIER, C. S. 2021. Caffeoylquinic acids: chemistry, biosynthesis, occurrence, analytical challenges, and bioactivity. *Plant J*, 107, 1299-1319.
- ALI, E., BAGCHI, D., & PAKRASHI, S. C. 1979. New flavonoids from *Anaphalis araneosa*. *Phytochemistry*, 18, 356-357. .
- ALTSCHUL, S. F., GISH, W., MILLER, W., MYERS, E. W. & LIPMAN, D. J. 1990. Basic local alignment search tool. *J Mol Biol*, 215, 403-410.
- ALY, A. H., EDRADA-EBEL, R., INDRIANI, I. D., WRAY, V., MÜLLER, W. E., TOTZKE, F., ZIRRGIEBEL, U., SCHÄCHTELE, C., KUBBUTAT, M. H., LIN, W. H., PROKSCH, P. & EBEL, R. 2008. Cytotoxic metabolites from the fungal endophyte

- Alternaria* sp. and their subsequent detection in its host plant *Polygonum senegalense*. *J Nat Prod*, 71, 972-980.
- ALZOHAIRY, M. A. 2016. Therapeutics Role of *Azadirachta indica* (Neem) and Their Active Constituents in Diseases Prevention and Treatment. *Evid Based Complement Alternat Med*, 2016, 7382506.
- AMAGATA, T., USAMI, Y., MINOURA, K., ITO, T. & NUMATA, A. 1998. Cytotoxic substances produced by a fungal strain from a sponge: physico-chemical properties and structures. *J Antibiot (Tokyo)*, 51, 33-40.
- AMANING DANQUAH, C., KOFFUOR, G., ANNAN, K. & KETOR, E. 2012. The Anthelmintic Activity of *Vernonia Amygdalina* (Asteraceae) and *Alstonia Boonei* De Wild (Apocynaceae). *J Med Biomed Sci*, 1, 21-27.
- AMININ, D. & POLONIK, S. 2020. 1,4-Naphthoquinones: Some Biological Properties and Application. *Chemical and Pharmaceutical Bulletin*, 68, 46-57.
- ARSENAULT, G. P. 1968. Fungal metabolites—III: Quinones from *fusarium solani* D2 purple and structure of (+)-solaniol2. *Tetrahedron*, 24, 4745-4749.
- ATANASOV, A. G., ZOTCHEV, S. B., DIRSCH, V. M., ORHAN, I. E., BANACH, M., ROLLINGER, J. M., BARRECA, D., WECKWERTH, W., BAUER, R., BAYER, E. A., MAJEED, M., BISHAYEE, A., BOCHKOV, V., BONN, G. K., BRAIDY, N., BUCAR, F., CIFUENTES, A., D'ONOFRIO, G., BODKIN, M., DIEDERICH, M., DINKOVA-KOSTOVA, A. T., EFFERTH, T., EL BAIRI, K., ARKELLS, N., FAN, T.-P., FIEBICH, B. L., FREISSMUTH, M., GEORGIEV, M. I., GIBBONS, S., GODFREY, K. M., GRUBER, C. W., HEER, J., HUBER, L. A., IBANEZ, E., KIJOA, A., KISS, A. K., LU, A., MACIAS, F. A., MILLER, M. J. S., MOCAN, A., MÜLLER, R., NICOLETTI, F., PERRY, G., PITTALÀ, V., RASTRELLI, L., RISTOW, M., RUSSO, G. L., SILVA, A. S., SCHUSTER, D., SHERIDAN, H., SKALICKA-WOŹNIAK, K., SKALTSOUNIS, L., SOBARZO-SÁNCHEZ, E., BREDT, D. S., STUPPNER, H., SUREDA, A., TZVETKOV, N. T., VACCA, R. A., AGGARWAL, B. B., BATTINO, M., GIAMPIERI, F., WINK, M., WOLFENDER, J.-L., XIAO, J., YEUNG, A. W. K., LIZARD, G., POPP, M. A., HEINRICH, M., BERINDAN-NEAGOE, I., STADLER, M., DAGLIA, M., VERPOORTE, R., SUPURAN, C. T. & THE INTERNATIONAL NATURAL PRODUCT SCIENCES, T. 2021. Natural products in drug discovery: advances and opportunities. *Nature Reviews Drug Discovery*, 20, 200-216.
- AYELESO, A. O., MATUMBA, M. G., NTAMBI, J. M. & MUKWEVHO, E. 2020. Chapter 17 - Insights into the metabolism of lipids in obesity and diabetes. In: NTAMBI, J. M. (ed.) *Lipid Signaling and Metabolism*. Academic Press. 345-357.
- AYER, W. A. & RACOK, J. S. 1990. The metabolites of *Talaromyces flavus*: Part 1. Metabolites of the organic extracts. *Can J Chem*, 68, 2085-2094.
- BAKER, D. D., CHU, M., OZA, U. & RAJGARHIA, V. 2007. The value of natural products to future pharmaceutical discovery. *Nat Prod Rep*, 24, 1225-44.
- BARKER, M. & RAYENS, W. 2003. Partial least squares for discrimination. *J Chemom*, 17, 166-173.
- BARRETO, J. C., TREVISAN, M. T., HULL, W. E., ERBEN, G., DE BRITO, E. S., PFUNDSTEIN, B., WÜRTELE, G., SPIEGELHALDER, B. & OWEN, R. W. 2008. Characterization and quantitation of polyphenolic compounds in bark, kernel, leaves, and peel of mango (*Mangifera indica* L.). *J Agric Food Chem*, 56, 5599-610.
- BASHYAL, B. P., WELLENSIEK, B. P., RAMAKRISHNAN, R., FAETH, S. H., AHMAD, N. & GUNATILAKA, A. A. 2014. Alttoxins with potent anti-HIV activity from *Alternaria tenuissima* QUE1Se, a fungal endophyte of *Quercus emoryi*. *Bioorg Med Chem*, 22, 6112-6.

- BAZZINI S., B. S., UDINE C., PASCA M., RICCARDI G. 2014. Molecular Basis for Antibiotic Resistance in the Genus Burkholderia. In: COENYE, T. & MAHENTHIRALINGAM, E. (eds.) *Burkholderia: From Genomes to Function*. Norfolk, UK: Caistee Academic Press. ISBN: 978-1-908230-97-3. 254 pp.
- BECKONERT, O., KEUN, H. C., EBBELS, T. M., BUNDY, J., HOLMES, E., LINDON, J. C. & NICHOLSON, J. K. 2007. Metabolic profiling, metabolomic and metabonomic procedures for NMR spectroscopy of urine, plasma, serum and tissue extracts. *Nat Protoc*, 2, 2692-2703.
- BELLEMAIN, E., CARLSEN, T., BROCHMANN, C., COISSAC, E., TABERLET, P. & KAUSERUD, H. 2010. ITS as an environmental DNA barcode for fungi: an in silico approach reveals potential PCR biases. *BMC Microbiology*, 10, 189.
- BERKEY, R., BENDIGERI, D. & XIAO, S. 2012. Sphingolipids and plant defense/disease: the "death" connection and beyond. *Front Plant Sci*, 3, 68.
- BERNARDINI, S., TIEZZI, A., LAGHEZZA MASCI, V. & OVIDI, E. 2018. Natural products for human health: an historical overview of the drug discovery approaches. *Nat Prod Res*, 32, 1926-1950.
- BERTRAND, S., BOHNI, N., SCHNEE, S., SCHUMPP, O., GINDRO, K. & WOLFENDER, J. L. 2014. Metabolite induction via microorganism co-culture: a potential way to enhance chemical diversity for drug discovery. *Biotechnol Adv*, 32, 1180-1204.
- BHAGAT, J., KAUR, A., KAUR, R., YADAV, A. K., SHARMA, V. & CHADHA, B. S. 2016. Cholinesterase inhibitor (Altenuene) from an endophytic fungus *Alternaria alternata*: optimization, purification and characterization. *J Appl Microbiol*, 121, 1015-1025.
- BILLS, G. F. & GLOER, J. B. 2016. Biologically active secondary metabolites from the fungi. *Microbiol Spectr*, 4, 6.
- BLAIR, J. M., WEBBER, M. A., BAYLAY, A. J., OGBOLU, D. O. & PIDDOCK, L. J. 2015. Molecular mechanisms of antibiotic resistance. *Nat Rev Microbiol*, 13, 42-51.
- BLEICHER, K. H., BÖHM, H. J., MÜLLER, K. & ALANINE, A. I. 2003. Hit and lead generation: beyond high-throughput screening. *Nat Rev Drug Discov*, 2, 369-378.
- BUITRAGO DÍAZ, A., ROJAS, J., COTE, V., BRUNO-COLMENÁREZ, J. & DÍAZ DE DELGADO, G. 2010. NMR elucidation and crystal structure analysis of 1-hydroxy-3,6-dimethoxy-8-methyl-9h-xanthen-9-one (lichexanthone) isolated from *Vismia baccifera* (Guttiferae). *Boletín Latinoamericano y del Caribe de Plantas Medicinales y Aromaticas*, 9, 470.
- CAESAR, L. K. & CECH, N. B. 2019. Synergy and antagonism in natural product extracts: when 1 + 1 does not equal 2. *Nat Prod Rep*, 36, 869-888.
- CAESAR, L. K., MONTASER, R., KELLER, N. P. & KELLEHER, N. L. 2021. Metabolomics and genomics in natural products research: complementary tools for targeting new chemical entities. *Nat Prod Rep*, 38, 2041-2065.
- CHALLIS, G. L. 2008. Mining microbial genomes for new natural products and biosynthetic pathways. *Microbiology (Reading)*, 154, 1555-1569.
- CHAN, E. C., KOH, P. K., MAL, M., CHEAH, P. Y., EU, K. W., BACKSHALL, A., CAVILL, R., NICHOLSON, J. K. & KEUN, H. C. 2009. Metabolic profiling of human colorectal cancer using high-resolution magic angle spinning nuclear magnetic resonance (HR-MAS NMR) spectroscopy and gas chromatography mass spectrometry (GC/MS). *J Proteome Res*, 8, 352-361.
- CHANDRA MOHANA, N., YASHAVANTHA RAO, H. C., RAKSHITH, D., MITHUN, P. R., NUTHAN, B. R. & SATISH, S. 2018. Omics based approach for biodiscovery of microbial natural products in antibiotic resistance era. *J Genet Eng Biotechnol*, 16, 1-8.

- CHATTERJEE, S., GHOSH, R. & MANDAL, N. C. 2019. Production of bioactive compounds with bactericidal and antioxidant potential by endophytic fungus *Alternaria alternata* AE1 isolated from *Azadirachta indica* A. Juss. *PLoS One*, 14, 4.
- CHEN, G. L., XU, Y. B., WU, J. L., LI, N. & GUO, M. Q. 2020. Hypoglycemic and hypolipidemic effects of *Moringa oleifera* leaves and their functional chemical constituents. *Food Chem*, 333, 127478.
- CHOI, H., MASCUCH, S. J., VILLA, F. A., BYRUM, T., TEASDALE, M. E., SMITH, J. E., PRESKITT, L. B., ROWLEY, D. C., GERWICK, L. & GERWICK, W. H. 2012. Honaucins A-C, potent inhibitors of inflammation and bacterial quorum sensing: synthetic derivatives and structure-activity relationships. *Chem Biol*, 19, 589-598.
- CIOFU, O. & TOLKER-NIELSEN, T. 2019. Tolerance and resistance of *Pseudomonas aeruginosa* biofilms to antimicrobial agents-How *P. aeruginosa* can escape antibiotics. *Front Microbiol*, 10, 913.
- CIOFU, O., TOLKER-NIELSEN, T., JENSEN, P., WANG, H. & HØIBY, N. 2015. Antimicrobial resistance, respiratory tract infections and role of biofilms in lung infections in cystic fibrosis patients. *Adv Drug Deliv Rev*, 85, 7-23.
- COFFINET, S., MEADOR, T. B., MÜHLENA, L., BECKER, K. W., SCHRÖDER, J., ZHU, Q. Z., LIPP, J. S., HEUER, V. B., CRUMP, M. P. & HINRICHS, K. U. 2020. Structural elucidation and environmental distributions of butanetriol and pentanetriol dialkyl glycerol tetraethers (BDGTs and PDGTs). *Biogeosciences*, 17, 317-330.
- COHEN, M. M. 2014. Tulsi - *Ocimum sanctum*: A herb for all reasons. *J Ayurveda Integr Med*, 5, 251-259.
- COLE, R. J. & COX, R. H. 1981. *Handbook of toxic fungal metabolites*, New York, Academic Press. ISBN 10: 0121797600 / ISBN 13: 9780121797607. 937 pp.
- COOPER, M. A. & SHLAES, D. 2011. Fix the antibiotics pipeline. *Nature*, 472, 32.
- COSTERTON, J. W., STEWART, P. S. & GREENBERG, E. P. 1999. Bacterial biofilms: a common cause of persistent infections. *Science*, 284, 1318-22.
- CRAGG, G. M. & PEZZUTO, J. M. 2016. Natural Products as a Vital Source for the Discovery of Cancer Chemotherapeutic and Chemopreventive Agents. *Med Princ Pract*, 25 Suppl 2, 41-59.
- CRAGG, G. M., SCHEPARTZ, S. A., SUFFNESS, M. & GREVER, M. R. 1993. The taxol supply crisis. New NCI policies for handling the large-scale production of novel natural product anticancer and anti-HIV agents. *J Nat Prod*, 56, 1657-1668.
- DALINOVA, A., CHISTY, L., KOCHURA, D., GARNYUK, V., PETROVA, M., PROKOFIEVA, D., YURCHENKO, A., DUBOVIK, V., IVANOV, A., SMIRNOV, S., ZOLOTAREV, A. & BERESTETSKIY, A. 2020. Isolation and Bioactivity of Secondary Metabolites from Solid Culture of the Fungus, *Alternaria sonchi*. *Biomolecules*, 10, 1.
- DALLA LANA, D. F., BATISTA, B. G., DA ROSA MACHADO, G., TEIXEIRA, M. L., DE OLIVEIRA, L. F. S., MACHADO, M. M., DE ANDRADE, S. F., LOPES, W., VAINSTEIN, M. H., DE ABREU LIMA, A. P., PANDOLFI, E., SILVA, E. E., FUENTEFRIA, A. M. & SILVEIRA, G. P. 2019. Design, synthesis, and evaluation of novel 2-substituted 1,4-benzenediol library as antimicrobial agents against clinically relevant pathogens. *Saudi Pharm J*, 27, 1064-1074.
- DAME, Z. T., SILIMA, B., GRYZENHOUT, M. & VAN REE, T. 2016. Bioactive compounds from the endophytic fungus *Fusarium proliferatum*. *Nat Prod Res*, 30, 1301-4.
- DAVISS, B. 2005. Growing pains for metabolomics. *Scientist*, 19, 25-28.
- DE VOS, R. C., MOCO, S., LOMMEN, A., KEURENTJES, J. J., BINO, R. J. & HALL, R. D. 2007. Untargeted large-scale plant metabolomics using liquid chromatography coupled to mass spectrometry. *Nat Protoc*, 2, 778-91.

- DEMARQUE, D. P., DUSI, R. G., DE SOUSA, F. D. M., GROSSI, S. M., SILVERIO, M. R. S., LOPES, N. P. & ESPINDOLA, L. S. 2020. Mass spectrometry-based metabolomics approach in the isolation of bioactive natural products. *Sci Rep*, 10, 1051.
- DESJARDINS, A. E. 2006. *Fusarium Mycotoxins: Chemistry, Genetics and Biology* St Paul, MN, USA, American Phytopathology Society. ISBN 0-89-54-335-6. 268 pp.
- DETTMER, K., ARONOV, P. A. & HAMMOCK, B. D. 2007. Mass spectrometry-based metabolomics. *Mass Spectrom Rev*, 26, 51-78.
- DUNN, W. B. & ELLIS, D. I. 2005. Metabolomics: Current analytical platforms and methodologies. *Trends Anal Chem*, 24, 285-294.
- EBADA, S. S., EZE, P., OKOYE, F. B. C., ESIMONE, C. O. & PROKSCH, P. 2016. The fungal endophyte *Nigrospora oryzae* produces quercetin monoglycosides previously known only from plants. *Chemistry Select*, 1, 2767-2771.
- EID, A. M., SALIM, S. S., HASSAN, S. E.-D., ISMAIL, M. A. & FOUDA, A. 2019. Role of Endophytes in Plant Health and Abiotic Stress Management. In: KUMAR, V., PRASAD, R., KUMAR, M. & CHOUDHARY, D. K. (eds.) *Microbiome in Plant Health and Disease: Challenges and Opportunities*. Singapore: Springer Singapore. 119-144.
- EL-ESAWI, M. A., AL-GHAMDI, A. A., ALI, H. M. & AHMAD, M. 2019. Overexpression of AtWRKY30 transcription factor enhances heat and drought stress tolerance in wheat (*Triticum aestivum* L.). *Genes (Basel)*, 10, 2.
- EL-MAHMOOD, A. M., HAMUEL, J. D. & LADAN, N. 2008. Antimicrobial screening of stem bark extracts of *Vitellaria paradoxa* against some enteric pathogenic microorganisms. *Afr J Pharm*, 2, 89-94.
- ELBERMAWI, A., HALIM, A. F., MANSOUR, E. S., AHMAD, K. F., ELSBAEY, M., ASHOUR, A., AMEN, Y., EL-GAMIL, M. M., TOMOFUMI, M. & SHIMIZU, K. 2022. *Lycium schweinfurthii*: new secondary metabolites and their cytotoxic activities. *Nat Prod Res*, 36, 5134-5141.
- ELGHAFFAR, R. Y. A., AMIN, B. H., HASHEM, A. H. & SEHIM, A. E. 2022. Promising Endophytic *Alternaria alternata* from Leaves of *Ziziphus spina-christi*: Phytochemical Analyses, Antimicrobial and Antioxidant Activities. *Appl Biochem Biotechnol*, 194, 3984-4001.
- ELLIS, D. I. & GOODACRE, R. 2006. Metabolic fingerprinting in disease diagnosis: biomedical applications of infrared and Raman spectroscopy. *Analyst*, 131, 875-885.
- ELWARD, A. M., MCANDREWS, J. M. & YOUNG, V. L. 2009. Methicillin-sensitive and methicillin-resistant *Staphylococcus aureus*: preventing surgical site infections following plastic surgery. *Aesthet Surg J*, 29, 232-44.
- ENGLEROVÁ, K., BEDLOVIČOVÁ, Z., NEMCOVÁ, R., KIRÁLY, J., MAĎAR, M., HAJDUČKOVÁ, V., STYKOVÁ, E., MUCHA, R. & REIFFOVÁ, K. 2021. *Bacillus amyloliquefaciens*-derived lipopeptide biosurfactants inhibit biofilm formation and expression of biofilm-related genes of *Staphylococcus aureus*. *Antibiotics (Basel)*, 10, 10: 1252.
- ERASTO, P., GRIERSON, D. S. & AFOLAYAN, A. J. 2007. Antioxidant constituents in *Vernonia amygdalina* leaves. *Pharm Biol*, 45, 195-199.
- FAETH, S. H. & FAGAN, W. F. 2002. Fungal endophytes: common host plant symbionts but uncommon mutualists. *Integr Comp Biol*, 42, 360-368.
- FAJARDO, A. & MARTÍNEZ, J. L. 2008. Chapter 8: Antibiotic Resistance in *Pseudomonas*. In: CORNELIS, P. (ed.) *Pseudomonas: Genomics and Molecular Biology*. Norfolk, UK: Caister Academic. ISBN: 978-1-913652-25-8. 244 pp.
- FATHY, S. M. & MAHMOUD, M. S. 2021. *Moringa oleifera* Lam. leaf extract mitigates carbon tetrachloride-mediated hepatic inflammation and apoptosis via targeting

- oxidative stress and toll-like receptor 4/nuclear factor kappa B pathway in mice. *Food Sci Human Wellness*, 10, 383-391.
- FEHR, M., PAHLKE, G., FRITZ, J., CHRISTENSEN, M. O., BOEGE, F., ALTEMÖLLER, M., PODLECH, J. & MARKO, D. 2009. Alternariol acts as a topoisomerase poison, preferentially affecting the H α isoform. *Mol Nutr Food Res*, 53, 441-451.
- FOUDA, A. H., HASSAN, S. E.-D., EID, A. M. & EWAIS, E. E.-D. 2015. Biotechnological applications of fungal endophytes associated with medicinal plant *Asclepias sinaica* (Bioss.). *Ann Agric Sci*, 60, 95-104.
- GABRANI, R., SHARMA, G., DANG, S. & GUPTA, S. 2015. Interplay Among Bacterial Resistance, Biofilm Formation and Oxidative Stress for Nosocomial Infections. In: RANI, V. & YADAV, U. C. S. (eds.) *Free Radicals in Human Health and Disease*. New Delhi: Springer India. 369-379.
- GALVÁN, G. A., KONING-BOUCOIRAN, C. F. S., KOOPMAN, W. J. M., BURGERMEIJER, K., GONZÁLEZ, P. H., WAALWIJK, C., KIK, C. & SCHOLTEN, O. E. 2008. Genetic variation among *Fusarium* isolates from onion, and resistance to *Fusarium* basal rot in related *Allium* species. *Eur J Plant Pathol*, 121, 499-512.
- GATENBECK, S. & BENTLEY, R. 1965. Naphthaquinone Biosynthesis in Moulds: The Mechanism for Formation of Javanicin. *Biochem J*, 94, 478-481.
- GENILLOU, O. 2019. Natural products discovery and potential for new antibiotics. *Curr Opin Microbiol*, 51, 81-87.
- GETINO, M., FERNÁNDEZ-LÓPEZ, R., PALENCIA-GÁNDARA, C., CAMPOS-GÓMEZ, J., SÁNCHEZ-LÓPEZ, J. M., MARTÍNEZ, M., FERNÁNDEZ, A. & DE LA CRUZ, F. 2016. Tanzawaic Acids, a Chemically Novel Set of Bacterial Conjugation Inhibitors. *PLoS One*, 11, 1.
- GHIASIAN, S. A., REZAYAT, S. M., KORD-BACHEH, P., MAGHSOOD, A. H., YAZDANPANA, H., SHEPHARD, G. S., VAN DER WESTHUIZEN, L., VISMER, H. F. & MARASAS, W. F. 2005. Fumonisin production by *Fusarium* species isolated from freshly harvested corn in Iran. *Mycopathologia*, 159, 31-40.
- GLAZEBROOK, J. 2005. Contrasting mechanisms of defense against biotrophic and necrotrophic pathogens. *Annu Rev Phytopathol*, 43, 205-27.
- GÓNGORA-CASTILLO, E. & BUELL, C. R. 2013. Bioinformatics challenges in de novo transcriptome assembly using short read sequences in the absence of a reference genome sequence. *Nat Prod Rep*, 30, 490-500.
- GOODACRE, R., YORK, E. V., HEALD, J. K. & SCOTT, I. M. 2003. Chemometric discrimination of unfractionated plant extracts analyzed by electrospray mass spectrometry. *Phytochemistry*, 62, 859-863.
- GOPALAKRISHNAN, L., DORIYA, K. & KUMAR, D. S. 2016. *Moringa oleifera*: A review on nutritive importance and its medicinal application. *Food Sci Human Wellness*, 5, 49-56.
- GOUDA, S., DAS, G., SEN, S. K., SHIN, H. S. & PATRA, J. K. 2016. Endophytes: A Treasure House of Bioactive Compounds of Medicinal Importance. *Front Microbiol*, 7, 1538.
- GOYAL, B. R., AGRAWAL, B. B., GOYAL, R. K. & MEHTA, A. A. 2007. Phytopharmacology of *Moringa oleifera* Lam. - An overview. *Nat Prod Radiance*, 6, 347-353.
- GREENSPAN, M. D., YUDKOVITZ, J. B., LO, C. Y., CHEN, J. S., ALBERTS, A. W., HUNT, V. M., CHANG, M. N., YANG, S. S., THOMPSON, K. L., CHIANG, Y. C. & ET AL. 1987. Inhibition of hydroxymethylglutaryl-coenzyme A synthase by L-659,699. *Proc Natl Acad Sci U S A*, 84, 7488-7492.
- GRKOVIC, T., POWWER, R. H., VIAL, M. L., GAMBINI, L., NOËL, A., HOOPER, J. N., WOOD, S. A., MELLICK, G. D. & QUINN, R. J. 2014. NMR fingerprints of the drug-

- like natural-product space identify iotrochotazine A: a chemical probe to study Parkinson's disease. *Angew Chem Int Ed Engl*, 53, 6070-6074.
- GU, L., JONES, A. D. & LAST, R. L. 2007. LC-MS/MS assay for protein amino acids and metabolically related compounds for large-scale screening of metabolic phenotypes. *Anal Chem*, 79, 8067-8075.
- HAMILL, F. A., APIO, S., MUBIRU, N. K., MOSANGO, M., BUKENYA-ZIRABA, R., MAGANYI, O. W. & SOEJARTO, D. D. 2003. Traditional herbal drugs of southern Uganda: Part III: Isolation and methods for physical characterization of bioactive alkanols from *Rubus apetalus*. *Journal of Ethnopharmacology*, 87, 15-19.
- HAMUEL, J. D. & MANZARA, S. 2008. In Vitro antibacterial activity of crude leaf extracts of *Mangifera indica* Linn. *Afr J Microbiol Res*, 2, 67-72.
- HARRISON, C. 2014. Patenting natural products just got harder. *Nat Biotechnol*, 32, 403-4.
- HASHIM, A. M., ALHARBI, B. M., ABDULMAJEED, A. M., ELKELISH, A., HOZZEIN, W. N. & HASSAN, H. M. 2020. Oxidative stress responses of some endemic plants to high altitudes by intensifying antioxidants and secondary metabolites content. *Plants (Basel)*, 9, 7:869.
- HASNAHANA, C., DEBAJYOTI, K., BIJU, S. O., MANASH, P. B., DHARITRI, S., TINKA, S., PONNALA, V., MOSAHARI, P. & SHARMA, U. B. 2019. Exploring the benefits of endophytic fungi through omics. In: SINGH, B. (ed.) *Advances in Endophytic Fungal Research*: Springer. ISBN 978-3-030-03589-1. 360 pp.
- HASSAN, S. E. 2017. Plant growth-promoting activities for bacterial and fungal endophytes isolated from medicinal plant of *Teucrium polium* L. *J Adv Res*, 8, 687-695.
- HASSANI, M. A., DURÁN, P. & HACQUARD, S. 2018. Microbial interactions within the plant holobiont. *Microbiome*, 6, 58.
- HATTI, K. S., MURALITHARAN, L., HEGDE, R. & KUSH, A. 2014. NeeMDB: Convenient Database for Neem Secondary Metabolites. *Bioinformation*, 10, 314-315.
- HENGZHUANG, W., WU, H., CIOFU, O., SONG, Z. & HØIBY, N. 2012. In vivo pharmacokinetics/pharmacodynamics of colistin and imipenem in *Pseudomonas aeruginosa* biofilm infection. *Antimicrob Agents Chemother*, 56, 2683-2690.
- HENRICH, C. J. & BEUTLER, J. A. 2013. Matching the power of high throughput screening to the chemical diversity of natural products. *Nat Prod Rep*, 30, 1284-1298.
- HØIBY, N., BJARNSHOLT, T., MOSER, C., BASSI, G. L., COENYE, T., DONELLI, G., HALL-STOODLEY, L., HOLÁ, V., IMBERT, C., KIRKETERP-MØLLER, K., LEBEAUX, D., OLIVER, A., ULLMANN, A. J. & WILLIAMS, C. 2015. ESCMID guideline for the diagnosis and treatment of biofilm infections 2014. *Clin Microbiol Infect*, 21 Suppl 1, S1-25.
- HOTELLING, H. 1933. Analysis of a complex of statistical variables into principal components. *J Educ Psychol*, 24, 417-441.
- HUANG, P. Q., ZHENG, X., LI WANG, S., LIANG YE, J., REN JIN, L. & CHEN, Z. 1999. A new approach to (S)-4-hydroxy-2-pyrrolidinone and its 3-substituted analogues. *Tetrahedron: Asymmetry*, 10, 3309-3317.
- HUSSAIN, H., DROGIES, K.-H., AL-HARRASI, A., HASSAN, Z., SHAH, A., RANA, U. A., GREEN, I. R., DRAEGER, S., SCHULZ, B. & KROHN, K. 2015. Antimicrobial constituents from endophytic fungus *Fusarium* sp. *Asian Pac J Trop Dis*, 5, 186-189.
- IBRAHIM, N. D. G., ABDURAHMAN, E. M. & IBRAHIM, G. 2000. Histological studies on the effects of chronic feeding of *Vernonia Amygdalina* Del. leaves on rats. *Niger J Surg Res*, 2, 68-74.
- IIJIMA, Y., NAKAMURA, Y., OGATA, Y., TANAKA, K., SAKURAI, N., SUDA, K., SUZUKI, T., SUZUKI, H., OKAZAKI, K., KITAYAMA, M., KANAYA, S., AOKI,

- K. & SHIBATA, D. 2008. Metabolite annotations based on the integration of mass spectral information. *Plant J*, 54, 949-62.
- IRAWATI, A. F., HARTATI, S. & WINDRIYATI, R. D. H. 2014. Pemanfaatan cendawan endofit dalam meningkatkan kualitas bibit tanaman padi. *Buletin Pertanian Perkotaan* 4, 30-40.
- IWU, M. M. 1986. Smooth muscle contracting lipid-soluble principles in chromatographic fractions of *Ocimum gratissimum*. *J Ethnopharmacol*, 18, 3-11.
- JABBAR, A., SHRESTA, A. P., RASHID, M. A., SHAMEEM, M. & YAHARA, S. 1998. Dehydroaltenusinic Acid- a Novel Microbial Metabolite from a *Streptomyces* sp. *Natural Product Letters*, 12, 311-316.
- JADULCO, R. 2002. Isolation and Structure Elucidation of Bioactive Secondary Metabolites from Marine Sponges and Sponge-derived Fungi. Dr. rer. nat, Julius-Maximilians-Universität Würzburg. ISBN-13- 9783736905603. 196 pp.
- JAGGAL, S., SRIVASTAVA, K., SARMA, B., PAL, C. & KUMAR, R. 2013. Studies on growth conditions of the tomato *Alternaria* leaf spot causing *Alternaria solani*. *The Bioscan*, 8, 101-104.
- JALGAONWALA, R., MOHITE, B. & MAHAJAN, R. 2011. A review: Natural products from plant associated endophytic fungi. *J. Microbiol. Biotech. Res.*, 1, 21-32.
- JAYASINGHE, L., ABBAS, H. K., JACOB, M. R., HERATH, W. H. & NANAYAKKARA, N. P. 2006. N-Methyl-4-hydroxy-2-pyridinone analogues from *Fusarium oxysporum*. *J Nat Prod*, 69, 439-42.
- JIANG, C. X., LI, J., ZHANG, J. M., JIN, X. J., YU, B., FANG, J. G. & WU, Q. X. 2019. Isolation, identification, and activity evaluation of chemical constituents from soil fungus *Fusarium avenaceum* SF-1502 and endophytic fungus *Fusarium proliferatum* AF-04. *J Agric Food Chem*, 67, 1839-1846.
- JIAO, P., GLOER, J. B., CAMPBELL, J. & SHEARER, C. A. 2006. Altenuene derivatives from an unidentified freshwater fungus in the family Tubeufiaceae. *J Nat Prod*, 69, 612-5.
- JOHANN, S., ROSA, L. H., ROSA, C. A., PEREZ, P., CISALPINO, P. S., ZANI, C. L. & COTA, B. B. 2012. Antifungal activity of altenusin isolated from the endophytic fungus *Alternaria* sp. against the pathogenic fungus *Paracoccidioides brasiliensis*. *Rev Iberoam Micol*, 29, 205-9.
- JOHNSON, S. R. & LANGE, B. M. 2015. Open-access metabolomics databases for natural product research: present capabilities and future potential. *Front Bioeng Biotechnol*, 3, 22.
- JOLLIFFE, I. T. 2002. Principal Component Analysis for Special Types of Data. *Principal Component Analysis*. New York, NY: Springer New York. ISBN- 978-0-387-22440-4. 338-372.
- JORDAN, K. W., NORDENSTAM, J., LAUWERS, G. Y., ROTHENBERGER, D. A., ALAVI, K., GARWOOD, M. & CHENG, L. L. 2009. Metabolomic characterization of human rectal adenocarcinoma with intact tissue magnetic resonance spectroscopy. *Dis Colon Rectum*, 52, 520-5.
- JOSEPH, B. & PRIYA, R. M. 2011. Bioactive compounds from endophytes and their potential in pharmaceutical effect: A Review. *Am J Mol Biol*, 1, 291-309.
- JUNIO, H. A., SY-CORDERO, A. A., ETTEFAGH, K. A., BURNS, J. T., MICKO, K. T., GRAF, T. N., RICHTER, S. J., CANNON, R. E., OBERLIES, N. H. & CECH, N. B. 2011. Synergy-directed fractionation of botanical medicines: a case study with goldenseal (*Hydrastis canadensis*). *Journal of natural products*, 74, 1621-1629.

- KAMAL, N., VIEGELMANN, C. V., CLEMENTS, C. J. & EDRADA-EBEL, R. 2017. Metabolomics-guided isolation of anti-trypanosomal metabolites from the endophytic fungus *Lasiodiplodia theobromae*. *Planta Med*, 83, 565-573.
- KAMBIZI, L. & AFOLAYAN, A. J. 2001. An ethnobotanical study of plants used for the treatment of sexually transmitted diseases (njovhera) in Guruve District, Zimbabwe. *J Ethnopharmacol*, 77, 5-9.
- KAUL, S., SHARMA, T. & M, K. D. 2016. "Omics" tools for better understanding the plant-endophyte interactions. *Front Plant Sci*, 7, 955.
- KAVANAGH, K. T., ABUSALEM, S. & CALDERON, L. E. 2018. View point: gaps in the current guidelines for the prevention of Methicillin-resistant *Staphylococcus aureus* surgical site infections. *Antimicrob Resist Infect Control*, 7, 112.
- KEHELPANNALA, C., RATHNAYAKE, G. R. N., DISSANAYAKE, D., KANATIWELA, D., KUMAR, N. S., ADIKARAM, N., JAYASINGHE, L., ARAYA, H. & FUJIMOTO, Y. 2021. Determination of the absolute stereochemistry of (+)-solaniol. *Chemical Papers*, 75, 2233-2235.
- KELL, D. B. 2004. Metabolomics and systems biology: making sense of the soup. *Curr Opin Microbiol*, 7, 296-307.
- KENGEN, R., THOONEN, E., DAVESON, K., LOONG, B., RODGERS, H., BECKINGHAM, W., KENNEDY, K., SUWANDARATHNE, R. & VAN HAREN, F. 2018. Chlorhexidine washing in intensive care does not reduce bloodstream infections, blood culture contamination and drug-resistant microorganism acquisition: an interrupted time series analysis. *Crit Care Resusc*, 20, 231-240.
- KHALIFA, S. A. M., ELIAS, N., FARAG, M. A., CHEN, L., SAEED, A., HEGAZY, M. F., MOUSTAFA, M. S., ABD EL-WAHED, A., AL-MOUSAWI, S. M., MUSHARRAF, S. G., CHANG, F. R., IWASAKI, A., SUENAGA, K., ALAJLANI, M., GÖRANSSON, U. & EL-SEEDI, H. R. 2019. Marine natural products: A source of novel anticancer drugs. *Mar Drugs*, 17, 9: 491.
- KHAN, J., TARAR, S. M., GUL, I., NAWAZ, U. & ARSHAD, M. 2021. Challenges of antibiotic resistance biofilms and potential combating strategies: a review. *3 Biotech*, 11, 169.
- KHAN, T. M., KOK, Y. L., BUKHSH, A., LEE, L. H., CHAN, K. G. & GOH, B. H. 2018. Incidence of methicillin resistant *Staphylococcus aureus* (MRSA) in burn intensive care unit: a systematic review. *Germs*, 8, 113-125.
- KHIRALLA, A., SPINA, R., VARBANOV, M., PHILIPPOT, S., LEMIERE, P., SLEZACK-DESCHAUMES, S., ANDRÉ, P., MOHAMED, I., YAGI, S. M. & LAURAIN-MATTAR, D. 2020. Evaluation of antiviral, antibacterial and antiproliferative activities of the endophytic fungus *Curvularia papendorffii*, and isolation of a new polyhydroxyacid. *Microorganisms*, 8, 9: 1353.
- KIM, H. K., CHOI, Y. H. & VERPOORTE, R. 2010a. NMR-based metabolomic analysis of plants. *Nat Protoc*, 5, 536-49.
- KIM, H. K., CHOI, Y. H. & VERPOORTE, R. 2011. NMR-based plant metabolomics: where do we stand, where do we go? *Trends Biotechnol*, 29, 267-75.
- KIM, H. K., WILSON, E. G., CHOI, Y. H. & VERPOORTE, R. 2010b. Metabolomics: A tool for anticancer lead-finding from natural products. *Planta Med*, 76, 1094-1102.
- KIM, J. H. & PERFECT, J. R. 1989. Infection and cyclosporine. *Rev Infect Dis*, 11, 677-90.
- KIPKORE, W., WANJOHI, B., RONO, H. & KIGEN, G. 2014. A study of the medicinal plants used by the Marakwet Community in Kenya. *J Ethnobiol Ethnomed*, 10, 24.
- KISTLER, H. C. 1997. Genetic diversity in the plant-pathogenic fungus *Fusarium oxysporum*. *Phytopathology*, 87, 474-479.

- KLAIKLAY, S., RUKACHAISIRIKUL, V., SUKPONDMA, Y., PHONGPAICHIT, S., BUATONG, J. & BUSSABAN, B. 2012. Metabolites from the mangrove-derived fungus *Xylaria cubensis* PSU-MA34. *Arch Pharm Res*, 35, 1127-31.
- KO, J. H. & MOON, S. M. 2018. Evaluation of methicillin-resistance rates among community-associated *Staphylococcus aureus* infections in Korean military personnel. *J Korean Med Sci*, 33, 39. e250.
- KOLEY, S. & MAHAPATRA, S. 2015. Evaluation of culture media for growth characteristics of *Alternaria solani*, causing early blight of tomato. *J Plant Pathol Microbiol*, S1: 005.
- KÖNIGS, P., RINKER, B., MAUS, L., NIEGER, M., RHEINHEIMER, J. & WALDVOGEL, S. R. 2010. Structural revision and synthesis of altechromone A. *J Nat Prod*, 73, 2064-2066.
- KOYAMA, N., YOTSUMOTO, M., ONAKA, H. & TOMODA, H. 2013. New structural scaffold 14-membered macrocyclic lactone ring for selective inhibitors of cell wall peptidoglycan biosynthesis in *Staphylococcus aureus*. *The Journal of Antibiotics*, 66, 303-304.
- LACHANCE, H., WETZEL, S., KUMAR, K. & WALDMANN, H. 2012. Charting, navigating, and populating natural product chemical space for drug discovery. *J Med Chem*, 55, 5989-6001.
- LAKHUNDI, S. & ZHANG, K. 2018. Methicillin-resistant *Staphylococcus aureus*: Molecular characterization, evolution, and epidemiology. *Clin Microbiol Rev*, 31.
- LARA, H. H., AYALA-NÚÑEZ, N. V., IXTEPAN TURRENT, L. D. C. & RODRÍGUEZ PADILLA, C. 2010. Bactericidal effect of silver nanoparticles against multidrug-resistant bacteria. *World J Microbiol Biotechnol*, 26, 615-621.
- LEBEAUX, D., GHIGO, J. M. & BELOIN, C. 2014. Biofilm-related infections: bridging the gap between clinical management and fundamental aspects of recalcitrance toward antibiotics. *Microbiol Mol Biol Rev*, 78, 510-543.
- LEE, T. S., DAS, A. & KHOSLA, C. 2007. Structure-activity relationships of semisynthetic mumbaistatin analogs. *Bioorg Med Chem*, 15, 5207-18.
- LESLIE, J. F. & SUMMERELL, B. A. 2006. *Fusarium* laboratory workshops—A recent history. *Mycotoxin Research*, 22, 73-74.
- LIN, W., EZEKWE, E. A. D., ZHAO, Z., LIMAN, E. R. & RESTREPO, D. 2008. TRPM5-expressing microvillous cells in the main olfactory epithelium. *BMC Neuroscience*, 9, 114.
- LINDON, J. C., NICHOLSON, J. K., HOLMES, E. & EVERETT, J. R. 2000. Metabonomics: Metabolic processes studied by NMR spectroscopy of biofluids. *Concepts Magn Reson*, 12, 289-320.
- LOGRIECO, A., MORETTI, A. & SOLFRIZZO, M. 2009. *Alternaria* toxins and plant diseases: an overview of origin, occurrence and risks. *World Mycotoxin J*, 2, 129-140.
- LOU, J., FU, L., PENG, Y. & ZHOU, L. 2013. Metabolites from *Alternaria* fungi and their bioactivities. *Molecules*, 18, 5891-5935.
- LOU, J., YU, R., WANG, X., MAO, Z., FU, L., LIU, Y. & ZHOU, L. 2016. Alternariol 9-methyl ether from the endophytic fungus *Alternaria* sp. Samif01 and its bioactivities. *Braz J Microbiol*, 47, 96-101.
- LOWRY, J. B., PETHERAM, R. J. & BUDI, T. 1992. "Plants fed to village ruminants in Indonesia. Notes on 136 species, their composition and significance in village farming system," Australian Centre for International Agricultural Research, Canberra, NT, Australia, : ACIAR Technical Reports. 22, 60 pp.
- LUMSANGKUL, C., CHIANG, H. I., LO, N. W., FAN, Y. K. & JU, J. C. 2019. Developmental toxicity of mycotoxin fumonisin B(1) in animal embryogenesis: An Overview. *Toxins (Basel)*, 11, 2: 114.

- MACIÀ, M. D., ROJO-MOLINERO, E. & OLIVER, A. 2014. Antimicrobial susceptibility testing in biofilm-growing bacteria. *Clin Microbiol Infect*, 20, 981-90.
- MACINTYRE, L., ZHANG, T., VIEGELMANN, C., MARTINEZ, I. J., CHENG, C., DOWDELLS, C., ABDELMOHSEN, U. R., GERNERT, C., HENTSCHEL, U. & EDRADA-EBEL, R. 2014. Metabolomic tools for secondary metabolite discovery from marine microbial symbionts. *Mar Drugs*, 12, 3416-48.
- MAHROUS, E. A. & FARAG, M. A. 2015. Two dimensional NMR spectroscopic approaches for exploring plant metabolome: A review. *J Adv Res*, 6, 3-15.
- MANGIATERRA, M., GIUSIANO, G., SMILASKY, G., ZAMAR, L., AMADO, G. & VINCENTÍN, C. 2001. Keratomycosis caused by *Cylindrocarpon lichenicola*. *Med Mycol*, 39, 143-5.
- MATSUDA, F., HIRAI, M. Y., SASAKI, E., AKIYAMA, K., YONEKURA-SAKAKIBARA, K., PROVART, N. J., SAKURAI, T., SHIMADA, Y. & SAITO, K. 2010. AtMetExpress development: a phytochemical atlas of Arabidopsis development. *Plant Physiol*, 152, 566-78.
- MEDENTSEV, A. G. & AKIMENKO, V. K. 1998. Naphthoquinone metabolites of the fungi. *Phytochemistry*, 47, 935-959.
- MEENA, M., SWAPNIL, P. & UPADHYAY, R. S. 2017. Isolation, characterization and toxicological potential of *Alternaria*-mycotoxins (TeA, AOH and AME) in different *Alternaria* species from various regions of India. *Sci Rep*, 7, 8777.
- MIAO, Y. H., HU, Y. H., YANG, J., LIU, T., SUN, J. & WANG, X. J. 2019. Natural source, bioactivity and synthesis of benzofuran derivatives. *RSC Adv*, 9, 27510-27540.
- MIRZA, S. B., BOKHARI, H. & FATMI, M. Q. 2015. Exploring natural products from the biodiversity of Pakistan for computational drug discovery studies: Collection, optimization, design and development of a chemical database (ChemDP). *Curr Comput Aided Drug Des*, 11, 102-109.
- MIZUSHINA, Y., MAEDA, N., KURIYAMA, I. & YOSHIDA, H. 2011. Dehydroaltenusin is a specific inhibitor of mammalian DNA polymerase α . *Expert Opin Investig Drugs*, 20, 1523-1534.
- MONGA, S., DHANWAL, P., KUMAR, R., BHAN-KHAR, A. & CHHOKAR, V. 2017. Pharmacological and physico-chemical properties of Tulsi (*Ocimum gratissimum* L.): An updated review. *Pharma Innovation*, 6, 181-186.
- MONI, F., SAIFULLAH, N., AFROZ, F., RONY, S. R., SHARMIN, S., SHAHINUZZAMAN, A. D. A., AL-MANSUR, M. A., AL-REZA, S. M. & SOHRAB, M. H. 2022. Antibacterial and cytotoxic compounds from endophyte *Fusarium solani* isolated from *Centella asiatica* (L.). *J Biol Act Prod Nat*, 12, 436-449.
- MUNKVOLD, G. P. 2003. Epidemiology of *Fusarium* diseases and their mycotoxins in maize ears. *Eur J Plant Pathol*, 109, 705-713.
- MURALI, M., MAHENDRA, C., HEMA, P., RAJASHEKAR, N., NATARAJU, A., SUDARSHANA, M. S. & AMRUTHESH, K. N. 2017. Molecular profiling and bioactive potential of an endophytic fungus *Aspergillus sulphureus* isolated from *Sida acuta*: a medicinal plant. *Pharm Biol*, 55, 1623-1630.
- MUSETTI, R., POLIZZOTTO, R., VECCHIONE, A., BORSELLI, S., ZULINI, L., D'AMBROSIO, M., DI TOPPI, L. S. & PERTOT, I. 2007. Antifungal activity of diketopiperazines extracted from *Alternaria alternata* against *Plasmopara viticola*: an ultrastructural study. *Micron*, 38, 643-50.
- NAMAN, C. B., LEBER, C. A. & GERWICK, W. H. 2017. Chapter 5 - Modern Natural Products Drug Discovery and Its Relevance to Biodiversity Conservation. In: KURTBÖKE, I. (ed.) *Microbial Resources: From Functional Existence in Nature to Applications*. Oxford, UK: Academic Press. ISBN 9780128047651. 103-120.

- NATIONAL NOSOCOMIAL INFECTIONS SURVEILLANCE, S. 2004. National Nosocomial Infections Surveillance (NNIS) System Report, data summary from January 1992 through June 2004, issued October 2004. *Am J Infect Control*, 32, 470-85.
- NEWMAN, D. 2017. Screening and identification of novel biologically active natural compounds. *F1000Res*, 6, 783.
- NEWMAN, D. J. & CRAGG, G. M. 2012. Natural products as sources of new drugs over the 30 years from 1981 to 2010. *J Nat Prod*, 75, 311-335.
- NEWMAN, D. J. & CRAGG, G. M. 2016. Natural Products as Sources of New Drugs from 1981 to 2014. *J Nat Prod*, 79, 629-661.
- NEWMAN, D. J. & CRAGG, G. M. 2020. Natural Products as Sources of New Drugs over the Nearly Four Decades from 01/1981 to 09/2019. *J Nat Prod*, 83, 770-803.
- NEWMAN, D. J., CRAGG, G. M. & SNADER, K. M. 2000. The influence of natural products upon drug discovery. *Nat Prod Rep*, 17, 215-234.
- NIRENBERG, H. 1976. *Untersuchungen über die morphologische und biologische Differenzierung in der Fusarium-Sektion Liseola*. Technischen Universitaet Berlin. ISBN 9783489169000. 117pp.
- NOORI, H. G., TADJROBEHKAR, O. & MOAZAMIAN, E. 2023. Biofilm stimulating activity of solanidine and Solasodine in *Pseudomonas aeruginosa*. *BMC Microbiol*, 23, 208.
- NÜTZMANN, H. W., REYES-DOMINGUEZ, Y., SCHERLACH, K., SCHROECKH, V., HORN, F., GACEK, A., SCHÜMANN, J., HERTWECK, C., STRAUSS, J. & BRAKHAGE, A. A. 2011. Bacteria-induced natural product formation in the fungus *Aspergillus nidulans* requires Saga/Ada-mediated histone acetylation. *Proc Natl Acad Sci U S A*, 108, 14282-7.
- OKAZAKI, Y., SHIMOJIMA, M., SAWADA, Y., TOYOOKA, K., NARISAWA, T., MOCHIDA, K., TANAKA, H., MATSUDA, F., HIRAI, A., HIRAI, M. Y., OHTA, H. & SAITO, K. 2009. A chloroplastic UDP-glucose pyrophosphorylase from *Arabidopsis* is the committed enzyme for the first step of sulfolipid biosynthesis. *Plant Cell*, 21, 892-909.
- OLA, A. R., THOMY, D., LAI, D., BRÖTZ-OESTERHELT, H. & PROKSCH, P. 2013. Inducing secondary metabolite production by the endophytic fungus *Fusarium tricinctum* through coculture with *Bacillus subtilis*. *J Nat Prod*, 76, 2094-2099.
- OLAMILOSOYE, K. P., AKOMOLAFE, R. O., AKINSOMISOYE, O. S., ADEFISAYO, M. A. & ALABI, Q. K. 2019. The aqueous extract of *Ocimum gratissimum* leaves ameliorates acetic acid-induced colitis via improving antioxidant status and hematological parameters in male Wistar rats. *Egypt J Basic Appl Sci*, 5, 220-227.
- ONAJOBI, F. D. 1986. Smooth muscle contracting lipid-soluble principles in chromatographic fractions of *Ocimum gratissimum*. *J Ethnopharmacol*, 18, 3-11.
- ORIAKHI, K., OIKEH, E., EZEUGWU, N., ANOLIEFO, O. N., AGUEBOR, O. & OMOREGIE, E. S. 2013. Comparative antioxidant activities of extracts of *Vernonia amygdalina* and *Ocimum gratissimum* leaves. *J Agric Sci*, 6, 13.
- ORWA, C., MUTUA, A., KINDT, R., JAMNADASS, R. & SIMONS, A. 2009. Agroforestry Database: A Tree Reference and Selection Guide, version 4.0. *World Agroforestry Centre ICRAF*, Nairobi, KE.
- OSTRY, V. 2008. *Alternaria* mycotoxins: an overview of chemical characterization, producers, toxicity, analysis and occurrence in foodstuffs. *World Mycotoxin J*, 1, 175-188.
- PANDA, S., KAR, A., SHARMA, P. & SHARMA, A. 2013. Cardioprotective potential of N, α -L-rhamnopyranosyl vincosamide, an indole alkaloid, isolated from the leaves of

- Moringa oleifera* in isoproterenol induced cardiotoxic rats: in vivo and in vitro studies. *Bioorg Med Chem Lett*, 23, 959-962.
- PANG, Z., RAUDONIS, R., GLICK, B. R., LIN, T. J. & CHENG, Z. 2019. Antibiotic resistance in *Pseudomonas aeruginosa*: mechanisms and alternative therapeutic strategies. *Biotechnol Adv*, 37, 177-192.
- PANT, S., MISHRA, D., GUPTA, S. & CHATURVEDI, P. 2021. Fungal endophytes as a potential source of therapeutically important metabolites. In: SHARMA, V. K., SHAH, M. P., PARMAR, S. & KUMAR, A. (eds.) *Fungi Bio-Prospects in Sustainable Agriculture, Environment and Nano-technology*. Academic Press. ISBN 9780128217344. 275-314.
- PARISOT, D., DEVYS, M. & BARBIER, M. 1988. Fusarubinoic acid, a new naphthoquinone from the fungus *Nectria haematococca*. *Phytochemistry*, 27, 3002-3004.
- PARISOT, D., DEVYS, M. & BARBIER, M. 1990. Naphthoquinone pigments related to fusarubin from the fungus *Fusarium solani* (Mart.) Sacc. *Microbios*, 64, 31-47.
- PATRIDGE, E., GAREISS, P., KINCH, M. S. & HOYER, D. 2016. An analysis of FDA-approved drugs: natural products and their derivatives. *Drug Discov Today*, 21, 204-7.
- PEARSON, H. 2007. Meet the human metabolome. *Nature*, 446, 8.
- PEARSON, K. 1901. LIII. On lines and planes of closest fit to systems of points in space. *The London, Edinburgh, and Dublin Philosophical Magazine and Journal of Science*, 2, 559-572.
- PETROVSKA, B. B. 2012. Historical review of medicinal plants' usage. *Pharmacogn Rev*, 6, 1-5.
- PINHO, B., SOUSA, C., OLIVEIRA, J., VALENTÃO, P. & ANDRADE, P. 2012. Naphthoquinones' biological activities and toxicological effects. In: BITTERLICH, A. & FISCHL, S. (eds.) *Bioactive Compounds: Types, Biological Activities and Health Effects*. Hauppauge, New York: Nova Science Publishers. 181-218.
- PROCTOR, R. H., MCCORMICK, S. P., ALEXANDER, N. J. & DESJARDINS, A. E. 2009. Evidence that a secondary metabolic biosynthetic gene cluster has grown by gene relocation during evolution of the filamentous fungus *Fusarium*. *Mol Microbiol*, 74, 1128-42.
- QADER, M. M., HAMED, A. A., SOLDATOU, S., ABDELRAOF, M., ELAWADY, M. E., HASSANE, A. S. I., BELBAHRI, L., EBEL, R. & RATEB, M. E. 2021. Antimicrobial and Antibiofilm Activities of the Fungal Metabolites Isolated from the Marine Endophytes *Epicoccum nigrum* M13 and *Alternaria alternata* 13A. *Mar Drugs*, 19, 4: 232.
- RANGIAH, K. & GOWDA, M. 2019. Method to Quantify Plant Secondary Metabolites: Quantification of Neem Metabolites from Leaf, Bark, and Seed Extracts as an Example. In: GOWDA, M., SHEETAL, A. & KOLE, C. (eds.) *The Neem Genome*. Cham: Springer International Publishing. ISBN 978-3-030-16122-4. 21-30.
- REHMAN, S., ASLAM, H., AHMAD, A., KHAN, S. A. & SOHAIL, M. 2014. Production of plant cell wall degrading enzymes by monoculture and co-culture of *Aspergillus niger* and *Aspergillus terreus* under SSF of banana peels. *Braz J Microbiol*, 45, 1485-92.
- RICE, L. B. 2008. Federal funding for the study of antimicrobial resistance in nosocomial pathogens: no ESKAPE. *J Infect Dis*, 197, 1079-81.
- RIM, S. O., LEE, J., CHOI, W. Y., HWANG, S.-K., SUH, S. J., LEE, I., RHEE, I. K. & KIM, J. G. 2005. *Fusarium proliferatum* KGL0401 as a new gibberellin-producing fungus. *J Microbiol Biotechnol*, 15, 809-814.
- ROEMER, T., XU, D., SINGH, S. B., PARISH, C. A., HARRIS, G., WANG, H., DAVIES, J. E. & BILLS, G. F. 2011. Confronting the challenges of natural product-based antifungal discovery. *Chem Biol*, 18, 148-64.

- ROSS, C., OPEL, V., SCHERLACH, K. & HERTWECK, C. 2014. Biosynthesis of antifungal and antibacterial polyketides by *Burkholderia gladioli* in coculture with *Rhizopus microsporus*. *Mycoses*, 57 Suppl 3, 48-55.
- ROSSITER, S. E., FLETCHER, M. H. & WUEST, W. M. 2017. Natural products as platforms to overcome antibiotic resistance. *Chem Rev*, 117, 12415-12474.
- RUBAKHIN, S. S., ROMANOVA, E. V., NEMES, P. & SWEEDLER, J. V. 2011. Profiling metabolites and peptides in single cells. *Nat Methods*, 8, S20-29.
- RUKACHAISIRIKUL, V., SOMMART, U., PHONGPAICHIT, S., SAKAYAROJ, J. & KIRTIKARA, K. 2008. Metabolites from the endophytic fungus *Phomopsis* sp. PSU-D15. *Phytochemistry*, 69, 783-787.
- RYBTKE, M., HULTQVIST, L. D., GIVSKOV, M. & TOLKER-NIELSEN, T. 2015. *Pseudomonas aeruginosa* Biofilm Infections: Community Structure, Antimicrobial Tolerance and Immune Response. *J Mol Biol*, 427, 3628-3645.
- SABBAGH, P., RIAHI, S. M., GAMBLE, H. R. & ROSTAMI, A. 2019. The global and regional prevalence, burden, and risk factors for methicillin-resistant *Staphylococcus aureus* colonization in HIV-infected people: A systematic review and meta-analysis. *Am J Infect Control*, 47, 323-333.
- SAKR, A., BRÉGEON, F., MÈGE, J. L., ROLAIN, J. M. & BLIN, O. 2018. *Staphylococcus aureus* Nasal Colonization: An Update on Mechanisms, Epidemiology, Risk Factors, and Subsequent Infections. *Front Microbiol*, 9, 2419.
- SALEM, M. A. & GIAVALISCO, P. 2018. Semi-targeted Lipidomics of Plant Acyl Lipids Using UPLC-HR-MS in Combination with a Data-Independent Acquisition Mode. *Methods Mol Biol*, 1778, 137-155.
- SALEM, M. A., JÜPPNER, J., BAJDZIENKO, K. & GIAVALISCO, P. 2016. Protocol: a fast, comprehensive and reproducible one-step extraction method for the rapid preparation of polar and semi-polar metabolites, lipids, proteins, starch and cell wall polymers from a single sample. *Plant Methods*, 12, 45.
- SÁNCHEZ-CALVO, J. M., BARBERO, G. R., GUERRERO-VÁSQUEZ, G., DURÁN, A. G., MACÍAS, M., RODRÍGUEZ-IGLESIAS, M. A., MOLINILLO, J. M. G. & MACÍAS, F. A. 2016. Synthesis, antibacterial and antifungal activities of naphthoquinone derivatives: a structure–activity relationship study. *Med Chem Res*, 25, 1274-1285.
- SCHIEBER, A., ULLRICH, W. & CARLE, R. 2000. Characterization of polyphenols in mango puree concentrate by HPLC with diode array and mass spectrometric detection. *Innov Food Sci Emerg Technol*, 1, 161-166.
- SCHIEWE, H. J. & ZEECK, A. 1999. Cineromycins, gamma-butyrolactones and ansamycins by analysis of the secondary metabolite pattern created by a single strain of *Streptomyces*. *J Antibiot (Tokyo)*, 52, 635-642.
- SCHMID, R., HEUCKEROTH, S., KORF, A., SMIRNOV, A., MYERS, O., DYRLUND, T. S., BUSHUIEV, R., MURRAY, K. J., HOFFMANN, N., LU, M., SARVEPALLI, A., ZHANG, Z., FLEISCHAUER, M., DÜHRKOP, K., WESNER, M., HOOGSTRA, S. J., RUDT, E., MOKSHYNA, O., BRUNGS, C., PONOMAROV, K., MUTABDŽIJA, L., DAMIANI, T., PUDNEY, C. J., EARLL, M., HELMER, P. O., FALLON, T. R., SCHULZE, T., RIVAS-UBACH, A., BILBAO, A., RICHTER, H., NOTHIAS, L.-F., WANG, M., OREŠIČ, M., WENG, J.-K., BÖCKER, S., JEIBMANN, A., HAYEN, H., KARST, U., DORRESTEIN, P. C., PETRAS, D., DU, X. & PLUSKAL, T. 2023. Integrative analysis of multimodal mass spectrometry data in MZmine 3. *Nat Biotechnol*, 41, 447-449.
- SHAH, K. A., PATEL, M. B., PATEL, R. J. & PARMAR, P. K. 2010. *Mangifera indica* (mango). *Pharmacogn Rev*, 4, 42-48.

- SHAHKARAMI, F., RASHKI, A. & RASHKI GHALEHNOO, Z. 2014. Microbial susceptibility and plasmid profiles of methicillin-resistant *Staphylococcus aureus* and Methicillin-susceptible *S. aureus*. *Jundishapur J Microbiol*, 7, 7. e16984.
- SHARMA, D., MISBA, L. & KHAN, A. U. 2019. Antibiotics versus biofilm: an emerging battleground in microbial communities. *Antimicrob Resist Infect Control*, 8, 76.
- SHESTAKOVA, K. M., MOSKALEVA, N. E., BOLDIN, A. A., REZVANOV, P. M., SHESTOPALOV, A. V., RUMYANTSEV, S. A., ZLATNIK, E. Y., NOVIKOVA, I. A., SAGAKYANTS, A. B., TIMOFEEVA, S. V., SIMONOV, Y., BASKHANOVA, S. N., TOBOLKINA, E., RUDAZ, S. & APPOLONOVA, S. A. 2023. Targeted metabolomic profiling as a tool for diagnostics of patients with non-small-cell lung cancer. *Sci Rep*, 13, 11072.
- SHIN, Y., TAMAI, Y. & TERAZAWA, M. 2001. Chemical constituents of *Inonotus obliquus* IV.: Triterpene and steroids from cultured mycelia. *Eur J Forest Res*, 2, 27-30.
- SIDDIQUI, A. H. & KOIRALA, J. 2022. *Methicillin Resistant Staphylococcus Aureus*, Treasure Island (FL), StatPearls Publishing.
- SILVA, D. A., CHAVES, M. C. O., COSTA, D. A., DE MORAES, M. R. R., DA NÓBREGA, F. B. P. & DE SOUZA, M. F. V. 2005. Flavonoids from *Herissantia tiubae*. *Pharm Biol*, 43, 197-200.
- SIMMLER, C., NAPOLITANO, J. G., MCALPINE, J. B., CHEN, S. N. & PAULI, G. F. 2014. Universal quantitative NMR analysis of complex natural samples. *Curr Opin Biotechnol*, 25, 51-59.
- SINGH, A., KUMAR, J., SHARMA, V. K., SINGH, D. K., KUMARI, P., NISHAD, J. H., GAUTAM, V. S. & KHARWAR, R. N. 2021. Phytochemical analysis and antimicrobial activity of an endophytic *Fusarium proliferatum* (ACQR8), isolated from a folk medicinal plant *Cissus quadrangularis* L. *S Afr J Bot*, 140, 87-94.
- SINGH, B. & SHARMA, R. A. 2020. *Azadirachta* Species. In: SINGH, B. & SHARMA, R. A. (eds.) *Secondary Metabolites of Medicinal Plants: Ethnopharmacological Properties, Biological Activity and Production Strategies*. Weinheim, Germany: Wiley-VCH Verlag GmbH & Co. KGaA. ISBN: 978-3-527-34732-2. 1560 pp.
- SON, S. W., KIM, H. Y., CHOI, G. J., LIM, H. K., JANG, K. S., LEE, S. O., LEE, S., SUNG, N. D. & KIM, J. C. 2008. Bikaverin and fusaric acid from *Fusarium oxysporum* show antioomycete activity against *Phytophthora infestans*. *J Appl Microbiol*, 104, 692-698.
- SONDERGAARD, T. E., FREDBORG, M., OPPENHAGEN CHRISTENSEN, A. M., DAMSGAARD, S. K., KRAMER, N. F., GIESE, H. & SØRENSEN, J. L. 2016. Fast screening of antibacterial compounds from *Fusaria*. *Toxins (Basel)*, 8, 12: 355.
- SONG, J. J., PONGNAK, W. & SOYTONG, K. 2016. Antifungal activity of endophytic fungi from palm trees against coffee anthracnose caused by *Colletotrichum coffeanum*. *Int J Agric Technol*, 12, 527-539.
- SOOKSAI, T., BANKEEREE, W., SANGWATANAROJ, U., LOTRAKUL, P., PUNNAPAYAK, H. & PRASONGSUK, S. 2019. Production of cutinase from *Fusarium falciforme* and its application for hydrophilicity improvement of polyethylene terephthalate fabric. *3 Biotech*, 9, 389.
- SOROKINA, M. & STEINBECK, C. 2020. Review on natural products databases: where to find data in 2020. *J Cheminf*, 12, 20.
- SPURR JR, H. W. & WELTY, R. E. 1975. Characterization of endophytic fungi in healthy leaves of *Nicotiana* spp. *Phytopathology*, 65, 417-422.
- STARKS, C. M., WILLIAMS, R. B., NORMAN, V. L., LAWRENCE, J. A., O'NEIL-JOHNSON, M. & ELDRIDGE, G. R. 2012. Phenylpropanoids from *Phragmipedium calurum* and their antiproliferative activity. *Phytochemistry*, 82, 172-175.

- STEPIEN, A., STEPIEN, M., WLAZEL, R. N., PARADOWSKI, M., BANACH, M. & RYSZ, J. 2014. Assessment of the relationship between lipid parameters and obesity indices in non-diabetic obese patients: a preliminary report. *Med Sci Monit*, 20, 2683-2688.
- STEPIEN, L., WASKIEWICZ, A. & WILMAN, K. 2015. Host extract modulates metabolism and fumonisin biosynthesis by the plant-pathogenic fungus *Fusarium proliferatum*. *Int J Food Microbiol*, 193, 74-81.
- STOHS, S. J. & HARTMAN, M. J. 2015. Review of the safety and efficacy of *Moringa oleifera*. *Phytother Res*, 29, 796-804.
- STOILOVA, I., GARGOVA, S. & KRASTANOV, A. 2005. Production of enzymes by mixed culture from micelial fungi in solid-state fermentation. *Biotechnol Biotechnol Equip*, 19, 103-108.
- STOVER, C. K., PHAM, X. Q., ERWIN, A. L., MIZOGUCHI, S. D., WARRENER, P., HICKEY, M. J., BRINKMAN, F. S., HUFNAGLE, W. O., KOWALIK, D. J., LAGROU, M., GARBER, R. L., GOLTRY, L., TOLENTINO, E., WESTBROCK-WADMAN, S., YUAN, Y., BRODY, L. L., COULTER, S. N., FOLGER, K. R., KAS, A., LARBIG, K., LIM, R., SMITH, K., SPENCER, D., WONG, G. K., WU, Z., PAULSEN, I. T., REIZER, J., SAIER, M. H., HANCOCK, R. E., LORY, S. & OLSON, M. V. 2000. Complete genome sequence of *Pseudomonas aeruginosa* PAO1, an opportunistic pathogen. *Nature*, 406, 959-64.
- STROBEL, G. 2018. The emergence of endophytic microbes and their biological promise. *J Fungi (Basel)*, 4(2): 57.
- SUZUKI, N. 1995. Structure, function and biosynthesis of sperm-activating peptides and fucose sulfate glycoconjugate in the extracellular coat of sea urchin eggs. *Zoolog Sci*, 12, 13-27.
- TANG, J., HUANG, L., LIU, Y., TOSHMATOV, Z., ZHANG, C. & SHAO, H. 2020. Two phytotoxins isolated from the pathogenic fungus of the invasive weed *Xanthium italicum*. *Chem Biodiversity*, 17, 4. e2000043.
- TATUM, J. H. & BAKER, R. A. 1983. Naphthoquinones produced by *Fusarium solani* isolated from citrus. *Phytochemistry*, 22, 543-547.
- TAWFIKE, A. F., VIEGELMANN, C. & EDRADA-EBEL, R. 2013. Metabolomics and Dereplication Strategies in Natural Products. In: ROESSNER, U. & DIAS, D. A. (eds.) *Metabolomics Tools for Natural Product Discovery: Methods and Protocols*. Totowa, NJ: Humana Press. 1055, 227-244.
- TECHAOEI, S., JARMKOM, K., DUMRONGPHUTTIDECHA, T. & KHOBJAI, W. 2021. Evaluation of the stability and antibacterial activity of crude extracts of hydro-endophytic fungi. *J Adv Pharm Technol Res*, 12, 61-66.
- TEITEN, M. H., MACK, F., DEBBAB, A., ALY, A. H., DICATO, M., PROKSCH, P. & DIEDERICH, M. 2013. Anticancer effect of altersolanol A, a metabolite produced by the endophytic fungus *Stemphylium globuliferum*, mediated by its pro-apoptotic and anti-invasive potential via the inhibition of NF- κ B activity. *Bioorg Med Chem*, 21, 3850-3858.
- TERRENI, M., TACCANI, M. & PREGNOLATO, M. 2021. New antibiotics for multidrug-resistant bacterial strains: latest research developments and future perspectives. *Molecules*, 26, 9: 2671.
- THIRUMALAI, T. K., E SENTHILKUMAR, B., DAVID, E. 2009. Ethnobotanical Study of Medicinal Plants used by the Local People in Vellore District, Tamilnadu, India. *Ethnobotanical Leaflets*, 13, 1302-11.
- THOMMA, B. P. 2003. *Alternaria* spp.: from general saprophyte to specific parasite. *Mol Plant Pathol*, 4, 225-36.

- TIWARI, R., VERMA, A. K., CHAKRABORTY, S., DHAMA, K. & SINGH, S. V. 2014. Neem (*Azadirachta indica*) and its potential for safeguarding health of animals and humans. A Review. *J Biol Sci*, 14, 110-123.
- TOGHUEO, R. M. K. 2020. Bioprospecting endophytic fungi from *Fusarium* genus as sources of bioactive metabolites. *Mycology*, 11, 1-21.
- TOLKER-NIELSEN, T. 2015. Biofilm Development. *Microbiol Spectr*, 3, 2. 10.1128/microbiolspec.mb-0001-2014.
- TOMODA, H., KUMAGAI, H., TAKAHASHI, Y., TANAKA, Y., IWAI, Y. & OMURA, S. 1988. F-244 (1233A), a specific inhibitor of 3-hydroxy-3-methylglutaryl coenzyme A synthase: taxonomy of producing strain, fermentation, isolation and biological properties. *J Antibiot (Tokyo)*, 41, 247-249.
- TOMODA, H., OHBAYASHI, N., MORIKAWA, Y., KUMAGAI, H. & OMURA, S. 2004. Binding site for fungal beta-lactone hymeglusin on cytosolic 3-hydroxy-3-methylglutaryl coenzyme A synthase. *Biochim Biophys Acta*, 1636, 22-8.
- TONG, S. Y., DAVIS, J. S., EICHENBERGER, E., HOLLAND, T. L. & FOWLER, V. G., JR. 2015. *Staphylococcus aureus* infections: epidemiology, pathophysiology, clinical manifestations, and management. *Clin Microbiol Rev*, 28, 603-61.
- TSAVKELOVA, E. A., BÖMKE, C., NETRUSOV, A. I., WEINER, J. & TUDZYNSKI, B. 2008. Production of gibberellic acids by an orchid-associated *Fusarium proliferatum* strain. *Fungal Genet Biol*, 45, 1393-403.
- UGBOKO, H. U., NWINYI, O. C., ORANUSI, S. U., FATOKI, T. H. & OMONHINMIN, C. A. 2020. Antimicrobial Importance of Medicinal Plants in Nigeria. *Sci World J*, 2020, 7059323.
- ULRICH-MERZENICH, G., PANEK, D., ZEITLER, H., VETTER, H. & WAGNER, H. 2010. Drug development from natural products: exploiting synergistic effects. 48, 3. 208-19.
- VERGARA-JIMENEZ, M., ALMATRAFI, M. M. & FERNANDEZ, M. L. 2017. Bioactive components in *Moringa Oleifera* leaves protect against chronic disease. *Antioxidants (Basel)*, 6, 4: 91.
- VILLATE, A., SAN NICOLAS, M., GALLASTEGI, M., AULAS, P. A., OLIVARES, M., USOBIAGA, A., ETXEBARRIA, N. & AIZPURUA-OLAIZOLA, O. 2021. Review: Metabolomics as a prediction tool for plants performance under environmental stress. *Plant Sci*, 303, 110789.
- VILLAVICENCIO, E. V., PORTERO, C. E. & NARVAEZ-TRUJILLO, A. 2021. Antibacterial and antifungal activity of organic and peptidic extracts of ecuadorian endophytic fungi. *Adv Microbiol*, 11, 266-282.
- VISALAKCHI, S. & JOHNPAUL, M. 2010. Taxol (Anticancer Drug) producing endophytic fungi. *Int J Pharma Bio Sci*, 1, 1-9.
- VISWANADHAN, V. N., RAJESH, H. & BALAJI, V. N. 2011. Atom type preferences, structural diversity, and property profiles of known drugs, leads, and nondrugs: a comparative assessment. *ACS Comb Sci*, 13, 327-336.
- VON BARGEN, K. W., NIEHAUS, E. M., KRUG, I., BERGANDER, K., WURTHWEIN, E. U., TUDZYNSKI, B. & HUMPF, H. U. 2015. Isolation and structure elucidation of Fujikurins A-D: products of the PKS19 gene cluster in *Fusarium fujikuroi*. *J Nat Prod*, 78, 1809-1815.
- WAGNER, H. & ULRICH-MERZENICH, G. 2009. Synergy research: approaching a new generation of phytopharmaceuticals. *Phytomedicine*, 16, 97-110.
- WANG, H.-J., GLOER, J. B., SCOTT, J. A. & MALLOCH, D. 1995. Coniochaetones A and B: New antifungal benzopyranones from the coprophilous fungus *Coniochaeta saccardoii*. *Tetrahedron Lett*, 36, 5847-5850.

- WANG, K., FU, S.-T., ZHANG, Z. & LI, Z.-Y. 2007. Synthesis and nuclear magnetic resonance shielding effect of three triazine-linked porphyrin compounds. *Journal of The Brazilian Chemical Society - JBCS*, 18, 5, 911-915.
- WANG, Q. X., LI, S. F., ZHAO, F., DAI, H. Q., BAO, L., DING, R., GAO, H., ZHANG, L. X., WEN, H. A. & LIU, H. W. 2011. Chemical constituents from endophytic fungus *Fusarium oxysporum*. *Fitoterapia*, 82, 777-781.
- WANG, Y., YANG, M. H., WANG, X. B., LI, T. X. & KONG, L. Y. 2014. Bioactive metabolites from the endophytic fungus *Alternaria alternata*. *Fitoterapia*, 99, 153-158.
- WEI, C. I., SWARTZ, D. D. & CORNELL, J. A. 1985. Effects of Culture Media, Exposure Time and Temperature on Near-Ultraviolet-Induced Sporulation of *Alternaria alternata*. *J Food Prot*, 48, 316-319.
- WISHART, D. S., KNOX, C., GUO, A. C., EISNER, R., YOUNG, N., GAUTAM, B., HAU, D. D., PSYCHOGIOS, N., DONG, E., BOUATRA, S., MANDAL, R., SINELNIKOV, I., XIA, J., JIA, L., CRUZ, J. A., LIM, E., SOBSEY, C. A., SHRIVASTAVA, S., HUANG, P., LIU, P., FANG, L., PENG, J., FRADETTE, R., CHENG, D., TZUR, D., CLEMENTS, M., LEWIS, A., DE SOUZA, A., ZUNIGA, A., DAWE, M., XIONG, Y., CLIVE, D., GREINER, R., NAZYROVA, A., SHAYKHUTDINOV, R., LI, L., VOGEL, H. J. & FORSYTHE, I. 2009. HMDB: a knowledgebase for the human metabolome. *Nucleic Acids Res*, 37, D603-10.
- WISHART, D. S., TZUR, D., KNOX, C., EISNER, R., GUO, A. C., YOUNG, N., CHENG, D., JEWELL, K., ARNDT, D., SAWHNEY, S., FUNG, C., NIKOLAI, L., LEWIS, M., COUTOULY, M. A., FORSYTHE, I., TANG, P., SHRIVASTAVA, S., JERONCIC, K., STOTHARD, P., AMEGBEY, G., BLOCK, D., HAU, D. D., WAGNER, J., MINIACI, J., CLEMENTS, M., GEBREMEDHIN, M., GUO, N., ZHANG, Y., DUGGAN, G. E., MACINNIS, G. D., WELJIE, A. M., DOWLATABADI, R., BAMFORTH, F., CLIVE, D., GREINER, R., LI, L., MARRIE, T., SYKES, B. D., VOGEL, H. J. & QUERENGESSER, L. 2007. HMDB: the Human Metabolome Database. *Nucleic Acids Res*, 35, D521-6.
- WOLD, S., JOHANSSON, E. & COCCHI, M. 1993. PLS: Partial Least Squares Projections to Latent Structures. In: KUBINYI, H. (ed.) *3D QSAR in Drug Design: Theory, Methods and Applications*. Dordrecht, The Netherlands Kluwer ESCOM Science Publisher.
- WOLD, S., SJÖSTRÖM, M. & ERIKSSON, L. 1994. Partial Least Squares Projections to Latent Structures (PLS) in Chemistry. In: VON RAGUÉ SCHLEYER, P., ALLINGER, N. L., CLARK, T., GASTEIGER, J., KOLLMAN, P. A., SCHAEFER, H. F. & SCHREINER, P. R. (eds.) *Encyclopedia of Computational Chemistry*. Chichester: Wiley. ISBN 9789072199140. 523-550.
- WOLD, S., SJÖSTRÖM, M. & ERIKSSON, L. 2001. PLS-regression: a basic tool of chemometrics. *Chemometr Intell Lab Syst*, 58, 109-130.
- WOLF-RAINER, A. & HANS-ADOLF, A. 1988. Fusalanipyrone, a monoterpene from *Fusarium solani*. *Phytochemistry*, 27, 3310-3311.
- WORLEY, B. & POWERS, R. 2013. Multivariate Analysis in Metabolomics. *Curr Metabolomics*, 1, 92-107.
- WØRMER, G. J. & POULSEN, T. B. 2021. The [4.3.0] Piperidine Alkaloids: Architectures, biology, biosyntheses, and the complete details of the asymmetric syntheses of Streptazone A and Abikoviromycin. *Synlett*, 33, 637-654.
- WU, C., KIM, H. K., VAN WEZEL, G. P. & CHOI, Y. H. 2015. Metabolomics in the natural products field—a gateway to novel antibiotics. *Drug Discov Today Technol*, 13, 11-7.
- WU, H., SOUTHAM, A. D., HINES, A. & VIANT, M. R. 2008. High-throughput tissue extraction protocol for NMR- and MS-based metabolomics. *Anal Biochem*, 372, 204-212.

- WU, Y., LI, T., GONG, L., WANG, Y. & JIANG, Y. 2019. Effects of different carbon sources on fumonisin production and FUM gene expression by *Fusarium proliferatum*. *Toxins (Basel)*, 11, 5: 289.
- XIE, T., SONG, S., LI, S., OUYANG, L., XIA, L. & HUANG, J. 2015. Review of natural product databases. *Cell Prolif*, 48, 398-404.
- XU, S., LI, M., HU, Z., SHAO, Y., YING, J. & ZHANG, H. 2023. The potential use of fungal co-culture strategy for discovery of new secondary metabolites. *Microorganisms*, 11, 2: 464.
- YABUTA, T. K., K; HAYASHI, T 1934. Biochemical studies of bakanae fungus on rice.I. Fusarinic acid, a new product of the bakanae fungus. *J Agric Chem Soc Jpn*, 10, 1059-1068.
- YADAV, G. & MEENA, M. 2021. Bioprospecting of endophytes in medicinal plants of Thar Desert: An attractive resource for biopharmaceuticals. *Biotechnol Rep (Amst)*, 30, e00629.
- YANG, B., WANG, X.-M., MA, H.-Y., JIA, Y., LI, X. & DAI, C. C. 2013. Effects of the fungal endophyte *Phomopsis liquidambari* on nitrogen uptake and metabolism in rice. *Plant Growth Regul*, 73, 165 - 179.
- YANG, J. Y., KARR, J. R., WATROUS, J. D. & DORRESTEIN, P. C. 2011. Integrating 'omics' and natural product discovery platforms to investigate metabolic exchange in microbiomes. *Curr Opin Chem Biol*, 15, 79-87.
- YANNAI, S. 2003. *Dictionary of food compounds with CD-ROM: Additives, flavors, and ingredients (1st ed.)*, New York, Chapman and Hall/CRC. ISBN 9780429149238. 1784 pp.
- ZÄHNER, H. 1977. Some aspects of antibiotics research. *Angew Chem Int Ed Engl*, 16, 687-94.
- ZAKARIA, L., JAMIL, M. I. & ANUAR, I. S. 2016. Molecular characterisation of endophytic fungi from roots of wild banana (*Musa acuminata*). *Trop Life Sci Res*, 27, 153-162.
- ZAMIN, M., FAHAD, S., KHATTAK, A. M., ADNAN, M., WAHID, F., RAZA, A., WANG, D., SAUD, S., NOOR, M., BAKHAT, H. F., MUBEEN, M., HAMMAD, H. M., SOLIMAN, M. H., ELKELISH, A. A., RIAZ, M. & NASIM, W. 2020. Developing the first halophytic turfgrasses for the urban landscape from native Arabian desert grass. *Environ Sci Pollut Res Int*, 27, 39702-39716.
- ZHANG, F., WEI, J., YIN, D., HUANG, H. & ZHANG, Y. 2009. A facile synthesis of goodyeroside A from (S)-malic acid. *Science in China Series B: Chemistry*, 52, 2176-2179.
- ZHANG, L., HATZAKIS, E. & PATTERSON, A. D. 2016. NMR-Based Metabolomics and Its Application in Drug Metabolism and Cancer Research. *Curr Pharmacol Rep*, 2, 231-240.
- ZHANG, L., WANG, J., ZHANG, C. & WANG, Q. 2013. Analysis of potential fumonisin-producing *Fusarium* species in corn products from three main maize-producing areas in eastern China. *J Sci Food Agric*, 93, 693-701.
- ZHANG, Y., CHEN, X., QIN, S., KIM, C., TEBAYASHI, S. & BI, K. 2006. LC-MS method for determination and pharmacokinetic study of chimaphilin in rat plasma after oral administration of the traditional Chinese medicinal preparation Lu xian cao decoction. *Biol Pharm Bull*, 29, 2523-2527.
- ZHANG, Y., HAN, T., MING, Q., WU, L., RAHMAN, K. & QIN, L. 2012. Alkaloids produced by endophytic fungi: a review. *Nat Prod Commun*, 7, 963-968.
- ZHAO, L. & ZHENG, L. 2023. A Review on Bioactive Anthraquinone and Derivatives as the Regulators for ROS. *Molecules*, 28, 24: 8139.

- ZHAO, Q., ZHANG, J. L. & LI, F. 2018. Application of metabolomics in the study of natural products. *Nat Prod Bioprospect*, 8, 321-334.
- ZHUANG, L. & ZHANG, H. 2021. Utilizing cross-species co-cultures for discovery of novel natural products. *Curr Opin Biotechnol*, 69, 252-262.
- ZOUHIR, A., JRIDI, T., NEFZI, A., BEN HAMIDA, J. & SEBEI, K. 2016. Inhibition of methicillin-resistant *Staphylococcus aureus* (MRSA) by antimicrobial peptides (AMPs) and plant essential oils. *Pharm Biol*, 54, 3136-3150.

11 APPENDIX

Appendix 1: Nucleotide sequence of BLS1- *F. proliferatum*

```
>1-BLS1_ITS1
AGAGAAACGAGTTTCACTCCCAAACCCCTGTGAACATACCAATTGTTGCCTCGGCGGATCAGCCCCT
CCCGGTAAAACGGGACGGCCCGCCAGAGGACCCCTAAACTCTGTTTCTATATGTAACCTTCTGAGTAAA
ACCATAAATAAATCAAACTTTCAACAACGGATCTCTTGGTTCTGGCATCGATGAAGAACGCAGCAAA
ATGCGATAAGTAATGTGAATTGCAGAATTCAGTGAATCATCGAATCTTTGAACGCACATTGCGCCCGC
CAGTATTCTGGCGGGCATGCCTGTTTCGAGCGTCATTTCAACCCTCAAGCCCCGGGTTTGGTGTGGG
GATCGGCGAGCCCTTGCGGCAAGCCGGCCCCGAAATCTAGTGGCGGTCTCGCTGCAGCTTCCATTGCG
TAGTAGTAAAACCCCTCGCAACTGGTACGCGGCGCGGCCAAGCCGTTAAACCCCCAACTTCTGAATGTT
GACCTCGGATCAGGTAGGAATACCCGCTGAACTTAAGCATATCAATAAGCGGAGGAAA
```

Following manual review of the sequencing chromatogram, the sequence read was trimmed at the 5' and 3' ends to removed low quality base-calls.

```
>1-BLS1_ITS1-EDIT
TTTCACTCCCAAACCCCTGTGAACATACCAATTGTTGCCTCGGCGGATCAGCCCCTCCCGGTAAAAC
GGGACGGCCCGCCAGAGGACCCCTAAACTCTGTTTCTATATGTAACCTTCTGAGTAAAACCATAAATAA
ATCAAACTTTCAACAACGGATCTCTTGGTTCTGGCATCGATGAAGAACGCAGCAAAATGCGATAAGT
AATGTGAATTGCAGAATTCAGTGAATCATCGAATCTTTGAACGCACATTGCGCCCGCCAGTATTCTGG
CGGGCATGCCTGTTTCGAGCGTCATTTCAACCCTCAAGCCCCGGGTTTGGTGTGGGGATCGGCGAGC
CCTTGCGGCAAGCCGGCCCCGAAATCTAGTGGCGGTCTCGCTGCAGCTTCCATTGCGTAGTAGTAAAA
CCCTCGCAACTGGTACGCGGCGCGGCCAAGCCGTTAAACCCCCAACTTCTGAATGTTGACCTCGGATC
AGGTAGGAATACCCGCTGAACTTAAGCATATCAATAAGCGGAGGAAA
```

BLAST result of BLS1_ITS1 –EDIT sequence

The highest similarity scores from the BLAST analysis included the following GenBank record hit:

Fusarium proliferatum isolate SRG1 internal transcribed spacer 1, partial sequence; 5.8S ribosomal RNA gene and internal transcribed spacer 2, complete sequence; and large subunit ribosomal RNA gene, partial sequence

Sequence ID: MK748309

Length: 535

Number of Matches: 1

Range 1: 13 to 535

Alignment statistics for match #1

Score	Expect	Identities	Gaps	Strand
966 bits(523)	0.0	523/523(100%)	0/523(0%)	Plus/Plus
Query 1	TTTCACTCCCAAACCCCTGTGAACATACCAATTGTTGCCTCGGCGGATCAGCCCCTCC	60		
Sbjct 13	TTTCACTCCCAAACCCCTGTGAACATACCAATTGTTGCCTCGGCGGATCAGCCCCTCC	72		
Query 61	GGTAAAACGGGACGGCCCGCCAGAGGACCCCTAAACTCTGTTTCTATATGTAACCTCTGA	120		
Sbjct 73	GGTAAAACGGGACGGCCCGCCAGAGGACCCCTAAACTCTGTTTCTATATGTAACCTCTGA	132		
Query 121	GTAAAACCATATAAATAAATCAAAACTTTCAACAACGGATCTCTTGGTCTGGCATCGATGA	180		
Sbjct 133	GTAAAACCATATAAATAAATCAAAACTTTCAACAACGGATCTCTTGGTCTGGCATCGATGA	192		
Query 181	AGAACGCAGCAAAATGCGATAAGTAATGTGAATTGCAGAATTCAGTGAATCATCGAATCT	240		
Sbjct 193	AGAACGCAGCAAAATGCGATAAGTAATGTGAATTGCAGAATTCAGTGAATCATCGAATCT	252		
Query 241	TTGAACGCACATTGCGCCCGCCAGTATTCTGGCGGGCATGCCTGTTTCGAGCGTCATTTCA	300		
Sbjct 253	TTGAACGCACATTGCGCCCGCCAGTATTCTGGCGGGCATGCCTGTTTCGAGCGTCATTTCA	312		
Query 301	ACCCTCAAGCCCCGGGTTTGGTGTGGGGATCGGCGAGCCCTTGCGGCAAGCCGGCCCC	360		
Sbjct 313	ACCCTCAAGCCCCGGGTTTGGTGTGGGGATCGGCGAGCCCTTGCGGCAAGCCGGCCCC	372		
Query 361	GAAATCTAGTGGCGGTCTCGCTGCAGCTTCCATTGCGTAGTAGTAAAACCCCTCGCAACTG	420		
Sbjct 373	GAAATCTAGTGGCGGTCTCGCTGCAGCTTCCATTGCGTAGTAGTAAAACCCCTCGCAACTG	432		
Query 421	GTACGCGGCGCGGCCAAGCCGTTAAACCCCAACTTCTGAATGTTGACCTCGGATCAGGT	480		
Sbjct 433	GTACGCGGCGCGGCCAAGCCGTTAAACCCCAACTTCTGAATGTTGACCTCGGATCAGGT	492		
Query 481	AGGAATACCCGCTGAACTTAAGCATATCAATAAGCGGAGGAAA	523		
Sbjct 493	AGGAATACCCGCTGAACTTAAGCATATCAATAAGCGGAGGAAA	535		

Appendix 2: Nucleotide sequence of MGS3A- *F. falciforme*

>1-MGS3A_ITS1

```
AGGGAAACGAGTTATACAACCTCATCAACCCTGTGAACATACCTATAACGTTGCCTCGGCGGGAACAGACGGCCCC
GTAACACGGGCCGCCCGCCAGAGGACCCCTAACTCTGTTTCTATAATGTTTCTTCTGAGTAAACAAGCAAAT
AAATTTAAACTTTCAACAACGGATCTCTTGGCTCTGGCATCGATGAAGAACGCAGCGAAATGCGATAAGTAATGT
GAATTGCAGAATTCAGTGAATCATCGAATCTTTGAACGCACATTGCGCCCGCCAGTATTCTGGCGGGCATGCCTG
TTCGAGCGTCATTACAACCCTCAGGCCCCCGGGCCTGGCGTTGGGGATCGGCGGAAGCCCCCTGCGGGCACAACG
CCGTCCCCCAAATACAGTGGCGGTCCCGCCGAGCTTCCATTGCGTAGTAGCTAACACCTCGCAACTGGAGAGCG
GCGCGGCCACGCCGTAAAACACCCAACCTTCTGAATGTTGACCTCGAATCAGGTAGGAATACCCGCTGAACTTAAG
CATATCAATAAGCCGGAGGAAAATCT
```

Following manual review of the sequencing chromatogram, the sequence read was trimmed at the 5' and 3' ends to removed low quality base-calls.

>1-MGS3A_ITS1-EDIT

```
AGTTATACAACCTCATCAACCCTGTGAACATACCTATAACGTTGCCTCGGCGGGAACAGACGGCCCCGTAACACGG
GCCGCCCCCGCCAGAGGACCCCTAACTCTGTTTCTATAATGTTTCTTCTGAGTAAACAAGCAAATAAATTTAAAA
CTTTCAACAACGGATCTCTTGGCTCTGGCATCGATGAAGAACGCAGCGAAATGCGATAAGTAATGTGAATTGCAG
AATTCAGTGAATCATCGAATCTTTGAACGCACATTGCGCCCGCCAGTATTCTGGCGGGCATGCCTGTTTCGAGCGT
CATTACAACCCTCAGGCCCCCGGGCCTGGCGTTGGGGATCGGCGGAAGCCCCCTGCGGGCACAACGCCGTCCCCC
AAATACAGTGGCGGTCCCGCCGAGCTTCCATTGCGTAGTAGCTAACACCTCGCAACTGGAGAGCGGCGCGGCCA
CGCCGTAAAACACCCAACCTTCTGAATGTTGACCTCGAATCAGGTAGGAATACCCGCTGAACTTAAGCATATCAAT
AAGC
```

BLAST result of MGS3A_ITS1 -EDIT sequence

The highest similarity scores from the BLAST analysis included the following GenBank record hit:

Fusarium falciforme strain DTO 422-H8 small subunit ribosomal RNA gene, partial sequence; internal transcribed spacer 1, 5.8S ribosomal RNA gene, and internal transcribed spacer 2, complete sequence; and large subunit ribosomal RNA gene, partial sequence

Sequence ID: MT251175

Length: 840

Number of Matches: 1

Range 1: 138 to 666

Alignment statistics for match #1

Score	Expect	Identities	Gaps	Strand
977 bits (529)	0.0	529/529(100%)	0/529(0%)	Plus/Plus
Query 1		AGTTATACAACCTCATCAACCCTGTGAACATACCTATAACGTTGCCTCGGCCGGAACAGAC		60
Sbjct 138		AGTTATACAACCTCATCAACCCTGTGAACATACCTATAACGTTGCCTCGGCCGGAACAGAC		197
Query 61		GGCCCCGTAACACGGGCCGCCCCGCCAGAGACCCCTAACTCTGTTTCTATAATGTTT		120
Sbjct 198		GGCCCCGTAACACGGGCCGCCCCGCCAGAGACCCCTAACTCTGTTTCTATAATGTTT		257
Query 121		CTTCTGAGTAAACAAGCAAATAAATTTAAACTTTCAACAACGGATCTCTGGCTCTGGCA		180
Sbjct 258		CTTCTGAGTAAACAAGCAAATAAATTTAAACTTTCAACAACGGATCTCTGGCTCTGGCA		317
Query 181		TCGATGAAGAACGCAGCGAAATGCGATAAGTAATGTGAATTGCAGAATTCAGTGAATCAT		240
Sbjct 318		TCGATGAAGAACGCAGCGAAATGCGATAAGTAATGTGAATTGCAGAATTCAGTGAATCAT		377
Query 241		CGAATCTTTGAACGCACATTGCGCCCGCCAGTATTCTGGCGGGCATGCCTGTTTCGAGCGT		300
Sbjct 378		CGAATCTTTGAACGCACATTGCGCCCGCCAGTATTCTGGCGGGCATGCCTGTTTCGAGCGT		437
Query 301		CATTACAACCCTCAGGCCCCCGGGCCTGGCGTTGGGGATCGGCCGGAAGCCCCCTGCGGGC		360
Sbjct 438		CATTACAACCCTCAGGCCCCCGGGCCTGGCGTTGGGGATCGGCCGGAAGCCCCCTGCGGGC		497
Query 361		ACAACGCCGTCCCCAAATACAGTGGCGGTCCCGCCGAGCTTCCATTGCGTAGTAGCTA		420
Sbjct 498		ACAACGCCGTCCCCAAATACAGTGGCGGTCCCGCCGAGCTTCCATTGCGTAGTAGCTA		557
Query 421		ACACCTCGCAACTGGAGAGCGGCGGCCACGCCGTAACACCCAACTTCTGAATGTTG		480
Sbjct 558		ACACCTCGCAACTGGAGAGCGGCGGCCACGCCGTAACACCCAACTTCTGAATGTTG		617
Query 481		ACCTCGAATCAGGTAGGAATACCCGCTGAACTTAAGCATATCAATAAGC	529	
Sbjct 618		ACCTCGAATCAGGTAGGAATACCCGCTGAACTTAAGCATATCAATAAGC	666	

Appendix 3: Nucleotide sequence of DGS2- *A. alternata*

>1-DGS2_ITS1

```
agggaAaaAAattGAAGGCGGGCTGGAATCTCTCGGGGTACAGCCTTGCTGAATTATTCACCCTTGT  
CTTTGCGTACTTCTTGTTCCTTGGTGGGTTCGCCACCCTAGGACAAACATAAACCTTTTGTAAT  
TGCAATCAGCGTCAGTAACAAATTAATAATTACAACCTTCAACAACGGATCTCTTGGTCTGGCATCG  
ATGAAGAACGCAGCGAAATGCGATAAGTAGTGTGAATTGCAGAATTCAGTGAATCATCGAATCTTTGA  
ACGCACATTGCGCCCTTTGGTATTCCAAAGGGCATGCCTGTTTCGAGCGTCATTTGTACCCTCAAGCTT  
TGCTTGGTGTGGGCGTCTTGTCTCTAGCTTTGCTGGAGACTCGCCTTAAAGTAATTGGCAGCCGGCC  
TACTGGTTTTCGGAGCGCAGCACAAAGTCGCACTCTCTATCAGCAAAGGTCTAGCATCCATTAAGCCTTT  
TTTCAACTTTTGACCTCGGATCAGGTAGGGATACCCGCTGAACTTAAGCATATCAAAAGCccGGAGGA  
Aa
```

Following manual review of the sequencing chromatogram, the sequence read was trimmed at the 5' and 3' ends to removed low quality base-calls.

>1-DGS2_ITS1-EDIT

```
GAAGGCGGGCTGGAATCTCTCGGGGTACAGCCTTGCTGAATTATTCACCCTTGTCTTTTGCCTACTT  
CTTGTTCCTTGGTGGGTTCGCCACCCTAGGACAAACATAAACCTTTTGTAATTGCAATCAGCGTC  
AGTAACAAATTAATAATTACAACCTTCAACAACGGATCTCTTGGTCTGGCATCGATGAAGAACGCAG  
CGAAATGCGATAAGTAGTGTGAATTGCAGAATTCAGTGAATCATCGAATCTTTGAACGCACATTGCGC  
CCTTTGGTATTCCAAAGGGCATGCCTGTTTCGAGCGTCATTTGTACCCTCAAGCTTTGCTTGGTGTGG  
GCGTCTTGTCTCTAGCTTTGCTGGAGACTCGCCTTAAAGTAATTGGCAGCCGGCCCTACTGGTTTTCGGA  
GCGCAGCACAAAGTCGCACTCTCTATCAGCAAAGGTCTAGCATCCATTAAGCCTTTTTTCAACTTTTGA  
CCTCGGATCAGGTAGGGATACCCGCTGAACTTAAGCATATCAAA
```

BLAST result of DGS2_ITS1 –EDIT sequence

The highest similarity scores from the BLAST analysis included the following GenBank record hit:

Alternaria alternata strain CD22M small subunit ribosomal RNA gene, partial sequence; internal transcribed spacer 1, 5.8S ribosomal RNA gene, and internal transcribed spacer 2, complete sequence; and large subunit ribosomal RNA gene, partial sequence

Sequence ID: MT102830

Length: 576

Number of Matches: 1

Range 1: 57 to 576

